# Synthesis of molecular complexes for small molecule activation

THÈSE N$^{O}$ 7250 (2016)

PRÉSENTÉE LE 11 NOVEMBRE 2016

À LA FACULTÉ DES SCIENCES DE BASE

GROUPE SCI-SB-MM

PROGRAMME DOCTORAL EN CHIMIE ET GÉNIE CHIMIQUE

ÉCOLE POLYTECHNIQUE FÉDÉRALE DE LAUSANNE

POUR L'OBTENTION DU GRADE DE DOCTEUR ÈS SCIENCES

PAR

Julie Renée Michelle ANDREZ

acceptée sur proposition du jury:

Prof. L. Helm, président du jury
M. Mazzanti, directrice de thèse
Prof. P. Arnold, rapporteuse
Prof. C. Copéret, rapporteur
Prof. K. Severin, rapporteur

ÉCOLE POLYTECHNIQUE
FÉDÉRALE DE LAUSANNE

Suisse
2016

# Acknowledgment

Firstly, I would like to thank the members of my jury, Prof. Arnold, Prof. Copéret, Prof. Helm and Prof. Severin, for accepting to examine this thesis.

I am grateful to my PhD supervisor, Prof. Marinella Mazzanti, for her guidance and advice all throughout my PhD studies. I would especially like to express my gratitude to her for involving me in all the steps of the laboratory move from Grenoble to Lausanne: planning the layout and organisation of the new laboratory, ordering new equipment, organising the transport of radioactive materials, etc. This was a very rewarding experience.

I would like to thank Prof. Maron and his group for performing the DFT calculations on the uranium sulfide complexes supported by siloxide ligands.

The meetings and discussions with Prof. Meyer and his student, Michael Rosenzweig, were enriching and helpful: I am grateful to them.

I must thank Dr. Gregory Nocton who kindly hosted me in his laboratory in Paris for one week and taught me low-temperature manipulations of derivatives of TPA complexes.

Je souhaiterais remercier Anne-Sophie Chauvin pour avoir toujours été une oreille attentive dans les moments difficiles et pour m'avoir permis d'encadrer des étudiants pendant un TP de chimie durant deux semestres. Cette nouvelle expérience d'enseignement à tes côtés m'a particulièrement plu.

Of course I would like to thank to all the "staff members" of the RICC and GCC laboratories I have met and who made the life in the lab enjoyable: Victor and Clément (who introduced me to f-element chemistry and lab techniques: thank you very much for your patience and kindness), Laetitia and Valentin (the parties at the Mark XIII would not have been the same without you), Maria and Marie (thank you for your constant support), Oliver and Sebastiano (thanks for the unforgettable D&D quests) and Mathieu, Marta, Anna, Sarah, Rory, Vipul, Bang and Davide (thank to all of you for the laughs, the support, the drinks and the refreshing discussions).

Lucile mérite un remerciement particulier. En plus d'être ma « collègue de déménagement du laboratoire », elle est ma co-voitureuse préférée, une amie et une confidente. Merci d'avoir été là.

Je tiens aussi à remercier Lydia, Yves, Joshua, Jessy et Florian pour leur bonne humeur au(x) laboratoire(s) et leurs compétences en chimie organique.

Merci à Pascale Maldivi pour sa bienveillance, à Colette Lebrun pour sa gentillesse et ses connaissances en spectro de masse, à Pierre-Alain Bayle pour les séquences RMN et les bons plans d'escalade ou de ski, à Jean-François Jacquot pour ses mains en or capables de réparer n'importe quel appareil du laboratoire, à Rosario Scopelliti et Euro Solari pour la cristallographie et les discussions sur l'actualité, à Pascal Mieville et Peter Péchy pour leur secours quand les spectromètres de RMN n'en faisaient qu'à leur tête et à Yoann Dind pour son aide précieuse en informatique.

Aux deux comparses Lionel Dubois et Serge Gambarelli qui m'ont respectivement initiée à l'électrochimie et à la RPE : merci pour votre soutien sans faille à base de chocolats !

Je suis extrêmement reconnaissante à Jacques Pécaut pour son enseignement sur l'art de la cristallographie des rayons X mais surtout pour avoir été présent dans les moments difficiles sans jamais faire payer ses séances de psychothérapie. Merci pour tout Jacques !

Un grand merci également à Zohra Termache et Nadia Gauljaux les secrétaires grenobloise et vaudoise qui ont fait preuve d'une efficacité et d'une gentillesse à toute épreuve.

Alain Arbona et Franck Guerin, sont devenus, avec le temps, plus que des collaborateurs hors-pairs toujours soucieux de fournir une pièce de verrerie adéquate. Merci pour votre aide.

Un immense merci à ma famille, à Papa, Maman, Fanny et Rémi pour m'avoir soutenue, quoi qu'il arrive, tout au long de ma jeune vie ; mais aussi à Papi, Mamie, Tonton, Tata et les cousins pour m'avoir accueillie dans le Haut-Doubs pendant les deux dernières années de cette thèse, pour les petits plats et la décompression pendant les week-end.

Quant à toi Quentin, les remerciements que tu mérites ne tiennent pas en quelques lignes. Cependant, pour te faire plaisir je serai concise : Merci de m'avoir supportée et merci d'être toi.

# Abstract

The redox chemistry of f-elements is drawing the attention of inorganic chemists due to their unusual reaction pathways. Notably low-valent f-element complexes have been shown to be able to activate small molecules such as $CO_2$ and $N_2$ in mild conditions. Compared to d-block metals, f-elements present a coordination chemistry dominated by electrostatic interactions and steric constraints. Molecular complexes of f-elements could thus provide new catalytic routes to transform small molecules into valuable chemicals. However the redox chemistry of low valent f-elements is dominated by single-electron transfers while the reductions of $CO_2$ and $N_2$ require multi-electronic processes.

Accordingly the first approach of this PhD work was the use of redox active ligands as electron reservoir to support f-element centres increasing the electron number available for reduction events. The coordination of uranium with tridentate Schiff base ligand was investigated and led to isolation of a dinuclear electron-rich species able to undertake up to eight-electron reduction combining the redox activity of the ligands and the uranium centres. In order to obtain electron-rich compounds potentially able to polarize the C=O bond of $CO_2$, the synthesis of heterobimetallic species supported by salophen Schiff base ligand was also studied.

In a second approach we have used bulky ligands with strong donor-character to tune the reducing abilities of low valent f-elements. In this case a bimolecular electron-transfer process is often observed. The reactivity of the U(III) siloxide complex $[U(OSi(OtBu)_3)_4K]$ was further investigated. Notably, reaction with $Ph_3PS$ led to the formation of a terminal U(IV) sulfide complex with multiple U-S bond which was analysed by DFT studies to better understand the bonding nature. Preliminary studies on the role of the counter-cation (M) in the system $[U(OSi(OtBu)_3)_4M]$ on the outcome of the reactivity with $CS_2$ and $CO_2$ have also been performed. The enhancement of the reducing power of the "classical" divalent lanthanide ions was studied using two different ligand systems. The coordination of siloxide ligands to divalent Eu, Yb and Sm metal centres led to highly reactive compounds featuring unique reactivity with small molecules such as azobenzene, $CS_2$ and $CO_2$. Finally, syntheses and electrochemistry analyses of a family of homoleptic lanthanide complexes supported by related tripodal aminophenolate ligands allowed us to quantify the influence of the ligand donor-character and charge on the reduction potential of the lanthanide centre. The reactivity of an Eu(II) system with $CS_2$ was also investigated.

**Keywords**

f-elements, redox active ligand, heterobimetallic complexes, cobalt, siloxide, cooperative effect, aminophenolate, small molecules.

# Résumé

La chimie d'oxydo-réduction des éléments f suscite actuellement l'attention des chimistes inorganiciens de par la particularité des chemins réactionnels mis en jeux. Il a notamment été montré que des complexes d'élément f à bas degré d'oxydation sont capables d'activer des petites molécules comme $CO_2$ et $N_2$ dans des conditions acceptables de pression et température. En comparaison des métaux du bloc d, les éléments f présentent une chimie de coordination dominée par des interactions électrostatiques et des contraintes stériques. Des complexes moléculaires d'éléments f pourraient donc offrir de nouvelles voies de synthèses catalytiques pour transformer de petites molécules en produits chimiques commercialisables. Cependant, la chimie d'oxydo-réduction des éléments f est dominée par des transferts mono-électroniques alors que les réductions de $CO_2$ et $N_2$ nécessitent des transferts multi-électroniques.

Le premier objectif de ce travail était l'utilisation de ligands redox-actifs en tant que réservoirs d'électrons dans des complexes d'élements f dans le but d'augmenter le nombre d'électrons disponibles pour des réactions de réduction. L'étude de la coordination de ligands base de Schiff tridentate à l'uranium a mené à la formation d'un composé dinucléaire riche en électrons capable de transférer jusqu'à huit électrons en combinant les propriétés d'oxydo-réduction du ligand et des ions uranium. Dans le but d'obtenir des composés riches en électrons susceptibles de polariser la liaison C=O du $CO_2$, une voie de synthèse d'espèces hétérobimetalliques supportées par une base de Schiff salophen a été explorée.

Dans une seconde approche, nous avons utilisé des ligands encombrants fortement donneurs pour améliorer les capacités réductrices des éléments f à bas degré d'oxydation. Dans ce cas, un transfert électronique bimoléculaire est souvent observé. La réactivité du complexe siloxide d'U(III) $[U(OSi(OtBu)_3)_4K]$ a été étudiée plus avant. Notamment, la réaction avec $Ph_3PS$ a mené à la formation d'un complexe sulfure terminal d'U(IV) présentant une liaison U-S multiple qui a été analysée par DFT pour mieux comprendre la nature de la liaison. Des études préliminaires sur le rôle du contre-cation (M) dans le système $[U(OSi(OtBu)_3)_4M]$ sur le résultat de la reduction de $CS_2$ et $CO_2$ ont également été réalisées. L'augmentation du pouvoir réducteur des ions lanthanides divalents « classiques » a été explorée en utilisant deux systèmes de ligand différents. La complexation des ligands silanolates aux centres métalliques divalents d'Eu, d'Yb et de Sm a mené à des composés hautement réactifs présentant une réactivité inhabituelle avec les petites molécules telles que l'azobenzène, le $CS_2$ et le $CO_2$. Finalement, la synthèse et l'analyse électrochimique d'une famille de complexes homoleptiques de lanthanides supportés par des ligands aminophenolates nous ont permis de quantifier l'influence de la charge et du caractère donneur du ligand sur le potentiel de réduction de l'ion lanthanide. La réactivité d'un système d'Eu(II) avec $CS_2$ a aussi été étudiée.

**Mots-clés**

Éléments f, ligand redox-actif, complexes hétérobimetalliques, cobalt, silanolate, effet de coopération, aminophenolate, petites molécules.

# Abbreviation list

18c6 = 18-crown-6 = 1,4,7,10,13,16-Hexaoxacyclooctadecane

Ad = 1-Adamantyl

Cryptand = 2.2.2-cryptand = 4,7,13,16,21,24-hexaoxa-1,10-diazabicyclo[8.8.8]hexacosane

Cp = $C_5H_5$

Cp* = $C_5Me_5$

Cp' = $C_5H_4(SiMe_3)$

Cy = cyclohexyl

DFT = Density Functional Theory

Dibenzo18c6 = 6,7,9,10,17,18,20,21-octahydrodibenzo[b,k][1,4,7,10,13,16]

hexaoxacyclooctadecine

DME = 1,2-dimethoxy ethane

Dmit = 1,3-dithiole-2-thione-4,5-dithiolate

DMSO = dimethyl sulphoxide

eq = equivalent

$E_{pa}$ = anodic potential

$E_{pc}$ = cathodic potential

$E_{1/2}$ = half wave potential

Fc = ferrocene

h = hour

HBPA = bis(2-pyridylmethyl)(2-hydroxybenzyl)amine

HBPPA = bis(2-pyridylmethyl)(3.5-di-tert-butyl-2-hydroxybenzyl)amine

$H_2$MPA = 2-pyridylmethyl)bis(3.5-di-tert-butyl-2-hydroxybenzyl)amine

hex =hexane

KHMDS = potassium bis(trimethylsilyl)amide

Me = methyl

min = minute

Np = *neo*-pentyl

OTf = triflate

Ph = phenyl

PhNNPh = diazobenzene

Py = pyridine

PyHCl = pyridinium chloride

PyNO = pyridine N-oxide

tBu = *tert*-butyl

THF = tetrahydrofuran

tol = toluene

TPA = tris(2-pyridylmethyl)amine

Trityl = triphenylmethyl

# Table of Content

# CHAPITRE I
# General Introduction

## I.1 Objectives of the project

The overarching aim of this study is to gain insight into the fundamental chemical properties of low-valent f-elements. Compared to d-block metals, low-valent lanthanide and uranium chemistry is much less developed. Investigation of the reactivity of low-valent f-element species is thus of great fundamental and practical interest.

Moreover, beyond the various applications of f-elements in manufactured goods or in nuclear industry, the study of small molecule ($CO_2$, CO, $N_2$) activation by low valent f-element complexes could lead to alternative routes to renewable energy sources. Indeed, the use of these simple molecules as renewable building blocks for the catalytic synthesis of fuels or commodity chemicals has become an important challenge.[1, 2] However, $CO_2$ and $N_2$ are highly kinetically and thermodynamically stable, necessitating the use of reactive metal complexes to overcome the high activation barriers to reduction.[3, 4] The reduction of $CO_2$ and $N_2$ into more elaborate molecules requires multi-electron transfer. While the long-term aim is the design of efficient f-element catalysts for the transformation of $CO_2$ or $N_2$ into value-added chemicals under mild conditions, current fundamental research in this area is focused on the synthesis of molecular f-element complexes that are able to coordinate $CO_2$ or $N_2$ and transfer a large number of electrons.

The few examples of small-molecule activation by f-elements reported in the literature before the beginning of this work were promising and underlined the unique reductive chemistry of lanthanide and uranium compounds. These studies showed the important role of the ancillary ligands and of their steric and electronic properties on the reactivity of f-element

complexes. Thus, it is a delicate balancing act trying to prepare electron-rich f-element complexes that are stable enough to handle while maintaining high reactivity.

Thus, the aim of this work is to synthesise new highly reducing mono- or polymetallic complexes of the f-elements and exploit their unique properties to promote the reduction of small molecules. Two different approaches were envisaged during this work.

In a first approach, as low-valent f-elements mainly engage in single-electron transfer reactions, the use of redox non-innocent ligands was investigated in order to promote metal-mediated multi-electron transfer to the targeted substrates. The aim is to use the ligand scaffold as a reservoir of electrons which are available to reduce small molecules and potentially combine the redox activity of the metal and the ligand. Tetradentate Schiff bases were previously identified by our group to be convenient redox-active ligands able to coordinate f-elements and to store at least two electrons.[5, 6] However the previously prepared homometallic complexes were not able to transfer electrons to unreactive molecules such as $CO_2$. One of the goals of this thesis was to increase the reducing ability of f-element complexes of redox-active ligands both by modifying the architecture of the Schiff base and by building heteropolymetallic complexes. Tridentate Schiff bases were identified as ligands of interest because they would lead to coordinatively unsaturated metal-centres.

The second approach adopted in this work for the development of highly reactive complexes of f-elements consists of synthesising low valent f-element complexes (U(III) and Ln(II)) supported by electron-rich ligands in order to enhance the reducing abilities of the metal centres. Such complexes, if a synthetic route could be identified, should lead to unusual reactivity with small molecules. In this work two different families of ligands have been chosen for the synthesis of highly reactive complexes of f-elements, siloxides and aminophenolates. Siloxide have been chosen because of their bulkiness and tunability. Moreover, they have multiple binding modes and their low basicity should prevent undesirable side reactions. Tripodal aminophenolates have been chosen due to their polydentate character and their versatile synthesis that allow to tune steric and electronics at the metal centre. The goal of the project was to explore the ability of these two families of ligands to stabilize low-valent complexes of f-elements and to explore their reducing properties. Preliminary studies had shown that the tris(tert-butoxy)siloxide ligand is particularly effective in stabilizing highly reactive trivalent uranium complexes. My objective was to further explore the reactivity of siloxide based uranium systems with different substrates and to investigate the possibility of extending this chemistry to divalent

lanthanides. Moreover, the uranium siloxide system was identified to provide adapted steric hindrance to stabilize terminal oxo complex.[7] Accordingly, one of the aims of this work consists of finding synthetic routes to terminal uranium sulfide species in order to gain insight into U-chalcogen multiple bonds.

# I.2 The f-elements

The f-elements were discovered in the late 1700's and their use in numerous diverse sectors has been intensified over the last 35 years. Their unique physical properties render their presence crucial in a large range of applications such as permanent magnets for data storage or engine in electric vehicles, luminophores in television screens, lasers, alloys in catalytic converters, superalloys for aeronautics or aerospace, miniaturized capacitors, probes for MRI imaging, nuclear weapon and fuel for nuclear industry. The increasing demand for those f-elements is now raising economic and geopolitical concerns.[8]

## I.2.1 Fundamental properties

The 30 elements whose atoms or ions possess valence electrons in f-orbitals are called the f-elements. They are divided in two families: the first row of the f-block gathers the elements possessing 4f valence electrons and is called the lanthanides series (La-Lu) while the second row gathering the elements possessing 5f valence electrons is called the actinide series (Ac-Lr). The lanthanum and the actinium, despite their electronic configuration of $[Xe]5d^{1}6s^{2}4f^{0}$ and $[Rn]6d^{1}7s^{2}$ respectively, are included by extension (Figure I-1). The elements in dark shaded cells are the unstable elements that do not occur naturally.

The f-elements feature large ionic radii leading to high coordination numbers (6 to 12 are the most common) and unusual coordination geometries compared to those observed in transition metal chemistry. The f-elements cations are hard Lewis acids and thus have a strong affinity for hard Lewis bases such as fluoride and alkoxides. Their tendency to form hydroxides or oxides by hydrolysis or abstraction of oxygen atoms led to describe the f-elements as oxophilic compounds.[9]

| | | | | | | | | | | | | | | |
|---|---|---|---|---|---|---|---|---|---|---|---|---|---|---|
| 57 **La** | 58 **Ce** | 59 **Pr** | 60 **Nd** | 61 **Pm** | 62 **Sm** | 63 **Eu** | 64 **Gd** | 65 **Tb** | 66 **Dy** | 67 **Ho** | 68 **Er** | 69 **Tm** | 70 **Yb** | 71 **Lu** |
| 89 **Ac** | 90 **Th** | 91 **Pa** | 92 **U** | 93 **Np** | 94 **Pu** | 95 **Am** | 96 **Cm** | 97 **Bk** | 98 **Cf** | 99 **Es** | 100 **Fm** | 101 **Mb** | 102 **No** | 103 **Lr** |

**Figure I-1: F-block elements. First row: the lanthanides, second row: the actinides. Dark shaded cells: unstable elements that do not occur naturally.**

The 5f orbitals of the early actinides in the +III oxidation state extend out farther from the nucleus than the 4f orbitals of the lanthanides in the +III oxidation state. Especially when relativistic effect are considered, the 5f electron density of Pu(III) ion shows an important tail compared to the 4f electron density of Sm(III) cation (Figure I-2)[1].[10] This induces a greater participation in chemical bonding of the 5f orbitals than the 4f ones that are deeper in the lanthanide atoms.

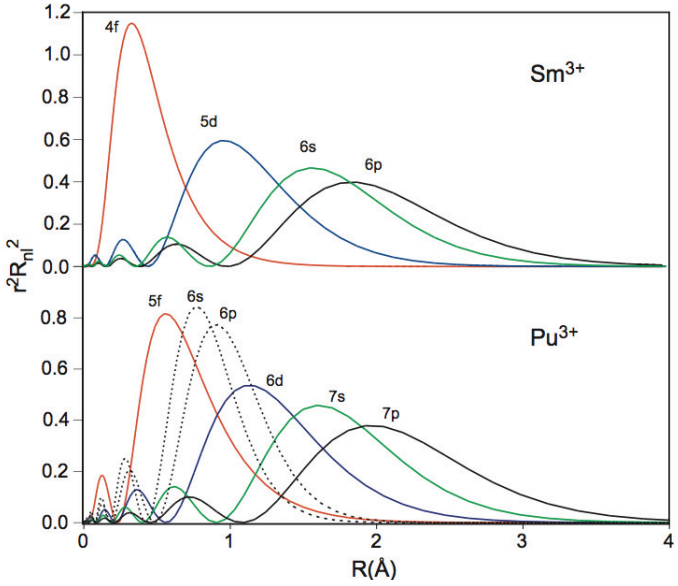


**Figure I-2[a]: Comparison of the relativistic radial extent of the electronic orbitals of Sm(III) (top) and Pu(III) (bottom) ions. [10]**

In consequence, the ligand-field does not significantly influence the electronic structure of Ln(III) complexes and the metal-ligand interaction in lanthanide chemistry is

[1] Reprinted from Coord. Chem. Rev., 257, Neidig M. L., Clark D. L., Martin R. L., Covalency in f-element complexes, 394-406, copyright (2013), with permission from Elsevier.

largely electrostatic. The magnetic and spectroscopic properties of Ln(III) complexes supported by different ligands are often comparable and very similar to the free ion properties due to the ionic character of the ligand-metal interaction. Thus, the coordination numbers and the coordination geometries adopted by the lanthanide centres are determined by the steric repulsion between the ligands and charge balance effects.[9, 11] As a result of their mainly electrostatic character the lanthanide complexes are kinetically labile. This renders attractive for catalytic applications.[12] The rational tuning of the charge and steric hindrance of the ligands is crucial in order to control the reactivity of the lanthanide complexes.

The increased radial probability of 5f and 6d orbitals in early actinides (Th-Pu), allows ligand and metal orbitals to overlap in some extent. This stronger interaction of the early actinides with the ligands leads to magnetic and spectroscopic properties more sensitive to the coordination environment of the actinide centre. Even if the actinide-ligand bond features some degree of covalency, the overall nature of the bonding remains mainly electrostatic and thus the coordination geometries and coordination numbers of the actinides are also essentially ruled by steric constraints.[9]

## I.2.2 The lanthanide series

The discovery of lanthanides ores started in 1787 in Sweden. The first serious characterisation of this ore was performed by Johan Gadolin in 1794. It is only in 1947 that the lanthanide series was completed with the synthesis of promethium.[13] The yttrium and scandium elements have similar physico-chemical properties to lanthanides. All together they form the rare earth group. The term “rare earths” makes a reference to the low concentration of these elements in the ores. However this adjective proved to be wrong as even the rarest lanthanides (Tm, Lu) are more abundant on earth than silver or platinum.[9] Nowadays, China possesses 97% of the worldwide production of lanthanides and access to rare earths resources is becoming one of the main geopolitical stakes of the 21$^{st}$ century.[8]

The +III oxidation state is the most stable in the lanthanide series. Looking at the evolution of the Ln(III) ionic radii along the series, we observe the so-called “lanthanide contraction” (Table I-1). Indeed, when the atomic number increase along the series, the electron is added in the buried 4f shell. As 4f electrons have poor screening abilities,

increasing the atomic charge of the nucleus leads to a greater attraction of the 5s and 5p electrons by the nucleus which decreases the ionic radius along the series.[9] Consequently, steric control around the metal centre can be tuned not only by the ligand bulkiness but also by using the gradually changing ionic radial size.

The lanthanide metals have mainly $[Xe]4f^{n+1}6s^2$ electron configurations except lanthanum, cerium, gadolinium and lutetium which have $[Xe]4f^n5d^16s^2$ electron configurations (Table I-1). With the exceptions of La(III) and Lu(III), all the Ln(III) cations possess unpaired 4f electrons and are thus paramagnetic. However other oxidation states, +IV and +II, are reachable. Notably, the configurations Ce(IV) $4f^0$, Tb(IV) $4f^7$, Eu(II) $4f^7$ and Yb(II) $4f^{14}$ (i.e. empty, half-filled or filled 4f shell) are known as well as Sm(II) $4f^6$.

**Table I-1: Electronic configurations of lanthanides and ionic radii of the Ln(III) cations.[14-16]**

| Element | Electronic configuration of the fundamental state | | | | Radii (Å) |
|---|---|---|---|---|---|
| | Ln | Ln(II) | Ln(III) | Ln(IV) | Ln(III)* |
| **La** | $[Xe]5d^16s^2$ | $[Xe]5d^1$ | [Xe] | | 1.16 |
| **Ce** | $[Xe]4f^15d^16s^2$ | $[Xe]4f^15d^1$ | $[Xe]4f^1$ | [Xe] | 1.14 |
| **Pr** | $[Xe]4f^36s^2$ | $[Xe]4f^25d^1$ | $[Xe]4f^2$ | $[Xe]4f^1$ | 1.13 |
| **Nd** | $[Xe]4f^46s^2$ | $[Xe]4f^4$ or $[Xe]4f^35d^1$ | $[Xe]4f^3$ | $[Xe]4f^2$ | 1.11 |
| **Pm** | $[Xe]4f^56s^2$ | | $[Xe]4f^4$ | | 1.09 |
| **Sm** | $[Xe]4f^66s^2$ | $[Xe]4f^6$ | $[Xe]4f^5$ | | 1.08 |
| **Eu** | $[Xe]4f^76s^2$ | $[Xe]4f^7$ | $[Xe]4f^6$ | | 1.07 |
| **Gd** | $[Xe]4f^75d^16s^2$ | $[Xe]4f^75d^1$ | $[Xe]4f^7$ | | 1.05 |
| **Tb** | $[Xe]4f^96s^2$ | $[Xe]4f^85d^1$ | $[Xe]4f^8$ | $[Xe]4f^7$ | 1.04 |
| **Dy** | $[Xe]4f^{10}6s^2$ | $[Xe]4f^{10}$ or $[Xe]4f^85d^1$ | $[Xe]4f^9$ | $[Xe]4f^8$ | 1.03 |
| **Ho** | $[Xe]4f^{11}6s^2$ | $[Xe]4f^{10}5d^1$ | $[Xe]4f^{10}$ | | 1.02 |
| **Er** | $[Xe]4f^{12}6s^2$ | $[Xe]4f^{11}5d^1$ | $[Xe]4f^{11}$ | | 1.00 |
| **Tm** | $[Xe]4f^{13}6s^2$ | $[Xe]4f^{13}$ | $[Xe]4f^{12}$ | | 0.99 |
| **Yb** | $[Xe]4f^{14}6s^2$ | $[Xe]4f^{14}$ | $[Xe]4f^{13}$ | | 0.99 |
| **Lu** | $[Xe]4f^{14}5d^16s^2$ | $[Xe]4f^{14}5d^1$ | $[Xe]4f^{14}$ | | 0.98 |

*Ionic radii for a coordination number of 8.

The three lanthanides europium, samarium and ytterbium were recognized more stable in the +II oxidation state than the others and thus called the "classical divalent lanthanides".[17] Recently, Evans and co-workers characterised by X-ray diffraction, UV-vis spectroscopy and DFT calculations, the divalent complexes [LnCp'$_3$][Kcryptand] (Cp'=$C_5H_4SiMe_3$) of all the lanthanides (except Pm).[15, 18, 19] This study allows the identification of three groups of Ln centres according to their electron configuration in the +II oxidation state. In this ligand environment Eu, Yb, Sm and Tm ions have [Xe]4f$^{n+1}$ electron configuration while La, Ce, Pr, Gd, Tb, Ho, Er, and Lu ions have [Xe]4f$^n$5d$^1$ electron configuration. However, Dy and Nd ions, depending on their ligand environment, can cross over between these two configurations. This work shows that, in the case of Ln(II) complexes, the ligand field can influence the ground electronic state.[15, 20, 21]

The redox potentials of the couples Ln(III)/Ln(II) have been calculated (measured in the case of Eu, Yb, Sm) in aqueous solution and are presented in Table I-2.[22] The classical divalent lanthanides are indeed the less reducing elements of the series which explain that complexes of Eu(II), Yb(II) and Sm(II) have been the most studied. However they remain very reactive species and samarium di-iodide $SmI_2$ has become a popular reducing agent in organic chemistry.[23, 24] The very low redox potentials observed for the majority of the divalent lanthanide ions explain the high reactivity of the Ln(II) complexes and together with their oxophilic character renders them very attractive for small molecules activation.[25]

**Table I-2: Reduction potentials (vs. NHE) calculated for Ln(III)/Ln(II) couples in order of increasing reducing power.[22, 26]**

| Ln | E (V vs. NHE) | Ln | E (V vs. NHE) |
|---|---|---|---|
| Eu | -0.35 | Pr | -2.7 |
| Yb | -1.15 | Ho | -2.9 |
| Sm | -1.55 | Er | -3.1 |
| Tm | -2.3 | La | -3.1 |
| Dy | -2.6 | Ce | -3.2 |
| Nd | -2.6 | Tb | -3.7 |
| Pm | -2.6 | Gd | -3.9 |

The isolation of divalent lanthanide complexes requires a careful choice of ligand with appropriate geometric and electronic properties. During the last decades, several ligands systems were proved to be able to stabilize Ln(II) complexes. They can be divided in two categories: the carbocyclic ligands and derivatives and the non-cyclopentadienyl-based ligands.

The Ln(II) coordination chemistry is largely dominated by carbocyclic ligands because of their suitable steric hindrance and electronic properties to form isolable Ln(II) complexes. The solubility of metallic europium and ytterbium in liquid ammonia allowed the synthesis of the first divalent Eu and Yb complexes supported by simple cyclopentadienyl ligands in 1964 and 1966.[27, 28] The divalent samarocene complex, has been synthesised in 1969 by reduction of the trivalent [$SmCp_3$] complex with potassium naphthalenide.[29] However the insolubility of these complexes incited researchers to add substituents on the Cp template. The introduction of alkyl or trimethylsilyl groups on the Cp ring allows the tuning of the complex solubility, of the steric hindrance and of the electronic density around the metal centre. Notably, Evans and co-workers reported the synthesis of decamethylsamarocene [$SmCp^*_2$] in 1984 and investigated in depth its interesting reactivity.[30, 31] For a long time it was assumed that this chemistry could not be expanded to the other lanthanides because of their very low reduction potentials. Notably, first "non-classical" divalent lanthanide di-iodide (Nd, Dy, Tm) compounds were isolated only thirty years later.[32-34] Evans et al. were then able to characterise the first Tm(II) organometallic complex supported by the silylated Cp" ligand (Cp"=$C_5H_3$-1,3-$(SiMe_3)_2$).[35] This complex is unstable in solution at room temperature. In order to increase the stability of Tm(II) complexes, Nief and co-workers successfully employed the use of phospholyl ligands, which are weaker π-donors than Cp ligands (Scheme I-1).[36]

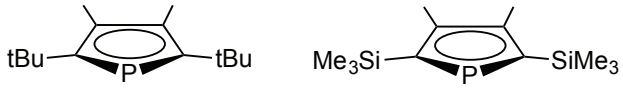


**Scheme I-1: Phospholyl ligands used for the synthesis of Tm(II) complexes.[36]**

However, the low solubility of the $DyI_2$ and $NdI_2$ salts in organic solvents prevented the synthesis of Dy(II) and Nd(II) molecular complexes by salt exchange. Consequently, the synthesis of the first Dy(II) and Nd(II) organometallic complexes was achieved by reduction of their trivalent analogous with potassium graphite in presence of 18c6 crown ether.[37, 38] Finally, it is only very recently that Evans and co-workers completed the series synthesising

the complexes [Kcryptand][LnCp'$_3$] of the most reducing divalent lanthanides (Ln=Pr, Gd, Tb, Ho, Er, Lu except Pm for radioactive reasons) (Scheme I-2).[15, 18, 19]

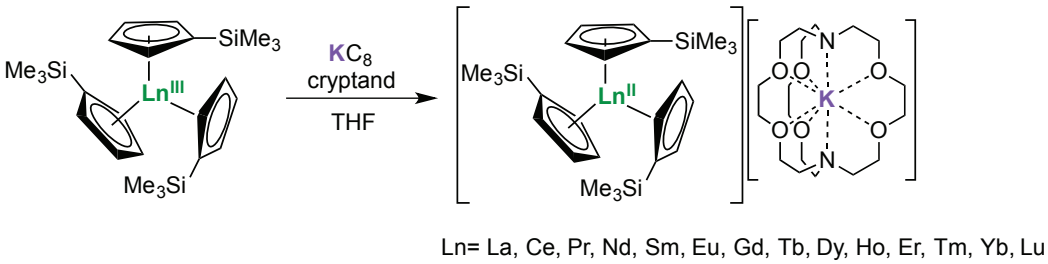


**Scheme I-2: Synthesis of the divalent lanthanide complexes [Kcryptand][LnCp'$_3$] for the entire series (except Pm).**

Examples of divalent lanthanide complexes supported by non-Cp ligands have also been reported since the early 1990's. Most of these are complexes of classical divalent lanthanides with alkyl, aryl, benzyl, alkenyl, allyl, aza-allyl, pentadienyl, cyclo-octatetraenyl, phosphoramide, alcoholate, benzamidinate, pyrolyl, pyrazolate or pyrazolylborate ligands and are described in the Edelmann review.[39] More recently, O- or/and N-donor ligands such as phenolate[40, 41], silanolate[42, 43], aminotroponiminate[44] amidinate and guanidinate[45], α-iminopyridine[46], pyrolyl schiff base[47], porphyrinogen[48], triazacyclononane-functionalized Cp[49], aminophenolate[50-53] or hydride ligands[54, 55] have been used.

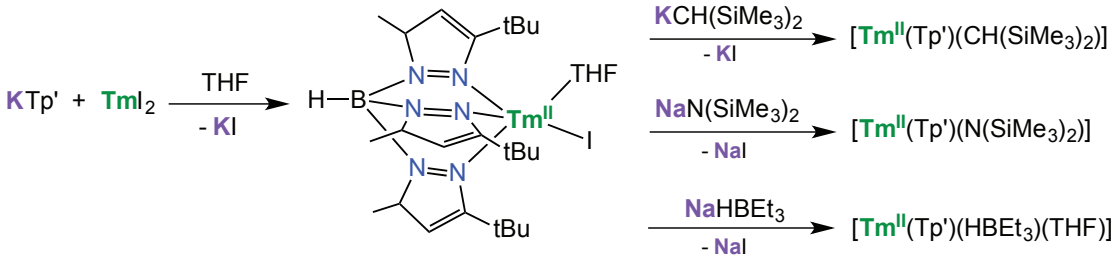


**Scheme I-3: Synthesis of the heteroleptic Tm(II) complexes supported by scorpionate ligand.[56]**

The only non-classical divalent lanthanide complexes supported by a non-Cp ligands has been isolated by Takats et al. in 2008 using scorpionate ligand (Scheme I-3).[56] The complex [Tm(Tp')I(THF)] slowly decomposes both in solution and solid state at -30°C but remains a useful precursor for the isolation of other heteroleptic Tm(II) complexes.

## I.2.3 The uranium element

Uranium, one of the rare actinides that occur naturally, has been isolated as uranium oxide in 1789 by Martin Heinrich Klaproth from the pitchblende ore. Uranium metal was obtained in 1841 by Eugène Melchior Péligot by reduction of $UCl_4$ with potassium.[57] Uranium occurs in nature with a proportion of 99.27% $^{238}U$ and 0.72% $^{235}U$ and both isotopes are radioactive. As the $^{235}U$ nucleus presents interesting decay properties, natural uranium enriched in $^{235}U$ isotope is used as nuclear fuel in nuclear power plants.[58] The isotope enrichment process affords highly pure $^{238}U$ depleted uranium as by-product. The $^{238}U$ isotope decays emitting α and $\beta^-$ particles of weak energy that can be stopped by simple glass thickness.[59] This property facilitates the safe handling of natural or depleted uranium compared to more radioactive elements which needs specific and constraining facilities to be safely handle.

Uranium features richer redox chemistry than lanthanides with a large number of known oxidation states from +II to +VI. Among the oxidation states, presented in Table I-3, +IV and +VI are the most stable. Under aerobic conditions, only the +VI oxidation state is stable and uranium is found in the form of the uranyl(VI) cation $UO_2^{2+}$. Under anaerobic conditions, due to the high stability of U(IV) ion, reduction reactions by U(III) compounds are dominated by mono-electronic transfers involving the U(IV)/U(III) couple. Bimolecular redox reactions from U(III) to U(IV) are thus more common than two-electron oxidation from U(III) to U(V).[60] With the exception of U(VI) ion which is iso-electronic with Rn and thus diamagnetic, all the other uranium cations possess unpaired 5f electrons and are thus paramagnetic.

**Table I-3: Electronic configurations of uranium and ionic radius of the U(III) cations.[14, 16, 61]**

| Electronic configuration of the fundamental state | | | | | | Radii (Å) | |
|---|---|---|---|---|---|---|---|
| U | U(II) | U(III) | U(IV) | U(V) | U(VI) | U(III)* | U(IV)# |
| $[Rn]5f^36d^17s^2$ | $[Rn]5f^36d^1$ | $[Rn]5f^3$ | $[Rn]5f^2$ | $[Rn]5f^1$ | [Rn] | 1.03 | 1.00 |

*Ionic radius for a coordination number of 6. # Ionic radius for a coordination number of 8.

The redox potential of the U(IV)/U(III) couple depends on the coordination environment around the metal centre and lies between -1.5 and -2.8 V vs. $Fc^{+}/Fc$.[60, 62] This range of values shows that U(III) complexes are potentially strong reducing agents. The high reducing power of U(III) associated to its oxophilic character has lead to interesting reactivity and small molecule reduction.[63, 64] However the reducing power of trivalent uranium limits the range of experimental conditions that can be used to prepare U(III) complexes.

The preparation of U(III) precursors in the 1970's were usually done at high temperature and led to insoluble polymeric anhydrous $UX_3$ (X=Cl, I) compounds[65, 66]. Although the solvated compound $[UCl_3(THF)_x]$, obtained by reduction of the $UCl_4$ salt, presents a better solubility, the reported syntheses for its preparation[67-69] were time consuming, extremely sensitive to reaction time or led to variable yields and contaminations with U(IV) species.[70] The first convenient soluble precursor $[UI_3(THF)_4]$ was reported in 1994 by Sattelberger and co-workers via addition of 1.5eq of di-iodide to amalgamated uranium turnings. Moreover, Sattelberger et al. also reported the improved synthesis of $[U(HMDS)_3]$ (HMDS=$N(SiMe_3)_2$) by addition of 3eq of sodium silylamide to this $[UI_3(THF)_4]$ precursor.[71] Significant improvements of the $[UI_3(THF)_4]$ synthesis were recently reported by Arnold et al.[72] and Kiplinger et al.[73] allowing large choice of solvent adducts (THF, Pyridine, DME, 1,4-dioxane), increased yields and room temperature and mercury-free conditions. The syntheses of $[UI_3(THF)_4]$ and $[U(HMDS)_3]$ precursors rendered possible the exploration of U(III) chemistry giving access to both salt metathesis and protonolysis routes to yield U(III) complexes. Another approach to the preparation of U(III) compounds is the reduction of the U(IV) analogue. This method is particularly useful when salt exchange between deprotonated ligands and $[UI_3(THF)_4]$ leads to oxidation of the uranium centre.[74, 75]

The first organometallic complex of U(III), $[UCp_3]$, was isolated in 1970 by Baumgärtner and co-workers.[76] This complex demonstrates the originality of uranium and f-elements as no tris-cyclopentadienyl analogous complex exists with transition metals. Consequently, the chemistry of U(III) supported by Cp derivatives and other aromatic carbocyclic ligands was largely studied.[77] Examples of heteroatom-based ligands stabilizing U(III) ions have emerged such as dicarbollide, polypyridine, pyrazine, imide, amide, silylamide, tacn-based amide, pyrazolylborate, pyrrolyl, calixpyrrol, phosphinoamide, diketiminate, N-heterocyclic carbene, phenolate, amino- aryl- or tacn-based trisphenolate,

chalcogeno-phosphinoyl-carbene, thiophenolate and thio-imidazolylborate. These examples are presented in the Baker and Liddle reviews.[74, 78]

Although an increasing number of non-Cp ligands have been identified that stabilize highly reactive U(III) complexes, the study of their reactivity remain still scarce. Moreover, the first U(II) complex was reported recently by Evans et al. and opens new perspectives in the chemistry of low valent uranium.[61]

# I.3 Reactivity of low valent lanthanide and uranium complexes with small molecules

In the next sections we will focus on the molecular reactivity of low valent f-element (divalent lanthanide and trivalent uranium) complexes with the substrates studied during this PhD work.

## I.3.1 $CO_2$ reduction

The increasing scarcity of fuel resources and the accumulation of greenhouse gases in the atmosphere make the chemical recycling of carbon dioxide in carbon feedstock a seductive solution. In addition to being abundant, $CO_2$ would be an economical, non-flammable and nontoxic building block. However, the main disadvantage is the great kinetic and thermodynamic stability of $CO_2$ leading to chemical inertness of this molecule.[1, 2, 79] The strong double C=O bonds have a large bond dissociation energy (126 kcal/mol)[80] and the carbon atom is in the most oxidized state for carbon. Thus a large input of energy is required to reduce this apolar molecule as evidenced by its very low single-electron redox potential (-1.9 V vs. NHE). Moreover, $CO_2$ reduction into valuable organic molecules require multi-electron transfers (Table I-4).[1, 81]

**Table I-4: Standard potentials (V vs. NHE) of single electron $CO_2$ reduction and proton-coupled multi-electron $CO_2$ reductions (T=25°C, pH=7, $P_{CO2}$=1 bar, $[H^+]$=1 M).[81]**

| Reaction | E° (V vs. NHE) |
|---|---|
| $CO_2 + e^- \rightarrow CO_2^{\bullet-}$ | -1.90 |
| $CO_2 + 2H^+ + 2e^- \rightarrow CO_2 + H_2O$ | -0.53 |
| $CO_2 + 2H^+ + 2e^- \rightarrow HCO_2H$ | -0.61 |
| $CO_2 + 4H^+ + 4e^- \rightarrow HC(O)H + H_2O$ | -0.48 |
| $CO_2 + 6H^+ + 6e^- \rightarrow CH_3OH + H_2O$ | -0.38 |
| $CO_2 + 8H^+ + 8e^- \rightarrow CH_4 + 2H_2O$ | -0.24 |

Despite these drawbacks, nature is able to use $CO_2$ as carbon feedstock in the photosynthesis process. Moreover, some enzymes (CO dehydrogenases) reduce catalytically $CO_2$ into CO.[4] Catalytic generation of CO is notably of great interest because carbon monoxide can be used in combination with $H_2$ in the Fischer-Tropsch process to produce hydrocarbons. Consequently the $CO_2$ activation is a main contemporary challenge in inorganic chemistry. Notably there has been a resurge of interest in identifying molecular complexes that can reduce carbon dioxide in ambient conditions and in their implementation in electrocatalytic processes.

## I.3.1.1 $CO_2^{\bullet-}$ complexes

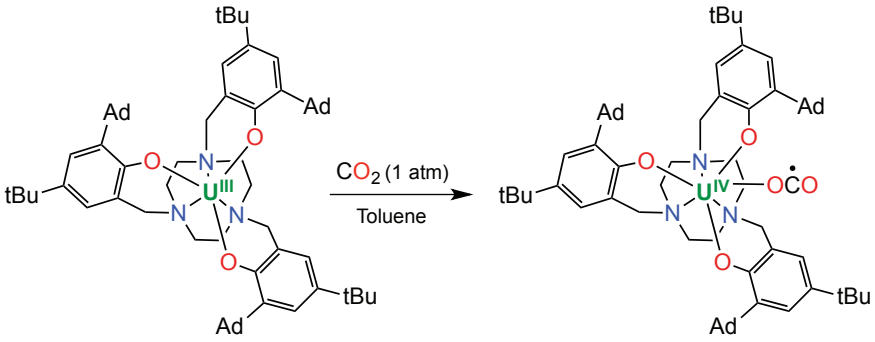


**Scheme I-4: $CO_2$ reduction by [U(($^{Ad,tBu}$ArO)$_3$tacn)].[82]**

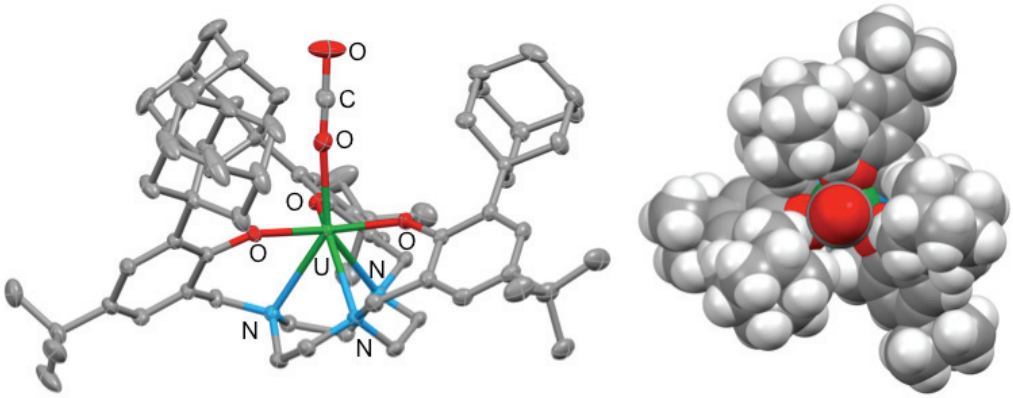


**Figure I-3: Solid state structure of [U(CO$_2$)(($^{Ad,tBu}$ArO)$_3$tacn)] side view (left, 50% ellipsoids) top view (right, spacefill representation). Hydrogen atoms on the side view and solvent molecules are omitted for clarity.[82]**

The anionic radical $CO_2^{\bullet-}$, formed by the single-electron reduction of $CO_2$, has been postulated as the highly reactive first intermediate in $CO_2$ reduction processes.[83] In 2004, Meyer et al. reported the first f-element complex containing a singly reduced $CO_2^{\bullet-}$ radical moiety.[82] Indeed the U(III) complex [U(($^{Ad,tBu}$ArO)$_3$tacn)] reacts with $CO_2$ to yield the complex [U(CO$_2$)(($^{Ad,tBu}$ArO)$_3$tacn)] which features a previously unseen nearly linear end-on OCO ligand (Scheme I-4). The quasi linearity of the $CO_2^{\bullet-}$ ligand is in contradiction to all the studies performed on this radical.[84, 85] However, the experimental data support the description of this complex as a U(IV) compound with $CO_2$ radical. The authors thus postulate that the linear shape of the reduced $CO_2^{\bullet-}$ radical is imposed by the steric hindrance provided by the adamantyl substituents of the ligand preventing the $CO_2^{\bullet-}$ radical to bend (Figure I-3).

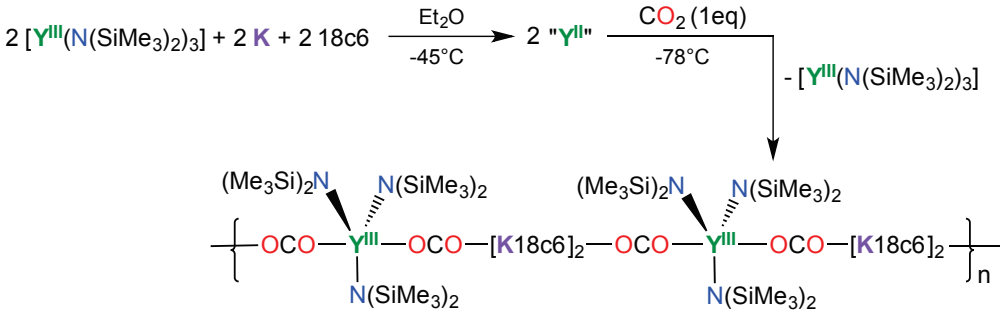


**Scheme I-5: $CO_2$ reduction by divalent yttrium complex. [86]**

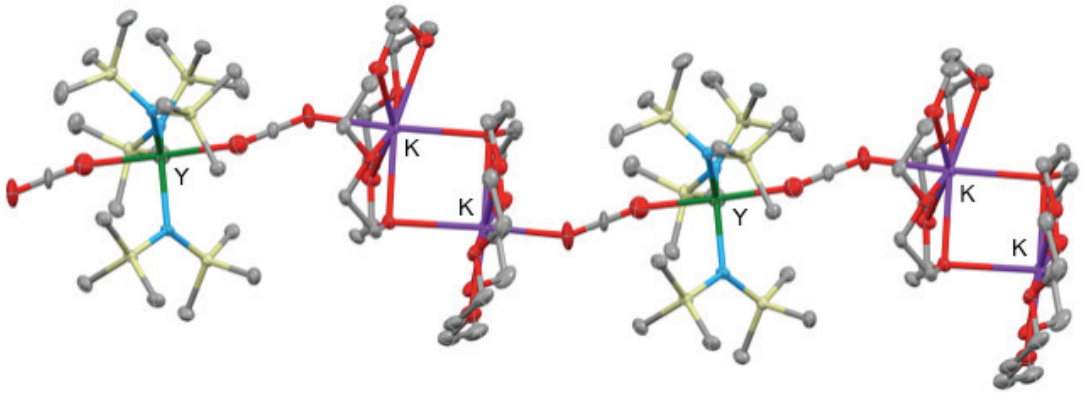


**Figure I-4: Solid state structure of the polymeric complex $[\{Y(CO_2)_2(HMDS)_3\}\{K18c6\}_2]_n$ (50% ellipsoids). Hydrogen atoms are omitted for clarity.** [86]

The only other example of linear end-on $CO_2^{\bullet-}$ radical was reported with an yttrium centre, an element which has similar physico-chemical properties than lanthanides. In 2012, Evans and co-workers reported the reduction of the Y(III) complex $[Y(HMDS)_3]$ by potassium metal in presence of crown ether putatively affording a non-isolated Y(II) complex which reacts *in situ* with carbon dioxide (Scheme I-5).[86] However in this case, the obtained polymeric Y(III) complex $[\{Y(CO_2)_2(HMDS)_3\}\{K18c6\}_2]_n$ displays a less sterically demanding environment (Figure I-4). Moreover the elemental analysis of this compound shows a higher nitrogen percentage than what is expected (calculated N, 3.32; obtained N, 5.35). It would be prudent to reconsider the interpretation of the authors on this $CO_2^{\bullet-}$ radical. Instead of $CO_2^{\bullet-}$ moiety it could be a linear isocyanate anion formed by the reaction of $CO_2$ with the silylamide ligands. Reaction of $CO_2$ with the silylamide ligand has been observed in the group of Prof. Arnold[90] and in our group.[87] Notably, the U(III) complex $[K18c6][U(HMDS)_4]$ reacts with $CO_2$ and subsequent multiple N-Si bond cleavage at the silylamide ligand affords the U(IV) bis-cyanate coordination polymer $[\{U(NCO)_2(HMDS)_3\}\{K18c6\}]_n$.[87]

If the yttrium complex example may need re-examination, the formation of the uranium complex $[U(CO_2)((^{Ad,tBu}ArO)_3tacn)]$ highlights the ability of trivalent uranium to undertake $CO_2$ reduction and underlines the importance of the ligand sterical environment to stabilize very reactive intermediates.

## I.3.1.2 Reductive deoxygenation of $CO_2$

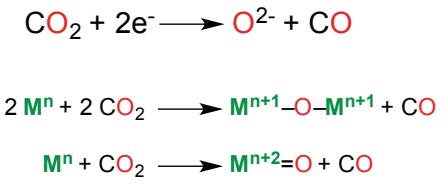


**Scheme I-6: Reductive splitting of $CO_2$.**

The reductive deoxygenation of $CO_2$ involves a two-electron transfer from the metal (one metal or two metals) per $CO_2$ molecule yielding an oxide ligand and carbon monoxide (Scheme I-6). Two mechanisms are possible. If two metal centres ($M^n$) are involved, each of them affects a single-electron transfer leading to the formation of a bridging oxide ligand between two oxidized metal centres ($M^{n+1}$) and the concomitant release of CO. This reaction can also occur at a single metal centre *via* a two-electron transfer from the metal to the $CO_2$ molecule affording a terminal oxide ligand bound to the doubly-oxidized metal centre ($M^{n+2}$) and the concomitant release of CO.

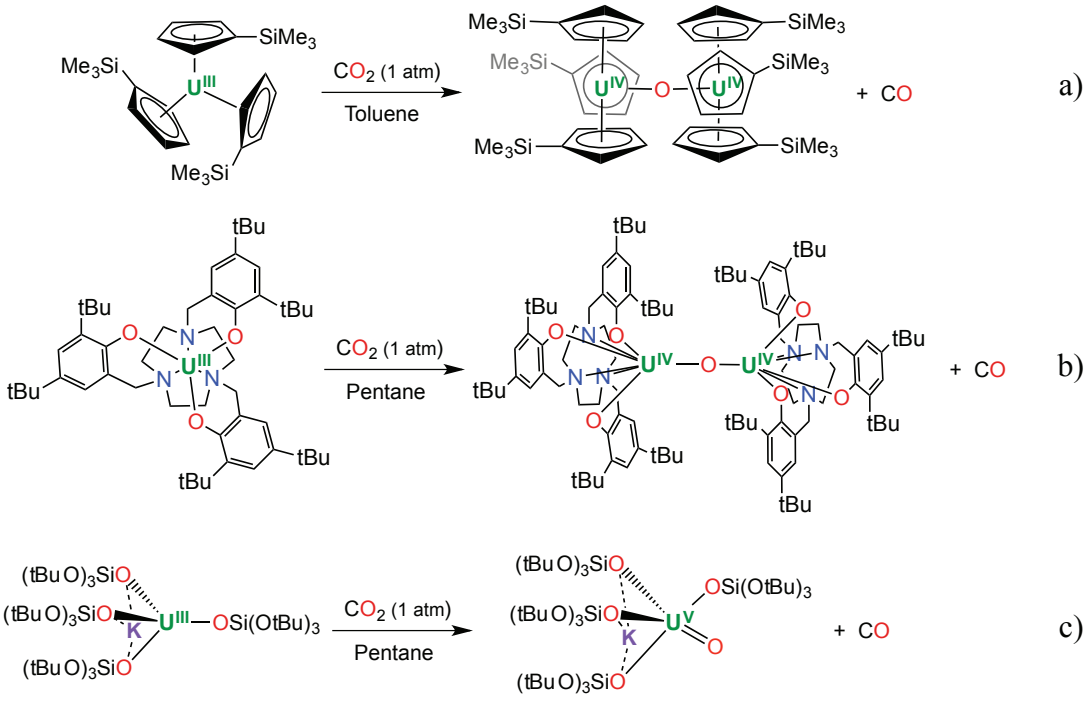


**Scheme I-7: Reductive splitting of $CO_2$ by U(III) complexes.** [7, 88, 89]

The first example of $CO_2$ reductive splitting by f-element complex was reported by Ephritikhine et al. in 1991. They discovered that the organometallic U(III) complex [UCp'$_3$] is able to cleave a C=O double bond of carbon dioxide to afford the oxo-bridged di-uranium(IV) complex [(UCp'$_3$)$_2$(μ-O)] (Scheme I-7a). The putative concomitant formation of CO was, however, not analysed.[88] A similar behaviour was observed by Meyer and co-workers for the U(III) complex [U(($^{tBu,tBu}$ArO)$_3$tacn)] (Scheme I-7b). [89] The CO formation was detected by IR spectroscopy. More recently our group reported the first two-electron reductive cleavage of $CO_2$ at a single uranium centre leading to the U(V) terminal oxo complex [UO(OSi(OtBu)$_3$)$_4$K] (Scheme I-7c).[7] The CO formation was detected by $^{13}$C NMR spectroscopy. Such a multi-electron redox transfer is rare in uranium chemistry. The computed enthalpy profile of the reaction shows that the potassium presence in the U(III) starting complex is crucial. Indeed one of the intermediates is stabilized by the coordination of the $CO_2^{2-}$ moiety to both uranium and potassium centres which ease the C-O bond cleavage. When the profile is computed in the absence of potassium atom, the enthalpy energy needed to break the C-O bond is much higher. Arnold and Cloke respectively reported the reaction of the U(III) complexes [{U(OAr)$_3$}$_2$(μ-N$_2$)][90] and [U(COT$^{TIPS2}$)(Cp$^{EMe4}$)] (E=N, P)[91] with $CO_2$. Oxygen abstraction of the carbon dioxide occurred affording bridging oxo species but in both cases $CO_2$ insertions into the U-heteroatom bonds were also observed. These examples are schematically represented in section I.3.1.5.

To our knowledge, such reductive splitting of $CO_2$ has never been reported for lanthanides.

## I.3.1.3 Reductive disproportionation of $CO_2$

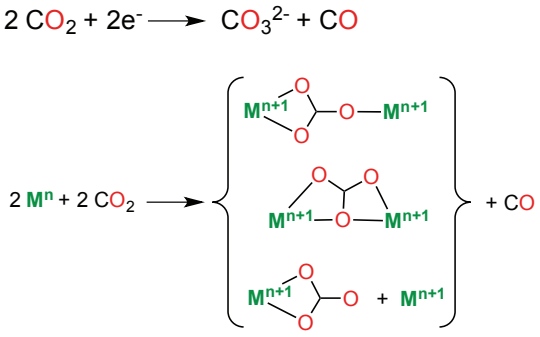


**Scheme I-8: Reductive disproportionation of $CO_2$.**

The reductive disproportionation of $CO_2$ involves a two-electron transfer to two $CO_2$ molecules yielding the carbonate dianion $CO_3^{2-}$ and concomitant formation of carbon monoxide. (Scheme I-8). In the examples of $CO_2$ reductive disproportionation by f-element complexes reported in the literature, two metal centres ($M^n$) undergoing a single-electron oxidation are involved to afford a terminal or bridging carbonate ligand bound to one or two oxidized metal centres ($M^{n+1}$) and CO release.

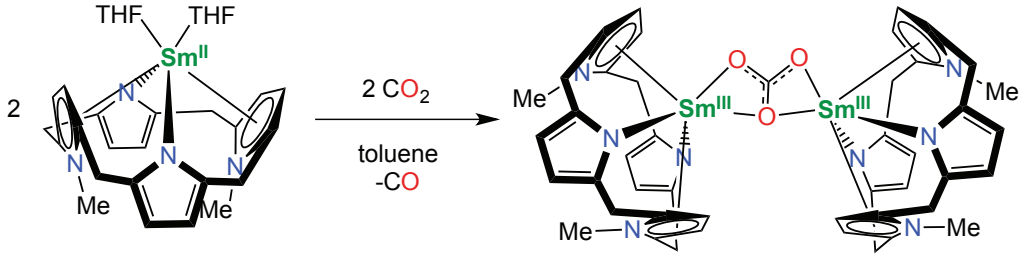


**Scheme I-9: Synthesis of the porphyrinogen Sm(III) carbonate via reductive disproportionation of $CO_2$. The meso-ethyl groups are omitted for clarity.[92]**

The first and only example of reductive disproportionation of $CO_2$ by 4f-element complex was reported by Gardiner et al. in 2006 and concerns a Sm(II) complex supported by porphyrinogen ligand (Scheme I-9).[92] The CO formation was confirmed by high-resolution GC-MS analyses. The mechanism of this reaction has not been investigated but the authors postulated that the strong steric hindrance provided by the ligands might destabilize potential bridging oxalate intermediate.

Three different U(III) systems were reported to undertake reductive disproportionation of $CO_2$: aromatic carbocyclic, anchored trisphenolate and siloxide platforms.

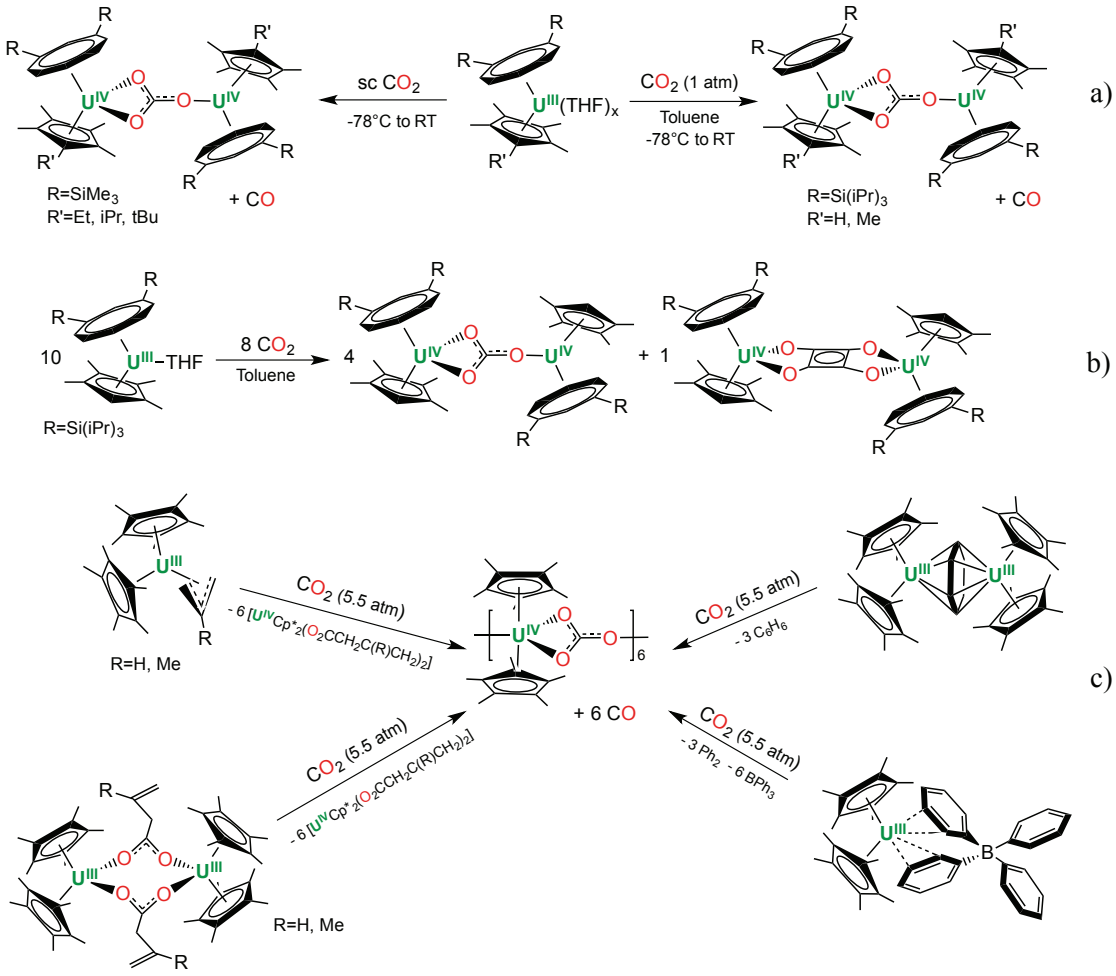


**Scheme I-10: Reductive disproportionation of $CO_2$ by organometallic the U(III) complexes: a) [U(COT$^{R}$)(Cp*$^{R'}$)] with excess $CO_2$,[93] b) [U(COT$^{Si(iPr)3}$)(Cp*$^{H}$)] with 8eq of $CO_2$,[94] and c) syntheses of [UCp*$_2$(μ-$CO_3$)]$_6$ from the reductive disproportionation of $CO_2$ by different U(III) metallocenes.[95]**

The ability of the mixed-sandwich U(III) complexes [U(COT$^{R}$)(Cp*$^{R'}$)] to reduce $CO_2$ into $CO_3^{2-}$ and CO was reported by Cloke and co-workers (Scheme I-10a and b).[93, 94] Interestingly, the use of supercritical $CO_2$ in the cases where R=SiMe$_3$ and R'=Et, iPr or tBu is crucial to obtain cleanly the corresponding U(IV) dinuclear carbonate complex. The use of stoichiometric amount of $CO_2$ leads to a mixture of carbonate, oxalate and oxide compounds. These reactions will be described in the next section. Moreover, when R=Si(iPr)$_3$ and R'=H, traces of a di-uranium(IV) squarate complex were observed and resulted from the reductive coupling of CO (formed during the reaction) by the starting U(III) complex. Since a large excess of $CO_2$ was used, this observation implies that [U(COT$^{Si(iPr)3}$)(Cp*$^{H}$)] reacts faster with CO than with $CO_2$. When the appropriate stoichiometry of $CO_2$ is added (8eq for 10 U(III) complexes), 4eq of the bridging carbonate complex and 1eq of the bridging squarate complex

are obtained cleanly (Scheme I-10b). Evans et al. isolated a unique hexametallic U(IV) carbonate wheel $[UCp^*_2(\mu\text{-}CO_3)]_6$ from the reductive disproportionation of $CO_2$ by different U(III) metallocenes (Scheme I-10c).[95]

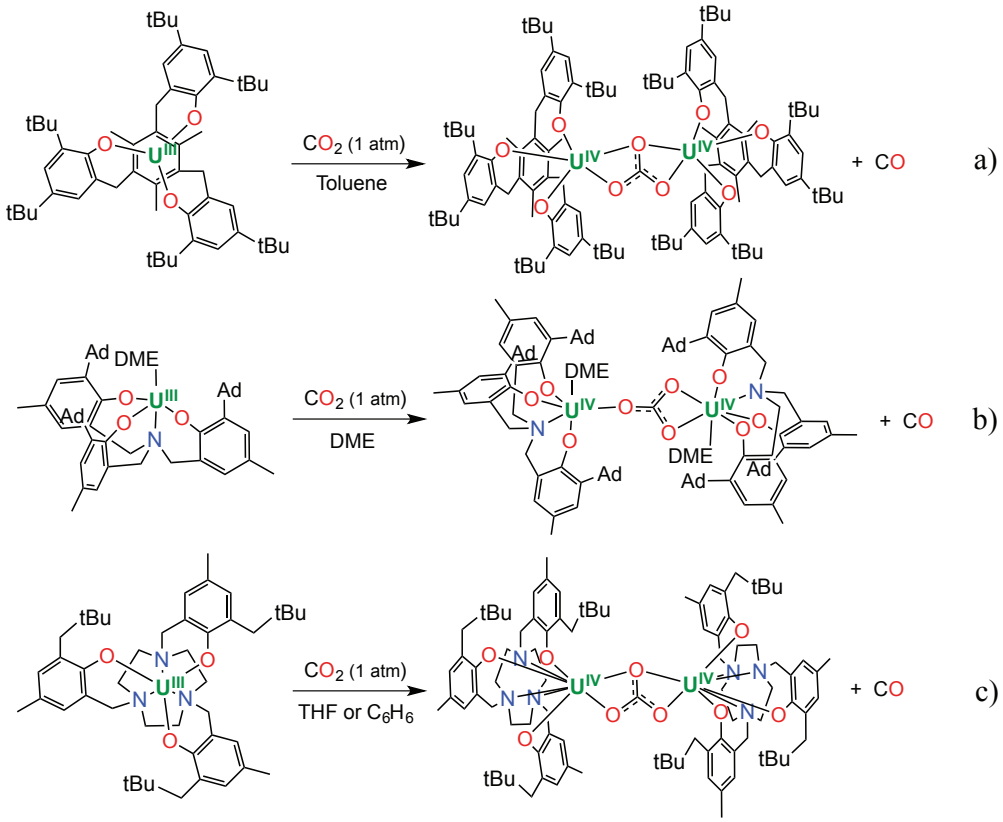


**Scheme I-11: Reductive disproportionation of $CO_2$ by U(III) trisphenolate complexes with a) mesitylene anchor,[96, 97] b) nitrogen atom anchor[96] and c) tacn anchor[98, 99]**

Changing the substituents on the phenolate groups and replacing the tacn anchor of the trisphenolate ($(^{tBu,tBu}ArO)_3tacn$) ligand with mesitylene or single nitrogen atom to support U(III) ion, Meyer and co-workers observed reductive disproportionation of $CO_2$ (Scheme I-11).[96, 98] The $CO_2$ reaction of the tacn-based complex with tert-butyl substituent on the phenolate groups leads to a bridging oxo complex (in the previous section) while the tacn-based complex with neopentyl and methyl substituents promote $CO_2$ disproportionation (Scheme I-11c).[98] Interestingly, the reduction of the obtained carbonate complex $[\{U((^{nP,Me}ArO)_3tacn)\}_2(\mu\text{-}CO_3)]$ by potassium graphite reforms the mononuclear U(III) starting compounds and eliminates $K_2CO_3$ salt. The complex $[U((^{nP,Me}ArO)_3tacn)]$ can be reacted again with $CO_2$ affording the carbonate complex and CO (Scheme I-12). This cycle is

terminated by the formation of the stable tetrametallic U(IV) carbonate complex [{U($CO_3$)(($^{nP,Me}$ArO)$_3$tacn)}$_4$].

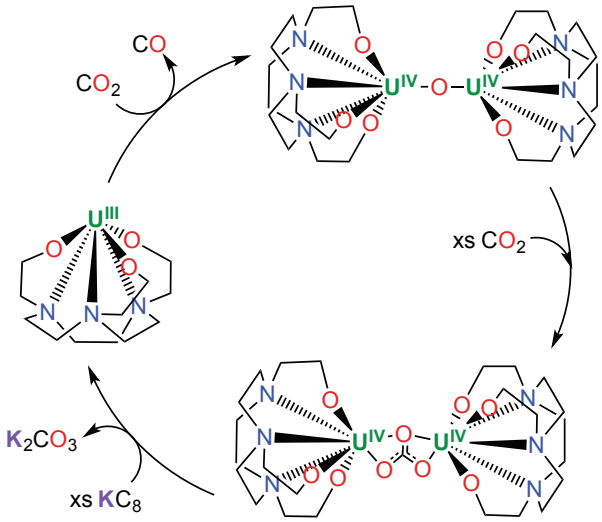


**Scheme I-12: Schematic representation of the closed synthetic reduction cycle of $CO_2$ by [U(($^{nP,Me}$ArO)$_3$tacn)].[98]**

The theoretical studies performed on the different systems have established different reaction pathways. The reaction mechanism for the mesitylene anchored complex involves CO release and a di-uranium(IV) bridging oxo intermediate which then undergoes $CO_2$ insertion.[97] In this case the reductive disproportionation of $CO_2$ involves a reductive deoxygenation of $CO_2$ followed by a $CO_2$ insertion in the U-$O_{oxo}$ bond. In order to confirm this mechanism, the independently prepared di-uranium(IV) bridging oxide complex [{U(($^{tBu,tBu}$ArO)$_3$mes)}$_2$(μ-O)] was reacted with $CO_2$ and underwent $CO_2$ insertion into the U(IV)-$O_{oxide}$ bond affording the expected bridging carbonate complex.[96] In contrast, in the calculated enthalpy profile for the tacn-based system, the calculated favoured pathway involves the formation of a dinuclear U(IV) complex with a bridging doubly reduced carbon dioxide ($CO_2^{2-}$) ligand. This $CO_2^{2-}$ moiety is then prone to undertake nucleophilic attack of on a second $CO_2$ molecule. The subsequent CO elimination and the formation of a bridging carbonate complex is then favoured.[99] The difference in reactivity observed for all these related trisphenolate U(III) complexes emphasizes the importance of the ligand steric hindrance on the outcome of the reaction. The described ligands are synthetically quite challenging but they allow a subtle tuning of the reactivity of the U(III) centre.

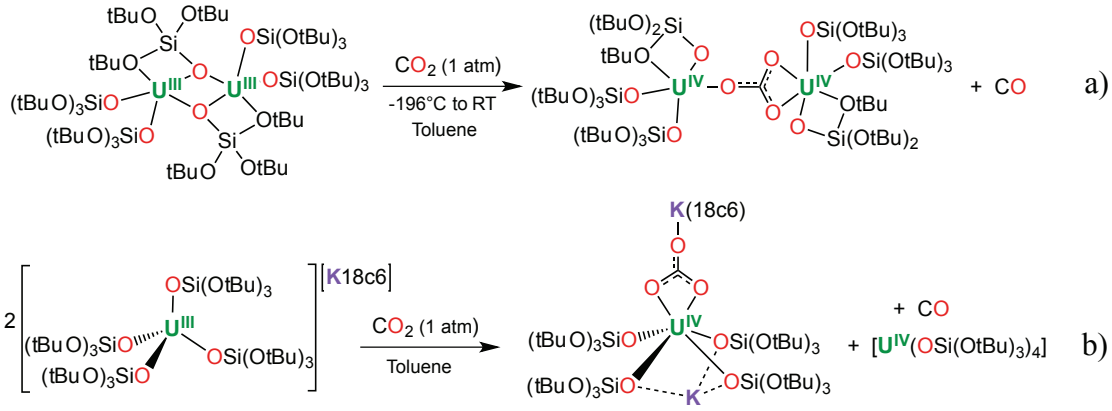


**Scheme I-13: Reductive disproportionation of $CO_2$ by U(III) siloxide complexes.** [7, 100]

Finally, a U(III) system able to promote reductive disproportionation of $CO_2$ was reported recently by our group using simple commercial monoanionic tert-butoxy siloxide supporting ligands. The dimeric homoleptic siloxide complex of U(III): $[\{U(OSi(OtBu)_3)_2(\mu\text{-}OSi(OtBu)_3)\}_2]$ reacts with 2eq of $CO_2$ affording CO and a U(IV)-U(IV) carbonate complex (Scheme I-13a).[100] The obtained carbonate complex is unstable and undergoes ligand scrambling to yield the mononuclear U(IV) complex $[U(OSi(OtBu)_3)_4]$ and unidentified U(IV) carbonate species. DFT calculations of the enthalpy profile shows that a stable dinuclear U(IV) $CO_2^{2-}$ intermediate is primary formed and undertakes nucleophilic attack of another $CO_2$ molecule. Indeed, the formation of a bridging oxo compound followed by $CO_2$ insertion was also computed but presents an overall higher energy barrier. The "ate" U(III) complex $[K18c6][U(OSi(OtBu)_3)_4]$ features the first reductive disproportionation of $CO_2$ to afford a mono-uranium(IV) carbonate complex $[U(CO_3)(OSi(OtBu)_3)_4K_2(18c6)]$ (Scheme I-13b).[7] This remarkable coordination is attributed to the strong bulkiness provided by the environment of four siloxide ligands preventing the bridging through the carbonate moiety to the concomitantly formed $[U(OSi(OtBu)_3)_4]$ complex.

## I.3.1.4 Reductive coupling of $CO_2$

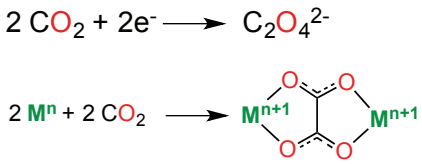


**Scheme I-14: Reductive coupling of $CO_2$.**

The reductive coupling of $CO_2$ involves the two-electron transfer from the metal to two $CO_2$ molecules yielding a bridging oxalate dianion $C_2O_4^{2-}$. In the rare reported examples of $CO_2$ reductive coupling performed by f-element complexes, two metal centres ($M^n$) are involved and each of them undertakes single-electron redox process to afford a bridging oxalate ligand between two oxidized metal centres ($M^{n+1}$) (Scheme I-14).

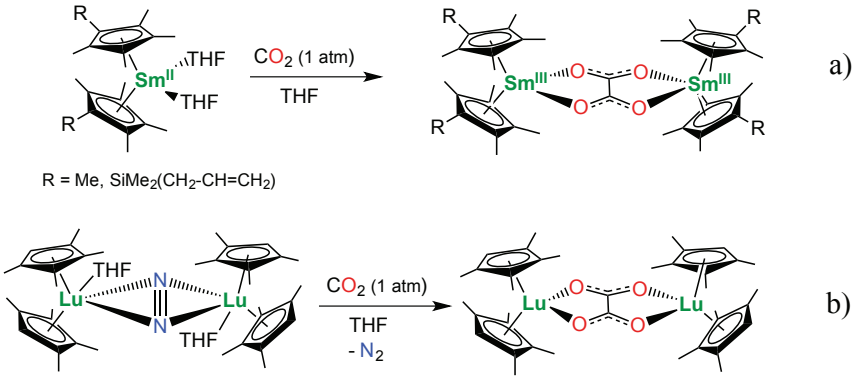


**Scheme I-15: Reductive coupling of $CO_2$ by lanthanocenes.** [83, 101-103]

The first example was reported by Evans et al. in 1998. The divalent decamethylsamarocene reacts with $CO_2$ affording the dinuclear complex [$(SmCp^*_2)_2(\mu$-$O_2CCO_2)$] (Scheme I-15a).[83] The related divalent complex [$SmCp^R_2$] (where $Cp^R$=$(C_5Me_4)SiMe_2(CH_2CH$=$CH_2)$) shows the same reactivity with $CO_2$.[101] In 2012, DFT calculations were performed to gain insight in the reaction mechanism between [$SmCp^*_2$] and $CO_2$.[102] The mechanism involving the coupling of two Sm(III) radical complexes [$Sm(CO_2^{\bullet})Cp^*_2$] was ruled out. The calculated favoured pathway involves the formation of a dinuclear Sm(III) complex with a bridging doubly reduced carbon dioxide ($CO_2^{2-}$) ligand. This dinuclear complex results from the cooperative reduction of $CO_2$ by two divalent

decamethylsamarocene complexes. Once this dinuclear intermediate formed, a free $CO_2$ molecule undergoes a nucleophilic attack from the bridging $CO_2^{2-}$ moiety affording the experimentally isolated di-samarium(III) oxalate compound. In 2009, Evans group also reported that the reaction of the lutetium dinitrogen adduct $[\{Lu(C_5Me_4H)_2\}_2(\mu\text{-}N_2)]$ with $CO_2$ cleanly leads to the formation of a dinuclear Lu(III) oxalate complex (Scheme I-15).[103] However, if the analogous lanthanum dinitrogen adduct was found to react with $CO_2$, the reaction products are numerous probably because of $CO_2$ insertion in the La-C bonds. Jones and co-workers reported this year the formation of a disamarium(III) oxalate complex supported by guanidinate ligands.[104] However, the isolated yield is very low (9%) and elemental analyses are not reproducible due to co-crystallisation of protonated ligand. DFT calculations of the enthalpy reaction profile are in agreement with the mechanism involving a nucleophilic attack of a $CO_2^{2-}$ moiety to a free molecule of $CO_2$ to yield an oxalate compound. However, in this case a subsequent $CO_2$ insertion in the Sm-N bond is thermodynamically favourable and observed experimentally.

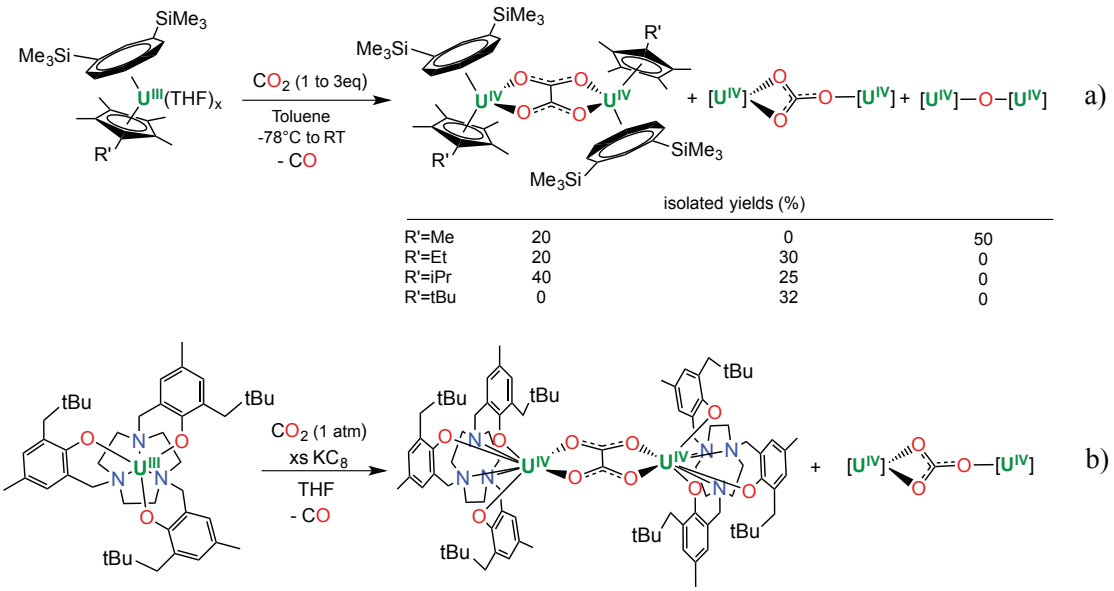


**Scheme I-16: Reductive coupling of $CO_2$ by U(III) complexes.** [94, 99]

The reductive coupling of $CO_2$ by uranium complexes is limited to two systems both reported in 2014. A diuranuim(IV) oxalate compounds was isolated by Cloke et al. from the reduction of $CO_2$ by U(III) metallocene complexes (Scheme I-16a).[94] Despite the fact that the reaction can be accompanied by carbonate and oxide formation, the selectivity can be

controlled by tuning the substituents of the Cp ring. Meyer et al. reported that the U(III) complex [U(($^{nP,Me}$ArO)$_3$tacn)] can undertake, in presence of excess $KC_8$ and in THF, reductive coupling of $CO_2$ affording a diuranium(IV) oxalate species (Scheme I-16b).[99]. In both studies presented by Cloke and Meyer, DFT calculations were performed and are in agreement with the mechanism previously reported by Evans et al. Although both theoretical studies predict the oxalate compound to be thermodynamically favoured, this pathway is kinetically less favoured than the reductive disproportionation as higher activation barriers are found. These results explain the concomitant formation of bound carbonate and oxalate species and the difficulties to obtain pure di-uranium oxalate complexes. Notably, the presence of $KC_8$ in the reaction reported by Meyer is essential: the formation of the carbonate complex is kinetically favoured but this carbonate compound can be reduced by the $KC_8$ in excess (as seen in the previous section) to reform the U(III) complex [U(($^{nP,Me}$ArO)$_3$tacn)]. This cycle allows, in some extent, the formation of the thermodynamically favoured oxalate product.

### I.3.1.5 Insertion into U-X or Ln-X bonds (X=C, N, P, O, S, Se)

Insertion of $CO_2$ into Ln-ligand or U-ligand bonds is an important aspect of the $CO_2$ reactivity with f-element complexes. This insertion has been mainly reported with U(IV) and Ln(III) complexes. $CO_2$ insertion in M-$C_{alkyl}$[105-107], M-$C_{allyl}$[108, 109] or M-$C_{alkynyl}$[110, 111] bonds (M=Ln(III) or U(IV)) provides another access to carboxylate complexes. Evans and co-workers, who studied in details the chemistry of lanthanocenes, reported the $CO_2$ insertion into the Ln(III)-Cp* bonds.[112, 113]. In addition, Arnold et al. studied the insertion of $CO_2$ into the Ln(III)-$C_{carbene}$ bonds.[114] The insertion of one molecule of $CO_2$ is also possible in the M-N bond (M=Ln(III) or U(IV)).[115-117] The insertion chemistry of $CO_2$ into the Ln(III)-O or Ln(III)-OH bonds led to isolation of high nuclearity carbonate clusters.[118-122] The U(IV)-mediated $CO_2$ insertion into polyketones-derived enolates was proved promising for the synthesis of small organic molecules.[123] Some examples reported the $CO_2$ insertion into chalcogenates in U(IV)[124] and Ln(III)[125] complexes. Moreover, unusual chalcogenocarbonate uranium complexes were synthesised by $CO_2$ insertion into the U(IV)-chalcogenide bonds (S, Se).[126]

Investigating the $CO_2$ insertion into metal-ligand bonds with low oxidation state of the f-element (U(III) and Ln(II)) is more difficult as both reduction and insertion reactions can occur.

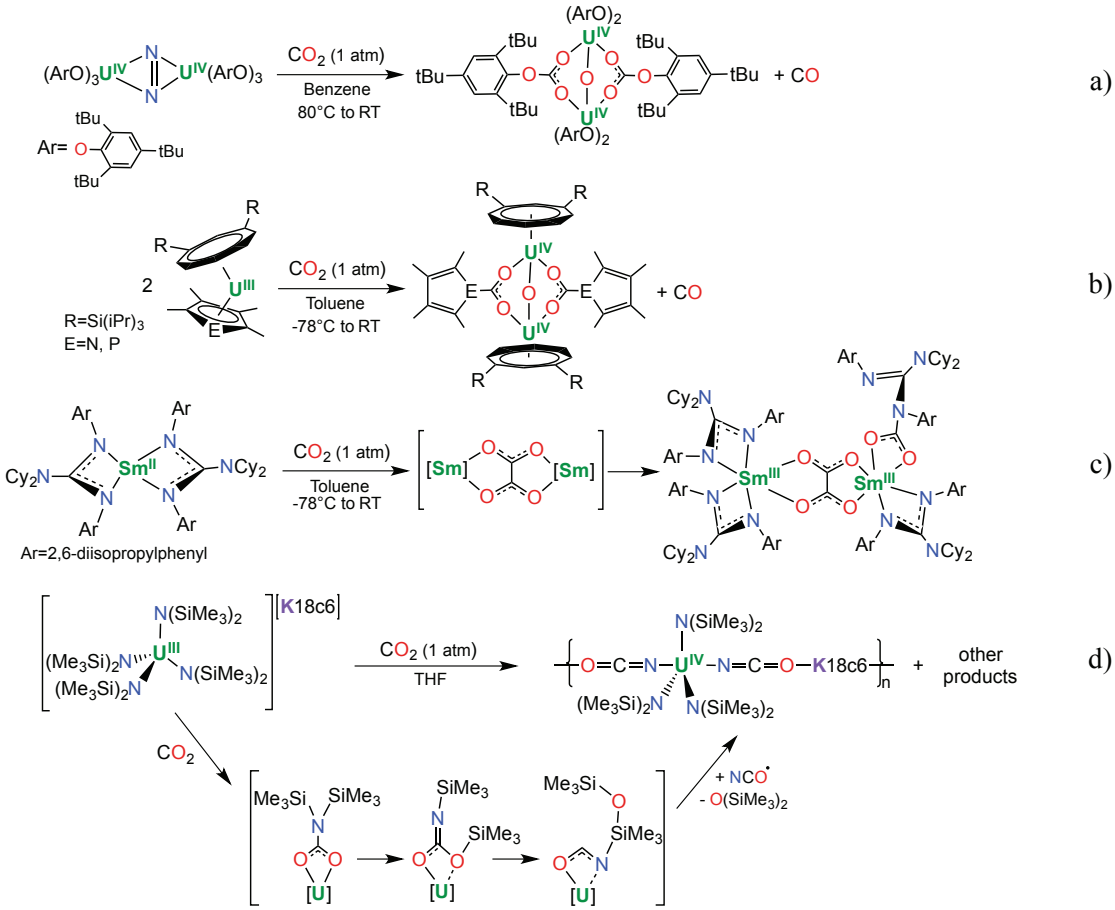


**Scheme I-17: $CO_2$ insertion and reduction with U(III) complexes.** [87, 90, 91, 104]

The U(IV) dinitrogen adduct $[\{U(OAr)_3\}_2\{\mu\text{-}N_2\}]$ does not react with $CO_2$ at room temperature. However upon heating, the $N_2$ molecule is released leading to in situ formation of the U(III) complex $[U(OAr)_3]$ which reacts with $CO_2$ to afford a bridging oxo arylcarbonate complex (Scheme I-17a).[90] Reductive splitting of $CO_2$ has occurred since the oxygen atom bridging two U(IV) centres probably arise from $CO_2$ reductive deoxygenation. In addition one $CO_2$ molecule has inserted in one of the three supporting phenolate ligands of each U(III) complex. Similar behaviour was observed by Cloke and co-workers for the U(III) complexes $[U(COT^{TIPS2})(Cp^{EMe4})]$ (E=N, P) and in these cases the $CO_2$ molecules insert in the U-N and U-P bonds yielding cyclopentadienyl carbamate and phosphacarbonate moieties respectively (Scheme I-17b).[91] The reaction mechanism of the Arnold and Cloke systems has

not been investigated and the nature of the first step (reduction or insertion) is not established yet. With the Sm(II) guanidinate complex, DFT studies have shown that the reductive coupling of $CO_2$ is initially promoted and followed by insertion of 1eq of $CO_2$ in one U-N bond of the Sm(III) dimer (Scheme I-17c).[104] As previously mentioned, our group reported recently that the "ate" complex [K18c6][U(HMDS)$_4$] slowly reacts with $CO_2$ to afford the U(IV) polymeric compound [{U(NCO)$_2$(HMDS)$_3$}{K18c6}] (Scheme I-17d).[87] Theoretical studies revealed that the mechanism leading to this polymeric complex is initiated by $CO_2$ insertion in one of the U(III)-N bonds. Then the cleavage of a N-Si bond allows the migration of a trimethylsilyl group to one oxygen atom of the carbamate function. Changing the coordination mode to the uranium centre of the carbamate group from O,O to O,N mode renders possible the migration of the $(OSiMe_3)^-$ moiety. After siloxane release and structural rearrangement a putative NCO radical (formed by another uranium complex) can complete the uranium coordination sphere and afford the polymeric U(IV) isocyanate species. Similar $CO_2$ insertion reactions followed by N-Si cleavage and structural rearrangements are also postulated for the U(III) silylamide complexes [U(HMDS)$_3$][90] and [UL(HMDS)$_2$] (L=bidentate alkoxy-tetherred NHC ligand).[114] Indeed, the formation of isocyanate moieties were detected by FTIR spectroscopy.

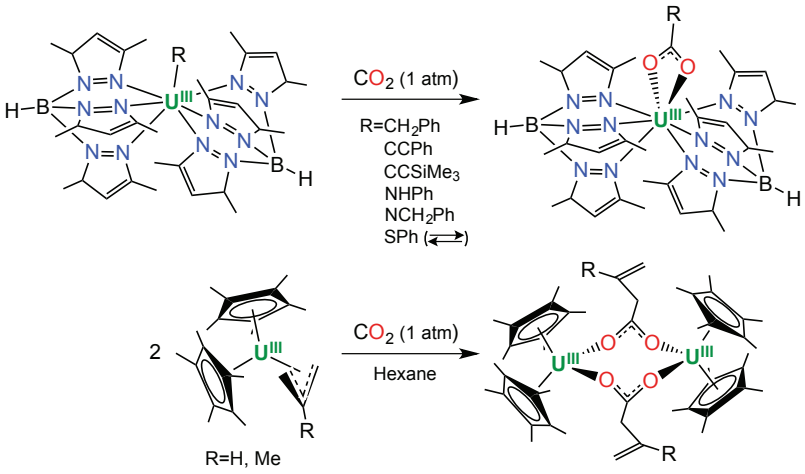


**Scheme I-18: Non-oxidative insertion of $CO_2$ in U(III) complexes.**[95, 127, 128]

Rare examples of $CO_2$ insertion reactions into metal-ligand bonds have also been reported for U(III) complexes. $CO_2$ insertion reactions into U(III)-C,[95, 127, 128] U(III)-N and U(III)-S bonds[128] are presented in Scheme I-18.

Altogether these examples of $CO_2$ insertion into Ln-L or U-L show us that a particular attention must be given to the choice of the supporting ligand. Indeed, $CO_2$ insertion in the ancillary ligand is unwanted reaction. Nevertheless, such an insertion in targeted substrates bound to the metal centre can have interest for synthesising new organic molecules.

## I.3.2 $CS_2$ Reduction

The heteroallene $CS_2$ is commonly used as isoelectronic model of $CO_2$. This thio-analogues is more reactive then $CO_2$ with C=S bond dissociation energy of 107 kcal/mol.[80]

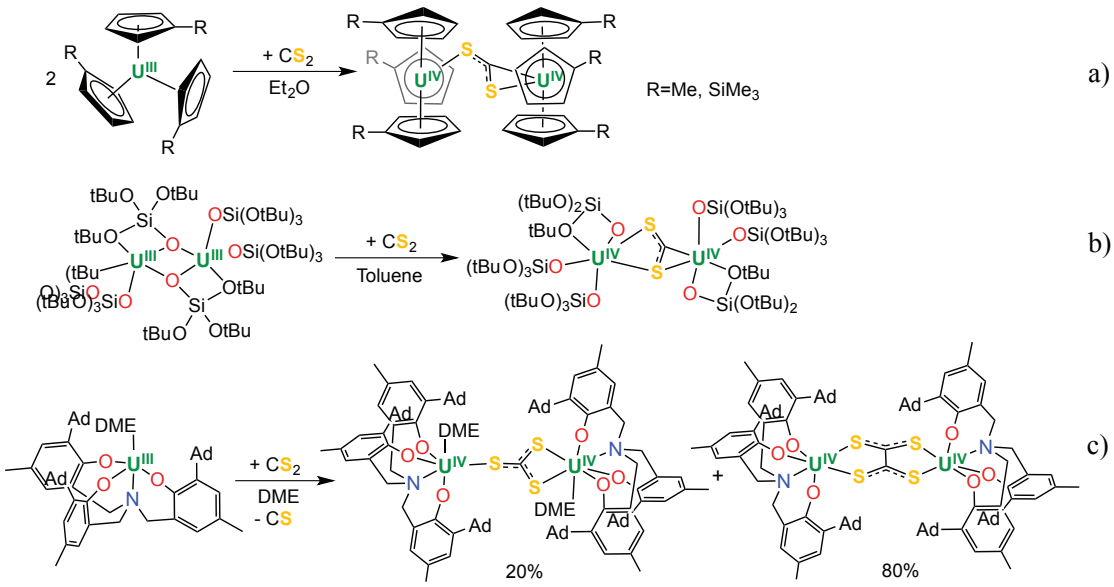


**Scheme I-19: Reductions of $CS_2$ by U(III) complexes: a) $[(UCp^R_3)]$,[129] b) $[U(OSi(OtBu)_3)_3]_2$[100] and c) $[U((^{Ad,Me}ArO)_3N)]$[130, 131]**

Examples of carbon disulfide reduction by U(III) complexes are limited to three examples presented in Scheme I-19. The first example was reported by Andersen et al. in 1986.[129] The $CS_2^{2-}$ di-uranium(IV) complexes $[(UCp^R_3)_2(\mu\text{-}CS_2)]$ ($Cp^R$=$C_5H_4Me$ or $C_5H_4SiMe_3$ (Cp')) were obtained from $CS_2$ reduction by the U(III) complexes $[UCp^R_3]$ (Scheme I-19a). Similar behaviour was observed more recently in our group with the reduction of $CS_2$ by the U(III)-U(III) dimer $[U(OSi(OtBu)_3)_3]_2$ leading also to $CS_2^{2-}$ bridging unit but featuring a different binding mode (Scheme I-19b).[100] These results contrast with the previously described reactions of the same U(III) complexes $[U(Cp')_3]$ and $[U(OSi(OtBu)_3)_3]_2$

with $CO_2$ which respectively led to reductive splitting and reductive disproportionation of $CO_2$. The DFT calculations performed for both systems confirm that the experimentally observed bridging $CS_2^{2-}$ complexes are the most stable product in the described experimental conditions.[100, 132] Notably, the theoretical studies performed by Maron and co-workers on the reactivity of the U(III) metallocene complex revealed that the difference in reactivity is due to the low stability of carbon monosulfide compared to carbon monoxide.[132] The U(III) trisphenolate complex [U(($^{Ad,Me}$ArO)$_3$N)] developed by Meyer et al. was also found to react with $CS_2$ affording a mixture di-uranium(IV) trithiocarbonate and tetrathiooxalate complexes as minor (20%) and major (80%) products respectively (Scheme I-19c).[130, 131] These two reaction products result from two different competitive mechanisms. The reaction pathway of the reductive disproportionation of $CS_2$ was investigated by DFT calculations and compared to the pathway (earlier mentioned) of the reductive disproportionation of $CO_2$. Similarly to the $CO_2$ reduction, the $CS_2$ reduction involves a bridging sulfido intermediate arising from an initial reductive splitting of $CS_2$. A subsequent $CS_2$ insertion in the U-S bond affords the thiocarbonate compound. However, the release of unstable CS is less favourable than the release of CO leading to a weaker driving force in $CS_2$ disproportionation. This explains that only 20% of the U(III) starting complex is converted in the thiocarbonate compound. The reaction of $CS_2$ with the independently prepared U(IV)-U(IV) bridging sulfide [{U(($^{Ad,Me}$ArO)$_3$N)}$_2$(μ-S)] affords the same bridging thiocarbonate complex confirming the theoretical studies.

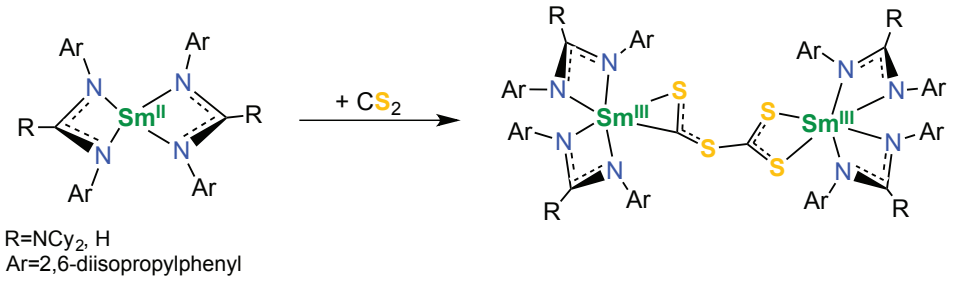


**Scheme I-20: Reduction of $CS_2$ by Ln(II) complexes.**[133, 134]

The reduction of carbon disulfide by divalent lanthanide complexes is limited to Sm(II) complexes supported by amidinate ligands. These examples were reported by Jones[133] and Junk[134] and in both cases a reductive coupling of $CS_2$, through C-S bond formation, affording a $(SCSCS_2)^{2-}$ bridging moiety , was observed rather than the more common C-C

bond formation (Scheme I-20). DFT calculations were recently performed by Jones and co-workers to investigate the enthalpy reaction profile of this $CS_2$ reduction.[104] The first step gives rise to the Sm(III)-Sm(III) bridging $CS_2^{2-}$ intermediate which then undertakes nucleophilic attack of a free $CS_2$ molecule *via* C-S bond formation. In this case, the formation of thiooxalate involves high-energy barrier preventing this pathway and the low kinetic stability of CS prevents the thiocarbonate formation.

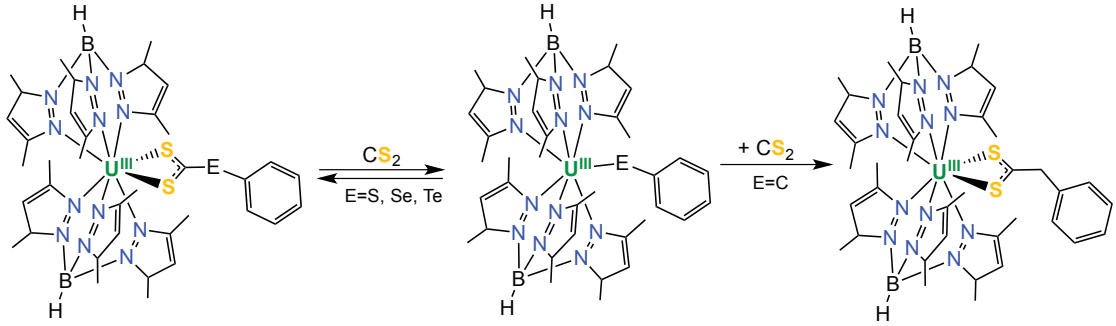


**Scheme I-21: Non-oxidative insertion of $CS_2$ in U(III) complexes.**[127, 135]

Ephritikhine and Meyer groups reported $CS_2$ insertion in U(IV)-chalcogen bonds for terminal thiolate ligands[124] and bridging chalcogenides ($S^{2-}$, $Se^{2-}$) ligands[126] respectively. Finally, Bart et al. demonstrated that insertion of $CS_2$ into U(III)-C bond is also possible (Scheme I-21 right).[127] This insertion chemistry was also expanded to U(III)-chalcogen (S, Se, Te) bonds although the reactions were found reversible (Scheme I-21 left).[135]

## I.3.3 $N_2$ reduction

Nitrogen atom is one of the main components of life and ecosystems as it is present in amino acids, the protein building blocks. Nitrogen is also present in numerous chemicals industrially produced such as pesticides or fertilizers. In nature, the nitrogen atom source is dinitrogen which is reduced by enzymes.[136] In industry, ammonia is produced by the Haber-Bosch process which uses a iron catalyst at harsh temperature and pressure conditions.[137] Reducing dinitrogen under mild conditions is a real challenge due to the extremely strong N-

N bond (226 kcal/mol).[1] However, uranium was found to be an efficient heterogeneous catalyst in the Haber-Bosch process.[138] This has attracted increasing interest on $N_2$ activation by f-elements.

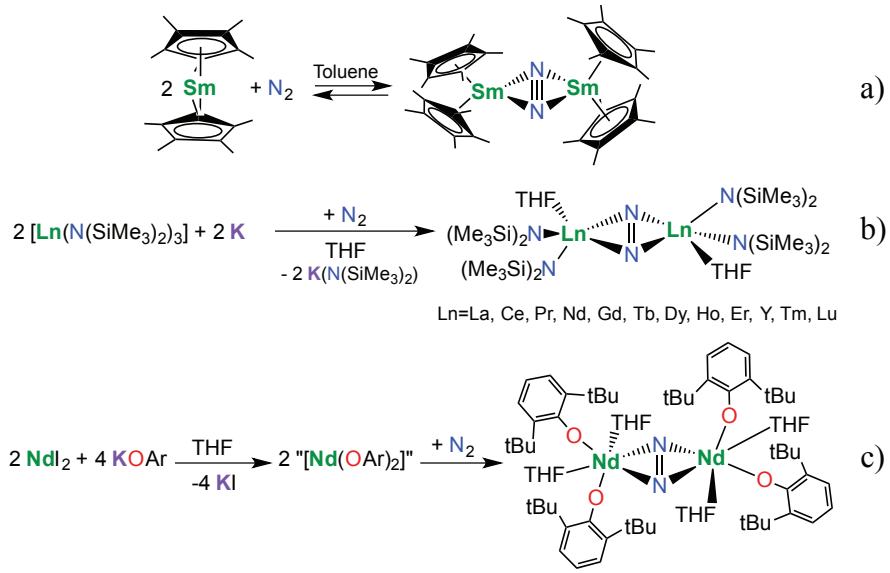


**Scheme I-22: Selected examples of dinitrogen activation by lanthanide complexes.[139-141]**

Binding molecular activation of dinitrogen by f-elements was first reported in 1988 (Scheme I-22a).[139] In this case the dinitrogen binding was reversible. Thereafter, $N_2$ activation was further studied using various metallocene complexes of non-classical divalent lanthanides.[142] The reduction of Ln(III) complexes of non-classical divalent lanthanide by strong reducing agent under $N_2$ atmosphere leads to two electron reduction of dinitrogen affording more or less cleanly the bridging $N_2^{2-}$ complexes (Scheme I-22b).[140, 143] Simple aryloxides were also found to be convenient ligand systems to form a Nd(II) homoleptic complex able to reduce dinitrogen (Scheme I-22c).[141] More recently, the isolations of yttrium silylamide and dysprosium aryloxide complexes bound to the further reduced $N_2^{3-}$ moiety were reported.[144]

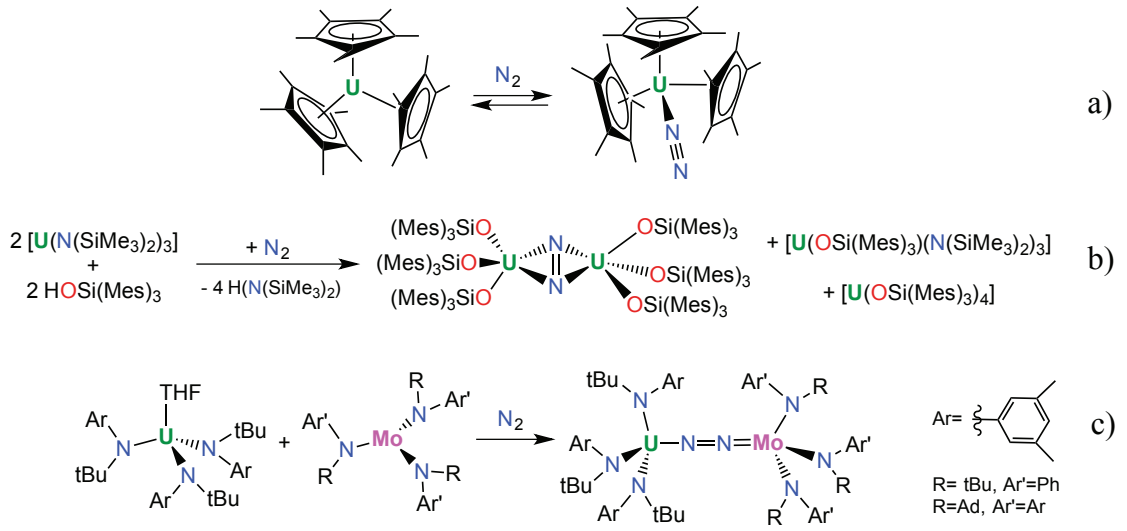


**Scheme I-23: Selected examples of dinitrogen activation by uranium complexes.**[145-147]

Dinitrogen activation was also observed for U(III) complexes. Notably, a singular end-on binding mode of $N_2$ to uranium centre was reported by Evans et al. after exposure of [UCp*$_3$] to $N_2$ (Scheme I-23a).[145] However this coordination is very weak and a dinitrogen pressure of 5.5 atm was needed to stabilize the $N_2$ adduct. Binding molecular activation of dinitrogen was also reported using triamidoamine as U(III) supporting ligands.[148, 149] A reversible reduction of $N_2$ featuring a side on binding mode of the formed $N_2^{2-}$ group was reported for uranium complexes supported by Cp derivatives.[150, 151] Arnold and co-workers reported the two-electron reduction of dinitrogen by very bulky U(III) aryloxide[90] and more recently siloxide complexes.[146] Despite the fact that by-products are formed during the $N_2$ reduction by the *in situ* formed U(III) siloxide complex (Scheme I-23b), these examples show that bulky oxygen donor ligands are suitable to form highly reducing U(III) complexes. The combination of two different metal centres to ease the N-N bond polarisation and thus $N_2$ reduction was explored by Cummins et al. using mononuclear complexes of U(III) and Mo(III) (Scheme I-23c). This strategy was successful as dinitrogen was doubly reduced in the isolated heterobimetallic complexes.[147] Finally, dinitrogen cleavage was reached *via* $N_2$ reduction by a U(III) complex supported by calixtetrapyrrole ligands in presence of potassium naphthalenide affording the mixed valent U(IV)-U(V) bridging dinitrido complex (Scheme I-24).[152] The putative U(II) intermediate is highly reactive and was found to reduce DME and silicon grease. The molecular complex active in $N_2$ reduction was never isolated.

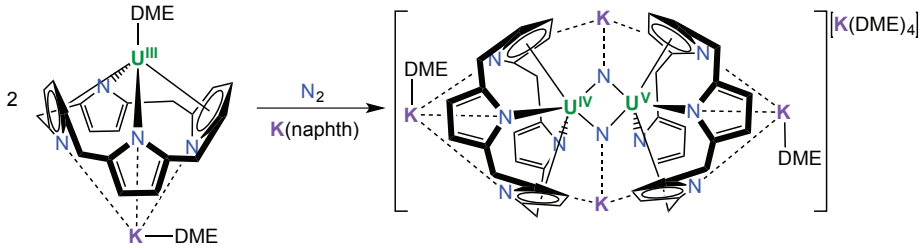


**Scheme I-24: Dinitrogen cleavage by uranium complex supported by calixtetrapyrrole ligand in presence of potassium naphthalenide. The meso-ethyl groups are omitted for clarity.[152]**

These examples confirm the potential of low valent f-element complexes for small molecules activation despite the fact that the degree of $N_2$ reduction varies from one complex to another. Even if these initial results are of high interest, improvement of the systems to implement catalytic reduction of $N_2$ is still one of the main challenges in f-element chemistry.

## I.3.4 PhNNPh reduction

Reduction of azobenzene has been investigated as a possible model of $N_2$ coordination and reduction. Thanks to the phenyl substituents on the nitrogen atoms, the double N=N bond is more reactive than its triple analogue in dinitrogen. The reactivity studies with PhNNPh thus provide information on f-element interactions with unsaturated substrates. Low valent f-element complexes were found to undertake one-, two- and even four-electron reductions of azobenzene leading in the last case to N=N bond cleavage.

### I.3.4.1 One-electron reduction of PhNNPh

During the reactivity studies of the organometallic Sm(II) complex $[SmCp^*_2(THF)_2]$, Evans and co-workers observed the one-electron reduction of azobenzene affording a Sm(III) complex bound to a $(N_2Ph_2)^-$ anion (Scheme I-25a).[153] If other examples of single-electron reduction of azobenzene by lanthanides were also reported with phospholide,[155] aryloxide[156] or pyrazolylborate[157] ligands, the radical character of the obtained azobenzene anion was not mentioned. In contrast, the U(IV) radical azobenzene complex $[U(N_2Ph_2^{\bullet})((SiMe_2NPh)_3tacn)]$, obtained from the reduction of 1eq of PhNNPh by

[U((SiMe$_2$NPh)$_3$tacn)] (Scheme I-25b), features uranium-radical coupling leading to unique single molecule magnet behaviour for a U(IV) complex.[154]

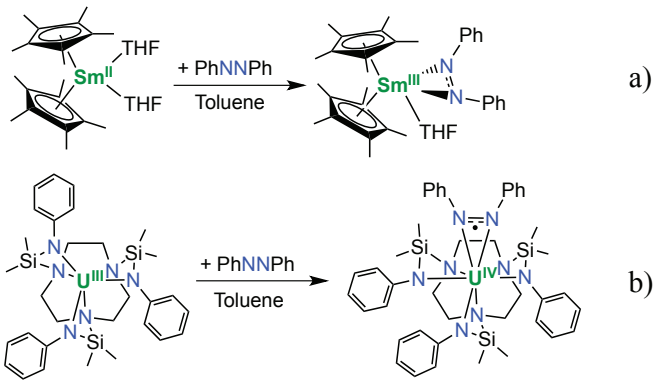


**Scheme I-25: Mono-electronic reduction of azobenzene by [SmCp*$_2$(THF)$_2$] and [U((SiMe$_2$NPh)$_3$tacn)].[153, 154]**

## I.3.4.2 Two-electron reduction of PhNNPh

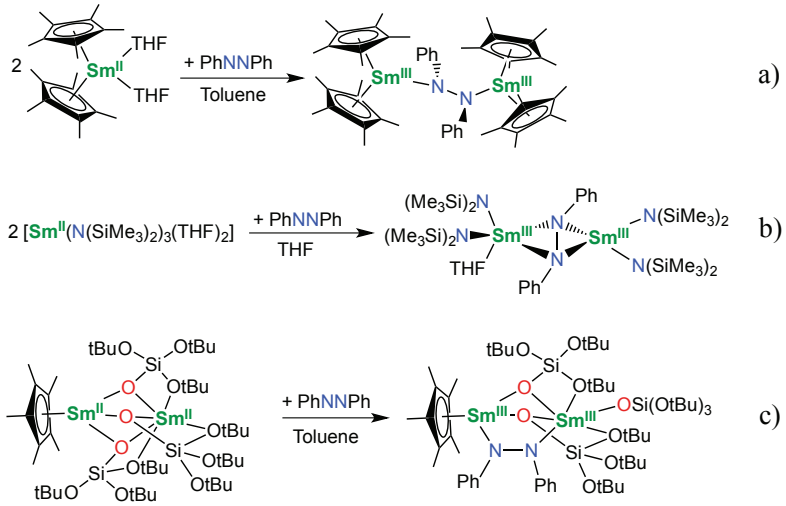


**Scheme I-26: Selected examples of azobenzene two-electron reductions by Sm(II) complexes.[43, 153, 158]**

The two-electron reduction of azobenzene by divalent lanthanide complexes is more common than the mono-electronic one and leads to bridging (PhNNPh)$^{2-}$ dianion between two Ln(III) centres. Reacting the [SmCp*$_2$(THF)$_2$] complex with 0.5eq of azobenzene per Sm(II) ion, leads to single-electron transfer from two Sm(II) centres to azobenzene affording the bridging (PhNNPh)$^{2-}$ moiety (Scheme I-26a).[153] This shows that the reduction of azobenzene can be controlled by the stoichiometry of the reaction. However, the steric environment

provided by the ligands plays also an important role in PhNNPh reduction as the bulky Sm(II) pyrazolylborate complex reported by Takats et al. undertakes only single-electron reduction of azobenzene even in presence of an excess of Sm(II) complex. The steric hindrance of the complex probably prevent the bridging of the azobenzene radical anion and thus further reduction[157] The reactivity studies of lanthanide complexes leading to two-electron reduction of this azo compound are dominated by Sm(II) complexes supported by various ligand systems such as silylamide[158] or siloxide[43] (Scheme I-26b and c). In the absence of electron rich ligands, non-classical divalent lanthanides are needed to activate azobenzene. Notably $LnI_2$ salts (Ln=Nd, Dy, Tm) were found to doubly reduce PhNNPh in 5 min at room temperature in THF to yield a mixture of the respective $LnI_3$ salt and the dimeric complex $[Ln(N_2Ph_2)I(THF)_2]_2$.[159] The authors mentioned that ytterbium diiodide is also able to promote similar azobenzene reduction but more drastic conditions are required (80°C, 15h) to overcome the lower reduction potential of Yb(II) ion.

It is to note that two-electron reduction of PhNNPh by U(III) complex has not been reported so far.

### I.3.4.3 Reductive splitting of PhNNPh

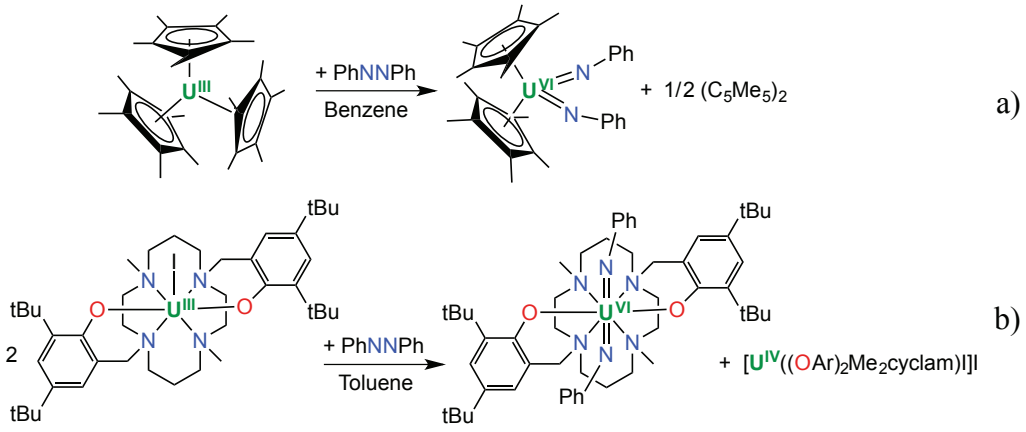


**Scheme I-27: Reductive splitting of azobenzene by [UCp*$_3$] and [U((OAr)$_2$Me$_2$cyclam)I].[160, 161]**

Low valent uranium complexes promote PhNNPh reductive splitting.[143] The mononuclear U(III) metallocene complex [UCp*$_3$], for example, is able to cleave the N=N bond thanks to four-electron transfer: three electrons from the U(III) to U(VI) oxidation and one from the oxidative coupling of Cp* ligands (Scheme I-27a).[160] However, concomitant

ligand-based reduction is not mandatory as proven by the reaction of 2eq of the U(III) complex supported by the redox-innocent bisphenolate cyclam ligand with 1eq of azobenzene which afford the U(IV) analogue and the U(VI) bis-imido complex (Scheme I-27b).[161] In this case, the authors propose a mechanism where three electrons are transferred by one U(III)-U(VI) transformation and the last electron by a more common U(III)-U(IV) oxidation process. However, the authors precise that a mechanism involving a two-electron transfer at one uranium centre followed by disproportionation of an unstable U(V) complex bound to a $(PhNNPh)^{2-}$ moiety cannot be ruled out. The possibility of uranium to undergo two-electron transfer (not observed for lanthanides), even if rare, renders it attractive for the activation of small molecules.

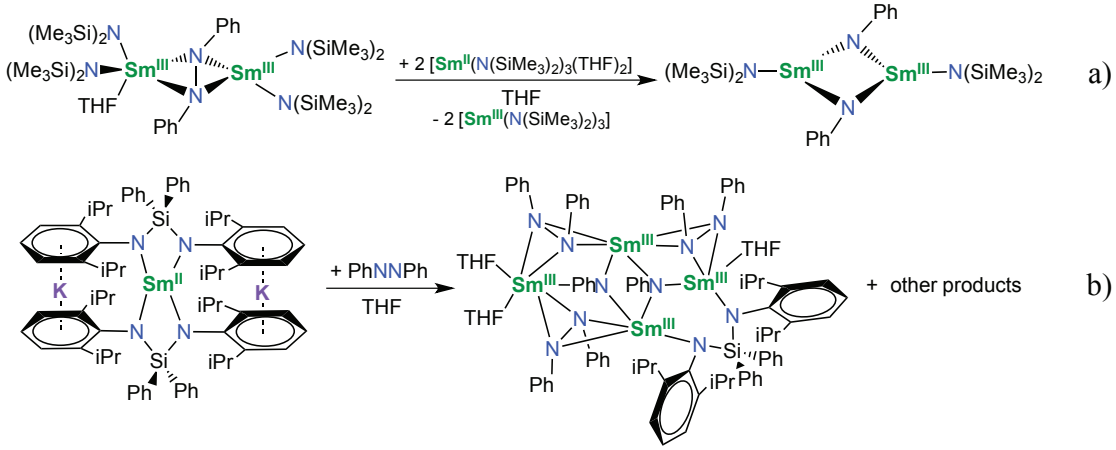


**Scheme I-28: Reductive splitting of azobenzene by samarium complexes.[158, 162]**

With less available oxidation states, the mononuclear divalent lanthanide complexes mainly undertake single-electron transfer. Nevertheless, examples of azobenzene reductive cleavage were also reported for divalent lanthanide species. Notably, the addition of 2eq of the Sm(II) bis-silylamide complex $[Sm(HMDS)_2(THF)_2]$ to the dinuclear Sm(III) bridging $(PhNNPh)^{2-}$ species provides the two electrons missing to achieve the N-N bond cleavage of the azobenzene moiety affording the dimeric imido compound $[Sm(NPh)(HMDS)]_2$ and two $[Sm(HMDS)_3]$ (Scheme I-28a).[158] The complex $[Sm(NPh)(HMDS)]_2$ was not characterised by X-ray diffraction, yet hydrolysis of this compound affords aniline proving the N-N bond dissociation. Divalent samarium "ate" complex supported by bisamide ligands undertakes azobenzene reductive splitting affording a tetranuclear Sm(III) compound with three $(N_2Ph_2)^{2-}$

moieties and two imido $(PhN)^{2-}$ groups (Scheme I-28b).[162] However, the stoichiometry of the reaction is not elucidated and side-products remain not identified.

# I.4 Activation of sulfur in uranium chemistry

The activation of elemental sulfur or sulfur-containing compounds is of interest for the development of synthetic pathways to produce sulfured organic molecules that have commercial and industrial applications. Notably, sulfur atom transfer catalysis performed by transition metal complexes is used in the syntheses of valuable thio-compounds.[163, 164] Transition-metal complexes with ligand presenting multiple bonding character are usually involved in sulfur transfer catalysis. With a large ionic radius, a wide range of oxidation states, an uncommon coordination geometry and 5f orbitals potentially available for participation in bonding, uranium-mediated sulfur activation could leads to interesting and singular outcomes.[165]

Moreover, there is currently a fundamental interest in multiple bonding with actinide ions to better understand the electronic structure, the nature of the bonding and the involvement of the f-orbitals in it.[166] Thus, the syntheses of terminal actinide nitride,[167, 168] oxide[7, 169-176] and sulfide[177-179] complexes received an increasing attention as they provide a promising way to study the covalent character of An-N, An-O and An-S bonds. The study of the An-S interaction is particularly important as S-donor ligands were shown to be very efficient in the An/Ln separation process of spent nuclear fuel retreatment.[180] The partial covalent character of the An-S multiple bond could be the reason of the high selectivity of these S-containing ligands for actinide extraction.[181-184]

However, the isolation of a terminal uranium sulfide complex from two-electron reduction of elemental sulfur or triphenylsulfide is not obvious as the nucleophilic character of the obtained $S^{2-}$ ligand often leads to sulfide-bridged complexes[185-190] or mononuclear disulfide complexes.[186, 191]

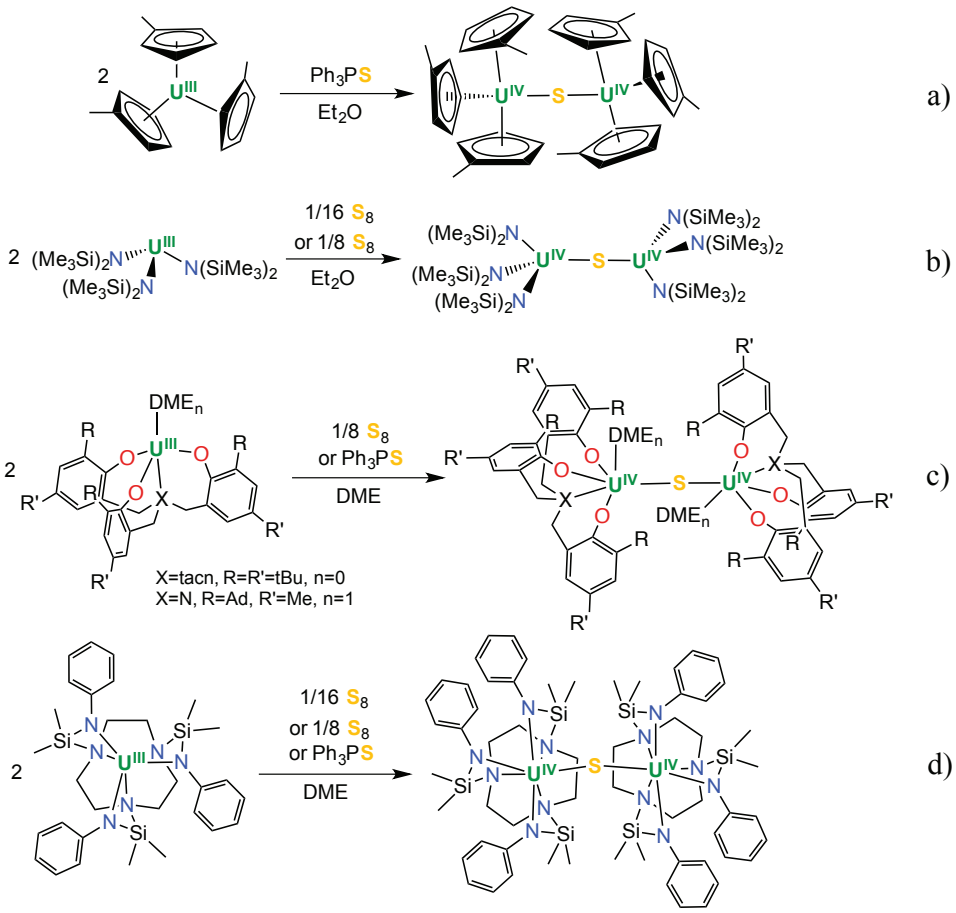


**Scheme I-29: Reduction of sulfur agents by U(III) complexes leading to U(IV)-U(IV) bridging sulfide species.** [185-187, 189]

Indeed even with bulky ligand systems such as cyclopentadienyl,[189] sylilamide,[187, 188] trisaryloxide[185] or silylated tacn ligands,[186] di-uranium(IV) sulfide-bridged complexes were formed (Scheme I-29).

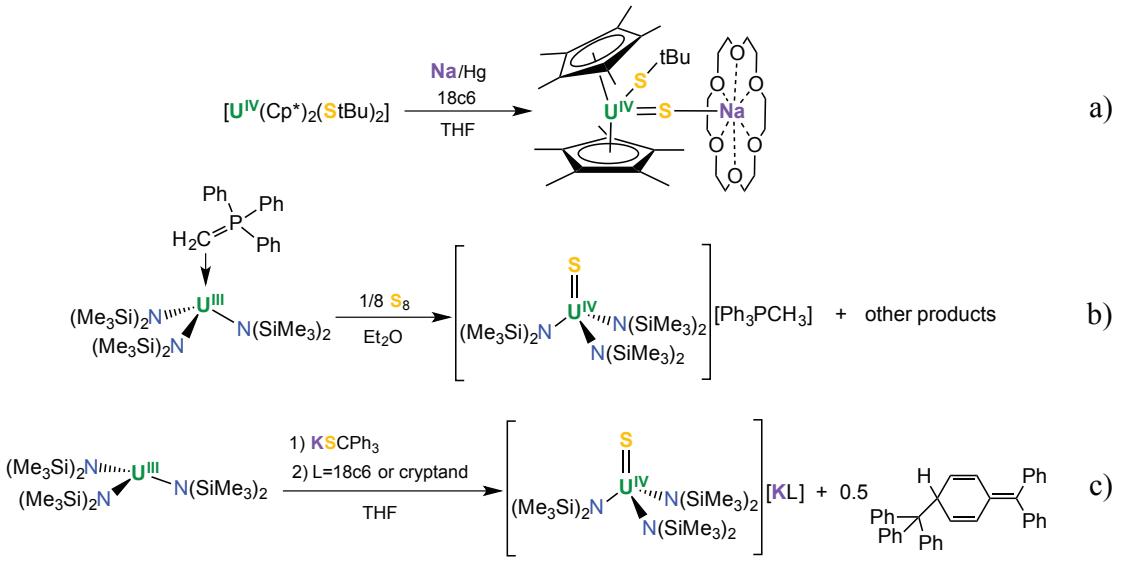


**Scheme I-30: Syntheses of U(IV) terminal sulfide complexes a) by reduction of a thiolate ligand with Na/Hg,[192] b) by reduction of elemental sulfur with a U(III) complex protected by a ylide moiety[177] and c) by cleavage of a trityl protecting group.[179]**

To date, only two ligand systems allowed the isolation of terminal uranium sulfide and, in each case, an unusual synthetic pathway was used. In 1999, the group of Ephritikhine isolated a sodium-capped terminal U(IV) sulfide complex [Na18c6][USCp*$_2$(StBu)] from the reduction of a thiolate ligand in the U(IV) complex [UCp*$_2$(StBu)$_2$] with Na/Hg amalgam (Scheme I-30a).[192] In 2012, Hayton and co-workers synthesised a series of anionic uranium chalcogenide complexes [UE(N(SiMe$_3$)$_2$)$_3$]$^-$ (E=S, Se, Te) by addition of 1eq of elemental chalcogens to the U(III) ylide adduct [U(H$_2$C=PPh$_3$)(NR$_2$)$_3$] (Scheme I-30b).[177] This ylide protecting ligand increases the bulk around the uranium atom preventing the bridging of the chalcogenide ligand during the chalcogen transfer. The yield of the terminal sulfide remains low. In 2014, the group of Hayton reported another synthetic route to form the anionic uranium sulfide complex [US(N(SiMe$_3$)$_2$)$_3$]$^-$ that involves the addition of 1eq of KSCPh$_3$ to [U(N(SiMe$_3$)$_2$)$_3$] (Scheme I-30c).[179] The trityl protecting group of the thiol is released as Gomberg's dimer via reductive cleavage leading to the U(IV) terminal sulfide complex.

In conclusion there are few examples of terminal uranium sulfide complexes because the two-electron reduction affording the $S^{2-}$ ligand often involves the mono-electronic oxidation of two U(III) complexes in their U(IV) analogues bridged by the obtained sulfide ligand. If the choice of a bulky ligand system is important to prevent sulfide bridging, the selection of the appropriate synthetic route is crucial as exemplified by the uranium

silylamide system which can lead to bridged compound (Scheme I-29b) or terminal sulfide complex if protecting groups are involved (Scheme I-30b and c).

# I.5 Schiff base ligand non-innocence in f-element chemistry

As seen in the previous sections, the reduction of small molecules often requires more than one electron. While uranium and lanthanide chemistry is dominated by mono-electronic redox processes, the use of redox active ligands, such as Schiff bases, affords a suitable route to store electrons into C-C bonds between two imino groups via a reversible reductive coupling.[193] Schiff base ligands have been mainly used in uranium chemistry to coordinate the uranyl(VI) moiety.[194, 195] The only examples of U(III) Schiff base complexes have been reported by Arnold et al. with pyrrolic macrocyclic ligands of the Pacman family.[196, 197] However, attempt to form the mononuclear U(III) complex supported by this Pacman ligand via protonolysis reaction between [U(HMDS)$_3$] and the protonated ligand leads to uranium oxidation and affords the mononuclear U(IV) complex (Scheme I-31).

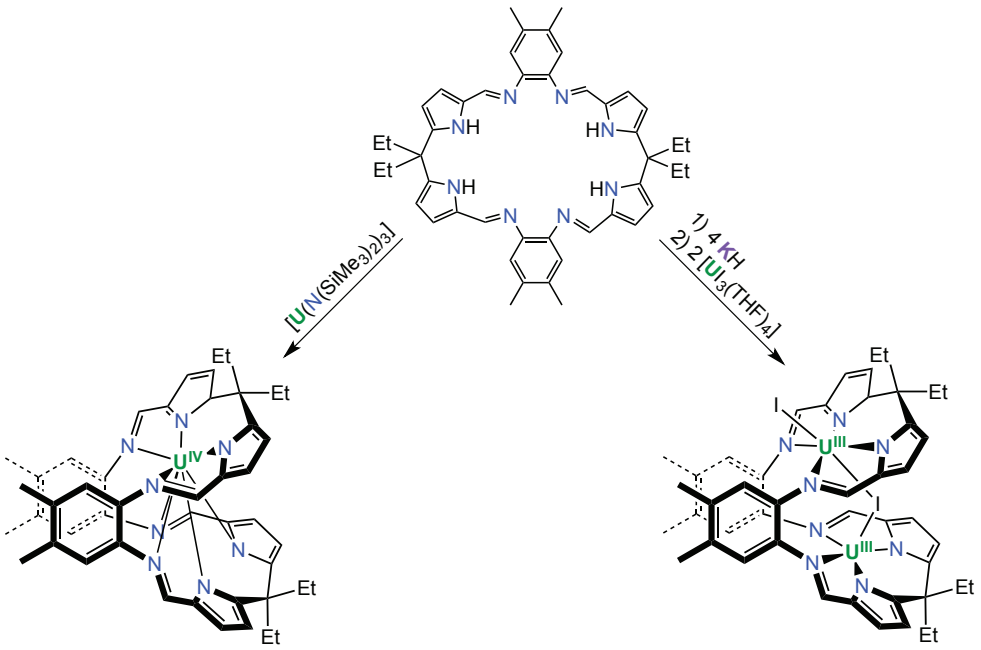


**Scheme I-31: Reaction of the Schiff base Pacman ligand with U(III) precursors.[196]**

Previous work in our group focused on the coordination of uranium by the salophen ligand (Scheme I-32).[5] Notably, the addition of 2eq of salophen$K_2$ to $[UI_4(OEt_2)_2]$ leads to the homoleptic U(IV) complex $[U(salophen)_2]$. Subsequent reduction of this complex by 2eq of metallic sodium, leads to the formation of an intramolecular C-C bond between one imino group of each ligand affording the new hexa-anionic bis-salophen ligand scaffold. The two electrons stored on the C-C bond are available to reduce oxidizing agents such as silver triflate or phenanthrene quinone. In these complexes, bi-electronic reductions occur without any change of the U(IV) oxidation state.

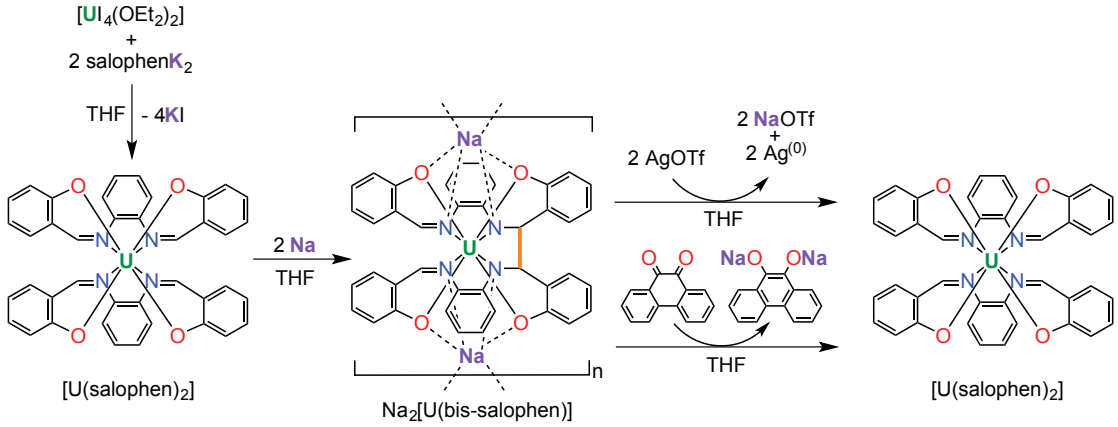


**Scheme I-32: Synthesis and reactivity of the $Na_2$[U(bis-salophen)] complex.[5]**

The redox chemistry of divalent samarium supported by tetradentate pyrrolic Schiff bases has been investigated by Gambarotta and co-workers.[47] The reaction of the Sm(II) silylamide complex $[Sm(HMDS)_2(THF)_2]$ with three related ligands have been explored (Scheme I-33). While the ligand with phenylene bridge allows electronic transfer from the samarium to the ligand scaffold affording dinuclear Sm(III) species with reductive C-C coupling of the ligands, the presence of methyl substituents in 3,4 positions of this phenylene bridge leads to disproportionation of the divalent samarium in Sm(III) ion pair species and Sm(0). The presence of ethylene bridge and the protection of the imine groups by methyl substituents allows the formation of the Sm(II) mono-ligand complex. This work exemplifies that small modifications of the steric and electronic properties of the ligand can drastically impact the redox behaviour of these systems.

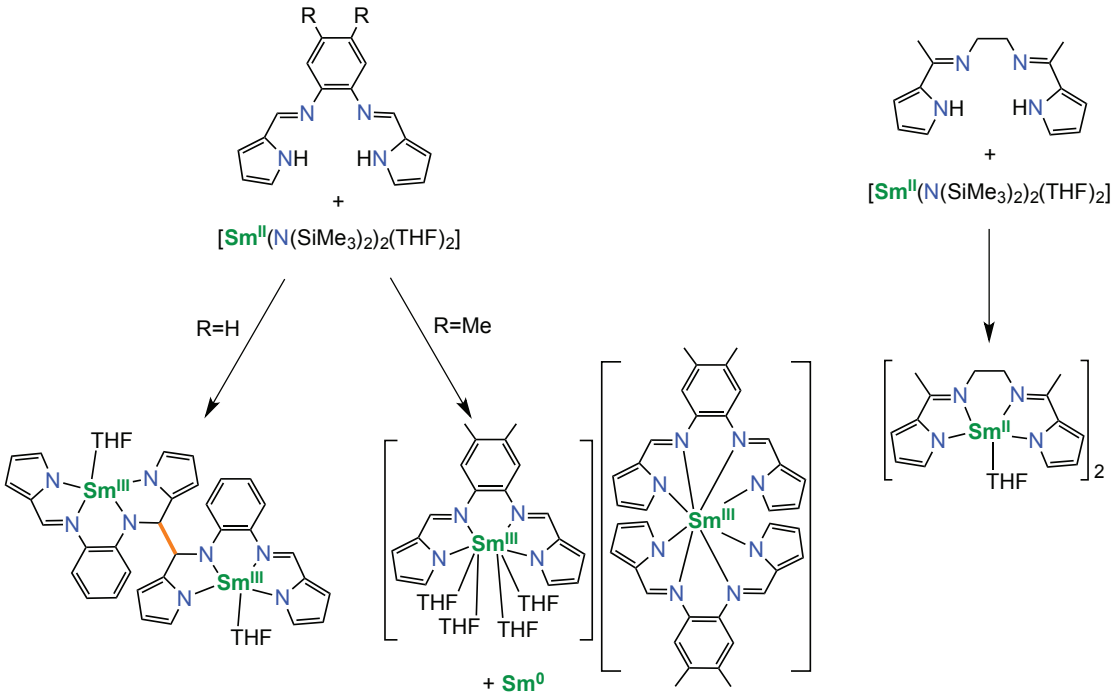


**Scheme I-33: Redox chemistry of samarium centres supported by pyrrolic Schiff bases.**[47]

More recently in our group, the redox chemistry of the uranium salophen system has been extended to lanthanides and a family of complexes $K_3$[Ln(bis-salophen)] (Ln=Nd, Eu, Tb, Yb) has been prepared[6] (Scheme I-34). Once again the bis-salophen ligand can be used as a 2 electrons reservoir: the electrons stored on the C-C bond can be released to reduce oxidizing agents. The effect of substituents in ortho and para positions on the phenolate groups was investigated by cyclic voltammetry studies. The presence of alkyl substituents, especially tert-butyl ones, was found to render the ligand oxidation easier as the oxidation potential of the C-C bond of the $^{R}$bis-salophen ligand ion is shifted to more negative values (from -0.97 V vs. $Fc^+/Fc$ for $K_3$[Nd(bis-salophen)] to -1.50 V vs. $Fc^+/Fc$ for $K_3$[Nd($^{tBu}$bis-salophen)]).

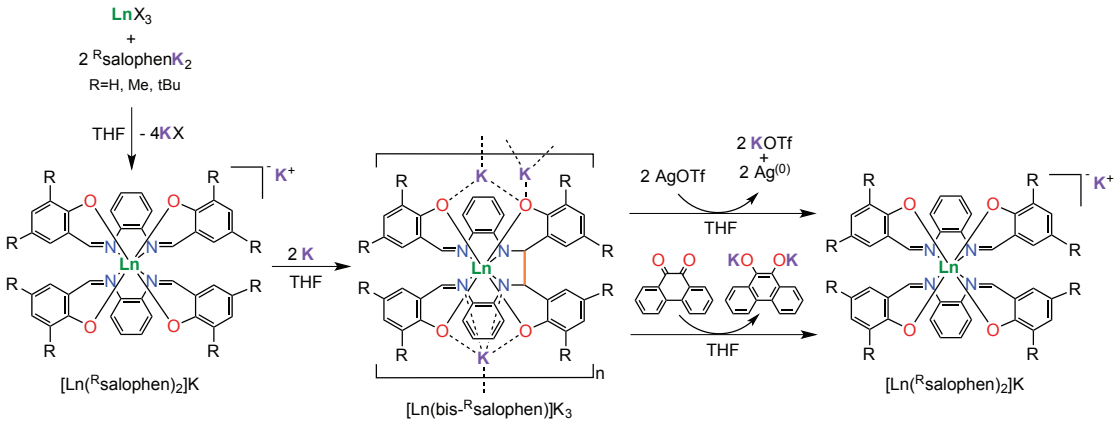


**Scheme I-34: Synthesis and reactivity of the $K_3$[Ln(bis-$^{R}$salophen)] complexes.[6]**

Shen et al. reported the use of the tridentate Schiff base ($^{tBu}$Phquinolen)$^{-}$ featuring a quinoline moiety and a phenolate group to coordinate Sm(III) centres. The addition of 2eq of the sodium ligand salt to the Sm(III) chloride precursor affords the heteroleptic complex [Sm($^{tBu}$Phquinolen)$_2$Cl]. Subsequent addition of 2eq of metallic sodium leads to a Sm(III) complex supported by a new ligand arising from the reduction and rearrangement of three ($^{tBu}$Phquinolen)$^{-}$ ligands (Scheme I-35).[198] This new penta-anionic ligand is obtained by $C_{imino}$-$C_{imino}$ and $C_{imino}$-$C_{quinoline}$ couplings and proton migration from the position 2 of one quinoline moiety to the basic amido function of another $^{tBu}$Phquinolen ligand. The formation of the $C_{imino}$-$C_{quinoline}$ bond between the carbon atom of one imino function and the carbon atom in position 2 of one quinoline moiety has then been reported for yttrium, ytterbium, and neodymium complexes supported by this ($^{tBu}$Phquinolen)$^{-}$ ligand.[199, 200]

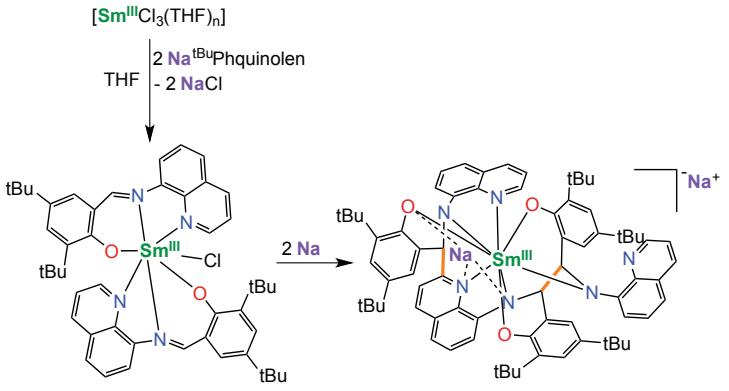


**Scheme I-35: Reduction of the complex [Sm($^{tBu}$Phquinolen)$_2$Cl].[198]**

To summarize, redox active Schiff base ligands are convenient tools to store electrons in C-C bonds and thus increase the number of electrons potentially available rendering possible multi-electronic reductions. However, this redox chemistry is extremely sensitive to electronic and steric properties of the ligand system and a particular attention to the ligand design is necessary.

# CHAPTER II

# Multi-electron Redox Reactions Involving C-C Bond Formation and Cleavage in Uranium and Transition Metal Schiff Base Complexes

## II.1 Electron-rich U(IV) complexes supported by tridentate Schiff base ligands

### II.1.1 Context

As mentioned in the introduction, our group studied the use of tetradentate Schiff bases as supporting ligand for uranium or lanthanide centres in order to achieve multi-electronic reduction. Notably, during his PhD, Valentin Guidal investigated the reactivity of some Ln(III) complexes supported by reduced Schiff bases. The complex $K_3$[Nd($^{tBu}$bis-salophen)] was shown to react with $CO_2$ leading to a mixture of multiple products including product resulting from carboxylation of the ligand.[201] This suggests that, in some extent, the $CO_2$ reaction is ligand-based probably due to the lack of available coordination site on the Nd(III) centre. In order to improve the reactivity of the uranium complexes supported by Schiff base ligands, we thus envisaged to design complexes that would present free coordination sites at the metal centre.

## II.1.2 Ligand design

Using a tridentate Schiff base ligand should free two coordination sites at the metal centre in contrary to the $Na_2$[U(bis-salophen)] system. The possibility for the substrate to coordinate the uranium ion should lead to a better control of the reactivity favouring the electron transfer from the ligand scaffold to the substrate *via* the metal centre. The tridentate Schiff base ligand $^{Me}$naphtquinolen, presented in Scheme II-1, matches all the selected criterions. The imine function is highly conjugated thanks to the quinoline moiety which favours electronic delocalization and renders the ligand a better electron acceptor. The protection of position 2 of the quinoline by a methyl substituent should prevent nucleophilic or radical side reactions typically known to occur at this position.[199]

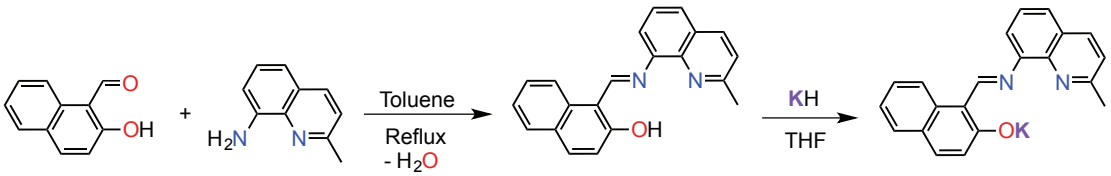


**Scheme II-1: Synthesis of $^{Me}$naphtquinolenK.**

This $^{Me}$naphtquinolen ligand was obtained by condensation between 2-methylquinolin-8-amine and 3-hydroxy-2-naphtaldehyde. The deprotonation of the phenol group was performed under inert atmosphere using potassium hydride.

## II.1.3 Synthesis of [U(bis-$^{Me}$naphtquinolen)]$_2$ and its equilibrium in polar solvents.

The work described in this section, on the synthesis and characterization of the [U(bis-$^{Me}$naphtquinolen)]$_2$ complex, was carried out in collaboration with Clement Camp, a PhD student in the group.

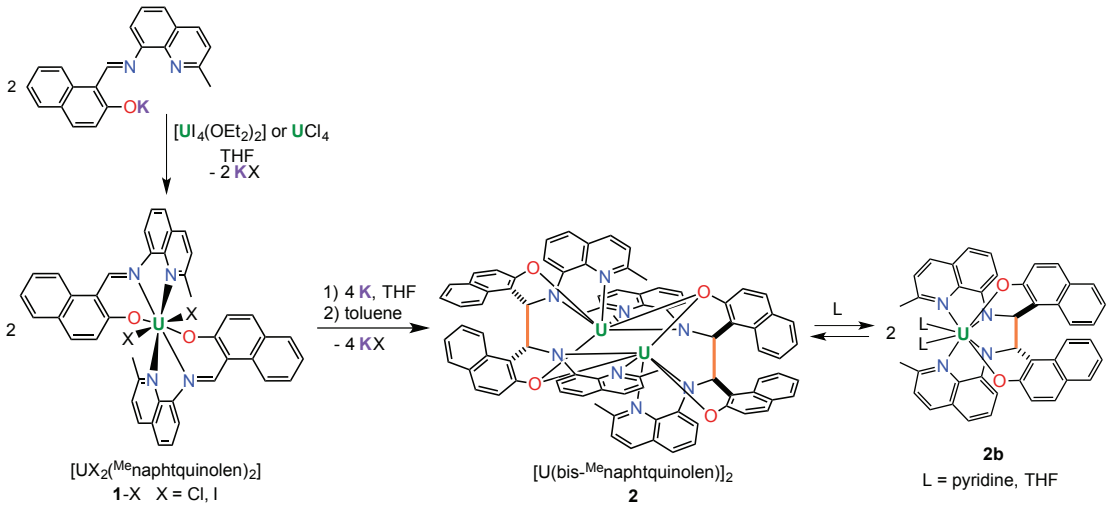


**Scheme II-2: Synthesis of [U(bis-$^{Me}$naphtquinolen)]$_2$, 2, and equilibrium in coordinating solvents.**

The addition of 2eq of $^{Me}$naphtquinolenK to 1eq of [UI$_4$(OEt$_2$)$_2$] or UCl$_4$ affords the heteroleptic U(IV) complex [UX$_2$($^{Me}$naphtquinolen)$_2$], **1**-X (X=I, Cl). The complex **1**-Cl can be isolated pure in 72% yield thanks to its higher solubility in THF and toluene than **1**-I, which renders its extraction from KCl salt easier. Single crystals suitable for X-ray diffraction were obtained by slow diffusion of hexane into a pyridine solution of **1**-Cl.

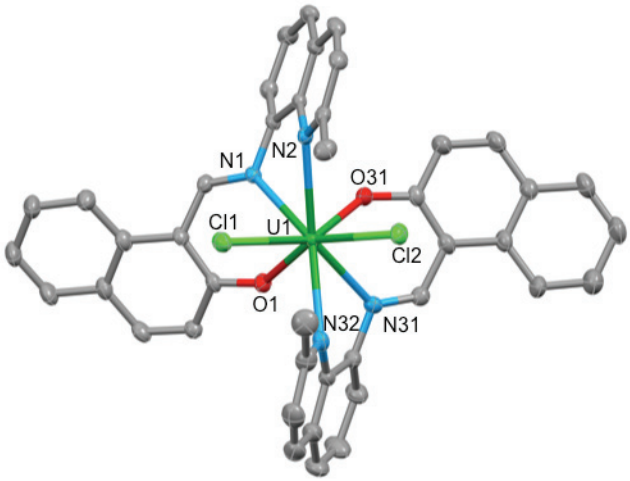


**Figure II-1: Solid state structure of [$UCl_2$($^{Me}$naphtquinolen)$_2$].(py), 1-Cl.(py) (50% ellipsoids). Hydrogen atoms and solvent molecules are omitted for clarity.**

**The X-ray structural analysis of 1-Cl.(py) shows that the uranium atom is octa-coordinated by two $^{Me}$naphtquinolen and two chloride ligands in a slightly distorted square antiprism possessing a pseudo $C_2$ axis (Figure II-1). The mean values of U-O (2.20(2) Å) ; U-N (2.6(1) Å) and U-Cl (2.67(4) Å) bond distances (**

Table II-2 at the end of section II.1.5.2) are in the range of the ones found in other U(IV) Schiff base complexes.[5, 202, 203] The $^{Me}$naphtquinolen ligands are strongly distorted from planarity with in average 68(4)° between the quinoline and the naphtol cycles. This is most probably due to sterical repulsion between the two tridentate ligands in the present coordination environment. This geometry is very different from the one reported for analogous tridentate ligands bound to Yb(III) or Y(III).[199] In the crystal structure of the [$LnL_2(HMDS)_2$] (Ln = Yb(III) or Y(III) L = bis(3,5-di-tert-butylsalicylidene)-8-aminoquinoline), the two tridentate Schiff bases are almost planar and bind the metal in a parallel fashion. These two binding modes are reminiscent of those found in sandwich and meridional isomers of uranium bis-ligand complexes of tetradentate Schiff bases.[5, 202]

The addition of 2eq of potassium metal per U atom to a THF solution of **1**-I leads to a dark brown suspension and the $^1$H NMR spectrum of the crude mixture in deuterated THF features two sets of 26 signals with an integration ratio near 2:1. However, once deuterated THF is removed under vacuum, the $^1$H NMR spectrum of the evaporated crude in deuterated toluene shows only one set of 26 signals. The complex [U(bis-$^{Me}$naphtquinolen)]$_2$, **2**, can be isolated pure in 67% yield by recrystallization from toluene.

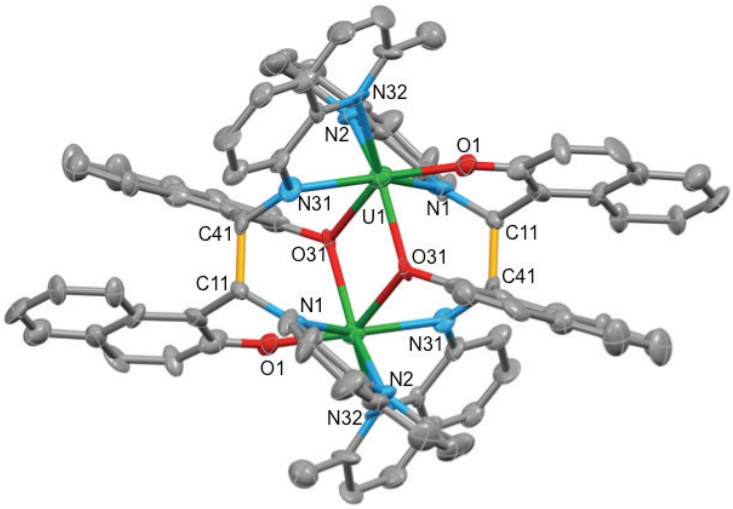


**Figure II-2: Solid state structure of [U(bis-$^{Me}$naphtquinolen)]$_2$.(tol)$_2$, 2.(tol)$_2$ (50% ellipsoids). The C-C bonds formed by the reduction of the imino functions are represented in orange. Hydrogen atoms and solvent molecules are omitted for clarity.**

The solid state structure of **2**.(tol)$_2$, determined by X-ray structural studies, is presented in Figure II-2. It shows that the dimeric compound **2** is composed of two U(IV) [U(bis-$^{Me}$naphtquinolen)] moieties bridged by the phenolate oxygens of the two tetra-anionic bis-$^{Me}$naphtquinolen ligands. The crystal structure is centrosymmetric, with an inversion centre located halfway between the two uranium atoms. Each metal cation is hepta-coordinated in a distorted capped trigonal prismatic environment by the four nitrogen (average U-N = 2.5(1) Å) and two oxygen atoms from a bis-$^{Me}$naphtquinolen ligand (average U-O = 2.3(1) Å) and by a bridging phenolate oxygen from the other [U(bis-$^{Me}$naphtquinolen)] moiety. The two bidentate phenolate bridging ligands hold the two uranium centres in the dimer at 3.7983(8) Å apart. The analysis of the structural parameters of complex **2** clearly shows that the reduction has occurred on the imino groups of the ligands rather than on the metal ions. Notably, the two-electron reduction of the ligand results in the formation of two C–C bonds, 1.64(1) Å long, by intramolecular coupling of the original imino groups. The value of the C–C bond distance is larger than the one found in the [U(bis-salophen)]Na$_2$ (1.559(7) Å) complex for the C-C bonds formed after reductive coupling of the imino groups[5] but remains in the range of reported values for C–C bonds in molecules with strong steric hindrance.[204, 205] The C–N$_{amido}$ bond distances (average C–N$_{amido}$ = 1.474(5) Å) of the ligand

backbone are much longer than those observed in **1**-Cl, and are in agreement with the presence of two amido groups. The shorter U–$N_{amido}$ distances in **2** (U–$N_{amido}$ = 2.36(2) Å) compared to the U–$N_{quinoline}$ distances in **2** (U–$N_{quinoline}$ = 2.538(3) Å) and the U–$N_{imino}$ distances in **1**-Cl (U–$N_{imino}$ = 2.51(3) Å) further confirm the presence of two amido groups. Finally, these distances are comparable to the U-$N_{amido}$ (2.387(8) Å) and U-$N_{imino}$ (2.624(7) Å) found in $Na_2$[U(bis-salophen)][5] and bond valence calculations are in agreement with a +IV oxidation state for the uranium ions in **2**.

The complex **2** is soluble in toluene, contrary to the $Na_2$[U(bis-salophen)] complex, probably because of its neutral formulation. Complex **2** is stable at room temperature both in solid state and solution. The centrosymmetric dimeric structure of **2** is in agreement with the set of 26 signals observed on its $^1$H NMR spectrum in deuterated toluene indicating that this structure is maintained in toluene solution. Dissolving dark crystals of **2** in deuterated THF or pyridine leads to $^1$H NMR spectra with two sets of 26 signals. When THF or pyridine is removed under vacuum and deuterated toluene is added to the resulting solid leading to a dark solution, the $^1$H NMR spectrum in toluene shows again one set of 26 signals. These results suggest that two forms of **2** are present in coordinating polar solvents. Monitoring the $^1$H NMR spectrum in deuterated pyridine overtime shows an evolution of the ratio between the two species from 3:1 half an hour after dissolution to a stable ratio of 1:2 after 4 days (Figure II-3). Thirty minutes after dissolution, the main species of **2** in pyridine features similar chemical shifts than the ones measured for **2** in toluene indicating that the dinuclear compound is initially the main one in pyridine solution but slowly undertakes structural rearrangement to form a second species. This new complex could be a solvated dinuclear compound or a mononuclear form of the complex.

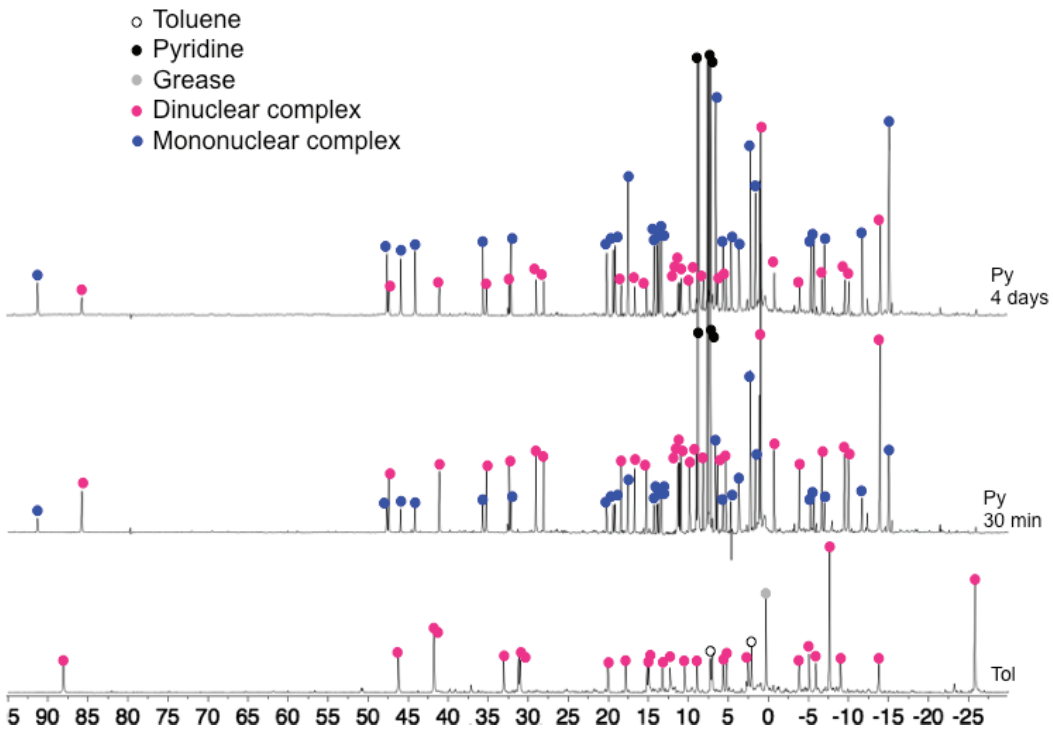


**Figure II-3: $^{1}$H NMR spectra (200 MHz, 298K) of complex [U(bis-$^{Me}$naphtquinolen)]$_2$, 2, in tol-d$_8$ (bottom) and after dissolution of 2 in py-d$_5$: after 30 min (middle), after 4 days (top).**

The diffusion coefficients, D, of both species were measured in pyridine solution by diffusion ordered spectroscopy in order to correlate D and the molecular weight M and thus discriminate the molecular arrangement of each species.[206] The values found for the diffusion coefficients in pyridine ($(D_{2b}/D_2)^3 = 1.63$) are in agreement with the presence in solution of a mononuclear and a dinuclear complexes ($M_2/M_{2b} = 1.69$). Unfortunately, all attempts to crystallize the mononuclear complex **2b** from coordinating solvents failed.

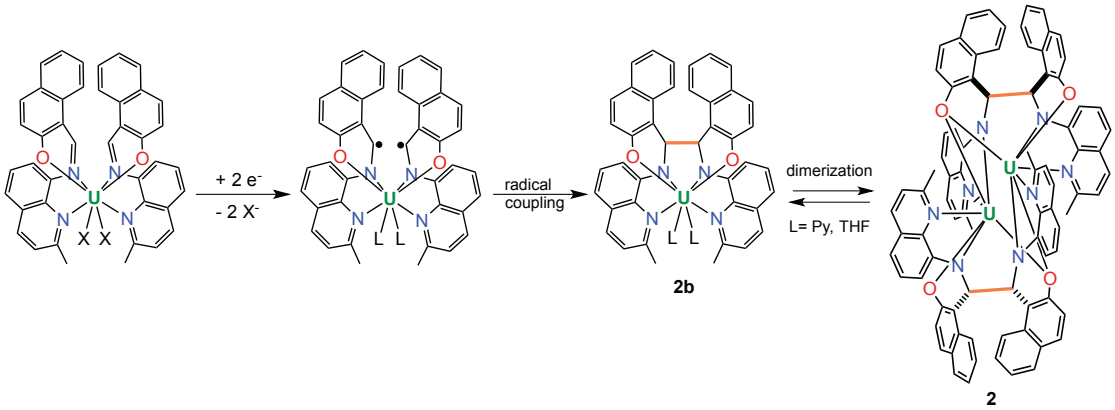


**Scheme II-3: Postulated pathway for the C-C bond formation leading to complex 2.**

The dinuclear architecture of complex **2** is probably the result of the dimerization of two [U(bis-$^{Me}$naphtquinolen)] complexes themselves arising from intramolecular C-C coupling of U(IV) radical anionic species after reduction of the two imino functions in **1**-X (Scheme II-3). In the absence of coordinating solvent molecules, at least two coordination sites are available at the U(IV) centre. This allow dimerization through the phenolate groups and lead only to the dinuclear complex **2**. However, in coordinating solvents, the equilibrium between the dinuclear (**2**) and the solvated mononuclear (**2b**) species is observed.

In order to investigate if complex **2** can be further reduced to reach a highly electron-rich U(III) complex, the electrochemical properties of **2** was explored.

## II.1.4 Electrochemistry studies

The cyclic voltammetry analyses of complexes **1**-I and **2** in pyridine are presented in Figure II-4 and the redox potentials are summarized in Table II-1.

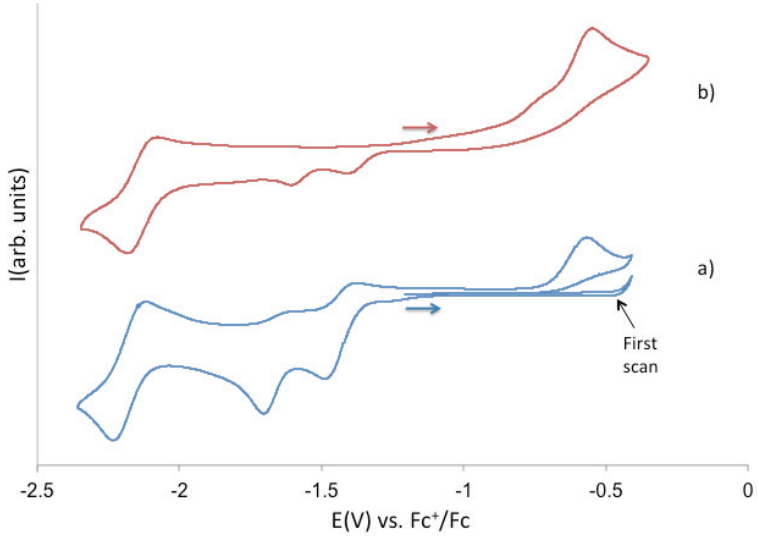


**Figure II-4: Cyclic voltammograms for 10 mM solutions of a) complex 1-I and b) complex 2 in ~0.1 M $[Bu_4N][PF_6]$ pyridine solution at 100 mV.s-1 scan-rate**

**Table II-1: Voltammetric data for complexes 1-I and 2 (in V vs. $Fc^+/Fc$)**

| Compounds | Metal-based event | Ligand-based events | | |
|---|---|---|---|---|
| | $E_{1/2}$ (V) | $E_{pc2}$ (V) | $E_{pc1}$ (V) | $E_{pa}$ (V) |
| **1-I** | -2.16 | -1.65 | -1.45 | -0.56 |
| **2** | -2.17 | -1.70 | -1.49 | -0.56 |

The voltammogram of complex **1**-I does not feature any oxidation process during the first scan of potential from -1.2 to -0.4 V vs. $Fc^+/Fc$. However when the voltammogram is then swept toward negative potentials, three distinct reduction waves are observed: two nearly irreversible events at $E_{pc1}$= -1.45 V vs. $Fc^+/Fc$ and $E_{pc2}$= -1.65 V vs. $Fc^+/Fc$ and a quasi-reversible event at $E_{1/2}$= -2.16 V vs. $Fc^+/Fc$. The two irreversible reduction processes are associated to an irreversible oxidation wave at $E_{pa}$= -0.56 V vs. $Fc^+/Fc$ as confirmed by the presence of this oxidation process after scanning the potentials from -1.2 to -2 V vs. $Fc^+/Fc$ and then from -2 to -0.4 V vs. $Fc^+/Fc$. The cyclic voltammogram of the potassium salt $^{Me}$naphtquinolenK, measured in the same conditions, does not present any redox event between -0.5 and -2.4 V vs. $Fc^+/Fc$. The limited degree of reversibility observed in the voltammogram of **1**-I can be explained by the formation of the C-C bond between two ligands which probably require an important structural rearrangement. The redox events visible on the voltammogram of the reduced dinuclear complex **2** are very similar to the ones observed on

the voltammogram of **1**-I with, notably, a quasi-reversible reduction at $E_{1/2}$= -2.17 V vs. $Fc^+/Fc$ and an irreversible oxidation at $E_{pa}$= -0.56 V vs. $Fc^+/Fc$. This latter oxidation wave presents a shoulder at -0.68 V vs. $Fc^+/Fc$ which was attributed to the oxidation of the mononuclear complex **2b** known to be in equilibrium with the dinuclear complex **2** in pyridine solution. To confirm this hypothesis, the voltammogram of **2** was measured twice: immediately after dissolution of **2** in pyridine and once again after one hour as shown in Figure II-5. The intensity of the shoulder at -0.68 V vs. $Fc^+/Fc$ is increasing with time while the intensity of the anodic peak at -0.56 V vs. $Fc^+/Fc$ is decreasing with time. This is in agreement with an increase of the mononuclear/dinuclear complex ratio, as observed by $^1H$ NMR spectroscopy, confirming the preceding assignation.

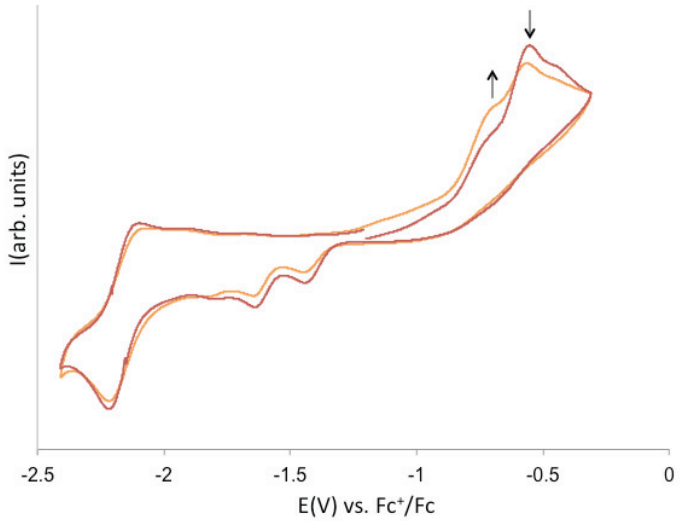


**Figure II-5: Cyclic voltammograms of complex 2 in ~0.1 M [$Bu_4N$][$PF_6$] pyridine solution at 100 mV.s-1 scan-rate. Red curve: on a freshly prepared solution. Orange curve: on the same solution after 1 hour.**

When the voltammogram of **2** is initially swept from -1.3 V vs. $Fc^+/Fc$ toward negative potentials, the two irreversible cathodic waves, at $E_{pc1}$= -1.49 V vs. $Fc^+/Fc$ and $E_{pc2}$= -1.70 V vs. $Fc^+/Fc$, are not present and thus attributed to the two successive one-electron reductions of the ligand as the C-C bonds are already formed in complex **2**. In consequence, the irreversible oxidation event at -0.56 V vs. $Fc^+/Fc$ is assigned to the cleavage of the C-C bond, that is to say, the oxidation of the bis-$^{Me}$naphtquinolen ligand scaffold. Differentiating ligand-centred and metal-centred events is not obvious considering that, in this system, both the ligand and the metal centre are electroactive. However, the irreversibility of the reduction/oxidation events at -1.7, -1.5 and -0.6 V vs. $Fc^+/Fc$ indicates a rapid chemical

transformation after the electrochemical reduction/oxidation in agreement with the formation/cleavage of the C-C bond between two imino groups. The difference between the much lower potential required to reduce the ligand and the potential required to oxidize it ($\Delta E_p$= 0.9 V) illustrates the strong stabilisation induced by the radical coupling into C-C bond. The quasi-reversible event at $E_{1/2}$= -2.16 V vs. $Fc^+/Fc$ is in the range of previously reported redox potentials for the couple U(IV)/U(III) in quasi reversible systems (-1.5 to -2.8 V vs. $Fc^+/Fc$).[60, 207] This further reduction of complex **2** is thus attributed to a metal-based reduction leading to an hypothetical U(III) complex $[U(\mu\text{-bis-}^{Me}\text{naphtquinolen})]_2^{2-}$.

Preliminary studies toward the isolation of this hypothetical highly electron-rich U(III) complex were performed. Unfortunately, the chemical reduction of complex **2** with 2eq or an excess of reducing agents in toluene (with $KC_8$ and K) or in THF (with K and Na) led only to the formation of species with uninformative NMR spectra and all attempts to crystallize any reaction product were unsuccessful. Performing these reductions under $N_2$ atmosphere did not lead to more informative $^1$H NMR spectra and no products crystallized from the reaction mixture.

## II.1.5 Reactivity of $[U(bis\text{-}^{Me}naphtquinolen)]_2$

### II.1.5.1 Reactivity with pyridinium chloride

Surprisingly, the addition of 1eq of pyridinium chloride per U atom to a freshly prepared pyridine solution of complex **2** does not lead to a rapid colour change of the reaction mixture, contrary to what was observed after the addition of pyHCl to the [Nd(bis-salophen)]$K_3$ complex.[6] The $^1$H NMR spectrum of the crude mixture in deuterated pyridine after 30 min of stirring shows the signals of the dinuclear complex **2** and another unidentified set of 26 signals with an integration ratio of 0.9:1 respectively. The signals of the mononuclear complex **2b** are absent from the spectrum while the equilibrium between **2** and **2b** is observed in pyridine before the addition of pyHCl. After 18h at room temperature, the colour of the mixture turned from dark brown to brown/yellow and the $^1$H NMR spectrum in deuterated pyridine shows only the 26 signals of the new species as shown in Figure II-6.

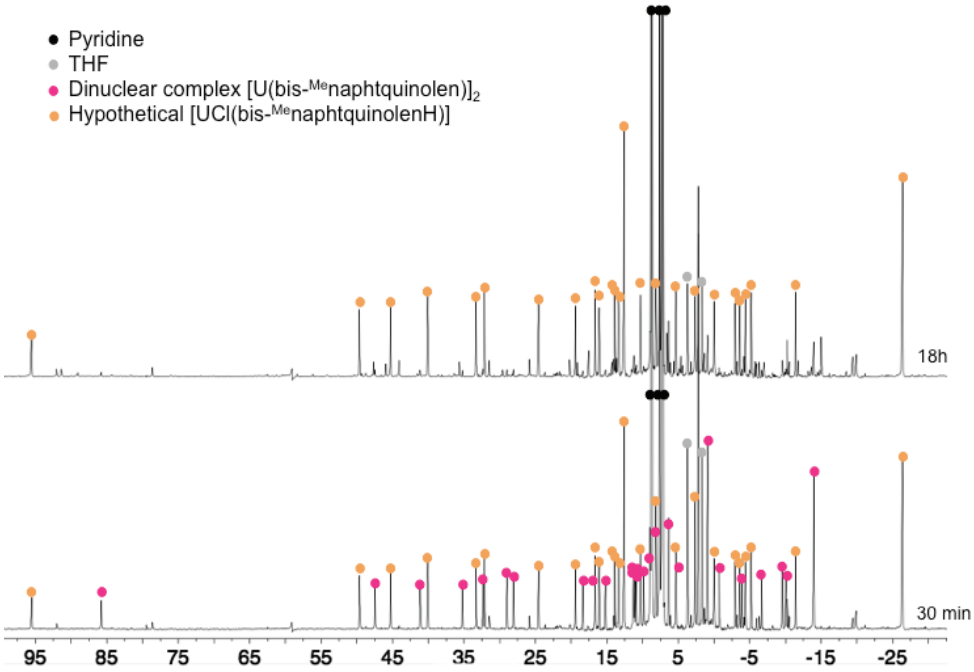


**Figure II-6: $^{1}$H NMR spectra (200MHz, 298K) of the crude reaction between [U(bis-$^{Me}$naphtquinolen)]$_2$, 2 and 2eq of pyHCl in py-d$_5$, after 30 min (bottom) and after 1 night (top).**

These results indicate a favoured protonation of the bis-$^{Me}$naphtquinolen ligand in the mononuclear form **2b** which leads to a mixture of the remaining dinuclear complex **2** and the hypothetical protonated complex [UCl(bis-$^{Me}$naphtquinolenH)]. The consumption of complex **2b** by the protonation reaction drives the equilibrium between **2b** and **2** to the mononuclear complex formation, which then reacts with the pyHCl still in solution (Scheme II-4). This is probably the reason of the observed slow rate of this reaction. The fact that only one product is obtained by reacting a mixture of **2** and **2b** confirms their isomeric relation. The absence of direct protonation of the dinuclear complex could be due to the lack of coordination site at the U(IV) centres in **2** for the chloride ligand while the mononuclear complex **2b** is likely to have two available sites at the U(IV) centre. This need of free coordination sites for chloride ligand was not observed during the protonation of $K_3$[Nd(bis-salophen)] by pyHCl.[6] Indeed, this latter possesses potassium counter-cations and thus KCl salt was eliminated.

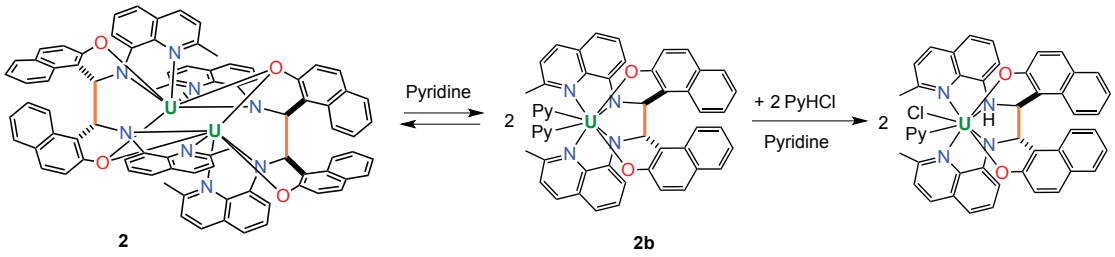


**Scheme II-4: Postulated reactivity of complex 2 with pyridinium chloride.**

Interestingly, after the subsequent addition of 1eq of pyHCl to the hypothetical [UCl(bis-$^{Me}$naphtquinolenH)], any change was observed on the $^{1}$H NMR spectrum of the crude mixture. The $^{1}$H NMR spectrum of the crude reaction after the direct addition of an excess of pyHCl to a pyridine solution of complex **2** shows the formation of the [UCl(bis-$^{Me}$naphtquinolenH)] as the main species. This could be due to structural issues such as a sterically crowded protonated complex rendering a further protonation kinetically or thermodynamically non-favoured. However, as neither the mononuclear complex **2b** nor the putative protonated complex [UCl(bis-$^{Me}$naphtquinolenH)] have been characterised by X-ray diffraction, this hypothesis has not been confirmed.

## II.1.5.2 Reactivity with oxidizing agents

In order to investigate the possibility of releasing the electrons stored in the C-C bonds, the reactivity of [U(bis-$^{Me}$naphtquinolen)]$_2$, **2**, with different oxidizing agents has been studied.

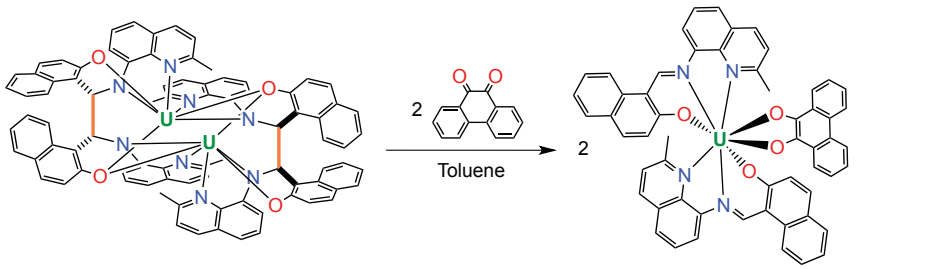


**Scheme II-5: Reactivity of complex 2 with 9,10-phenanthrenequinone.**

The reaction between complex **2** and 2eq of 9,10-phenanthrenequinone in toluene affords the U(IV) complex [U(9,10-phenanthrenediol)($^{Me}$naphtquinolen)$_2$], **3**, in 54% yield (Scheme II-5). Performing the reaction in pyridine solution leads to the same reaction product. A slow evaporation of a pyridine solution of complex **3** led to suitable crystals for X-ray diffraction. The solid state structure of **3**.(py)$_{4.5}$, presented in Figure II-7, consists of a $C_2$-symmetric complex where the uranium atom is octacoordinated in a distorted square antiprismatic geometry by two tridentate monoanionic $^{Me}$naphtquinolen ligands and one dianionic 9,10-phenanthrenediolate ligand. The reduction of the quinone to its catecholate form is confirmed by the analysis of the metrical parameters of the ligands. The average U-$O_{phenanthrenediolate}$ bond distance (2.26(4) Å) is relatively short, as expected for a doubly charged phenolate ligand, and is comparable with the average U-$O_{phenolate}$ distance from the $^{Me}$naphtquinolen ligand (2.23(1) Å). The C-O bond distances for the catecholate ligand (1.359(1) Å in average) are in agreement with the presence of simple C-O bonds. The imino functions of the $^{Me}$naphtquinolen ligands have been restored, as is illustrated by the short C-N double bond distances (1.294(9) Å in average) and long U-N bond distances (2.52(1) Å) which compare well with those found in complex **1**-Cl. The overall neutral charge of the complex is in agreement with an unchanged +IV oxidation state of the uranium cation in **3**.

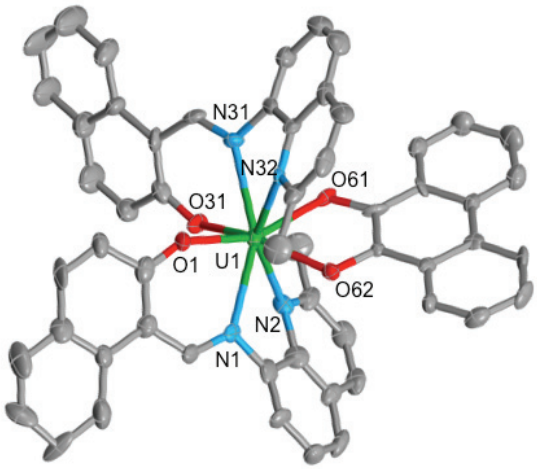


**Figure II-7: Solid state structure of [U(9,10-phenanthrenediol)($^{Me}$naphtquinolen)$_2$].(py)$_{4.5}$, 3.(py)$_{4.5}$ (50% ellipsoids). Hydrogen atoms and solvent molecules are omitted for clarity.**

During the reduction of 9,10-phenanthrenequinone by **2**, the coordination of the substrate to each uranium atom is probably concomitant with the disruption of the dinuclear structure and the cleavage of the two C-C bonds. In consequence, each mononuclear U(IV) moiety [U(bis-$^{Me}$naphtquinolen)] undertakes metal-assisted two-electron reduction of the quinone using the electrons stored in the C-C bond without changing the oxidation state of the metal centre. The structure of **3** shows that the available coordination sites at the U(IV) ion in this tridentate Schiff base system allow the coordination of the incoming product.

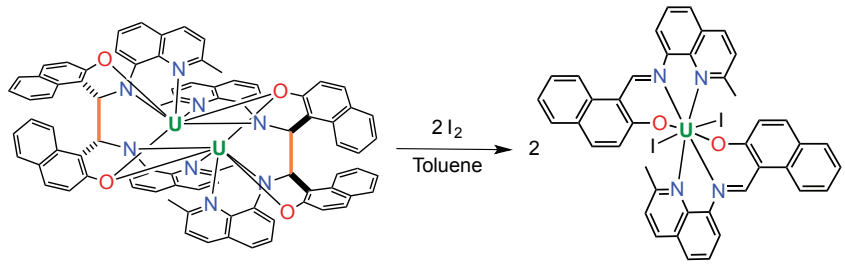


[U(bis-$^{Me}$naphtquinolen)]$_2$
**2**

[UI$_2$($^{Me}$naphtquinolen)$_2$]
**1**-I

**Scheme II-6: Reactivity of complex 2 with iodine.**

The chemical reversibility of this system has been demonstrated by the reaction of **2** with iodine (Scheme II-6). Indeed, the addition of 2eq of $I_2$ to complex **2** in toluene leads to the formation of a brown/yellow precipitate. The $^1$H NMR spectrum in deuterated pyridine of the obtained solid shows the signals assigned to complex **1**-I in which the C-C bonds have been cleaved but can be reformed by addition of metallic potassium.

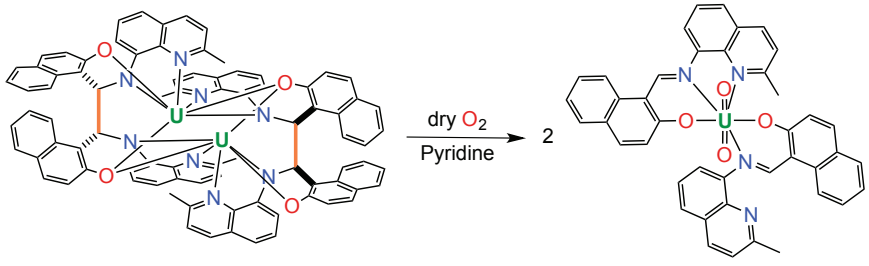


[U(bis-$^{Me}$naphtquinolen)]$_2$
**2**

[UO$_2$($^{Me}$naphtquinolen)$_2$]
**4**

**Scheme II-7: Reactivity of complex 2 with dry dioxygen.**

When both the ligand and the uranium centre are involved in the reduction process, the number of transferred electrons can be increased up to 4 electrons per mononuclear complex.

The addition of an excess of dry dioxygen to a pyridine solution of **2** (in equilibrium with complex **2b**) leads to an immediate colour change of the solution from dark brown to dark orange and the formation of the U(VI) complex [$UO_2$($^{Me}$naphtquinolen)$_2$], **4** which can be isolated pure in 69% yield (Scheme II-7). Crystals suitable for X-ray diffraction were obtained by slow diffusion of hexane into a saturated solution of **4** in toluene. In the solid state structure, presented in Figure II-8, the uranium atom has a pentagonal bipyramidal coordination provided by the two oxo groups in axial positions and five oxygen and nitrogen atoms from two $^{Me}$naphtquinolen ligands in the equatorial plane. While the first $^{Me}$naphtquinolen ligand adopts a classical tridentate ONN coordination mode, as found in **1**-Cl and **3**, the second $^{Me}$naphtquinolen ligand is bound to the uranium centre in a bidentate fashion by the phenolate and the imino groups with the nitrogen atom from the quinoline moiety remaining non-coordinated. Pentagonal bipyramid is the most common coordination geometry for uranyl(VI) compounds, higher coordination numbers in the equatorial plane being disfavoured for sterical reasons. The C-$N_{imino}$ (1.276(6) and 1.308(6) Å) bond distances from both $^{Me}$naphtquinolen ligands are in the same range than the ones found in **1**-Cl and **3** (see Table II-2), confirming their imino character. U-$N_{imino}$, U-$N_{quinoline}$ and U-$O_{phenolate}$ mean bond distances (respectively 2.547(2), 2.646(4) and 2.238(6) Å) compare well with those found in other uranyl(VI) Schiff base complexes.[6, 195] The $UO_2$ moiety in **4** is nearly linear (O–U–O angle 177.3(1)°) with uranyl bond distances (1.776(3) Å in average) falling in the characteristic range of heptacoordinated hexavalent uranyl complexes.[6, 195]

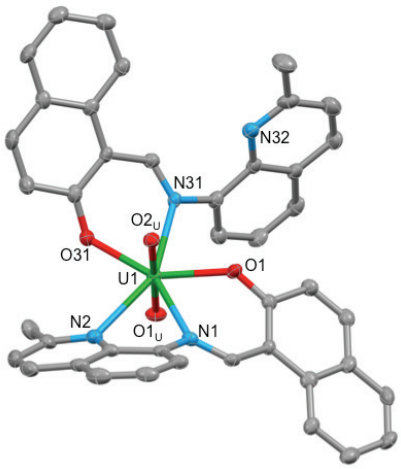


**Figure II-8: Solid state structure of [$UO_2$($^{Me}$naphtquinolen)$_2$], 4 (50% ellipsoids). Hydrogen atoms are omitted for clarity.**

**Table II-2: Selected bond lengths (or average) in the U(IV) complexes 1-Cl, 2, 3 and the U(VI) complex 4 (in Å).**

| Bonds | **1**-Cl | **2**.tol | **3**.py$_{4.5}$ | **4** |
|---|---|---|---|---|
| U-N$_{quinoline}$ | 2.70(3) | 2.538(3) | 2.58(7) | 2.646(4) |
| U-N$_{imino/amido}$ | 2.51(3) | 2.36(2) | 2.52(2) | 2.55(2) |
| U-O$_{phenolate}$ | 2.204(18) | 2.26(10) | 2.227(13) | 2.238(6) |
| U-X | 2.67(4) X=Cl | - | 2.26(4) X=O$_{diol}$ | 1.776(3) X=O$^{2-}$ |
| C-C | - | 1.636(14) | - | - |
| C-N$_{imino/amido}$ | 1.293(2) | 1.474(5) | 1.294(9) | 1.292(2) |

The $^{1}$H NMR spectrum of **4** in deuterated pyridine features 13 signals in the diamagnetic zone, in agreement with the +VI oxidation state of the uranium atom and suggesting that the two $^{Me}$naphtquinolen ligands are equivalent in solution probably because of a fluxional coordination of the quinoline moieties which competes with coordination of pyridine molecules.

In this reaction, the complex **2** transfers 8 electrons (4 electron from the uranium atoms and four electrons from the ligands) to two oxygen molecules to form 2eq of complex **4**. The transfer of such a high number electrons from an uranium systems has been rarely observed and only when the uranium is associated to redox-active ligands.[208, 209] The overall reactivity observed in this section demonstrates that reversible C-C bond formation and cleavage is not limited to tetradentate Schiff base ligands and provides a new example of non-innocent ligand which features multi-electronic reductions at a U(IV) centre.

# II.2 Preliminary studies on heterobimetallic f-d complexes supported by the salophen ligand

## II.2.1 Context

Preliminary studies conducted by Clément Camp in our group have shown that addition of 1eq of $[UI_4(OEt_2)_2]$ precursor to the U(IV) complex $Na_2$[U(bis-salophen)] leads to the formation of the dinuclear U(IV) complex $[U_2$(bis-salophen)$(py)_6]I_2$ as shown in Scheme II-8. In this complex, the hexa-anionic bis-salophen ligand unfolds adapting its coordination to encapsulate another U(IV) centre. The X-ray structure of $[U_2$(bis-salophen)$(py)_6]I_2$ was obtained and features three positions at each U(IV) centre occupied by solvent molecules indicating six potentially available coordination sites for substrates in this complex in solution.[210]

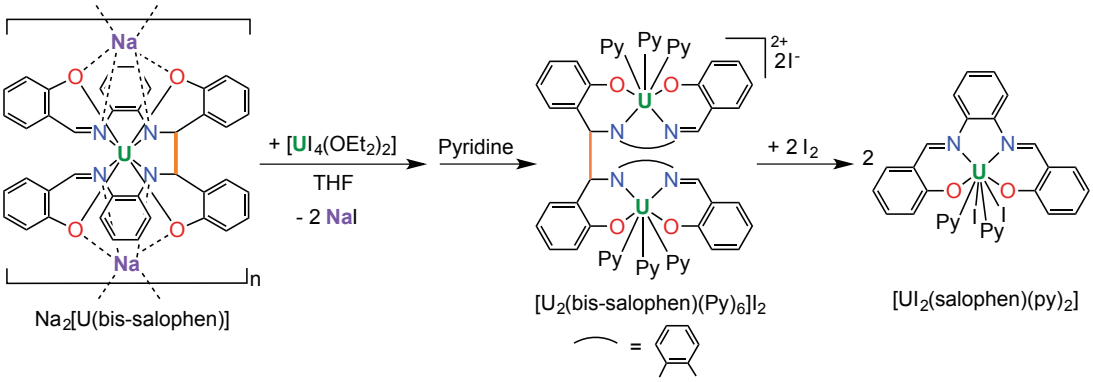


**Scheme II-8: Synthesis of the dinuclear complex $[U_2$(bis-salophen)$(py)_6]I_2$ and the reaction with $I_2$.**

Unfortunately, even if the electrons stored in the C-C bond are released to reduce iodine leading to the formation of the mononuclear oxidized compound $[UI_2$(salophen)$(py)_2]$, the complex $[U_2$(bis-salophen)$(py)_6]I_2$ does not react with $CO_2$. This could be due to the homobimetallic character of this complex which leads to an apolar species. If one of the uranium atom was replaced by a d-block element, the proximity of a more nucleophilic transition metal and an oxophilic actinide centre could improve the polarization of the very

stable C=O bonds in carbon dioxide. Moreover, Floriani and coworkers reported in 1978 the $CO_2$ activation by the Co(I) complex supported by the tetradentate Schiff base $^{nPr}$salen ligand.[211] The X-ray structure of the obtained 1D polymer [Co($^{nPr}$salen)$KCO_2$(THF)]$_n$ clearly shows a bent $CO_2$ molecule binding the Co ion *via* the carbon atom, and the potassium ion via one oxygen atom. In 1996, the group of Floriani extended this reactivity with $CO_2$ to the complexes [$Co_2$(bis-$^R$salophen)$Na_2$(THF)$_x$] (R=H, x=6; R=OMe, x=4) (Scheme II-9). These Co(II) starting complexes were characterised by X-ray diffraction and their solid state structures present an intermolecular C-C bond between two imino functions of the [Co($^R$salophen)Na] units. The $CO_2$ reduction products [Co($^R$salophen)$NaCO_2$(THF)] have been characterised by IR spectroscopy and elemental analyses but, unfortunately, no X-ray structure was obtained.

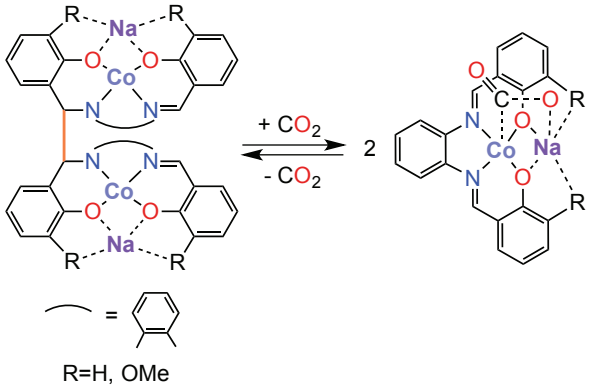


**Scheme II-9: Postulated reactivity of the [$Co_2$(bis-$^R$salophen)$Na_2$(THF)$_x$] (R=H, x=6; R=OMe, x=4) with $CO_2$. When R=H no coordination to the Na cation, when R=OMe coordination to the Na cation.**

The fact that the carbon atom of the $CO_2$ molecule coordinates the Co cation in [Co($^{nPr}$salen)$KCO_2$(THF)]$_n$ and supposedly in [Co($^R$salophen)$NaCO_2$(THF)], leads us to consider designing a f-d heterobimetallic complex. The stoichiometric addition of transition metal halogenide salts to the complex $Na_2$[U(bis-salophen)] could be a convenient synthetic route for such heterobimetallic complexes.

## II.2.2 A route to 5f-3d heterobimetallic complexes

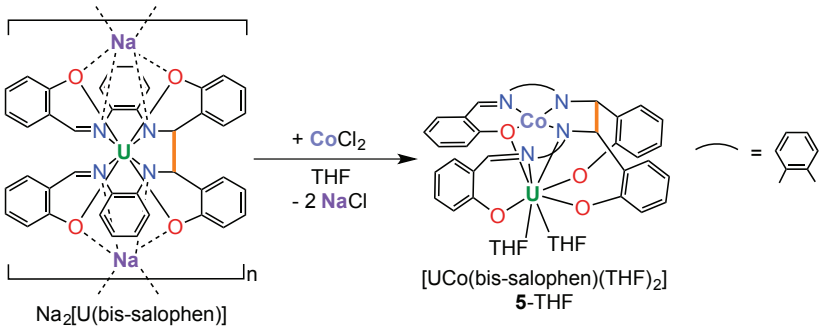


**Scheme II-10: Synthesis of [UCo(bis-salophen)(THF)$_2$], 5-THF.**

The addition of 1eq of $CoCl_2$ to $Na_2$[U(bis-salophen)] in THF affords the heterobimetallic complex [UCo(bis-salophen)(THF)$_2$], **5**-THF (Scheme II-10). Single crystals suitable for X-ray diffraction analysis were obtained either by slow diffusion of DIPE into a THF solution of the complex, or by slow diffusion of hexane into a pyridine solution of the complex, giving respectively **5**-THF and **5**-py (Figure II-9). These two X-ray crystal structures are isomorphous and their metrical parameters are reported in Table II-3 but only the bond lengths of **5**-py will be discussed. The solid state structure shows that the octadentate hexa-anionic bis-salophen ligand coordinates both the cobalt and the uranium centres. The cobalt cation is tetracoordinated by an ONNN pocket in a square planar geometry. The uranium ion is hexacoordinated by the bis-salophen ligand, and its coordination sphere is completed to eight in a distorted square antiprismatic geometry by the coordination of two solvent molecules. The overall structure is highly asymmetric and the bis-salophen ligand is highly distorted. The C7-N1 and C27-N21 bond distances of 1.300(4) Å confirm the double bond character of the imino moieties while the C14-N2 and C34-N22 bond distances (respectively 1.505(4) Å and 1.467(4) Å) are consistent with a single C-N bonding in the amido moieties. The C14-C34 bond length of 1.565(4) Å is comparable to the C-C bond distance found in $Na_2$[U(bis-salophen)] (1.559(7) Å).[5] The global neutral charge of the complex is in agreement with the +II and +IV oxidation states of the cobalt and uranium centres respectively. The two metallic ions are connected through a $\mu_2$-$N_{amido}$ and a $\mu_2$-$O_{phenolate}$ bridging atoms. The presence of a U-Co bond has been reported in U(IV)-Co(-I)[212, 213] and U(IV)-Co(I) complexes.[214] In the example reported by Liddle et al. the unsupported

metal-metal U(IV)-Co(-I) bond distance is 2.9450(9) Å long[212] while in the example reported by Arnold et al. the U(IV)-Co(-I) complex presents a bond supported by a bridging ligand with a U-Co bond distance of 3.0319(7) Å.[213] In the two U(IV)-Co(I) complexes supported by bridging phosphinoamide ligands reported by Bart et al., the U-Co bond distances were found to be 3.0812(7) and 2.874(3) Å long.[214] The U…Co distance of 3.0439(5) Å in complex **5**-py is the shortest reported for U(IV)-Co(II) systems and is comparable to the U-Co distances mentioned above. DFT analyses of complex **5** could allow us to gain insight on a possible metal-metal interaction in complex **5**-py.

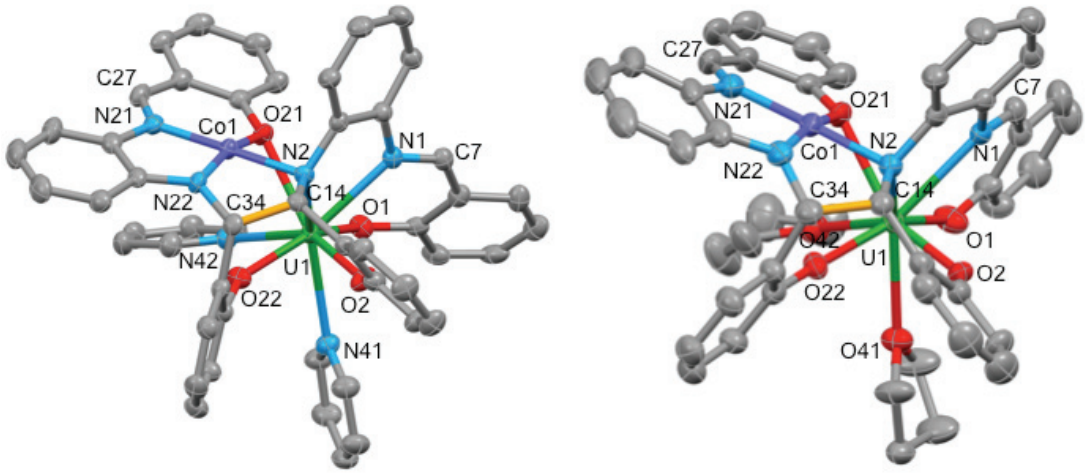


**Figure II-9: Solid state structure of [UCo(bis-salophen)(THF)$_2$], 5-THF (left) and [UCo(bis-salophen)(py)$_2$], 5-py (right) (50% ellipsoids). The C-C bond formed by the reduction of the imino functions is represented in orange. Hydrogen atoms and lattice solvent molecules are omitted for clarity.**

The $^1$H NMR spectrum of **5** in deuterated pyridine or THF shows 28 signals in agreement with a completely dissymmetric bis-salophen ligand. Monitoring the $^1$H NMR spectrum of **5** in deuterated THF over time shows a slow decomposition of the bimetallic complex in the mononuclear U(IV) complex [U(salophen)$_2$] (Figure II-10). The precipitation over time of a black solid from the mixture suggests that Co(0) metal is the side-product of the decomposition which is complete after nearly one month.

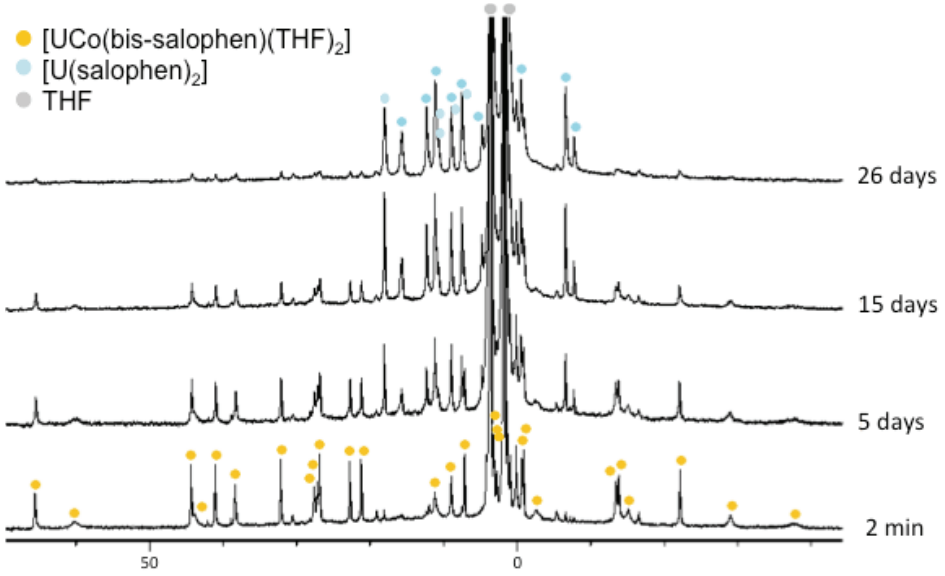


**Figure II-10: $^{1}$H NMR spectrum (200MHz, THF-$d_8$, 298K) of complex 5, and evolution over time.**

These results indicate that the C-C bond is maintained in complex **5** and the two electrons stored on the ligand scaffold are still available. These electrons are probably slowly released to reduce the Co(II) centre to yield cobalt(0). Subsequent ligand redistribution affords the [U(salophen)$_2$] complex without change of the uranium oxidation state. A synthetic procedure at low temperature is currently under investigations to isolate cleanly the complex **5**.

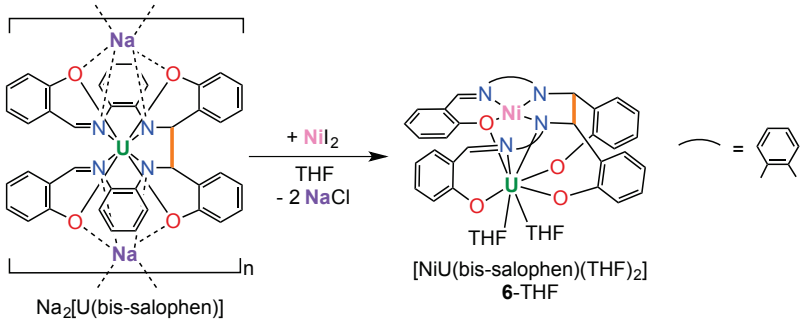


**Scheme II-11: Synthesis of [UNi(bis-salophen)(THF)$_2$], 6-THF.**

We have also investigated the possibility of using the same method to obtain d-f heterometallic complexes with different d-block metal ions. The addition of 1eq of $NiI_2$ to $Na_2$[U(bis-salophen)] in THF affords the heterobimetallic complex [UNi(bis-

salophen)$(THF)_2$], **6**-THF (Scheme II-11). X-ray quality crystals of **6**-THF were obtained by slow diffusion of DIPE into a THF solution of the complex.

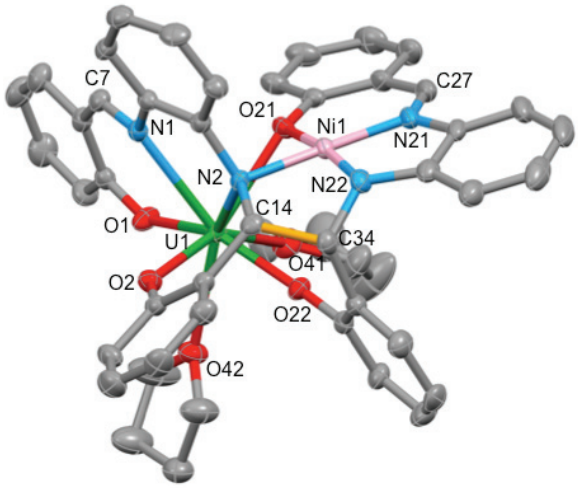


**Figure II-11: Solid state structure of [UNi(bis-salophen)$(THF)_2$], 6-THF (50% ellipsoids). The C-C bond formed by the reduction of the imino functions is represented in orange. Hydrogen atoms and lattice solvent molecules are omitted for clarity.**

The solid state structure of complex **6**-THF is isostructural with the structure of **5**-THF. Thus, the hexa-anionic bis-salophen ligand encapsulates both the nickel and the uranium atoms. The nickel cation is tetracoordinated in a square planar geometry and the uranium ion is octacoordinated in a distorted square antiprismatic geometry with two THF solvent molecules completing its coordination sphere. The metrical parameters of **6**-THF are reported in Table II-3. The C7-N1 and C27-N21 bond distances of 1.292(6) Å and 1.310(6) Å respectively confirm the double bond character of the imino moieties while the C14-N2 and C34-N22 bond distances (respectively 1.504(5) Å and 1.477(5) Å) are consistent with a single C-N bonding in the amido moieties. The C14-C34 bond length of 1.550(6) Å is comparable to the C-C bond distances found in complexes **5** and $Na_2$[U(bis-salophen)].[5] The global neutral charge of the complex is in agreement with +II and +IV oxidation states of the nickel and uranium centres respectively. Arnold and co-workers recently reported the first examples of U-Ni metal-metal bond (U-Ni distance = 2.520(1) - 2.556(1) Å) in the U(IV)-Ni(0) bimetallic complexes [UNi($\mu$-$OAr^P$)$_3$X] (X=I, F, $OSiMe_3$) supported by bridging phosphinophenolate ligands.[214] In the U(IV)-Ni(II) complex **6**-THF, the U…Ni distance of 3.1340(6) Å is significantly longer than those found in the [UNi($\mu$-$OAr^P$)$_3$X] (X=I, F, $OSiMe_3$) complexes

but is significantly shorter than the one found in all previously reported U(IV)-Ni(II) bimetallic complexes.[215-219] DFT analyses of complex **6** could allow us to gain insight on a possible metal-metal interaction in complex **6**-THF.

**Table II-3: Selected bond lengths (or average) in the U(IV)-M(II) complexes 5-py, 5-THF (M=Co) and 6-THF (M=Ni) (in Å).**

| Bonds | 5-py | 5-THF | 6-THF |
|---|---|---|---|
| U-$N_{imino}$ | 2.474(3) | 2.463(4) | 2.474(3) |
| U-$N_{amido}$ | 2.559(3) | 2.605(4) | 2.613(3) |
| U-$O_{phenolate}$ | 2.3(2) | 2.3(2) | 2.3(2) |
| M-$N_{imino}$ | 1.9(1) | 1.9(1) | 1.87(8) |
| M-$N_{amido}$ | 1.859(3) | 1.865(6) | 1.858(4) |
| M-$O_{phenolate}$ | 1.861(2) | 1.880(4) | 1.875(3) |
| U…M | 3.0439(5) | 3.1349(9) | 3.1340(6) |
| C-$N_{imino}$ | 1.49(3) | 1.48(2) | 1.49(2) |
| C-$N_{amido}$ | 1.300(4) | 1.32(2) | 1.30(1) |
| C-C | 1.565(4) | 1.571(8) | 1.550(6) |

The $^{1}$H NMR spectrum in deuterated THF of **6** shows 28 sharp signals in agreement with a completely dissymmetric bis-salophen ligand. However, a small amount of the oxidized [U(salophen)$_2$] complex is present after the addition of $NiI_2$ to $Na_2$[U(bis-salophen)]. This by-product formation could arise from an impurity in the nickel salt or from a local excess of $NiI_2$ in the reaction mixture and is currently under studies. Contrary to its Co analogue **5**, the complex **6** is stable for months in THF solution. The greater stability of the U-Ni complex **6** is probably due to the higher stability of the Ni(II) ion in a square planar geometry.

Interestingly, the $^{1}$H NMR spectrum in deuterated THF of the crude reaction between $Na_2$[U(bis-salophen)] and 1eq of $ZnI_2$ shows one set of signals of an unidentified species and the 14 signals of unreacted $Na_2$[U(bis-salophen)] (Figure II-12 bottom). The subsequent addition of another equivalent of $ZnI_2$ to the mixture leads to the complete consumption of the $Na_2$[U(bis-salophen)] precursor and to an increase in intensity of the set of 28 signals as shown in Figure II-12 (top). Unfortunately all attempts to crystallize this new compound were unsuccessful.

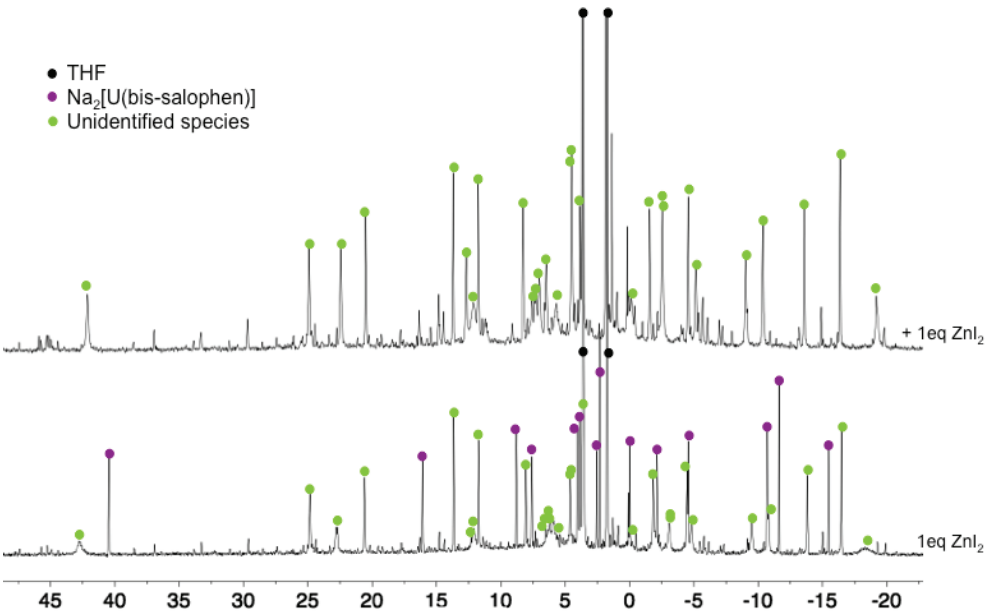


**Figure II-12: $^1$H NMR spectrum (200 MHz, THF-$d_8$, 298 K) of the 1:1 reaction mixture of $Na_2$[U(bis-salophen)] and $ZnI_2$ (bottom) and after another addition of $ZnI_2$ (top).**

In conclusion the addition of halogenated salts of d-block metal to the U(IV) reduced species $Na_2$[U(bis-salophen)] provides a simple synthetic route to 5f-3d complexes. The complexes **5** and **6** do not react with $CO_2$ despite the close proximity of the Ni and Co atoms with the U centre. The electrons stored in the C-C bond formed between the two imino moieties in the bis-salophen ligand remain in these complexes not accessible for the reduction of $CO_2$. However, the close vicinity of the Co and U atoms in **5** and of the Ni and U atoms in **6** may result in magnetic communication that will be studied in the future.

## II.2.3 Isolation of the 4f-3d heterobimetallic complex [NdCo(salophen)$_2$(THF)]

We became then interested in extending this synthetic procedure to the synthesis of 4f-3d heterobimetallic complexes. In order to do this transition metal halogenide salts were added to the previously reported complex $K_3$[Nd(bis-salophen)].[6] The $^1$H NMR spectrum in deuterated THF of the crude reaction mixture of $K_3$[Nd(bis-salophen)] and 1eq of $CoCl_2$

shows one set of only 14 signals as the major species. This result indicates the formation of a complex with a higher ligand symmetry than the one found in the complexes [UM(bis-salophen)(THF)$_2$] (M=Co, Ni). A slow diffusion of hexane or DIPE into a pyridine or THF solution of the complex afforded dark single crystals of the complex [NdCo(salophen)$_2$(S)], **7**-py (S=py) or **7**-THF (S=THF) (Figure II-13). The complex **7**-py crystallizes in the P2$_1$/c space group with two complexes in the unit cell while complex **7**-THF crystallizes in the Pnma space group. These two X-ray crystal structures are isomorphous and their metrical parameters are reported in Table II-4 but only the bond lengths of **7**-THF will be discussed.

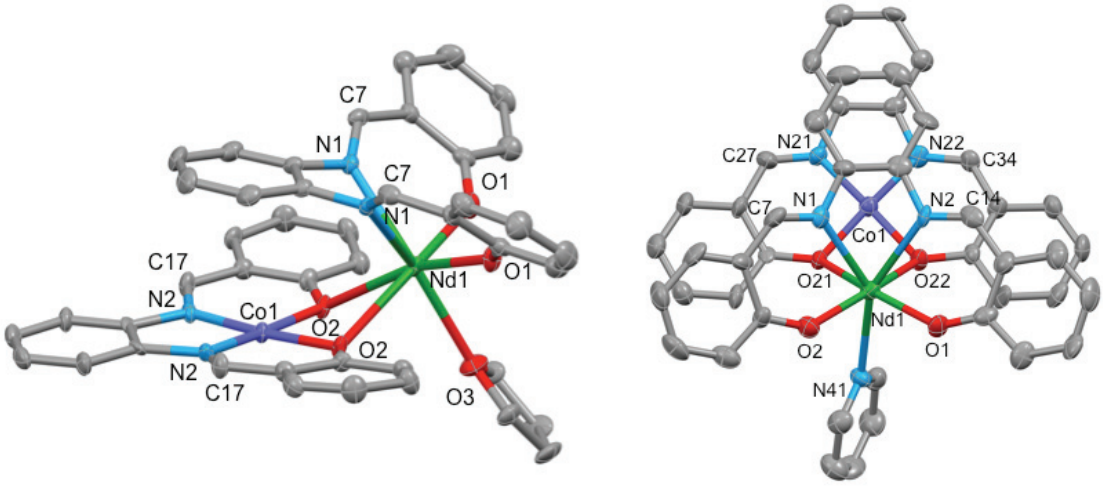


**Figure II-13: Solid state structure of [NdCo(salophen)$_2$(THF)], 7-THF (side view, left) and one of the complexes [NdCo(salophen)(py)], 7-py (top view, right) (50% ellipsoids). Hydrogen atoms, disorder and lattice solvent molecules are omitted for clarity.**

The solid state structure of [NdCo(salophen)$_2$(THF)], **7**-THF shows the presence of a [Nd(salophen)(THF)] unit and of a [Co(salophen)] unit connected through the $\mu_2$-O$_{phenolate}$ atoms of the [Co(salophen)] complex. The presence of a mirror plane containing the Nd1, Co1 and O3 atoms is concordant with the set of 14 signals on the $^1$H NMR spectrum of the complex indicating that the C$_s$ symmetry of the complex in the solid state is maintained in solution. The cobalt cation is tetracoordinated by a OONN pocket in a square planar geometry. The neodymium ion is heptacoordinated in a distorted geometry by one salophen ligand, the two bridging oxygen atoms of the [Co(salophen)] unit and one solvent molecule. The average value of the C-N$_{imino}$ distances (1.306(8) Å) is in agreement with the double bond

character of the imino moieties indicating that the C-C bond present in the [Nd(bis-salophen)]$K_3$ precursor has been cleaved. The global neutral charge of the complex indicates

the presence of Nd(III) and Co(I) cations. The complex **7**-THF is, to our knowledge, the first example of a Nd(III)-Co(I) bimetallic complex. The Nd...Co distance of 3.413(1) Å is elongated compared to the only examples of Yb(II)-Co(-I) and Sm(III)-Co(-I) bonds recently reported by Mountford et al. (d(Yb-Co)= 2.9893(4) Å, d(Sm-Co)= 2.8969(9) and 2.954(1) Å).[220] However, the Nd…Co distance in **7**-THF is comparable to the Ln(III)…Co(II) distances previously reported by Costes and co-workers (from 3.4201(9) to 3.4471(8) Å).[221]

**Table II-4: Selected bond lengths (or average) in the Nd(III)-Co(I) complexes 7-THF and 7-py (in Å).**

| Bonds | 7-THF | 7-py |
|---|---|---|
| **Nd-$N_{imino}$** | 2.524(5) | 2.52(1) |
| **Nd-$O_{phenolate}$** | 2.264(4) | 2.265(2) |
| **Nd-$O_{phen.\ bridging}$** | 2.467(4) | 2.44(2) |
| **Co-$N_{imino}$** | 1.833(5) | 1.844(6) |
| **Co-$O_{phenolate}$** | 1.913(4) | 1.916(2) |
| **Nd…Co** | 3.413(1) | 3.229(2) |
| **C-$N_{imino}$** | 1.306(8) | 1.315(9) |

Changing the stoichiometry of the reaction by adding 0.5eq or 2eq of $CoCl_2$ to $K_3$[Nd(bis-salophen)] in THF drastically influences the outcome of the reaction as suggested by the $^1$H NMR spectra of the crude mixtures in deuterated THF (Figure II-14). Notably the $^1$H NMR spectrum in deuterated THF of the reaction of 2eq of $CoCl_2$ and $K_3$[Nd(bis-salophen)] shows a set of six broad signals indicating the formation of a symmetric paramagnetic species. Unfortunately, all attempts to crystallize this compound failed.

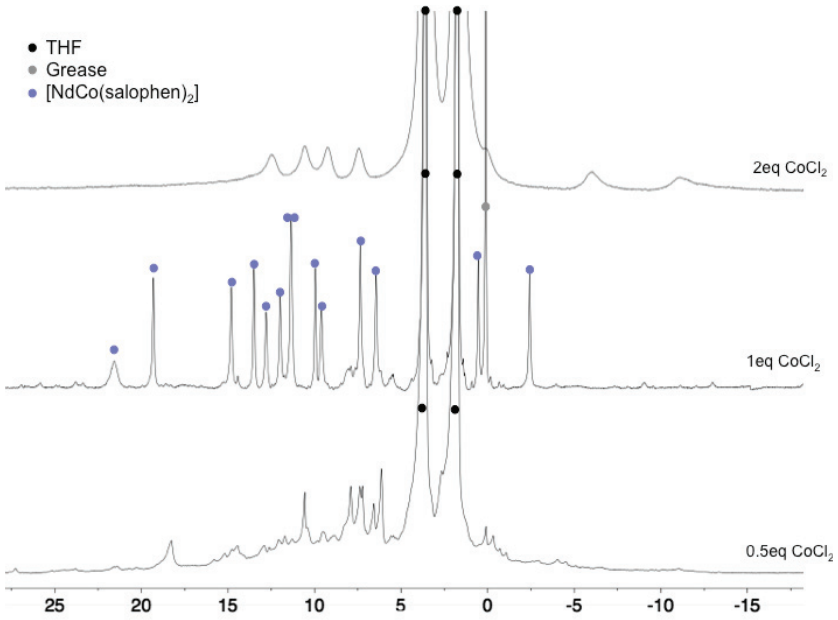


**Figure II-14: $^{1}$H NMR spectra (200 MHz, THF-$d_8$, 298 K) of the 1:0.5 (bottom), 1:1 (middle) and 1:2 (top) reaction mixtures of $K_3$[Nd(bis-salophen)] and $CoCl_2$.**

In the structure of complex **7**, the C-C bond present in the $K_3$[Nd(bis-salophen)] precursor has been cleaved releasing the two electrons stored on the ligand scaffold. However, only one of these electrons has been used to reduce the Co(II) ion in a Co(I) ion. In consequence other unidentified side-products are formed (Scheme II-12) preventing the clean isolation of complex **7**.

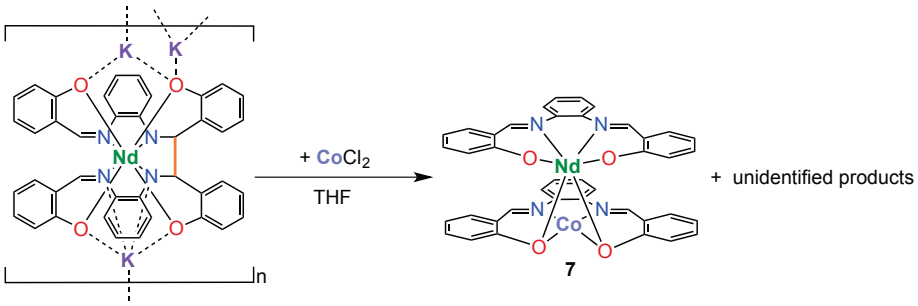


**Scheme II-12: Reaction of $K_3$[Nd(bis-salophen)] with 1eq of $CoCl_2$.**

According to the work reported by Floriani on cobalt complexes supported by salophen ligands, the reduction of the Co(II) compound [Co(salophen)] by sodium metal leads to the ligand reduction rather than the metal one affording the [$Co_2$(bis-salophen)$Na_2$]

complex.[222] This suggests that the C-C bond formation is favoured compared to the Co(I) complex formation. In the Nd-Co heterometallic complex, the electrons stored in the C-C bond are used for the reduction of the cobalt metal centre. This could arise from the presence of the Nd cation in the heterometallic complex leading to a different electronic environment of the cobalt ion. These results suggest that the occurrence of C-C bond formation versus metal reduction in these complexes might be affected by small variation in the coordination sphere. This incited us to revisit the chemistry of cobalt ions supported by salophen ligand.

# II.3 Revisiting the chemistry of cobalt complexes supported by salophen ligands.

## II.3.1 One electron reduction of Co(II) salophen complexes by alkali metals.

### II.3.1.1 Reduction by potassium metal and comparison with the reported reduction with sodium metal.

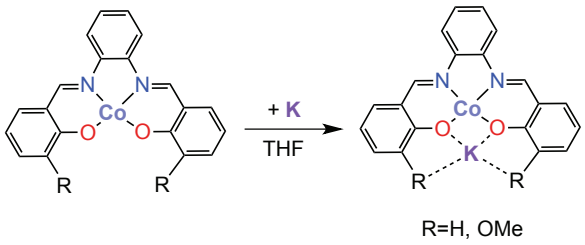


**Scheme II-13: Reduction of [Co($^{R}$salophen)] (R=H and OMe) by potassium metal. When R=H no coordination to the K cation, when R=OMe coordination to the K cation.**

In collaboration with Valentin Guidal (a PhD student in the group) we showed that the reduction of the Co(II) complexes [Co(salophen)] and [Co($^{OMe}$salophen)] with one equivalent of potassium metal in THF affords the Co(I) polymeric complex [Co(salophen)K(THF)]$_n$,

and the Co(I) monomeric complex [Co($^{OMe}$salophen)K(THF)] (Scheme II-13).[201] Both complexes were notably characterised by X-ray diffraction confirming their heterobimetallic nature and the absence of C-C bond revealing the +I oxidation state for the cobalt atoms. The structure of the polymeric complex [Co(salophen)K(THF)]$_n$ is very similar to the solid state structure previously reported for the [Co(salen)Na(THF)]$_n$ polymeric complex obtained by reduction of [Co(salen)] with sodium metal.[211, 223] The methoxy substituents of the $^{OMe}$salophen ligand in [Co($^{OMe}$salophen)K(THF)] provide a convenient encapsulation of the potassium preventing a polymeric assembly.

The structures of complexes [Co(salophen)K(THF)]$_n$ and [Co($^{OMe}$salophen)K(THF)] differ from the solid state structures previously reported for the compound obtained from the reduction of the Co(II) complexes [Co(salophen)] and [Co($^{OMe}$salophen)] with sodium metal.[222] Notably, as earlier mentioned, the reductions of [Co(salophen)] and [Co($^{OMe}$salophen)] were reported to yield the dimeric complexes of Co(II) [Co$_2$(bis-salophen)Na$_2$(THF)$_6$] and [Co$_2$(bis-$^{OMe}$salophen)Na$_2$(THF)$_4$] respectively. The difference in the solid state structure of the compounds obtained from the reduction of [Co(salophen)] and [Co($^{OMe}$salophen)] with K and Na, suggests that the nature of the alkali ion has an important effect on the outcome of the reduction. While in the presence of potassium the reduction occurs on the metal, in the presence of sodium it occurs on the ligand. This could be explained in terms of the lower Lewis acid character of the potassium cation compared to the sodium one leading to a more electron rich ligand scaffold less susceptible to be reduced. However the cleavage of the C-C bond in K$_3$[Nd(bis-salophen)] after the addition of CoCl$_2$ observed in the previous section and leading to [NdCo(salophen)$_2$(THF)] is more difficult to rationalize.

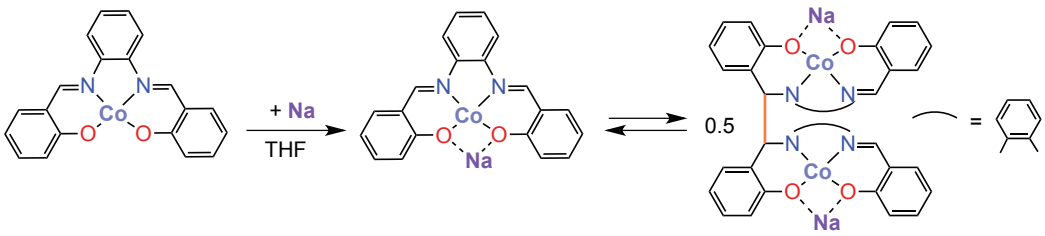


**Scheme II-14: Reduction of [Co(salophen)] by sodium metal.**

$^1$H NMR studies on the complexes [Co(salophen)K(THF)]$_n$ and [Co($^{OMe}$salophen)K(THF)] were carried out and compared to those of the previously reported

$[Co_2(bis\text{-}salophen)Na_2(THF)_6]$ and $[Co_2(bis\text{-}^{OMe}salophen)Na_2(THF)_4]$ complexes. The proton NMR spectrum in THF of complex $[Co(salophen)K(THF)]_n$ shows 7 signals in the diamagnetic region indicating the presence in THF solution of the Co(I) form of the complex and the absence of C-C coupling between salophen ligands. In contrast the $^1H$ NMR spectrum in THF of the reported $[Co_2(bis\text{-}salophen)Na_2(THF)_6]$ complex prepared *in situ* by reduction of [Co(salophen)] with 1eq of sodium metal shows a significantly more complex pattern. The presence of two sets of signals, one of 7 signals in the diamagnetic region and one of 14 signals in the paramagnetic region suggests the presence in solution of both a square planar diamagnetic Co(I) complex of formula analogous to the potassium complex, [Co(salophen)Na(THF)], and of the Co(II) complex $[Co_2(bis\text{-}salophen)Na_2(THF)_6]$ (Scheme II-14).

The proton NMR spectrum of complex $[Co(^{OMe}salophen)K(THF)]$ shows 7 signals in the diamagnetic region indicating that also this complex retains its Co(I) form in THF solution. The $^1H$ NMR spectrum in THF-$d_8$ of the previously reported $[Co_2(bis\text{-}^{OMe}salophen)Na_2(THF)_4]$ (prepared *in situ* by reduction of the $[Co(^{OMe}salophen)]$ with one equivalent of sodium metal) shows also the presence of only one set of 7 signals in the diamagnetic region indicating the presence in solution of the Co(I) complex $[Co(^{OMe}salophen)Na]$ as only species. In this case dimerization is not detectable by NMR spectroscopy in solution up to the solubility limit of the complex but occurs in the solid state probably due to the lower solubility of the dimeric species.

## II.3.1.2 Reduction by Lithium metal

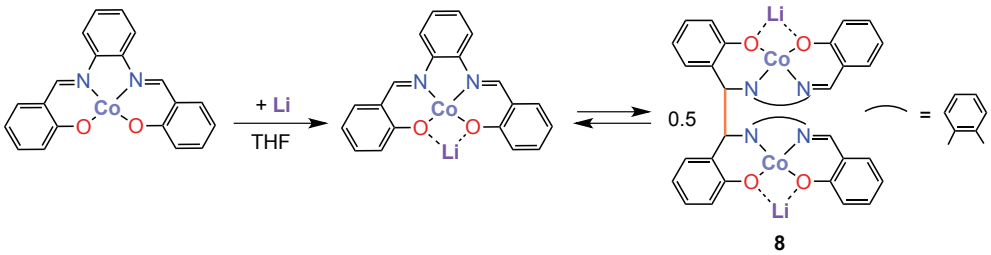


**Scheme II-15: Reduction of [Co(salophen)] by lithium metal.**

In order to further investigate the effect of the alkali ions we have also investigated the reduction of the [Co(salophen)] complex with Li metal (Scheme II-15). $^1H$ NMR studies of

the reaction mixture obtained from the reduction of the [Co(salophen)] complex with 1eq of Li metal show the presence of two sets of 7 and 14 signals that where assigned to a monomeric Co(I) [Co(salophen)Li(THF)$_x$] complex and to a Co(II) dimeric complex [Co$_2$(bis-salophen)Li$_2$(THF)$_x$]. This suggests that the reduced complex behaves similarly in the presence of $Na^+$ and $Li^+$ cations.

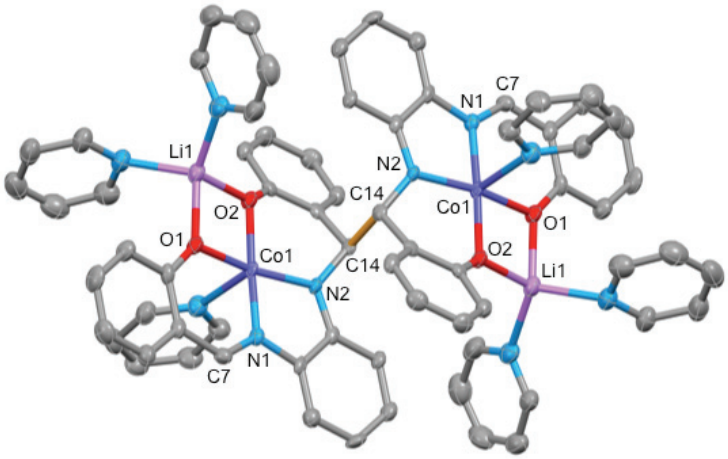


**Figure II-15: Solid state structure of [Co$_2$(bis-salophen)Li$_2$(py)$_4$], 8 (50% ellipsoids). The C-C bond formed by the reduction of the imino functions is represented in orange. Hydrogen atoms are omitted for clarity.**

X-ray quality crystals of the dimeric complex [Co$_2$(bis-salophen)Li$_2$(Py)$_4$], **8** were obtained by slow diffusion of hexane into a pyridine solution of the complex. The structure of **8** (Figure II-15) shows the presence of a reduced hexa-anionic bis-salophen ligand resulting from the formation of a C-C bond between the two carbon atoms of the reduced imino groups from two different [Co(salophen)] units. The C-C bond length of 1.581(8) Å is slightly elongated compared to the one found in the Na$_2$[U(bis-salophen)] complex (1.559(7) Å)[5] or in the heterobimetallic [UM(bis-salophen)] (M=Co, Ni) complexes (1.565(4) and 1.550(6) Å respectively). Each cobalt centre is pentacoordinated by two oxygen and two nitrogen atoms of the bis-salophen ligand and one pyridine nitrogen in a square pyramidal geometry. Each lithium cation is tetracoordinated by two oxygen atom of the bis-salophen ligand and two pyridine nitrogen atoms with a tetrahedral geometry. Significantly different C-N distances are found for the imino (1.298(6) Å) and amido (1.449(5) Å) moieties in agreement with the presence of double and simple bond respectively.

Variable temperature NMR studies show that the ratio of Co(II) versus Co(I) species in solution changes with the temperature in agreement with the presence of an equilibrium between the monomeric Co(I) complex and the dimeric Co(II) complex (Scheme II-15). Notably, the ratio Co(II)/Co(I) increases when the temperature decreases. A variable temperature NMR study allows the determination of the thermodynamic parameters for the interconversion Co(II)/Co(I) (Figure II-16). The thermodynamic constants of this equilibrium was determined thanks to the Van't Hoff equation:

$$Ln\big(Keq(T)\big) = -\frac{\Delta H^\circ}{RT} + \frac{\Delta S^\circ}{R} \quad with \;\; Keq = \frac{[Co_2(\mu\text{-}bis\text{-}salophen)Na_2]}{[Co(salophen)Na]^2} \times C^\circ$$

$$C^\circ = standard\ concentration = 1\ mol.L^{-1}$$

Plotting Ln(Keq) as a function of 1/T leads to values of ΔH°= -4.1 kcal/mol and of ΔS°= -11.5 cal/mol/K. The value of ΔG° is of -0.68 kcal/mol indicating that the C-C bond formation is slightly thermodynamically favoured at room temperature but the bond dissociation energy is close to zero suggesting the very weak character of the C-C bond. Several examples of reversible C-C coupling with low dissociation energies (10-20 kcal $mol^{-1}$) have been reported in metal complexes [224, 225] and in sterically hindered organic compounds such as the Gomberg's dimer.[226] However, such a ΔG° value close to zero is less common.

A variable temperature NMR study was also performed on the Co(II)/Co(I) equilibrium with $Na^+$ counter ion revealing similar thermodynamic parameters than for the interconversion Co(II)/Co(I) Li system. The Van't Hoff analysis for this equilibrium with Na cation leads to values of ΔH°= -5.0 kcal/mol and of ΔS°= -15.7 cal/mol/K. The value of ΔG° is of -0.32 kcal/mol indicating once again a very weak character of the C-C bond.

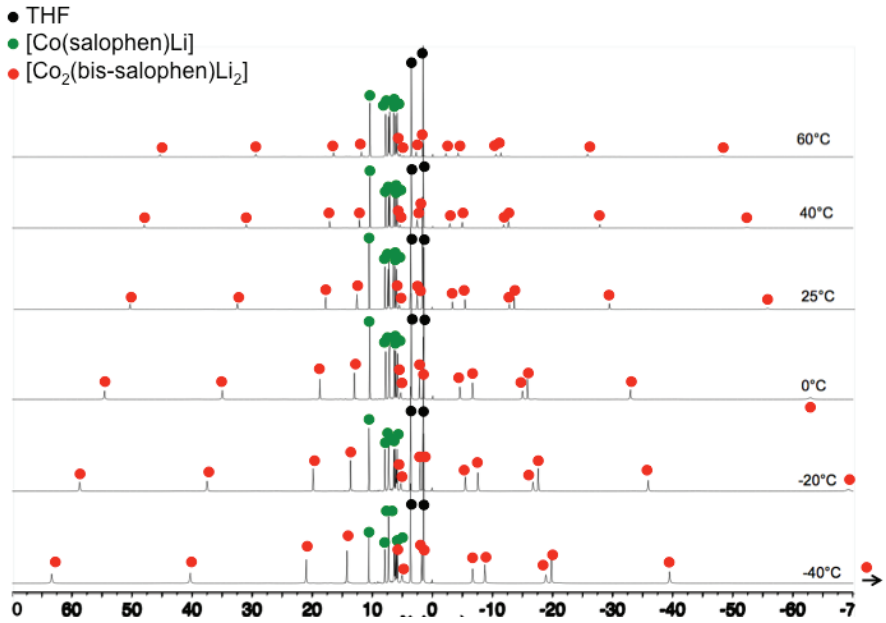


**Figure II-16: Variable temperature $^{1}$H NMR spectra (400 MHz) from -40°C to 60°C of a [Co(salophen)] solution in THF-$d_8$ reacted with one equivalent of lithium.**

This study on mono-electronic reduction of Co(II) salophen complexes reveals the crucial role of the alkali metal chosen: the reduction occurred only at the cobalt centre using potassium or both at the metal centre and on the ligand scaffold affording a mixture of [Co(salophen)M] and [$Co_2$(bis-salophen)$M_2$] (M=Na, Li) complexes using sodium or lithium.

## II.3.2 Two electron reduction of the Co(II) complex [Co($^{OMe}$salophen)]

Despite the fact that reported electrochemistry studies on cobalt complexes supported by salophen ligand indicate that several reduction events are reachable,[227, 228] further chemical reduction has never been reported for these complexes. Moreover, reduced species were reported to be involved in the electrocatalytic reduction of $CO_2$ by cobalt complex supported by salophen ligand.[227]

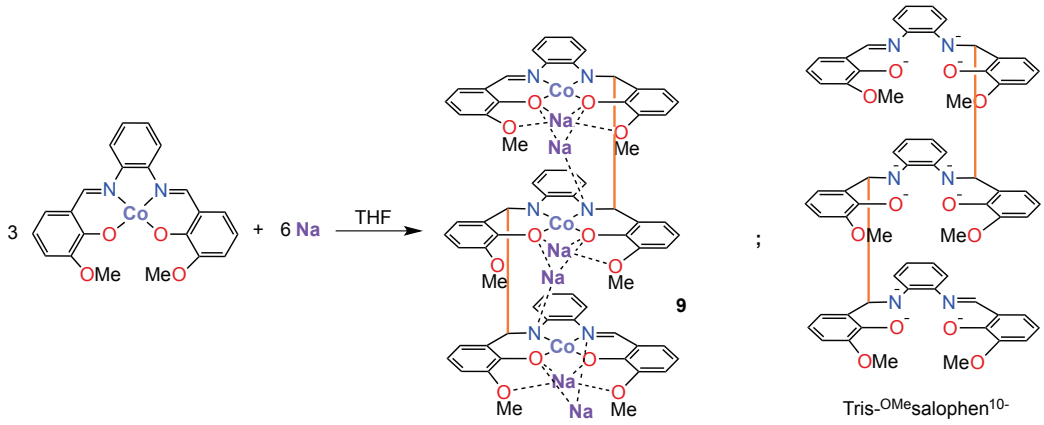


**Scheme II-16: Synthesis of the trinuclear complex [$Co_3$(tris-$^{OMe}$salophen)$Na_6$(THF)$_6$], 9 and schematic representation of the ligand tris-$^{OMe}$salophen$^{10-}$.**

The addition of 2eq of sodium metal to a suspension of the Co(II) complex [Co($^{OMe}$salophen)] leads to a green solution of the trinuclear species [$Co_3$(tris-$^{OMe}$salophen)$Na_6$(THF)$_6$], **9** (Scheme II-16). Crystals of **9**.hex were obtained from the slow diffusion of hexane into a THF solution of the complex (Figure II-17).

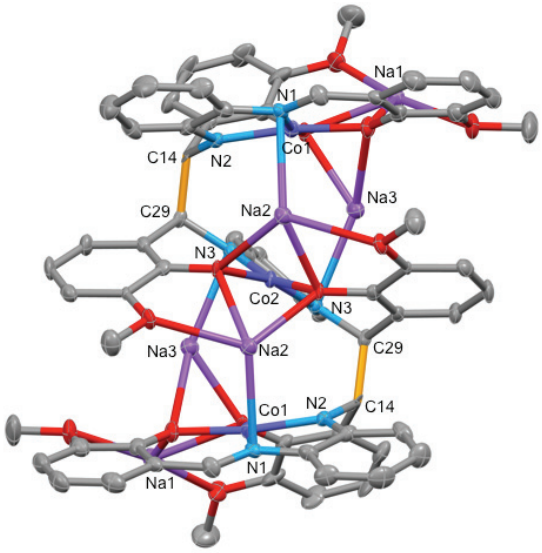


**Figure II-17: Solid state structure of [$Co_3$(tris-$^{OMe}$salophen)$Na_6$(THF)$_6$].hex, 9.hex (50% ellipsoids). The C-C bonds formed by the reduction of the imino functions are represented in orange. Hydrogen atoms and lattice solvent molecules are omitted for clarity.**

The crystal structure of complex **9** shows that reduction has occurred both on the metal and on the imino groups of the ligands affording a Co(I)-Co(II)-Co(I) complex supported by a bridging deca-anionic tris-$^{OMe}$salophen$^{10-}$ ligand. This ligand forms from the coupling of three

$^{OMe}$salophen ligands through formation of two C-C bonds. Six sodium cations counter-balance the charge of the complex. The asymmetric unit is formed by one Co(I) moiety and half of the central Co(II) moiety, indeed a 2-fold axis passes through the Co(II) atom. In each Co(I) moiety, one sodium cation is positioned into the $O_4$ pocket formed by the phenolate and methoxy groups of one $^{OMe}$salophen ligand, the other sodium is bound to the same phenolate groups and to the amido function of the Co(II) entity. Each sodium cation of the Co(II) moiety is bound by the two phenolate groups and one methoxy group of the $^{OMe}$salophen of the Co(II) unit and by the imino function of the Co(I) entity. The $^{OMe}$salophen$^{4-}$ fragment binding the Co(II) unit is bent in a zig-zag fashion due to the presence of the two C-C bonds (1.587(9) Å) connecting this tetra-anionic fragment to the two $^{OMe}$salophen$^{3-}$ fragments in the tris-$^{OMe}$salophen$^{10-}$ ligand. Each cobalt centre is tetracoordinated by two oxygen and two nitrogen atoms of the tris-$^{OMe}$salophen ligand with a distorted square planar geometry (distances of the cobalt atoms from the NNO mean planes of the ligand fragments: 0.098(4) Å for Co1 and 0.219(3) Å for Co2 due to the zig-zag arrangement). Once again significantly different average C-N bond distances are found for the imino (1.359(8) Å) and the amido (1.457(1) Å) functions.

The complex **9** is stable for weeks in THF and pyridine but decomposes in acetonitrile affording the Co(I) complex [Co($^{OMe}$salophen)] identified by $^1$H NMR and by X-ray diffraction in its dinuclear form [$Co_2$(bis-$^{OMe}$salophen)]. $^1$H NMR studies of the crude reaction mixture obtained by reacting [Co($^{OMe}$salophen)] with 2eq of sodium and of crystals of **9** show the formation of a new species with a $^1$H NMR signature of 28 signals between 13 and 2 ppm. These 28 signals are divided in two sets of 14 signals; one set is composed of sharp signals which integrated for two protons, the other set is composed of broad signals with an integration of one proton. Variable temperature NMR studies from -40°C to 60°C of a solution of complex **9** in THF-$d_8$ do not reveal any change in the ratio of the two sets of 14 signals, but shifts and overlapping of the broad signals. These results suggest that the trinuclear structure is maintained in solution without equilibrium between isomeric forms.

Complex **9** contains 4 electrons stored in two C-C bonds, two Co(I) and one Co(II) atoms. Globally each cobalt ion has been reduced by two electrons, which are located either on the metal or on the ligand. In order to investigate if also in this reduced species an alternative species containing only Co(0) could be isolated or identified we envisaged, using cryptand, to encapsulate the sodium cations and therefore alter the nuclearity and the electronic structure of the ligand.

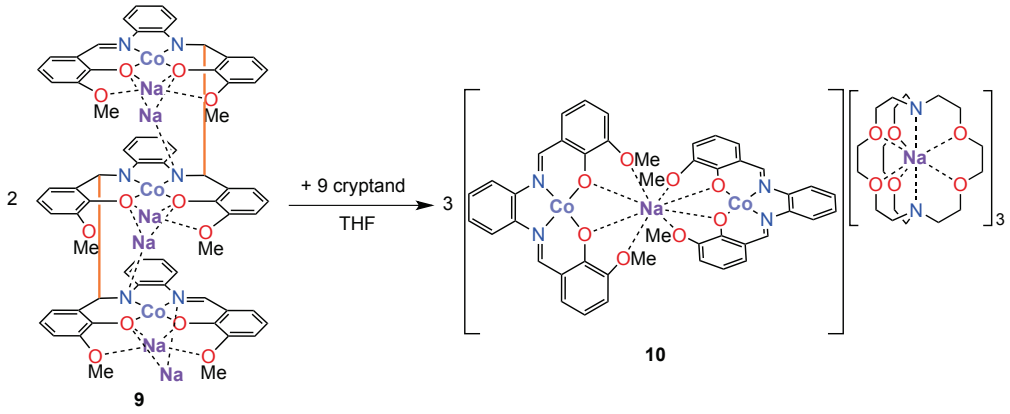


**Scheme II-17: Synthesis of the Co(0) complex [Na(cryptand)]$_3$[(Co($^{OMe}$salophen))$_2$Na], 10.**

The addition of cryptand (4.5eq or excess) to complex **9** in THF leads to the formation of a dinuclear Co(0) species [Na(cryptand)]$_3$[(Co($^{OMe}$salophen))$_2$Na], **10** (Scheme II-17). Dark needles suitable for X-ray diffraction of complex **10** were obtained by slow diffusion of cryptand in THF into a THF solution of **9**.

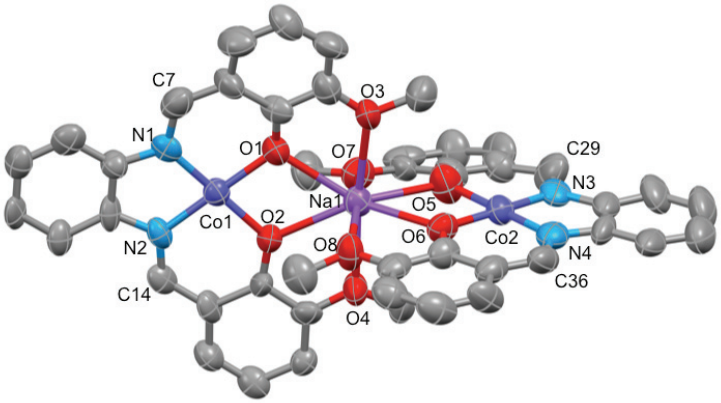


**Figure II-18: Solid state structure of [Na(cryptand)]$_3$[(Co($^{OMe}$salophen))$_2$Na], 10 (50% ellipsoids). [Na(cryptand)]$^+$ counter-cations and hydrogen atoms are omitted for clarity.**

The complex **10** crystallizes as a dimer in the P2$_1$/c space group (Figure II-18). The two Co(0) moieties [Co($^{OMe}$salophen)]$^{2-}$ are bridged in a quasi-perpendicular fashion (92.6(3)° between the mean planes defined by the NNOO sites of the ligands) by one sodium cation which is encapsulated in a $O_8$ pocket formed by the phenolate and the methoxy groups of both [Co($^{OMe}$salophen)] units. Three [Na(cryptand)]$^+$ cations counter-balance the charge of the overall complex. The cobalt atoms are tetracoordinated in a square planar geometry (the cobalt atoms are at 0.014(6) and 0.018(5) Å from the mean plane). In the rare examples of

previously reported Co(0) square planar species supported by N- and O-donor ligands, the discrimination between a [$Co^0L$] or a [$Co^IL^{\bullet-}$] compound is not obvious.[229] DFT and EPR studies are usually performed in addition to the structural parameters analyses leading so far to the assignment of these species as [$Co(I)L^{\bullet-}$] compounds.[230-232] Unfortunately, the precision of the bond distances Co-N (1.84(1) Å in average), Co-O (1.86(2) Å in average) and C-N (1.34(2) Å in average) in the structure of **10** is not sufficient to discriminate between a [$Co^0L$] or [$Co^IL^{\bullet-}$] structure. However, the isolation of complex **10** demonstrates that the C-C bonds in complex **9** can be cleaved by simple addition of cryptand to **9**. This facile redistribution of the electrons stored on the ligand scaffold suggests weak bond dissociation energy of the C-C bonds in **9** even if no equilibrium between isomeric forms is visible on the $^1$H NMR spectrum this complex in THF-$d_8$.

## II.3.3 Reactivity of [$Co_3$(tris-$^{OMe}$salophen)$Na_6(THF)_6$] with $CO_2$.

The high number of electrons stored and the facile cleavage of the C-C bonds in complex **9** incited us to investigate its reactivity with $CO_2$. Contrary to complexes [$Co_2$(bis-$^R$salophen)$Na_2(THF)_x$] (R=H, x=6; R=OMe, x=4), reported by Floriani, which only undertake reversible coordination of $CO_2$, the complex **9** reacts irreversibly with an excess of $^{13}CO_2$ in THF to yield a brown suspension. The $^1$H NMR spectrum in THF-$d_8$ of the supernatant after 1 night is silent. The removal of volatiles under vacuum and the dissolution of the residue in THF-$d_8$ do not lead to $CO_2$ release or to the appearance of signals in the $^1$H NMR spectrum. The dissolution in deuterated water of the residue leads to partial dissolution of the solid. The $^{13}$C NMR spectrum of this water solution shows a signal at 167 ppm, assigned to the $CO_3^{2-}$ di-anion.[233] The addition of $^{13}$C labelled sodium acetate as internal standard allows determining the yield in carbonate product that amounts to 53% of $CO_3^{2-}$ (per Co atom). When only 1eq of $^{13}CO_2$ per Co atom is added onto a THF-$d_8$ solution of **9**, a comparable yield in carbonate was measured (58%). However if the carbonate formation can be clearly identified by $^{13}$C NMR spectroscopy this is not the case for the concomitant formation of CO probably because of the CO coordination to low valent cobalt centres.[234-237] The addition of cryptand to the crude mixture of the reaction with excess $CO_2$ allowed the isolation of few crystals of a complex featuring the product of a ligand-based $CO_2$ reduction (Scheme II-18). Single crystals suitable for X-ray diffraction of the complex [Na(cryptand)]$_2$[Co($^{OMe}$salophen-$CO_2$)Na]$_2$, **11**, were

obtained by slow diffusion of DIPE into the THF solution of **9** reacted with $CO_2$ and then treated with cryptand.

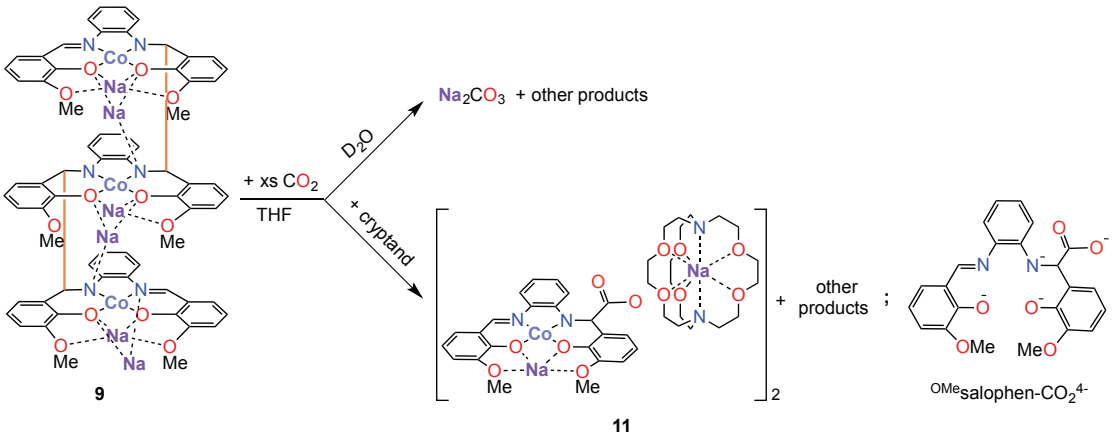


**Scheme II-18: $CO_2$ reduction by the trinuclear complex [$Co_3$(tris-$^{OMe}$salophen)$Na_6$(THF)$_6$] and schematic representation of the ligand $^{OMe}$salophen-$CO_2^{4-}$.**

The complex **11**.$(THF)_2$, crystallizes in the $P2_1/c$ space group. The structure is composed of two bridged [Co($^{OMe}$salophen-$CO_2$)Na]$^-$ anions and two [Na(cryptand)]$^+$ cations (Figure II-19 right). Each Co(II) atoms are tetracoordinated in a square planar geometry by the new tetra-anionic $^{OMe}$salophen-$CO_2^{4-}$ ligand (Scheme II-18). The two [Co($^{OMe}$salophen-$CO_2$)Na]$^-$ anions (Figure II-19 left) are bridged by the coordination of the carboxylate and one phenolate functions to the sodium cation of the other unit. The significantly different C-N bonds (1.456(7) and 1.474(8) Å for the $C_{CO2}$-N compared to 1.302(8) and 1.320(8) Å for the C-$N_{imino}$) are in agreement with the presence of a $C_{CO2}$-N single bond and a C=N double bond for the intact imino function. The C-$C_{carboxylate}$ bond lengths are dissymmetric, the longest of 1.590(7) Å is comparable to the C-C bond lenghts found in complexes **8** and **9** and the shortest 1.556(8) Å is comparable to the one found in $Na_2$[U(bis-salophen)][5] and [UM(bis-salophen)] (M=Co, Ni) (1.550(6)- 1.565(4) Å). The O-C-O angle values of the carboxylate moieties are 126.4(5)° and 128.9(6)°. The two carboxylate functions feature a slightly longer C-$O_{carboxylate}$ bond distance for the oxygen atoms coordinated to the sodium cation (1.257(6) Å in average) compared to the unbound oxygen atoms (1.230(4) Å in average). However these C-O distances remain short in agreement with a delocalized double bond on each carboxylate function.

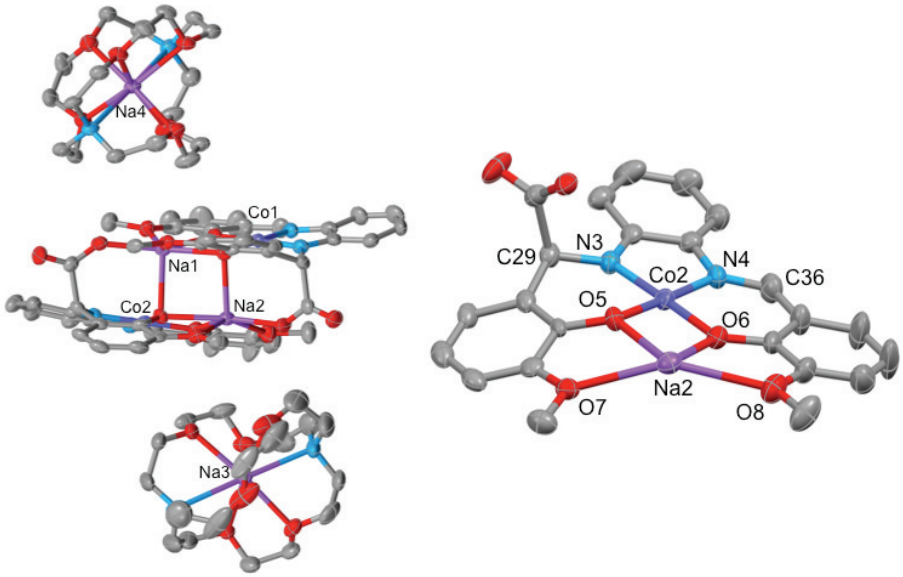


**Figure II-19: Solid state structure of [Na(cryptand)]$_2$[Co($^{OMe}$salophen-CO$_2$)Na]$_2$.THF$_2$, 11.THF$_2$. Structural arrangement (left) and one [Co($^{OMe}$salophen-CO$_2$)Na]$^-$ anions (right) (50% ellipsoids). Hydrogen atoms and solvent molecules are omitted for clarity.**

Unfortunately, because of the low solubility of all the reaction products complex **11** cannot be isolated cleanly. The structural parameters found in complex **11**, notably the O-C-O angles of the bent $CO_2$ group, confirm the reduction of the $CO_2$ molecule on the ligand platform leading to carboxylate formation. This reactivity differs from the one of the $K_3$[Nd(bis-$^{tBu}$salophen)] complex with $CO_2$ which leads to the formation of carboxylate functions on the phenyl bridge of one $^{tBu}$salophen ligand. These results show that the lack of available coordination site at the Nd centre in $K_3$[Nd(bis-$^{tBu}$salophen)] may not be the reason for the observed ligand-based reactivity as the Co centres in [$Co_3$(tris-$^{OMe}$salophen)$Na_6$(THF)$_6$] are more accessible but ligand-based reaction is still observed. Even if the two compounds, $K_3$[Nd(bis-$^{tBu}$salophen)] and [$Co_3$(tris-$^{OMe}$salophen)$Na_6$(THF)$_6$], are very different their respective reaction with $CO_2$ confirms a strong electron delocalisation on the ligand scaffold.

## II.3.4 A new synthetic route to [NdCo(salophen)$_2$(THF)]

In addition of the interesting reactivity of complex **9** with $CO_2$, revisiting the chemistry of cobalt supported by salophen ligand contributed to the syntheses of Co(I)

precursors such as [Co(salophen)K(THF)]. A new synthetic route for the preparation of the [NdCo(salophen)$_2$] **7** complex without side-product formation was thus envisaged.

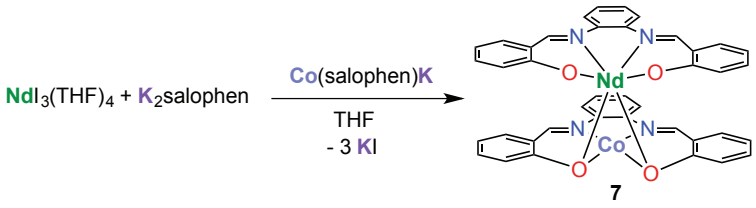


**7**

**Scheme II-19: Synthesis of [NdCo(salophen)$_2$] 7.**

The addition of 1eq of [Co(salophen)K(THF)] to the 1:1 reaction mixture of $NdI_3$ and 1eq of $K_2$salophen salts in THF affords the complex [NdCo(salophen)$_2$] **7** as confirmed by $^1$H NMR spectroscopy (Scheme II-19). Future studies will focus on the reactivity of the complex **7** with small molecules.

# II.4 Conclusion

The work presented in this chapter focuses on the syntheses of f-elements and/or transition metals supported by Schiff base redox active ligands to perform uncommon multi-electronic reductions.

In the first part of this chapter, we have demonstrated that the tridentate $^{Me}$naphtquinolen ligand framework can be used as supporting ligand for U(IV) centres. This ligand behaves as non-innocent ligand during the reduction reaction of its U(IV) complex leading to the reversible C-C bond formation between the imino moieties of the Schiff base. In addition the use of this tridentate Schiff base ligand instead of the tetradentate salophen one opens coordination sites at the U(IV) metal centre. Notably, the product of the two-electron reduction of 9,10-phenanthrenequinone by the dinuclear U(IV) complex is bound to the uranium metal centre. The complex [U(bis-$^{Me}$naphtquinolen)]$_2$ is able to promote multi-electronic reductions. Up to 4 electrons can be transferred when both the ligand and the uranium centre are participating in the reduction process like in the case of the reaction with dry $O_2$. Reduction of $CO_2$ by this system is not observed.

In the second part of this chapter, we identified a new synthetic route to heterobimetallic 5f-3d complexes supported by the octadentate bis-salophen ligand with free coordination sites at the metal centres. In these complexes an oxophilic U(IV) centre and a more nucleophilic transition metal centre are brought in close proximity with the aim of promoting a more effective polarization of the C=O bonds in $CO_2$. The simple synthetic pathway developed here led to the isolation of the [UM(bis-salophen)$(THF)_2$] (M=Co, Ni) in which the two metallic centres are in close vicinity and two electrons are stored in the reversible C-C bond of the bis-salophen ligand. In these complexes the electrons stored on the C-C bond remain unavailable for $CO_2$ reduction. Future studies will be directed to tune the accessibility of these electrons for $CO_2$ reduction. The further reduction of the metal centres also needs to be explored. The isolated complexes are also of interest for investigating the magnetic communication between metal centres. We have also demonstrated that the synthetic pathway used for the isolation of heterobimetallic [UM(bis-salophen)$(THF)_2$] complexes can be extended to access heterobimetallic 4f-3d complexes. The isolation of the Nd(III)-Co(I) complex [NdCo(salophen)$_2$] suggests that in this case the reduction of the Co(II) to Co(I) metal-centred is favoured over the C-C bond formation. This is discordant with the work reported by Floriani et al. on the reduction of the Co(II) complex [Co(salophen)] by sodium metal which leads to the formation of a Co(II)-Co(II) dinuclear compound with a reduced bis-salophen ligand.[222]

In the last part of this chapter, the chemistry of cobalt supported by salophen ligand was thus re-investigated. This study allowed us to gain insight in the importance of the counter-cation role in the one-electron reduction of the [Co(salophen)] complex. We revealed that according to the alkali metal chosen, the reduction occurred only at the cobalt centre (using potassium) or both at the metal centre and on the ligand scaffold affording a mixture of [Co(salophen)M] and [$Co_2$(bis-salophen)$M_2$] complexes (using M=Na or Li). Moreover a redox equilibrium was observed in solution between [Co(salophen)M] and [$Co_2$(μ-bis-salophen)$M_2$]. The determination of the thermodynamic constants of this equilibrium demonstrated that the C-C bond formed is very weak with bond dissociation energy close to zero. The two-electron reduction of the Co(II) complex [Co($^{OMe}$salophen)] was also investigated and led to the isolation of a trinuclear Co(I)-Co(II)-Co(I) compound with four additional electrons stored in two C-C bonds. These C-C bonds were found to be also very weak as simple addition of cryptand to remove the sodium cations allowed their cleavage and led to the isolation of a Co(0) complex. The trinuclear complex [$Co_3$(tris-

$^{OMe}$salophen)$Na_6(THF)_6$] was found to react with $CO_2$ and preliminary analyses of the $CO_2$ reduction products revealed the formation of carbonate and ligand-based reduction product. These results provide evidence that C-C bonds can be used to store electrons on a metal complex and that these electrons can also become available for the reduction of very unreactive molecules such as $CO_2$.

# CHAPTER III

# Small Molecule Activation by Trivalent Uranium Complexes Supported by Siloxide Ligands

## III.1 Context

As shown in the general introduction, low valent uranium complexes, when supported by the appropriate ancillary ligands optimizing steric and electronic properties, are able to reduce small molecules like $CO_2$, $CS_2$, $N_2$, etc. Recent work in our team focused on the use of a bulky siloxide ligand with U(III) centre. The tris(tert-butoxy)siloxide ligand presents several advantages: It is commercially available and cheap, it is soluble in aliphatic solvents, it can be used to model catalysts supported on silica nanoparticules. In addition to their steric role, the tert-butoxy groups can coordinate the metal centre leading to various binding modes as shown in Figure III-1. Siloxide ligands are less donating than alkoxide ligands because of the less polar Si-O and the small π-accepting capability of the silicon atom.[238] Nevertheless, siloxides are considered more robust than alkoxides as the Si-O bond is stronger than the C-O one limiting its cleavage to afford metal oxo species. Morever, as siloxides are less basic than the alkoxide ligands, they are less prone to undergo insertion in the metal-oxygen bond.

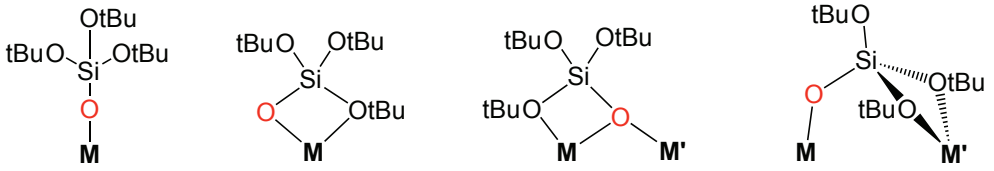


Monodentate Bidentate Bidentate-bridging Tridentate-bridging

**Figure III-1: Possible binding modes of the tris(tert-butoxy)siloxide ligand.**

Siloxide ligands have been mainly used with d-transition metals as precursors for the synthesis, among others, of M-containing silica via thermal treatment of $[M(OSi(OtBu)_3)_4]$ (M=Ti,[239] M=Zr,[240]) $[Ti(tBuO)_2\{\mu\text{-}O_2Si[OSi(OtBu)_3]_2\}]_2$,[241] $[\{Cr(OSi(OtBu)_3)_2\}_2]$[242] which are used in olefin epoxidation[243] or olefin polymerization.[242] Molecular complexes of transition metals supported by siloxide ligands have also been isolated and show catalytic activity for alkyne metathesis ($[MoN(OSiPh_3)_3(Py)]$,[244] $[WCPh(OSi(OtBu)_3)_3]$[245]).

However, the siloxide ligands have been rarely used in uranium chemistry and no U(III) siloxide complex had been isolated before 2012[246] probably because the high reactivity of these complexes rendered their synthesis and handling challenging. In 2012, our team succeeded to isolate the dimeric homoleptic siloxide complex of U(III): $[\{U(OSi(OtBu)_3)_2(\mu\text{-}OSi(OtBu)_3)\}_2]$.[100] As mentioned in the introduction, the reaction of $[\{U(OSi(OtBu)_3)_2(\mu\text{-}OSi(OtBu)_3)\}_2]$ with 2eq of $CO_2$ proceeds with the reductive disproportionation of $CO_2$ affording CO and a U(IV)-U(IV) carbonate complex (Scheme III-1a). In order to investigate the steric and electronic effects induced by a different number of siloxide ligands around the uranium centre, our group synthesised the heterobimetallic U,K complex $[U(OSi(OtBu)_3)_4K]$ and its ion-pair analoguous complex $[K18c6][U(OSi(OtBu)_3)_4]$. Both complexes react with $CO_2$ but lead to different reaction products (Scheme III-1b and c). Indeed, the addition of 1 atm of $CO_2$ to the U,K complex $[U(OSi(OtBu)_3)_4K]$ in toluene leads to the two-electron reductive cleavage of $CO_2$ yielding CO and a U(V) terminal oxo complex $[UO(OSi(OtBu)_3)_4K]$. The addition of 1 atm of $CO_2$ to the $[K18c6][U(OSi(OtBu)_3)_4]$ complex in toluene affords the terminal carbonate $[U(CO_3)(OSi(OtBu)_3)_4K_2(18c6)]$ along with the release of CO. This difference in reactivity can be explained by the close proximity between the uranium and potassium centres in the $[U(OSi(OtBu)_3)_4K]$ complex. The coordination of $CO_2$ by the two metal centres weakens significantly the C=O bond, rendering the C=O cleavage easier. This cooperativity has been supported by DFT calculations of the enthalpy profile for this reaction.

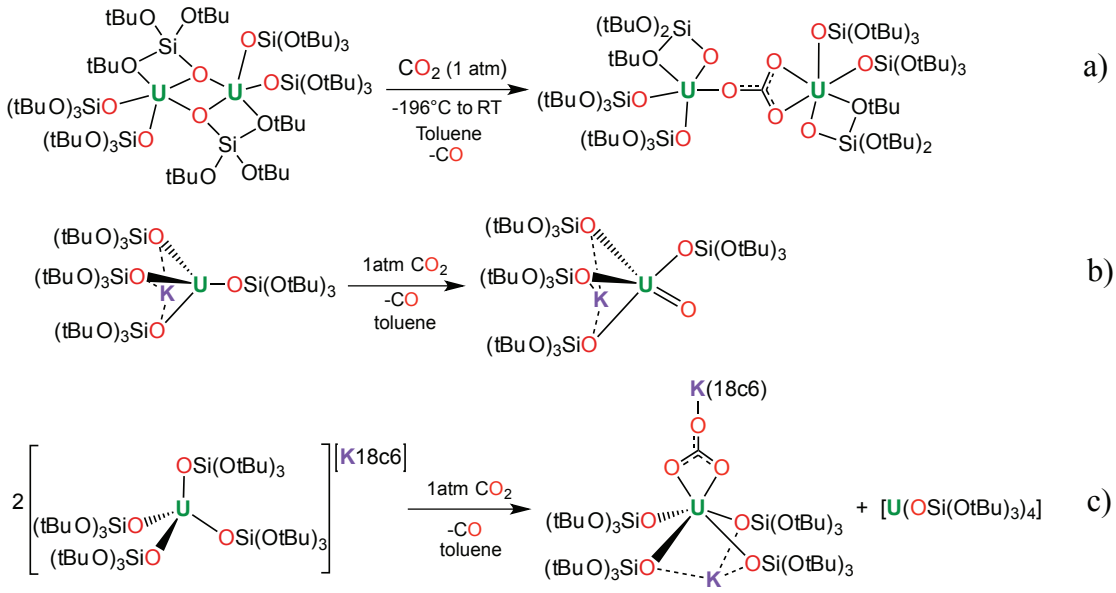


**Scheme III-1: $CO_2$ Reduction by [{U(OSi(OtBu)$_3$)$_2$(μ-OSi(OtBu)$_3$)}$_2$], [U(OSi(OtBu)$_3$)$_4$K] and [K18c6][U(OSi(OtBu)$_3$)$_4$] complexes.**

In comparison to the dinuclear tris-siloxide [{U(OSi(OtBu)$_3$)$_2$(μ-OSi(OtBu)$_3$)}$_2$] complex, the U(III) tetrasiloxide complexes show a more important steric hindrance and only mononuclear complexes are formed during the $CO_2$ reduction reactions. Moreover the reactivity with $CO_2$ can be controlled by the presence or absence of the potassium cation in the close proximity of the uranium centre. In my work I have investigated the effects of cooperativity in the reduction of other substrates such as $CS_2$ or $Ph_3PS$.

# III.2 Reactivity of U(III) tetrasiloxide "ate" complexes : Role of the counter-cation

Although Bianchini and co-workers underlined, in 1984, the important role of Lewis acids present ($NaBPh_4$, $HgCl_2$, $BF_3$, $HBF_4$ or $NaPF_6$) in the reaction mixture to promote $CS_2$ reductive coupling into $C_2S_4^{2-}$ by the complex $[RhCl(C_2H_4)_2]_2$,[247] the cooperative effect between f-element and alkali centres had never been studied on $CS_2$ reduction.

## III.2.1 Reactivity with $CS_2$

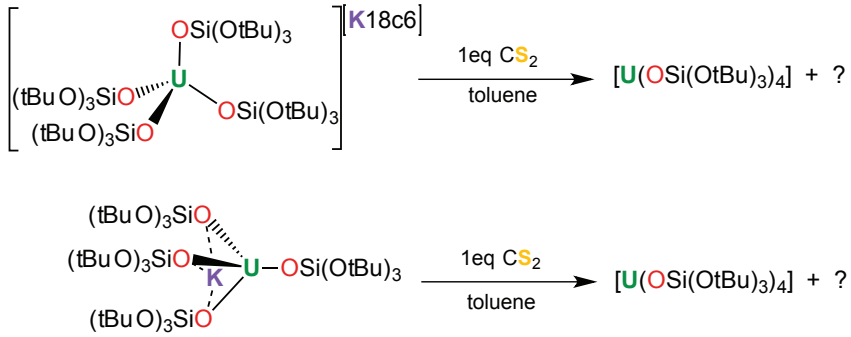


**Scheme III-2: Reactions of [K18c6][U(OSi(OtBu)$_3$)$_4$] (top) and [U(OSi(OtBu)$_3$)$_4$K] (bottom) with 1eq of $CS_2$.**

The addition of 1eq of $CS_2$ to the [K18c6][U(OSi(OtBu)$_3$)$_4$] (or the [U(OSi(OtBu)$_3$)$_4$K]) complexes in toluene (Scheme III-2) leads to an immediate change of the brown suspension (or brown solution) to a pink/red solution (or orange solution). The reaction with $CS_2$ is instantaneous. The $^1$H NMR studies of both reactions clearly show that several U(IV) intermediate species are formed and that the mixtures evolve over time as presented in Figure III-2 and Figure III-3. A signal assigned to the [U(OSi(OtBu)$_3$)$_4$] complex is present, among others, on the $^1$H NMR spectra right after the $CS_2$ addition. After 2 days, only the [U(OSi(OtBu)$_3$)$_4$] signal is present on the spectra. A 65% and 66% conversion respectively is determined using naphthalene as internal standard.

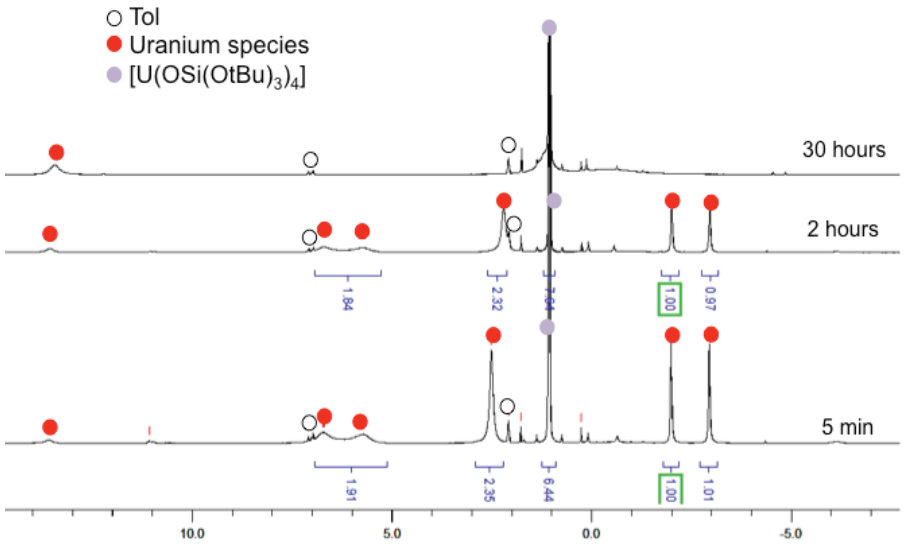


**Figure III-2: $^{1}$H NMR spectrum (200MHz, tol-$d_8$, 298K) of the crude reaction mixture of $CS_2$ and [K18c6][U(OSi(OtBu)$_3$)$_4$] over the course of 2 days.**

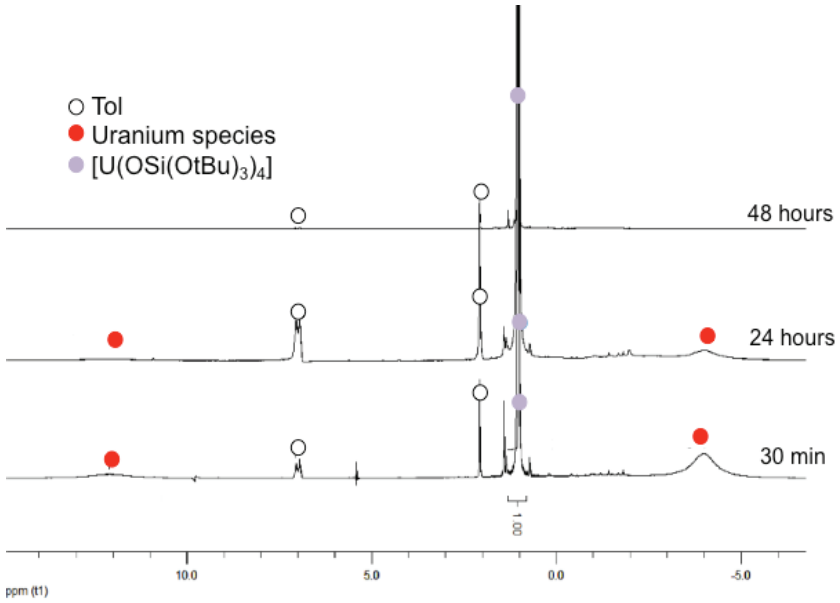


**Figure III-3: $^{1}$H NMR spectrum (200MHz, tol-$d_8$, 298K) of the crude reaction mixture of $CS_2$ and [U(OSi(OtBu)$_3$)$_4$K] over the course of 2 days.**

## III.2.1.1 Short reaction times: Isolation of intermediates

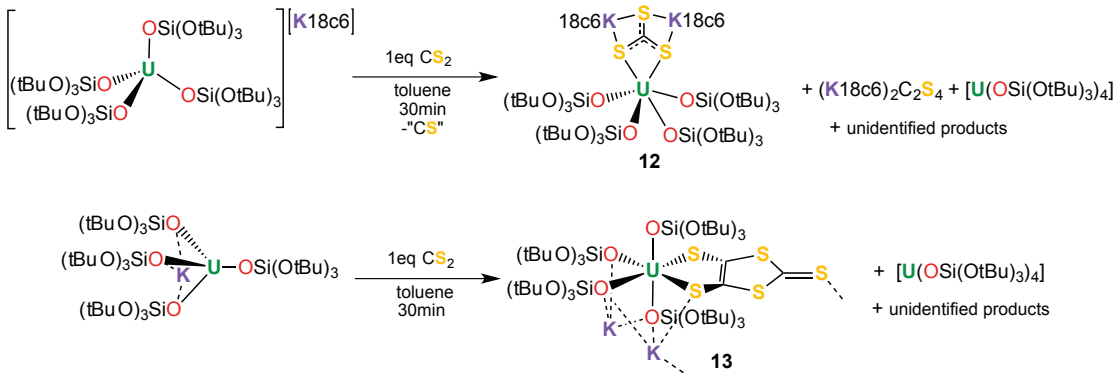


**Scheme III-3: Reactions of [K18c6][U(OSi(OtBu)$_3$)$_4$] (top) and [U(OSi(OtBu)$_3$)$_4$K] (bottom) with $CS_2$ after 30min in toluene.**

Initial work performed by Clément Camp and Oliver Cooper led to the isolation of reaction intermediates. The reaction mixtures of [K18c6][U(OSi(OtBu)$_3$)$_4$] or [U(OSi(OtBu)$_3$)$_4$K] and $CS_2$ were worked up 30 min after the $CS_2$ addition (Scheme III-3).

After the removal of toluene, hexane was added to extract the hexane soluble species from an insoluble precipitate. The $^{13}C$ NMR spectrum of the hexane insoluble residue in deuterated pyridine shows only the signals at 70.6 ppm and 248.5 ppm assigned to the 18c6 and to the tetrathioxalate dianion $^{13}C_2S_4^{2-}$ respectively. The formation of this latter compound was confirmed by crystallization from pyridine/hexane leading to isolation of dark green crystals of [(K18c6)$_2$($C_2S_4$)].Py suitable for X-Ray diffraction (Figure III-4 left). $^{13}C$ NMR spectra of those crystals in deuterated pyridine and DMSO attest the chemical shift of the dianion $^{13}C_2S_4^{2-}$ to be 248.5 ppm in pyridine and 264.4 ppm in DMSO. Even if the [U(OSi(OtBu)$_3$)$_4$] complex is the major product of the hexane extract, few yellow crystals of the U(IV) trithiocarbonate species [U(OSi(OtBu)$_3$)$_4$($CS_3$)$K_2$(18c6)$_2$], **12**, were obtained after recrystallization from toluene at -40°C (Figure III-4 right). The $^{13}C$ NMR spectrum of the hexane extract in deuterated DMSO shows the signals of the [(K18c6)$_2$($^{13}CS_3$)] compound (70.6ppm for 18c6 and 267.7 ppm for $CS_3^{2-}$[233]) proving that the trithiocarbonate is released from **12** in DMSO.

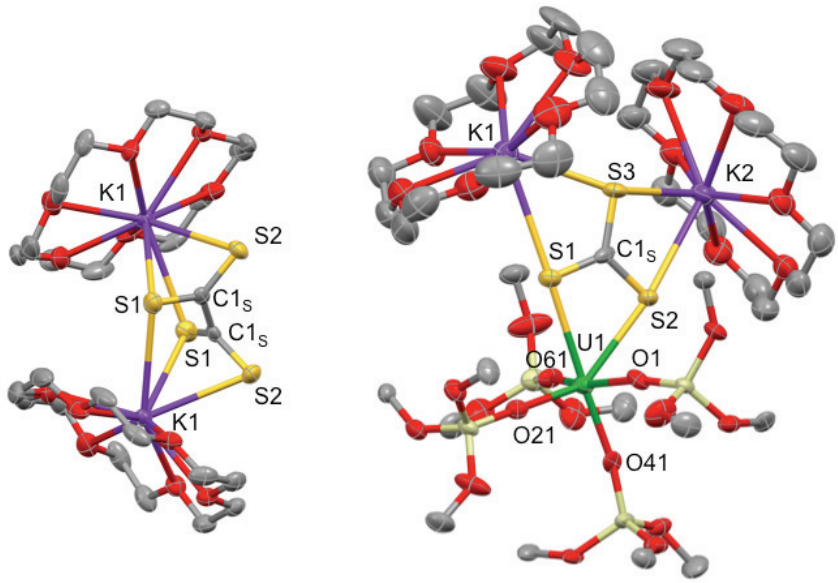


**Figure III-4: Solid state structure of isolated intermediates $[(K18c6)_2(C_2S_4)]$.Py and $[U(OSi(OtBu)_3)_4(CS_3)K_2(18c6)_2].(tol)_4$, 12.$(tol)_4$ (50% ellipsoids). Hydrogen atoms, methyl groups and solvent molecules are omitted for clarity.**

The $C_2S_4^{2-}$ unit lies on a crystallographically imposed two-fold axis in the middle of the C-C bond of the thioxalate. The $C_2S_4^{2-}$ moiety is coordinated to two $[K18c6]^+$ cations in a bridging $\kappa^3$:$\kappa^3$ mode which, to our knowledge, has not been reported before for this ligand. The $C_2S_4^{2-}$ moiety adopts a non-planar structure, with a torsion S2–$C1_S$–$C1_S$–S2 angle of 83.8(3)°. A similar feature is found in the related $[PPh_4]_2[C_2S_4]$[248] and $[NEt_4]_2[C_2S_4]$[249] structures. The central C–C bond length and the C–S bond distances ($C1_S$–$C1_S$ 1.511(6) Å, S1–$C1_S$ 1.670(3) Å and S2–$C1_S$ 1.679(3) Å) are also in agreement with the presence of a dianionic tetrathioxalate.

The structure of **12**.$(tol)_4$ shows the presence of a U(IV) centre hexacoordinated by the two S atoms of a trithiocarbonate unit and the four oxygen atoms of four terminal siloxide ligands. The trithiocarbonate unit bridges in a $\mu^3$-$\kappa^2$:$\kappa^2$:$\kappa^2$ fashion the uranium and two $[K18c6]^+$ cations. Overall, the metrical parameters of **12** and its global charge are in agreement with a tetravalent oxidation state for uranium. Notably, the average U–O bond distance (2.199(14) Å) falls in the range of those typically found for U(IV) siloxy systems.[100, 250, 251]. The C–S bond lengths are comparable (1.727(8), 1.709(9) and 1.706(8) Å), and are in agreement with an electronic delocalisation over the $CS_3^{2-}$ unit. These values are also similar to those found in other trithiocarbonate complexes.[131, 252, 253] Unfortunately, because of the

presence of multiple reaction products and the labile coordination of the $CS_2$ reduction products, compound **12** cannot be isolated cleanly, preventing further characterisation.

According to the isolation of the intermediates $[(K18c6)_2(C_2S_4)]$ and **12**, we know that $[K18c6][U(OSi(OtBu)_3)_4]$ is able to reduce $CS_2$ through both reductive dimerization and disproportionation pathways affording tetrathioxalate and trithiocarbonate dianions respectively.

To probe the role of the potassium cation, the U,K complex $[U(OSi(OtBu)_3)_4K]$ was reacted with $CS_2$ (Scheme III-3). Work up of the reaction 30 min after the addition of $^{13}CS_2$ to the U,K complex in toluene led to the isolation of a new intermediate, the U(IV) complex $[U(OSi(OtBu)_3)_4K_2(C_3S_5)]_n$, **13** (Figure III-5).

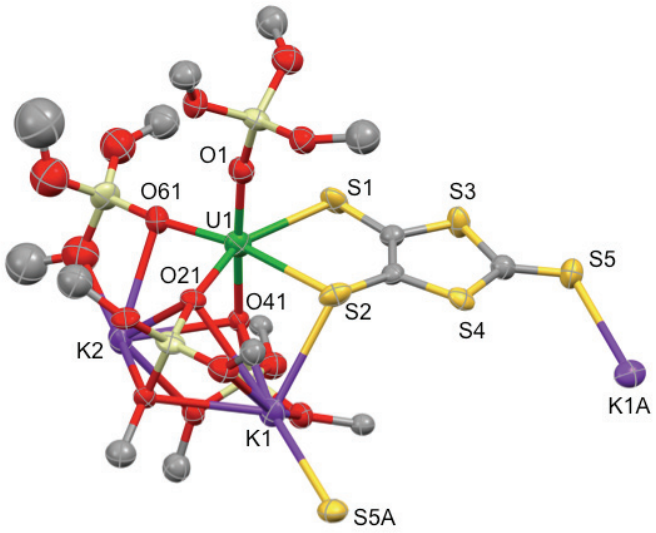


**Figure III-5: solid state structure of the isolated intermediate $[U(OSi(OtBu)_3)_4K_2(C_3S_5)]_n$·hexane, 13.hex (50% ellipsoids). Hydrogen atoms, methyl groups and solvent molecules are omitted for clarity.**

The complex **13**.hex crystallizes as an infinite 1D polymer. While the quality of the structure is not sufficient to discuss the metrical parameters, it clearly shows the atom connectivity. In the structure, the uranium centre is hexacoordinated by the four oxygens of the siloxide ligands and the two sulfur atoms of the $C_3S_5^{2-}$ ligand ($dmit^{2-}$) in a slightly distorted octahedral geometry. Two potassium cations are bound in the pockets formed by five oxygen atoms from the siloxide ligands. The thione sulfur of the $C_3S_5^{2-}$ ligand binds one of the potassium cations of the adjacent complex yielding a 1-D chain. The structure of **13** shows that the coordination environment provided by the siloxide ligands can adapt allowing the coordination of the dmit

dianion to the uranium centre. The formation of the dmit $C_3S_5^{2-}$ dianion probably comes from the reaction of $C_2S_4^{2-}$ with local excess $CS_2$[254, 255] or with CS (which is also formed during the reaction via the reductive disproportionation, see III.2.1.2 Long reaction times). In both cases the reductive dimerization of $CS_2$ in $C_2S_4^{2-}$ seems to be the first step of this reaction. The complex **13** is, to our knowledge, the first example of structurally characterised dmit complex of f-element and the first dmit complex formed directly from reduction of $CS_2$ by a metallic complex.

We remark that different intermediate species have been isolated in these reactions depending on the presence of 18c6 crown ether in the starting U(III) tetrasiloxide complex. Yet, to be certain that the potassium-uranium proximity plays an important role in the $CS_2$ reduction, an analysis of the total reaction mixture is necessary.

## III.2.1.2 Long reaction times: Comparison of the reaction product ratios.

One equivalent of $^{13}CS_2$ was added to a brown suspension of [K18c6][U(OSi(OtBu)$_3$)$_4$] or a brown solution of [U(OSi(OtBu)$_3$)$_4$K] in toluene. The obtained solutions were let stand at room temperature during 48h. The $^1$H NMR spectra of both reaction media confirmed that the reaction was complete as only the signal of the [U(OSi(OtBu)$_3$)$_4$] complex was present. All the volatiles were then removed *in vacuo* and deuterated DMSO was added leading to the release of the reduction products. Quantitative $^{13}$C NMR spectra recorded in DMSO-$d_6$ showed the four signals of the products $CS_3^{2-}$ (267.7 ppm), $C_2S_4^{2-}$ (264.5 ppm) and $C_3S_5^{2-}$ (146 and 203 ppm). The $^{13}$C NMR shifts of $CS_3^{2-}$ and $C_3S_5^{2-}$ are in good agreement with those reported in the literature.[233, 254, 255] The $^{13}$C NMR shift of $C_2S_4^{2-}$ is in agreement with that recorded on the isolated [(K18c6)$_2$($C_2S_4$)] complex. The calculated product ratios of the $^{13}CS_2$ reduction by [K18c6][U(OSi(OtBu)$_3$)$_4$] and [U(OSi(OtBu)$_3$)$_4$K] are shown in Scheme III-4. Quantitative $^{13}$C NMR spectroscopy using naphthalene as an internal standard confirms the quantitative transformation of $CS_2$ into the reduction products.

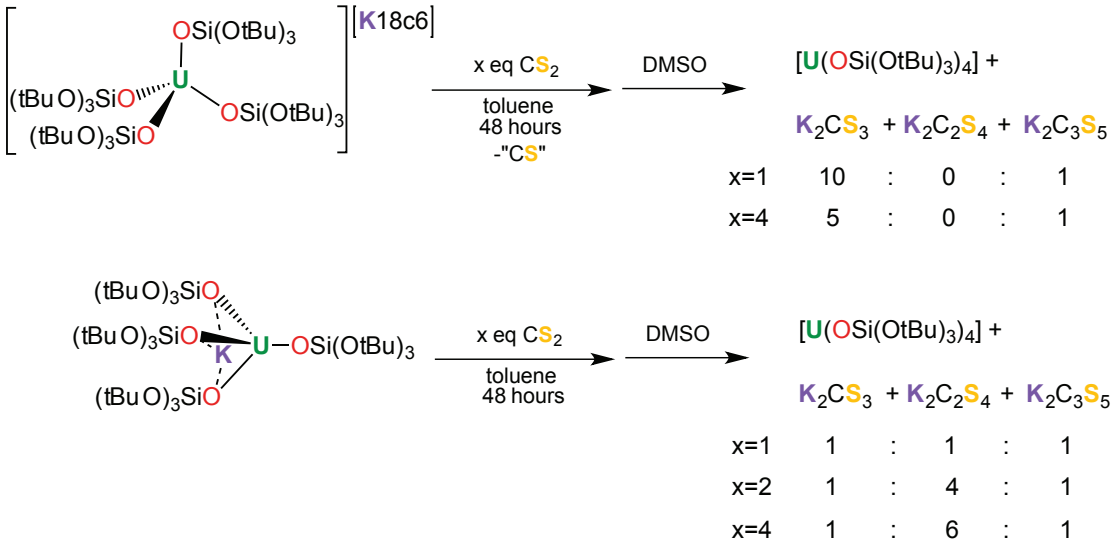


**Scheme III-4: Reactions of [K18c6][U(OSi(OtBu)$_3$)$_4$] (top) and [U(OSi(OtBu)$_3$)$_4$K] (bottom) with $CS_2$ after 2 days in toluene and subsequent addition of DMSO-d$_6$.**

We remark that the crown ether complex [K18c6][U(OSi(OtBu)$_3$)$_4$] favours the reductive disproportionation of $CS_2$ and thus the formation of the $CS_3^{2-}$ compound (ratio $CS_3^{2-}$/$C_2S_4^{2-}$/$C_3S_5^{2-}$= 10/0/1). Reductive dimerization of $CS_2$ into $C_2S_4^{2-}$ occurs in a much less important proportion and the small quantity of $C_2S_4^{2-}$ formed reacts with the highly reactive CS or with a local excess of $CS_2$ to form the dmit dianion, $C_3S_5^{2-}$. When an excess of $CS_2$ (4eq) is added to [K18c6][U(OSi(OtBu)$_3$)$_4$], the trithiocarbonate remains the main product, with a ratio $CS_3^{2-}$/$C_2S_4^{2-}$/$C_3S_5^{2-}$ of 5/0/1, but the reductive dimerization in $C_2S_4^{2-}$ (eventually followed by a reaction with CS or $CS_2$ to also form $C_3S_5^{2-}$) increases. As the dimerization of $CS_2$ presumably involves a U(IV) radical anionic $CS_2^{\bullet-}$ intermediate, increasing the amount of $CS_2$ molecules should increases the potential amount of U-$CS_2^{\bullet-}$ intermediates and as a result the quantity of $C_2S_4^{2-}$ formed. Yet the formation of $CS_3^{2-}$ remains more favoured and this could be due to the non-proximity of the U-K centres. Moreover, once the $CS_3^{2-}$ compound is formed, the presence of the $[K18c6]^+$ cation could stabilize the complex **12** by binding the uranium-bound trithiocarbonate and thus may contribute to drive the reaction toward the reductive disproportionation pathway.

On the other hand, we observe that the U,K complex [U(OSi(OtBu)$_3$)$_4$K] clearly favours the reductive dimerization of 1eq $CS_2$ in $C_2S_4^{2-}$ with a ratio $CS_3^{2-}$/$C_2S_4^{2-}$/$C_3S_5^{2-}$ of 1/1/1 in other words a ratio disproportionation/dimerization of 1/2. We also observe that increasing the $CS_2$ excess up to 4eq changes the ratio $CS_3^{2-}$/$C_2S_4^{2-}$/$C_3S_5^{2-}$ to 1/6/1 (i.e. ratio disproportionation/dimerization of 1/7) showing that once again the $CS_2$ dimerization rises

with the $CS_2$ stoichiometry. However, with the U,K complex, the dimerization is favoured even in stoichiometric amount of $CS_2$. This is in agreement with Bianchini and co-workers conclusions: the presence of a Lewis acids like $Na^+$, $Hg^{2+}$or $BF_3$ ($K^+$ in our case) together with an electron rich metal centre Rh(I) (U(III) in our case) favours the dimerization of $CS_2$. Moreover they have shown that the $NBu_4^+$ Lewis acid does not induce the formation of $C_2S_4^{2}$. This is probably due to the steric hindrance of this cation which prevent a close proximity between the metal centre and the Lewis acid.

The reaction of $CS_2$ with $[U(OSi(OtBu)_3)_4K]$ indicates that the $dmit^{2-}$ formation is probably due to the reaction of $C_2S_4^{2-}$ with CS rather than excess $CS_2$. Indeed, even when 4eq of $CS_2$ are added to the $[U(OSi(OtBu)_3)_4K]$ complex, the amount of $C_3S_5^{2-}$ compound corresponds to the amount of $CS_3^{2-}$ obtained. This shows that only the CS formed during the disproportionation of $CS_2$ in $CS_3^{2-}$ reacts with $C_2S_4^{2-}$.

When the reaction mixture obtained from the reaction of 1eq of $CS_2$ with $[U(OSi(OtBu)_3)_4K]$ in toluene is evaporated, the recrystallization of this residue in DMSO layered with toluene affords yellow crystals of $[K_2C_2S_4(DMSO)_3]_n$ suitable for X-ray diffraction. The X-ray studies show the presence of a 2D polymeric structure (Figure III-6). Each $C_2S_4^{2-}$ ligand bridges three potassium cations yielding a 1D polymer chain. Two DMSO molecules bridge two potassium cations from adjacent chains to afford the 2D polymeric structure. The central C–C bond length and the C–S bond distances (C1–C3 1.496(3) Å, S1–C1 1.700(2) Å and S2–C1 1.671(2) Å, S3–C3 1.678(3) Å and S4–C3 1.686(2) Å) are in agreement with the presence of a dianionic tetrathioxalate.[248]

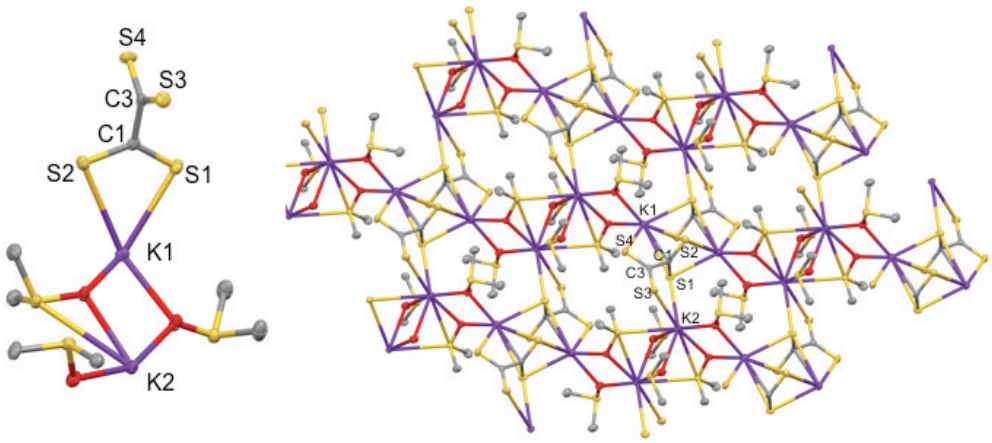


**Figure III-6: Solid state structure of $[K_2C_2S_4(DMSO)_3]_n$, asymmetric unit (left) and 2D coordination polymer (right) (50% ellipsoids). Hydrogen atoms are omitted for clarity.**

In summary, [K18c6][U(OSi(OtBu)$_3$)$_4$] and [U(OSi(OtBu)$_3$)$_4$K] complexes react with $CS_2$ affording both reductive disproportionation and dimerization. The reduction products ($CS_3^{2-}$, $C_2S_4^{2-}$ and $C_3S_5^{2-}$) are labile and easily released from the uranium coordination sphere by addition of coordinating solvents such as pyridine or DMSO. The bulky environment providing by four tris(tert-butoxy)siloxide ligands is surely the reason of the easy displacement of the reduction products rendering these systems well suited for the development of catalytic cycles. The reactivity of the ion-pair complex [K18c6][U(OSi(OtBu)$_3$)$_4$] and the U,K complex [U(OSi(OtBu)$_3$)$_4$K] is significantly different from the reaction of the homoleptic tris-siloxide complex [{U(OSi(OtBu)$_3$)$_2$(μ-OSi(OtBu)$_3$)}$_2$] which leads to a $CS_2^{2-}$ moiety strongly bound to two U(IV) centres. This difference shows the ability of siloxide ligands to tune the reactivity of the U(III) metal centre. Indeed, the outcome of the reaction is affected by the number of siloxides and thus by sterical and the charge effects. Moreover, the crucial role of the potassium cation has been demonstrated. The close proximity of uranium and potassium centres in [U(OSi(OtBu)$_3$)$_4$K] leads preferentially to the reductive dimerization of $CS_2$ while the ion-pair [K18c6][U(OSi(OtBu)$_3$)$_4$] complex favours the reductive disproportionation pathway. The X-ray structures of isolated intermediate complexes **12** and **13** show the coordination of the $K^+$ and $[K18c6]^+$ cations to the reduction products which suggest that the alkali ion plays an important but probably different role in both systems. We have then become interested in investigating the effects of cooperativity in other reactions like sulfur transfer reaction.

## III.2.2 Reactivity with sulfur donor agents

### III.2.2.1 Context

As shown in the general introduction, investigations on the U-S multiple bond received an increasing interest as complexes with Metal-Sulfur multiple bond are involved in sulfur atom transfer catalyses. Besides, studies on U-S multiple bond allow us to gain insight in the nature of the bonding and the f-orbital contribution to it. However, the isolation of a terminal uranium sulfide complex is not obvious as the nucleophilic character of the sulfide ligands often leads to sulfide-bridged complexes[185-188, 190, 256] or mononuclear disulfide

complexes.[186, 191] The recent characterisation, in our group, of the U(V) terminal oxo complex [UO(OSi(OtBu)$_3$)$_4$] from the reaction of $CO_2$ with the U(III) complex [U(OSi(OtBu)$_3$)$_4$K] shows that the bulk provided by four siloxide ligands is sufficient to prevent the formation of oxo-bridged compounds. This suggest that the [U(OSi(OtBu)$_3$)$_4$K] complex might be an appropriate precursor for the synthesis of a uranium terminal sulfide complex from a sulfur transfer agent. Moreover, the important role played by the siloxide-bound potassium cation in the reactivity of [U(OSi(OtBu)$_3$)$_4$K] and [K18c6][U(OSi(OtBu)$_3$)$_4$] with $CO_2$ or $CS_2$ suggests that the U/K proximity could also influence the reactivity in the sulfur transfer reactions.

### III.2.2.2 Syntheses of terminal hydrosulfide and sulfide complexes supported by tacn-based ligand.

During my studies toward the synthesis of a uranium tetrasiloxide terminal sulfide complex, I had the opportunity to collaborate with Pr. Meyer's group in the development of uranium-chalcogens multiple bonding. Discussions and mutual exchanges of information and advices lead to the syntheses of terminal U(IV) hydrosulfide and sulfide complexes supported by the ($^{Ad,Me}$ArO)$_3$tacn ligand.[257] Indeed, the addition of 1eq of $H_2S$ to the U(III) complex [U(($^{Ad,Me}$ArO)$_3$tacn)] affords the hydrosulfide complex [U(SH)(($^{Ad,Me}$ArO)$_3$tacn)] in 82% yield (Scheme III-5).

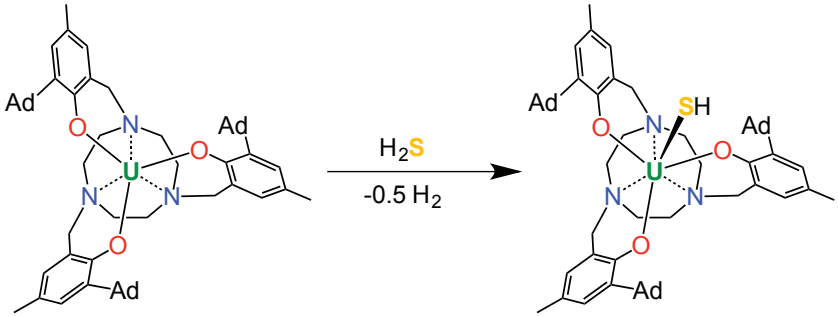


[U(($^{Ad,Me}$ArO)$_3$tacn)] [U(SH)(($^{Ad,Me}$ArO)$_3$tacn)]

**Scheme III-5: Synthesis of the hydrosulfide complex [U(SH)(($^{Ad,Me}$ArO)$_3$tacn)].**

This complex was characterised by X-ray diffraction and the U-S bond lengths of the two independent molecules in the asymmetric unit (2.844(4) and 2.775(2) Å) are in agreement with previously reported U-(SH) single bond (2.588(1)-2.907(3) Å)[258] and, as expected, significantly longer than the U-S distances reported for uranium terminal sulfide complexes (2.382(11)-2.481(1) Å)[177, 179, 192] (Figure III-7).

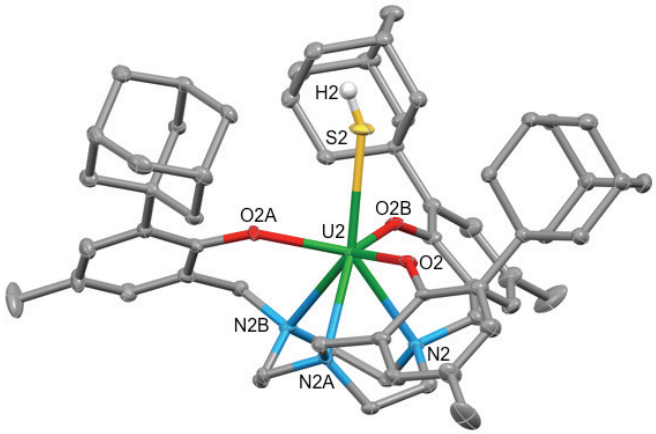


**Figure III-7: Solid state structure of one of the two complexes [U(SH)(($^{Ad,Me}$ArO)$_3$tacn)] (50% ellipsoids). Hydrogen atoms of the ($^{Ad,Me}$ArO)$_3$tacn ligand and solvent molecules are omitted for clarity.**

In this complex the uranium ions are located slightly beneath the plane formed by the three aryloxide oxygen atoms ($U_{oop}$= -0.282(3) and -0.268(4) Å respectively) which is an usual out-of-plane shift for U(IV) ions supported by ($^{R,R'}$ArO)$_3$tacn$^{3-}$ ligand system (R = Ad, tBu, Np; R' = tBu, Me). The deprotonation of the hydrosulfido ligand with potassium bis(trimethylsilyl)amide (KHMDS) in the presence of crown ethers, dibenzo18c6 or cryptand, yields the U(IV) terminal sulfide species [{US(($^{Ad,Me}$ArO)$_3$tacn)}{Kdibenzo18c6}] and [Kcryptand][US(($^{Ad,Me}$ArO)$_3$tacn)] respectively (Scheme III-6).

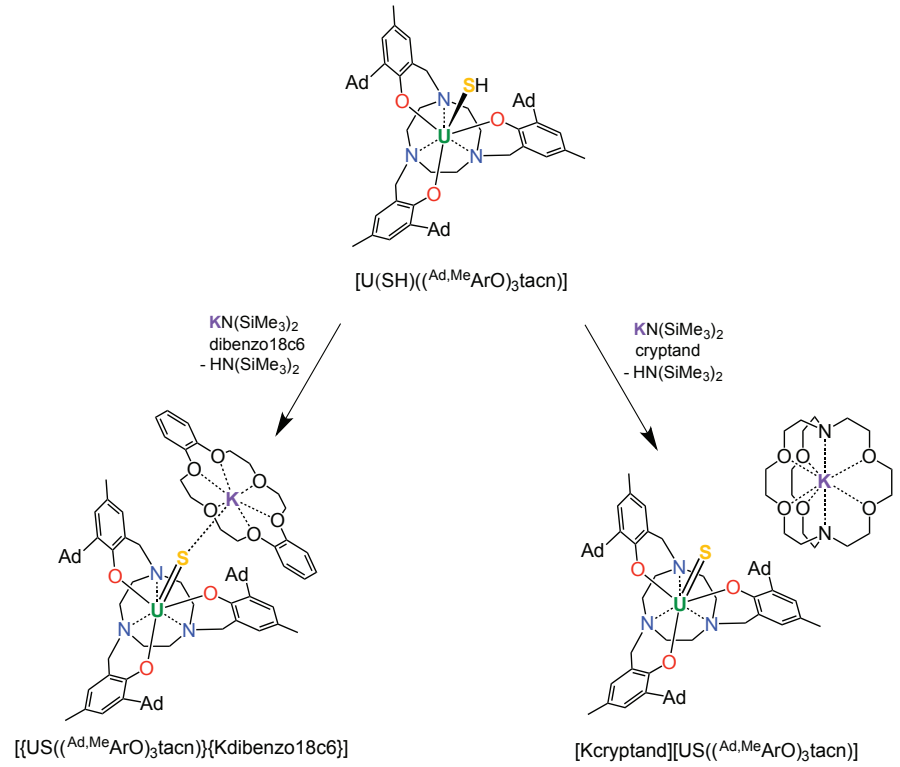


**Scheme III-6: Synthesis of the terminal sulfide complexes [{US((Ad,MeArO)3tacn)}{Kdibenzo18c6}] and [Kcryptand][US((Ad,MeArO)3tacn)].**

The X-ray crystal structure of [{US((Ad,MeArO)3tacn)}{Kdibenzo18c6}] (Figure III-8 left) reveals a much shorter U-S distance of 2.507(1) Å compared to the hydrosulfide starting complex, confirming the presence of a $S^{2-}$ ligand. Yet this U-S bond length is slightly longer than the one previously reported for uranium terminal sulfide complexes (2.382(11)-2.481(1) Å).[177, 179, 192] The presence of the dibenzo crown ether does not prevent the coordination of the $S^{2-}$ moiety to the potassium cation with a S-K distance of 3.136(1) Å. Surprisingly, the uranium ion is almost located in the plane of the aryloxide oxygen atoms: the U out-of-plane shift of -0.055(2) Å is very unusual for a U(IV) centre supported by tacn-based ligand but more common for higher oxidation states with strong π-donor ligands. This change might suggest a more covalent U-S bond than in the hydrosulfide complex leading to a weaker interaction with the tacn cycle. The X-ray crystal structure of [Kcryptand][US((Ad,MeArO)3tacn)] (Figure III-8 right) features that, contrary to [{US((Ad,MeArO)3tacn)}{Kdibenzo18c6}], the complex is a separated ion pair of the $[Kcryptand]^+$ cation and the $[US((^{Ad,Me}ArO)_3tacn)]^-$ anion. Yet, unexpectedly, even if the $S^{2-}$ moiety does not coordinate the $K^+$ cation anymore, the U-S distance in

[Kcryptand][US((Ad,MeArO)3tacn)] is slightly longer (2.536(2) Å) than the one in [{US((Ad,MeArO)3tacn)}{Kdibenzo18c6}] (2.507(1) Å). Concerning the uranium position, the $U_{oop}$ slightly increases to -0.086(8) Å but remains unusually low for a U(IV) complex.

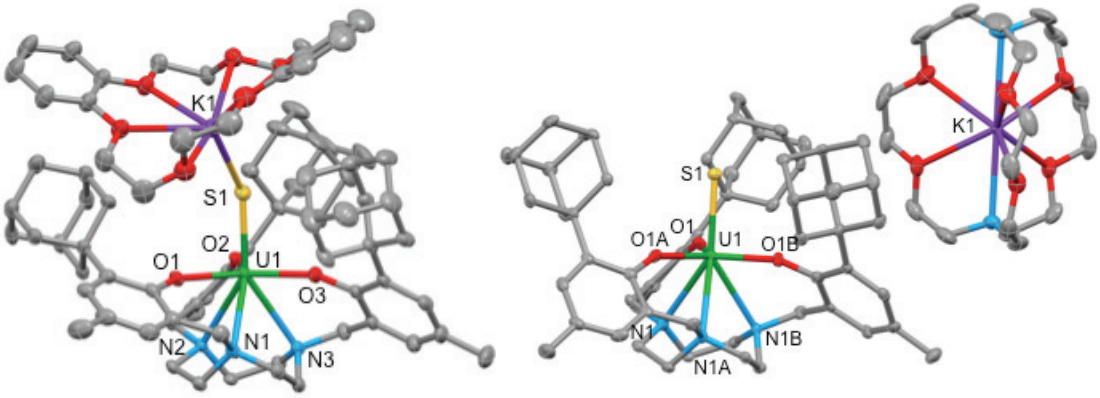


**Figure III-8: Solid state structure of [{US((Ad,MeArO)3tacn)}{Kdibenzo18c6}] (left) and [Kcryptand][US((Ad,MeArO)3tacn)] (right) (50% ellipsoids). Hydrogen atoms and solvent molecules are omitted for clarity.**

Theoretical studies were performed on [U(SH)((Ad,MeArO)3tacn)], [{US((Ad,MeArO)3tacn)}{Kdibenzo18c6}] and [Kcryptand][US((Ad,MeArO)3tacn)] complexes in order to better understand the nature of the U-S bonds and the possible involvement of the f-orbitals. The structural parameters and DFT studies of these uranium terminal hydrosulfide and sulfide complexes will be compared, in the following sections, to the analogous tetrasiloxide systems.

## III.2.2.3 Synthesis of tetrasiloxide U(IV) sulfide complexes

### *III.2.2.3.1 Reactivity with $S_8$ as sulfur donor agent*

Proton NMR studies show that the reaction of 0.125eq of $S_8$ with the U,K complex $[U(OSi(OtBu)_3)_4K]$ in toluene affords a mixture of products. Among these multiple products, few crystals of a dimeric U(IV) persulfide complex $[U(S_2)(OSi(OtBu)_3)_4K_2]_2$, **14** were isolated. Complex **14**.tol crystallizes in the orthorombic Pbca space group as a dimer. The solid state structure presented in Figure III-9 shows that two $[U(S_2)(OSi(OtBu)_3)_4K]$ moieties

are bridged by two potassium cations capping the terminal persulfide ligands to yield a dimer. Two potassium cations and the two terminal persulfides form a $S_2KS_2K$ diamond core around the inversion centre. The second potassium ion of the asymmetric unit is located in an $O_6$ coordination pocket formed by three bidentate siloxide ligands. The S1-S2 distance of 2.1047(18) Å is slightly elongated compared to that found in previously reported U(IV) terminal persulfide complexes (2.075(3)-2.082(1) Å)[191, 259] but is similar to the S-S bond lengths found in the K-capped terminal persulfide complexes $[K18c6][U(S_2)(N(SiMe_3)_2)_3]$ and $[K(Et_2O)_2][U(S_2)(N(SiMe_3)_2)_3]$ (2.160(7) and 2.1031(7) Å respectively).[188, 260] The U1-S1 and U1-S2 bond lengths of 2.7836(12) and 2.7526(13) respectively are in the range of U-S distances in U(IV) persulfide complexes (2.589(4)-2.9228(15) Å).[186-188, 191, 259-261] The average U-O bond length of 2.22(2) Å falls in the range of U-O bond distances reported for U(IV) siloxide complexes (2.11(5)-2.23(1)).[7, 100, 250, 262]

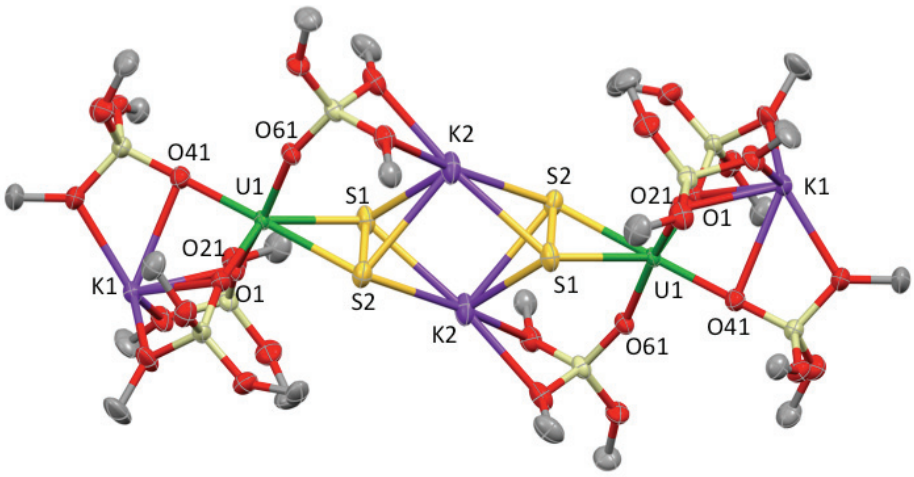


**Figure III-9: Solid state structure of $[U(S_2)(OSi(OtBu)_3)_4K_2]_2$.tol, 14.tol (50% ellipsoids). Methyl groups and solvent molecules are omitted for clarity.**

In order to optimize the synthesis of complex **14**, the U,K complex $[U(OSi(OtBu)_3)_4K]$ was reacted with the stoichiometric amounts of $S_8$ (0.25eq) in toluene. Unfortunately, the $^1$H NMR spectrum of the crude mixture shows multiple resonances in agreement with the presence of multiple products. After removal of the volatiles, and washing of the obtained residue with hexane, the $^1$H NMR spectrum of this solid in tol-$d_8$ shows a resonance at 0.44 ppm as the main signal. Crystals suitable for X-ray diffraction of a dimeric U(IV) disulfide- trisulfide complex $[\{U(OSi(OtBu)_3)_3\}_2(\mu\text{-}S_2)(\mu\text{-}S_3)K]$.tol, **15**.tol were obtained from the crude mixture at 233K. The **15**.tol complex crystallizes in the Monoclinic P

$2_1/n$ space group as a dimer. The solid state structure shown in Figure III-10 features two $[U(OSi(OtBu)_3)_3K]$ moieties bridged by disordered $S_3^{2-}$ and $S_2^{2-}$ ligands (occupancy factor of 0.183(5) and 0.817(5) respectively). The potassium ion of the asymmetric unit is located in an $O_6$ coordination pocket formed by three siloxide ligands. The S1-S2 bond length of the persulfide ligand is 2.131(3) Å which is in the range of those reported for persulfide-bridged uranium complexes (2.072(6)-2.1051(19) Å).[186, 187, 261] The S-S bond lengths in the $S_3^{2-}$ ligand are very dissymmetric with a S1B-S3B distance of 2.046(14) Å which is similar to the S-S distances in the only reported example of uranium trisulfide complex $[K18c6][U(S_3)(N(SiMe_3)_2)_3]$[260] and a shorter S2B-S3B distance of 1.666(16) Å. The average U-S distances for the $S_2^{2-}$ ligand (2.83(6) Å) and for the $S_3^{2-}$ ligand (2.93(7) Å) are in the range of U-S bond lengths reported for U(IV) disulfide complexes and slightly longer than those of U(IV) trisulfide complex $[K18c6][U(S_3)(N(SiMe_3)_2)_3]$ (2.760(1)-2.835(1) Å). We also note that each uranium centre has lost one siloxide ligand and the average U-O distance of 2.178(6) Å is similar to previously reported U-O bonds in U(IV) siloxide complexes.

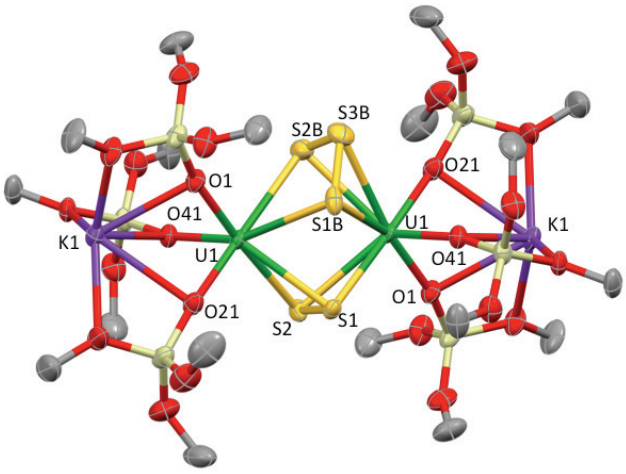


**Figure III-10: Solid state structure of $[\{U(OSi(OtBu)_3)_3\}_2(\mu\text{-}S_2)(\mu\text{-}S_3)K]$.tol, 15.tol (50% ellipsoids). Methyl groups, disorder and solvent molecules are omitted for clarity.**

These results show that the reaction of the uranium tetrasiloxide complex with $S_8$ leads to multiple products. This is probably due, in part, to the low solubility of $S_8$ that renders difficult the control of the reaction stoichiometry. Therefore we have investigated $Ph_3PS$ as soluble sulfur transfer agent.

### *III.2.2.3.2 $Ph_3PS$ as sulfur donor agent*

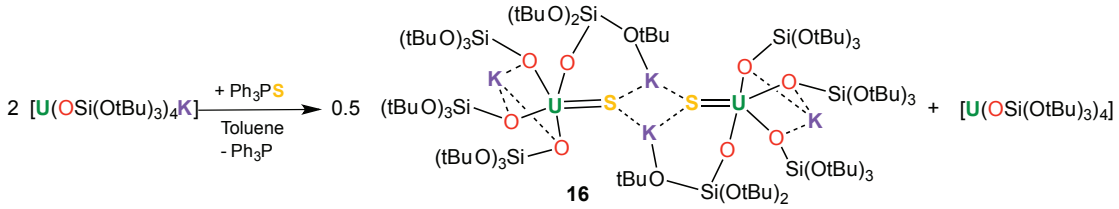


**Scheme III-7: Synthesis of the U(IV) sulfide complex $[US(OSi(OtBu)_3)_4K_2]_2$, 16.**

The addition of 0.5 eq. or 1eq of $Ph_3PS$ to $[U(OSi(OtBu)_3)_4K]$ leads, as confirmed by $^1H$ NMR spectroscopy, to the formation of the same uranium species (and unreacted $Ph_3PS$ in the case of addition of 1eq).The K-capped U(IV) sulfide complex $[US(OSi(OtBu)_3)_4K_2]_2$, **16** was obtained by the addition of 0.5eq of $Ph_3PS$ to a brown solution of $[U(OSi(OtBu)_3)_4K]$ in toluene. Green crystals of the K-capped U(IV) sulfide complex, **16**.tol were obtained from the toluene crude mixture at room temperature with a yield up to 62%. In both cases (addition of 1 or 0.5eq of $Ph_3PS$), the $^1H$ NMR spectrum of the crude reaction mixture reveals the concomitant formation of $[U(OSi(OtBu)_3)_4]$. Indeed, since U(III) complexes favour one-electron oxidations, two equivalents of the U(III) siloxide complex $[U(OSi(OtBu)_3)_4K]$ react with one equivalent of $Ph_3PS$. One complex is oxidized to the stable U(IV) complex, $[U(OSi(OtBu)_3)_4]$, whereas the second equivalent reacts with the sulfur transfer agent, generating 0.5eq of complex **16** like shown in Scheme III-7.

Complex **16**.tol crystallized as a dimer in the centrosymmetric, triclinic space group, P-1. The solid-state structure of complex **16** (Figure III-11) shows that two $[US(OSi(OtBu)_3)_4K_2]$ moieties are bridged by two potassium cations capping the sulfides to yield a dimer. Two potassium cations (each one also bound to two OtBu groups) and the two sulfides form an SKSK diamond core around the inversion centre. The second potassium ion of the asymmetric unit is located in an $O_6$ coordination pocket formed by three siloxide ligands.

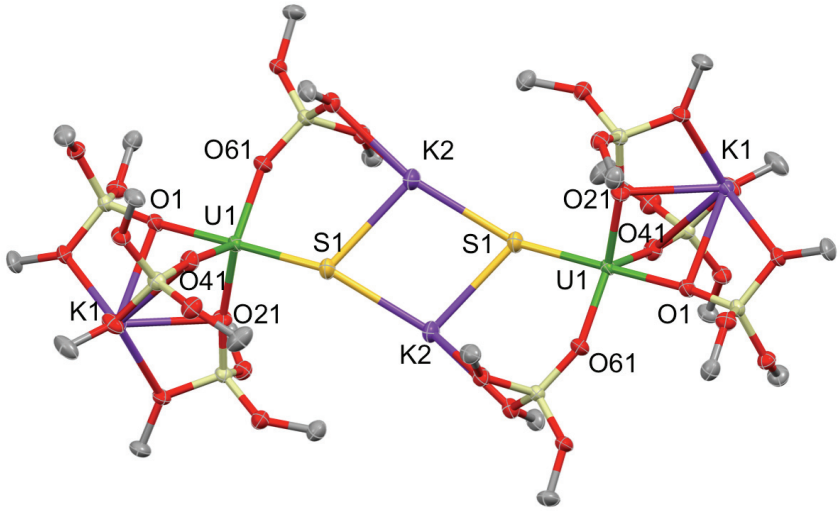


**Figure III-11: Solid state structure of $[US(OSi(OtBu)_3)_4K_2]_2$.tol, 16.tol (50% ellipsoids). Methyl groups and solvent molecules are omitted for clarity.**

The pentacoordinated uranium centre is ligated by four oxygen atoms of the siloxide ligands and one sulfide. The coordination geometry can best be described as distorted trigonal bipyramidal. The U-S bond length (2.5440(8) Å) is significantly longer than those found in the previously reported sodium or potassium capped U(IV) sulfide complexes (2.4805(5)–2.4463(6) Å),[179, 192] but closer from the U-S bond length of the potassium capped complex [{US(($^{Ad,Me}$ArO)$_3$tacn)}{Kdibenzo18c6}] (2.507(1) Å).[257] This is probably due to steric hindrance provided by the four siloxide ligands. The S1-K2 bond length of 3.0455(12) Å is comparable to those found in the U(IV) complexes [K18c6][US(N(SiMe$_3$)$_2$)$_3$] (3.0684(8) Å and 3.1551(8) Å)[179] and [{US(($^{Ad,Me}$ArO)$_3$tacn)}{Kdibenzo18c6}] (3.136(1) Å),[257] in which the sulfide is capped by the $[K18c6]^+$ and the $[Kdibenzo18c6]^+$ cations respectively. The average U-$O_{siloxide}$ bond length (2.22(1) Å) falls in the range of U-O bond lengths reported for U(IV) siloxide complexes. The $^1$H NMR spectrum of crystals of **16** in tol-$d_8$ features a very broad signal from 3 to -1 ppm which suggests fluxional binding in solution of the siloxide ligands to the potassium cations. Low temperature NMR studies (Figure III-12) reveal the appearance of several signals but the spectra are not fully resolved and complex **16** is poorly soluble in toluene at low temperature.

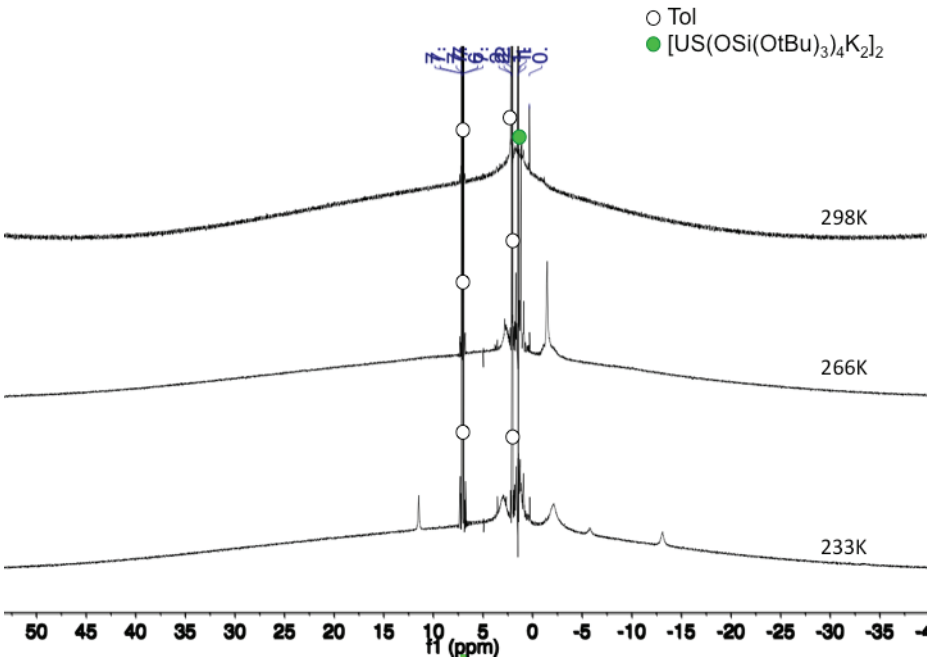


**Figure III-12: Variable temperature $^{1}$H NMR spectra (400 MHz, tol-$d_8$) of $[US(OSi(OtBu)_3)_4K_2]_2$, 16.**

The complex **16** is stable in solid state for weeks but it slowly decomposes in toluene at room temperature. $^{1}$H NMR studies of a toluene solution of **16** over time show the increase of $[U(OSi(OtBu)_3)_4]$, $KOSi(OtBu)_3$ and unidentified signals.

In order to isolate an uncapped terminal sulfide and gain insight in the potassium role in the stability of sulfide complexes, complex **16** was reacted with 18c6. The addition of 1eq of 18c6 to a toluene solution of complex **16** leads to the formation of $[\{US(OSi(OtBu)_3)_4K_2\}_2(\mu\text{-}18c6)]$, **16** which was isolated from the toluene crude mixture at -40°C. **17**.tol crystallizes in the centrosymmetric, monoclinic space group, $P2_1/n$. In the structure of **17**, a 18c6 bridges two $[US(OSi(OtBu)_3)_4K_2]$ units to yield a dimer with the inversion centre located in the middle of the crown ether (Figure III-13). The coordination environment of the U(IV) ion in **17** is very similar to that found in **16**. In contrast, the $S_2K_2$ core present in the structure of **16** is disrupted by the presence of the bridging 18c6. Each potassium cation capping the sulfides in **17** is also bound to two OtBu groups from a siloxide ligand and to four oxygen atoms of the bridging crown ether. Thus, the crown ether is coordinated to two different potassium cations, and adopts a non-planar wave shape

conformation. The U-S distance (2.534(2) Å) in **17** is similar to that found in complex **16**, indicating that the presence of crown ether coordinated to the potassium cation does not significantly affect the U-S bonding interaction. The S1-K2 bond length (3.128(3) Å) in **17** is slightly elongated compared to **16** because of the presence of the crown ether.

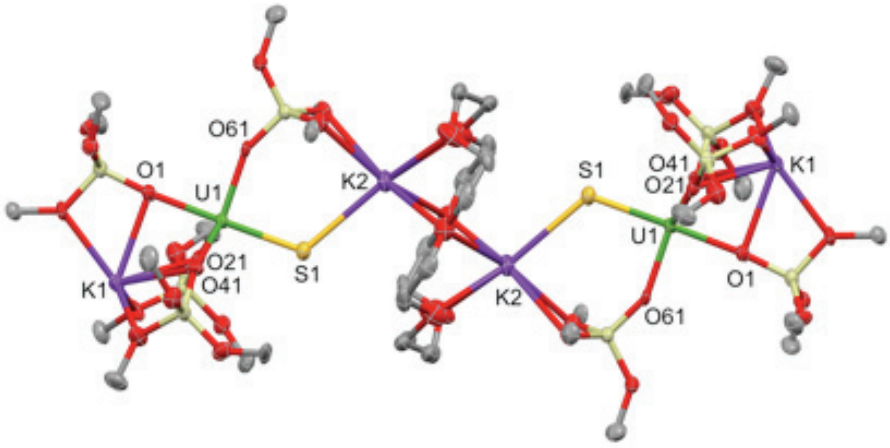


**Figure III-13: Solid state structure of [{US(OSi(OtBu)$_3$)$_4$K$_2$}$_2$(μ-18c6)].tol, 17.tol (50% ellipsoids). Hydrogen atoms, methyl groups, disoreder and solvent molecules are omitted for clarity.**

The $^1$H NMR spectrum of crystals of [{US(OSi(OtBu)$_3$)$_4$K$_2$}$_2$(μ-18c6)] **17** in tol-d$_8$, reveals two signals for the siloxide ligands at -0.9 ppm and -10.3 ppm with an integration ratio of 3:1 respectively and no visible signal for the crown ether. This is in agreement with a $C_3$ symmetry of the complex in solution and a labile coordination of the 18c6. The fluxional binding of the potassium cations would leads to two different chemical environments for the siloxide in trans of the sulfide ligand and for those in the equatorial plane explaining the 3:1 ratio. The addition of an excess of 18c6 does not lead to a more symmetric species in solution but only to an increasingly broad peak for the crown ether signal, as shown in Figure III-14, in agreement with a labile coordination of 18c6.

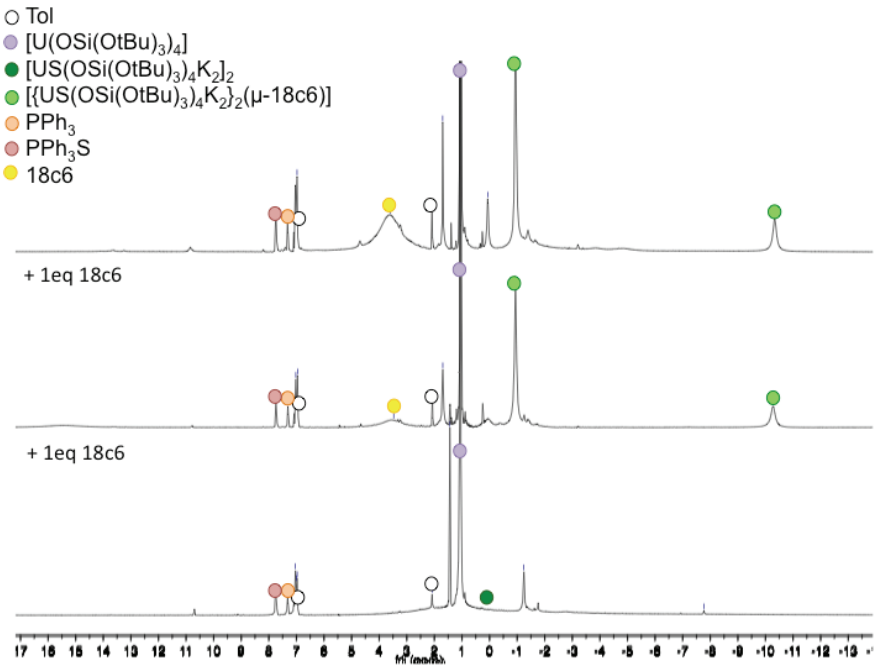


**Figure III-14: $^{1}$H NMR spectrum (400 MHz, tol-$d_8$, 298 K) of the 1:1 reaction mixture of $[U(OSi(OtBu)_3)_4K]$ and $Ph_3PS$ (bottom), after addition of 1eq of 18c6 per U to the crude mixture (middle) and after another addition of 1eq of 18c6 per U.**

The complex **17** can also be obtained by addition of 0.5 or 1eq of $Ph_3PS$ to the U(III) complex $[U(OSi(OtBu)_3)_4][K18c6]$ in toluene. In both reactions, the addition of 18c6 to complex **16** or the reaction of $Ph_3PS$ with $[K18c6][U(OSi(OtBu)_3)_4]$, the 18c6 crown ether is not able to prevent the capping of the sulfide by the potassium cation. Therefore we decided to use cryptand in order to better encapsulate the potassium ion.

The uncapped terminal U(IV) sulfide complex $[Kcryptand][US(OSi(OtBu)_3)_4K]$, **18**, was obtained by addition of 1eq of cryptand per U atom to $[US(OSi(OtBu)_3)_4K_2]_2$, **16**, in toluene (Scheme III-8).

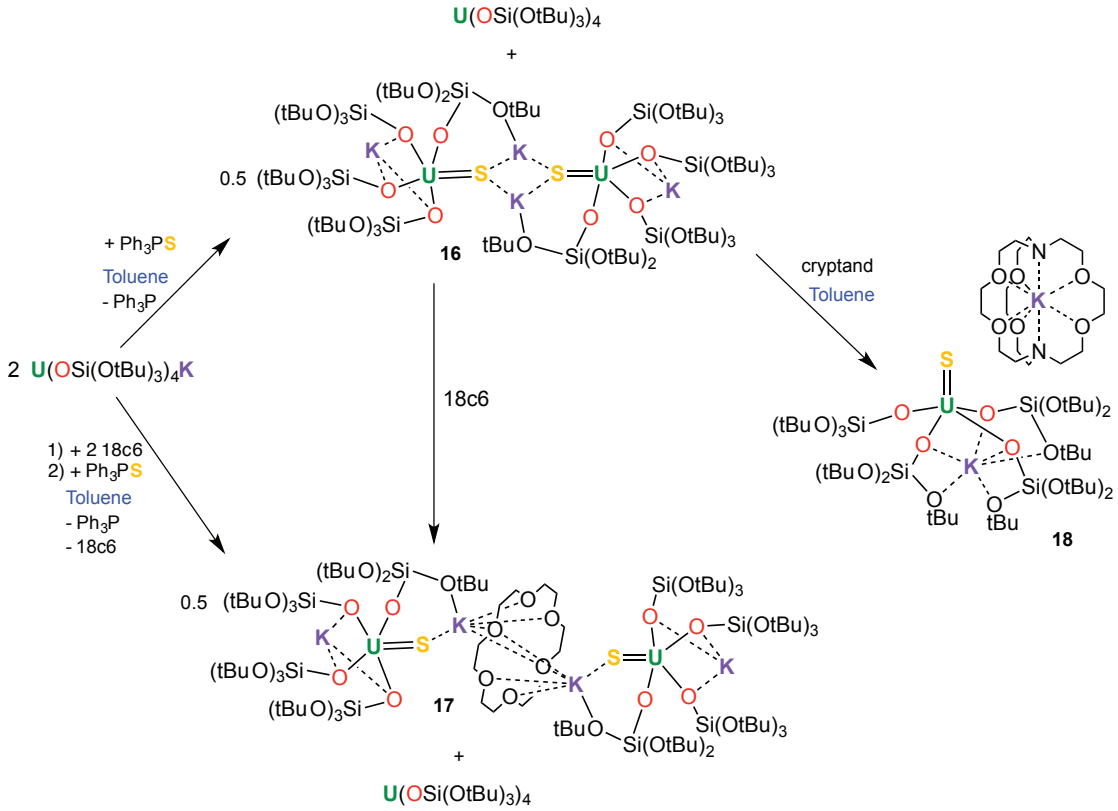


**Scheme III-8: Syntheses of the U(IV) sulfide complexes $[US(OSi(OtBu)_3)_4K_2]_2$ 16, $[\{US(OSi(OtBu)_3)_4K_2\}_2(\mu\text{-}18c6)]$ 17, and [Kcryptand][$US(OSi(OtBu)_3)_4K$] 18.**

The complex **18** crystallizes from hexane in 74% yield. Complex **18**.hex crystallized in the centrosymmetric triclinic space group, P-1, as a separated ion pair, consisting of the $[Kcryptand]^+$ cation and the $[US(OSi(OtBu)_3)_4K]^-$ anion (Figure III-15). In **18**, the pentacoordinated uranium ion is ligated by four siloxide ligands and a terminal sulfide, giving a distorted trigonal bipyramidal coordination geometry. One potassium atom remains encapsulated in the $O_6$ pocket made by three bridging siloxide ligands. The U-S bond length in **18** (2.5220(14) Å) is comparable to the U-S bond distance in complex **16** (2.5440(8) Å). This indicates that potassium binding and dimer formation in **16** only lead to a slight lengthening of the U-S bond. The U-O bond length is 2.197(4) Å for the terminal siloxide oxygen, while the average for the three UK-bridging siloxide ligands is 2.26(2) Å, which is in the range of previously reported $U\text{-}O_{siloxide}$ bond lengths.

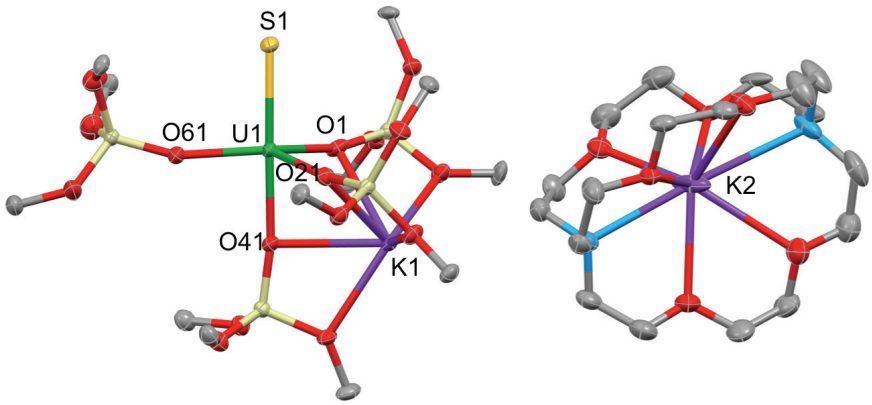


**Figure III-15: Solid state structure of [Kcryptand][US(OSi(OtBu)$_3$)$_4$K].hexane, 18.hex (50% ellipsoids). Hydrogen atoms, methyl groups, disorder and solvent molecule are omitted for clarity.**

The $^1$H NMR spectrum of crystals of **18** in tol-d$_8$ reveals two signals for the siloxide ligands at -0.5 ppm and -10.6 ppm with an integration ratio of 3:1 respectively and three paramagnetically shifted signals for the cryptand (13.1, 12.9 and 11.8 ppm). The 3:1 ratio for the siloxide ligands is in agreement with a $C_3$ symmetry of the complex in solution due to a fluxional binding of the potassium cation leading to two different chemical environments for the siloxide in trans of the sulfide ligand and for those in the equatorial plane. The important shift of the cryptand signals could be due to an interaction in solution of the [Kcryptand]$^+$ cation with the terminal sulfide ligand as already observed by Liddle and coworkers for the phosphinidene complex [U(Tren$^{TIPS}$)(PH)(Kcryptand)].[263]

Proton NMR studies show that the uncapped terminal sulfide complex **18** is stable in solid state at room temperature for weeks but slowly decomposes in solution. The $^1$H NMR spectra in Figure III-16 show the evolution of **18** in toluene and reveal that 50% of the complex decomposed in 1 month.

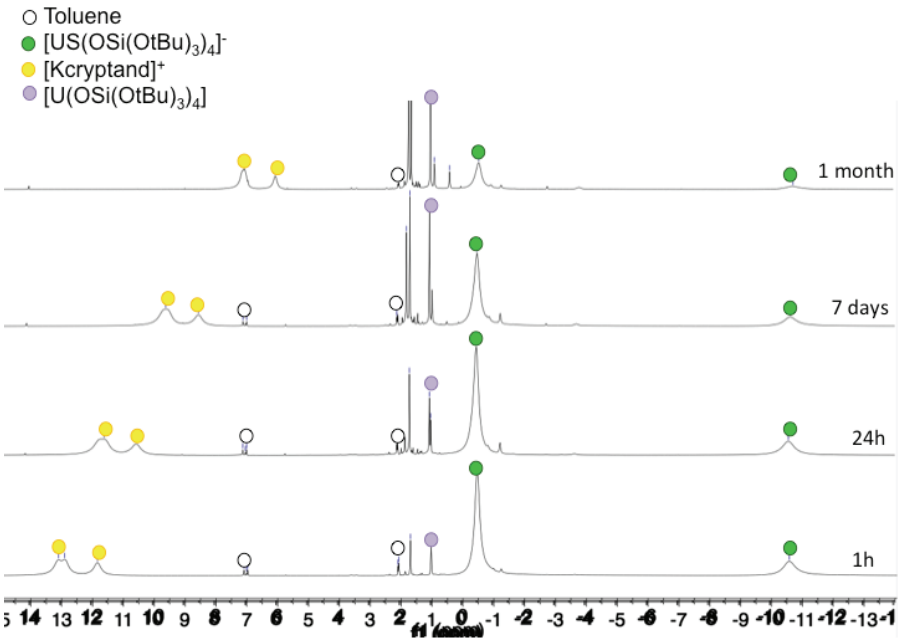


**Figure III-16: $^{1}$H NMR spectrum (400 MHz, tol-$d_8$, 298K) after addition of 1eq of cryptand per U atom to $[US(OSi(OtBu)_3)_4K_2]_2$, 16 in anhydrous tol-$d_8$ and evolution over time.**

The decomposition of complex **18** is similar in THF-$d_8$ leading to the appearance on the $^{1}$H NMR spectrum of the U(IV) complex $[U(OSi(OtBu)_3)_4]$ signal and several other decomposition product signals. Brown crystals of the U(IV)-U(IV) complex $[Kcryptand][U_2(\mu\text{-}S_3)(OSi(OtBu)_3)_6K_3]$, **19**, were obtained from a THF/hexane mixture of complex **18** at -40°C allowing us to identify one of the decomposition products of **18** in THF. Complex **19** crystallizes in the orthorhombic space group, $P2_12_12$, as an ion pair consisting of the $[U_2(\mu\text{-}S)_3(OSi(OtBu)_3)_6K_3]^-$ anion and the $[Kcryptand]^+$ cation. In the $[U_2(\mu\text{-}S)_3(OSi(OtBu)_3)_6K_3]^-$ anion, three $S^{2-}$ anions bridge the two uranium atoms. Each U(IV) ion is six-coordinate by three oxygen atoms from three siloxide ligands, and three sulfide anions in a distorted octahedral fashion. The average value of the U-S bond lengths is 2.748(7) Å, which is in agreement with the values of U-S bond lengths found in reported sulfide-bridged di-uranium(IV) complexes.[185-188, 190, 256] The average U-O bond length (2.258(3) c) is in the range of reported bond lengths for siloxide compounds. The average value for the S-K bond lengths (3.053(4) Å) is similar to the S-K distance in complex **16** (3.0455(12) Å).

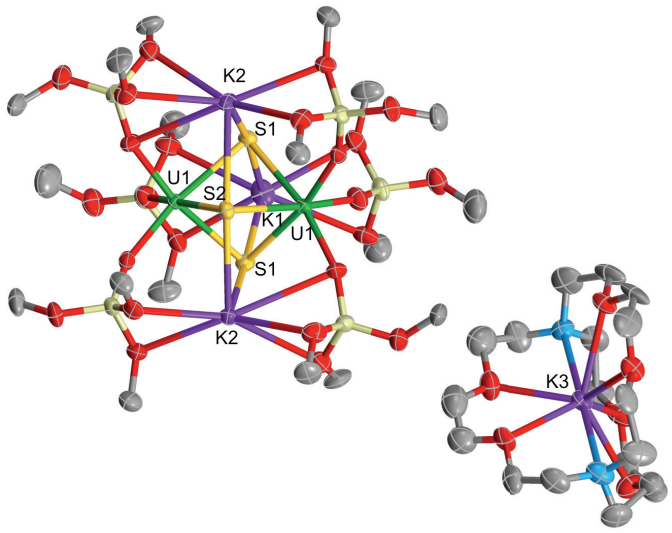


**Figure III-17: Solid state structure of [Kcryptand][$U_2(\mu\text{-}S_3)(OSi(OtBu)_3)_6K_3$], 19 (50% ellipsoids). Hydrogen atoms, methyl groups and disorder are omitted for clarity.**

The structure of complex **19** shows that the decomposition process leads to the loss of one siloxide ligand per U atom and to a sulfide bridged di-uranium(IV) species. We also remark a sulfide redistribution with a U:S ratio of 2:3 instead of 1:1 in complexes **16**, **17** and **18** which requires the presence of other decomposition products. The $^1$H NMR spectrum, performed after 7 months of decomposition, of complex **18** in THF-$d_8$ and the addition of naphthalene as internal standard revealed a 20% conversion rate of **18** in complex **19**. Unfortunately, the other decomposition products remained unidentified.

Interestingly and in contrast to the complex [{$US(OSi(OtBu)_3)_4K_2$}$_2$(μ-18c6)] **17**, the complex [Kcryptand][$US(OSi(OtBu)_3)_4K$] **18** cannot be obtained by reaction of the corresponding U(III) tetrasiloxide starting complex [Kcryptand][$U(OSi(OtBu)_3)_4$] with $Ph_3PS$. This observation leads to question the role of the potassium cation in the S-transfer reaction and a possible cooperative effect between the uranium and potassium atoms.

## III.2.2.4 The role of the potassium cation in the U(III) siloxide reactivity

As summarized in Scheme III-9, the reactivity of the U(III) starting material $[U(OSi(OtBu)_3)_4K]$ with $Ph_3PS$ is very different depending on the presence of 18c6 or cryptand and on the solvent of the reaction.

The heterobimetallic $[U(OSi(OtBu)_3)_4K]$ complex, fully soluble in THF and toluene, reacts with $Ph_3PS$ in both solvents. When $[U(OSi(OtBu)_3)_4K]$ is reacted with 1eq of 18c6 to form $[K18c6][U(OSi(OtBu)_3)_4]$, the latter reacts with $Ph_3PS$ only in toluene. Finally, when $[U(OSi(OtBu)_3)_4K]$ is pre-treated with 1eq of cryptand to form $[Kcryptand][U(OSi(OtBu)_3)_4]$ no reaction is observed neither in THF nor in toluene. Brown crystals of the U(III) complex $[Kcryptand][U(OSi(OtBu)_3)_4]$, **20**, were obtained by slow diffusion of hexane into a THF solution mixture of $[U(OSi(OtBu)_3)_4K]$ and 1eq of cryptand. Its solid state structure confirms the separated ion pair character ($[U(OSi(OtBu)_3)_4]^-$ anion and $[Kcryptand]^+$ cation) of this compound. Two $[Kcryptand][U(OSi(OtBu)_3)_4]$ complexes crystallize in the asymmetric unit and the average U-O bond lengths in both complexes (2.20(2) and 2.208(5) Å) are in agreement with U-O distances in previously reported U(III) siloxide complexes. Similarly to $[U(OSi(OtBu)_3)_4K]$ and $[K18c6][U(OSi(OtBu)_3)_4]$, the uranium centre is tetracoordinated in a distorted tretrahedral geometry. It is to note that the U(III) complex $[Kcryptand][U(OSi(OtBu)_3)_4]$ is fully soluble in THF but insoluble in toluene.

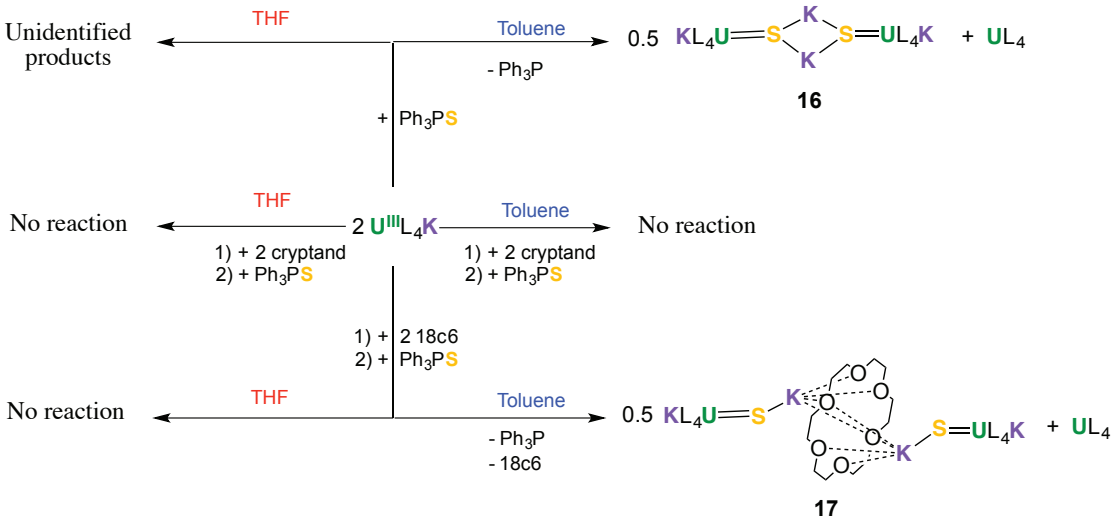


**Scheme III-9: Reactivity of the U(III) complex $[U(OSi(OtBu)_3)_4K]$ with $Ph_3PS$ in the absence and presence of 18c6 and cryptand in THF and toluene.**

Such differences in reactivity clearly underline the crucial role of the potassium cation in this S-transfer reaction. In $[U(OSi(OtBu)_3)_4K]$, the potassium ion is bound to the siloxide ligands in toluene and nothing can prevent its interaction with the U(III) complex even in THF, a more dissociating solvent. Indeed we observe a reaction of $[U(OSi(OtBu)_3)_4K]$ in both solvents. After the addition of 18c6 or cryptand, the potassium is encapsulated in the crown ether and both complexes $[K18c6][U(OSi(OtBu)_3)_4]$ and $[Kcryptand][U(OSi(OtBu)_3)_4]$ exists as separated ion pairs in THF. In consequence the U/K cooperative effect is not possible and these U(III) complexes do no react with $Ph_3PS$ in THF. In toluene, the $[K18c6][U(OSi(OtBu)_3)_4]$ complex is partially soluble and the 18c6 crown ether may not fully prevent the coordination of the potassium in solution, that is probably why we observe a reaction of $[K18c6][U(OSi(OtBu)_3)_4]$ and $Ph_3PS$ in toluene. Concerning the absence of reactivity of $[Kcryptand][U(OSi(OtBu)_3)_4]$ with $Ph_3PS$ in toluene, the insolubility of the U(III) starting material renders delicate the interpretation. The absence of reaction could be due to the impossible U/K interaction because of the ion pair character of the $[Kcryptand][U(OSi(OtBu)_3)_4]$ complex even in toluene, but its insolubility in toluene could also prevents the reaction.

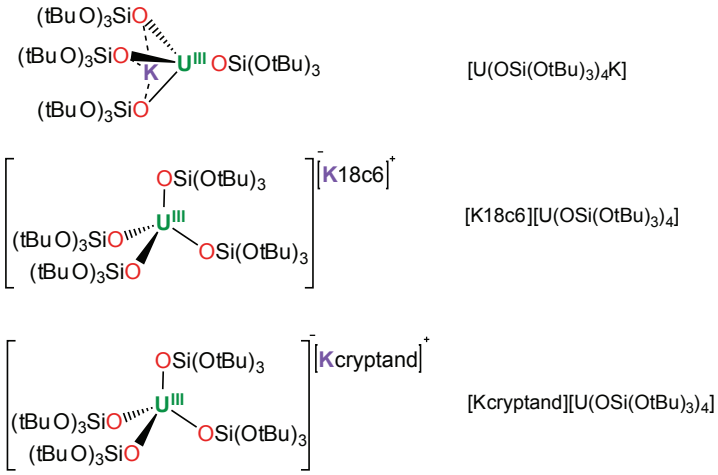


**Scheme III-10: Drawing of complexes $[U(OSi(OtBu)_3)_4K]$ (top), $[U(OSi(OtBu)_3)_4][K18c6]$ (middle) and $[U(OSi(OtBu)_3)_4][Kcryptand]$ (bottom).**

The steric effect, reducing the access to the uranium centre, could also be one explanation for these differences in reactivity. To compare the steric hindrance around the uranium atom of the three complexes $[U(OSi(OtBu)_3)_4K]$, $[K18c6][U(OSi(OtBu)_3)_4]$ and $[Kcryptand][U(OSi(OtBu)_3)_4]$ (Scheme III-10), we have compared their solid state structures.

To identify steric differences around the uranium centres, we compared the O-U-O angles of the three U(III) precursors in Table III-1.

**Table III-1: Comparison of the O-U-O angles (°) in $[U(OSi(OtBu)_3)_4K]$, $[K18c6][U(OSi(OtBu)_3)_4]$ and $[Kcryptand][U(OSi(OtBu)_3)_4]$**

| | $[U(OSi(OtBu)_3)_4K]$ | $[K18c6][U(OSi(OtBu)_3)_4]$ | $[Kcryptand][U(OSi(OtBu)_3)_4]$ | |
|---|---|---|---|---|
| | | | Complex 1 | Complex 2 |
| **O-U-O Angles (°)** | 127.2(3) | 111.3(3) | 112.0(4) | 113.4(3) |
| | 122.5(3) | 110.4(3) | 111.5(4) | 110.9(3) |
| | 115.0(3) | 110.1(3) | 110.6(3) | 110.4(3) |
| | 95.0(3) | 108.6(2) | 110.3(3) | 107.8(4) |
| | 94.9(3) | 108.4(2) | 107.8(4) | 107.1(3) |
| | 94.9(2) | 108.0(2) | 104.5(4) | 107.0(4) |

We observe a significant difference of the O-U-O angles between $[U(OSi(OtBu)_3)_4K]$ and the two other complexes in which the potassium is encapsulated in a crown ether. In $[K18c6][U(OSi(OtBu)_3)_4]$ and $[Kcryptand][U(OSi(OtBu)_3)_4]$ the four siloxide ligands form a weakly distorted tetrahedron with six similar angles and average values of 109(1)° for $[K18c6][U(OSi(OtBu)_3)_4]$ and 109(3)° for $[Kcryptand][U(OSi(OtBu)_3)_4]$. In $[U(OSi(OtBu)_3)_4K]$, the potassium cation coordinates three siloxide ligands and bring them in closer proximity leading to a highly distorted tetrahedral coordination geometry. The three angles between the K-bridging siloxides are similar (mean value of 94.91(7)°) and smaller than the angles with the terminal siloxide (127.2(3)°, 122.5(3)° and 115.0(3)°) leading to an average angle value of 108(15)° farer from the ideal value of 109.5° and with an important standard deviation. This is in agreement with a more accessible uranium centre in the U,K complex $[U(OSi(OtBu)_3)_4K]$ as shown in Figure III-18 and could be an explanation of the greater reactivity of this complex with $Ph_3PS$ in THF and toluene.

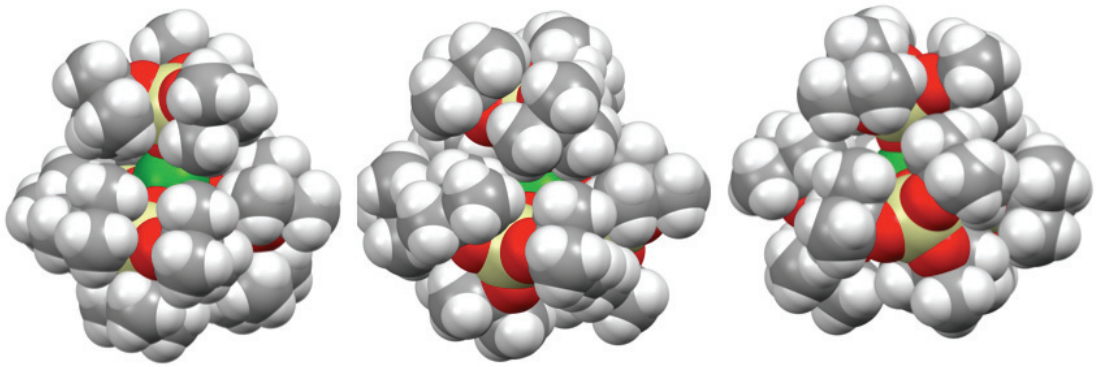


**Figure III-18: Spacefilling representation of $[U(OSi(OtBu)_3)_4K]$, $[K18c6][U(OSi(OtBu)_3)_4]$ and $[Kcryptand][U(OSi(OtBu)_3)_4]$. Solvent molecules and $[K18c6]^+$ and $[Kcryptand]^+$ cations are omitted for clarity.**

However, understanding if the formation of the terminal sulfide complex $[US(OSi(OtBu)_3)_4K_2]_2$ is mainly dominated by sterics or by the a cooperative effect of the potassium cation is not obvious. In theses systems, the steric bulk provided by the four siloxide ligands could prevent the formation of sulfide-bridging species but the coordination of the sulfur atom to the potassium could also reduce the nucleophilic character of the sulfur and render the formation of a bridging compound less favourable. Computational studied should help to identify the parameters governing this reactivity.

### III.2.2.5 Sulfur transfer reactions: reactivity with $S_8$, $CS_2$, $CO_2$

In order to assess if, despite the multiple character of the U-S bond, the transfer of the sulfur atom was possible, we studied the reactivity of the sulfide complex $[US(OSi(OtBu)_3)_4K_2]_2$, **16**, with different substrates. In the literature, it has been shown that disulfide-,[264] trithiocarbonate-[131] and monothiocarbonate-bridged[126] di-uranium(IV) complexes can be obtained by nucleophilic addition of elemental sulfur, $CS_2$ and $CO_2$ respectively onto sulfide-bridged di-uranium(IV) complexes. However, for previously reported terminal U(IV) sulfide, only the sulfur atom transfers to chalcogens (S or Se) has been investigated leading to the formation of the terminal dichalcogenide complexes $[K18c6][U(S_2)(N(SiMe_3)_3]$ or $[K18c6][U(SSe)(N(SiMe_3)_3]$ and the terminal trisulfide complex $[K18c6][U(S_3)(N(SiMe_3)_3]$. The added chalcogen atoms can be removed from the

dichalogenides or trisulfide complexes by addition of $Ph_3P$ or $Et_3P$ to restore the initial terminal U(IV) sulfide or disulfide complex.[260]

We have investigated the reactivity of the complex **16** with elemental sulfur in order to identify new routes to siloxide supported U(IV) persulfide complexes. The addition of 0.5 eq of $S_8$ to complex **16** results in immediate reaction with colour change from green to deep brown. The $^1$H NMR spectrum of the crude reaction mixture shows several resonances in agreement with the presence of multiple reaction products. Among these products were identified the signals of the free siloxide ligand and of the U(IV) complex $[U(OSi(OtBu)_3)_4]$. Brown crystals of the U(IV) disulfide-trisulfide complex $[\{U(OSi(OtBu)_3)_3\}_2(\mu\text{-}S_2)(\mu\text{-}S_3)K]$, **21**, were obtained from the toluene crude mixture solution at -40°C.

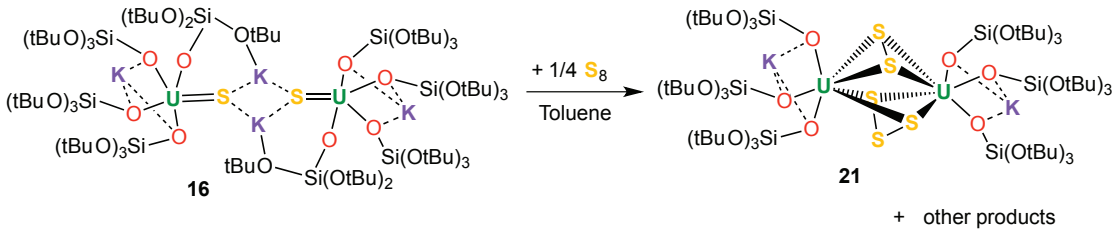


**Scheme III-11: Addition of 1eq of elemental sulfur per U atom to the terminal sulfide complex $[US(OSi(OtBu)_3)_4K_2]_2$, 16.**

The solid state structure of complex **21** is very similar to the one of complex **15** obtained by addition of $S_8$ to $[U(OSi(OtBu)_3)_4K]$ in toluene. However, the structure of **21** shows the presence of two complexes in the unit cell and the occupancy factors of the bridging disordered $S_3^{2-}$ and $S_2^{2-}$ ligands (0.451(6) and 0.549(6) respectively) are different from the one in the structure of **15** (0.183(5) and 0.817(5)). Moreover, in one of the complexes present in the asymmetric unit, the disorder is so high that the establishment of a model is much more difficult (ring of electronic density around the U-U axis). Interestingly the $^1$H NMR spectrum of complex **21** shows the presence of only one shift at 0.44 ppm previously attributed to complex **15**. This could be explained by the fluxional coordination in solution of the $S_3^{2-}$ and $S_2^{2-}$ ligands to the uranium centres. A mixture of complexes U-$(\mu\text{-}S_3)_2$-U, U-$(\mu\text{-}S_2)_2$-U and U-$(\mu\text{-}S_3)(\mu\text{-}S_2)$-U is probably present in solution and crystallization process could lead to solid state structures with different product ratios and thus different occupancy factors of $S_3^{2-}$ and $S_2^{2-}$. We can conclude that the nucleophilic addition of sulfur does occur leading to disulfide and trisulfide bridged complexes.

Meyer et al. reported the reductive disproportionation of $CS_2$ by the U(III) complex $[U((^{Ad}ArO)_3N)(DME)]$ affording a bridged-thiocarbonate U(IV) complex in 20% yield.[130] They postulated that a bridging sulfide U(IV) compound is an intermediate in the reaction and to gain insight in this question, they independently synthesised the sulfide-bridged $[\{U((^{Ad}ArO)_3N)\}_2(\mu\text{-}S)]$ complex and added $CS_2$. The bridged-thiocarbonate was obtained in high yield suggesting the veracity of their hypothesis.[131] In light of this antecedent result we have investigated the possibility of obtaining terminal thiocarbonate species from the reaction of the terminal U(IV) sulfide with $CS_2$ or $CO_2$. The addition of 1eq of $^{13}CS_2$ per U atom to complex **16** in toluene leads to a rapid colour change from light green to light yellow. The $^1H$ NMR spectrum of the reaction mixture immediately after the $^{13}CS_2$ addition shows the signals of a labile species with two very broad peaks at 11.1 and -2.8 ppm with an integration ratio of 1:3 respectively. The obtained compound is unstable and the $^1H$ NMR spectra of the mixture over time show the disappearance of the two broad peaks and the increase in intensity of the $[U(OSi(OtBu)_3)_4]$ signal. When toluene is removed and DMSO-$d_6$ added, the $^{13}C$ NMR spectrum shows only the signal of free thiocarbonate at 267 ppm[233] confirming the nucleophilic addition of $^{13}CS_2$ on the terminal sulfide ligand (Scheme III-12).

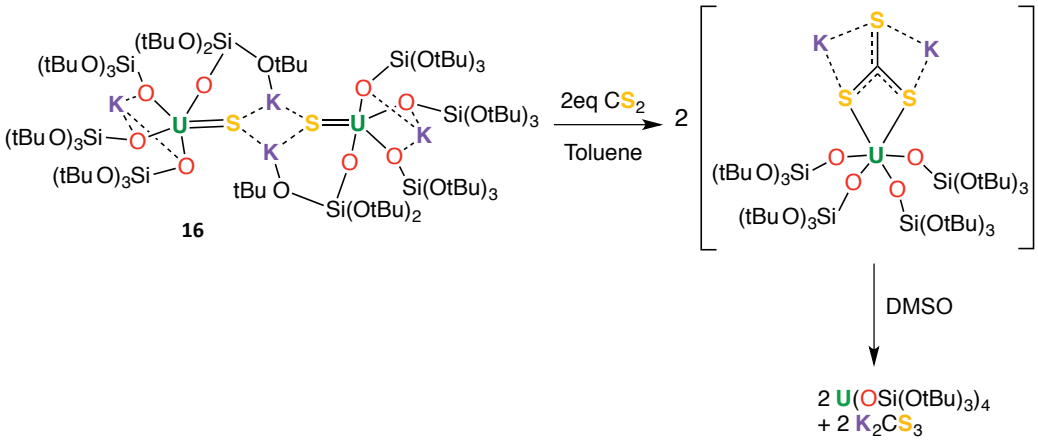


**Scheme III-12: Insertion of $CS_2$ into the terminal sulfide complex 16.**

This indicates that the likely formed terminal thiocarbonate U(IV) complex is unstable and quickly dissociates in toluene to yield $[U(OSi(OtBu)_3)_4]$ and $K_2CS_3$. Unfortunately all attempts to isolate the hypothetical $[U(CS_3)(OSi(OtBu)_3)_4K_2]$ complex were unsuccessful. The same reactivity was observed after the addition of 1eq of $^{13}CS_2$ to [Kcryptand][US(OSi(OtBu)$_3$)$_4$K], **18**.

When an excess of $^{13}CO_2$ is added to complex **16** in deuterated toluene, the solution turns immediately from light green to light pink and the $^{1}H$ NMR spectrum of the reaction mixture is very similar to the one obtained after $CS_2$ addition on complex **16** with two broad peaks at 8.7 and -2.9 ppm with an integration ratio of 1:3 respectively as shown in Figure III-19. Unfortunately, once again the obtained species is unstable and decomposes quickly in toluene. The $^{13}C$ NMR spectrum of the crude reaction mixture in toluene shows the increase in intensity of a peak at 153.5 ppm that was attributed to free COS.[265]

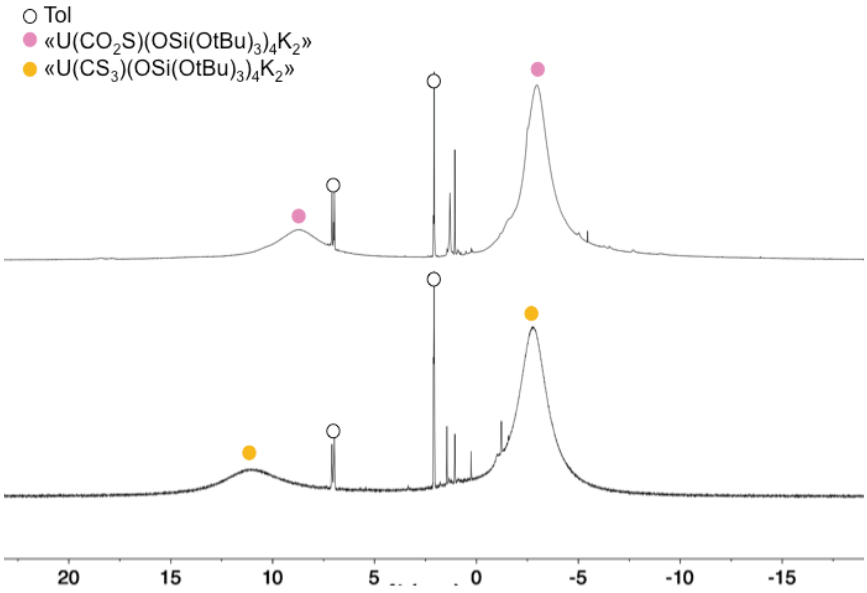


**Figure III-19: $^{1}H$ NMR spectra (400MHz, tol-$d_8$, 298K) of the crude mixture right after addition of 1eq of $^{13}CS_2$ per U atom to 16 (bottom) and after addition of an excess of $^{13}CO_2$ to 16.**

The release of COS could be a consequence of the decomposition of the hypothetical $[U(CO_2S)(OSi(OtBu)_3)_4K_2]$ complex. So far, the other decomposition products are unknown as the follow up of the crude mixture by $^{1}H$ NMR spectroscopy does not present any previously identified signal and attempts to isolate compounds from the decomposition mixture failed. Once again the same reactivity, with COS formation, was observed after the addition of an excess of $CO_2$ to complex **18**.

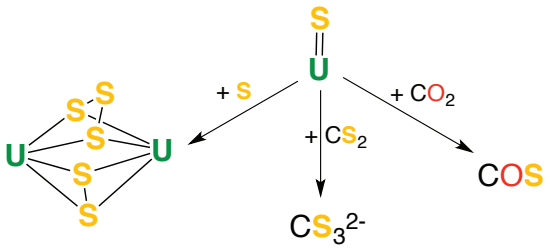


**Figure III-20: Reactivity of terminal U(IV) sulfide complexes.**

As summarized in Figure III-20, the nucleophilic additions of elemental sulfur, $CS_2$ and $CO_2$ on the terminal sulfide complexes occurred but, probably because of steric hindrance, the respectively obtained species present ligand loss and bridging event, dissociation or decomposition.

## III.2.2.6 Protonation of a terminal sulfide complex to obtain a terminal hydrosulfide one

The protonation of the terminal sulfide function, commonly used in transition metal chemistry to yield a terminal hydrosulfide complex,[266, 267] has not been investigated on uranium sulfide complexes. The only reported uranium hydrosulfide complex so far, was isolated by Meyer et al. via reduction of $H_2S$ by the tacn-based U(III) complex [U(($^{Ad}$ArO)$_3$N)(DME)].[258] We found that the addition of 1eq of PyHCl per U atom to a THF solution of complex **16** that has been pre-treated with 18c6 leads to the protonation of the sulfide function and to the formation of the hydrosulfide complex [{K18c6}{U(SH)(OSi(OtBu)$_3$)$_4$}], **22** (Scheme III-13).

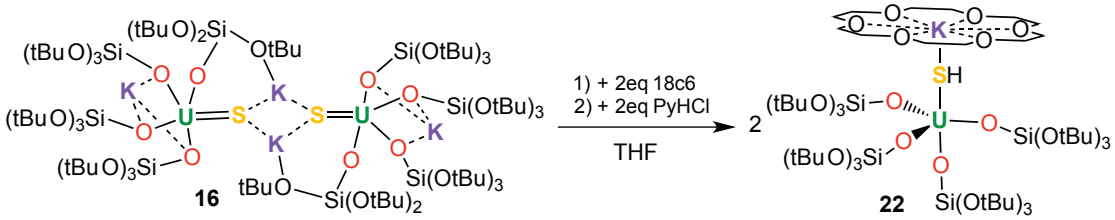


**Scheme III-13: Synthesis of the terminal hydrosulfide complex [{K18c6}{U(SH)(OSi(OtBu)$_3$)$_4$}], 22.**

Single crystals of complex **22**.tol were obtained from cooling down the filtered crude reaction mixture at -40°C. Complex **22**.tol crystallized in the non-centrosymmetric,

monoclinic space group, Cc (Figure III-21). The pentacoordinated uranium atom is ligated by four terminal siloxide ligands and one $SH^-$ moiety in a distorted trigonal bipyramidal geometry. The 18c6-encapsulated potassium counter-ion is bound to the sulfur atom with a S1-K1 bond length of 3.229(5) Å. The U1-S1 distance was measured to be 2.834(3) Å, which is much longer than the U-S bond distance in **18** (2.5220(14) Å), but is very similar to that found in the only other example of a mononuclear U(IV)-SH complex (2.797(1) Å).[258] The average $U\text{-}O_{siloxide}$ bond length (2.15(3) Å) is similar in length to that found for the terminal siloxide ligands in the terminal sulfide complex **18** (2.197(4) Å).

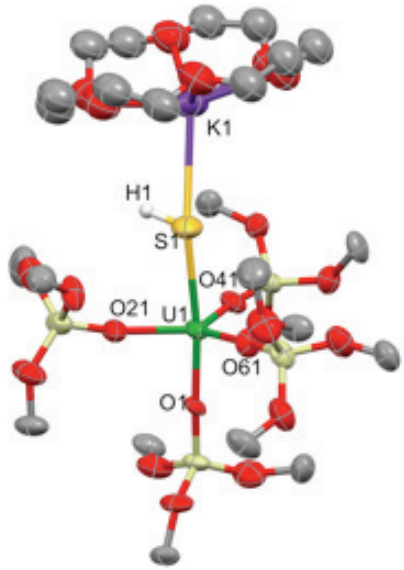


**Figure III-21: Solid state structure of [{K18c6}{U(SH)(OSi(OtBu)$_3$)$_4$}], 22 (50% ellipsoids). Hydrogen atoms (except the one of the hydrosulfide ligand), methyl groups and disorder are omitted for clarity.**

The $^1$H NMR spectrum of **22** present two signals at 3.1 and 0.7 ppm assigned to the crown ether and the four siloxide ligands respectively. A conversion of 53% was determined by $^1$H NMR spectroscopy using naphthalene as an internal standard. This relatively low yield could be explained by the low stability of complex **16** in the presence of pyridine released by the reaction. However, elimination of $H_2S$ to afford bridging sulfides by-products cannot be ruled out.

The complex **22** can also be obtained, similarly to the previously reported U(IV) hydrosulfide complex,[258] from the reduction of 1eq of $H_2S$ by the U(III) complex [K18c6][U(OSi(OtBu)$_3$)$_4$]. However the isolated yield and overall conversion (determined by $^1$H NMR spectroscopy using naphthalene as an internal standard) are much lower with 17% and 22% respectively. Attempts to increase the yield, using a sub-stoichiometric amount of

$H_2S$ or more diluted conditions to avoid a fast reaction with more than one equivalent of $H_2S$, failed. A dimeric side-product of this $H_2S$ reduction was isolated from toluene at -40°C. The X-ray structure of this by-product clearly shows the presence of two [U((OSi(OtBu)$_3$)$_3$K] moieties, bridged by three sulfur atoms (Figure III-22). The intermediate average value of the U-S distances (2.83(2) Å) falling in between the reported values for bridging $S^{2-}$ (2.59(1)–2.736(2) Å)[185, 256] and bridging $SH^-$ (2.877(1) - 2.964(1) Å)[258] moieties, suggests that two $SH^-$ and one $S^{2-}$ groups are bridging the U(IV) centres forming the [{U(OSi(OtBu)$_3$)$_3$}$_2$(μ-SH)$_2$(μ-S)] complex **23**. The bond valence sum calculation is also in agreement with the presence of two U(IV) ions. The hydrogen atoms of the $SH^-$ moieties are probably fluxional, and therefore very difficult to locate in the crystal structure.

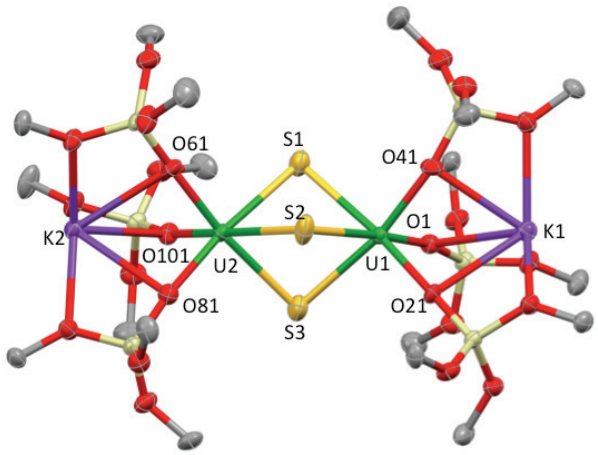


**Figure III-22: Solid state structure of [{U(OSi(OtBu)$_3$)$_3$}$_2$(μ-SH)$_2$(μ-S)].tol, 23.tol (50% ellipsoids). Methyl groups are omitted for clarity.**

The presence of this by-product in the crude indicates that fast reaction between the U(III) complex and more than 1eq of $H_2S$ occurs explaining the low yield and conversion observed in this reaction. This formation of polysulfide compounds via aggregation of hydrosulfide compounds is a well-known problem in mononuclear sulfide synthesis.[267] The protonation of the terminal sulfide ligand in complex **16** represents a better synthetic pathway leading to higher yield and avoiding the use of the very toxic $H_2S$ gas.

The obtention of terminal sulfide and terminal hydrosulfide complexes supported by siloxide ligands allow for the comparison of the structural data of the tacn-based terminal sulfide and terminal hydrosulfide complexes obtained by Pr. Meyer's group.

### III.2.2.7 Comparison of structural parameters tacn vs. siloxide system

The structural parameters for the terminal sulfide or hydrosulfide complexes in both tacn-based and siloxide systems are summarized in Table III-2 and Table III-3. We can observe that the U-S bond lengths in all the terminal sulfide complexes are similar and that no particular trend is visible when crown ether is present or not. Concerning the S-K bond distances we observe, as expected, an elongation of the bond length when the potassium is encapsulated in 18c6 or dibenzo18c6 crown ether. The U-SH distances in the terminal hydrosulfide complexes are comparable even if, in complex **22**, the potassium binds the $SH^-$ moiety.

**Table III-2: Selected bond distances for the terminal sulfide complexes complexes 16, 17, 18, [{US((Ad,Me ArO)3tacn)}{Kdibenzo18c6}] and [Kcryptand][US((Ad,Me ArO)3tacn)] (in Å).**

| | 16 | 17 | 18 | [{US((Ad,Me ArO)3tacn)}{Kdibenzo18c6}] | [Kcryptand][US((Ad,Me ArO)3tacn)] |
|---|---|---|---|---|---|
| **U-S** | 2.5440(8) | 2.534(2) | 2.5220(14) | 2.507(1) | 2.536(2) |
| **S-K** | 3.0455(12) | 3.128(3) | - | 3.136(1) | - |

**Table III-3: Selected bond distances for the terminal hydrosulfide complexes 22 and [U(SH)((Ad,Me ArO)3tacn)] (in Å).**

| | 22 | [U(SH)((Ad,Me ArO)3tacn)] |
|---|---|---|
| **U-SH** | 2.834(3) | 2.844(4) and 2.775(2) |
| **SH-K** | 3.229(5) | - |

With these structural data in mind, computational bonding analysis can be performed to gain insight in the nature of the U-S bonds in terminal sulfide and hydrosulfide complexes supported by both siloxide and tacn-based ligand systems.

## III.2.2.8 DFT studies

DFT calculations on these systems were carried out by the group of Pr. Maron. The geometrical optimizations of complexes **16**, **18** and **22** were performed to validate the theoretical protocol (the f-electrons of the U(IV) atoms are included in the valence shell: small core basis set). For complex **18** and **22**, the respective $[Kcryptand]^+$ and the $[K18c6]^+$ cation were excluded from the calculations and a negative charge was assigned on each overall complexes. The metrical parameters of the experimental X-ray data and those predicted by the calculated optimizations are in close agreement. In consequence, analyses of molecular orbital (MO) and of natural bond orbital (NBO) were performed and concluded to a triple bond character ($\sigma^2\pi^4$ configuration) for the U≡S bonds in the terminal sulfide complexes **16** and **18** with a bond order of 2.25 and 2.55 respectively. Moreover, in both cases, the two highest singly-occupied orbitals (in NBO analysis) present almost pure 5f character. Yet, interestingly, when the f-electrons of the U(IV) atoms are excluded from the valence shell (large core basis set), the bonding pictures for complexes **16** and **18** remain almost the same (Figure III-23). This result suggests that the triple-bond character is mainly due to U(IV) d orbitals involvement in the bonding rather 5f orbitals.

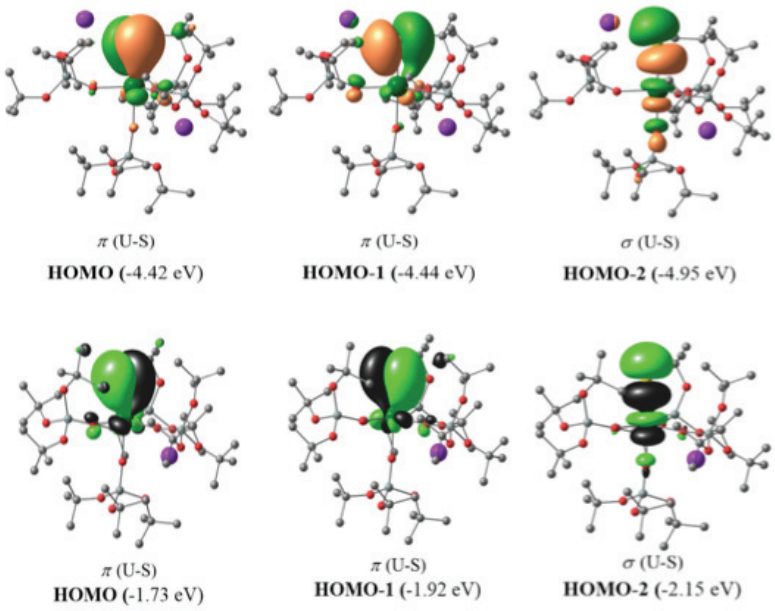


**Figure III-23: σ and π molecular orbitals calculated for the monomer unit of complex 16 (large core basis set) and complex 18 (small core basis set).**

Additionally, the similarity of the bonding pictures of complexes **16** and **18** indicates that the absence of the potassium cation near the sulfur atom in complex **18** does not affect the U≡S bond configuration. The group of Pr. Maron also computed the terminal U(IV) sulfide complexes supported by tacn-based ligand [{US(($^{Ad,Me}$ArO)$_3$tacn)}{Kdibenzo18c6}] and [Kcryptand][US(($^{Ad,Me}$ArO)$_3$tacn)]. Interestingly, the negligible effect of the potassium presence, the U≡S bond configuration and the U(IV) d orbitals involvement in bonding remain similar independently of the supporting ligand nature. This comparison suggests that the U≡S bond is not affected by the ligand field.

Concerning the hydrosulfide complexes, the computational analyses of complex **22** and [U(SH)(($^{Ad,Me}$ArO)$_3$tacn)] led to a different bond configuration. In complex **22**, the U=SH bond presents a double bond character ($\sigma^2\pi^2$ configuration) with a bond order of 1.39. However, MO and NBO analyses on [U(SH)(($^{Ad,Me}$ArO)$_3$tacn)] concluded to a single bond between U and S atoms with a bond order of 0.77. In both systems, the metal orbital has similar contribution of the uranium orbitals with 10% 7s, 40% 6d and 50% 5f for **22** and 12% 7s, 38% 6d and 50% 5f for [U(SH)(($^{Ad,Me}$ArO)$_3$tacn)]. In the previous section we also remarked that the U-SH distances obtained by X-ray data are comparable. Actually, the diminished degree of multiple bonding in the U-S bond of [U(SH)(($^{Ad,Me}$ArO)$_3$tacn)] can be explained by a greater interaction of the uranium centre with the N donor atoms of the tacn ligand than in [{US(($^{Ad,Me}$ArO)$_3$tacn)}{Kdibenzo18c6}] and [Kcryptand][US(($^{Ad,Me}$ArO)$_3$tacn)] (in agreement with the higher $U_{oop}$ of -0.282(3) and -0.268(4) Å in their X-ray structures). This results in a less available U orbital to overlap with the lone pairs of the S atom. This trans-effect was confirmed by the computation of the hypothetical complex [U(SH)($^{Ad,Me}$ArO)$_3$] (where the tacn-base is replaced by hydrogen atoms) that features a double bond character between the U(IV) (in a tetrahedral geometry) and the sulfur atom of the hydrosulfide function. In conclusion, contrary to what was observed for the terminal sulfide complexes, the ligand plays a bigger role on the multiple bonding character of the U-SH bond.

In order to gain insight in the nature of other uranium-chalcogen bonds, the group of Pr. Maron performed bonding analysis with the hypothetical terminal oxo-homologues of [{US(($^{Ad,Me}$ArO)$_3$tacn)}{Kdibenzo18c6}] and [Kcryptand][US(($^{Ad,Me}$ArO)$_3$tacn)]. A much more ionic U-O bonding is predicted which is in agreement with the observed trend in the $[U(E)(NSiMe_3)_2]^-$ (E=O, S, Se, Te) series recently reported by Hayton et al.[268] To confirm this

trend, on-going work focuses on the synthesis of the complete series of U(IV) terminal hydrochalcogenide and chalcogenide complexes with siloxide and tacn-based ligand systems.

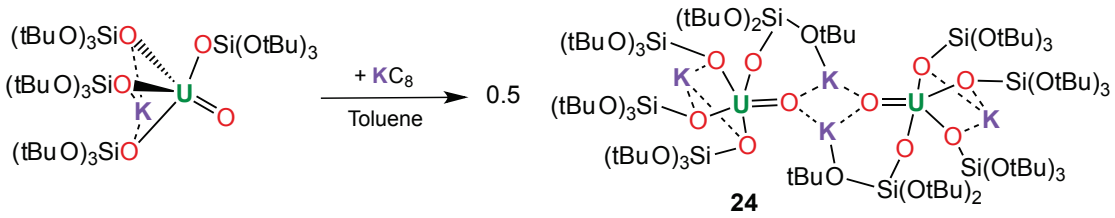


**Figure III-24: Synthesis of $[UO(OSi(OtBu)_3)_4K_2]_2$, 24.**

Preliminary studies toward the synthesis of the siloxide series $[UE(OSi(OtBu)_3)_4K_2]_2$ or [Kcryptand][$UE(OSi(OtBu)_3)_4K$] (E=O, S, Se, Te) leads to the isolation of the oxo-homologues of complex **16** : $[UO(OSi(OtBu)_3)_4K_2]_2$, **24**. Complex **24** was obtained by reduction with 1eq of $KC_8$ of the terminal U(V) oxide complex $[UO(OSi(OtBu)_3)_4K]$[7] in toluene (Figure III-24). Complex **24** crystallizes from toluene at -40°C. The X-ray structure finalization of complex **24** is on-going, nevertheless we can already observe that the structure is isomorphous with the structure of **16** and thus features two $[UO(OSi(OtBu)_3)_4K_2]$ moieties bridged by two potassium cations capping the oxides to form a dimer (Figure III-25). An OKOK diamond core is formed around an inversion centre with two potassium cations and the two oxides ligands. The second potassium ion of the asymmetric unit is located in an $O_6$ coordination pocket formed by three siloxide ligands.

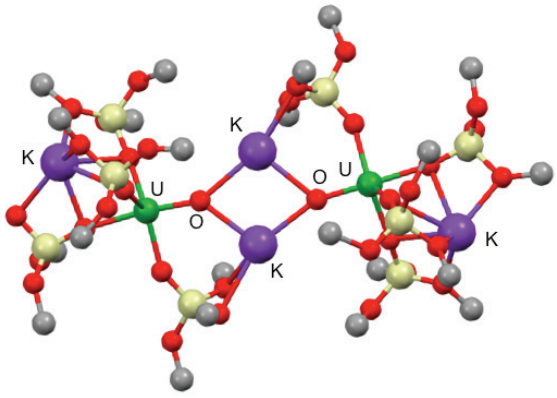


**Figure III-25: Solid state structure of $[UO(OSi(OtBu)_3)_4K_2]_2$, 24 (Ball and stick representation). Methyl groups and solvent molecules are omitted for clarity.**

The provisional average U-O distance (1.96(1) Å) is slightly elongated compared to previously reported U-O bond length in terminal mono-oxide U(IV) complexes (1.860(3)-1.890(5) Å)[171, 172, 177, 179] probably due to steric hindrance. A similar elongation was also observed for the U-S distance in complex **16**. Future works will focus on the optimization of the synthesis of complex **24**, on DFT calculations and on the syntheses of the entire chalcogen series. Further effort will also be directed toward the isolation of terminal chalcogenide complexes containing uranium in oxidation state higher than +IV. So far, attempts to oxidize the U(IV) sulfide complexes **16-18** in order to obtain terminal U(V) sulfide species only led to decomposition reactions. Electrochemistry measurements were performed on complex **16** (See appendices) to know if this oxidation state was reachable. However, the decomposition of **16** in THF renders difficult the attribution of the redox events observable on the cyclic-voltammograms.

We observed in this section III.2 that even if, once the terminal sulfide complexes formed, the binding of the potassium cation to the sulfide ligand does not affect the U-S bond configuration, the presence or not of the potassium cation in the vicinity of the U(III) complexes [U(OSi(OtBu)$_3$)$_4$K], [K18c6][U(OSi(OtBu)$_3$)$_4$] and [Kcryptand][U(OSi(OtBu)$_3$)$_4$] plays an important role in their reactivity with $CO_2$, $CS_2$ or $Ph_3PS$. To further investigate the role of steric and electronic effects in these reactions, we decided to synthesise the U(III) tetrasiloxide complex with different counter-cations (Li, Na and Cs) and to compare the reactivity of these different complexes. Indeed, an influence of the counter cation nature has already been observed in f-element reactivity.[269-271]

## III.2.3 Changing the counter-cation $M^+$ in the U(III) complex [U(OSi(OtBu)$_3$)$_4$M]

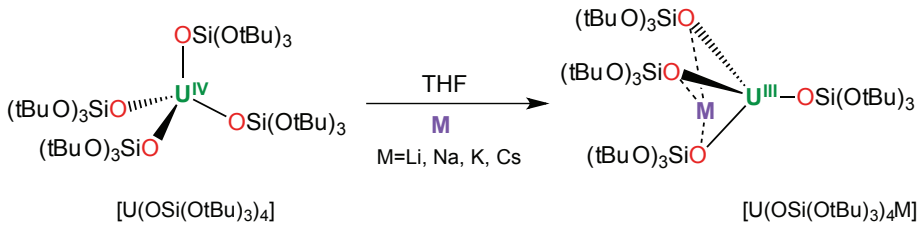


**Scheme III-14: Synthetic route of the [U(OSi(OtBu)$_3$)$_4$M] complexes (M=Li, Na, K or Cs).**

The addition of 1eq of the appropriate alkali metal M to a THF solution of the U(IV) complex $[U(OSi(OtBu)_3)_4]$ provides a convenient route for the synthesis of the U(III) series $[U(OSi(OtBu)_3)_4M]$ (M=Li, Na, K or Cs). The $[U(OSi(OtBu)_3)_4M]$ (M=Li **25**, Na **26** and Cs **27**) complexes crystallized from toluene (for M=Li, and Cs) and from DIPE (for M=Na) at -40°C. The X-ray structures of **25**-THF, **26**, $[U(OSi(OtBu)_3)_4K]$[7] and **27** are presented in Figure III-26. The crystal structures of $[U(OSi(OtBu)_3)_4K]$ and $[U(OSi(OtBu)_3)_4Cs]$ are isostructural with a tetrahedral uranium centre coordinated to one terminal siloxide and three bridging bidentate siloxide ligands. The K and Cs atoms are located in the $O_6$ coordination site made by the three bridging siloxide.

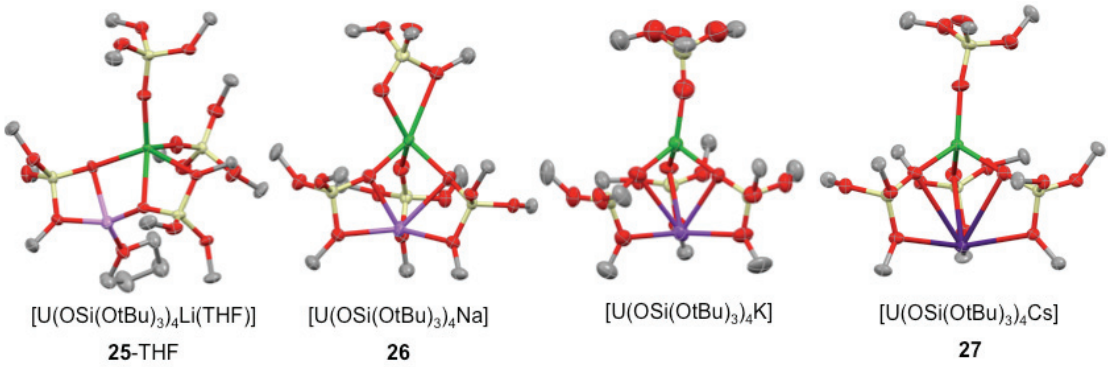


**Figure III-26: Solid state structures of $[U(OSi(OtBu)_3)_4M]$ complexes (M=Li 25, Na 26, K or Cs 27) (50% ellipsoids). Hydrogen atoms, methyl groups and lattice solvent molecules are omitted for clarity.**

In the X-ray structure of complex **26**, the sodium cation is also encapsulated in the $O_6$ pocket built by three bridging bidentate siloxide ligands but the fourth siloxide coordinating the U centre is bidentate. This leads to a pentacoordinated U centre in a highly distorted geometry. In complex **25**-THF, the Li cation is not located in the usual $O_6$ pocket but in an $O_4$ coordination site created by one bridging bidentate siloxide, one bridging monodentate siloxide and one residual molecule of THF. This arrangement is probably due to the very small size of $Li^+$. Notably binding of the $Li^+$ in the $O_6$ pocket would bring the siloxide ligands in a too close proximity. The uranium centre is pentacoordinated by one bridging bidentate, one bridging monodentate and two terminal monodentate siloxide ligands in a highly distorted geometry.

Even if the four $[U(OSi(OtBu)_3)_4M]$ complexes do not present the same coordination geometry around the uranium, the accessibility to the U centre can be illustrated with their O-U-O angles (where O is the negatively charged oxygen of the siloxide ligand). These angles

can then be compared with the O-U-O angles in [K18c6][U(OSi(OtBu)$_3$)$_4$] where the U centre is tetracoordinated by four terminal monodentate siloxide in a weakly distorted tetrahedral geometry. The O-U-O angles and U-M distances are reported in Table III-4. For the Na, K and Cs compounds, the three first reported values correspond to the angles between the non-bridging and the bridging siloxide ligands. The next three are the angles between the bridging siloxides.

**Table III-4: Comparison of the O-U-O angles (°) and U-M distances in [U(OSi(OtBu)$_3$)$_4$M] (M=Li, Na, K, Cs) and [K18c6][U(OSi(OtBu)$_3$)$_4$].**

| | **25-THF** (Li) | **26** (Na) | **[U(OSi(OtBu)$_3$)$_4$K]** (K) | **27** (Cs) | **[U(OSi(OtBu)$_3$)$_4$]$^-$** **(Ø)** |
|---|---|---|---|---|---|
| **O-U-O Angles (°)** | 136.0(1) | 138.0(1) | 127.2(3) | 122.90(1) | 111.3(3) |
| | 112.8(1) | 129.1(1) | 122.5(3) | 117.75(1) | 110.4(3) |
| | 109.5(1) | 93.35(9) | 115.0(3) | 116.92(1) | 110.1(3) |
| | 107.6(1) | 92.8(1) | 95.0(3) | 99.39(1) | 108.6(2) |
| | 106.1(1) | 89.5(1) | 94.9(3) | 97.62(1) | 108.4(2) |
| | 75.3(1) | 86.83(9) | 94.9(2) | 97.46(1) | 108.0(2) |
| **U-M (Å)** | 3.221(9) | 3.396(2) | 3.577(2) | 3.8058(5) | - |

Comparing the values of the O-U-O angles of the Na–Cs complexes in Table III-4, we observe that the last three angles between the bridging ligands increase with increasing cation size. Exception is noted for the Li complex **25**-THF in which the Li cation occupies a very different position to the metals in the other complexes. Indeed, when the cation is smaller, the three bridging siloxides between U and M are closer to each other, giving smaller O-U-O angles. Looking at the largest O-U-O angle in each complex, we observe that this value decreases steadily across the series from the Na compound (138(1)°) to the ion pair complex [K18c6][U(OSi(OtBu)$_3$)$_4$] (111.3(3)°). The Li compound, despite its altered arrangement, has the second largest angle in the series: 136.0(1)°. The Na compound, with the largest angle of the series, seems to have the most accessible U centre, yet the smaller size of the sodium cation frees up enough space for the terminal siloxide to become bidentate, thereby decreasing this accessibility in the solid state. However, in toluene solution, the bonding of the OtBu group is probably labile and access to the U centre should increase. Looking at the U-M distances, we observe an expected increase of the U-M bond length with increasing cation

size. Even for compound **25**-THF, in which the Li cation is not in the same location as in the other complexes, this trend is confirmed.

In order to assess if the nature of the cation affects the reactivity of the complex, an excess of $^{13}CO_2$ was added to complexes **25**-THF, **26** and **27** (Scheme III-15). $^{1}H$ NMR spectra of the deuterated toluene crude reaction mixtures are presented in Figure III-27.

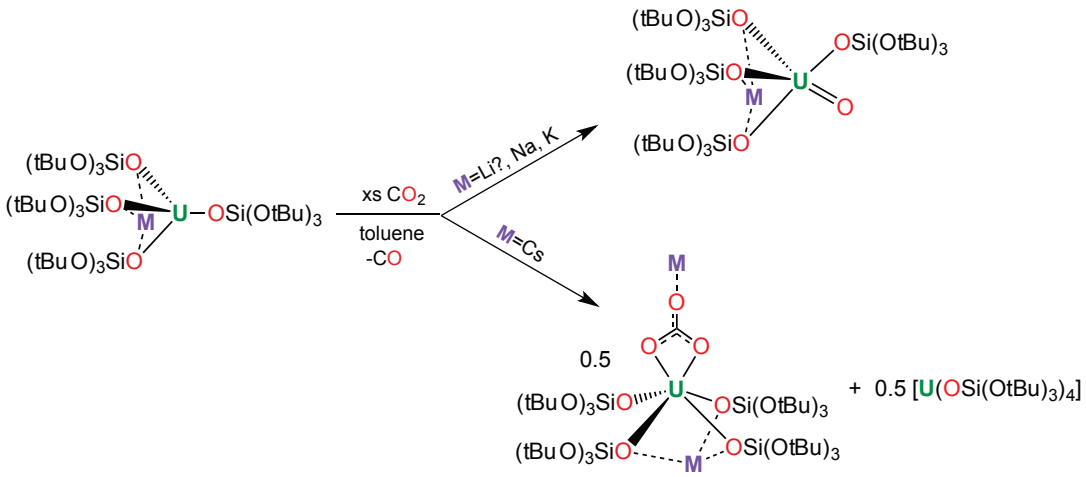


**Scheme III-15: Addition of an excess of $CO_2$ to the $[U(OSi(OtBu)_3)_4M]$ complexes (M=Li, Na, K, Cs).**

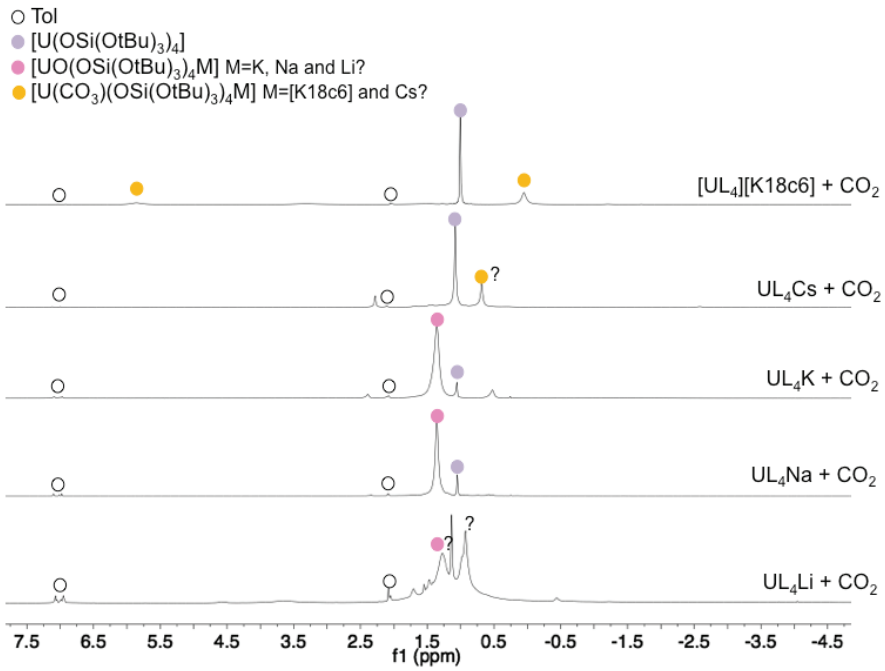


**Figure III-27: $^{1}H$ NMR spectra (400MHz, tol-$d_8$, 298K) of the crude mixtures after addition of an excess of $^{13}CO_2$ to $[U(OSi(OtBu)_3)_4M]$ complexes (M=Li, Na, K, Cs) and to $[K18c6][U(OSi(OtBu)_3)_4]$ (from bottom to top).**

On the $^{1}H$ NMR spectra of all the resulting reaction mixtures we observe a signal at the characteristic shift of the terminal U(V) oxo complex [UO(OSi(OtBu)$_3$)$_4$K].[7] The hypothetical U(V) [UO(OSi(OtBu)$_3$)$_4$Li] and [UO(OSi(OtBu)$_3$)$_4$Na] complexes are likely to be formed, similarly to [UO(OSi(OtBu)$_3$)$_4$K], by the two electron reductive deoxygenation of one $CO_2$ molecule at one U centre. In the Li case, the reaction is less clean and unattributed peaks are present. This could be due to the smaller size of the $Li^+$ cation, which could affect the reactivity. The presence of residual THF in the structure of **25**-THF could also lead to THF-adduct compounds with unidentified shifts in deuterated toluene. The reductive disproportionation of $CO_2$ by the ion pair complex [K18c6][U(OSi(OtBu)$_3$)$_4$] is known[7] and leads to formation of the terminal U(IV) carbonate complex [U(OSi(OtBu)$_3$)$_4$($CO_3$)$K_2$(18c6)] and the U(IV) [U(OSi(OtBu)$_3$)$_4$] complex. The reaction of the Cs compound with $CO_2$ yield mainly the [U(OSi(OtBu)$_3$)$_4$] complex and an unknown species with a proton NMR signal at 0.66 ppm which could be attributed to a carbonate compound. The $^{13}C$ NMR spectra of all the crude reaction mixtures present the signals of excess $CO_2$ at 125 ppm and of free CO at 185 ppm.

The Cs complex behaves similarly to the [K18c6][U(OSi(OtBu)$_3$)$_4$] complex while the reactivity of the Li and Na complexes are comparable to the one of [U(OSi(OtBu)$_3$)$_4$K]. This could mean that a critical size of the counter-cation exists (between K and Cs size) beyond which the formation of the U(V) terminal oxide complex is disfavoured and the formation of [U(OSi(OtBu)$_3$)$_4$] and a terminal U(IV) carbonate complex is favoured. However the difference in reactivity could also arise from a weaker Lewis acid character of the Cs cation which could modify its interaction with the substrate. Such an impact of the Lewis character of the counter cation has been observed during reduction of azobenzene by Ce(III) complex.[271]

We also investigated the reaction of the Na complex **26** with a stoichiometric amount of $CO_2$ in deuterated toluene. The $^{1}H$ NMR spectrum of the crude reaction mixture shows, in addition to the signal of the putative U(V) oxo complex [UO(OSi(OtBu)$_3$)$_4$Na], the signal of [U(OSi(OtBu)$_3$)$_4$] and two broad signals at -2.3 and -5.7 ppm (Figure III-28). After several hours, a purple microcrystalline solid formed in the reaction mixture.

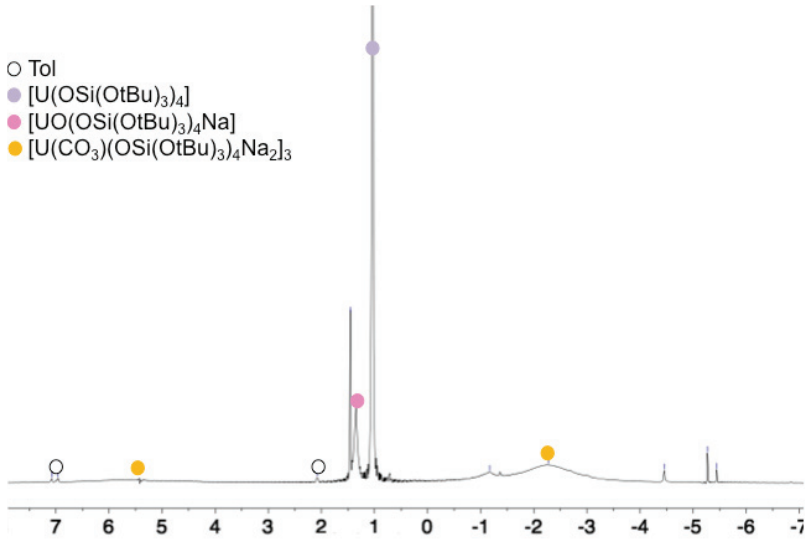


**Figure III-28: $^{1}$H NMR spectrum (400MHz, tol-$d_8$, 298K) of the crude mixture after addition of 1eq of $CO_2$ to $[U(OSi(OtBu)_3)_4Na]$**

Recrystallization of this solid residue in DIPE afforded a terminal U(IV) carbonate trimeric compound $[U(CO_3)(OSi(OtBu)_3)_4Na_2]_3$, **28**. Complex **28**.DIPE crystallizes in the trigonal space group R-3. The solid-state structure of complex **28.**DIPE (Figure III-29) shows that three $[U(CO_3)U(OSi(OtBu)_3)_4Na_2]$ moieties are bridged by three sodium cations capping the carbonates to yield a trimer. The second sodium ion of each moiety is located in the $O_6$ coordination pocket formed by three siloxide ligands. A similar carbonate-bridged U(IV) tetrameric assembly was obtained from the $CO_2$ reduction by the U(III) complex $[U((^{Neop,Me}ArO)_3tacn)]$.[98] The U2 and U3 uranium centres are hexacoordinated in a distorted octahedral geometry by a bidentate carbonate, one terminal monodentate siloxide and three other siloxide ligands bridging each uranium centre with Na2 or Na3 atom respectively. The U1 unit presents a similar structural arrangement with a distorted octahedral coordination geometry around the U centre except that the fourth siloxide ligand is tridentate bridging between the U1 and Na5 atoms. The average U-$O_{carbonate}$ distance (2.38(2) Å) is in the range of those found in previously reported terminal U(IV) carbonate complexes (2.271(1)-2.421(3) Å).[7, 98] The C–O bond lengths in the carbonate moieties are comparable with an average value of 1.30(5) Å is in agreement with other reported C-O distances in terminal U(IV) carbonate compounds. [7, 98]

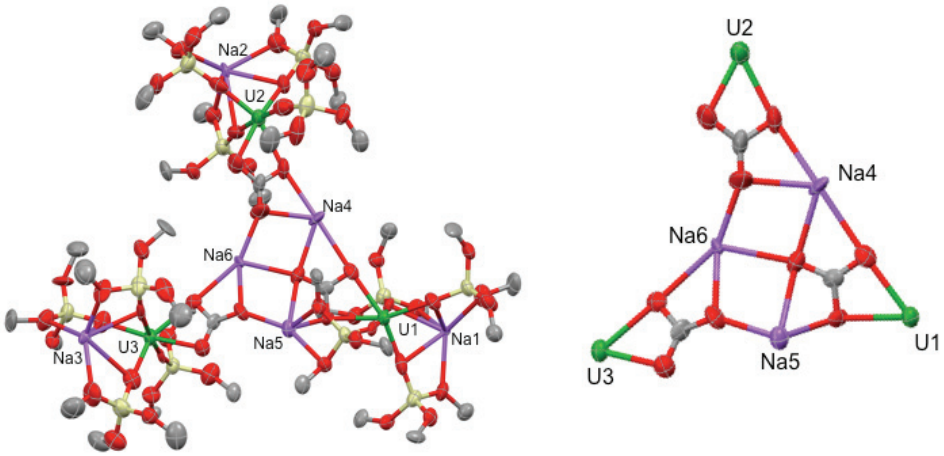


**Figure III-29: Solid state structure of $[U(CO_3)(OSi(OtBu)_3)_4Na_2]_3$.DIPE, 28.DIPE (left) and core view (right) (50% ellipsoids). Methyl groups, disorder and lattice solvent molecules are omitted for clarity.**

The $^1$H NMR spectrum of complex **28** shows two very broad peaks at -2.3 and -5.7 ppm (with an integration ratio of 3:1 respectively) confirming that the carbonate complex **28** and $[U(OSi(OtBu)_3)_4]$ are the main products formed after the addition of 1eq of $CO_2$ to complex **26**. The quantity of $CO_2$ added to complex **26** plays a crucial role on the reactivity (Scheme III-16).

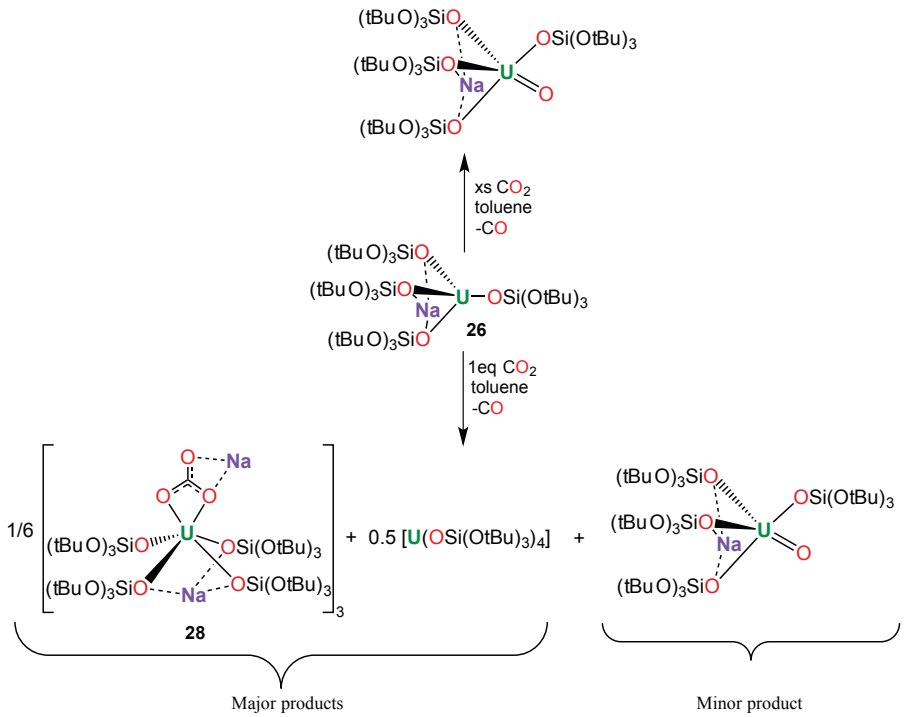


**Scheme III-16: Difference in reactivity of the $[U(OSi(OtBu)_3)_4Na]$ complex with 1eq or an excess of $CO_2$.**

These preliminary studies on the effect of the cation nature in $[U(OSi(OtBu)_3)_4M]$ complexes suggest that the reactivity with an excess of $CO_2$ can be tuned by the cation size. To confirm this hypothesis and better compare the uranium accessibility in the Li complex, the reduction of $[U(OSi(OtBu)_3)_4]$ with Li metal should be performed directly in toluene to prevent the coordination of the THF molecule to the $Li^+$ ion. A different structural arrangement and a different $CO_2$ reactivity could be observed. Finally the amount of added $CO_2$ also seems to strongly influence the reactivity of the Na complex **26** leading to a U(IV) carbonate complex or a U(V) oxo complex. To verify this trend the same stoichiometric addition of $CO_2$ will be performed on $[U(OSi(OtBu)_3)_4M]$ complexes (M=Li, K and Cs).

## III.3 Preliminary studies on the reactivity of $[U(OSi(OtBu)_3)_4K]$ and $[U(OSi(OtBu)_3)_3]_2$ with hydroxo- and oxo-donor agents.

The stoichiometric reaction of organometallic U(III) complexes with water was reported by Andersen and co-workers to afford the analogous U(III) bis-hydroxide complexes. Upon heating, these complexes decompose to afford U(IV) bis-oxo complexes and dihydrogen by oxidative elimination.[272] Recent work of Meyer et al. shows that the controlled hydrolysis of the U(III) complex $[U((^{Ad,Me}ArO)_3mes)]$ can lead to a terminal U(IV) hydroxo complex $[U(OH)((^{Ad,Me}ArO)_3mes)]$ which is likely to be involved in an electrocatalytic cycle for $H_2$ formation.[273] Former studies in our group, focusing on the controlled hydrolysis of U(III) complexes also lead to the isolation of oxo and hydroxo complexes of uranium.[274]

The reaction of U(III) complexes with $N_2O$ provide also a route to bridging[88, 96] or terminal[170, 275] oxo complexes. Recently, Severin et al. reported the synthesis of a N-heterocyclic carbene-activated $N_2O$ ($IMesN_2O$)[276] leading to an unusual reactivity of the $N_2O$ moiety with transition metal complexes.[277-279] However, the $N_2O$ activation by low valent U(III) complexes remains poorly explored.

## III.3.1 Reactivity of $[U(OSi(OtBu)_3)_4K]$ with water

The addition of 1eq of $H_2O$ to $[U(OSi(OtBu)_3)_4K]$ in toluene led to the isolation of a dimeric $[\{U(OSi(OtBu)_3)_3\}_2(\mu\text{-}OH)_2(\mu\text{-}O)]$.tol, **29**.tol which is isostructural with complex **23**.tol, its sulfur-analogue. Complex **29**.tol crystallizes from the toluene crude mixture at -40°C and the X-ray crystal structure presents two $[U((OSi(OtBu)_3)_3K]$ moieties bridged by three oxygen atoms. This demonstrated the loss of one siloxide ligand. The average value of the U-O1A, B, C distances (2.32(6) Å) is slightly longer than reported values for $\mu_2$–oxo bridged U(IV) complexes (2.1036(2)–2.179(3) Å)[88, 96, 176] and $\mu_2$–hydroxo bridged U(IV) (2.267(3)-2.299(3) Å)[176, 272] moieties. This is probably due to the bulky environment provided by the siloxide and the bridging $O^{2-}$ and $OH^-$ moieties. The bond valence sum is in agreement with the presence of two U(IV) centres but, similarly to complex **23**, the hydrogen atoms of the $OH^-$ groups are probably fluxional, and therefore very difficult to locate in the crystal structure.

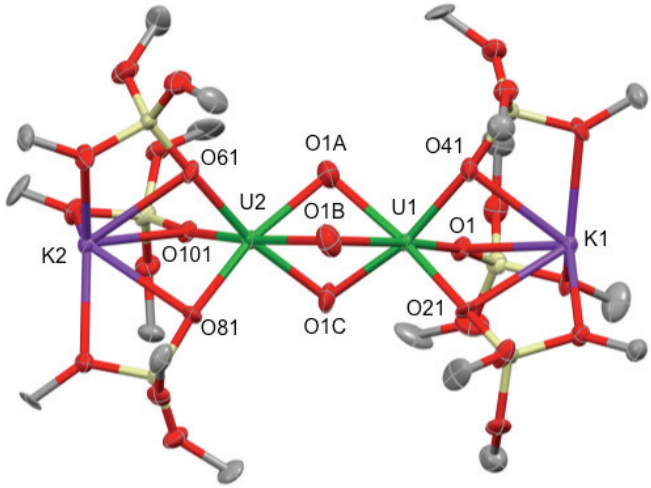


**Figure III-30: Solid state structure of $[\{U(OSi(OtBu)_3)_3\}_2(\mu\text{-}OH)_2(\mu\text{-}O)]$.tol, 29.tol (50% ellipsoids). Methyl groups and lattice solvent molecules are omitted for clarity.**

The $^1H$ NMR spectrum of the crude reaction mixture after 18h hours reveals only the presence of complex **29**, free siloxide ligands and unreacted $[U(OSi(OtBu)_3)_4K]$. This shows that, contrary to the reduction of $H_2S$ by [K18c6][$U(OSi(OtBu)_3)_4$], the reduction of $H_2O$ by $[U(OSi(OtBu)_3)_4K]$ does not form the hypothetical terminal hydroxo complex $[U(SH)(OSi(OtBu)_3)_4K]$. This observation led us to reconsider the reaction as consisting in

the reduction of one molecule of $H_2O$ by two $[U(OSi(OtBu)_3)_4K]$ complexes yielding $H_2$ and an oxide ligand. The subsequent, or concomitant, deprotonation of two water molecules by one siloxide ligand from each U centre releases two protonated siloxide ligands and forms two hydroxide ligands bridging the two U(IV) centres as shown in Scheme III-17. The synthesis was then repeated on a bigger scale and using the correct stoichiometry. A bubbling attributed to $H_2$ release was observed. The $^1$H NMR spectrum of the crude reaction mixture does not present unreacted $[U(OSi(OtBu)_3)_4K]$ but only the signal of free ligand and complex **29**. Complex **29** was isolated pure by crystallization from the toluene crude mixture in 49% yield.

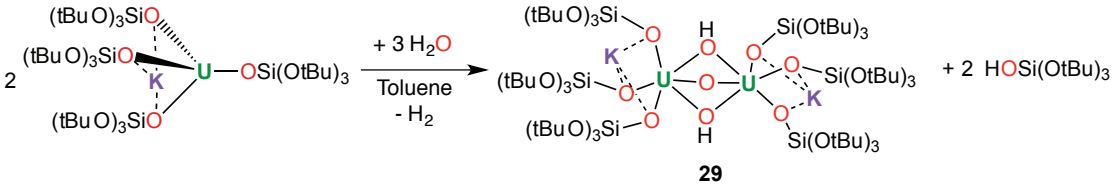


**Scheme III-17: Synthesis of the $[\{U(OSi(OtBu)_3)_3\}_2(\mu\text{-}OH)_2(\mu\text{-}O)]$ complex, 29.**

## III.3.2 Reactivity of the dimeric $[U(OSi(OtBu)_3)_3]_2$ with $N_2O$ sources

The reaction of the di-uranium(III) complex $[U(OSi(OtBu)_3)_3]_2$ with 1eq of the carbene-activated $N_2O$ ($IMesN_2O$) leads to the immediate formation of the U(IV) bridging oxo complex $[\{U(OSi(OtBu)_3)_3\}_2(\mu\text{-}O)]$, **30**, and $N_2$ evolution (Scheme III-18).

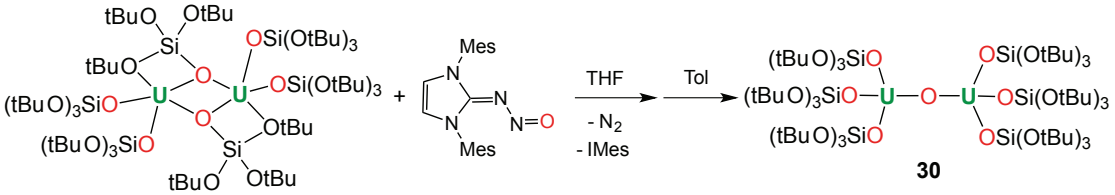


**Scheme III-18: Synthesis of the oxo complex $[\{U(OSi(OtBu)_3)_3\}_2(\mu\text{-}O)]$, 30.**

Light pink crystals of complex **30** were obtained from the toluene crude solution at -40°C. The molecular structure of **30** is represented in Figure III-31 and shows two $[U(OSi(OtBu)_3)_3]$

moieties bridged by an oxygen atom. The coordination spheres of the two uranium centres are different. U1 is hexacoordinated in a highly distorted geometry by the bridging oxide ligand, one monodentate siloxide and two bidentate siloxide ligands, while U2 is pentacoordinated in a highly distorted geometry by the bridging oxide ligand, one bidentate siloxide and two monodentate siloxide ligands. As a consequence the distance between the more electron-rich U1 centre and the oxo group is elongated compared to the one with the U2 centre (2.1375(4) Å and 2.0851(4) Å respectively). Yet, both U1-O1A and U2-O1A distances are in agreement with those reported in other U(IV) bridging $O^{2-}$ moieties.[88, 96, 176] The U-O-U angle is nearly linear with a value of 172.265(2)°.

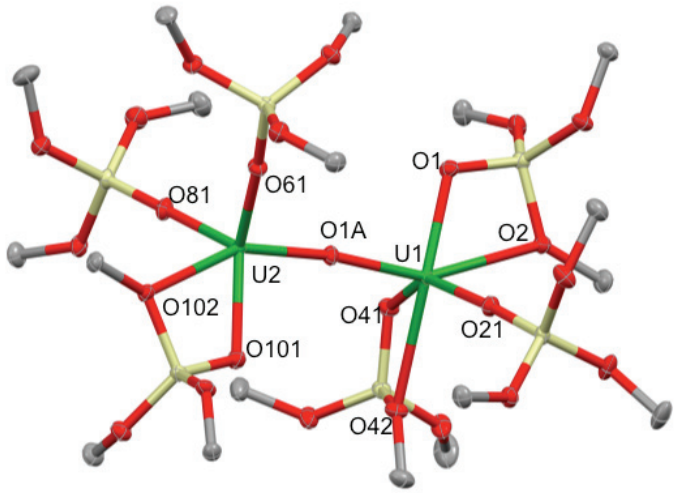


**Figure III-31: Solid state structure of [{U(OSi(OtBu)$_3$)$_3$}$_2$(μ-O)], 30 (50% ellipsoids). Methyl groups are omitted for clarity.**

The $^1$H NMR spectrum of complex **30** features only one signal at 0.5 ppm suggesting a fluxional binding of the tert-butoxy groups in solution. Complex **30** can be isolated pure in 49% yield. Monitoring its $^1$H NMR spectrum overtime shows that complex **30** is unstable at room temperature in toluene and slowly decomposes in the U(IV) [U(OSi(OtBu)$_3$)$_4$] complex and unidentified species (Figure III-32).

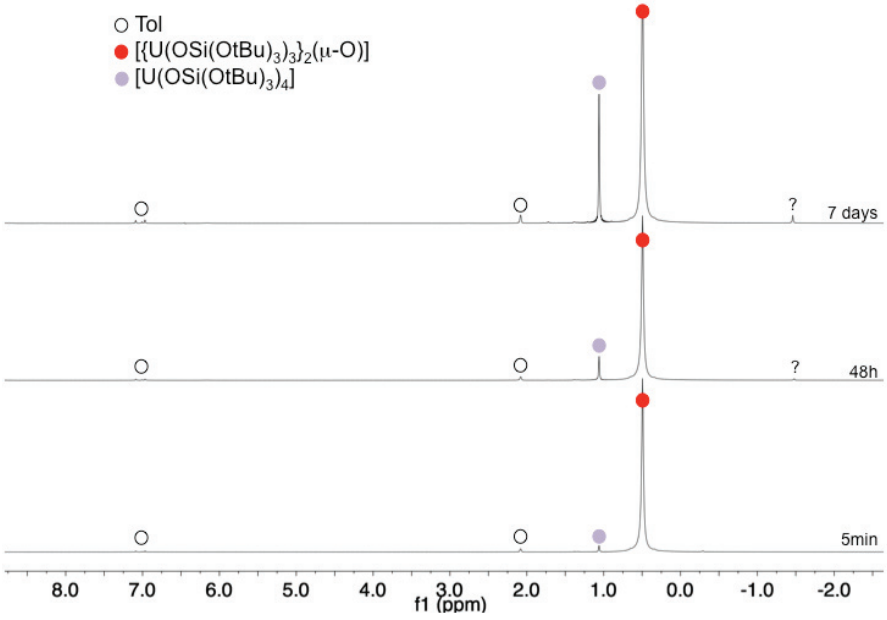


**Figure III-32: $^1$H NMR (400 MHz, tol-$d_8$, 298K) spectrum of [{U(OSi(OtBu)$_3$)$_3$}$_2$(μ-O)], 30 and evolution over time.**

Complex **30** can also be obtained by addition of 1eq of PyNO to the [U(OSi(OtBu)$_3$)$_3$]$_2$ complex in THF but in much lower yield (9%) probably because of the presence of released pyridine in the reaction mixture. Interestingly, the addition of an excess of $N_2O$ to a U(III) complex [U(OSi(OtBu)$_3$)$_3$]$_2$ solution in THF shows an immediate colour change from dark brown to yellow. The $^1$H NMR spectrum in deuterated toluene of the crude mixture does not present the signal of complex **30** but unidentified peaks. Suspecting an over-oxidation of the U(III) starting material by the $N_2O$ excess, [U(OSi(OtBu)$_3$)$_4$] was exposed to 1 atm of $N_2O$ to confirm that a U(IV) siloxide complex can reduce nitrous oxide (Scheme III-19).

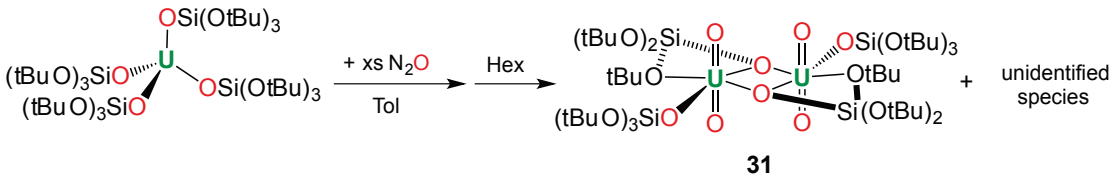


**Scheme III-19: Synthesis of [(UO$_2$)$_2$(OSi(OtBu)$_3$)$_4$], 31.**

Under a $N_2O$ atmosphere, a light blue solution of $[U(OSi(OtBu)_3)_4]$ in toluene turns instantaneously dark purple. Yellow crystals suitable for X-ray diffraction of the dimeric uranyl(VI) bis-siloxide complex $[(UO_2)_2(OSi(OtBu)_3)_4]$, **31**, were obtained from hexane at -40°C. The structure finalisation of complex **31** is ongoing but two uranyl moieties bridged by two bidentate siloxides are clearly recognizable. The equatorial plane of each uranium coordination sphere is completed by one terminal monodentate siloxide ligand. The provisional average U-O distance in the uranyl groups (1.768(3) Å) is comparable to those found in other uranyl(VI) complexes.[280]

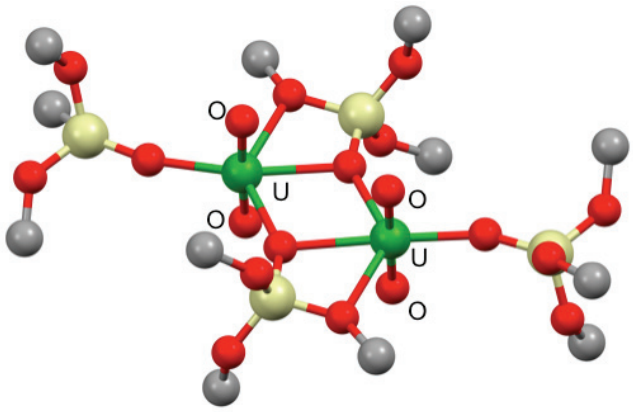


**Figure III-33: Solid state structure of $[(UO_2)_2(OSi(OtBu)_3)_4]$, 31 (Ball and stick representation). Methyl groups are omitted for clarity.**

The $^1H$ NMR spectrum of the toluene crude reaction mixture reveals the appearance of only one signal at 1.6 ppm after the $N_2O$ addition. However, as the reduction of $N_2O$ into $N_2$ and oxo ligand needs two electrons, eight electrons were used to form the four oxo groups in complex **31** while the two U centres only gave two electrons each. Thus, another U species has to be present in the crude mixture. Unfortunately, this by-product has not been isolated so far. The isolation of complex **31** from $N_2O$ addition to $[U(OSi(OtBu)_3)_4]$ indicates that over-oxydation to U(VI) is possible contrary to what was observed in some $N_2O$ reactivity studies with U(III) starting materials.[88, 96, 275] Interestingly, complex **30** does not react with an additional equivalent of $IMesN_2O$. In this case, the use of this carbene-activated $N_2O$ is a better route for controlled oxidative oxygen transfer reactions.

# III.4 Conclusion

The work presented in this chapter focused on the reactivity of trivalent uranium complexes supported by the tris(tert-butoxy)siloxide ligand, $OSi(OtBu)_3$.

In the first part of this chapter we demonstrated that cooperative effects play an important role in the reduction of carbon disulfide and triphenylphosphine sulfide. The comparison of the reaction product ratio for the reduction of $CS_2$ by $[U(OSi(OtBu)_3)_4K]$ or $[U(OSi(OtBu)_3)_4][K18c6]$ complexes shows that the presence of the K cation favours the reductive coupling of $CS_2$ to yield tetrathiooxalate as the main product. Conversely, the removal of $K^+$ by 18c6 in $[K18c6][U(OSi(OtBu)_3)_4]$ favours the reductive disproportionation of $CS_2$ to yield trithiocarbonate as the main product. During this work two particularly interesting U(IV) compounds, complexes **12** and **13**, were isolated showing that the coordination of $CS_3^{2-}$ and $C_3S_5^{2-}$ moieties on a U(IV) centre supported by four siloxides is possible despite the important steric bulk. The importance of the cation role was also visible in the $Ph_3PS$ reduction reaction. In addition to the isolation of rare U(IV) terminal and potassium capped sulfide complexes (**16**, **17** and **18**), the study of their reactivity with $S_8$, $CS_2$, and $CO_2$ has been performed demonstrating that, despite the multiple character of the U-S bond, the sulfur atom can be transferred to substrates. The protonation of the sulfide by pyHCl was found to be a convenient route to form a U(IV) hydrosulfide complex. DFT calculations allowed us to gain insight in the nature of the triple U-S and the double U-(SH) bonds. Moreover, the absence of reaction of $[K18c6][U(OSi(OtBu)_3)_4]$ and [Kcryptand][$U(OSi(OtBu)_3)_4$] complexes with $Ph_3PS$ in THF (contrary to $[U(OSi(OtBu)_3)_4K]$) confirmed the need of the U/K proximity for the reduction to occur. To better understand if this proximity influences the reactivity because of steric hindrance (siloxide coordination to cation leading to a more accessible U centre) or because of coordination and electronic reasons, we investigated the effect of the nature of the cation (M) in $[U(OSi(OtBu)_3)_4M]$. These preliminary studies on the reactivity of the isolated complexes $[U(OSi(OtBu)_3)_4M]$ (M=Li, Na, K, Cs) with $CO_2$ indicate a critical size of the M cation beyond which the favoured reaction product changes. This could point out that steric reasons dominate this effect, yet further investigations need to be done to confirm this hypothesis.

Indeed, the different Lewis acidity of the counter-cations could also play a role in the reactivity.

In the second part of this chapter, preliminary studies on the reactivity of the U(III) complexes $[U(OSi(OtBu)_3)_4K]$ and $[U(OSi(OtBu)_3)_3]_2$ with water and $N_2O$ were reported. The reaction of $[U(OSi(OtBu)_3)_4K]$ with 1eq of water led to the isolation of a bis-hydroxo mono-oxo U(IV) complex showing that controlling U(III) complex hydrolysis is not obvious especially because of the lability of the monodentate siloxide ligand. The reaction of $[U(OSi(OtBu)_3)_3]_2$ with $N_2O$ or its carbene-activated analogue, $IMesN_2O$, show that the carbene-activated $N_2O$ offers a better control of the oxidative oxygen atom transfer allowing the isolation of a bridging oxo U(IV) dimer. Further investigations of the reactivity of U(III) siloxide complexes with oxo donor agents will be pursued in the future. In parallel, the isolated oxo and hydroxo complexes could be attractive precursor to investigate the magnetic properties.

# CHAPTER IV

# Small Molecule Activation by Divalent Lanthanide Complexes

## IV.1 Synthesis and reactivity of new divalent lanthanide complexes supported by siloxide ligands

### IV.1.1 Context

In the preceding chapter, the reactivity of U(III) complexes supported by siloxide ligands with carbon disulphide, triphenylphosphinesulfide, carbon dioxide, nitrous oxide or water was investigated. The possibility of tuning their reactivity with $CO_2$ and $CS_2$ by changing the number of siloxide ligands and by coordinating the counter cation renders these systems very attractive. As shown in the general introduction, divalent lanthanide complexes are also known to undertake small molecule activation.[92, 133, 281] Because of the wide range of ionic radii and redox potential of lanthanides, the complexes of divalent lanthanides supported by tris(tert-butoxy)siloxide ligands could feature an unusual and possibly tunable reactivity.

The most common siloxides used as supporting ligands for lanthanide centres are shown in Scheme IV-1.[282]

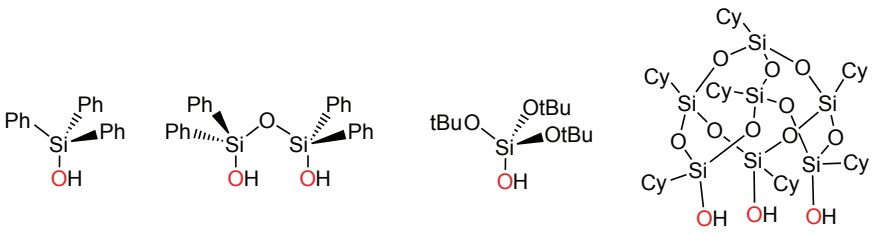


**Scheme IV-1: Siloxide ligands commonly used in the synthesis of lanthanide complexes.**

Most reported complexes contain the lanthanide ions in the oxidation state +III. These systems have found application as homogeneous catalysts for olefin hydrosilylation,[282] precursors for ceramic synthesis,[283, 284] or dopant in thin films.[285, 286] They have also been used as homogeneous molecular models for heterogeneous supported catalysts,[287-291] and in the development of luminescent silica nanoparticules.[292] Selected examples of Ln(III) supported by tris(tert-butoxy)siloxide ligands are shown in Scheme IV-2.

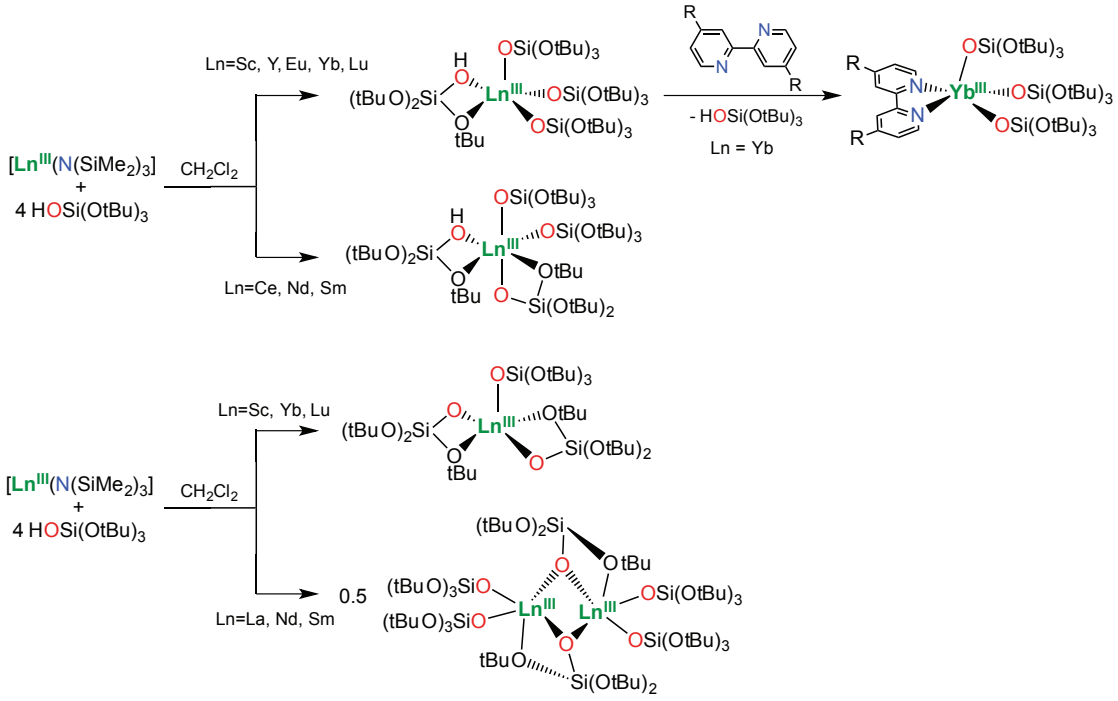


**Scheme IV-2: Syntheses of Ln(III) complexes supported by tris(tert-butoxy)siloxide ligands.[288, 292]**

To date isolated divalent lanthanide siloxide complexes are limited to few examples of Sm(II) and Yb(II) complexes[42, 43, 293] presented in Scheme IV-3. Interestingly, Anwander et al. reported the formation of the bis-siloxide complexes $[Ln(OSi(OtBu)_3AlEt_3)_2]$ (Ln=Yb, Sm) and underlined that even when only one equivalent of siloxide ligand is added, the latter bis-siloxide complex is formed.

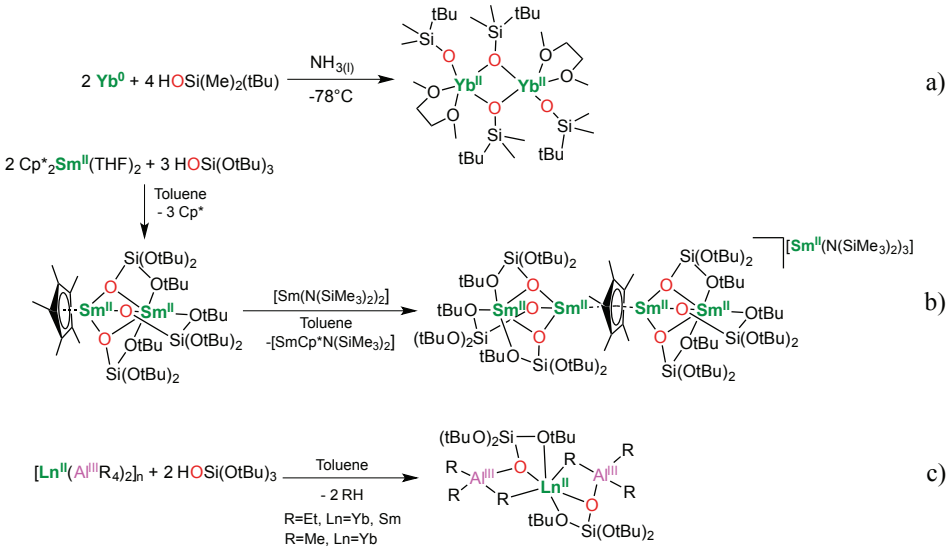


**Scheme IV-3: Syntheses of the Ln(II) complexes a) $[Yb(OSi(Me)_2(tBu)(DME)]_2$,[42] b) $[Sm_2(Cp^*)(OSi(OtBu)_3)_3]$ and $[Sm_2(Cp^*)(OSi(OtBu)_3)_3]_2[Sm(N(SiMe_3)_2)_3]$,[43] c) $[Ln(OSi(OtBu)_3AlR_3)_2]$ (R=Et, Ln=Yb and Sm; R=Me, Ln=Yb).[293]**

The reactivity of the complexes $[Yb(OSi(Me)_2tBu)(DME)]_2$, $[Ln(OSi(OtBu)_3AlR_3)_2]$ (R=Et, Ln=Yb and Sm; R=Me, Ln=Yb) and $[Sm_2(Cp^*)(OSi(OtBu)_3)_3]_2[Sm(N(SiMe_3)_2)_3]$ has not been investigated. The complex $[Sm_2(C_5Me_5)(OSi(OtBu)_3)_3]$ reacts with azobenzene in toluene leading to a bi-electronic reduction of the latter with the formation of the Sm(III) dinuclear complex $[Sm_2(PhNNPh)(Cp^*)(OSi(OtBu)_3)_3]$. This promising reactivity, the possibility of tuning Ln ion sizes and redox potentials, incited us to further explore the synthesis and the reactivity of new Ln(II) complexes supported by tris(tert-butoxy)siloxide ligands. These studies will also allow to compare U(III) and Ln(II) reactivity.

## IV.1.2 Synthesis of the series of divalent lanthanide complexes $[Ln(OSi(OtBu)_3)_4K_2]$ (Ln=Eu, Yb, Sm)

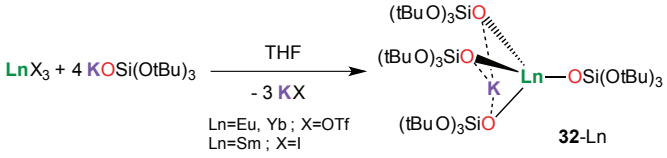


**Scheme IV-4: Synthesis of Ln(III) tetrasiloxide complexes $[Ln(OSi(OtBu)_3)_4K]$ (Ln=Eu, Yb, Sm), 32-Ln.**

The addition of four equivalents of the deprotonated $KOSi(OtBu)_3$ ligand to Ln(III) salts $LnX_3$ (Ln=Eu, Yb, X=OTf; Ln=Sm, X=I) affords the trivalent lanthanide tetrasiloxide complexes $[Ln(OSi(OtBu)_3)_4K]$, **32**-Ln (Ln=Eu, Yb, Sm), in high yields (80-85%) (Scheme IV-4). Interestingly the addition of only three siloxide ligands per Ln centre also leads to complex **32**-Ln and unreacted lanthanide salts. Similarly to the example reported by Anwander et al.[293] the higher coordination number is favoured even at non stoechiometric ratios. The protonolysis reaction between $[Ln(N(SiMe_3)_2)_3]$ and the protonated ligand $HOSi(OtBu)_3$ is, therefore the only way to prepare the tris-siloxide species $[Ln(OSi(OtBu)_3)_3]$.[288]

Colorless crystals of the complex **32**-Yb were obtained from a toluene solution at -40°C. The structure of **32**-Yb, presented in Figure IV-1, is isomorphous with the structure of the U(III) complex $[U(OSi(OtBu)_3)_4K]$. The Yb(III) ion is tetracoordinated by four siloxide ligands. Three siloxides are bidentate and bridge the Yb and K ions. The values of the Yb-O distances (2.06(2) Å in average) are in the range of the values reported for mononuclear Yb(III) siloxide complexes.[43, 288, 294]

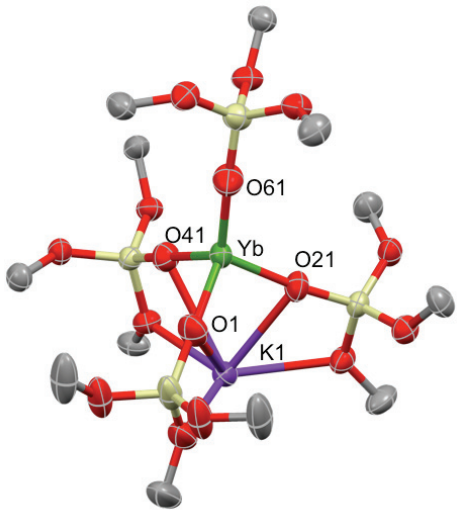


**Figure IV-1: Solid state structure of $[Yb(OSi(OtBu)_3)_4K]$, 32-Yb (50% ellipsoids). Methyl groups and solvent molecules are omitted for clarity.**

The $^1H$ NMR spectra of **32**-Ln show only one signal for the 108 protons of the complexes in both deuterated toluene and THF. The addition of 1eq of 18c6 to **32**-Yb leads to a shift of the signal on the $^1H$ NMR spectrum from 5.5 to 1.9 ppm in THF. This suggest that complex **32**-Yb maintains a heterobimetallic Yb-K structure in solution with a fluxional coordination of the potassium cation that renders all the hydrogen atoms equivalent. When the

$^1$H NMR spectrum of **32**-Yb is acquired at -30°C in deuterated toluene, two broad signals are present with an integration ratio of 3:1 in agreement with the solid state structure. At low temperature the fluxional motion of the K is therefore reduced. The $^1$H NMR spectrum of **32**-Eu at -30°C in toluene does not show the same de-coalescence but only a broadening of the signal. The $^1$H NMR spectrum of **32**-Sm is not significantly affected by the temperature suggesting an increased fluxionality in agreement with the larger size of the Sm cation.

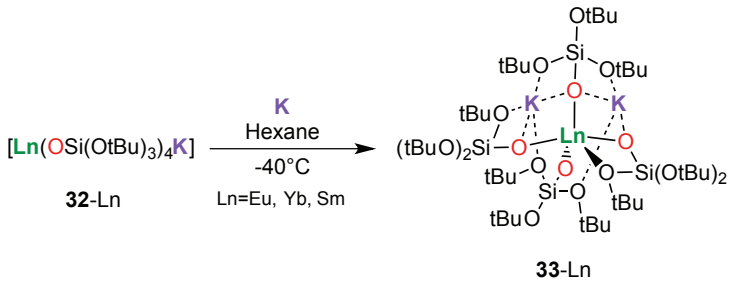


**Scheme IV-5: Synthesis of Ln(II) tetrasiloxide complexes [Ln(OSi(OtBu)$_3$)$_4$K$_2$], 33-Ln (Ln=Eu, Yb, Sm).**

The complexes **32**-Ln can be reduced by 1eq of potassium metal, in hexane at -40°C, to afford the divalent complexes [Ln(OSi(OtBu)$_3$)$_4$K$_2$], **33**-Ln (Ln=Eu, Yb, Sm) which, after recrystallization in hexane, were isolated pure in high yields (81-88%) (Scheme IV-5).

Yellow-brown crystals of complex **33**-Eu.THF were obtained from a concentrated hexane/THF mixture at -40°C. Deep pink crystals of **33**-Yb.tol and **33**-Sm were obtained, at -40°C, from concentrated toluene and hexane solutions respectively. The X-ray structures of **33**-Ln show the presence of a pentacoordinated Ln(II) centre by four siloxide oxygen atoms and one OtBu group in a highly distorted geometry. The siloxide ligands bridge the Ln centre to two potassium cations affording a neutral heterometallic structure (Figure IV-2). The structures of complexes **33**-Yb.tol and **33**-Sm are isomorphous while the structure of **33**-Eu.THF presents an additional THF molecule bound to one potassium cation. The values of the Ln-O distances in the **33**-Ln complexes are given in Table IV-1. The Ln-O distances in the complexes **33**-Ln are significantly longer than in the Yb(III) complex **32**-Yb. The shorter Yb-O distances compared to Sm-O and Eu-O ones are in agreement with the decrease of the ion size among the Ln series. The longer Ln-O61 and Ln-O62 distances in each complex are explained by the bidentate binding mode of the ligand with the Ln centres.

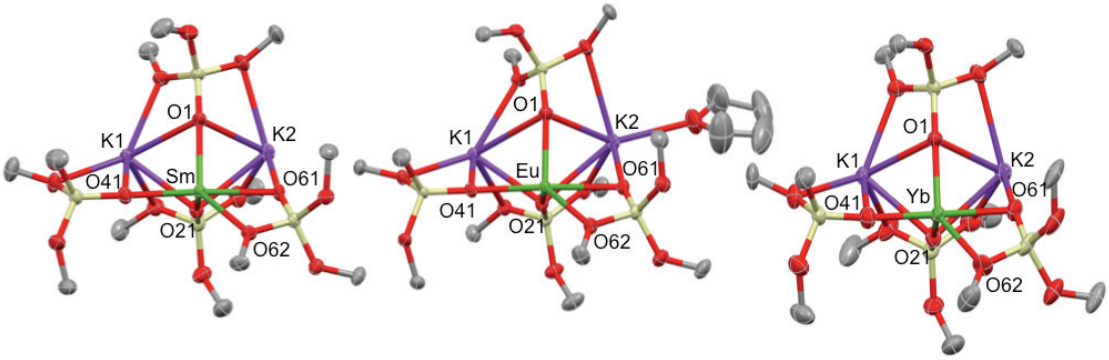


**Figure IV-2: Solid state structure of $[Ln(OSi(OtBu)_3)_4K_2]$ complexes, 33-Sm (left), 33-Eu.THF (middle), 33-Yb.tol (right) (50% ellipsoids). Methyl groups and solvent molecules are omitted for clarity.**

**Table IV-1: Ln-O bond lengths (Å) in $[Ln(OSi(OtBu)_3)_4K_2]$ complexes.**

| Ln-O (Å) | 33-Sm | 33-Eu.THF | 33-Yb.tol |
|---|---|---|---|
| **Ln-O1** | 2.381(2) | 2.3418(19) | 2.271(5) |
| **Ln-O21** | 2.3876(18) | 2.3870(19) | 2.272(5) |
| **Ln-O41** | 2.3888(18) | 2.3969(17) | 2.251(6) |
| **Ln-O61** | 2.5236(19) | 2.5263(17) | 2.422(5) |
| **Ln-O62** | 2.6659(18) | 2.6381(19) | 2.571(6) |

The $^1$H NMR spectra of **33**-Ln (Ln=Yb, Sm) show only one signal for the 108 protons of the complexes in both deuterated toluene and THF. The complex **33**-Eu is NMR silent due to the strong paramagnetism of its $4f^7$ electronic configuration. The complexes **33**-Eu and **33**-Yb are stable in toluene and THF solutions at room temperature but the complex **33**-Sm decomposes at 25°C in toluene. Monitoring the $^1$H NMR spectrum of **33**-Sm over time reveals the increasing formation of **32**-Sm and free ligand (Figure IV-3).

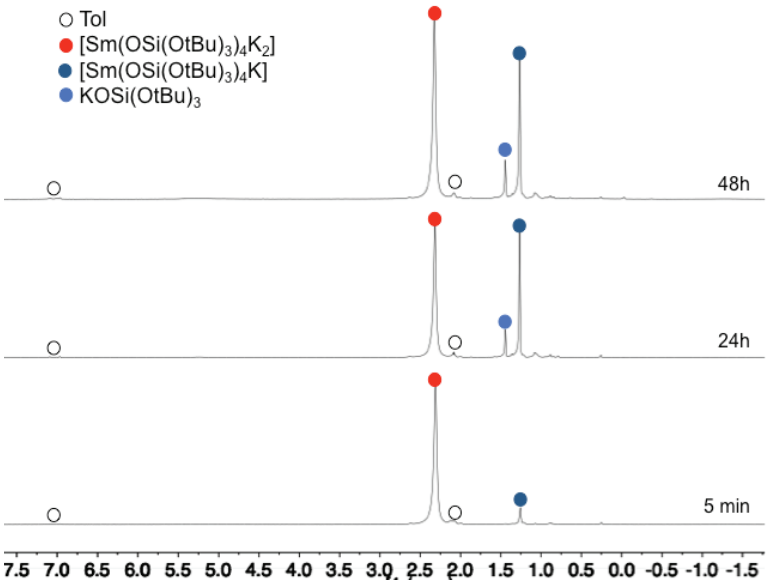


**Figure IV-3: $^{1}$H NMR spectrum (200MHz, tol-$d_8$, 298K) of [Sm(OSi(OtBu)$_3$)$_4$K$_2$], 33-Sm, and evolution over time.**

Interestingly, **33**-Yb features a much lower solubility in THF and dioxane than in toluene, which can be improved by the addition of 2eq of 18c6. Varying the temperature does not significantly affect the $^{1}$H NMR spectrum of **33**-Yb in toluene. When 2eq of 18c6 are added to a toluene solution of **33**-Yb, the obtained complex becomes insoluble indicating an ion-pair structure in presence of crown ether and a heterometallic Yb-$K_2$ structure (as found in solid state) in absence of crown ether. The presence of only one NMR signal in toluene and in the absence of 18c6 can be explained by a fluxional coordination of the potassium cation rendering all the hydrogen atoms equivalent.

Cyclic voltammetry studies were performed on the divalent **33**-Eu and **33**-Yb complexes in THF (6 mM concentration) but not on **33**-Sm for stability reasons. The obtained cyclic voltammograms were compared to those of the divalent salts $EuI_2$ and $YbI_2$ in THF at the same concentration (Figure IV-4). A strong shift of the oxidation potentials towards the negative values is observed for **33**-Eu and **33**-Yb compared to those found for $EuI_2$ and $YbI_2$ (from $E_{ox}$ = -0.14 V for $EuI_2$ to $E_{ox}$ = -1.26 V for **33**-Eu and from $E_{ox}$ = -0.68 V for $YbI_2$ to $E_{ox}$ = -2.19 V for **33**-Yb). Thus, the divalent tetrasiloxide complexes are easier to oxidize than their iodide analogues. This shows that the coordination of siloxide ligands leads to an increased reducing power. A smaller, enhancement of the reducing power of $SmI_2$ was reported for the hexamethylphosphoramide ligand.[295, 296] Interestingly, the cyclic voltammograms of **33**-Eu and **33**-Yb show only an irreversible oxidation and no reduction is

observed even when the scan rate is increased up to 1V.s$^{-1}$. This could be due to a kinetic inertia of the system.

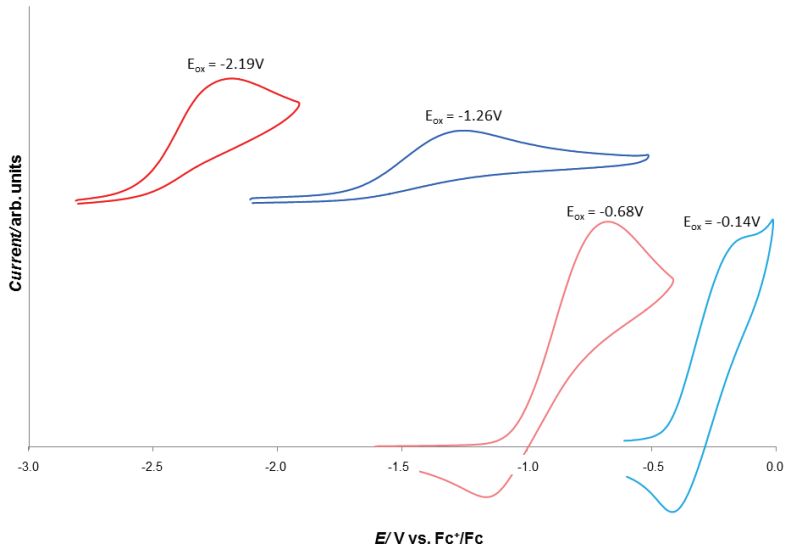


**Figure IV-4: Cyclic voltammogram for $EuI_2$ (light blue), $YbI_2$ (light red), 33-Eu + 2eq 18C6 (blue) and 33-Yb + 2eq 18C6 (red) recorded at 6mM concentration in ~0.1 M $[Bu_4N][PF_6]$ THF solution at 100 mV.s$^{-1}$ scan-rate with a glassy carbon working electrode.**

With these highly reducing divalent tetrasiloxide complexes in hands, we decided to investigate their reactivity with small molecules.

## IV.1.3 Reactivity with PhNNPh

The complexes **33**-Eu and **33**-Yb did not show any reactivity with $N_2$ in toluene or THF/18c6.

However, the addition of 1eq of PhNNPh to **33**-Ln (Ln=Eu, Yb) in toluene leads to the immediate formation of the trivalent complex **32**-Ln (Ln=Eu, Yb), identified by $^1$H NMR spectroscopy, and the precipitation of the reduced potassium radical anion KPhNNPh (Scheme IV-6).

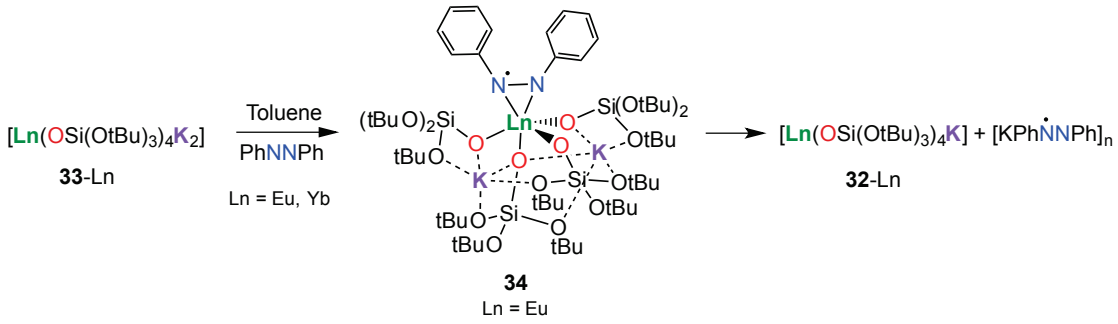


**Scheme IV-6: Reactivity of complexes 33-Ln with diazobenzene.**

The KPhNNPh compound is soluble in THF and NMR silent in agreement with its radical character. It can be isolated pure in 74% yield by slow diffusion of toluene into a THF solution of KPhNNPh. Crystals suitable for X-ray diffraction were obtained using the same procedure. The solid state structure of KPhNNPh shows the presence of a 2D polymeric network (Figure IV-5). The nitrogen atoms of the azobenzene radical are found on two positions with respectively 0.66(2) and 0.34(2) occupation coefficients. The structural data show that the N-N distance between the principal positions of the nitrogen atoms N1 (1.331(17) Å) is elongated compared to free azobenzene (1.25Å)[297] in agreement with the presence of a monoanionic reduced ligand. The value of the N-N distance in KPhNNPh is in the range of those found in carbocyclic complexes of Tm(III) or Sm(III) containing a monoanionic reduced diazobenzene (1.32-1.39 Å).[153, 155]

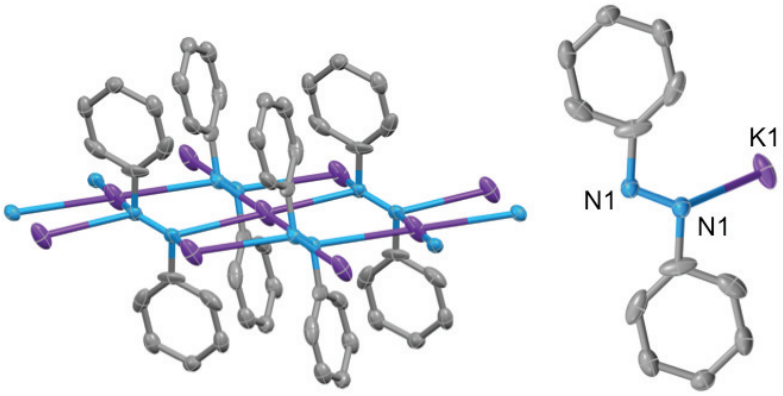


**Figure IV-5: Solid state structure of KPhNNPh (50% ellipsoids). Disorder and hydrogen atoms are omitted for clarity.**

EPR studies of the *in situ* generated KPhNNPh radical in DME have been reported[298] but its solid state structure was, until now, unknown. The EPR spectra measured on the

isolated KPhNNPh compound are in agreement with those reported by Gerson et al. with an intense signal at g~2, characteristic of an organic radical. The EPR spectrum measured in DME/THF solution (Figure IV-6) also shows the same hyperfine pattern as described by Gerson.

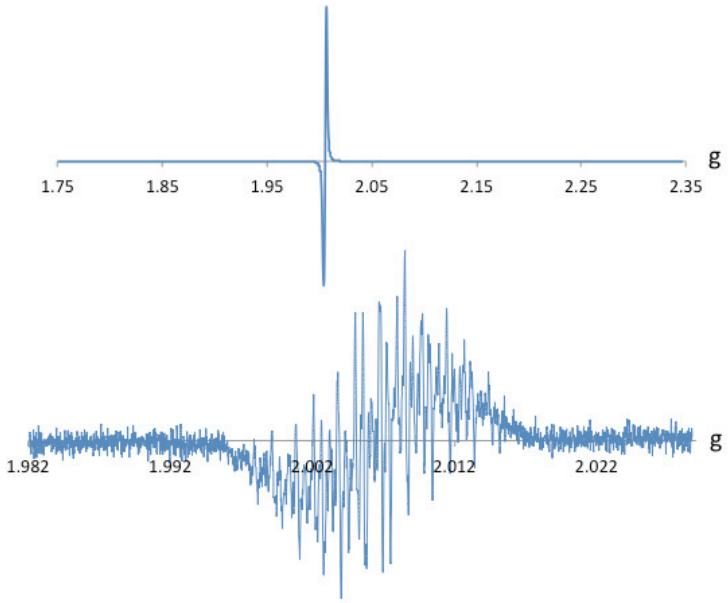


**Figure IV-6: EPR spectra of solid KPhNNPh suspended in a toluene/hexane mixture (20/2) (top) and in DME/THF (100/1) solution (bottom) at 292K with 33dB of attenuation.**

Performing the reaction of **33**-Eu with PhNNPh at -40°C allowed the isolation from hexane of few crystals of the intermediate Eu(III) complex [Eu(PhNNPh)(OSi(OtBu)$_3$)$_4$K$_2$], **34**. In the structure of complex **34**.hex, presented in Figure IV-7, the europium ion is hexacoordinated in a highly distorted trigonal prismatic fashion. The N81-N82 bond distance (1.450(8)Å) is similar to the N-N simple bond of hydrazine (1.45 Å) and longer than in the free radical KPhNNPh (1.331(17) Å) or in the carbocyclic complexes of Tm(III) or Sm(III) containing a monoanionic reduced PhNNPh (1.32-1.39 Å). [153, 155] The Eu-N82 distance is significantly longer than Eu-N81 (2.599(5) and 2.328(5) Å respectively), suggesting the presence of a radical localized on N82.

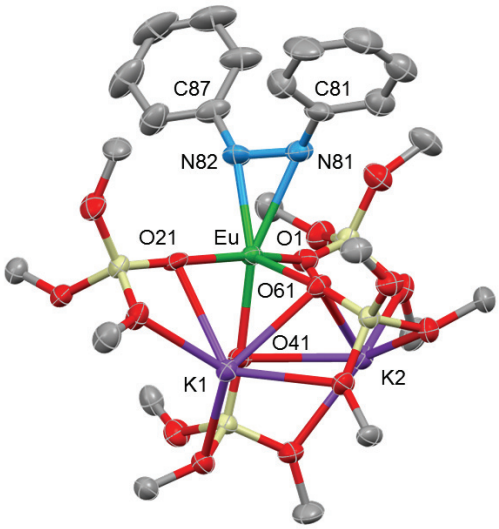


**Figure IV-7: Solid state structure of [Eu(PhNNPh)(OSi(OtBu)$_3$)$_4$K$_2$].hex, 34.hex (50% ellipsoids). Methyl groups, hydrogen atoms and solvent molecule are omitted for clarity.**

The structure of complex **34** demonstrates that coordination of the substrate to the lanthanide centre is possible despite the bulky environment provided by the four siloxide ligands. Therefore, the reduction can occur via an inner sphere mechanism. However, the sterically crowded environment renders this complex unstable and leads to the release of the reduction product affording the free radical anion KPhNNPh and **32**-Ln. Such a spontaneous release of the azobenzene reduction product from a lanthanide complex has never been reported so far. Moreover, this reactivity is the first example of azobenzene reduction by an Eu(II) complex illustrating the enhancement of reducing abilities of the Eu(II) ion thanks to the electron rich environment provided by the four siloxide ligands.

## IV.1.4 Reactivity with $CS_2$

This unprecedented reactivity with azobenzene incited us to investigate the reaction of **33**-Ln (Ln=Eu, Yb) with $CS_2$. So far, the reduction of $CS_2$ by 4f-elements has been limited to Sm(II) complexes.[104, 133, 134] The addition of 1eq of $^{13}CS_2$ to a THF solution of the divalent **33**-Ln (Ln=Eu, Yb) complexes pre-treated with 18c6 crown ether leads to the immediate formation of a precipitate. The $^{1}$H NMR spectra of the supernatants in deuterated THF show only the signal of the respective trivalent complexes **32**-Ln, which are formed with ~94%

conversion (determined using naphthalene as an internal standard). The $^{13}C$ NMR spectra of the precipitates in deuterated DMSO show the presence of $CS_3^{2-}$ as the main species and of $C_2S_4^{2-}$ (264 ppm) and $C_3S_5^{2-}$ (203 and 145 ppm) as minor species[233, 254, 255] (Scheme IV-7). Pale pink crystals of the 3D polymer $[(K_2CS_3)_5(DMSO)_{12}]_n$ were obtained from a slow diffusion of toluene into these DMSO solutions. The X-ray structure of $[(K_2CS_3)_5(DMSO)_{12}]_n$ features five $CS_3^{2-}$ units bridged together by potassium cations, DMSO molecules complete the potassium coordination spheres. The C-S bond lengths in the thiocarbonate moieties are comparable and the average value of 1.72(1) Å is in the range with the C-S distances in $[U(OSi(OtBu)_3)_4(CS_3)K_2(18c6)_2]$ **12** (1.706(8)-1.727(8) Å).

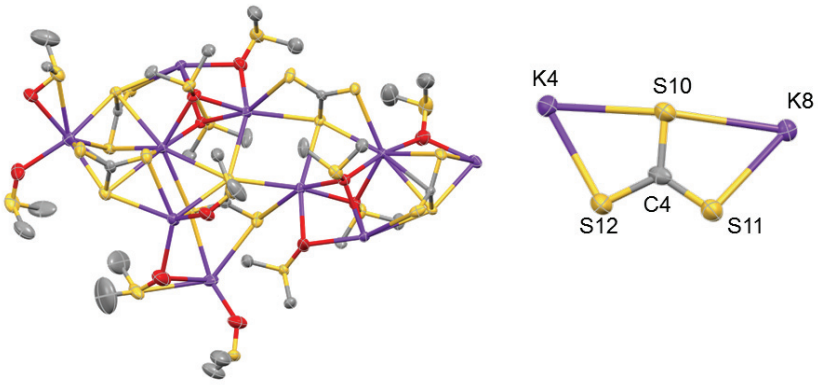


**Figure IV-8: Solid state structure of $[(K_2CS_3)_5(DMSO)_{12}]_n$, asymmetric unit (left), and detail of one $K_2CS_3$ unit (right) (50% ellipsoids). Disorder and hydrogen atoms are omitted for clarity.**

Comparably to the U(III) complex $[U(OSi(OtBu)_3)_4K]$, the divalent tetrasiloxide **33**-Ln (Ln=Eu, Yb) are able to promote both reductive disproportionation and reductive coupling of $CS_2$ to yield respectively to $CS_3^{2-}$/CS and $C_2S_4^{2-}$ ($C_3S_5^{2-}$ probably forms from the reaction of $C_2S_4^{2-}$ with CS). The relative ratios of the reduction products depending on the metal centre of the complex are shown in Scheme IV-7. We can observe that the complex **33**-Eu features a better selectivity for the reductive disproportionation pathway and thus thiocarbonate formation (ratio $CS_3^{2-}/C_2S_4^{2-}/C_3S_5^{2-}$= 40/1/2). Surprisingly, the relative ratios of the products do not significantly change when the reaction is carried out in toluene or when an excess of $CS_2$ is added. In consequence, the observed difference in selectivity is probably only due to the different size of the Eu(II) and Yb(II) ions (1.17 and 1.02 Å respectively)[16] leading to different steric demands in the respective $CS_2$-bound reaction intermediates but a possible role of the different redox potentials cannot be ruled out.

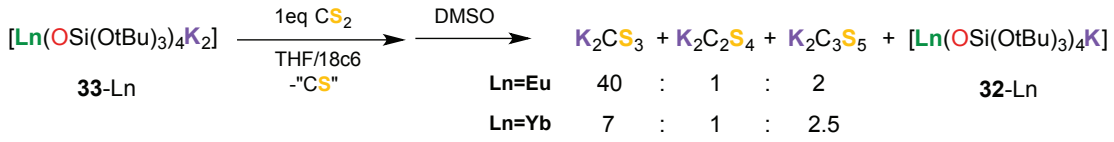


**Scheme IV-7: Reaction of 33-Ln (Ln=Eu, Yb) with $CS_2$ and ratios of reduction products.**

Unfortunately, all attempts to isolate an intermediate presenting the reduction products bound to the lanthanide centre failed even if one can assume that the $CS_2$ molecule, sterically less demanding than PhNNPh, could coordinate the lanthanide ion. The steric bulk provided by the four siloxide ligands and the dianionic charge of the reduction products are probably responsible for the release of thiocarbonate and thioxalate.

The reactivity with $CS_2$ shows that having access to complexes with different Ln(II) centres in the same ligand environment can be an advantage in term of tuning selectivity. Unfortunately, as the complexes **33**-Ln (Ln=Eu, Yb) precipitate from toluene after the addition of 18c6, the role of the potassium cation cannot be easily investigated. However, the steric hindrance and the electron-rich environment of the Ln centres provided by the siloxide ligands lead to unprecedented $CS_2$ reductions by Eu(II) and Yb(II) ions together with unique thiocarbonate and thioxalate formation and release.

## IV.1.5 Reactivity with $CO_2$

The observed reactivity with $CS_2$ incited us to further study the reactivity of complexes **33**-Ln with heteroallenes and focus on $CO_2$ activation. The divalent complex **33**-Eu does not react with $CO_2$ , but an immediate colour change occurs when a toluene solution of complex **33**-Yb is exposed to an excess of carbon dioxide. During this reaction, the formation of the trivalent complex **32**-Yb was identified by $^{1}H$ NMR spectroscopy in ~50% conversion determined using naphthalene as an internal standard. The $^{13}C$ NMR spectrum of the toluene crude mixture confirms the presence of the Yb(III) complex and shows the signal of free $^{13}CO$ at 185 ppm. These results indicate that Yb(III) complexes with bound reduction products should be present in the crude mixture despite the absence of other signals on the NMR spectra. To confirm the presence of $CO_3^{2-}$ and $C_2O_4^{2-}$ bound Yb(III) complexes in the toluene crude reaction mixture, the IR spectrum of the crude residue was performed and compared to the one of pure **32**-Yb (Figure IV-9). The IR spectrum of the reaction of **33**-Yb

with $CO_2$ (in green) clearly shows an absorption band around 1650 $cm^{-1}$, characteristic of C=O stretching, which is absent on the IR spectrum of pure **32**-Yb (in blue). This suggests that Yb(III) species containing bound carbonate and oxalate dianions are present in the toluene crude mixture.

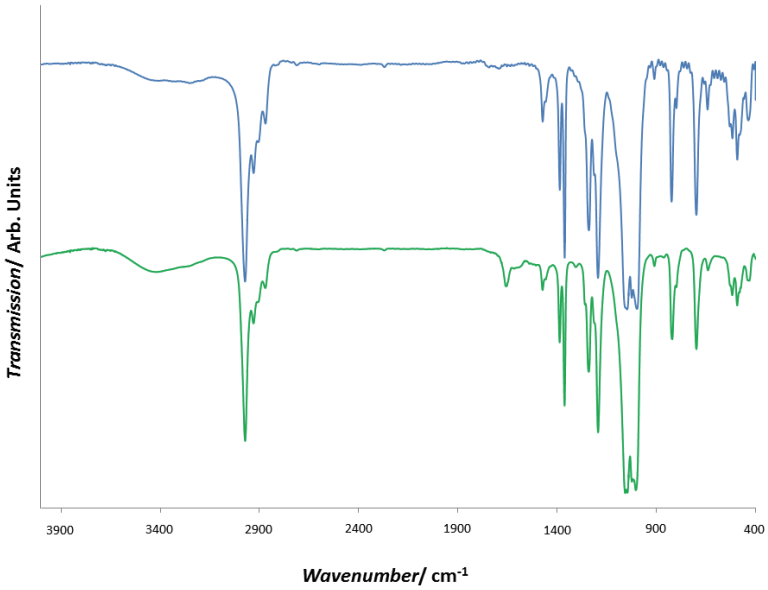


**Figure IV-9: IR spectra of the pure 32-Yb complex (blue) and the crude reaction of 33-Yb with $CO_2$ (green) in KBr disc.**

Attempts to crystallize these complexes only resulted in the isolation of **32**-Yb. This is probably due to a labile coordination of the $CO_2$ reduction products to the metal centre that also explains the absence of signals on the NMR spectra.

The addition of $D_2O$ to the crude residue leads to the release of the bound reaction products. The $^{13}C$ NMR spectrum in $D_2O$ shows the presence of the potassium oxalate and potassium carbonate signals (at 173 and 168 ppm respectively) in a 1:2.2 ratio (Scheme IV-8). The total conversion in $CO_2$ reduction products of ~95% was determined by quantitative $^{13}C$ NMR spectroscopy using $^{13}C$ labelled sodium acetate as an internal standard. The measured conversion rate confirms that the $CO_2$ reduction by **33**-Yb affords quantitatively CO, carbonate and oxalate and does not lead to the formation of by-products resulting from $CO_2$ insertion in the siloxide ligands.

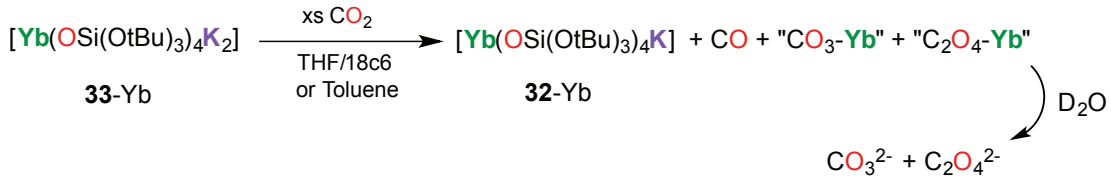


**Scheme IV-8: Reaction of 33-Yb with an excess of $CO_2$.**

The ratio oxalate/carbonate was found to slightly vary with the reaction conditions (Table IV-2). In particular, the concentration of the Yb(II) precursor affects the ratio in toluene which varies from 1:2.2 for a 158 mM solution of **33**-Yb to 1:0.7 for a 5 mM solution of **33**-Yb. When the reaction is performed in a THF solution of **33**-Yb pre-treated with 18c6 the ratio oxalate/carbonate slightly varies with the amount of carbonate increasing for diluted solution (oxalate/carbonate 1:1.7 and 1:3.1 for 158 mM and 15 mM solutions of **33**-Yb respectively).

**Table IV-2: Oxalate/carbonate ratios from the reaction of 33-Yb with excess $CO_2$.**

| Reagents | Solvent | Concentration | Oxalate:Carbonate |
|---|---|---|---|
| **33-Yb** | Toluene | 158 mM | 1:2.2 |
| | | 15 mM | 1:1.5 |
| | | 5 mM | 1:0.7 |
| **33-Yb + 2eq 18c6** | THF | 158 mM | 1:1.7 |
| | | 15 mM | 1:3.1 |

The intermediate in the reduction of $CO_2$ could be a Yb(III)-radical anion (Yb-$CO_2^{\bullet-}$). Such an intermediate has been proposed in the reduction of $CO_2$ by the Sm(II) complex $[Sm(Cp^*)_2(THF)_x]$[102, 299] and the isolation of a stable $CO_2^{\bullet-}$ radical complex has been reported for U(III)[82] and Y(II).[86] The dependency of the oxalate/carbonate ratio from the concentration in THF also fits with the proposed intermediate. In concentrated solutions two Yb-$CO_2^{\bullet-}$ radical are more likely to react together to yield the oxalate product, while in diluted conditions the Yb-$CO_2^{\bullet-}$ radical is more prone to react with a second molecule of $CO_2$ to afford the carbonate. In toluene the effect of the concentration on the selectivity is more difficult to explain. An important effect of the solvent on the outcome of the reduction of $CO_2$ has already been observed for the $[Sm(Cp^*)_2(THF)_x]$.[83] Moreover, as mentioned in the introduction, the reductive disproportionation of $CO_2$ can involve a bridging oxide complex which undergoes $CO_2$ insertion in the Ln-O bond or a nucleophilic attack of a dinuclear $CO_2^{2-}$

intermediate on a free $CO_2$ molecule. The solvent-effect on the reactivity in toluene or THF could also be explained by the stabilisation of one intermediate of the carbonate formation.

Since in the reduction of $CO_2$ by **33**-Yb, the trivalent Yb(III) complex **32**-Yb is reformed, we envisaged implementing this reaction in a closed synthetic cycle. After the first reaction of **33**-Yb and $CO_2$ in toluene, which leads to **32**-Yb and unidentified Yb(III) complexes with bound reduction products, 2eq of $KC_8$ are added to the reaction mixture. The $^1$H NMR spectrum of the centrifuged crude shows the resonance of the divalent complex **33**-Yb and new signals of side-products (among them the one of potassium siloxide can be identified). $CO_2$ is then added and this cycle can be repeated as long as the signal of **32**-Yb is observable on the $^1$H NMR spectrum after the addition of $CO_2$. After each $CO_2$ exposure, **32**-Yb is reformed with ~50% conversion compared to the amount of **33**-Yb in the previous step. On a 20 mg scale experiment, five cycles can be performed and the $^1$H NMR spectra show the decrease of the **33**-Yb signal and the increase of the side-products signals over the cycles (Figure IV-10). The formation of polynuclear carbonate- or oxalate-bound Yb(III) compounds, that cannot be reduced to reform **33**-Yb, probably terminates the synthetic cycle and prevents the implementation of a catalytic cycle. Similarly, a termination of $CO_2$ reduction cycles by a tetrameric $CO_3$-bound U(IV) complex has been reported by Meyer et al.[98] Once again, the electron-rich environment around the Yb(II) centre leads to unique reactivity with this first example of $CO_2$ reduction by divalent Yb(II) complex.

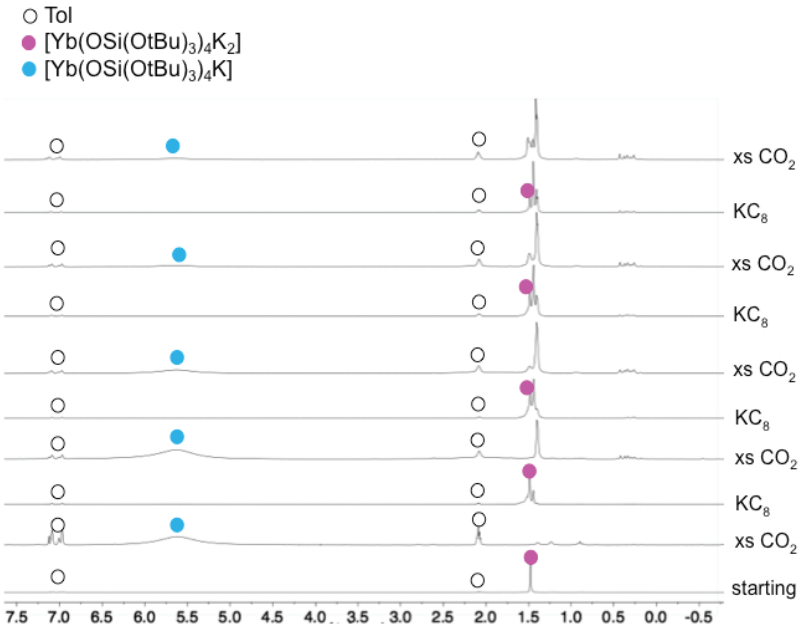


**Figure IV-10: $^1$H NMR spectra (200MHz, tol-$d_8$, 298K) of the $CO_2$ reduction cycles.**

During preliminary experiments to further study the influence of the number of siloxide ligands on reactivity, the dinuclear Yb(II) complex $[Yb_2(OSi(OtBu)_3)_4)(DME)]$, **35**, was isolated from the reaction of the divalent complex $[Yb(HMDS)_2]$ with 2eq of silanol $HOSi(OtBu)_3$ in DME. Orange crystals of **35**, suitable for X-ray diffraction, were obtained from the concentrated DME crude mixture at -40°C. The complex **35** crystallizes in the triclinic P-1 space group with two complexes per asymmetric unit (Figure IV-11). Each Yb centre is hexacoordinated by six oxygen atoms in a highly distorted geometry. The Yb ions are bridged by two bidentate siloxide ligands and one DME molecule. A terminal siloxide (monodentate for Yb1 and bidentate for Yb2) completes their coordination sphere. The Yb-$O_{siloxide}$ bond distances in complex 22 are reported in Table IV-3 and are in the range of the Yb-O distances found in complex **33**-Yb. The two Yb atoms are in close proximity with a Yb…Yb distance of 3.4167(15) Å.

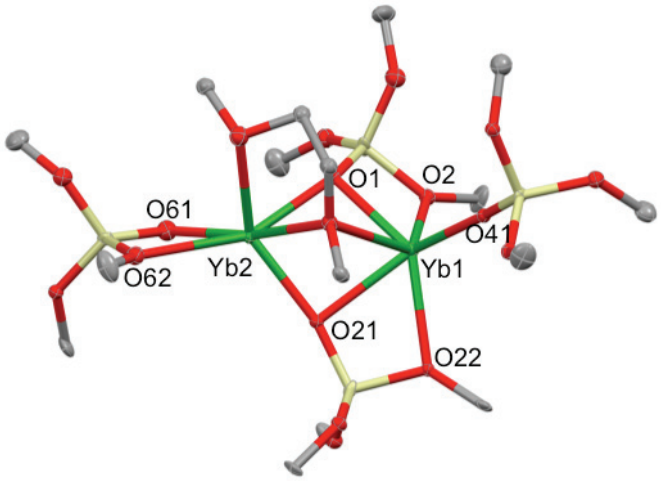


**Figure IV-11: Solid state structure of one of the two complexes $[Yb_2(OSi(OtBu)_3)_4)(DME)]$, 35 (50% ellipsoids). Disorder and hydrogen atoms are omitted for clarity.**

**Table IV-3: Yb-$O_{siloxide}$ bond lengths (Å) in $[Yb_2(OSi(OtBu)_3)_4)(DME)]$, 35.**

| Ln-O (Å) | 35 |
|---|---|
| Yb1-$O_{bridging\ bidentate}$ | 2.44(2) |
| Yb1-OtBu | 2.526(0) |
| Yb1-O41 | 2.222(17) |
| Yb2-$O_{bridging\ bidentate}$ | 2.36(6) |
| Yb2-O61 | 2.268(15) |
| Yb2-O62 | 2.589(17) |

The addition of 2eq of potassium siloxide to $YbI_2$ precursor in THF leads to a mixture of products suggesting that the protonolysis pathway is the most appropriate to cleanly obtain complexes with low ligand/metal ratios. Preliminary reactivity tests on complex **35** show an immediate reaction with $CS_2$ and $CO_2$ but further efforts need to be done to identify the reaction products.

In summary, the reactivity of the complexes **33**-Ln demonstrates that siloxide ligands clearly enhance the reducing ability of Eu(II) and Yb(II) ions rendering these systems very attractive as stable and easy-to-handle precursors that can be used to reduce small molecules. In addition, the bulkiness of the four siloxides prevents the stable coordination of the reduction products to the Ln(III) complex in the cases of PhNNPh and $CS_2$ activation. The release of the reaction products is a prerequisite for the implementation of a catalytic cycle and even if this step is not achieved for the $CO_2$ reduction, an optimization of the steric bulk could promote the decoordination of the reduction products.

# IV.2 Design and reactivity of divalent lanthanide complexes supported by N- and O- donor ligands

## IV.2.1 Context

In the previous chapter we show that electron-rich siloxide ligands can improve the reducing abilities of Eu(II) and Yb(II) ions and promote rare reactivity in homoleptic “ate” complexes of “classical” divalent lanthanides. Our investigations for new ligand systems capable of enhancing reducing power of Eu(II) and Yb(II) ions, led us to study the influence of tripodal tetradentate ligands with different charge on the redox potential of these ions in homoleptic bis-ligand complexes.

Divalent lanthanide chemistry has been dominated for a while by carbocyclic supporting ligands. More recently N- and O- donor chelating ligands have attracted interest in Ln(II) reactivity studies.[300, 301] Notably tripodal polypyridyl such as tris(2-pyridylmethyl)amine (TPA) and aminophenolate ligands, which have been largely studied

with transition metals,[302] are less used as supporting ligands with f-elements. Even though Ln(III) complexes of TPA and tripodal aminophenolate ligands present a singular reactivity,[303-308] Ln(II) complexes supported by those ligands remain rare.[50-53, 309-311] The reported X-ray-characterised Ln(II) complexes supported by tripodal aminophenolate ligands are represented in Scheme IV-9.

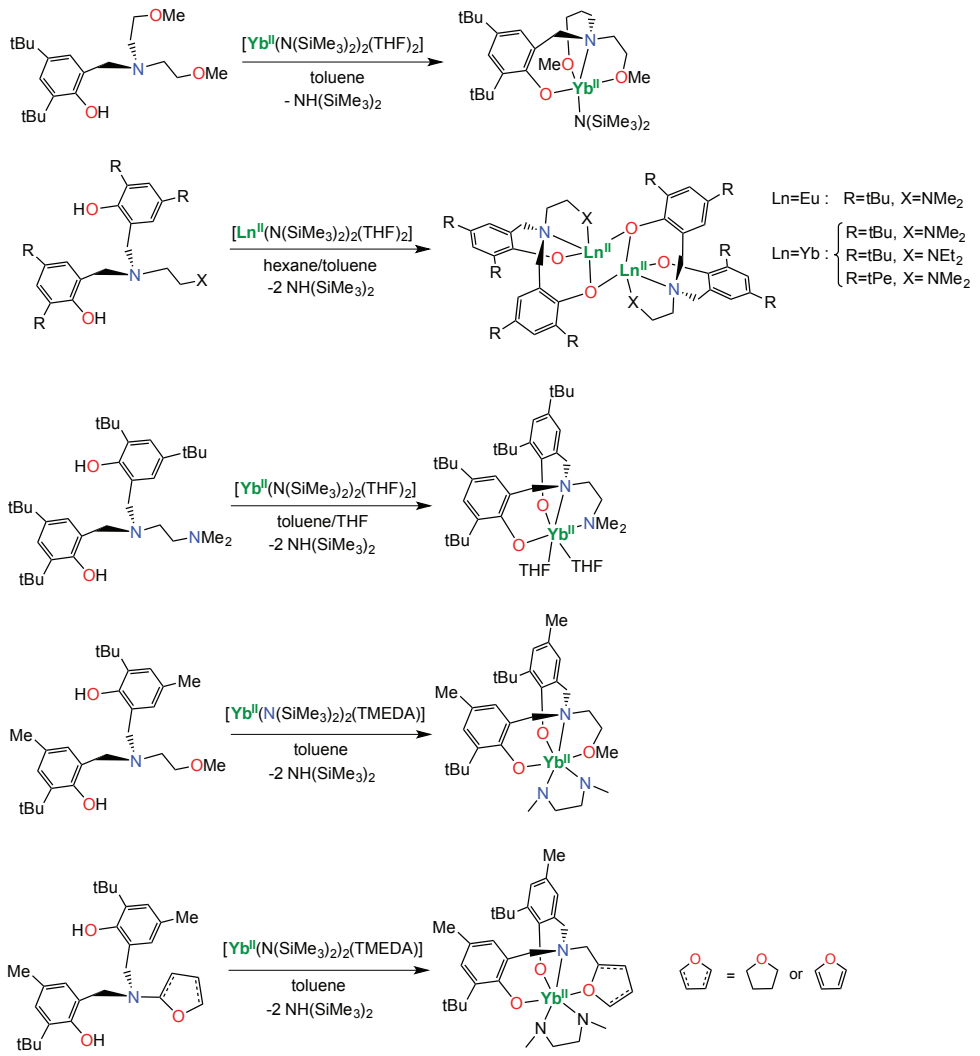


**Scheme IV-9: Ln(II) complexes supported by tripodal aminophenolate ligands.**[50-53, 309-311]

Surprisingly homoleptic bis-ligand complexes of tripodal aminophenolate were never studied in divalent lanthanide chemistry. Moreover, the reactivity of the Ln(II) mono-ligand complexes presented in Scheme IV-9 has never been studied with heteroallenes. Based on the

experience of our group in f-elements supported by TPA ligands (tris(2-pyridylmethyl)amine)[274, 303, 312] and on the preliminary results obtained in the group on the synthesis of homoleptic complexes of TPA we decided to investigate the influence of aminophenolate ligands with different donor properties on the reducing power of the Ln(II) centres.

## IV.2.2 Syntheses of mono- and bis-ligand Ln complexes of TPA, BPA, BPPA and MPA

### III.2.2.1 Ligand design

In order to study the influence of the charge and the number of phenolate functions of the ligands on the reducing abilities of divalent lanthanides, TPA, a neutral tetradentate ligand, was first investigated. TPA-derivative ligands, in which the pyridyl arms were gradually replaced by phenol ones, were synthesised (Scheme IV-10).

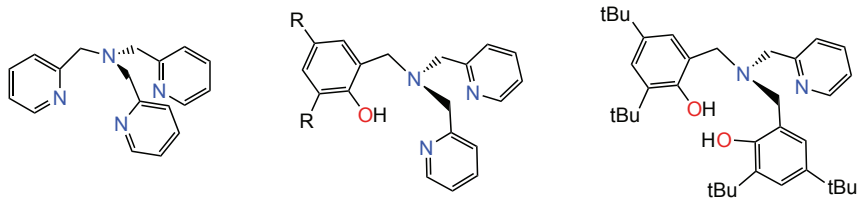


**Scheme IV-10: Synthesised N- and O-donor tripodal ligands.**

Tert-butyl groups on the phenol cycles were envisaged to improve the solubility of the ligands and the final lanthanide complexes. The presence of these donating groups could also influence the redox properties of the lanthanide compounds.

## IV.2.2.2 Syntheses of Ln complexes supported by TPA

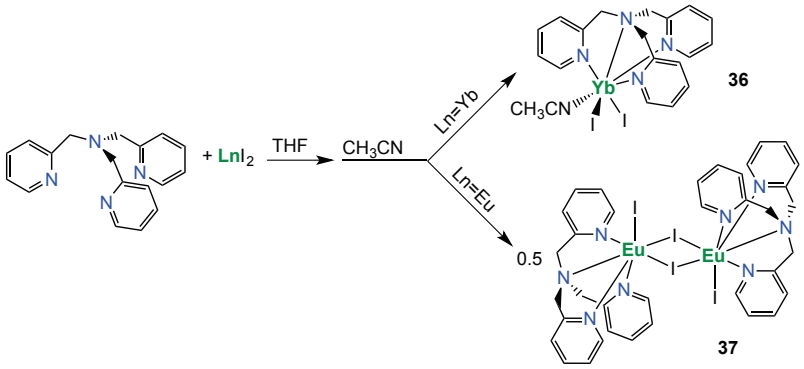


**Scheme IV-11: Synthesis of the mono-ligand complexes [Yb(TPA)$I_2$($CH_3CN$)], 36 and [Eu(TPA)(μ-I)I]$_2$, 37.**

Preliminary studies, performed by Gülay Bozoklu during her PhD, led to the isolation of Ln(II) complexes supported by TPA.[313] The addition of 1eq of TPA ligand to the divalent lanthanide iodide salts $LnI_2$ (Ln=Eu, Yb, Sm) in THF leads to the precipitation from the crude mixture of the mono-ligand complexes [Ln(TPA)$I_2$] (Scheme IV-11). Crystals suitable for X-ray diffraction were obtained by layering a $CH_3CN$ solution of the Eu(II) and Yb(II) mono-TPA complexes with DIPE. Attempts to isolate single crystals of [Sm(TPA)$I_2$] were unsuccessful.

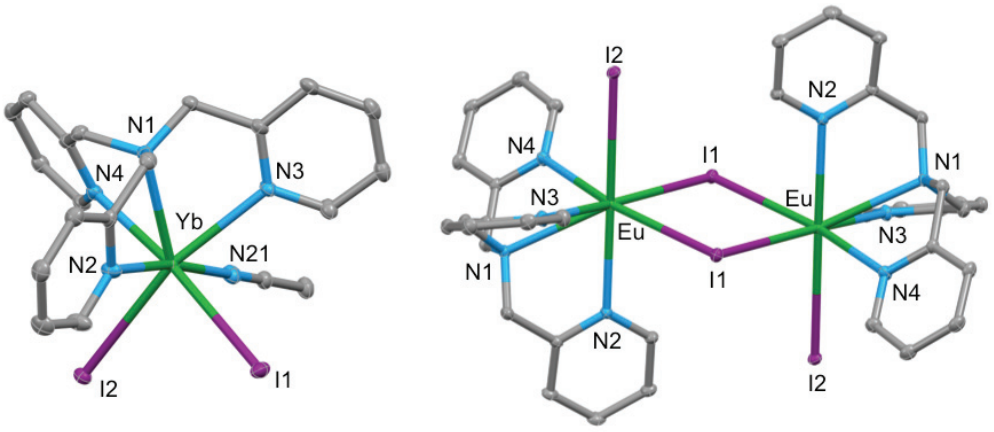


**Figure IV-12: Solid state structure of [Yb(TPA)$I_2$($CH_3CN$)].($CH_3CN$)$_{0.5}$, 36.$CH_3CN_{0.5}$ (left) and [Eu(TPA)(μ-I)I]$_2$, 37 (right) (50% ellipsoids). Hydrogen atoms and solvent molecules are omitted for clarity.**

The complex [Yb(TPA)$I_2$($CH_3CN$)].($CH_3CN$)$_{0.5}$, **36**.($CH_3CN$)$_{0.5}$, crystallizes in the triclinic space group P-1. The structure of complex **36**.($CH_3CN$)$_{0.5}$, given in Figure IV-12 (left), presents a heptacoordinated Yb(II) ion with a distorted monocapped octahedron geometry by four nitrogen atoms of TPA, two iodide ions and a nitrogen atom of an acetonitrile molecule. The Yb-$N_{amine}$ bond (2.620(4) Å) is longer than the average Yb-$N_{pyridyl}$ bond (2.565(6) Å). The complex [Eu(TPA)(μ-I)I]$_2$, **37**, crystallizes as a dimer in the orthorhombic Pbca space group (Figure IV-12 right). This value is larger than one observed for the Yb(II) in **36**.$CH_3CN_{0.5}$ (1.087(3) Å) due to the smaller ionic radius of the Yb(II) ion compared to the Eu(II). These differences are probably responsible for the observed nuclearity of the Yb and Eu complexes in the solid state crystal structure. The structure of **37** has a $C_2$ symmetry with a two-fold axis passing through the two bridging iodides. The europium atoms are heptacoordinated, with a distorted mono capped octahedron geometry, by the four nitrogens of the TPA ligand, one terminal and two bridging iodide ligands. The ligand TPA adopts an helical arrangement around the metal cation as found in the reported Eu(III) complex [Eu(TPA)$Cl_3$].[312] The Eu-$N_{amine}$ distance of 2.748(3) Å is longer than the average Eu-$N_{pyridyl}$ distance (2.67(1) Å). Significantly shorter Eu-N distances were found in the Eu(III) complex [Eu(TPA)$Cl_3$] (Eu-$N_{amine}$ = 2.612(1) Å; mean Eu-$N_{pyridyl}$ = 2.57(2) Å) but the difference in bond length values remains smaller than the difference in ionic radii (0.2 Å). As expected, the Eu-I distance in **37** is shorter for the terminal iodide (Eu-I2=3.2888(3) Å) than for the bridging ones (Eu-I1 3.3142(1) Å and 3.3111(1) Å).

The complex **37** is NMR silent in agreement with the strong paramagnetism of the $4f^7$ electronic configuration of Eu(II) ion. The $^1$H NMR spectrum of **36** in deuterated acetonitrile presents 5 signals in the diamagnetic zone. This is in agreement with a diamagnetic Yb(II) complex with a $C_3$ symmetry in solution. Both complexes **36** and **37** are stable in acetonitrile solution for weeks. The Sm(II) analogue [Sm(TPA)$I_2$], which precipitates from the THF crude mixture of $SmI_2$ and 1eq of TPA, is stable in solid state but decomposes in acetonitrile at room temperature.

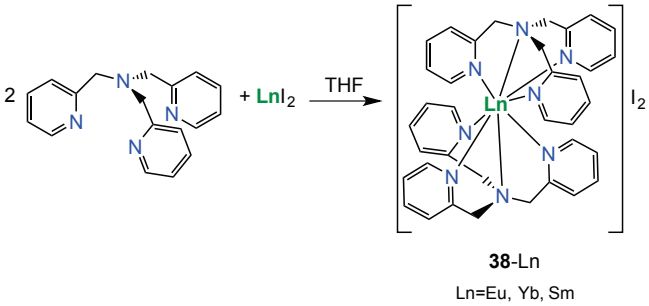


**Scheme IV-12: Synthesis of $[Ln(TPA)_2]I_2$, 38-Ln (Ln=Eu, Yb, Sm).**

In order to prepare the homoleptic bis-ligand complexes, 2eq of TPA were added to the divalent iodide salts $LnI_2$ (Ln=Eu, Yb, Sm) in THF resulting in the precipitation of the complexes $[Ln(TPA)_2]I_2$, **38**-Ln, from the crude mixture (Scheme IV-12). X-ray quality crystals of **38**-Eu and **38**-Sm were obtained by slow diffusion of a THF ligand solution into a solution of the respective $LnI_2$ salt in THF. Crystals of **38**-Yb.$(CH_3CN)_3$ were obtained by slow diffusion of DIPE into an acetonitrile solution of the Yb(II) complex. The structures of **38**-Eu and **38**-Sm are isostructural with each other and are isomorphous with the structure of **38**-Yb.$(CH_3CN)_3$ (Figure IV-13).

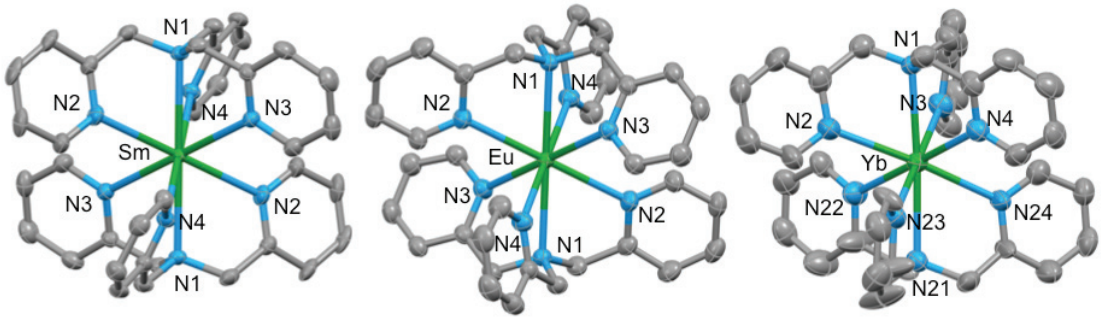


**Figure IV-13: Solid state structure of $[Ln(TPA)_2]I_2$ complexes, 38-Sm (left), 38-Eu (middle), 38-Yb.$(CH_3CN)_3$ (right) (50% ellipsoids). Iodine counter-anions, hydrogen atoms, disorder and solvent molecules are omitted for clarity.**

The complexes **38**-Sm and **38**-Eu crystallize in the monoclinic centrosymmetric $P2_1/c$ space group while **38**-Yb crystallizes in the non-centrosymmetric monoclinic Cc space group. In the **38**-Ln complexes the metal cations are octacoordinated by the eight nitrogen atoms from the two TPA ligands with a distorted cubic geometry. The mean values of the Ln-N distances found for pyridyl nitrogen are 2.69(2) Å for **38**-Sm, 2.67(2) Å for **38**-Eu, and 2.60(2) Å for **38**-Yb. The mean value of the Ln-N distance found for the apical tertiary amine

nitrogen is 2.730(8) Å, 2.727(3) Å, and 2.65(2) Å for the Sm, Eu and Yb complexes respectively (these structural parameters are summarized in Table IV-4 and Table IV-5 in section IV.2.2.6). As expected in ionic bonding model, the Ln-N distances show a linear decrease with decreasing ionic radii from Sm(II) to Yb(II). In the structures of the **38**-Ln complexes the two ligands show opposite right and left handed helical arrangement around the cation as illustrated with **38**-Sm in Figure IV-14 (left). This differs from the structure of the previously reported Ln(III) complexes $[Ln(TPA)_2]X_3$ (Ln= La, Ce, Nd; X=I and Ln=Eu, X=OTf)[303] where both ligands have the same helical arrangement. Such a difference in the ligand arrangement is probably the result of the larger ionic radius of the Ln(II) ions compared to the Ln(III) ones. Notably the same difference is also observed between the structure of **38**-Sm and that of the Sm(III) complex $[Sm(TPA)_2]I_3$, (Figure IV-14 right) prepared according to the procedure described for the above mentioned $[Ln(TPA)_2]I_3$ complexes. The Ln-N distances found in $[Sm(TPA)_2]I_3$ ($Sm\text{-}N_{pyridine}$= 2.55(3) Å and $Sm\text{-}N_{amine}$=2.59(2) Å) are shorter than those found in **38**-Sm ($Sm\text{-}N_{pyridine}$=2.69(2) Å and $Sm\text{-}N_{amine}$=2.730(8) Å) in agreement with the difference in the ionic radii between Sm(III) (1.079 Å) and Sm(II) (1.27 Å).

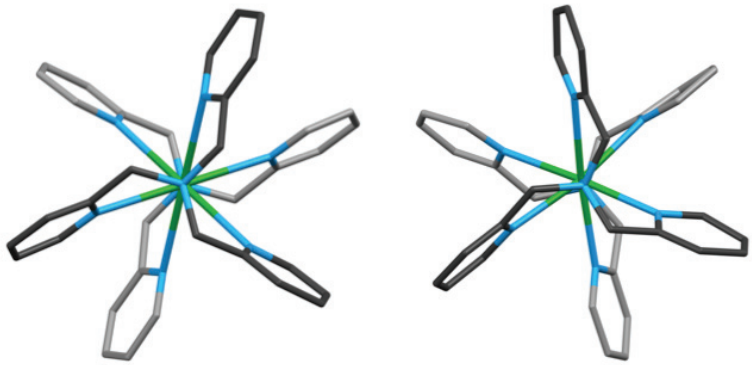

**Figure IV-14: Top view of the structures $[Sm(TPA)_2]I_2$ 38-Sm (left) and $[Sm(TPA)_2]I_3$ (right), (wireframe representation). Hydrogen atoms and iodine counter-ion are omitted for clarity.**

In the $^1H$ NMR spectra of complexes **38**-Ln (Ln=Yb, Sm), in deuterated acetonitrile, five resonances are present: four signals for the pyridyl hydrogens and one signal for the methylene hydrogens meaning that all the chelating arms of both TPA ligands are equivalent with a $D_3h$ symmetry of the complexes in solution. The complexes **38**-Eu and **38**-Yb are stable in acetonitrile solution at room temperature but complex **38**-Sm decomposes in one night leading to a yellow solution of unidentified products (Figure IV-15). This lower stability in solution of the Sm(II) complex compared to its Eu(II) and Yb(II) analogues is in agreement

with the more negative redox potential of Sm and is confirmed by the electrochemistry studies on the homoleptic complexes in section IV.2.3.

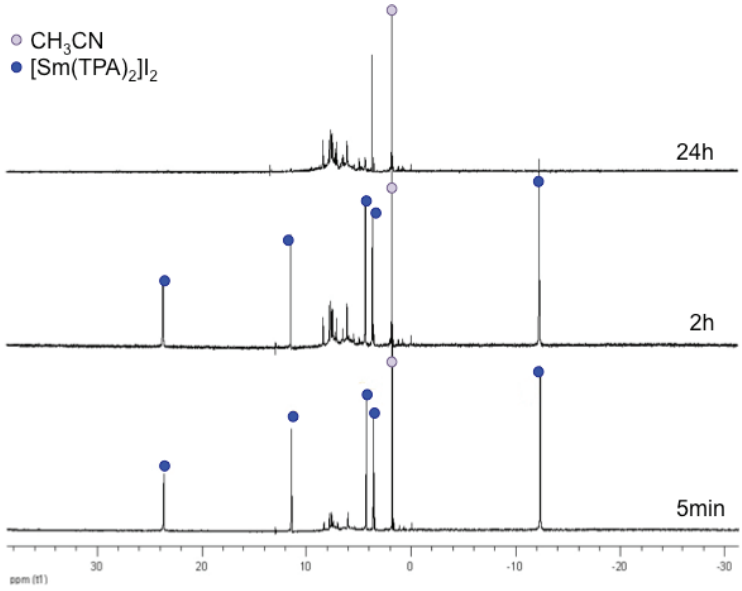


**Figure IV-15: $^1$H NMR spectrum (400 MHz, $CD_3CN$, 298K) of $[Sm(TPA)_2]I_2$, 38-Sm and evolution over time.**

## IV.2.2.3 Syntheses of Ln complexes supported by BPA

In order to investigate the effect of the substitution of one pyridyl arm of the TPA ligand by a phenol arm on the Ln(II) ion redox properties, we studied the complexation of Yb and Eu in the oxidation state +III and +II by the BPA ligand.

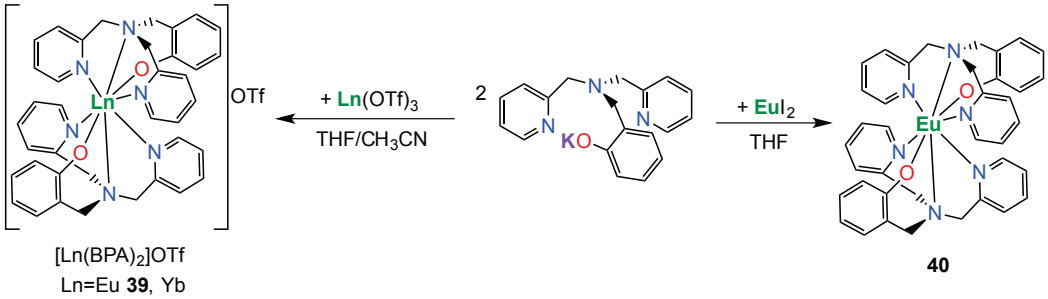


**Scheme IV-13: Synthesis of the trivalent $[Ln(BPA)_2]OTf$ complexes and the divalent $[Eu(BPA)_2]$, 40 complex.**

The addition of 2eq of KBPA to the lanthanide triflate salts $Ln(OTf)_3$ (Ln=Eu, Yb) in acetonitrile leads to the formation of the bis-ligand complexes $[Ln(BPA)_2]OTf$ (Scheme IV-13). The cyclic voltammograms of the crude reaction mixtures in acetonitrile are given in section IV.2.3. The trivalent Eu complex $[Eu(BPA)_2]OTf$, 39, was isolated and orange X-ray quality crystals of **39** were obtained from a slow diffusion of DIPE into a THF solution of the Eu(III) complex. The complex **39** crystallizes in the monoclinic $P2_1/n$ space group. The structure presents an octacoordinated europium centre surrounded by two BPA ligands in a distorted dodecahedral geometry (Figure IV-16). Similar values are found for the average Eu-$N_{pyridyl}$ bond distances (mean value = 2.62(3) Å) and the Eu-$N_{amine}$ distance (2.64(5) Å). The mean value of the Eu-O distances is 2.234(8) Å and fall in the range of Eu-$O_{phenoxide}$ bond distances reported in the literature.[294] The two BPA ligands wrap around the Eu(III) cation with a pincer arrangement rather than the helical one found in bis-TPA complexes.

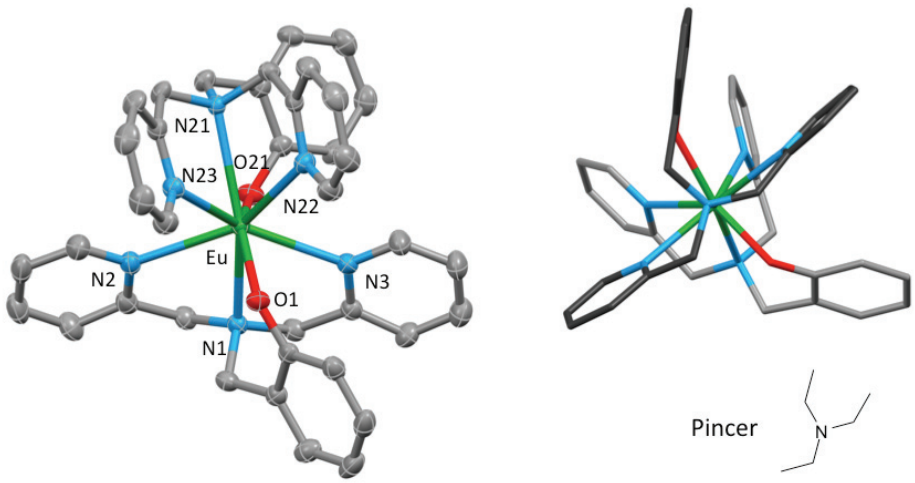


**Figure IV-16: Solid state structure of $[Eu(BPA)_2]OTf$, 39 (left) and top view (right) illustrating the pincer arrangement (50% ellipsoids and wireframe representation). Triflate counter-anions and hydrogen atoms are omitted for clarity.**

The addition of 2eq of KBPA to the divalent lanthanide iodide salt $EuI_2$ in THF leads to the formation of the neutral complex $[Eu(BPA)_2]$, **40** (Scheme IV-13). The complex **40** is poorly soluble in THF but presents a better solubility in acetonitrile and pyridine. The Eu(II) complex is stable in acetonitrile and pyridine solution for weeks. The $^1H$ NMR spectrum of **40** shows a very broad and uninformative signal because of the paramagnetism of the Eu(II) ion. Crystals suitable for X-ray diffraction were obtained from a slow diffusion of hexane into a

pyridine solution of **40**. This homoleptic complex crystallizes in monoclinic system and P $2_1/n$ space group.

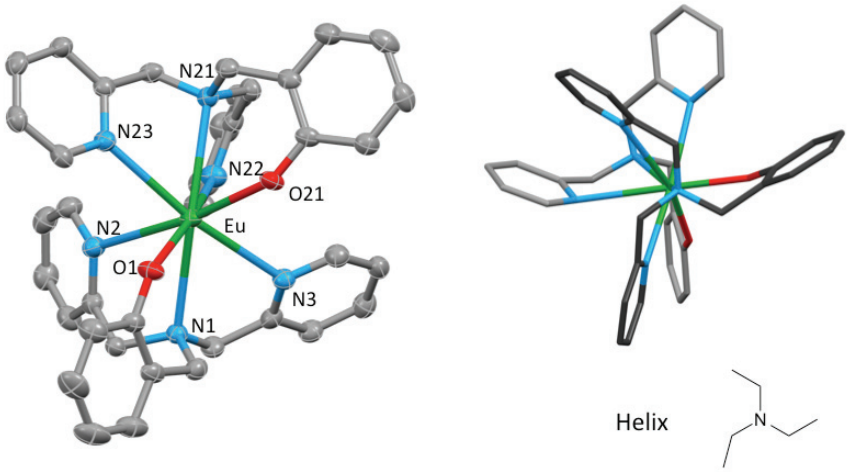


**Figure IV-17: Solid state structure of [Eu(BPA)$_2$], 40 (left) and top view (right) illustrating the helical arrangement (50% ellipsoids and wireframe representation). Hydrogen atoms are omitted for clarity.**

The overall neutral charge is in agreement with the presence of an Eu(II) metal centre. The octacoordinated europium centre is surrounded by two ligands arranged in a distorted cubic fashion (Figure IV-17). The two ligands wrap around the metal ion in a geometry that brings the two oxygen atoms from the phenolate arms side by side. In each ligand, a Eu-$N_{pyridyl}$ distance is significantly shorter than the other: 2.755(3) and 2.866(3) Å for the first ligand, 2.742(3) and 2.887(3) Å for the second one. These distances are slightly elongated compared to the bis-TPA europium complex **38**-Eu where the average Eu-$N_{pyridyl}$ is 2.68(2) Å. This is probably due to the steric effect of the phenol arms. The average value of the Eu-$N_{amine}$ 2.83(5) Å is 0.1 Å longer than the value found for **38**-Eu. The large lengthening of the Eu-N and Eu-O (2.83(5) Å) distances found in complex **40** compared to its Eu(III) analogue **39** can be interpreted in term of the difference in ionic radii of the Eu(III) and Eu(II) cations (0.19 Å). The two ligands in the divalent **40** complex adopt the same helical conformation leading to a chiral complex. Both enantiomers ΛΛ and ΔΔ are present in the structure.

The $^1$H NMR spectrum of the crude reaction mixture of $YbI_2$ with 2eq of KBPA in THF (at room temperature or at -40°C) shows numerous signals in the paramagnetic region demonstrating the formation of a mixture of Yb(III) species. Performing the reaction in $CD_3CN$ at -40°C leads to a $^1$H NMR spectrum showing one set of paramagnetic signals attributed to the Yb(III) complex $[Yb(BPA)_2]^+$ but also signals of an unstable diamagnetic

intermediate which decompose rapidly even at -40°C. Attempts to isolate single crystals of these diamagnetic intermediates failed. The reaction mixtures, both in THF and acetonitrile, turn deep blue after 1 night at room temperature or at -40°C. As $[Yb(BPA)_2]^+$ is colourless, the deep blue colour of the mixture suggests additional decomposition products such as solvent or ligand reduction products. Indeed highly reactive Yb(II) complexes have been shown to effect the C-C coupling of phenanthroline[224] or solvent molecules such as pyridine[314] and acetonitrile.[315] Yet, as we were not able to isolate any reduction products, the formation of $[Yb(BPA)_2]^+$ via a disproportionation reaction of an Yb(II) complex to Yb(III) and Yb(0) species cannot be ruled out. Attempt to form the putative divalent ytterbium complex $[Yb(BPA)_2]$ in THF at -80°C under $CO_2$ atmosphere affords silent NMR species which could not be crystallographically characterised.

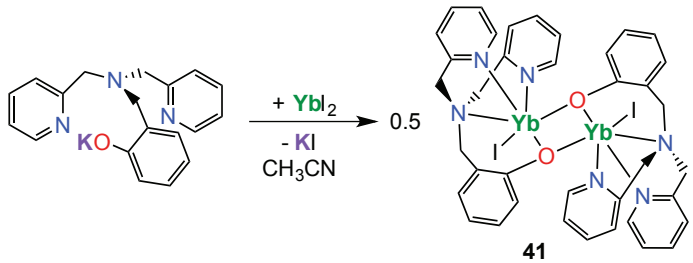


**Scheme IV-14: Synthesis of $[Yb(BPA)I(CH_3CN)]_2$, 41.**

However, when only 1eq of KBPA is added to the $YbI_2$ salt in deuterated acetonitrile, a dark green suspension is obtained and the $^1H$ NMR spectrum of the crude reaction mixture shows only one set of signals in the diamagnetic zone indicating the formation of a stable mono-ligand Yb(II) compound (Scheme IV-14). Dark green crystals suitable for X-ray diffraction were obtained from a saturated acetonitrile solution. The crystal structure of the divalent complex $[Yb(BPA)I(CH_3CN)]_2.(CH_3CN)_{0.4}$, **41**.$(CH_3CN)_{0.4}$ shows that the phenolate oxygen atoms of the ligand BPA bridge two Yb(II) ions affording a dimer with an inversion center in the middle of the YbOYbO diamond core (Figure IV-18). The two Yb ions are heptacoordinated by three nitrogen and two oxygen atoms from the BPA ligands, one nitrogen from an acetonitrile molecule and one iodide in a distorted pentagonal bipyramidal geometry. The value of the Yb-$N_{amine}$ distance (2.594(3) Å) and the average value of the Yb-$N_{pyridyl}$ distance (2.626(9) Å) in complex **41** are similar to those found for the Yb-$N_{amine}$ and Yb-$N_{pyridyl}$ distances in the bis-TPA Yb(II) complex **38**-Yb. The Yb-O distances is 2.346(3) Å and falls in the range of bridging Yb-$O_{phenoxide}$ bond distances reported in literature.[51]

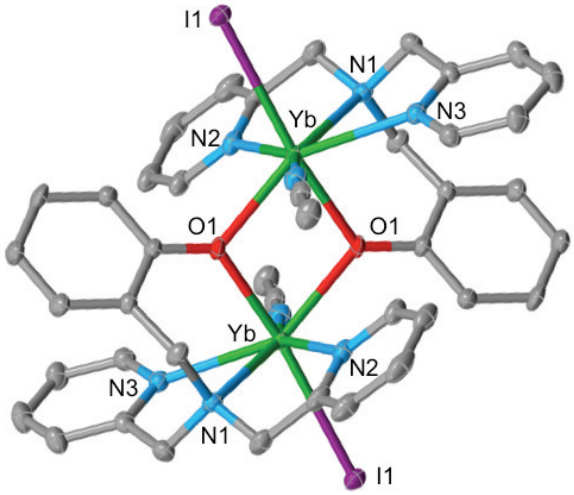


**Figure IV-18: Solid state structure of $[Yb(BPA)I(CH_3CN)]_2.(CH_3CN)_{0.4}$, 41.$(CH_3CN)_{0.4}$ (50% ellipsoids). Hydrogen atoms and solvent molecule are omitted for clarity.**

When 1eq of KBPA is added to the $EuI_2$ salt in THF at -40°C, the $^1H$ NMR spectrum of the crude mixture in deuterated acetonitrile shows only the signals of the solvent in agreement with the presence of NMR silent Eu(II) species.

These results show that the substitution of one pyridyl arm in the TPA ligand by a phenol one to afford the BPA ligand significantly decreases the stability of the homoleptic bis-BPA Yb(II) complex compared to its TPA analogue **38**-Yb. The greater stability of the bis-BPA Eu(II) complex, **40**, can be explained by its less negative redox potential (as shown in IV.2.3 section). In contrast, the heteroleptic mono-BPA Yb(II) complex **41** is stable at room temperature in solution and in the solid state for weeks. This complex is an attractive species for reactivity studies and for its potential catalytic activities. Notably, some divalent lanthanide mono-aminophenolate complexes have been shown to undertake catalytic ring opening polymerisation of cyclic esters[51, 53, 309-311] or catalytic hydrophosphination of styrene.[50] Preliminary reactivity tests show that complex **41** reacts with azobenzene, $CS_2$ and $CO_2$ but further efforts need to be done to identify the reaction products.

## IV.2.2.4 Syntheses of Ln complexes supported by BPPA

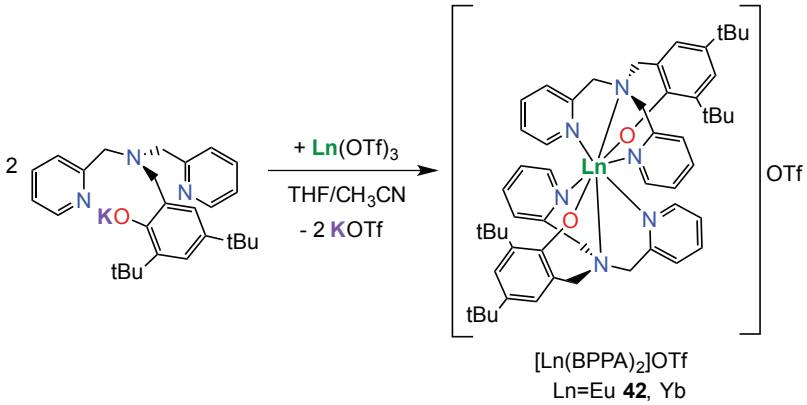


**Scheme IV-15: Synthesis of [Ln(BPPA)$_2$]OTf complexes.**

In order to improve the solubility of the lanthanide aminophenolate complexes and investigate the effect of the donor tert-butyl groups on the redox properties, coordination of lanthanide ions by the BPPA ligand was studied. The addition of 2eq of KBPPA to the lanthanide triflate salts Ln(OTf)$_3$ (Ln=Eu, Yb) in acetonitrile leads to the formation of the bis-ligand complexes [Ln(BPPA)$_2$]OTf (Scheme IV-15). The cyclic voltammograms of the crude reaction mixtures in acetonitrile are given in section IV.2.3. The trivalent Eu complex [Eu(BPPA)$_2$]OTf, **42**, was isolated and orange needles of **42**.(Py)$_{2.5}$ were obtained from a slow diffusion of hexane into a pyridine solution of this Eu(III) complex. The quality of the collected X-ray data is unfortunately insufficient to discuss the structural parameters but good enough to determine the global structure and connectivity (Figure IV-19). The crystal structure shows that the europium centre is octacoordinated by two tetradentate BPPA ligands with a distorted cubic geometry. The ligand arms are both in a helical conformation presenting opposite rotation direction. This results in an achiral complex. The overall monocationic charge of the Eu(III) complex is counterbalanced by the triflate anion. Complex **42** is fully soluble in $CH_3CN$ but present a lower solubility in THF. The isolation of complex **42** attests that the presence of the tertbutyl groups does not prevent formation of homoleptic bis-BPPA complexes. Attempts to isolate the divalent europium bis-ligand complexes led to the formation of silent NMR species. Crystallization experiments were not successful.

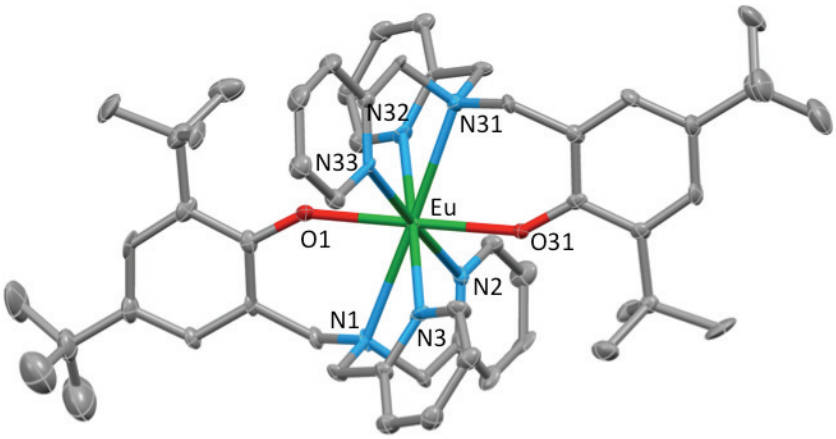


**Figure IV-19: Solid state structure of [Eu(BPPA)$_2$]OTf.(Py)$_{2.5}$, 42.(Py)$_{2.5}$ (50% ellipsoids). Triflate counter-anion, hydrogen atoms and lattice solvent molecule are omitted for clarity.**

## IV.2.2.5 Syntheses of Ln complexes supported by MPA

We were then interested in the synthesis of lanthanide complexes supported by MPA ligands possessing two phenol arms in order to study the influence of the charge and of the donor character of the ligand on the redox properties.

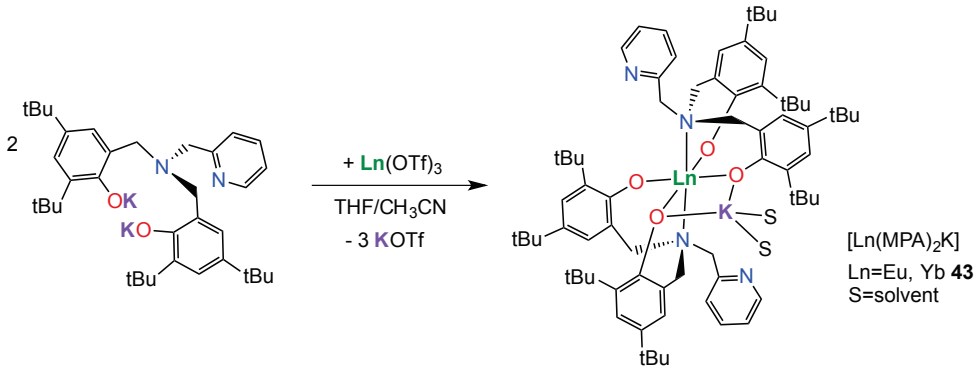


**Scheme IV-16: Synthesis of [Ln(MPA)$_2$K] complexes.**

The addition of 2eq of $K_2$MPA to the lanthanide triflate salts Ln(OTf)$_3$ (Ln=Eu, Yb) in THF leads to the formation of the heterobimetallic bis-ligand complexes [Ln(MPA)$_2$K] (Scheme IV-16). The cyclic voltammograms of the crude reaction mixtures in acetonitrile are given in section IV.2.3. The trivalent Yb complex [Yb(MPA)$_2$K(DME)$_2$], **43**-DME, was isolated and colourless crystals suitable for X-ray diffraction were obtained from a solution of the complex in a DME/hexane mixture (~1/30) at -40°C. The solubility in non-polar solvents

of the complexes supported by MPA ligands is largely increased thanks to the presence of the four tert-butyl substituents. The X-ray crystal structure (Figure IV-20) shows that two MPA ligands bind to the Yb(III) ion, but in the resulting complex the pyridine nitrogens remain not binding with a Ln-N distance of 5.393(19) Å. As a result the ytterbium centre is only hexacoordinated by two MPA ligands in a distorted octahedral geometry. The average values of the Yb-O distances and of the Yb-$N_{amine}$ distances are respectively 2.16(2) Å and 2.448(16) and are slightly shorter than the Yb-O and Yb-$N_{amine}$ average distances of the mono-BPA Yb(II) complex **41** (Table IV-4 and Table IV-5 in section IV.2.2.6). This is in agreement with the smaller ionic radii of Yb(III) centre. A potassium cation is also present in the structure and binds a phenolate oxygen from each ligand with a K-O distance of 2.794(14) Å. Two DME molecules complete the K coordination sphere. A two-fold axis is passing through the Yb and K atoms.

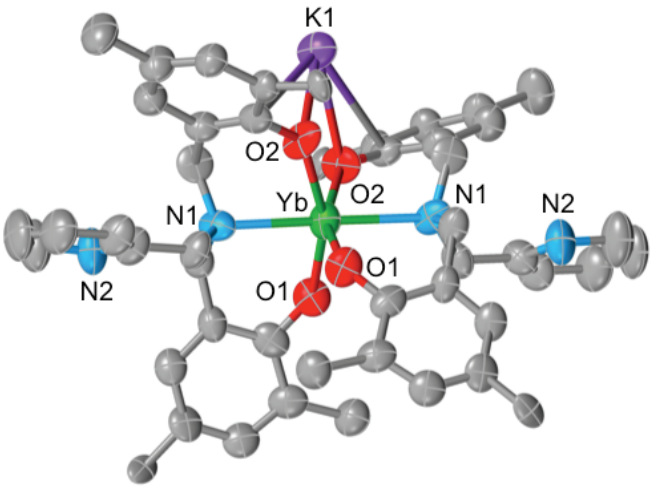


**Figure IV-20: Solid state structure of [Yb(MPA)$_2$K(DME)$_2$], 43-DME (50% ellipsoids). Methyl groups of the tert-butyl substituents, DME solvent molecules coordinated to K and hydrogen atoms are omitted for clarity.**

The $^1$H NMR spectrum of complex **43** in deuterated acetonitrile shows the presence of both broad and sharp paramagnetic signals from -50 to 186 ppm confirming the +III oxidation state of the Yb centre. The $^1$H NMR spectrum in $CD_3CN$ of the crude reaction mixture of $Eu(OTf)_3$ and 2eq of $K_2MPA$ shows one set of 18 signals from -9 to 10 ppm assigned to the trivalent [Eu(MPA)$_2$K] complex. Unfortunately, attempts to obtain crystals of this Eu(III) complex failed.

Interestingly, the addition of only 1eq of $K_2$MPA ligand to $LnOTf_3$ (Ln=Eu, Yb) in THF or $CH_3CN$ leads, regardless of the stoichiometry, to the formation of the bis-ligand complexes [Ln(MPA)$_2$K] identified by $^1$H NMR spectroscopy. The MPA ligand seems to feature a strong preference for bis-ligand complex formation which is quite rare in coordination chemistry. However, similar behaviours were reported for complexes of Ln(III) supported by tripodal aminoimidazole or aminophenolate ligands.[316-318]

The addition of 2eq of $K_2$MPA to $YbI_2$ in THF at -40°C leads to the immediate formation of the Ln(III) complex **43**, identified by $^1$H NMR spectroscopy and X-ray diffraction. This indicates the oxidation of the Yb(II) centre by solvent/ligand reduction or by disproportionation in Yb(0) and Yb(III) species (Figure IV-21 top). Such an oxidation of a hypothetical Yb(II) bis-ligand complexes supported by tripodal aminobisphenolate ligands in its respective Yb(III) bis-ligand complexes has also been observed by Delbridge et al.[51, 309] The addition of 2eq of $K_2$MPA to $EuI_2$ in THF at -40°C leads to an intermediate NMR silent species suggesting the presence of Eu(II) complexes. This intermediate slowly decomposes at room temperature to afford the Eu(III) bis-ligand complex [Eu(MPA)$_2$K] (identified by $^1$H NMR spectroscopy). Crystallisation experiments were unsuccessful.

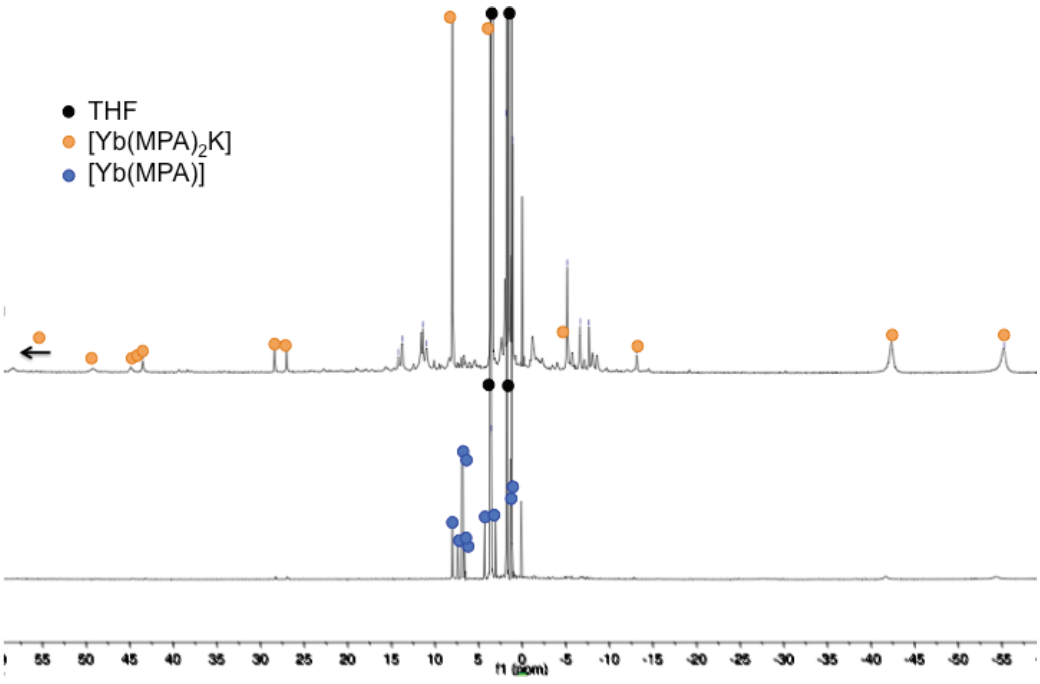


**Figure IV-21: $^1$H NMR spectra (400 MHz, THF-d$_8$, 298K) of the 1:2 (top) and 1:1 (bottom) $YbI_2$ and $K_2$MPA reaction mixtures at -40°C in THF-d$_8$.**

In contrast preliminary NMR studies indicate that it is possible to obtain Ln(II) mono-MPA complexes (Ln=Eu, Yb) stable in THF at room temperature (Figure IV-21 bottom for Yb). Unfortunately, no single crystal of the complexes [Ln(MPA)] (Ln=Eu, Yb) was obtained so far. Nevertheless, preliminary reactivity tests show that the [Yb(MPA)] complex reacts with $CO_2$ but further efforts need to be done to identify the reaction products.

In summary, the substitution of two pyridyl arms of the TPA ligand by two phenolate groups results in highly electron-rich metal centres with increased reactivity. This prevents the isolation of the desired homoleptic divalent bis-ligand complexes [Ln(MPA)$_2$K$_2$] (Ln=Eu, Yb) and leads to the oxidation (by solvent or ligand) or disproportionation of the Ln(II) centres. However, the formation of divalent mono-ligand [Ln(MPA)] complexes is promising and future work will focus on the reactivity of these compounds with small molecules. Indeed, previously reported stable Ln(II) mono-ligand complexes supported by aminobisphenolate complexes with bulky substituents have been shown to react stoichiometrically with carbodiimides to yield oxalamidinate or diamidocarbene[307] and to be pre-catalyst for ring-opening polymerization of cyclic esters.[51, 309-311]

## IV.2.2.6 Summary of syntheses and structural parameters

The Scheme IV-17 summarizes the reactivity of Ln(II) salts with the aminophenolate ligands BPA and MPA compared to TPA. Instability of the Sm complexes was observed even for the neutral TPA ligand which led us to do not investigate the coordination of the Sm(II) ion with the more electron-rich aminophenolate ligands. The replacement of even just one pyridine arm by a phenolate one leads to homoleptic complexes of Yb(II) that are unstable and decompose in their trivalent analogues [Yb(BPA)$_2$]I and [Yb(MPA)$_2$K]. However, the mono-ligand complexes of Yb(II) with these ligands are stable. In the case of the Eu(II) centre, stable homoleptic complexes cannot be isolated with the MPA ligand. However the putative mono-MPA complexes of Eu(II) and Yb(II), identified by $^1$H NMR are stable in THF at room temperature.

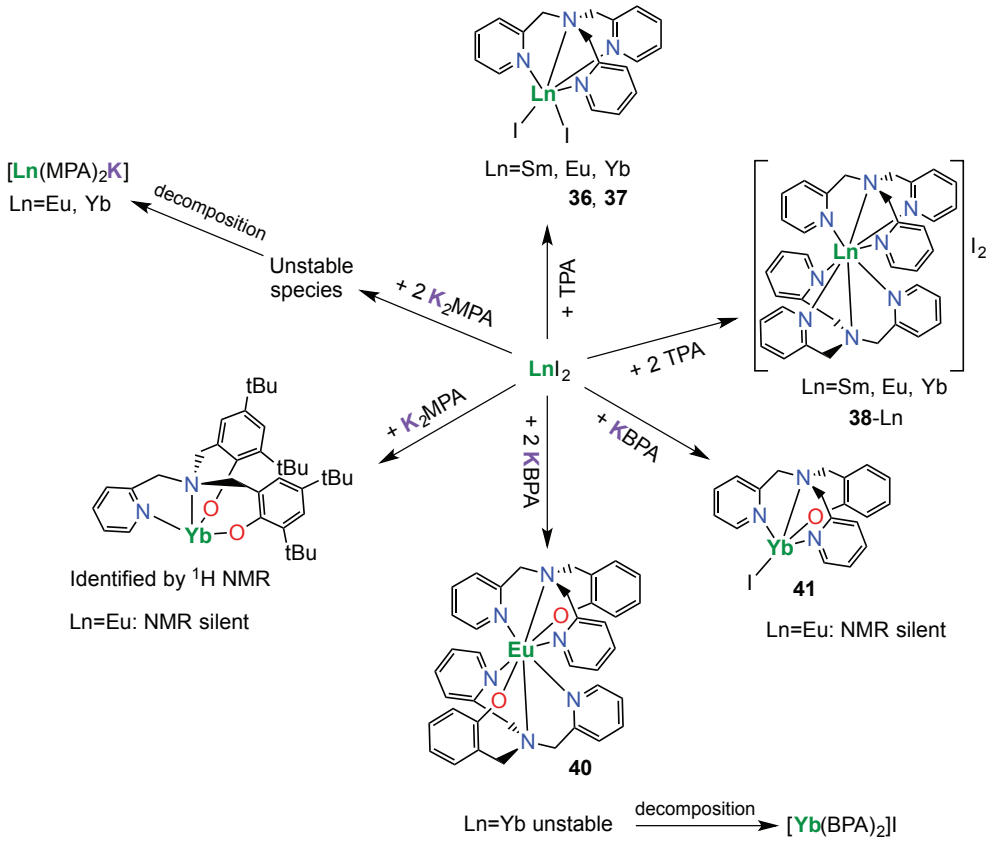


**Scheme IV-17: Syntheses of the Ln(II) mono- and bis-ligand complexes supported by the TPA and TPA-derivative ligands.**

The Scheme IV-18 summarizes the "in situ" reactivity of Ln(III) with the aminophenolate ligands BPA and MPA compared to TPA. At least one complex was isolated and fully characterised for each ligand system. The solid state structures of $[Sm(TPA)_2]I_3$, $[Eu(BPA)_2]OTf$, $[Eu(BPPA)_2]OTf$ and $[Yb(MPA)_2K]$, together with the $^1H$ NMR spectra, confirm the 2:1 stoichiometry of these complexes.

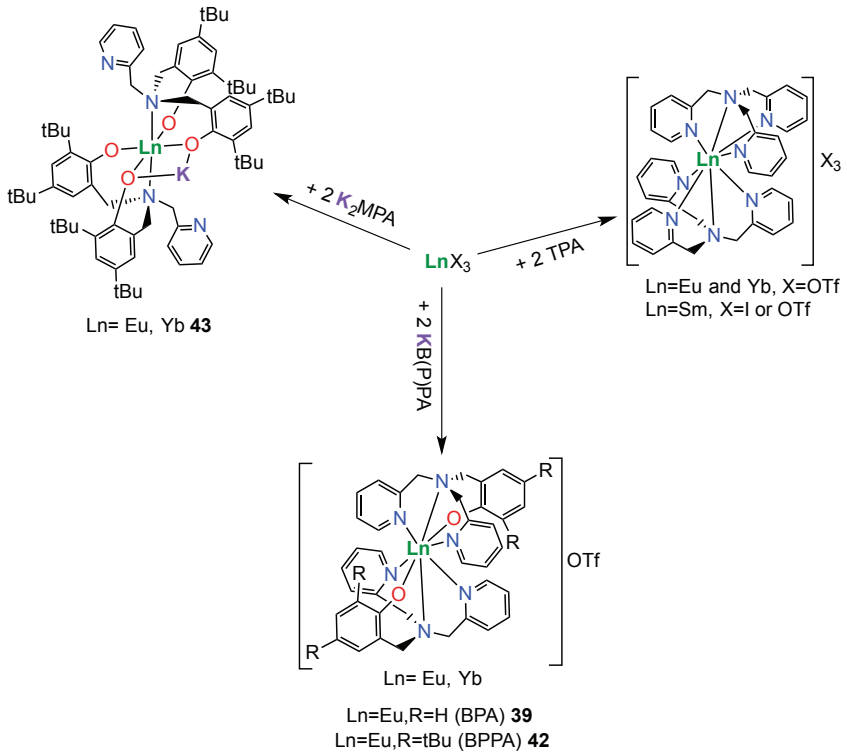


**Scheme IV-18: Syntheses of the Ln(III) bis-ligand complexes supported by the TPA and TPA-derivative ligands.**

The Ln-$N_{amine}$, Ln-$N_{pyridyl}$ and eventual Ln-O distances (or average distance) in the earlier described solid state structures are summarized in Table IV-4 for the europium complexes and in Table IV-5 for the ytterbium ones. The observed variations in bond lengths between the two tables are in agreement with the size evolution of the lanthanide ions: the distances are found shorter for the smaller Yb ions. Besides, in each table the variations in bond lengths are in agreement with the change in oxidation state: The distances are shorter for the smaller and more acidic Ln(III) complexes.

**Table IV-4: Selected bond lengths (or average) for the Eu complexes (in Å).**

| Bonds | 37<br>Eu(II)<br>mono-TPA | 38-Eu<br>Eu(II)<br>bis-TPA | 40<br>Eu(II)<br>bis-BPA | 39<br>Eu(III)<br>bis-BPA |
|---|---|---|---|---|
| Eu-$N_{amine}$ | 2.748(3) | 2.731(3) | 2.83(5) | 2.64(5) |
| Eu-$N_{pyridyl}$ | 2.67(1) | 2.68(2) | 2.749(9)<br>and 2.88(1) | 2.62(3) |
| Eu-O | - | - | 2.41(3) | 2.234(8) |

**Table IV-5: Selected bond lengths (or average) for the Yb complexes (in Å).**

| Bonds | 36 Yb(II) mono-TPA | 38-Yb Yb(II) bis-TPA | 41 Yb(II) mono-BPA | 43 Yb(III) bis-MPA |
|---|---|---|---|---|
| Yb-$N_{amine}$ | 2.620(4) | 2.65(3) | 2.594(3) | 2.448(16) |
| Yb-$N_{pyridyl}$ | 2.565(6) | 2.68(2) | 2.626(9) | - |
| Yb-O | - | - | 2.346(3) | 2.16(2) |

## IV.2.3 Electrochemistry studies of the homoleptic Ln(III) complexes

To correlate the observed reducing abilities of the divalent lanthanide complexes with their redox properties, cyclic voltammetry analyses were performed in acetonitrile on the *in situ* prepared homoleptic Ln(III) complexes supported by TPA, BPA, BPPA and MPA ligands. The Table IV-6, at the end of this section, summarizes the obtained voltammetric data for Eu and Yb complexes.

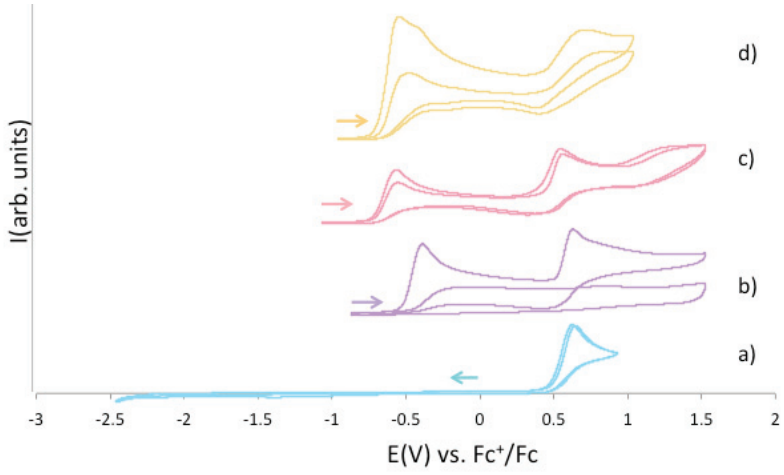


**Figure IV-22: Cyclic voltammograms of TPA (4mM) (a), KBPA (<4mM) (b), KBPPA (4mM) (c) and $K_2$MPA (4mM) (d) in ~0.1 M [$Bu_4N$][$PF_6$] acetonitrile solution at 100 mV.s-1 scan-rate.**

Prior to the electrochemistry studies of the lanthanide complexes, the cyclic voltammograms of the free TPA and of the potassium salts KBPA, KBPPA and $K_2$MPA were measured in acetonitrile under similar conditions (Figure IV-22). The oxidation process around 0.5 V on each voltammogram is attributed to the oxidation of the central amine while the oxidation wave around -0.5 V on the KBPA, KBPPA and $K_2$MPA voltammograms is attributed to the phenolate oxidation. All these events are irreversible even when the scan rate is increased to 1 $V.s^{-1}$.

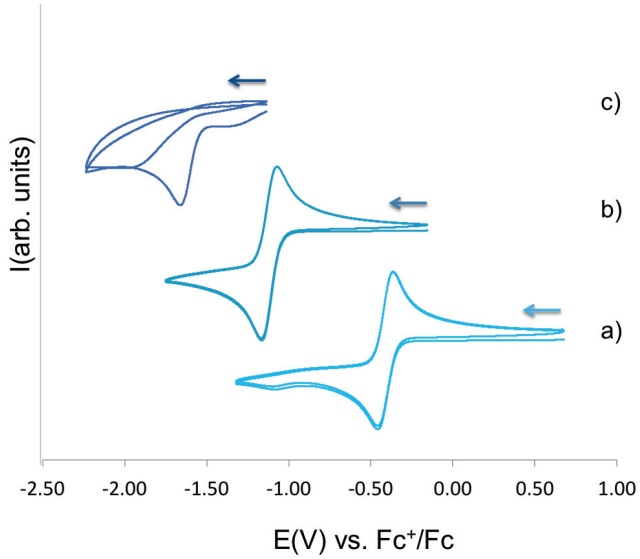


**Figure IV-23: Cyclic voltammograms for 4 mM solutions of a) $[Eu(TPA)_2]OTf_3$, b) $[Yb(TPA)_2]OTf_3$ and c) $[Sm(TPA)_2]OTf_3$ in ~0.1 M $[Bu_4N][PF_6]$ acetonitrile solution at 100 mV.s-1 scan-rate.**

The cyclic voltammograms of the complexes $[Ln(TPA)_2]OTf_3$ (Ln=Eu, Yb, Sm), presented in Figure IV-23, show a quasi-reversible reduction of the Ln(III) metal centre for the less reducing Eu (-0.41 V vs. $Fc^+/Fc$) and Yb (-1.11 V vs. $Fc^+/Fc$) systems. The voltammogram of the Sm(II) complex show an irreversible reduction of the metal centre at -1.7 V vs. $Fc^+/Fc$ even at 1 $V.s^{-1}$ scan rate. This is in agreement with the stability observed for the divalent **38**-Eu and **38**-Yb complexes and the instability of **38**-Sm in acetonitrile. Moreover, the differences in reduction potentials between $[Eu(TPA)_2]OTf_3$ and $[Yb(TPA)_2]OTf_3$ ($\Delta E$= -0.70 V), and $[Yb(TPA)_2]OTf_3$ and $[Sm(TPA)_2]OTf_3$ ($\Delta E$= -0.55 V), are in reasonable agreement with the corresponding differences in reduction potentials between Eu(III) and Yb(III), and Yb(III) and Sm(III) ions ($\Delta E$= -0.80 V and $\Delta E$= -0.40 V, respectively).[22] These reduction events are absent from the cyclic voltammogram of the free TPA ligand in $CH_3CN$ confirming their metal-based characters. An irreversible oxidation,

attributed to the oxidation of the central tertiary amine, is present on the free TPA voltammogram at 0.63 V but absent from the one of $[Ln(TPA)_2]OTf_3$. This is probably due to the coordination of the lanthanide centre to the central amine leading to stabilization of the latter. In consequence, the amine is more difficult to oxidize; the irreversible oxidation event is thus shifted from 0.63 V to higher potentials.

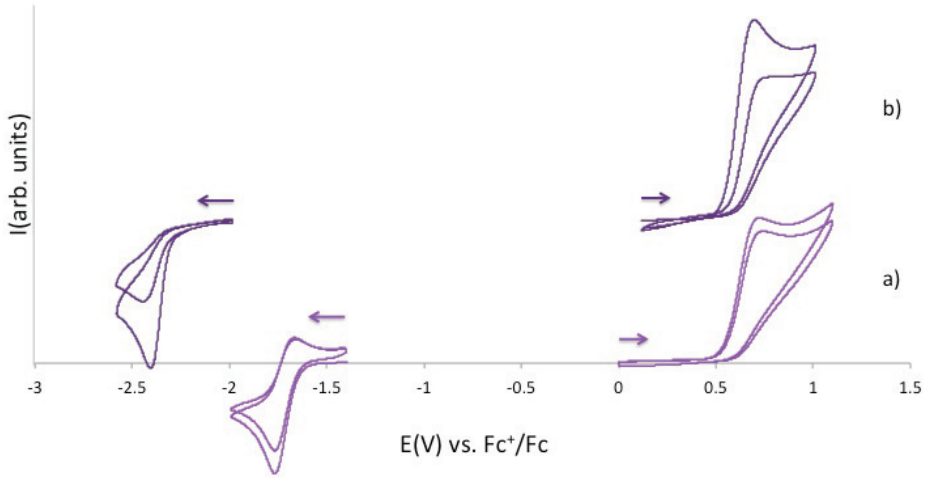


**Figure IV-24: Cyclic voltammograms for 4 mM solutions of a) $[Eu(BPA)_2]OTf$ and b) $[Yb(BPA)_2]OTf$ in ~0.1 M $[Bu_4N][PF_6]$ acetonitrile solution at 100 mV.s-1 scan-rate.**

The cyclic voltammogram of $[Eu(BPA)_2]OTf$ shows a quasi-reversible reduction of the Eu(III) centre at -1.73 V vs. $Fc^+/Fc$ which corresponds to a shift of this event of -1.25 V compared to the Eu(III) TPA analogous complex. In the case of the $[Yb(BPA)_2]OTf$ complex, the reduction is irreversible with a cathodic potential at -2.41 V vs. $Fc^+/Fc$ close to the solvent reduction (Figure IV-24). This event remains irreversible even at 1 $V.s^{-1}$ scan rate which indicates the formation of a highly reactive Yb(II) complex. The shift of -1.24 V of the cathodic potential of $[Yb(BPA)_2]OTf$ compared to the Yb(III) TPA analogue is comparable to the shift observed in the europium systems. The lanthanide centre is significantly more electron-rich and thus more difficult to reduce when one pyridyl group of the TPA ligand is replaced by a phenolate one. Although a shift in the metal-based redox event towards more negative potential was expected using BPA instead of TPA, such a large shift (> 1.2 V) is surprising but it helps to explain the instability of the much more reducing Yb(II)-BPA species. The voltammograms of $[Ln(BPA)_2]OTf$ present irreversible oxidation process at 0.72 V vs. $Fc^+/Fc$ for Eu and 0.70 V vs. $Fc^+/Fc$ for Yb. These oxidation events were not present in the voltammograms of $[Ln(TPA)_2]OTf_3$. They are assigned to the oxidation of the phenolate

moiety of BPA which is easier to oxidize than the tertiary amine. The anodic potential in the voltammogram of the potassium salt KBPA was originally at -0.43 V vs. $Fc^+/Fc$. This demonstrates a stabilization of the phenol function of the BPA ligand by coordination to the lanthanide centre.

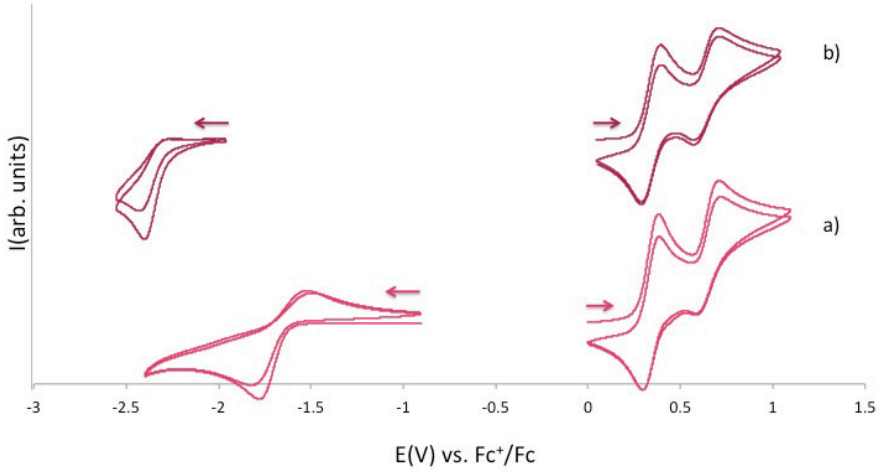


**Figure IV-25: Cyclic voltammograms for 4 mM solutions of a) $[Eu(BPPA)_2]OTf$ and b) $[Yb(BPPA)_2]OTf$ in ~0.1 M $[Bu_4N][PF_6]$ acetonitrile solution at 100 mV.s-1 scan-rate.**

The cyclic voltammograms of $[Ln(BPPA)_2]OTf$ (Ln=Eu, Yb), presented in Figure IV-25, feature very similar reduction potentials of the Ln(III) centres compared to the analogous $[Ln(BPA)_2]OTf$ voltammograms. Indeed, the cathodic potentials are almost unchanged (-2.40 V for Yb and -1.78 V for Eu with BPPA ligand compared to -2.41 V for Yb and -1.77 V for Eu with the BPA ligand). This demonstrates that the tert-butyl groups, despite their electron-donor character, do not impact significantly the reduction potential of the metal centre. On the cyclic voltammograms of $[Ln(BPPA)_2]OTf$, two quasi-reversible oxidation processes are visible at 0.34 V and 0.65 V vs. $Fc^+/Fc$ for Eu and at 0.34 V and 0.64 V vs. $Fc^+/Fc$ for Yb. These events are assigned to the successive oxidation of the phenolate functions forming phenoxyl radical cations. The quasi-reversibility of the waves can be explained by the stabilization of these radical cations by the tert-butyl groups in ortho and para positions of the phenolate cycle in BPPA ligand. However, the coordination of the ligand to the lanthanide ion also increase this stabilization. Indeed, the phenolate oxidation process on the voltammogram of the potassium salt KBPPA is not reversible (Figure IV-22 c).

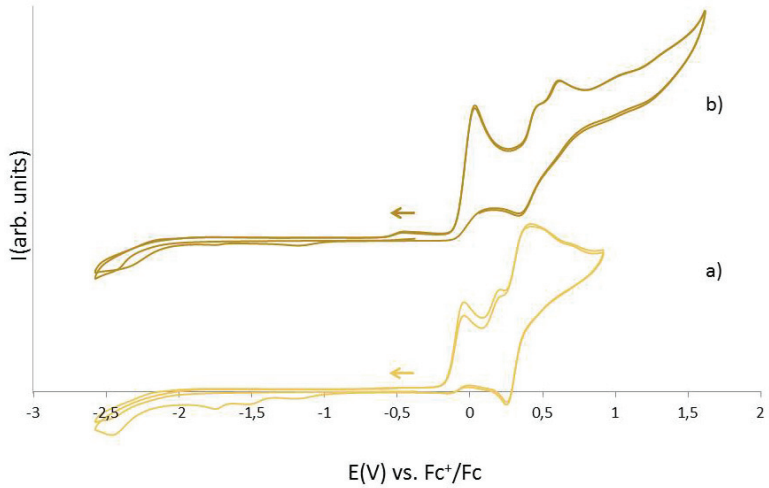


**Figure IV-26: Cyclic voltammograms for 4 mM solutions of a) [Eu(MPA)$_2$K] and b) [Yb(MPA)$_2$K] in ~0.1 M [Bu$_4$N][PF$_6$] acetonitrile solution at 100 mV.s-1 scan-rate.**

The cyclic voltammograms of [Ln(MPA)$_2$K] (Ln=Eu, Yb) do not present any metal-based reduction event (Figure IV-26). Even when the experiment was performed in THF, a more inert solvent, no reduction of the metal centre was visible. Some small reduction processes appears on the second cycle but are linked to oxidation events on the ligand. This absence of metal-based reduction indicates a shift of the redox potential beyond the solvent reduction potential in agreement with the instability observed during the reaction between the iodide salt $LnI_2$ (Ln=Eu, Yb) and 2eq of $K_2MPA$ both in THF and acetonitrile. The ligand-based redox processes are much more difficult to interpret than for the analogous BPPA complexes.

**Table IV-6: Voltammetric data for Eu and Yb complexes (in V vs. Fc$^+$/Fc)**

| Compounds | Metal-based event | | Ligand-based events | |
|---|---|---|---|---|
| | $E_{pc}$ (V) | $E_{pa}$ (V) | $E_{pa1}$ (V) | $E_{pa2}$ (V) |
| **[Eu(TPA)$_2$]OTf$_3$** | -0.46 | -0.36 | - | - |
| **[Eu(BPA)$_2$]OTf** | -1.77 | -1.66 | 0.72 | - |
| **[Eu(BPPA)$_2$]OTf** | -1.78 | -1.52 | $E_{1/2}$=0.34 | $E_{1/2}$=0.65 |
| **[Yb(TPA)$_2$]OTf$_3$** | -1.17 | -1.05 | - | - |
| **[Yb(BPA)$_2$]OTf** | -2.41 | - | 0.70 | - |
| **[Yb(BPPA)$_2$]OTf** | -2.40 | - | $E_{1/2}$=0.34 | $E_{1/2}$=0.64 |

In conclusion the electrochemistry analyses illustrates the increasing electron-rich character of the homoleptic Ln complexes when the ligands present an increased number of phenolate arms. The changes in redox potential are very large suggesting that these ligands should promote interesting reactivity in "classical" easy to handle Ln(II) ions.

## IV.2.4 Preliminary reactivity studies

The reactivity of the Ln(II) homoleptic complexes was investigated with $CO_2$ and $CS_2$ which were found to be reduced respectively by $[Yb(OSi(OtBu)_3)_4K_2]$ and $[Ln(OSi(OtBu)_3)_4K_2]$ (Ln=Eu and Yb).

The divalent complexes $[Ln(TPA)_2]I_2$ (**38**-Ln with Ln=Eu, Yb), $[Eu(BPA)_2]$ (**40**) and $[Eu(MPA)_2K_2]$ (at low temperature) do not react with $CO_2$. However, while the divalent complexes $[Ln(TPA)_2]I_2$ (**38**-Ln with Ln=Eu, Yb) do not react with $CS_2$, the complex $[Eu(BPA)_2]$ (**40**) is able to reduce $CS_2$. The addition of 1eq of $CS_2$ to the complex **40** in THF or pyridine leads to a colour change from purple to red. The $^1H$ NMR spectrum in deuterated pyridine of the crude reaction mixture shows only the signals of the Eu(III) complex $[Eu(BPA)_2]^+$ probably due to the fluxional nature of the putative $[Eu(CS_3)(BPA)_2]^-$ complex. When DMSO-$d_6$ is added to the residue after solvent removal, the $^1H$ NMR spectrum shows, in addition of the $[Eu(BPA)_2]^+$ signals, a set of paramagnetic peaks attributed to the complex $[Eu(BPA)(CS_3)(DMSO)_2]$, **44** (Scheme IV-19).

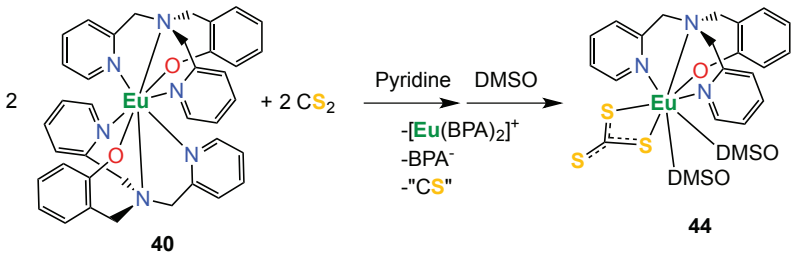


**Scheme IV-19: Reactivity of complex 40 with $CS_2$, synthesis of complex 44.**

Indeed, crystals of **44**.DMSO suitable for X-ray diffraction were obtained by slow diffusion of toluene into a DMSO solution of the reaction products. The structure of **44**.DMSO, presented in Figure IV-27, shows the presence of a Eu(III) ion surrounded by one BPA ligand and a terminal trithiocarbonate moiety. Two DMSO molecules complete the

coordination sphere of the europium centre which is thus octacoordinated in a distorted dodecahedral geometry. The values of the Eu-$N_{amine}$, of Eu-$N_{pyridyl}$ and Eu-$O_{phenol}$ distances (respectively 2.672(6) Å, 2.601(7) Å and 2.588(7) Å and 2.272(5) Å) are very similar to those found in the Eu(III) bis-ligand complex $[Eu(BPA)_2]OTf$, **40**. The average Eu-S bond (2.88(1) Å) falls in the range of Eu-S distances previously reported for Eu(III) thiocarbamate complexes.[319] The S-C bonds of the thiocarbonate moiety, S1-C2 and S2-C2 measure respectively 1.735(10) Å and 1.725(10) Å. The S3 atom is disordered between two positions. The main position (55% occupancy) leads to a C-S distance of 1.748(15) Å, the minor position (45% occupancy) leads to a shorter C-S distance of 1.630(16) Å. The C-S bond distances remain in the range of previously reported trithiocarbonate complexes of f-element and complex **12**.[131]

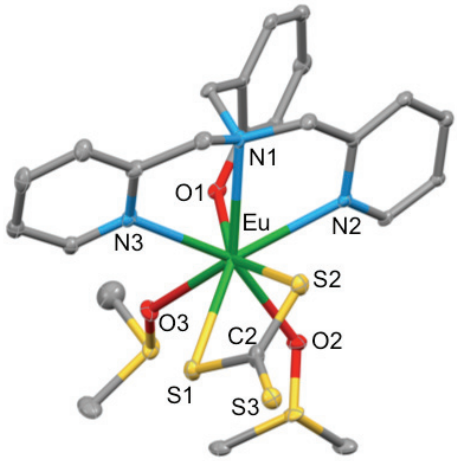


**Figure IV-27: Solid state structure of $[Eu(BPA)(CS_3)(DMSO)_2]$.DMSO, 44.DMSO (50% ellipsoids). Hydrogen atoms, disorder and solvent molecules are omitted for clarity.**

Complex **44** can be isolated analytically pure in 33% yield by slow diffusion of toluene into a DMSO solution of the reaction mixture. When 1 eq of $CS_2$ is added to a 1:1 solution of $EuI_2$ and KBPA in pyridine, the formation of the $[Eu(BPA)_2]^+$ complex is observed by $^1H$ NMR spectroscopy. However, the signals of complex **44** are absent from the $^1H$ NMR spectrum in DMSO-$d_6$. This indicates that the hypothetical heteroleptic Eu(II) complex [Eu(BPA)I] is also able to reduce $CS_2$ affording different reduction products which remain unidentified so far. As shown in the general introduction, the reported $CS_2$ reductions yielding trithiocarbonate complexes containing f-elements are limited to few examples[131, 320, 321] including complex **12** in chapter III. Moreover, among the four reported examples of $CS_2$ reduction by divalent lanthanide, one involves the Eu(II) and Yb(II) tetrasiloxide complexes

described in the first part of this chapter.[322] The others involve Sm(II) complexes supported by formamidinate[134] or guanidinate[104, 133] ligands which reduce $CS_2$ and afford the thioformyl carbonotrithioate through C-S coupling. The complex **44** is thus the first example of trithiocarbonate complex containing lanthanide and only the second example of $CS_2$ reduction by a Eu(II) complex.

This study on tripodal pyridylamine or pyridylaminophenolate complexation with lanthanide ions shows that an enhancement of the Ln(II) reducing abilities is possible with the appropriate electron-rich environment which is tunable in this ligand family. The reactivity of complex **40** is promising and further investigations will focus on the reactivity of the heteroleptic Eu(II) and Yb(II) complexes of BPA and MPA with small molecules.

# IV.3 Conclusion

The work presented in this chapter was dedicated to the enhancement of the reducing abilities of "classical" divalent lanthanides complexes by electron rich ligands in order to synthesise highly reducing complexes able to activate small molecules such as $CS_2$, $CO_2$, etc.

In the first part of this chapter we demonstrated that the coordination of four tris(tert-butoxy)siloxide ligands to the classical divalent lanthanides (Eu, Yb, Sm) leads to the isolation of the highly reactive complexes $[Ln(OSi(OtBu)_3)_4K_2]$, **33**-Ln. Indeed, the reactivity of these Eu(II) and Yb(II) compounds with small molecules such as azobenzene, $CS_2$ or $CO_2$ was unique for these usually less reducing lanthanide ions. Notably, the complex **33**-Yb is able to reduce $CO_2$ into oxalate and carbonate, a reducing ability never reported for Yb(II) complexes. The cooperative effect with the K cation, observed in the reactivity of $[U(OSi(OtBu)_3)_4K]$, is more difficult to investigate in the case of the complexes **33**-Ln as the addition of 18c6 in toluene lead to completely insoluble species. The steric bulk provided by the four siloxide ligands was appropriate to prevent the stable coordination of the reduction products of PhNNPh and $CS_2$ to the trivalent lanthanide complexes. The release of the reduction products is an important step for implementation of catalytic cycle. The Eu(II) and Yb(II) tetrasiloxide complexes are remarkable compounds as stable and easy-to-handle precursors can be used to activate small molecules.

In the second part of this chapter we investigated the improvement of the reducing power of the classical divalent lanthanides with another family of ligand. The coordination of

the tripodal pyridyl amine TPA ligand with trivalent lanthanide and uranium have been previously studied in our group[274, 303] and few examples of divalent lanthanide supported by one tripodal aminophenolate ligand have been reported. However, the formation of homoleptic bis-aminophenolate complexes of divalent lanthanide has never been studied. We thus explored the formation of homoleptic divalent lanthanide Eu(II) and Yb(II) complexes supported by TPA and tripodal pyridylaminophenolate ligands to quantify the effect of the ligand charge and electron-donor character on the redox properties of Ln(II) centres. Ln(II) and Ln(III) complexes were isolated. Electrochemistry studies on the homoleptic trivalent Eu(III) and Yb(III) complexes prepared *in situ* confirm the important increasing reducing abilities of the divalent lanthanide complexes with the increasing electron-donor character of the ligands. Indeed, the reduction potential of the metal centre was shifted to much more negative values for the complexes supported by BPA ligand compared to the one supported by TPA. The homoleptic complexes supported by MPA ligand, do not present redox process at the metal centre suggesting that the reduction potential of the metal is even lower than the solvent one. Preliminary studies on the reactivity of the obtained divalent complexes showed that the reducing power of the Ln(II) compounds is drastically increased by the simple substitution of one pyridine arm of the TPA ligand by a phenolate one. Notably, $[Eu(BPA)_2]$, immediately reduces $CS_2$ to afford the first example of lanthanide trithiocarbonate complex. Further investigations will focus on the reactivity of divalent mono-BPA and mono-MPA complexes. The aimed enhancement of the reducing properties of the "classical" divalent lanthanide has been reached. However, this was to the detriment of the bis-ligand complex stability, especially with MPA ligand. Further tuning of the steric and electronic properties of the ligand system needs to be investigated to obtain the right balance between high reactivity and sufficient stability.

# General conclusion

This PhD work contributes to a better understanding of the fundamental chemical properties of f-elements thanks to the synthesis and reactivity studies of electron-rich lanthanide and uranium complexes.

We first have shown that despite the tendency of f-elements to undertake mono-electronic transfer, multi-electron redox processes can be promoted by U(IV) centre thanks to the use of redox-active ligands. The redox chemistry of a tridentate Schiff base as supporting ligand for U(IV) ion was successfully investigated: Up to eight-electron reduction can be performed in combining the electron stored in C-C bond on the ligand scaffold and the electron of the metal centres. Using the salophen tetradentate Schiff base we have identified a route to heterobimetallic complexes containing f- and d-block elements and an electron reservoir on the ligand platform. If the synthetic conditions have to be optimized to minimize decomposition or by-products formations, magnetic studies of the obtained heterobimetallic compounds could allow us to gain insight into metal-metal communication and further reduction of the metal centres, if achievable, should enhance the reducing abilities of the species leading to original $CO_2$ reduction.

Another approach consisted of using low valent f-element complexes supported by electron-rich ligands to enhance the reducing power of the f-element centres and thus promote unusual reactivity. We further investigated the reactivity of the U(III) tetrasiloxide complexes $[U(OSi(OtBu)_3)_4K]$ and $[K18c6][U(OSi(OtBu)_3)_4]$ with the reduction reactions of other substrates such as $CS_2$ and $Ph_3PS$. The U/K proximity was shown to affect the selectivity of the $CS_2$ reduction. The reduction studies of $Ph_3PS$ by the U(III) tetrasiloxide complexes led to rare U(IV) terminal sulfide and hydrosulfide complexes. The U-S interactions were found to consist of a triple bond (with bond order >2) for the sulfides and of a double bond (with bond order of 1.39) for the hydrosulfide species. Moreover, the 5f orbitals were found to not take

part in the U-S bonding. The synthesis and theoretical analyses of the U(IV) terminal chalcogenide family is part of our future aims. During the reactivity studies of U(III) tetrasiloxide complex with $Ph_3PS$ and $H_2S$, decomposition processes or side-reactions were found to involve ligand loss and bridging events. Future work will be directed to identify bulky chelating siloxide ligand to prevent ligand scrambling.

Preliminary studies suggest that the nature of the counter-cation (Li, Na, K, Cs) in the U(III) tetrasiloxide system may have an influence on the outcomes of the $CO_2$ reduction as well as the $CO_2$ stoichiometry in the reaction. Future investigations could be focused in this direction. The influence of the counter-cation charge could also be studied using metallic Ca or Mg as reducing agent to reduce the U(IV) complex $[U(OSi(OtBu)_3)_4]$.

Furthermore in this work, we have identified two ligand systems that allow to increase the reducing abilities of classical lanthanides.

We have demonstrated that the coordination of four siloxide ligands to Eu(II), Yb(II) and Sm(II) ions enhances their reducing abilities affording highly reactive complexes able to reduce azobenzene, $CS_2$ and $CO_2$. Indeed, this reactivity with $CS_2$ and $CO_2$, previously limited to Sm(II) species for lanthanides, is unique for Eu(II) and Yb(II) compounds. Moreover, the steric environment provided by the siloxides leads to the release of the reduction products in the cases of PhNNPh and $CS_2$ reductions.

Using a tripodal aminopyridine/aminophenolate ligand family, we studied the evolution of the redox properties of homoleptic complexes of europium and ytterbium with the increasing electron-donor character and charge of the supporting ligand. Reactivity studies with $CS_2$ led to the first lanthanide thiocarbonate complex. Electrochemistry analyses confirm that the reducing abilities of Eu(II) and Yb(II) have been improved by successive substitution of pyridyl arms by phenolate one. However, the stability of the Ln(II) bis-ligand complexes rapidly decreases, especially for Yb(II) species, with the increasing number of phenolate arm. The future challenge thus consists of tuning the steric and electronic properties of the ligand to optimize the balance between high reducing reactivity and appropriate stability.

# Experimental Section

## General considerations

Unless otherwise noted, all manipulations were carried out at ambient temperature under an inert argon atmosphere using Schlenk techniques and an MBraun glovebox equipped with a purifier unit. The water and oxygen level were always kept at less than 1 ppm. Glassware was systematically dried in oven overnight at 150°C followed by 3 vacuum/argon cycles before use. Reductions or syntheses involving U(III) and Ln(II) compounds were performed using glass-covered stirring bars.

**Starting materials.** Unless otherwise noted, reagents were purchased from commercial suppliers and used without further purification. Molecular sieves were activated upon heating at 200°C under high vacuum. The solvents were purchased from Aldrich in their anhydrous form, conditioned under argon and vacuum distilled from K/benzophenone (DIPE, DME, dioxane, toluene, pyridine and THF) or sodium dispersion (hexane) or $CaH_2$ (acetonitrile) and degassed by three freeze-pump-thaw cycles. The deuterated solvents were purchased from Eurisotop or Cortecnec and prepared identically, except pyridine-$d_5$ and DMSO-$d_6$ which were degassed by three freeze-pump-thaw cycles and further dried over 3 Å molecular sieves. All reagents were dried under high-vacuum ($10^{-7}$ mBar) for 5 days prior to use. The $[Bu_4N][PF_6]$ electrolyte, 9,10-phenanthrenequinone were purified by recrystallization from toluene and dried under high vacuum prior to use. The 18c6 crown ether was purified by recrystallization from acetonitrile and dried under high vacuum prior to use. Cryptand was dried under high vacuum and recrystallizes in the glovebox from THF prior to use. $I_2$ PhNNPh, PyNO and $HOSi(OtBu)_3$ were sublimed prior to use. $IMesN_2O$ carbene was provided by the group of Prof. Severin. TPA was recrystallizes from $Et_2O$ prior to use. Dry

dioxygen was prepared upon storing an $O_2$ atmosphere upon $P_4O_{10}$ for one week prior to use. Dry $^{13}CO_2$ was prepared by storing over molecular sieves for one week prior to use. Non-labeled $CS_2$ was degassed by three freeze-pump-thaw cycles and further dried over 3 Å molecular sieves. Anhydrous $CoCl_2$ and $NiI_2$ salts were purified by hot extraction in THF to afford $[CoCl_2(THF)]$ and $[NiI_2(THF)_{0.2}]$. $[SmI_3(THF)_{3.7}]$ and $[NdI_3(THF)_4]$ were obtained by hot extraction of anhydrous $SmI_3$ and $NdI_3$ with distilled THF under argon. The amount of THF was determined by $^1H$ NMR using naphthalene as internal reference. Depleted uranium turnings were purchased from the "Société Industrielle du Combustible Nucléaire" of Annecy (France). Natural uranium oxide was provided by the CEA of Grenoble (France). $[UI_3(THF)_4]$ was prepared either from the direct reaction of uranium metal with iodine in THF,[71] or by hot extraction of $[UI_3(1,4\text{-dioxane})_{1.5})]$[73] with THF. $[U(N(SiMe_3)_2)_3]$,[71], $[Yb(N(SiMe_3)_2)_2]$,[323] $[Co(N(SiMe_3)_2)_2]$,[324] $[UCl_4]$,[325] $[UI_4(OEt_2)_2]$[72], $Na_2[U(bis\text{-}salophen)]$[5], $[U(OSi(OtBu)_3)_4K]$,[7] $[U(OSi(OtBu)_3)_4][K18c6]$,[250] $[UO(OSi(OtBu)_3)_4K]$[7] and $[U(OSi(OtBu)_3)_3]_2$[100] were prepared according to the published procedures.

# Characterisations

**Elemental analyses** were performed under argon by Analytische Laboratorien GMBH at Lindlar (Germany) or by the elemental analyses department of the EPFL using a Thermo Scientific Flash 2000 Organic Elemental Analyzer.

**FTIR spectra** were recorded with a Thermo Scientifique IS50-FTIR spectrophotometer from KBr pellets under nitrogen flow.

**Mass spectra** were acquired on a LXQ-linear ion trap (Thermo Scientific, San Jose, CA,USA), equipped with an electrospray source in a THF solution which was prepared and filtered on microporous filters in the glove-box and maintained under argon until injection in the spectrometer. Electrospray full scan spectra, in the range of m/z 50 –3000 amu, were obtained by infusion through fused silica tubing at 2-10 μL $min^{-1}$. The LXQ calibration (m/z 50-2000) was achieved according to the standard calibration procedure from the manufacturer (mixture of caffeine/MRFA and Ultramark 1621). The LXQ calibration (m/z 2000-4000) was performed with ES tuning mix (Agilent). The temperature of the heated capillary of the LXQ

was set to the range of 180-220 °C, the ion spray voltage was in the range of 1-3 kV with an injection time of 5-100 ms. The experimental isotopic profile was compared in each case to the theoretical one.

**NMR experiments** were carried out using NMR tubes adapted with J. Young valves. $^{1}H$ NMR spectra were recorded on Bruker 200 MHz and 400 MHz and Varian Mercury 400 MHz spectrometers, at various temperatures. NMR chemical shifts (δ) are reported in ppm with solvent as internal reference. Abbreviations used for describing multiplicity and shape of the NMR signals are: s (singulet), d (doublet), t (triplet), m (multiplet) and br (broad). Diffusion coefficients measurements were performed by NMR using a Pulsed-Field Gradient STimulated Echo (PFGSTE) sequence, using bipolar Gradients, at 298 K and no spinning was applied to the NMR tube.[326] The coefficient diffusion and the molecular weight are related. The ratio of the molecular weights of two molecules ($M_A$ and $M_B$) can thus be conveniently expresses as the reciprocal cubic ratio of their diffusion coefficients: $M_A/M_B=(D_B/D_A)^3$.[327]

**Electrochemical Methods.** Cyclic voltammetry data were carried out at room temperature in an argon-filled glovebox described above. Data were collected using a Biologic SP-300 potentiostat connected to a personal computer. All samples were 2 to 10 mM in complex with 0.1 M $[Bu_4N][PF_6]$ supporting electrolyte in pyridine, acetonitrile or THF solution. The experiments were carried out with a platinum disk (d=5 mm or d=1 mm) or a vitrous carbon disk (d=1 mm) working electrode, a platinum wire counter-electrode and an Ag/AgCl reference electrode. Potential calibration was performed at the end of each data collection cycle using the ferrocene/ferrocenium $Fc/Fc^+$ couple as an internal standard.
The solutions of the trivalent complexes $[Ln(TPA)_2]OTf_3$; $[Ln(BPA)_2]OTf$ ; $[Ln(BPPA)_2]OTf$ and $[Ln(MPA)_2K]$ (Ln = Eu and Yb) for voltammetric studies were prepared in situ by the addition of 2 equivalents of ligand to the corresponding $LnOTf_3$ salt.

**EPR measurements** at X-band was recorded with an EMX Bruker spectrometer fitted with an OXFORD Instrument ESR900 cryostat. The spectrum was recorded under unsaturated conditions at room temperature, with the following set of parameters:

- For the solid state EPR: ν = 9.6543GHz, scan range 2940-3940 G (from g=2.346 to g=1.751), P receiver gain 33 dB, amplitude modulation 1 G, frequency modulation 100 kHz. EPR data was expressed as the first derivative of the absorption related to

the increase in applied magnetic field. The sample for EPR measurements was introduced as a suspension in a 150 μL mixture of solvents in 5mm Suprasil-Quartz tubes adapted with young valves.

- For the solution EPR: ν = 9.6475GHz, scan range 3400-3480 G (from g=2.029 to g=1.982), P receiver gain 33 dB, amplitude modulation 0.1 G, frequency modulation 100 kHz. EPR data was expressed as the first derivative of the absorption related to the increase in applied magnetic field. The sample for EPR measurements was introduced as a 150 μL solution of a mixture of solvents in 5mm Suprasil-Quartz tubes adapted with young valves.

**X-ray Crystallography Diffraction data** were taken using an Oxford-Diffraction XCallibur S kappa geometry or a Bruker APEX II CCD kappa geometry diffractometers (Mo-Kα radiation, graphite monochromator, λ = 0.71073 Å). To prevent evaporation of co-crystallised solvent molecules the crystals were coated with light hydrocarbon oil and the data were collected at between 100 K and 150 K. The datasets were reduced by CrysAlis[328] or EvalCCD[329] and then corrected for absorption.[330] The solution and refinement were performed by SHELX or Superflip.[331, 332] The crystal structures were refined using full-matrix least-squares based on $F^2$ with all non-hydrogen atoms anisotropically defined. Hydrogen atoms were placed in calculated positions by means of the "riding" model. Additional electron density found in the difference Fourier map (due to highly disordered solvent) was eventually treated by the SQUEEZE algorithm of PLATON.[333] Details of the data collection and crystal parameters are given in appendix.

# Ligand Syntheses

Tetradentate Schiff base ligands were prepared by the condensation of 1,2-phenylenediamine (**$H_2$salophen** and **$H_2^{OMe}$salophen**) with the corresponding salicylaldehyde derivatives (1:2 stoichiometric ratio) in ethanol under reflux according to previously reported procedure.[334]

**$H^{Me}$naphtquinolen**

The ligand was prepared by a modified literature procedure.[335, 336] A solution of 2-methylquinolin-8- amine (1.0 g, 6.32 mmol, 1eq) and 3-hydroxy-2-naphtaldehyde (1.1 g, 6.39 mmol, 1.01eq) in 30 mL of anhydrous toluene was stirred in a Dean Stark set-up at 110°C during 2 days. Then the solvent was removed under vacuum giving an orange-brown solid. This solid was suspended in 100 mL cyclohexane and heated to reflux. Toluene was added dropwise until most solid was soluble and the temperature was raised to maintain the reflux. A hot filtration was carried out to remove the black insoluble impurities and the mixture was cooled down to room temperature, affording red crystals that were filtered and dried under vacuum to give $H^{Me}$naphtquinolen (1.38 g, 4.42 mmol, 70 % yield). $^{1}$H NMR (200 MHz, $CDCl_3$, 298 K): δ = 15.8 (br s, 1H, OH), 9.3 (d, 1H), 8.1 (d, 1H), 8.0 (d, 1H), 7.7-7.4 (m, 7H), 7.3-7.2 (m, 1H), 6.9 (d, 1H), 2.9 (s, 3H, CH3). $^{13}$C NMR (50 MHz, $CDCl_3$, 298 K): δ = 182.3 (C=N), 159.3 ($C_{aro}$), 145.9 ($C_{aro}$), 139.5 ($C_{aro}$), 139.3 ($C_{aro}$), 136.6 ($C_{aro}$), 136.0 ($C_{aro}$), 134.5 ($C_{aro}$), 129.5 ($C_{aro}$), 128.4 ($C_{aro}$), 127.2 ($C_{aro}$), 126.9 ($C_{aro}$), 126.7 ($C_{aro}$), 125.7 ($C_{aro}$), 124.1 ($C_{aro}$), 123.6 ($C_{aro}$), 122.3 ($C_{aro}$), 118.4 ($C_{aro}$), 113.2 ($C_{aro}$), 8.0 ($C_{aro}$), 25.9 ($CH_3$). ESI-MS : m/z = 313.2 [$M+H^+$].

The potassium salts of the Schiff base ligands were prepared as previously described[337] by addition of KH or NaH to a THF solution of the corresponding Schiff base. The resulting **$K^{Me}$naphtquinolen**, **$K_2$salophen**, **$Na_2$salophen**, **$K_2^{OMe}$salophen** and **$Na_2^{OMe}$salophen** salts were obtained in 65-95% yield.

**$K^{Me}$naphtquinolen**

$^{1}$H NMR (200 MHz, py-$d_5$, 298 K): δ = 9.7 (s, 1H, HC=N), 8.6 (d, 1H), 8.0 (d, 1H), 7.7 (m, 2H), 7.5-7.7 (m, 3H), 7.3-7.0 (m, 4H), 2.5 (s, 3H, $CH_3$).

**$K_2$salophen**

$^{1}$H NMR (200 MHz, THF-$d_8$, 298 K): δ = 8.4 (s, 2H, HC=N), 7.2 (s, 2H), 7.1 (s, 2H), 7.0 (s, 2H), 6.8 (s, 2H), 6.4 (s, 2H), 6.1 (s, 2H).

**$Na_2$salophen.**

$^{1}$H NMR (200 MHz, THF-$d_8$, 298 K): δ = 8.6 (s, 2H, HC=N), 7.4 (d, 2H), 6.9-7.3 (m, 8H), 6.5 (t, 2H).

**$K_2^{OMe}$salophen**

$^1$H NMR (200 MHz, DMSO-$d_6$, 298 K): δ = 8.5 (s, 2H, HC=N), 7.0-6.9 (m, 4H), 6.7 (t, 2H), 6.4 (d, 2H), 5.7 (t, 2H), 3.6 (s, 6H).

**$Na_2^{OMe}$salophen**

$^1$H NMR (200 MHz, py-$d_5$, 298 K): δ = 8.6 (s, 2H, HC=N), 7.3 (s, 4H), 7.1 (d, 2H), 6.6 (d, 2H), 6.4 (t, 2H), 3.3 (s, 6H).

**KOSi(tBuO)$_3$** was prepared upon reaction of HOSi(tBuO)$_3$ (1.636 g, 6.2 mmol, 1eq) with one equivalent of KH (248 mg, 6.2 mmol, 1eq) in THF (10 mL). After 24 hours stirring, the mixture was filtered and the filtrate was taking to dryness. The resulting white powder was collected and dried for 3 hours to give KOSi(tBuO)$_3$ (1.460 g, 4.8 mmol, 78 % yield). $^1$H NMR (400 MHz, THF-$d_8$, 298 K): δ = 1.3 (s, 27H). $^1$H NMR (200 MHz, tol-$d_8$, 298 K): δ = 1.4 (s, 27H). $^{13}$C NMR (50MHz, tol-$d_8$, 298K): δ = 70.54 (C), 32.27 ($CH_3$).

The ligand **HBPPA** was prepared according to the published procedure.[338] The previously reported **HBPA** ligand[339] was prepared in 78% yield with the same procedure used for ligand **HBPPA**.[338] The previously reported ligand **$H_2$MPA**[340] was synthesised from 2-(3,5- di-tert-butyl-2-hydroxybenzylaminomethyl)pyridine in 24% yield according to the literature procedure used for a similar system.[341] The potassium salts of all ligands were prepared by addition of KH to a THF solution of the corresponding ligand according to a published procedure.[342]

**KBPA**

$^1$H NMR (200 MHz, py-$d_5$, 298 K): δ = 8.3 (d, 2 H), 7.5–7.1 (m, 7H), 6.9 (dd, 2H), 6.5 (td, 1H), 3.7 (m, 6H).

**KBPPA**

HBPPA (1.1 g, 2.5 mmol, 1eq) and potassium hydride (0.11 g, 2.8 mmol, 1.1eq) were mixed in anhydrous THF (25 mL). The reaction mixture was heated at reflux under argon for 12 h. The mixture was then filtered to remove the excess of KH, the filtrate was taken to dryness and washed with hexane (10 mL). The obtained solid was dried under vacuum for 2 days to give KBPPA(THF)$_{0.65}$ (0.9 g, 1.7 mmol, 68 % yield), in which the amount of THF was

determined by quantitative $^1$H NMR spectroscopy. $^1$H NMR (200 MHz, py-$d_5$, 298 K): δ = 8.3 (d, 2 H), 7.5–7.2 (m, 6 H), 6.9 (dd, 2H), 3.9 (s, 2H), 3.8 (s, 4H), 1.8 (s, 9H), 1.5 (s, 9H).

**$K_2$MPA**

$^1$H NMR (200 MHz, py-$d_5$, 298 K): δ = 7.9 (d, 1 H), 7.4–7.3 (m, 4H), 7.1 (d, 2H), 6.7 (t, 1H), 4.1 (s, 2H), 3.9 (brs, 4H), 1.7 (s, 18 H), 1.4 (s, 18 H).

# Complex Syntheses

**[$UCl_2$(Menaphtquinolen)$_2$] 1-Cl**

A solution of $K^{Me}$naphtquinolen (92.3 mg, 0.263 mmol, 2eq) in THF (10 mL) was added to $UCl_4$ (50.0 mg, 0.132 mmol, 1eq) and the reaction mixture was stirred at room temperature overnight, affording an orange suspension. The mixture was filtered to remove KCl, the THF volume of the filtrate was reduced to 2 mL and the solution was layered with hexane. The resulting orange precipitate was filtered and dried under vacuum to afford **1-Cl** as an orange solid. (89.0 mg, 0.096 mmol, 72% yield). $^1$H NMR (200 MHz, THF-$d_8$, 298 K): δ = 25.7 (s, 2H), 19.4 (d, 2H), 13.0 (d, 2H), 11.8 (d, 2H), 10.1 (t, 2H), 9.7 (t, 2H), 9.5 (m, 2H), 5.6 (s, 6H), 1.0 (d, 2H)-0.4 (t, 2H), -0.8 (m, 2H), -3.0 (d, 2H), -6.1 (s, 2H). Anal. Calcd for [$UCl_2$(Menaphtquinolen)$_2$] **1-Cl** : $C_{42}H_{30}Cl_2N_4O_2U$: C, 54.15; H, 3.25; N, 6.01. Found: C, 54.03; H, 3.41; N, 6.06. Single crystals suitable for X-ray diffraction were obtained by slow diffusion of hexane into a pyridine solution of **1-Cl**.

**[U(μ-bis-$^{Me}$naphtquinolen)]$_2$ 2**

A solution of $K^{Me}$naphtquinolen (150.0 mg, 0.428 mmol, 2eq) in THF (8 mL) was added to [$UI_4(OEt_2)_2$] (191.3 mg, 0.214 mmol, 1eq) and the reaction mixture was stirred at room temperature overnight, affording a yellowish-brown suspension. Intermediate data for [$UI_2$($^{Me}$naphtquinolen)$_2$] **1-I**: $^1$H NMR (200 MHz, py-$d_5$, 298 K): δ = 108.9 (br s, 2H), 37.9 (s, 2H), 37.3 (s, 6H), 31.1 (s, 2H), 29.7 (br s, 2H), 22.1 (s, 2H), 21.6 (s, 2H), 18.0 (br s, 6H), 16.9 (s, 2H), 4.3 (s, 4H), 0.6 (s, 2H), -3.2 (s, 2H) -7.4 (s, 2H). This mixture was added onto potassium chunks and then stirred at room temperature for 12 hours. The reaction mixture gradually turned dark olive brown. The mixture was filtered to remove KI and the filtrate

evaporated to dryness. The resulting brown solid was extracted with toluene (12 mL) to give a brown suspension that was filtered. The filtrate was taken to dryness to give [U(μ-bis-$^{Me}$naphtquinolen)]$_2$ **2** as a brown solid (122.9 mg, 0.071 mmol, 67% yield). $^1$H NMR (200 MHz, tol-d$_8$, 298 K): δ = 88.0 (s, 2H), 46.2 (s, 2H), 41.7 (m, 4H), 33.1 (d, 2H), 31.2 (d, 2H), 30.9 (d, 2H), 20.0 (t, 2H), 17.8 (d, 2H), 15.1 (d, 2H), 14.9 (m, 2H), 13.2 (t, 2H), 12.3 (t, 2H), 10.4 (t, 2H), 8.9 (dt, 2H), 7.2 (d, 2H), 5.6 (d, 2H), 5.2 (d, 2H), 2.5 (d, 2H), -3.9 (d, 2H), -5.1 (d, 2H), -5.9 (t, 2H), -7.7 (s, 6H, CH$_3$), -9.0 (d, 2H), -13.8 (d, 2H), -25.8 (s, 6H, CH$_3$). Anal. Calcd for **2** $C_{84}H_{60}N_8O_4U_2$: C, 58.61; H, 3.51; N, 6.51. Found: C, 58.37; H, 3.73; N, 6.38. Single crystals suitable for X-ray diffraction were obtained by slow diffusion of hexane into a toluene solution of **2**.

Upon dissolution of **2** into pyridine, 2 sets of proton signals are observed in solution assigned to the dimeric complex **2** and the monomeric analogue **2b** : $^1$H NMR (500 MHz, py-d$_5$, 298 K): Ratio of complexes **2**:**2b**: 3:1 after 30 minutes, 0.5:1 after 4 days. Complex **2**: δ = 85.7 (s, 2H), 47.4 (d, 2H), 41.1 (d, 2H), 35.2 (d, 2H), 32.3 (d, 2H), 28.9 (s, 2H), 28.1 (d, 2H), 18.4 (t, 2H), 16.7 (d, 2H), 15.2 (t, 2H), 11.3 (t, 2H), 11.2 (t, 2H), 11.1 (t, 2H), 10.9 (d, 2H), 9.8 (d, 2H), 8.9 (d, 2H), 8.1 (d, 2H), 6.3 (d, 2H), 5.2 (d, 2H), 0.9 (s, 6H, CH$_3$), -0.7 (d, 2H), -3.8 (t, 2H), -6.7 (d, 2H), -9.5 (d, 2H), -10.0 (d, 2H), -13.9 (s, 6H, CH$_3$). Complex **2b**: δ = 91.3 (s, 2H), 47.6 (d, 2H), 45.9 (d, 2H), 44.1 (s, 2H), 35.6 (d, 2H), 32.1 (d, 2H), 20.2 (d, 2H), 19.3 (d, 2H), 19.1 (t, 2H), 17.5 (m, 2H), 14.3 (t, 2H), 13.9 (t, 2H), 13.7 (d, 2H), 13.4 (t, 2H), 13.3 (d, 2H), 6.5 (s, 6H, CH$_3$), 5.7 (d, 2H), 4.6 (d, 2H), 3.7 (t, 2H), 2.2 (s, 2H), 1.6 (d, 2H), -5.3 (t, 2H), -5.7 (d, 2H), -7.0 (d, 2H), -11.8 (d, 2H), -15.0 (s, 6H, CH$_3$).

**Reduction of [UCl$_2$(Menaphtquinolen)$_2$] 1-Cl**

To a solution of **1-Cl** (24.5 mg, 0.026 mmol, 1eq) in THF (2 mL) was added a suspension of potassium graphite (7.1 mg, 0.053 mmol, 2eq) in THF (2 mL) and the reaction mixture was stirred at room temperature for 15 minutes, affording a deep brown suspension. Graphite was removed by centrifugation. The $^1$H NMR spectrum (200 MHz, THF-d$_8$, 298 K) recorded for the crude reaction mixture showed the formation of **2** and **2b** as the only $^{Me}$naphtquinolen-containing species.

To a solution of **1-Cl** (24.5 mg, 0.026 mmol, 1eq) in THF (4 mL) was added a potassium chunk (2.1 mg, 0.053 mmol, 2eq) and the reaction mixture was stirred at room temperature overnight, affording a deep brown suspension. The $^1$H NMR spectrum (200 MHz, THF-d$_8$,

298 K) recorded for the crude reaction mixture showed that a complex mixture of compounds had formed, among which the resonances of **2** and **2b** could be identified.

**Reaction of 2 with pyHCl**

A pyridine solution (1 mL) of pyridinium hydrochloride (6.8 mg, 0.059 mmol) was prepared. 200 μL of this stock solution (i.e. 1eq of pyHCl per U atom) were added to a pyridine solution (0.5 mL) of complex **2**. No immediate visible change was observed. After 30 min of stirring the $^{1}$H NMR spectrum of the crude mixture in deuterated pyridine showed two sets of signals: one set was attributed to the dinuclear form of complex **2**, the other one was unidentified. The integration ratio **2**:new species was 0.9:1. After 1 night at room temperature, the reaction mixture turned yellowish and the $^{1}$H NMR spectrum in py-$d_5$ presented only the signals of the new species. $^{1}$H NMR after 18h (200 MHz, py-$d_5$, 298 K): δ = 95.5 (s, 2H), 49.6 (s, 2H), 45.3 (s, 2H), 40.1 (s, 2H), 33.3 (s, 2H), 32.1 (s, 2H), 24.6 (t, 2H), 19.4 (d, 2H), 16.6 (s, 2H), 16.1 (s, 2H), 13.9 (s, 2H), 13.4 (d, 2H), 13.3 (t, 2H), 12.6 (s, 6H), 10.3 (s, 2H), 8.0 (s, 2H), 5.3 (s, 2H), 2.6 (s, 2H), 0.0 (d, 2H), -2.9 (s, 2H), -3.6 (d, 2H), -4.4 (s, 2H), -5.2 (s, 2H), -11.4 (s, 2H), -26.3 (s, 6H).

**[U(9,10-phenanthrenediol)($^{Me}$naphtquinolen)$_2$] 3**

A toluene (6 mL) 9,10-phenanthrenequinone (12.2 mg, 0.059 mmol, 2eq) solution was prepared and added to a toluene (4 mL) solution of complex 15 (50.6 mg, 0.029 mmol, 1eq). Immediately the deep brown solution turned yellowish green. The mixture was stirred 3 hours before filtration. The brown solid was washed with 2 x 0.5 mL toluene and dried in vacuo to give [U(9,10- phenanthrenediol)($^{Me}$naphtquinolen)$_2$] **3** as a brown-gold solid (33.8 mg, 0.032 mmol, 54% yield). Similar results were obtained when performing the reaction in pyridine. Single crystals suitable for X-ray diffraction were obtained by slow evaporation of a saturated pyridine solution of the complex. $^{1}$H NMR (200 MHz, tol-$d_8$, 298 K): δ = 27.6 (s, 2H), 19.9 (s, 2H), 19.1 (s, 2H), 18.6 (s, 2H), 16.2 (d, 2H), 13.0 (t, 2H), 12.5 (d, 2H), 11.7 (t, 2H), 9.4 (t, 2H), 9.3 (t, 2H), 8.0 (d, 2H), 0.7 (t, 2H), 0.6 (d, 2H), -1.1 (d, 2H), -2.4 (d, 2H), -5.2 (d, 2H), -10.5 (s, 6H). Anal. Calcd for **3**.tol$_{0.2}$ $C_{57.2}H_{39.6}N_4O_4U$: C, 63.32; H, 3.68; N, 5.16. Found: C, 63.54; H, 3.85; N, 5.25.

**Reaction of 2 with $I_2$**

To a stirring solution of **2** (9.7 mg, 0.006 mmol, 1eq) in toluene (0.5 mL) was added dropwise a solution of iodine (2.9 mg, 0.011 mmol, 2eq) in toluene (1 mL). Immediately, the dark brown solution turned pale brown and a yellowish-brown precipitate formed. After 10 minutes stirring, the crude reaction was taken to dryness and dissolved back into pyridine. The $^1$H NMR spectrum (200 MHz, py-$d_5$, 298 K) recorded for the crude reaction mixture showed that complex **1-I** was restored.

**$[UO_2(^{Me}$naphtquinolen$)_2]$ 4**

A pyridine (6 mL) solution of complex **2** (58.0 mg, 0.034 mmol, 1eq) was transferred into a reaction vessel. The suspension was degassed using a freeze-pump-thaw procedure. Then 1 atmosphere of dry dioxygen was introduced into the flask. Immediately, a colour change from dark brown to dark red/orange was observed. The reaction was stirred for 12 hours at room temperature before the solvent was removed in vacuo. The solid was washed with toluene (3 x 2 mL), recovered and dried *in vacuo* to afford $[UO_2(^{Me}$naphtquinolen$)_2]$ **4** as a bright orange solid (42.0 mg, 0.047 mmol, 69% yield). Crystals suitable for X-ray diffraction were obtained by slow diffusion of hexane into a saturated solution of **4** in toluene. $^1$H NMR (200 MHz, THF-$d_8$, 298 K): $\delta$ = 10.3 (s, 2H, N=CH), 8.5 (d, 2H), 8.2 (d, 2H), 7.9-7.8 (m, 6H), 7.7-7.5 (m, 6H), 7.4 (t, 2H), 7.2 (t, 2H), 6.2 (d, 2H), 3.4 (s, 6H, $CH_3$). Anal. Calcd for **4**.$(KI)_{0.25}$ $C_{42}H_{30}N_4O_4UK_{0.25}I_{0.25}$: C, 54.00; H, 3.24; N, 6.00. Found: C, 53.88; H, 3.49; N, 5.98. The presence of KI arises from the residual presence of KI in the batch of complex **2** used in this reaction.

**Reaction of $Na_2$[U(bis-salophen)] with $CoCl_2$, isolation of [UCo(bis-salophen)$(THF)_2$] 5**

A deep purple solution of $Na_2$[U(bis-salophen)] (105.1 mg, 0.115 mmol, 1eq) in THF (2 mL) was added to a blue suspension of $[CoCl_2(THF)]$ (23.3 mg, 0.115 mmol, 1eq) in THF (6 mL). The reaction mixture was stirred 1h at room temperature, affording a deep black-green suspension. The mixture was filtered; the solvent volume of the filtrate was reduced to 6 mL and 8 mL of hexane were added. The obtained black precipitate was collected by filtration, giving a black-green microcrystalline solid which was dried under vacuum [UCo(bis-salophen)$(THF)_2$] **5** (20.3 mg). Re-crystallization of this solid by slow diffusion of DIPE into a THF solution of the complex or slow diffusion of hexane into a pyridine solution of the complex afforded black single crystals suitable for X-ray diffraction. ES-MS : m/z= 1141.7

$[M+THF]^+$. $^1H$ NMR (200 MHz, THF-$d_8$, 298 K): δ = 65.5 (s, 1H), 60.2 (s, 1H), 44.3 (s, 1H), 43.9 (s, 1H), 41.0 (s, 1H), 38.3 (s, 1H), 32.1 (s, 1H), 27.6 (s, 1H), 27.1 (s, 1H), 26.8 (s, 1H), 22.7 (s, 1H), 21.2 (s, 1H), 11.2 (s, 1H), 8.9 (s, 1H), 7.2 (s, 1H), 4.1 (s, 1H), 3.1 (s, 1H), 2.8 (s, 1H), -0.7 (s, 1H), -0.9 (s, 1H), -2.6 (s, 1H), -13.5 (s, 1H), -13.8 (s, 1H), -15.1 (s, 1H), -22.1 (s, 1H), -29.0 (s, 1H), -37.7 (s, 1H). $^1H$ NMR (200 MHz, py-$d_5$, 298 K): δ = 66.3 (s, 1H), 65.6 (br s, 1H), 42.0 (s, 1H), 40.5 (s, 1H), 38.9 (s, 1H), 36.0 (s, 1H), 31.1 (s, 1H), 30.6 (s, 1H), 27.6 (s, 1H), 26.1 (s, 1H), 24.7 (s, 1H), 21.4 (s, 1H), 16.7 (s, 1H), 9.8 (s, 1H), 9.2 (s, 1H), 5.7 (s, 1H), 3.7 (s, 1H), 2.5 (s, 1H), 1.6 (s, 1H), -1.2 (s, 1H), -4.2 (s, 1H), -6.2 (s, 1H), -10.5 (br s, 1H), -11.2 (s, 1H), -11.6 (s, 1H), -22.4 (s, 1H), -24.0 (s, 1H), -27.1 (s, 1H). Monitoring the $^1H$ NMR spectrum of **5** in deuterated THF over time shows a slow decomposition of the bimetallic complex in the mononuclear U(IV) complex [U(salophen)$_2$].

**Reaction of $Na_2$[U(bis-salophen)] with $NiI_2$, isolation of [UNi(bis-salophen)$(THF)_2$] 6**

To a deep purple solution of $Na_2$[U(bis-salophen)] (12.1 mg, 0.013 mmol, 1eq) in THF (0.5 mL) was added a yellow solution of [$NiI_2(THF)_{0.2}$] (4.3 mg, 0.013 mmol, 1eq) in THF (0.5 mL). The reaction mixture was stirred at room temperature 25 min, affording a deep green solution above a brown precipitate. The mixture was filtered and the supernatant was layered with DIPE. Black-green crystals suitable for X-ray diffraction analysis were obtained from this slow diffusion. $^1H$ NMR (200MHz, THF-$d_8$, 298K) δ= 57.9 (s, 1H); 48.3 (s, 1H); 43.4 (s, 1H); 38.2 (s, 1H); 34.6 (s, 1H); 33.9 (s, 1H); 31.1 (s, 1H); 28.6 (s, 1H); 26.1 (s, 1H); 25.5 (s, 1H); 23.9 (s, 1H); 19.0 (s, 1H); 16.0 (s, 1H); 11.3 (s, 1H); 9.8 (s, 1H); 7.3 (s, 1H); 6.6 (s, 1H); 3.9 (s, 1H); 3.2 (s, 1H); 1.9 (s, 1H); -0.3 (s, 1H); -1.5 (s, 2H); -3.1 (s, 1H); -3.8 (s, 1H); -7.2 (s, 1H); -11.3 (s, 1H); -28.4 (s, 1H). Additional signals of a small amount of [U(salophen)$_2$] are present on the $^1H$ NMR spectrum of the crude reaction mixture.

**Reaction of $Na_2$[U(bis-salophen)] with $ZnI_2$**

To a deep purple solution of $Na_2$[U(bis-salophen)] (10.0 mg, 0.011 mmol, 1eq) in THF (0.5 mL) was added a colourless solution of $ZnI_2$ (3.5 mg, 0.011 mmol, 1eq) in THF (0.5 mL). The reaction mixture was stirred at room temperature 1h. The $^1H$ NMR spectrum of the crude reaction mixture in THF-$d_8$ shows one set of signals of a new species and one set of 14 signals of unreacted $Na_2$[U(bis-salophen)]. The subsequent addition of another equivalent of $ZnI_2$ (3.5 mg, 0.011 mmol, 1eq) to the mixture led, after 2h of stirring, to the disappearance of the $Na_2$[U(bis-salophen)] signals on the $^1H$ NMR spectrum in THF-$d_8$. Only the signals of the

new species was observed: $^{1}$H NMR (200MHz, THF-$d_8$, 298K) δ= 42.1 (s, 1H); 28.9 (s, 1H); 22.4 (s, 1H); 20.5 (s, 1H); 13.6 (s, 1H); 12.6 (s, 1H); 12.0 (br s, 1H); 11.7 (s, 1H); 8.2 (s, 1H); 7.8-5.2 (m, 5H); 4.4 (s, 2H); 3.8 (s, 1H); -0.2 (br s, 1H); -1.7 (s, 1H); -2.6 (s, 2H); -4.7 (s, 1H); -5.2 (s, 1H); -9.1 (s, 1H); -10.5 (s, 1H); -13.7 (s, 1H); -16.5 (s, 1H); -19.3 (br s, 1H).

**[NdCo(salophen)$_2$(THF)] 7**

To a [$NdI_3$(THF)$_4$] (197.8 mg, 0.245 mmol, 1eq) suspension in THF (1 mL), a yellow suspension of $K_2$salophen (97.2 mg, 0.245 mmol, 1eq) in THF (3 mL) was added and the obtained yello suspension was stirred 1h. A brown suspension of [Co(salophen)K].$(KCl)_{0.33}$ (107.4 mg, 0.245 mmol, 1eq) in THF (2 mL) was then added to the stirred reaction mixture which turned dark green immediately. After 1h of stirring, the mixture was filtered affording 200 mg of a dark precipitate and a green filtrate. The solid residue was stirred during 1h in 6 mL of pure THF and the resulting suspension was filtered leading to a second dark green filtrate. The two filtrates were then layered with DIPE. After one week dark crystals of [NdCo(salophen)$_2$(THF)] **7** formed from the slow diffusions. The crystals were collected and dried under vacuum (67.2 mg, 0.077 mmol, 32% yield). Slow diffusion of DIPE into a THF solution of the complex or slow diffusion of hexane into a pyridine solution of the complex afforded dark single crystals suitable for X-ray diffraction $^{1}$H NMR 200MHz at 298K (THF-$d_8$): δ= 21.59 (br s, 2H); 19.30 (s, 2H); 14.81 (s, 2H); 13.49 (s, 2H); 12.79 (s, 2H); 11.98 (s, 2H); 11.35 (s, 4H); 9.95 (s, 2H); 9.59 (s, 2H); 7.35 (s, 2H); 6.43 (s, 2H); 0.53 (s, 2H); -2.43 (s, 2H). Anal. Calcd for [NdCo(salophen)$_2$(THF)$_{0.5}$] $C_{42}H_{32}N_4O_{4.5}$NdCo: C, 58.12; H, 3.72; N, 6.46. Found: C, 57.86; H, 4.09; N, 6.37. ES-MS : m/z = 831.2 $[M\text{-}THF]^+$.

The complexes **[Co(salophen)]**, and **[Co($^{OMe}$salophen)]** were prepared from addition of potassium salt of the corresponding ligand to [$CoCl_2$(THF)] according to the published procedure,[222] or from addition of protonated $H_2$salophen/$H_2{}^{OMe}$salophen ligand to [Co(HMDS)$_2$(THF)]. The Co(I) species **[Co(salophen)K]**, and **[Co($^{OMe}$salophen)K]** were obtained *via* the reduction of the corresponding Co(II) complex by 1eq of metallic potassium.[201]

**[$Co_2$(bis-salophen)$Li_2$(Py)$_4$] 8**

Lithium chunks (2.7 mg, 0.391 mmol, 1eq) were added on a solution of [Co(salophen)] (145.8 mg, 0.391 mmol, 1eq) in THF (6 mL). The mixture was stirred for 24h affording a green

solution. The solution was taken to dryness and the obtained residue was crystallized by slow diffusion of hexane into a pyridine solution of the complex (135.9 mg, 0.266 mmol, 68%). Single crystals of $[Co_2(bis\text{-}salophen)Li_2(py)_4]$ suitable for X-ray diffraction were obtained by slow diffusion of hexane into a pyridine solution of $[Co(salophen)Li]/[Co_2(bis\text{-}salophen)Li_2]$ mixture.$^1$H NMR (0.34 M solution) (400 MHz, THF-$d_8$, 298 K): diamagnetic species δ = 10.4 (s, 2H), 7.9 (d, 2H), 7.3 (m, 4H), 6.7 (s, 2H), 6.1 (m, 4H); paramagnetic species δ = 50.8 (s, 2H), 32.8 (s, 2H), 17.9 (s, 2H), 12.6 (s, 2H), 7.5 (s, 2H), 7.0 (s, 2H), 2.4 (s, 2H), -3.5 (s, 2H), -5.6 (s, 2H),-13.0 (s, 2H), -14.0 (s, 2H), -30.0 (s, 2H), -56.9 (s, 2H), -131.5(s, 2H). Anal. Calcd for $[Co(salophen)Li].(Py)_{1.65}$ $C_{28.25}H_{22.25}N_{3.65}O_2CoLi$: C, 66.46; H, 4.39; N, 10.01. Found: C, 66.07; H, 4.44; N, 10.40.

**$[Co_3(tris\text{-}^{OMe}salophen)Na_6(THF)_6]$ 9**

$[CoCl_2(THF)]$ (633.1 mg, 2.9 mmol, 1eq) is added onto a suspension of $Na_2{}^{OMe}salophen$ (1.2 g, 2.9 mmol, 1eq) in THF (30 mL) and the resulting brown suspension was stirred for 5h at 50°C. Then sodium chunks (137.0 mg, 5.8 mmol, 2eq) were added. The resulting mixture was stirred for 5 days at room temperature to yield a dark green suspension that was filtered to obtain a green solid after washing with THF. A slow diffusion of hexane into a THF solution of the complex affords $[Co_3(tris\text{-}^{OMe}salophen)Na_6(THF)_6]$, **9** crystals suitable for X-ray diffraction (68% yield after recristallisation). $^1$H NMR (400 MHz, THF-$d_8$, 298 K): δ = 12.8 (s, 2H), 12.5 (br s, 1H), 9.5 (br s, 1H), 9.2 (br s, 1H), 8.6 (d, 2H), 8.5 (br s, 1H), 8.3 (d, 2H), 7.9 (d, 2H), 7.8 (d, 2H), 7.4 (br s, 1H), 7.2 (br s, 1H), 7.0 (s, 2H), 6.7-6.6 (m, 4H), 6.5 (br s, 1H), 6.4 (d, 2H), 6.2 (d, 2H), 6.1 (br s, 1H), 5.9 (t, 2H), 5.3 (t, 2H), 4.9 (br s, 1H), 4.7 (br s, 2H), 4.5 (br s, 1H), 3.4 (s, 6H, $CH_3$), 3.1 (s, 6H, $CH_3$), 2.4 (br s, 3H, $CH_3$), 2.2 (br s, 3H, $CH_3$). Anal. Calcd for $[Co_3(tris\text{-}^{OMe}salophen)Na_6(THF)_{2.5}].(NaCl)_{0.3}$ $C_{76}H_{74}N_6O_{14.5}Co_3Na_{6.3}Cl_{0.3}$: C, 55.81; H, 4.56; N, 5.14. Found: C, 55.55; H, 4.78; N, 4.76.

**$[(Co(^{OMe}salophen))_2Na][Na(cryptand)]_3$ 10**

A THF solution of cryptand (95.1 mg, 0.222 mmol, 6eq) was diffused into a green THF solution of $[Co_3(tris\text{-}^{OMe}salophen)Na_6(THF)_{2.5}].(NaCl)_{0.3}$ (60.5 mg, 0.037 mmol, 1eq) leading to the formation of brown needles of $[(Co(^{OMe}salophen))_2Na][Na(cryptand)]_3$ **10** (78.6 mg, 0.038 mmol, 68% yield) suitable for X-ray diffraction. Complex **10** is insoluble in THF. The $^1$H NMR spectrum of **10** in deutarated pyridine is silent. Anal. Calcd for

[(Co($^{OMe}$salophen))$_2$Na][Na(cryptand)]$_3$ $C_{98}H_{144}N_{10}O_{26}Co_2Na_4$: C, 56.37; H, 6.95; N, 6.71. Found: C, 56.44; H, 6.98; N, 6.46.

**Reaction of 9 with $CO_2$, isolation of [Co($^{OMe}$salophen-$CO_2$)Na]$_2$[Na(cryptand)]$_2$ 11**

[$Co_3$(tris-$^{OMe}$salophen)$Na_6$(THF)$_{2.5}$].$(NaCl)_{0.3}$ (6.3 mg, 0.004 mmol) was dissolved in THF-$d_8$ (0.5 mL) in a J.Young NMR tube under argon. The solution was degassed and an excess of $^{13}CO_2$ (approx. 74eq) was introduced in the tube. The mixture turned purple instantaneously and then slowly brown with concomitant precipitate formation. The $^1$H NMR spectrum after 1 night is silent. THF was then removed under vacuum and the residue was dried 5min under dynamic vacuum. THF-$d_8$ (0.5 mL) was re-added but the $^1$H and $^{13}$C NMR spectra remained silent excluding labile coordination of $CO_2$ to the Co centres. THF was removed under vacuum and the residue was dried 30min under dynamic vacuum before addition of $D_2O$. $^{13}$C NMR (400 MHz, $D_2O$, 298 K): δ = 167.5 ($CO_3^{2-}$). Carbonate was formed in 53% yield ( determined using $^{13}$C labelled sodium acetate as internal standard). When only 1eq of $^{13}CO_2$ per Co atom was added onto a THF-$d_8$ solution of **9**, a comparable yield in carbonate was measured (58%).

When the reaction scale was increased (43.5 mg, 0.027 mmol of complex **9**), single crystals of [Co($^{OMe}$salophen-$CO_2$)Na]$_2$[Na(cryptand)]$_2$, complex **11**, were obtained by slow diffusion of DIPE into the filtered THF solution.

**Reaction of [K18c6][U(OSi(OtBu)$_3$)$_4$] with $CS_2$, isolation of 12**

*Short reaction times*. 100 µL of a 0.15 M toluene solution of $^{13}CS_2$ (0.015 mmol, 1eq) were added to a 2 mL suspension of [K18c6][U(OSi(OtBu)$_3$)$_4$] (25.0 mg, 0.015 mmol, 1eq) in toluene to afford a red/pink solution. After 30 min stirring, the solvent was removed *in vacuo*. The residue was extracted with hexane to give a pink/red solution (A) and an insoluble brown solid. The solid was recovered by centrifugation and then dissolved in pyridine to give a brown solution; slow diffusion of hexane into this pyridine solution produced deep green needles of [(K18c6)$_2$($C_2S_4$)].Py suitable for X-ray diffraction (13% yield). $^1$H NMR (200 MHz, py-$d_5$, 298 K): δ= 3.6 (s, 24H, $CH_2$-18c6). $^{13}$C NMR (50 MHz, py-$d_5$, 298 K): δ 70.6 (s, $CH_2$-18c6), 248.5 (s, $C_2S_4^{2-}$). $^{13}$C NMR (50 MHz, $D_2O$, 298 K): δ= 70.0 (s, $CH_2$-18c6), 251.0 (s, $C_2S_4^{2-}$). After removing all volatiles from the pink/red hexane extract (A) the solid was dissolved in toluene and left standing at -40°C to afford crystals of [U(OSi(OtBu)$_3$)$_4$($CS_3$)$K_2$(18c6)$_2$], **12** suitable for X-ray diffraction. Unfortunately, attempts to

separate **12** from [U(OSi(OtBu)$_3$)$_4$] were unsuccessful, preventing further characterisation of this species. The quantitative $^1$H NMR spectrum recorded on a toluene solution of [K18c6][U(OSi(OtBu)$_3$)$_4$] reacted with one equivalent of $CS_2$ for 30 minutes after addition of an internal standard (naphthalene) shows the formation of [U(OSi(OtBu)$_3$)$_4$] in 50% yield.

*Long reaction times*. 10.4 µL of a 0.64 M toluene solution of $^{13}CS_2$ (0.006 mmol, 1eq) were added to a 0.5 mL suspension of [K18c6][U(OSi(OtBu)$_3$)$_4$] (9.5 mg, 0.006 mmol, 1 eq.) in toluene to afford a red/pink solution. The quantitative $^1$H NMR spectrum of the toluene reaction mixture after two days shows the presence of the U(IV) complex [U(OSi(OtBu)$_3$)$_4$] as the major product (65%). Quantitative $^{13}$C NMR spectra in deuterated DMSO of the reaction mixture after toluene evaporation show the presence of free $^{13}CS_3^{2-}$ as the major species, compared to $^{13}C_3S_5^{2-}$ in a 10 : 1 ratio. Quantitative $^{13}$C NMR using naphthalene as an internal standard shows the quantitative transformation of $^{13}CS_2$ into the reduction products $^{13}CS_3^{2-}$, and $^{13}C_3S_5^{2-}$.

**Reaction of [U(OSi(OtBu)$_3$)$_4$K] with $CS_2$ , isolation of 13**

*Short reaction times*. 30 µL (0.038 mmol, 2eq) of a 1.25 M tol-d$_8$ solution of $^{13}CS_2$ were added to a solution of [U(OSi(OtBu)$_3$)$_4$K] (25.4 mg, 0.019 mmol, 1eq) in tol-d$_8$ (0.5 mL) and stirred for 30 minutes. All volatiles were then removed *in vacuo*. The residue was suspended in hexane and the undissolved solid was discarded. Pink/red crystals of [U(OSi(OtBu)$_3$)$_4$K$_2$(C$_3$S$_5$)]$_n$, **13** suitable for X-ray diffraction were isolated by letting this hexane solution to stand for few days at room temperature. Attempts to separate **13** from the other reaction products were unsuccessful, preventing further characterisation of this species.

*Long reaction times*. 30 µL (0.038 mmol, 1eq) of a 1.25 M tol-d$_8$ solution of $^{13}CS_2$ were added to a solution of [U(OSi(OtBu)$_3$)$_4$K] (50.8 mg, 0.038 mmol, 1eq) in tol-d$_8$ (0.5 mL) to afford an orange solution. After letting the solution stand at room temperature for 2 days a few red crystals formed which were identified by $^{13}$C NMR as $K_2CS_3$. The $^1$H NMR spectrum of the toluene reaction mixture shows the presence of the U(IV) complex [U(OSi(OtBu)$_3$)$_4$] as the major product (66%). All the volatiles were then removed *in vacuo* to afford a brown solid. Recrystallization of this residue by slow diffusion of toluene (4 mL) into DMSO (0.5 mL) affords [K$_2$C$_2$S$_4$(DMSO)$_3$]$_n$, as yellow crystals suitable for X-ray diffraction. $^{13}$C NMR (50 MHz, DMSO-d$_6$, 298 K): δ = 264.5 (s, $C_2S_4^{2-}$). An analogous reaction performed with a 1 : 2 ratio [U(OSi(OtBu)$_3$)$_4$K]:$^{13}CS_2$ allows the isolation of the insoluble K$_2$C$_2$S$_4$.(THF)$_5$ salt (5 THFs confirmed from the $^1$H NMR spectrum in DMSO-d$_6$) as yellow crystals in 65% yield (a

yield consistent with the 1:3.7:1 $^{13}CS_3^{2-}$:$^{13}C_2S_4^{2-}$: $^{13}C_3S_5^{2-}$ ratio obtained from the quantitative $^{13}C$ NMR spectra as indicated below). The quantitative $^{13}C$ NMR spectrum recorded in deuterated pyridine or DMSO immediately after solvent evaporation of a toluene solution of $[U(OSi(OtBu)_3)_4K]$ reacted with one equivalent of $^{13}CS_2$ shows the presence of free $^{13}CS_3^{2-}$, $^{13}C_2S_4^{2-}$ and $^{13}C_3S_5^{2-}$ in a 1:1.2:1 ratio. The quantitative $^{13}C$ NMR spectrum recorded in deuterated pyridine or DMSO immediately after solvent evaporation of toluene solutions of $[U(OSi(OtBu)_3)_4K]$ reacted with two or four equivalents of $^{13}CS_2$, showing the presence of an increasingly higher amount of free $^{13}C_2S_4^{2-}$ compared to $^{13}CS_3^{2-}$ and $^{13}C_3S_5^{2-}$. (A 1:3.7:1 $^{13}CS_3^{2-}$:$^{13}C_2S_4^{2-}$: $^{13}C_3S_5^{2-}$ ratio was found for 2eq $^{13}CS_2$ and a 1:5.9:1 for 4eq)

**Reaction of $[U(OSi(OtBu)_3)_4K]$ with 1/8eq of $S_8$, isolation of $[U(S_2)(OSi(OtBu)_3)_4K_2]_2$ 14**

A brown solution of $[U(OSi(OtBu)_3)_4K]$ (83.0 mg, 0.062 mmol, 1eq) in deuterated toluene (0.5 mL) was added onto elemental sulfur (2.0 mg, 0.008 mmol, 0.125eq), stirred 18 hours and then sonicated 10 minutes. The reaction mixture turned light brownish. The $^1H$ NMR spectrum of the crude mixture in tol-$d_8$ shows the presence of free $KOSi(OtBu)_3$ (1.4 ppm), U(IV) complex $[U(OSi(OtBu)_3)_4]$ (1.1 ppm) and of two unknown species at -1.4 ppm and 0.4 ppm. Suitable crystals for X-ray diffraction of $[U(S_2)(OSi(OtBu)_3)_4K_2]_2$.tol **14**.tol were obtained from the toluene reaction mixture at -40°C.

**Reaction of $[U(OSi(OtBu)_3)_4K]$ with 1/4eq of $S_8$, isolation of $[\{U(OSi(OtBu)_3)_3\}_2(\mu\text{-}S_2)(\mu\text{-}S_3)K]$ 15**

A brown solution of $[U(OSi(OtBu)_3)_4K]$ (76.7 mg, 0.058 mmol, 1eq) in toluene (2 mL) was added onto elemental sulfur (3.7 mg, 0.001 mmol, 0.25eq), and stirred for 18 hours. The solvent was removed under reduced pressure and the resulting solid was washed with hexane, centrifuged and dried under vacuum. The $^1H$ NMR spectrum of the obtained solid in tol-$d_8$ shows the presence of a peak at 0.4 ppm as the main species. Suitable crystals for X-ray diffraction of $[\{U(OSi(OtBu)_3)_3\}_2(\mu\text{-}S_2)(\mu\text{-}S_3)K]$.tol **15**.tol were obtained from the crude reaction solution at -40°C. It is noteworthy, that the 1H NMR shift of complex **15** is similar to **21**, even if the disulfide and trisufide ratios are different in these two structures.

**$[US(OSi(OtBu)_3)_4K_2]_2$ 16**

A colourless solution of $Ph_3PS$ (26.3 mg, 0.089 mmol, 0.5eq) in toluene (2 mL) was added to a stirred brown solution of $[U(OSi(OtBu)_3)_4K]$ (238.1 mg, 0.179 mmol, 1eq) in toluene (4

mL). The mixture was stirred at room temperature for 18 h. The resulting green solution was concentrated to approximately 3 mL and big green crystals formed overnight from toluene at room temperature. The crystals were filtered and dried for 2 hours (79.3 mg, 62% yield in 2 crops). The isolated yield can be increased by recovering additional crops but it leads to co-crystallization of small amounts of the by-product [U(OSi(OtBu)$_3$)$_4$]. Green single crystals of 16.tol suitable for X-ray diffraction were obtained from a concentrated toluene solution of the complex at room temperature. $^1$H NMR (400 MHz, tol-d$_8$, 298 K): δ ≈ 1 (very broad, 216H). Anal. calcd for **16**.(tol)$_{0.6}$ $C_{100.2}H_{220.8}O_{32}Si_8S_2K_4U_2$: C, 42.09; H, 7.78; S, 2.24. Found C, 42.17; H, 7.68; S, 2.10.

**[{US(OSi(OtBu)$_3$)$_4$K$_2$}$_2$(μ-18c6)] 17**

A colourless solution of $Ph_3PS$ (2.1 mg, 0.007 mmol, 0.5eq) in toluene (1 mL) was added to a stirred brown suspension of [K18c6][U(OSi(OtBu)$_3$)$_4$] (22.3 mg, 0.014 mmol, 1eq) in toluene (0.5 mL). The mixture was stirred at room temperature for 18 h to yield a green solution. The $^1$H NMR spectrum shows the presence of $PPh_3$, [U(OSi(OtBu)$_3$)$_4$] and complex **17** (90% conversion determined by $^1$H NMR spectroscopy using naphthalene as an internal standard) in the reaction mixture. $^1$H NMR (400 MHz, tol-d$_8$, 298 K): δ= -0.9 (s, 162H), -10.3 (s, 54H). Blue-green single crystals of **17**.tol were obtained from the toluene reaction mixture at -40°C. Due to the similar solubility of [U(OSi(OtBu)$_3$)$_4$] and complex **17**, the latter can only be isolated in low yield from this reaction (25%). Complex **17** can also be obtained with similar conversion rates by addition of 1eq of 18c6 per U atom to complex **16** in toluene.

Anal. Calcd for [{US(OSi(OtBu)$_3$)$_4$K$_2$}$_2$(μ-18c6)] **17** $C_{108}H_{240}O_{38}Si_8S_2K_4U_2$: C, 42.28; H, 7.88; found C, 42.33; H, 8.07.

**[Kcryptand][US(OSi(OtBu)$_3$)$_4$K] 18**

A colourless solution of 2.2.2-cryptand (7.8 mg, 0.021 mmol, 2eq, 1eq per U) in toluene (1 mL) was added to a stirred green solution of complex **16** (29.5 mg, 0.010 mmol, 1eq) in toluene (1 mL). After 20 min of stirring, toluene was removed and hexane (1 mL) was added. Green single crystals of complex **18**.hex formed from hexane at room temperature. The crystals were filtered, washed with hexane and dried under vacuum for 1h (27 mg, 74%). $^1$H NMR (400 MHz, tol-d$_8$, 298 K): δ= 13.1 (br s, 12H), 12.9 (br s, 12H), 11.8 (br s, 12H), -0.5 (br s, 81H), -10.6 (br s, 27H). Anal. calcd for [Kcryptand][US(OSi(OtBu)$_3$)$_4$K] **18** $C_{66}H_{144}N_2O_{22}Si_4SK_2U$: C, 44.57; H, 8.16; N, 1.58. Found C, 44.16; H, 8.15; N, 1.65.

**Decomposition of 18 in THF, isolation of [Kcryptand][$U_2(\mu\text{-}S_3)(OSi(OtBu)_3)_6K_3$] 19**

A colourless solution of 2.2.2-cryptand (3.8 mg, 0.010 mmol, 2eq, 1eq per U) in THF (0.3 mL) was added to a stirred green solution of complex **16** (14.4 mg, 0.005 mmol, 1eq) in THF (0.2 mL) to form complex **18** *in situ*. After 10 min of stirring, the green solution was layered with hexane and was allowed to stand for one week at room temperature. Then the mixture was cooled down to -40°C, resulting in the formation of brown single crystals overnight. $^1$H NMR (400 MHz, THF-$d_8$, 298 K): δ = 1.4 (s, 162H). The formation of the U(IV) complex, [$U(OSi(OtBu)_3)_4$], was also identified as decomposition product by $^1$H NMR spectroscopy. The observed U/S ratio of 2:3 in **19** (compared to a U/S ratio of 1:1 in **18**) requires the presence of other decomposition products that remain unidentified.

**[Kcryptand][$U(OSi(OtBu)_3)_4$] 20**

To a stirred brown solution of [$U(OSi(OtBu)_3)_4K$] (49.4 mg, 0.037 mmol, 1eq) in toluene (1 mL), a colourless solution of 2.2.2-cryptand (14.0 mg, 0.037 mmol, 1eq) in toluene (2 mL) was added. An immediate brown precipitate formed instantaneously. After 15 min of stirring the brown suspension was filtered. The obtained brown solid of [Kcryptand][$U(OSi(OtBu)_3)_4$] **20** was washed with toluene and dried for 4 hours (48.7 mg, 0.028 mmol, 76% yield). Brown crystals of complex **20** suitable for X-ray diffraction were obtained from slow diffusion of hexane into a THF solution of the complex. $^1$H NMR (400 MHz, THF-$d_8$, 298 K): δ = 3.6 (m, 24H, cryptand), 2.6 (t, 12H, cryptand), 1.2 (s, 108H). Anal. calcd for [Kcryptand][$US(OSi(OtBu)_3)_4K$].$(KCl)_{0.2}$ **18**.$(KCl)_{0.2}$ $C_{66}H_{144}N_2O_{22}Si_4K_{1.2}Cl_{0.2}U$: C, 46.03; H, 8.43; N, 1.63. Found C, 45.63; H, 8.53; N, 1.78. The presence of KCl arises from the residual presence of KCl in the batch of [$U(OSi(OtBu)_3)_4K$] used in this reaction.

**Reaction of 16 with 1/4eq of $S_8$ , isolation of 21**

A green solution of complex **16** (17.8 mg, 0.006 mmol, 1eq) in toluene (1 mL) was added to a stirred yellow suspension of $S_8$ (0.4 mg, 0.0015 mmol, 0.25eq) in toluene (1 mL), resulting in a brown solution. After 1.5 h of stirring, a $^1$H NMR spectrum was recorded (400 MHz, tol-$d_8$, 298 K) and it showed the formation of the complex [$\{U(OSi(OtBu)_3)_3\}_2(\mu\text{-}S_2)(\mu\text{-}S_3)K$] **21** (0.4 ppm) with 36% conversion (determined by NMR spectroscopy using naphthalene as an internal standard) among other reaction products. Brown single crystals of complex **21** were

obtained from the toluene reaction mixture at -40°C. A similar compound (**14**) was also obtained (together with other unidentified products) from the reaction of [U(OSi(OtBu)$_3$)$_4$K] with 0.25eq of $S_8$ in toluene but the occupancy factors of the disulfide and trisulfide moieties found in the structure of **14** and **21** are different. Attempts to isolate [{U(OSi(OtBu)$_3$)$_3$}$_2$(μ-$S_2$)(μ-$S_3$)K] **21** analytically pure failed due to the presence of other reaction products.

**Reaction of 16 with $CS_2$**

To a green solution of complex **16** (8.5 mg, 0.003 mmol, 1eq) in deuterated toluene (0.5 mL), 9.3 mL of a 636.5 mM solution of $^{13}CS_2$ (0.006 mmol, 2eq) in deuterated toluene were added. The reaction mixture immediately turned light yellow. $^1$H NMR (400 MHz, tol-d$_8$, 298 K): δ = 11.1 (br s, 27H), -2.8 (br s, 81H). The solution was periodically monitored by $^1$H NMR spectroscopy over the course of a week, and it showed a decrease in the intensity of the two broad peaks and an increase in the intensity of the signal corresponding to the U(IV) complex [U(OSi(OtBu)$_3$)$_4$]. This evolution shows the lability of the likely formed thiocarbonate complex, resulting in the release of the thiocarbonate anion. When toluene was removed and DMSO-d$_6$ added, the $^{13}$C NMR spectrum only showed the signal assigned to thiocarbonate.$^{13}$C NMR (100 MHz, DMSO-d$_6$, 298 K): δ = 267.4 (s, $CS_3^{2-}$).

**Reaction of 16 with $CO_2$**

An excess (1 atm) of $^{13}CO_2$ was added to a frozen green solution of complex **16** (11.7 mg, 0.004 mmol, 1eq) in deuterated toluene (0.5 mL). The solution was allowed to warm up to room temperature to yield a light pink solution. $^1$H NMR (400 MHz, tol-d$_8$, 298 K): δ = 8.7 (br s, 27H), -2.9 (br s, 81H). $^{13}$C NMR (100 MHz, tol-d$_8$, 298 K): δ = 153.5 (s, CSO).

**[{K18c6}{U(SH)(OSi(OtBu)$_3$)$_4$}] 22**

A colourless solution of 18c6 (5.2 mg, 0.020 mmol, 2eq) in THF (1 mL) was added to a stirred green solution of complex **16** (28.2 mg, 0.010 mmol, 1eq) in THF (1 mL). The resulting green solution of complex **17** was stirred for ten minutes and was added to a stirred white suspension of PyHCl (2.3 mg, 0.020 mmol, 2eq) in THF (1 mL). The resulting yellow suspension was stirred for 2 h to yield a light green suspension. The $^1$H NMR spectrum of the crude reaction mixture in THF-d$_8$ at 298 K showed the formation of complex [{K18c6}{U(SH)(OSi(OtBu)$_3$)$_4$}] **22** with 53% conversion (determined by NMR spectroscopy using naphthalene as an internal standard) as the main reaction product. Blue-

green single crystals of complex **22**.tol were obtained by storing the toluene reaction mixture at -40°C. The crystals were collected and dried under vacuum for 2 h (11.1 mg, 0.007 mmol, 34% yield). $^1$H NMR (400 MHz, THF-$d_8$, 298 K): δ = 3.07 (s, 24H, 18c6), 0.74 (s, 108H). Anal. calcd for **22**.$(tol)_{0.5}$ $C_{63.5}H_{137}O_{22}Si_4SKU$: C, 45.55; H, 8.25. Found C, 45.66; H, 8.61.

Complex **22** was also obtained in lower yield (17%) (22% overall conversion determined by NMR spectroscopy using naphthalene as an internal standard) by addition of 1eq of $H_2S$ to the U(III) complex [K18c6][$U(OSi(OtBu)_3)_4$] in THF. Crystals of the side-product [$\{U(OSi(OtBu)_3)_3\}_2(\mu\text{-}SH)_2(\mu\text{-}S)$] **23** of this $H_2S$ reaction were isolated from toluene at -40°C.

The reaction of complex [$US(OSi(OtBu)_3)_4K_2]_2$ **16** with PyHCl was carried out under analogous conditions. The $^1$H NMR spectrum of the crude reaction mixture performed in THF-$d_8$ at 298 K after addition of 18c6 showed the formation of **22** with 48% conversion. The reaction of [Kcryptand][$US(OSi(OtBu)_3)_4K$] **18** with PyHCl affords [Kcryptand][$U(SH)(OSi(OtBu)_3)_4$] with 52% conversion as determined by $^1$H NMR. $^1$H NMR (400 MHz, THF-$d_8$, 298 K): δ = 3.36–3.33 (m, cryptand), 2.35 (s, cryptand), 0.70 (s, 108H) (the identity of this complex was confirmed by comparing this $^1$H NMR spectrum to the one obtained after adding cryptand to a solution of complex **22**).

**Isolation of [$UO(OSi(OtBu)_3)_4K_2]_2$ 24**

To a stirred pink solution of [$UO(OSi(OtBu)_3)_4K$] (52.7 mg, 0.039 mmol, 1eq) in toluene (2 mL), $KC_8$ (5.3 mg, 0.039 mmol, 1eq) was added. After 2h of stirring the reaction mixture was centrifuged affording graphite as a black solid and a brown/green solution. $^1$H NMR spectrum in tol-$d_8$ of the crude mixture shows the formation of multiple products. Pale crystals of [$UO(OSi(OtBu)_3)_4K_2]_2$ **24** suitable for X-ray diffraction formed from the toluene crude mixture stored at -40°C.

**Synthetic route to [$U(OSi(OtBu)_3)_4M$] 25 (M=Li), 26 (M=Na), 27 (M=Cs)**

To a stirred green/blue solution of [$U(OSi(OtBu)_3)_4$] (around 50 mg, 1eq) in THF (1 mL), alkali metal chunks (1.1eq of Li, Na or Cs) were added. After 18h of stirring, the resulting dark brown solution was filtered to remove the potential excess of alkali metal. Dark brown crystals of [$U(OSi(OtBu)_3)_4M$] were obtained from toluene (for M=Li **25**, and Cs **27**) and from DIPE (for M=Na **26**) at -40°C. $^1$H NMR (400 MHz, tol-$d_8$, 298 K): for **25**: δ = 0.0 (s, 108H); for **26**: δ = -0.5 (s, 108H); for **27**: δ = -0.2 (s, 108H).

**Reaction of 25, 26 and 27 with excess $CO_2$**

An excess (>1 atm) of $CO_2$ was added to a frozen brown solution of complex **25-27** in deuterated toluene (0.5 mL). The solution was allowed to warm up to room temperature to yield a light yellow (for **25**), light pink (for **26**) and colourless (for **27**) solutions. $^1$H NMR spectra (400 MHz, tol-$d_8$, 298 K) of the crude mixture: for **25**: δ = 1.3 (br s), 0.9 (br s); for **26**: δ = 1.4 (s); for **27**: δ = 1.1 (s, 108H, [U(OSi(OtBu)$_3$)$_4$]), 0.7 (s). All the $^{13}$C NMR spectra in tol-$d_8$ of the crude reaction mixtures show the signal of free CO at 184 ppm.

**Reaction of 26 with 1eq of $CO_2$, isolation of [U(CO$_3$)(OSi(OtBu)$_3$)$_4$Na$_2$]$_3$ 28**

A stoichiometric amount of $CO_2$ (1eq per U atom) was added to a frozen brown solution of complex **26** in deuterated toluene (0.5 mL). The solution was allowed to warm up to room temperature to yield a light pink solution. After several hours, a purple microcrystalline solid formed in the crude mixture. Recristallisation of this solid residue from DIPE at -40°C afforded light purple crystals of **28**.DIPE. $^1$H NMR (400 MHz, tol-$d_8$, 298 K): δ = 5.5 (br s, 27H), -2.2 (br s, 27H).

**[{U(OSi(OtBu)$_3$)$_3$}$_2$(μ-OH)$_2$(μ-O)] 29**

To a stirred brown solution of [U(OSi(OtBu)$_3$)$_4$K] (192.4 mg, 0.145 mmol, 1eq) in toluene (2 mL), 435 μL of a 0.5 M solution of $H_2O$ in THF (0.217 mmol, 1.5eq) were slowly added and a bubbling attributed to $H_2$ release was observed. After 1 week of stirring, the reaction mixture consisted of a light brownish solution above a pink precipitate. The mixture of solvents was removed *in vacuo*. Toluene (1 mL) was added to the solid residue and the resulting suspension was filtered affording a first crop of [{U(OSi(OtBu)$_3$)$_3$}$_2$(μ-OH)$_2$(μ-O)] **29** as pink microcrystalline solid. The isolated yield of the reaction can be improved by concentrating the toluene filtrate and storing it at -40°C to recover additional crops of pink needles (80.5 mg, 49% yield in 3 crops). Pink crystals of [{U(OSi(OtBu)$_3$)$_3$}$_2$(μ-OH)$_2$(μ-O)] **31** suitable for X-ray diffraction were obtained from toluene at -40°C. $^1$H NMR (400 MHz, tol-$d_8$, 298 K): δ = -0.3 (s, 162H). Anal. calcd for **29**.(tol)$_{0.8}$ $C_{77.6}H_{170.4}O_{27}Si_6K_2U_2$: C, 41.27; H, 7.60. Found C, 41.07; H, 7.56.

**[{U(OSi(OtBu)$_3$)$_3$}$_2$(μ-O)] 30**

To a stirred brown solution of [U(OSi(OtBu)$_3$)$_3$]$_2$ (826.9 mg, 0.402 mmol, 1eq) at -40°C in THF (6 mL), a yellow suspension of IMes$N_2$O (140.1 mg, 0.402 mmol, 1eq) at -40°C in THF

(6 mL) was added. An immediate strong bubbling, attributed to $N_2$ release, was observed. After 4h of stirring at room temperature the reaction mixture consisted in a dark suspension which was taken to dryness. Toluene (2 mL) was added to the solid residue and the resulting suspension was filtered affording $[\{U(OSi(OtBu)_3)_3\}_2(\mu\text{-}O)]$ **30** as a pink/purple microcrystalline solid (406.0 mg, 49% yield). Purple crystals of $[\{U(OSi(OtBu)_3)_3\}_2(\mu\text{-}O)]$ **30** suitable for X-ray diffraction were obtained from toluene at -40°C. $^1$H NMR (400 MHz, tol-$d_8$, 298 K): δ = 0.5 (s, 162H). $^1$H NMR (400 MHz, THF-$d_8$, 298 K): δ = -1.3 (s, 162H). Anal. calcd for **30** $C_{72}H_{162}O_{25}Si_6U_2$: C, 41.72; H, 7.88. Found C, 41.46; H, 7.76.

**Reaction of $[U(OSi(OtBu)_3)_4]$ with $N_2O$, isolation of $[(UO_2)_2(OSi(OtBu)_3)_4]$ 31**

An excess of $N_2O$ (1 atm) was added to a frozen blue solution of $[U(OSi(OtBu)_3)_4]$ (13.5 mg, 0.010 mmol, 1eq) in deuterated toluene (0.5 mL). The solution turned immediately dark purple. The $^1$H NMR spectrum of the crude mixture shows only two signals: the signal attributed to residual $[U(OSi(OtBu)_3)_4]$ and an intense unattributed signal at 1.6 ppm. Yellow crystals of $[(UO_2)_2(OSi(OtBu)_3)_4]$ **31** suitable for X-ray diffraction were obtained from hexane at -40°C.

**$[Ln(OSi(OtBu)_3)_4K]$ (Ln=Eu, Yb, Sm) 32-Ln**

A colourless solution of $KOSi(OtBu)_3$ (4eq) in THF (3 mL) was added to $Ln(OTf)_3$ (1 eq) (Ln =Eu, Yb) or $[SmI_3(THF)_{3.7}]$. The resulting mixture was stirred 12h. THF was then removed under vacuum and 3 mL of hexane were added, giving a suspension which was filtered to remove KOTf or KI salts. Hexane was finally removed under vacuum leading to a white powder (78-85% yield). X-ray quality crystals of the complex **32-Yb** were obtained from a toluene solution at -40°C. **32-Eu**: $^1$H NMR (200 MHz, tol-$d_8$, 298K): δ = 2.7 (s, 108H). Anal. Calcd for $[Eu(OSi(OtBu)_3)_4K]$: $C_{48}H_{108}O_{16}Si_4KEu$: C, 46.32; H, 8.75. Found: C, 45.99; H, 8.44. ESI/MS: 1205 $[M\text{-}K]^-$. **32-Yb**: $^1$H NMR (200 MHz, tol-$d_8$, 298K): δ = 5.6 (br s, 108H). $^{13}$C NMR (100 MHz, tol-$d_8$, 298K): δ = 72.3 (C), 35.4 ($CH_3$). Anal. Calcd for $[Yb(OSi(OtBu)_3)_4K].(KOTf)_{0.1}$: $C_{48.1}H_{108}O_{16.3}Si_4S_{0.1}F_{0.3}K_{1.1}Yb$: C, 44.97; H, 8.47. Found: C, 44.82; H, 8.34. ESI/MS: 1226 $[M\text{-}K]^-$. **32-Sm**: $^1$H NMR (200 MHz, tol-$d_8$, 298K): δ = 1.2 (s, 108H). $^{13}$C NMR (50 MHz, tol-$d_8$, 298K): δ = 72.0 (C), 32.2 ($CH_3$). Anal. Calcd for $[Sm(OSi(OtBu)_3)_4K]$: $C_{48}H_{108}O_{16}Si_4KSm$: C, 46.38; H, 8.76. Found: C, 46.17; H, 8.41. ESI/MS: 1204 $[M\text{-}K]^-$.

**[Ln(OSi(OtBu)$_3$)$_4$K$_2$] (Ln=Eu, Yb, Sm) 33-Ln**

To a cold (-40°C) colourless solution of [Ln(OSi(OtBu)$_3$)$_4$K] **32-Ln** (1eq) in hexane (3 mL) potassium chunks were added (1eq) and the mixture was stirred for 12h. The resulting yellow (**33-Eu**) or deep pink solution (**33-Yb** and **33-Sm**) was filtered and the filtrate was concentrated and put at -40°C to crystallize. The yellow (**33-Eu**) or pink crystals (**33-Yb** and **33-Sm**) obtained were washed with cold (-40°C) hexane and dried under vacuum (81-88% yield). **33-Eu**: $^1$H NMR (200 MHz, tol-d$_8$, 298K): NMR silent species. Anal. Calcd for [Eu(OSi(OtBu)$_3$)$_4$K$_2$]: $C_{48}H_{108}O_{16}Si_4K_2Eu$: C, 44.91; H, 8.48. Found: C, 44.96; H, 8.36. Single crystals suitable for X-ray diffraction were obtained from a concentrated solution of the complex in 20:1 hexane/THF at -40°C. **33-Yb**: $^1$H NMR (200 MHz, tol-d$_8$, 298K): δ = 1.5 (s, 108H). $^{13}$C NMR (50 MHz, tol-d$_8$, 298K): δ = 71.4 (C), 32.3 ($CH_3$). Anal. Calcd for [Yb(OSi(OtBu)$_3$)$_4$K$_2$] : $C_{48}H_{108}O_{16}Si_4K_2Yb$: C, 44.18; H, 8.34. Found: C, 44.06; H, 8.15. Single crystals suitable for X-ray diffraction grown from a concentrated toluene solution at -40°C. **33-Sm**: $^1$H NMR (200 MHz, tol-d$_8$, 298K): δ = 2.3 (s, 108H). Anal. Calcd for [Sm(OSi(OtBu)$_3$)$_4$K$_2$] : $C_{48}H_{108}O_{16}Si_4K_2Sm$: C, 44.96; H, 8.49. Found: C, 44.71; H, 8.60. Single crystals suitable for X-ray diffraction grown from a concentrated solution of hexane at -40°C.

**Reaction of 33-Eu with PhNNPh, isolation of [Eu(PhNNPh)(OSi(OtBu)$_3$)$_4$K$_2$] 34**

To a yellow solution of **33-Eu** (136.3 mg, 0.106 mmol, 1eq) in toluene (2.5 mL), PhNNPh (19.3 mg, 0.106 mmol, 1eq) was added at room temperature. The reaction mixture turned brown immediately and was left stirred 1h at room temperature. After centrifugation of the reaction mixture, a light yellow solution and a brown precipitate were obtained. The $^1$H NMR spectrum (200 MHz, tol-d$_8$, 298K) of the evaporated yellow solution in deuterated toluene shows only the presence of **33-Eu**. The brown precipitate was washed with 8 mL of toluene and dissolved in 3 mL of THF. The obtained yellow/brown solution was layered with toluene to yield after 3 days a dark microcrystalline solid. The solid was washed with toluene and dried under vacuum for two days to yield the KPhNNPh radical as a brown solid (17.5 mg, 0.078 mmol, 74% yield). Crystals of [Eu(PhNNPh)(OSi(OtBu)$_3$)$_4$K$_2$] **34** were obtained by letting stand a concentrated hexane solution at -40°C. Anal. Calcd for KPhNNPh $C_{12}H_{10}N_2K$: C, 65.12; H, 4.55; N, 12.66. Found: C, 64.75; H, 4.89; N, 12.87. Dark crystals of KPhNNPh suitable for X-ray diffraction were obtained by slow diffusion of toluene into a diluted THF solution.

The same reactivity leading to the KPhNNPh radical anion and **32-Yb** was also observed for **33-Yb**.

**Reactions of 33-Yb and 33-Eu with $CS_2$**

11 µL of a 0.15 M solution of $^{13}CS_2$ (0.017 mmol, 1eq) in THF-$d_8$ was added at room temperature to a dark solution of **33-Yb** (21.5 mg, 0.017 mmol, 1eq) and 18C6 (8.7 mg, 0.033 mmol, 2eq) in THF-$d_8$ (0.5mL), resulting in a rapid colour change of the solution from dark grey to light orange and the formation of a precipitate. The $^1$H NMR spectrum (200 MHz, THF-$d_8$, 298K) showed the formation of **32-Yb** (1.9 ppm) with 94% conversion determined by NMR using naphthalene as an internal standard). $^{13}$C NMR (50 MHz, THF-$d_8$, 298K): δ = 268.7 ($CS_3^{2-}$), 193.5 (free $CS_2$), 71.2 (18C6), 70.8 (C), 33.5 ($CH_3$). The precipitate was washed with THF and dissolved in DMSO-$d_6$. $^{13}$C NMR (100 MHz, DMSO-$d_6$, 298K): δ = 266.9 ($CS_3^{2-}$), 263.9 ($C_2S_4^{2-}$), 203.0 and 145.7 ($C_3S_5^{2-}$). Suitable crystals of $[(K_2CS_3)_5(DMSO)_{12}]_n$ were obtained by slow diffusion of toluene into a DMSO solution of the precipitate.

The same reactivity was observed for **33-Eu** in THF. The reaction of **33-Eu** with one equivalent of $^{13}CS_2$ at 298 K leads to the immediate formation of a yellow solid identified by NMR as $K_2CS_3$. Suitable crystals of $[(K_2CS_3)_5(DMSO)_{12}]_n$ were obtained by slow diffusion of toluene into the DMSO solution of the precipitate. The relative ratio of the products obtained from the reduction of $CS_2$ by **33-Yb** in THF/18C6 is $CS_3^{2-}$:$C_2S_4^{2-}$:$C_3S_5^{2-}$ 7:1:2.5. The selectivity for the formation of the $CS_3^{2-}$ species is significantly higher when the **33-Eu** complex is used to reduce $CS_2$ ($CS_3^{2-}$:$C_2S_4^{2-}$:$C_3S_5^{2-}$ 40:1:2). Any attempt to isolate (by conducting the reactions at low temperature) an intermediate presenting an Yb or Eu bound thiocarbonate failed.

**Reaction of 33-Yb with $CO_2$ in toluene**

An excess of $^{13}CO_2$ was added to liquid nitrogen frozen solution of **33-Yb** (samples with concentrations of 158, 15 or 5 mM were used) in deuterated toluene. The solutions were allowed to warm up at room temperature during which time a colour fading of the solution from pink to colourless was observed. The $^1$H NMR spectrum (200 MHz, tol-$d_8$, 298K) shows the formation of **32-Yb** (5.6 ppm). $^{13}$C NMR (50 MHz, tol-$d_8$, 298K): δ = 184.6 (free CO), 125.1 (free $CO_2$), 72.3 (C), 35.4 ($CH_3$). Quantitative $^{13}$C NMR of the evaporated reaction mixture in $D_2O$ (100 MHz, $D_2O$, pD=12, 298K): δ = 173.5 ($C_2O_4^{2-}$), 168.3 ($CO_3^{2-}$).

**Reaction of 33-Yb with $CO_2$ in THF**

An excess of $^{13}CO_2$ was added to liquid nitrogen frozen solutions of **33-Yb** (samples with concentrations of 158, or 5 mM were used) and 2eq of 18C6 in deuterated THF. The solutions were allowed to warm up at room temperature during which time a colour fading of the solution from deep grey to colourless was observed. The $^1$H NMR spectrum (200 MHz, THF-$d_8$, 298K) showed the formation of **32-Yb** (1.9 ppm) and the 18C6 signal (3.5 ppm). $^{13}$C NMR (50 MHz, tol-$d_8$, 298K): δ = 185.1 (free CO), 126.7 (free $CO_2$), 71.2 (C), 33.5 (CH3). Quantitative $^{13}$C NMR of the evaporated reaction mixture in $D_2O$ (100 MHz, $D_2O$, pD=12, 298K): δ = 173.5 ($C_2O_4^{2-}$), 168.3 ($CO_3^{2-}$).

**Sequential cyclic reaction of 33-Yb with $CO_2$ in toluene**

An excess of $^{13}CO_2$ was added to a liquid nitrogen frozen solution of **33-Yb** (20.4 mg) in deuterated toluene (0.7 mL). The solution was allowed to warm up at room temperature during which time a colour fading of the solution from pink to colourless was observed. The $^1$H NMR spectrum (200 MHz, tol-$d_8$, 298K) shows the formation of **32-Yb** (5.6 ppm). Then the colourless toluene solution was stirred 15 hours with 2eq of $KC_8$ in order to reduce back the **32-Yb** complex reformed. The $^1$H NMR spectrum (200 MHz, tol-$d_8$, 298K) shows the presence of **33-Yb** (1.5 ppm) and side products at 1.5 and 1.4 ppm. After 5 cycles, the **33-Yb** peak decreased drastically while the side products signals increased.

**Isolation of $[Yb_2(OSi(OtBu)_3)_4)(DME)]$ 35**

To a stirred cold (-40°C) green solution of $[Yb(HMDS)_2]$ (red solution at RT) in DME (0.5 mL), a cold (-40°C) colourless solution of $HOSi(OtBu)_3$ in DME (0.5 mL) was added leading to an orange solution which was stirred at -40°C for 30min. Orange crystals of $[Yb_2(OSi(OtBu)_3)_4)(DME)]$ **35** were obtained from a concentrated solution of complex in DME stored at -40°C. $^1$H NMR (200 MHz, tol-$d_8$, 298K): δ = 3.5 (DME), 3.1 (DME), 1.5 (s, 108H).

**$[Yb(TPA)I_2(CH_3CN)]$ 36**

Slow addition of a solution of TPA (11.3 mg, 0.039 mmol, 1eq) in $CH_3CN$ (2 mL) to a stirred orange solution of $YbI_2$ (16.6 mg, 0.039 mmol, 1eq) in $CH_3CN$ (2 mL) resulted in a dark blue solution. After stirring for 3 h, the reaction mixture was layered with DIPE. Big dark crystals formed in three days and were collected by filtration and dried under vacuum to yield

$[Yb(TPA)I_2(CH_3CN)_{0.6}]$ (20.4 mg, 0.028 mmol, 70% yield). Crystals suitable for X-ray diffraction were obtained by slow diffusion of DIPE into a $CH_3CN$ solution of the complex. $^1H$ NMR (200 MHz, $CD_3CN$, 298K): δ = 8.8 (s, 3H), 7.8 (t, 3H), 7.3 (d, 6H), 4.0 (s, 6 H). Anal. Calcd for $[Yb(TPA)I_2(CH_3CN)_{0.6}]$ $C_{19.2}H_{19.8}I_2N_{4.6}Yb$: C, 31.09; H, 2.69; N, 8.69. Found: C, 30.86; H, 2.80; N, 8.84.

**$[Ln(TPA)I_2]$ Ln = Sm and Eu 37**

Addition of a solution of TPA (20.9 mg, 0.071 mmol) in THF (1 mL) to a stirred solution of $LnI_2$ (1eq) in THF (1 mL) resulted in an orange suspension for $[Eu(TPA)I_2]$ and a red-purple suspension for $[Sm(TPA)I_2]$. After filtration, the residue was washed several times with THF and hexane and dried under vacuum to yield $[Eu(TPA)I_2]$ as an orange powder in 90% yield and $[Sm(TPA)I_2]$ as a red-purple powder in 82% yield. Crystals suitable for X-ray diffraction were obtained for $[Eu(TPA)(\mu\text{-}I)I]_2$ **37** by slow diffusion of DIPE into an acetonitrile solution of the complex. Anal. Calcd for $[Eu(TPA)(\mu\text{-}I)I]_2$ **37** $C_{36}H_{36}I_4N_8Eu_2$: C, 31.06; H, 2.61; N, 8.05. Found: C, 31.11; H, 2.75; N, 8.18. Anal. Calcd for $[Sm(TPA)I_2(THF)_{0.2}]$ $C_{18.8}H_{19.6}I_2N_8O_{0.2}Sm$: C, 31.85; H, 2.79; N, 7.90. Found: C, 31.84; H, 3.4; N, 7.96.

**$[Ln(TPA)_2]I_2$ (Ln = Eu, Yb, Sm) 38-Ln**

Addition of TPA (20 mg, 0.068 mmol, 2eq) in THF (2 mL) to a stirred solution of $LnI_2$ (1eq) in THF (2 mL) resulted in a colour change (to dark red for Ln=Eu, to green for Ln=Yb and to purple-violet for Ln=Sm). A solid precipitates out of the solution after few minutes. After filtration, the solids were washed several times with THF and hexane and dried under vacuum to yield $[Ln(TPA)_2]I_2$ **38-Ln** as powder in 70-80% yield. Crystals suitable for X-ray diffraction were obtained by slow diffusion of a solution of TPA in THF into a solution of $LnI_2$ in THF (for **38-Eu** and **38-Sm**) and from slow diffusion of DIPE into an acetonitrile solution of **38-Yb**. **38-Eu**: $^1H$ NMR (200 MHz, $CD_3CN$, 298 K): NMR silent species. Anal. Calcd for $[Eu(TPA)_2]I_2$ $C_{36}H_{36}I_2N_8Eu$: C, 43.83; H, 3.68; N, 11.36. Found: C, 43.53; H, 3.85, N, 11.44. **38-Yb**: $^1H$ NMR (200 MHz, $CD_3CN$, 298 K): δ = 7.9 (s, 6H), 7.5 (d, 6H), 7.4 (s, 6H), 6.9 (s, 6H), 4.2 (s, 12H). Anal. Calcd for $[Yb(TPA)_2]I_2$ $C_{36}H_{36}I_2N_8Yb$: C, 42.92; H, 3.60; N, 11.12. Found: C, 42.54; H, 3.70; N, 11.26. **38-Sm**: $^1H$ NMR (200 MHz, $CD_3CN$, 298 K): δ = 23.8 (s, 6H), 11.5 (d, 6H), 4.6-4.2 (m, 6H), 3.9-3.6 (m, 6H), -12.2 (s, 12H). Anal. Calcd for $[Sm(TPA)_2]I_2$ $C_{36}H_{36}I_2N_8Sm$: C, 43.90; H, 3.68; N, 11.38. Found: C, 43.75; H, 3.81; N, 11.41.

**[Eu(BPA)$_2$]OTf 39**

A white suspension of KBPA (118.2 mg, 0.340 mmol, 2eq) in THF (2 mL) was added to a white suspension of [Eu(OTf)$_3$] (103.2 mg, 0.170 mmol, 1eq) in THF (2 mL) and stirred 30 min. The reaction mixture turned yellow in few seconds and a white precipitate formed (KOTf) that was filtered out. The resulting solution was layered with DIPE. Orange crystals formed in 2 days and they were filtered and dried under vacuum for 24 h leading to [Eu(BPA)$_2$]OTf **39** (151.3 mg, 0.160 mmol, 95% yield). Orange crystals suitable for X-ray diffraction were obtained by slow diffusion of DIPE into a THF solution of the complex. $^1$H NMR (200 MHz, py-d$_5$, 298 K): δ = 30.6 (br s, 4 H), 13.0-11.8 (m, 12H), 2.0-1.0 (m, 6H), -2.5 to -4.0 (m, 8H), -15.7 (br s, 4H), -18.2 (br s, 2 H). Anal. Calcd for [Eu(BPA)$_2$]OTf.(KOTf)$_{0.1}$ **39**.(KOTf)$_{0.1}$ $C_{39.1}H_{36}N_6O_{5.3}F_{3.3}S_{1.1}K_{0.1}Eu$: C, 50.57; H, 3.91; N, 9.05. Found: C, 50.62; H, 3.88; N 9.14.

**[Eu(BPA)$_2$] 40**

A solution of EuI$_2$ (200.0 mg, 0.49 mmol, 1eq) in THF (3 mL) was added to a white suspension of KBPA (338.2 mg, 0.98 mmol, 2eq) in THF (6 mL), affording a red-brown suspension. After 1h of stirring, the mixture was filtered. The brown solid obtained was extracted in pyridine (4 mL) to remove KI. The two filtrates were combined, concentrated, and layered with hexane. Brown crystals formed after one week, which were collected, washed with hexane, and dried under vacuum for 24h to yield [Eu(BPA)$_2$] **40** (318.0 mg, 0.420 mmol, 85% yield). Dark-brown crystals suitable for X-ray diffraction were obtained by slow diffusion of hexane into a pyridine solution of the complex. $^1$H NMR (200 MHz, py-d$_5$, 298 K): NMR silent species. Anal. Calcd for [Eu(BPA)$_2$] $C_{38}H_{36}N_6O_2Eu$: C, 60.00; H, 4.77; N, 11.05. Found: C, 59.61; H, 4.74; N, 10.95.

**[Yb(BPA)I(CH$_3$CN)]$_2$ 41**

A white suspension of KBPA (17.3 mg, 0.0505 mmol, 1eq) in CH$_3$CN (1.5 mL) was added dropwise to an orange solution of [YbI$_2$(THF)2.1] (29.2 mg, 0.0505 mmol, 1eq) in CH$_3$CN (1.5 mL) and stirred 18h. The resulting mixture turned dark green in few seconds. The mixture was then concentrated to 2 mL and filtered. The filtrate was layered with DIPE. A dark-green crystalline solid formed after 24 h. The proton NMR spectrum shows the presence of only one set of signals assigned to [Yb(BPA)I(CH$_3$CN)]$_2$ **41**. X-ray quality dark-green crystals of [Yb(BPA)I(CH$_3$CN)]$_2$.(CH$_3$CN)$_{0.4}$ **41**.(CH$_3$CN)$_{0.4}$ were obtained from a saturated

solution of the complex in $CH_3CN$. Unfortunately, a satisfactory elemental analysis was not obtained because of an important co-crystallization of KI, which we were not able to separate. $^1$H NMR (400 MHz, $CD_3CN$, 298 K): δ = 8.4 (d, 2 H), 7.8 (t, 2H), 7.3 (d, 2H), 7.2 (d, 1H), 7.1–7.0 (m, 3H), 6.8 (d, 1H), 6.5 (t, 1 H), 3.9–3.7 (m, 6 H).

**[Eu(BPPA)$_2$]OTf 42**

A white suspension of KBPPA.$(THF)_{0.65}$ (93.3 mg, 0.180 mmol, 2eq) in THF (2 mL) was added to a white suspension of [Eu$(OTf)_3$] (55.6 mg, 0.090 mmol, 1eq) in THF (2 mL) and stirred for 1h. The resulting suspension turned orange in few seconds. The solvent was then removed under vacuum and pyridine (2 mL) was added to afford a deep orange suspension that was filtered to partially remove KOTf. Complete removal of KOTf salt is not possible due to the very similar solubility of the desired complex and KOTf. The filtrate was layered with hexane to yield [Eu$(BPPA)_2$]OTf.$(KOTf)_{1.5}$ **42**.$(KOTf)_{1.5}$ (96.1 mg, 0.068 mmol, 73% yield) as an orange solid. X-ray quality orange crystals of **42**.$(py)_{2.5}$ were obtained by slow diffusion of hexane into a pyridine solution of the complex. $^1$H NMR (200 MHz, py-$d_5$, 298 K): δ = 30.0 to -24.0 (br m, 32 H), 4.9 (s, 18 H), -15.2 (s, 18 H). Anal. Calcd for [Eu$(BPPA)_2$]OTf.$(KOTf)_{1.5}$ $C_{56.5}H_{68}N_6O_{9.5}F_{7.5}S_{2.5}K_{1.5}Eu$: C, 47.91; H, 4.84; N, 5.93. Found: C, 47.85; H, 4.86; N, 6.21.

**[Yb(MPA)$_2$K] 43**

A light-yellow solution of $K_2$MPA (54.9 mg, 0.080 mmol, 2eq) in THF (3 mL) was added to a suspension of Yb$(OTf)_3$ (24.8 mg, 0.040 mmol, 1eq) in THF (2 mL), affording a pale-yellow suspension which was stirred for 4h. The reaction mixture was evaporated and the resulting solid was extracted with hexane. The insoluble KOTf was removed and the colourless filtrate was concentrated and let standing at -40°C. After 15h, colourless crystals formed that were washed with cold hexane and dried under vacuum for 24h to afford [Yb$(MPA)_2$K] **43** (42.5 mg, 0.030 mmol, 78% yield). Colourless crystals suitable for X-ray diffraction were obtained from a concentrated solution of the complex in 30:1 hexane/DME. $^1$H NMR (200 MHz, $CD_3CN$, 298 K): δ = 187.0-148.0 (br m, 8H), 52.9 (br m, 4H), 43.3 (br s, 2H), 42.4 (br s, 2H), 27.7 (s, 2H), 26.4 (s, 2H), 6.2 (s, 18H), 4.8 (s, 18H), 1.6 (s, 4H), -7.6 (br s, 2H), -10.8 (br s, 2H), -43.9 (br s, 18H), -50.9 (br s, 18H). Anal. Calcd for [Yb$(MPA)_2$K][KOTf]$_{0.3}$ $C_{72.3}H_{100}N_4O_{4.9}F_{0.9}S_{0.3}K_{1.3}Yb$: C, 64.13; H, 7.44; N, 4.14. Found: C, 64.26; H, 7.37; N, 4.15.

**Reaction of $YbI_2$ with 2eq of $K_2MPA$**

A light yellow solution of $[YbI_2(THF)_{2.4}]$ in THF-$d_8$ and a white suspension of 2eq of $K_2MPA$ in THF-$d_8$ were prepared separately and cooled down to -40°C. The cold ligand solution was added to the cold suspension of ytterbium iodide leading to a light orange suspension. The $^1H$ NMR spectrum of this reaction mixture show the presence of the signals assigned to the trivalent Yb complex $[Yb(MPA)_2K]$ **43** as the main species.

**$[Eu(BPA)(CS_3)(DMSO)_2]$ 44**

$^{13}CS_2$ (4.9 µL) was added to a pyridine solution (1.5 mL) of $[Eu(BPA)_2]$ **40** (61.5 mg, 0.081 mmol, 1eq). The solution turned from red-brown to red. Then pyridine was removed under vacuum and DMSO was added. Red crystals suitable for X-ray diffraction were obtained from a DMSO solution of the reaction mixture layered with toluene. $[Eu(BPA)(CS_3)(DMSO)_2].(DMSO)_{0.3}$ **44**$.(DMSO)_{0.3}$ was recovered (11.0 mg, 0.015 mmol, 37% yield). Anal. Calcd for $[Eu(BPA)(CS_3)(DMSO)_2].(DMSO)_{0.3}$ $C_{26.6}H_{37.8}N_3O_{4.3}S_{6.3}Eu$: C, 38.85; H, 4.63; N, 5.11. Found: C, 38.46; H, 4.48; N, 4.91.

# References


1. Tolman, W. B., *Activation of Small Molecules*. Wiley: Weinheim, 2006.
2. Sakakura, T.; Choi, J.-C.; Yasuda, H., *Chem. Rev.* **2007,** *107* (6), 2365-2387.
3. Costentin, C.; Drouet, S.; Robert, M.; Saveant, J. M., *Science* **2012,** *338* (6103), 90-94.
4. Appel, A. M.; Bercaw, J. E.; Bocarsly, A. B.; Dobbek, H.; DuBois, D. L.; Dupuis, M.; Ferry, J. G.; Fujita, E.; Hille, R.; Kenis, P. J. A.; Kerfeld, C. A.; Morris, R. H.; Peden, C. H. F.; Portis, A. R.; Ragsdale, S. W.; Rauchfuss, T. B.; Reek, J. N. H.; Seefeldt, L. C.; Thauer, R. K.; Waldrop, G. L., *Chem. Rev.* **2013,** *113* (8), 6621-6658.
5. Camp, C.; Mougel, V.; Horeglad, P.; Pecaut, J.; Mazzanti, M., *J. Am. Chem. Soc.* **2010,** *132* (49), 17374-17377.
6. Camp, C.; Guidal, V.; Biswas, B.; Pecaut, J.; Dubois, L.; Mazzanti, M., *Chem. Sci.* **2012,** *3* (8), 2433-2448.
7. Cooper, O.; Camp, C.; Pecaut, J.; Kefalidis, C. E.; Maron, L.; Gambarelli, S.; Mazzanti, M., *J. Am. Chem. Soc.* **2014,** *136* (18), 6716-6723.
8. van Hoecke, M. P.; Leroy, M. J. F., *Actualite Chimique* **2011,** (358), 24-29.
9. Cotton, S. A., *Lanthanide and Actinide Chemistry*. John Wiley & Sons: 2006.
10. Neidig, M. L.; Clark, D. L.; Martin, R. L., *Coord. Chem. Rev.* **2013,** *257* (2), 394-406.
11. Huang, C.-H., *Rare Earth Coordination Chemistry*. John Wiley & Sons: 2010.
12. Sastri, V. S.; Bünzli, J.-C.; Rao, V. R.; Rayudu, G. V. S.; R., P. J., *Modern Aspects of Rare Earths and their Complexes*. Elsevier: Amsterdam, 2003.
13. Aspinall, H. C., *Chemistry of the f-Block Elements*. Gordon and Breach Science Publishers: 2001.
14. Housecroft, C. E.; Sharpe, A. G., The f-block metals: lanthanoids and actinoids. In *Inorg. Chem.*, Pearson Education Limited: Essex, 2005.
15. Fieser, M. E.; MacDonald, M. R.; Krull, B. T.; Bates, J. E.; Ziller, J. W.; Furche, F.; Evans, W. J., *J. Am. Chem. Soc.* **2015,** *137* (1), 369-382.
16. Shannon, R. D., *Acta Cryst. A* **1976,** *32*, 751-767.
17. Nief, F., *Dalton Trans.* **2010,** *39* (29), 6589-6598.
18. MacDonald, M. R.; Bates, J. E.; Fieser, M. E.; Ziller, J. W.; Furche, F.; Evans, W. J., *J. Am. Chem. Soc.* **2012,** *134* (20), 8420-8423.
19. MacDonald, M. R.; Bates, J. E.; Ziller, J. W.; Furche, F.; Evans, W. J., *J. Am. Chem. Soc.* **2013,** *135* (26), 9857-9868.
20. Meyer, G.; Wickleder, M. S., *Handbook on the Physics and Chemistry of Rare Earths*. Elsevier Science B. V.: Amsterdam, 2000; Vol. 28.
21. Corbett, J. D., *Revue De Chimie Minerale* **1973,** *10* (1-2), 239-257.
22. Morss, L. R., *Chem. Rev.* **1976,** *76* (6), 827-841.
23. Kagan, H. B.; Namy, J. L., *Tetrahedron* **1986,** *42* (24), 6573-6614.
24. Kagan, H. B., *Tetrahedron* **2003,** *59* (52), 10351-10372.
25. Evans, W. J., *Coord. Chem. Rev.* **2000,** *206*, 263-283.
26. Nugent, L. J.; Vandersl.Kl, *J. Chem. Phys.* **1973,** *59* (6), 3440-3441.
27. Fischer, E. O.; Fischer, H., *Angew. Chem. Int. Ed.* **1964,** *3* (2), 132-133.

28. Fischer, E. O.; Fischer, H., *J. Organomet. Chem.* **1966,** *6* (2), 141-148.
29. Watt, G. W.; Gillow, E. W., *J. Am. Chem. Soc.* **1969,** *91* (3), 775-776.
30. Evans, W. J.; Hughes, L. A.; Hanusa, T. P., *J. Am. Chem. Soc.* **1984,** *106* (15), 4270-4272.
31. Evans, W. J., *Polyhedron* **1987,** *6* (5), 803-835.
32. Bochkarev, M. N.; Fedushkin, I. L.; Dechert, S.; Fagin, A. A.; Schumann, H., *Angew. Chem. Int. Ed.* **2001,** *40* (17), 3176-3178.
33. Evans, W. J.; Allen, N. T.; Ziller, J. W., *J. Am. Chem. Soc.* **2000,** *122* (47), 11749-11750.
34. Bochkarev, M. N.; Fedushkin, I. L.; Fagin, A. A.; Petrovskaya, T. V.; Ziller, J. W.; BroomhallDillard, R. N. R.; Evans, W. J., *Angew. Chem. Int. Ed.* **1997,** *36* (1-2), 133-135.
35. Evans, W. J.; Allen, N. T.; Ziller, J. W., *Angew. Chem. Int. Ed.* **2002,** *41* (2), 359-361.
36. Nief, F.; Turcitu, D.; Ricard, L., *Chem. Commun.* **2002,** (15), 1646-1647.
37. Jaroschik, F.; Nief, F.; Le Goff, X. F.; Ricard, L., *Organometallics* **2007,** *26* (5), 1123-1125.
38. Jaroschik, F.; Momin, A.; Nief, F.; Le Goff, X. F.; Deacon, G. B.; Junk, P. C., *Angew. Chem. Int. Ed.* **2009,** *48* (6), 1117-1121.
39. Edelmann, F. T.; Freckmann, D. M. M.; Schumann, H., *Chem. Rev.* **2002,** *102* (6), 1851-1896.
40. Deacon, G. B.; Forsyth, C. M.; Junk, P. C.; Skelton, B. W.; White, A. H., *Chem. Eur. J.* **1999,** *5* (5), 1452-1459.
41. Vandenhende, J. R.; Hitchcock, P. B.; Holmes, S. A.; Lappert, M. F., *J. Chem. Soc., Dalton Trans.* **1995,** (9), 1435-1440.
42. Duncalf, D. J.; Hitchcock, P. B.; Lawless, G. A., *J. Organomet. Chem.* **1996,** *506* (1-2), 347-349.
43. Nishiura, M.; Hou, Z. M.; Wakatsuki, Y., *Organometallics* **2004,** *23* (6), 1359-1368.
44. Datta, S.; Gamer, M. T.; Roesky, P. W., *Organometallics* **2008,** *27* (6), 1207-1213.
45. Edelmann, F. T., *Chem. Soc. Rev.* **2012,** *41* (23), 7657-7672.
46. Trifonov, A. A.; Gudilenkov, I. D.; Larionova, J.; Luna, C.; Fukin, G. K.; Cherkasov, A. V.; Poddel'sky, A. I.; Druzhkov, N. O., *Organometallics* **2009,** *28* (23), 6707-6713.
47. Berube, C. D.; Gambarotta, S.; Yap, G. P. A.; Cozzi, P. G., *Organometallics* **2003,** *22* (3), 434-439.
48. Wang, J.; Dick, A. K. J.; Gardiner, M. G.; Yates, B. F.; Peacock, E. J.; Skelton, B. W.; White, A. H., *Eur. J. Inorg. Chem.* **2004,** (10), 1992-1995.
49. Giesbrecht, G. R.; Cui, C. M.; Shafir, A.; Schmidt, J. A. R.; Arnold, J., *Organometallics* **2002,** *21* (18), 3841-3844.
50. Basalov, I. V.; Dorcet, V.; Fukin, G. K.; Carpentier, J.-F.; Sarazin, Y.; Trifonov, A. A., *Chem. Eur. J.* **2015,** *21* (16), 6033-6036.
51. Dugah, D. T.; Skelton, B. W.; Delbridge, E. E., *Dalton Trans.* **2009,** (8), 1436-1445.
52. Guo, H.; Zhou, H.; Yao, Y.; Zhang, Y.; Shen, Q., *Dalton Trans.* **2007,** (32), 3555-3561.
53. Yang, S.; Nie, K.; Zhang, Y.; Xue, M.; Yao, Y.; Shen, Q., *Inorg. Chem.* **2014,** *53* (1), 105-115.
54. Ferrence, G. M.; McDonald, R.; Takats, J., *Angew. Chem. Int. Ed.* **1999,** *38* (15), 2233-2237.
55. Konkol, M.; Okuda, J., *Coord. Chem. Rev.* **2008,** *252* (15-17), 1577-1591.
56. Cheng, J.; Takats, J.; Ferguson, M. J.; McDonald, R., *J. Am. Chem. Soc.* **2008,** *130* (5), 1544-1545.
57. Péligot, E. M., *Annales de Chimie et de Physique* **1842,** *3*, 5.
58. Settle, F. A., *J. Chem. Educ.* **2009,** *86* (3), 316-323.

59. Greenwood, N. N.; Earnshaw, A., *Chemistry of the Elements*. Elsevier: Amsterdam, 1997.
60. Evans, W. J.; Kozimor, S. A., *Coord. Chem. Rev.* **2006,** *250* (7-8), 911-935.
61. MacDonald, M. R.; Fieser, M. E.; Bates, J. E.; Ziller, J. W.; Furche, F.; Evans, W. J., *J. Am. Chem. Soc.* **2013,** *135* (36), 13310-13313.
62. Schelter, E. J.; Yang, P.; Scott, B. L.; Thompson, J. D.; Martin, R. L.; Hay, P. J.; Morris, D. E.; Kiplinger, J. L., *Inorg. Chem.* **2007,** *46* (18), 7477-7488.
63. Lam, O. P.; Meyer, K., *Polyhedron* **2012,** *32* (1), 1-9.
64. Fox, A. R.; Bart, S. C.; Meyer, K.; Cummins, C. C., *Nature* **2008,** *455* (7211), 341-349.
65. Taylor, J. C.; Wilson, P. W., *Acta Cryst. B* **1974,** *30*, 2803-2805.
66. Levy, J. H.; Taylor, J. C.; Wilson, P. W., *Acta Cryst. B* **1975,** *31*, 880-882.
67. Andersen, R. A., *Inorg. Chem.* **1979,** *18* (6), 1507-1509.
68. Moody, D. C.; Odom, J. D., *J. Inorg. Nucl. Chem.* **1979,** *41* (4), 533-535.
69. Moody, D. C.; Zozulin, A. J.; Salazar, K. V., *Inorg. Chem.* **1982,** *21* (10), 3856-3857.
70. Santos, I.; Marques, N.; Dematos, A. P., *Inorg. Chim. Acta* **1985,** *110* (2), 149-151.
71. Avens, L. R.; Bott, S. G.; Clark, D. L.; Sattelberger, A. P.; Watkin, J. G.; Zwick, B. D., *Inorg. Chem.* **1994,** *33*, 2248-2256.
72. Carmichael, C. D.; Jones, N. A.; Arnold, P. L., *Inorg. Chem.* **2008,** *47* (19), 8577-8579.
73. Monreal, M. J.; Thomson, R. K.; Cantat, T.; Travia, N. E.; Scott, B. L.; Kiplinger, J. L., *Organometallics* **2011,** *30* (7), 2031-2038.
74. Baker, R. J., *Coord. Chem. Rev.* **2012,** *256* (23-24), 2843-2871.
75. Yin, H.; Lewis, A. J.; Williams, U. J.; Carroll, P. J.; Schelter, E. J., *Chem. Sci.* **2013,** *4* (2), 798-805.
76. Kanellak.B; Fischer, E. O.; Dornberg.E; Baumgart.F, *J. Organomet. Chem.* **1970,** *24* (2), 507-514.
77. Ephritikhine, M., *Organometallics* **2013,** *32*, 2464−2488.
78. Liddle, S. T., *Angew. Chem. Int. Ed.* **2015,** *54*, 8604-8641.
79. Aresta, M.; Dibenedetto, A.; Angelini, A., *Chem. Rev.* **2014,** *114* (3), 1709-1742.
80. Ibers, J. A., *Chem. Soc. Rev.* **1982,** *11* (1), 57-73.
81. Benson, E. E.; Kubiak, C. P.; Sathrum, A. J.; Smieja, J. M., *Chem. Soc. Rev.* **2009,** *38* (1), 89-99.
82. Castro-Rodriguez, I.; Nakai, H.; Zakharov, L. N.; Rheingold, A. L.; Meyer, K., *Science* **2004,** *305* (5691), 1757-1759.
83. Evans, W. J.; Seibel, C. A.; Ziller, J. W., *Inorg. Chem.* **1998,** *37* (4), 770-776.
84. Mascetti, J., Metal Coordination of CO2. In *Encyclopedia of Inorganic and Bioinorganic Chemistry*, John Wiley & Sons: 2011.
85. Mascetti, J.; Galan, F.; Papai, I., *Coord. Chem. Rev.* **1999,** *192*, 557-576.
86. Fang, M.; Farnaby, J. H.; Ziller, J. W.; Bates, J. E.; Furche, F.; Evans, W. J., *J. Am. Chem. Soc.* **2012,** *134* (14), 6064-6067.
87. Camp, C.; Chatelain, L.; Kefalidis, C. E.; Pecaut, J.; Maron, L.; Mazzanti, M., *Chem. Commun.* **2015,** *51* (84), 15454-15457.
88. Berthet, J. C.; Lemarechal, J. F.; Nierlich, M.; Lance, M.; Vigner, J.; Ephritikhine, M., *J. Organomet. Chem.* **1991,** *408* (3), 335-341.
89. Castro-Rodriguez, I.; Meyer, K., *J. Am. Chem. Soc.* **2005,** *127* (32), 11242-11243.
90. Mansell, S. M.; Kaltsoyannis, N.; Arnold, P. L., *J. Am. Chem. Soc.* **2011,** *133* (23), 9036-9051.
91. Kahan, R. J.; Cloke, F. G. N.; Roe, S. M.; Nief, F., *New J. Chem.* **2015,** *39* (10), 7602-7607.
92. Davies, N. W.; Frey, A. S. P.; Gardiner, M. G.; Wang, J., *Chem. Commun.* **2006,** (46), 4853-4855.

93. Summerscales, O. T.; Frey, A. S. P.; Geoffrey, F.; Cloke, N.; Hitchcock, P. B., *Chem. Commun.* **2009,** (2), 198-200.
94. Tsoureas, N.; Castro, L.; Kilpatrick, A. F. R.; Cloke, F. G. N.; Maron, L., *Chem. Sci.* **2014,** *5* (10), 3777-3788.
95. Webster, C. L.; Ziller, J. W.; Evans, W. J., *Organometallics* **2013,** *32* (17), 4820-4827.
96. Lam, O. P.; Bart, S. C.; Kameo, H.; Heinemann, F. W.; Meyer, K., *Chem. Commun.* **2010,** *46* (18), 3137-3139.
97. Castro, L.; Lam, O. P.; Bart, S. C.; Meyer, K.; Maron, L., *Organometallics* **2010,** *29* (21), 5504-5510.
98. Schmidt, A. C.; Nizovtsev, A. V.; Scheurer, A.; Heinemann, F. W.; Meyer, K., *Chem. Commun.* **2012,** *48* (69), 8634-8636.
99. Schmidt, A.-C.; Heinemann, F. W.; Kefalidis, C. E.; Maron, L.; Roesky, P. W.; Meyer, K., *Chem. Eur. J.* **2014,** *20* (42), 13501-13506.
100. Mougel, V.; Camp, C.; Pecaut, J.; Coperet, C.; Maron, L.; Kefalidis, C. E.; Mazzanti, M., *Angew. Chem. Int. Ed.* **2012,** *51* (49), 12280-12284.
101. Evans, W. J.; Perotti, J. M.; Brady, J. C.; Ziller, J. W., *J. Am. Chem. Soc.* **2003,** *125* (17), 5204-5212.
102. Castro, L.; Labouille, S.; Kindra, D. R.; Ziller, J. W.; Nief, F.; Evans, W. J.; Maron, L., *Chem. Eur. J.* **2012,** *18* (25), 7886-7895.
103. Evans, W. J.; Lorenz, S. E.; Ziller, J. W., *Inorg. Chem.* **2009,** *48* (5), 2001-2009.
104. Castro, L.; Mills, D. P.; Jones, C.; Maron, L., *Eur. J. Inorg. Chem.* **2016,** (6), 792-796.
105. Schumann, H.; Meesemarktscheffel, J. A.; Dietrich, A.; Gorlitz, F. H., *J. Organomet. Chem.* **1992,** *430* (3), 299-315.
106. Nakajima, Y.; Okuda, J., *Organometallics* **2007,** *26* (5), 1270-1278.
107. Webster, C. L.; Ziller, J. W.; Evans, W. J., *Organometallics* **2014,** *33* (1), 433-436.
108. Webster, C. L.; Ziller, J. W.; Evans, W. J., *Organometallics* **2012,** *31*, 7191−7197.
109. Evans, W. J.; Seibel, C. A.; Ziller, J. W.; Doedens, R. J., *Organometallics* **1998,** *17* (10), 2103-2112.
110. Evans, W. J.; Walensky, J. R.; Ziller, J. W., *Organometallics* **2010,** *29* (4), 945-950.
111. Cheng, H.; Zhao, B.; Yao, Y.; Lu, C., *Green Chem.* **2015,** *17* (3), 1675-1682.
112. Evans, W. J.; Perotti, J. M.; Kozimor, S. A.; Champagne, T. M.; Davis, B. L.; Nyce, G. W.; Fujimoto, C. H.; Clark, R. D.; Johnston, M. A.; Ziller, J. W., *Organometallics* **2005,** *24* (16), 3916-3931.
113. Evans, W. J.; Rego, D. B.; Ziller, J. W.; DiPasquale, A. G.; Rheingold, A. L., *Organometallics* **2007,** *26* (19), 4737-4745.
114. Arnold, P. L.; Turner, Z. R.; Germeroth, A. I.; Casely, I. J.; Nichol, G. S.; Bellabarba, R.; Tooze, R. P., *Dalton Trans.* **2013,** *42* (5), 1333-1337.
115. Dellamico, D. B.; Calderazzo, F.; Marchetti, F.; Perego, G., *J. Chem. Soc., Chem. Commun.* **1979,** (23), 1103-1105.
116. Baisch, U.; Dell'Amico, D. B.; Calderazzo, F.; Labella, L.; Marchetti, F.; Merigo, A., *Eur. J. Inorg. Chem.* **2004,** (6), 1219-1224.
117. Frey, J. A. H.; Cloke, F. G. N.; Roe, S. M., *Organometallics* **2015,** *34* (11), 2102-2105.
118. Ke, H. S.; Zhao, L.; Xu, G. F.; Guo, Y. N.; Tang, J. K.; Zhang, X. Y.; Zhang, H. J., *Dalton Trans.* **2009,** (47), 10609-10613.
119. Bag, P.; Dutta, S.; Biswas, P.; Maji, S. K.; Florke, U.; Nag, K., *Dalton Trans.* **2012,** *41* (12), 3414-3423.
120. Natrajan, L.; Pecaut, J.; Mazzanti, M., *Dalton Trans.* **2006,** (8), 1002-1005.
121. Tang, X. L.; Wang, W. H.; Dou, W.; Jiang, J.; Liu, W. S.; Qin, W. W.; Zhang, G. L.; Zhang, H. R.; Yu, K. B.; Zheng, L. M., *Angew. Chem. Int. Ed.* **2009,** *48* (19), 3499-3502.

122. Andrews, P. C.; Beck, T.; Forsyth, C. M.; Fraser, B. H.; Junk, P. C.; Massi, M.; Roesky, P. W., *Dalton Trans.* **2007,** (48), 5651-5654.
123. Zuend, S. J.; Lam, O. P.; Heinemann, F. W.; Meyer, K., *Angew. Chem. Int. Ed.* **2011,** *50* (45), 10626-10630.
124. Lescop, C.; Arliguie, T.; Lance, M.; Nierlich, M.; Ephritikhine, M., *J. Organomet. Chem.* **1999,** *580* (1), 137-144.
125. Evans, W. J.; Miller, K. A.; Ziller, J. W., *Inorg. Chem.* **2006,** *45* (1), 424-429.
126. Lam, O. P.; Franke, S. M.; Heinemann, F. W.; Meyer, K., *J. Am. Chem. Soc.* **2012,** *134* (40), 16877-16881.
127. Matson, E. M.; Forrest, W. P.; Fanwick, P. E.; Bart, S. C., *J. Am. Chem. Soc.* **2011,** *133* (13), 4948-4954.
128. Matson, E. M.; Fanwick, P. E.; Bart, S. C., *Organometallics* **2011,** *30* (21), 5753-5762.
129. Brennan, J. G.; Andersen, R. A.; Zalkin, A., *Inorg. Chem.* **1986,** *25* (11), 1756-1760.
130. Lam, O. P.; Heinemann, F. W.; Meyer, K., *Angew. Chem. Int. Ed.* **2011,** *50* (26), 5965-5968.
131. Lam, O. P.; Castro, L.; Kosog, B.; Heinemann, F. W.; Maron, L.; Meyer, K., *Inorg. Chem.* **2012,** *51* (2), 781-783.
132. Castro, L.; Maron, L., *Chem. Eur. J.* **2012,** *18* (21), 6610-6615.
133. Heitmann, D.; Jones, C.; Mills, D. P.; Stasch, A., *Dalton Trans.* **2010,** *39* (7), 1877-1882.
134. Deacon, G. B.; Junk, P. C.; Wang, J.; Werner, D., *Inorg. Chem.* **2014,** *53* (23), 12553-12563.
135. Matson, E. M.; Breshears, A. T.; Kiernicki, J. J.; Newell, B. S.; Fanwick, P. E.; Shores, M. P.; Walensky, J. R.; Bartt, S. C., *Inorg. Chem.* **2014,** *53* (24), 12977-12985.
136. Howard, J. B.; Rees, D. C., *Proc. Natl. Acad. Sci. USA* **2006,** *103* (46), 17088-17093.
137. Erisman, J. W.; Sutton, M. A.; Galloway, J.; Klimont, Z.; Winiwarter, W., *Nature Geoscience* **2008,** *1* (10), 636-639.
138. Haber, F. *Ammonia*. German patent DE229126 **1909**.
139. Evans, W. J.; Ulibarri, T. A.; Ziller, J. W., *J. Am. Chem. Soc.* **1988,** *110* (20), 6877-6879.
140. Gardiner, M. G.; Stringer, D. N., *Materials* **2010,** *3* (2), 841-862.
141. Evans, W. J.; Zucchi, G.; Ziller, J. W., *J. Am. Chem. Soc.* **2003,** *125* (1), 10-11.
142. Evans, W. J.; Lee, D. S., *Can. J. Chem.* **2005,** *83* (4), 375-384.
143. Evans, W. J., *J. Alloys Compd.* **2009,** *488* (2), 493-510.
144. Evans, W. J.; Fang, M.; Zucchi, G.; Furche, F.; Ziller, J. W.; Hoekstra, R. M.; Zink, J. I., *J. Am. Chem. Soc.* **2009,** *131* (31), 11195-11202.
145. Evans, W. J.; Kozimor, S. A.; Ziller, J. W., *J. Am. Chem. Soc.* **2003,** *125* (47), 14264-14265.
146. Mansell, S. M.; Farnaby, J. H.; Germeroth, A. I.; Arnold, P. L., *Organometallics* **2013,** *32* (15), 4214-4222.
147. Odom, A. L.; Arnold, P. L.; Cummins, C. C., *J. Am. Chem. Soc.* **1998,** *120* (23), 5836-5837.
148. Roussel, P.; Scott, P., *J. Am. Chem. Soc.* **1998,** *120*, 1070-1071.
149. Roussel, P.; Errington, W.; Kaltsoyannis, N.; Scott, P., *J. Organomet. Chem.* **2001,** *635* (1-2), 69-74.
150. Cloke, G., F. N.; Hitchcock, P. B., *J. Am. Chem. Soc.* **2002,** *124*, 9352-9353.
151. Cloke, F. G. N.; Green, J. C.; Kaltsoyannis, N., *Organometallics* **2004,** *23* (4), 832-835.
152. Korobkov, I.; Gambarotta, S.; Yap, G. P. A., *Angew. Chem. Int. Ed.* **2002,** *41* (18), 3433-3436.

153. Evans, W. J.; Drummond, D. K.; Chamberlain, L. R.; Doedens, R. J.; Bott, S. G.; Zhang, H. M.; Atwood, J. L., *J. Am. Chem. Soc.* **1988,** *110* (15), 4983-4994.
154. Antunes, M. A.; Coutinho, J. T.; Santos, I. C.; Marcalo, J.; Almeida, M.; Baldovi, J. J.; Pereira, L. C. J.; Gaita-Arino, A.; Coronado, E., *Chem. Eur. J.* **2015,** *21* (49), 17817-17826.
155. Turcitu, D.; Nief, F.; Ricard, L., *Chem. Eur. J.* **2003,** *9* (20), 4916-4923.
156. Yuan, F. G.; Liu, X. J., *Appl. Organomet. Chem.* **2005,** *19* (7), 877-878.
157. Takats, J.; Zhang, X. W.; Day, V. W.; Eberspacher, T. A., *Organometallics* **1993,** *12* (11), 4286-4288.
158. Brady, E. D.; Clark, D. L.; Keogh, D. W.; Scott, B. L.; Watkin, J. G., *J. Am. Chem. Soc.* **2002,** *124* (24), 7007-7015.
159. Katkova, M. A.; Fukin, G. K.; Fagin, A. A.; Bochkarev, M. N., *J. Organomet. Chem.* **2003,** *682* (1-2), 218-223.
160. Evans, W. J.; Kozimor, S. A.; Ziller, J. W., *Chem. Commun.* **2005,** (37), 4681-4683.
161. Maria, L.; Santos, I. C.; Sousa, V. R.; Marcalo, J., *Inorg. Chem.* **2015,** *54* (18), 9115-9126.
162. Pan, C. L.; Chen, W.; Song, J. F., *Organometallics* **2011,** *30* (8), 2252-2260.
163. Adam, W.; Bargon, R. M., *Chem. Rev.* **2004,** *104* (1), 251-261.
164. Donahue, J. P., *Chem. Rev.* **2006,** *106* (11), 4747-4783.
165. Ephritikhine, M., *Coord. Chem. Rev.* **2016,** *319*, 35-62.
166. Hayton, T. W., *Chem. Commun.* **2013,** *49* (29), 2956-2973.
167. King, D. M.; Tuna, F.; McInnes, E. J. L.; McMaster, J.; Lewis, W.; Blake, A. J.; Liddle, S. T., *Science* **2012,** *337* (6095), 717-720.
168. Fortier, S.; Wu, G.; Hayton, T. W., *J. Am. Chem. Soc.* **2010,** *132* (20), 6888-6889.
169. Arney, D. S.; Burns, C. J., *J. Am. Chem. Soc.* **1993,** *115*, 9840-9841.
170. Arney, D. S. J.; Burns, C. J., *J. Am. Chem. Soc.* **1995,** *117* (37), 9448-9460.
171. Zi, G. F.; Jia, L.; Werkema, E. L.; Walter, M. D.; Gottfriedsen, J. P.; Andersen, R. A., *Organometallics* **2005,** *24* (17), 4251-4264.
172. Kraft, S. J.; Walensky, J.; Fanwick, P. E.; Hall, M. B.; Bart, S. C., *Inorg. Chem.* **2010,** *49* (17), 7620-7622.
173. Fortier, S.; Brown, J. L.; Kaltsoyannis, N.; Wu, G.; Hayton, T. W., *Inorg. Chem.* **2012,** *51* (3), 1625-1633.
174. Bart, S. C.; Anthon, C.; Heinemann, F. W.; Bill, E.; Edelstein, N. M.; Meyer, K., *J. Am. Chem. Soc.* **2008,** *130* (37), 12536-12546.
175. Kosog, B.; La Pierre, H. S.; Heinemann, F. W.; Liddle, S. T.; Meyer, K., *J. Am. Chem. Soc.* **2012,** *134* (11), 5284-5289.
176. Schmidt, A.-C.; Heinemann, F. W.; Lukens, W. W., Jr.; Meyer, K., *J. Am. Chem. Soc.* **2014,** *136* (34), 11980-11993.
177. Brown, J. L.; Fortier, S.; Lewis, R. A.; Wu, G.; Hayton, T. W., *J. Am. Chem. Soc.* **2012,** *134* (37), 15468-15475.
178. Brown, J. L.; Fortier, S.; Wu, G.; Kaltsoyannis, N.; Hayton, T. W., *J. Am. Chem. Soc.* **2013,** *135* (14), 5352-5355.
179. Smiles, D. E.; Wu, G.; Hayton, T. W., *J. Am. Chem. Soc.* **2014,** *136* (1), 96-99.
180. Dam, H. H.; Reinhoudt, D. N.; Verboom, W., *Chem. Soc. Rev.* **2007,** *36* (2), 367-377.
181. Ingram, K. I. M.; Kaltsoyannis, N.; Gaunt, A. J.; Neu, M. P., *J. Alloys Compd.* **2007,** *444*, 369-375.
182. Jones, M. B.; Gaunt, A. J.; Gordon, J. C.; Kaltsoyannis, N.; Neu, M. P.; Scott, B. L., *Chem. Sci.* **2013,** *4* (3), 1189-1203.
183. Pereira, C. C. L.; Marsden, C. J.; Marcalo, J.; Gibson, J. K., *PCCP* **2011,** *13* (28), 12940-12958.

184. Wang, X. F.; Andrews, L.; Thanthiriwatte, K. S.; Dixon, D. A., *Inorg. Chem.* **2013,** *52* (18), 10275-10285.
185. Lam, O. P.; Heinemann, F. W.; Meyer, K., *Chem. Sci.* **2011,** *2* (8), 1538-1547.
186. Camp, C.; Antunes, M. A.; Garcia, G.; Ciofini, I.; Santos, I. C.; Pecaut, J.; Almeida, M.; Marcalo, J.; Mazzanti, M., *Chem. Sci.* **2014,** *5* (2), 841-846.
187. Brown, J. L.; Wu, G.; Hayton, T. W., *Organometallics* **2013,** *32* (5), 1193-1198.
188. Smiles, D. E.; Wu, G.; Hayton, T. W., *New J. Chem.* **2015,** *39* (10), 7563-7566.
189. Brennan, J. G.; Andersen, R. A.; Zalkin, A., *Inorg. Chem.* **1986,** *25* (11), 1761-1765.
190. Spencer, L. P.; Yang, P.; Scott, B. L.; Batista, E. R.; Boncella, J. M., *Inorg. Chem.* **2009,** *48* (6), 2693-2700.
191. Matson, E. M.; Goshert, M. D.; Kiernicki, J. J.; Newell, B. S.; Fanwick, P. E.; Shores, M. P.; Walensky, J. R.; Bart, S. C., *Chem. Eur. J.* **2013,** *19* (48), 16176-16180.
192. Ventelon, L.; Lescop, C.; Arliguie, T.; Leverd, P. C.; Lance, M.; Nierlich, M.; Ephritikhine, M., *Chem. Commun.* **1999,** (7), 659-660.
193. Solari, E.; Maltese, C.; Franceschi, F.; Floriani, C.; ChiesiVilla, A.; Rizzoli, C., *J. Chem. Soc., Dalton Trans.* **1997,** (17), 2903-2910.
194. Jones, M. B.; Gaunt, A. J., *Chem. Rev.* **2013,** *113* (2), 1137-1198.
195. Sessler, J. L.; Melfi, P. J.; Pantos, G. D., *Coord. Chem. Rev.* **2006,** *250* (7-8), 816-843.
196. Arnold, P. L.; Potter, N. A.; Magnani, N.; Apostolidis, C.; Griveau, J. C.; Colineau, E.; Morgenstern, A.; Caciuffo, R.; Love, J. B., *Inorg. Chem.* **2010,** *49* (12), 5341-5343.
197. Arnold, P. L.; Stevens, C. J.; Farnaby, J. H.; Gardiner, M. G.; Nichol, G. S.; Love, J. B., *J. Am. Chem. Soc.* **2014,** *136* (29), 10218-10221.
198. Li, B. Y.; Yao, Y. M.; Wang, Y. R.; Zhang, Y.; Shen, Q., *Inorg. Chem. Commun.* **2008,** *11* (3), 349-352.
199. Han, F. B.; Li, B. Y.; Zhang, Y.; Wang, Y. R.; Shen, Q., *Organometallics* **2010,** *29* (15), 3467-3470.
200. Han, F. B.; Teng, Q. Q.; Zhang, Y.; Wang, Y. R.; Shen, Q., *Inorg. Chem.* **2011,** *50* (6), 2634-2643.
201. Guidal, V. *Conception et réactivité de nouveaux complexes de lanthanides et de cobalt contenant des ligands rédox-actifs; application aux réductions multi-électroniques*. Université de Grenoble, France, **2014**.
202. Salmon, L.; Thuery, P.; Ephritikhine, M., *Dalton Trans.* **2004,** (24), 4139-4145.
203. Salmon, L.; Thuery, P.; Ephritikhine, M., *Dalton Trans.* **2004,** (10), 1635-1643.
204. Baldridge, K. K.; Kasahara, Y.; Ogawa, K.; Siegel, J. S.; Tanaka, K.; Toda, F., *J. Am. Chem. Soc.* **1998,** *120* (24), 6167-6168.
205. Fokin, A. A.; Chernish, L. V.; Gunchenko, P. A.; Tikhonchuk, E. Y.; Hausmann, H.; Serafin, M.; Dahl, J. E. P.; Carlson, R. M. K.; Schreiner, P. R., *J. Am. Chem. Soc.* **2012,** *134* (33), 13641-13650.
206. Allouche, L.; Marquis, A.; Lehn, J.-M., *Chem. Eur. J.* **2006,** (12), 7520-7525.
207. Morris, D. E.; Da Re, R. E.; Jantunen, K. C.; Castro-Rodriguez, I.; Kiplinger, J. L., *Organometallics* **2004,** *23* (22), 5142-5153.
208. Cladis, D. P.; Kiernicki, J. J.; Fanwick, P. E.; Bart, S. C., *Chem. Commun.* **2013,** *49* (39), 4169-4171.
209. Anderson, N. H.; Odoh, S. O.; Yao, Y.; Williams, U. J.; Schaefer, B. A.; Kiernicki, J. J.; Lewis, A. J.; Goshert, M. D.; Fanwick, P. E.; Schelter, E. J.; Walensky, J. R.; Gagliardi, L.; Bart, S. C., *Nature chemistry* **2014,** *6* (10), 919-926.
210. Camp, C. *Conception et réactivité de complexes mono- et polymétalliques d'éléments f en bas degré d'oxydation*. Université de Grenoble, France, **2013**.
211. Fachinetti, G.; Floriani, C.; Zanazzi, P. F., *J. Am. Chem. Soc.* **1978,** *100* (23), 7405-7407.

212. Patel, D.; Moro, F.; McMaster, J.; Lewis, W.; Blake, A. J.; Liddle, S. T., *Angew. Chem. Int. Ed.* **2011,** *50* (44), 10388-10392.
213. Ward, A. L.; Lukens, W. W.; Lu, C. C.; Arnold, J., *J. Am. Chem. Soc.* **2014,** *136* (9), 3647-3654.
214. Napoline, J. W.; Kraft, S. J.; Matson, E. M.; Fanwick, P. E.; Bart, S. C.; Thomas, C. M., *Inorg. Chem.* **2013,** *52* (20), 12170-12177.
215. Le Borgne, T.; Riviere, E.; Marrot, J.; Thuery, P.; Girerd, J. J.; Ephritikhine, M., *Chem. Eur. J.* **2002,** *8* (4), 774-783.
216. Paine, R. T.; Duesler, E. N.; Moody, D. C., *Organometallics* **1982,** *1* (8), 1097-1098.
217. Kozimor, S. A.; Bartlett, B. M.; Rinehart, J. D.; Long, J. R., *J. Am. Chem. Soc.* **2007,** *129* (35), 10672-10673.
218. Salmon, L.; Thuery, P.; Riviere, E.; Girerd, J. J.; Ephritikhine, M., *Dalton Trans.* **2003,** (14), 2872-2880.
219. Salmon, L.; Thuery, P.; Ephritikhine, M., *Polyhedron* **2007,** *26* (3), 645-652.
220. Blake, M. P.; Katsoyannis, N.; Mountford, P., *J. Am. Chem. Soc.* **2015,** *137* (38), 12352-12368.
221. Costes, J. P.; Vendier, L.; Wernsdorfer, W., *Dalton Trans.* **2011,** *40* (8), 1700-1706.
222. DeAngelis, S.; Solari, E.; Gallo, E.; Floriani, C.; ChiesiVilla, A.; Rizzoli, C., *Inorg. Chem.* **1996,** *35* (21), 5995-6003.
223. Fachinetti, G.; Floriani, C.; Zanazzi, P. F.; Zanzari, A. R., *Inorg. Chem.* **1979,** *18* (12), 3469-3475.
224. Nocton, G.; Lukens, W. W.; Booth, C. H.; Rozenel, S. S.; Medling, S. A.; Maron, L.; Andersen, R. A., *J. Am. Chem. Soc.* **2014,** *136* (24), 8626-8641.
225. Dugan, T. R.; Bill, E.; MacLeod, K. C.; Christian, G. J.; Cowley, R. E.; Brennessel, W. W.; Ye, S.; Neese, F.; Holland, P. L., *J. Am. Chem. Soc.* **2012,** *134* (50), 20352-20364.
226. Neumann, W. P.; Uzick, W.; Zarkadis, A. K., *J. Am. Chem. Soc.* **1986,** *108* (13), 3762-3770.
227. Isse, A. A.; Gennaro, A.; Vianello, E.; Floriani, C., *J. Mol. Catal.* **1991,** *70* (2), 197-208.
228. Isse, A. A.; Gennaro, A.; Vianello, E., *J. Chem. Soc., Dalton Trans.* **1993,** (14), 2091-2096.
229. Ciurli, S.; Gambarotta, S.; Floriani, C.; Chiesivilla, A.; Guastini, C., *Angew. Chem. Int. Ed.* **1986,** *25* (6), 553-554.
230. Williams, O. M.; Cowley, A. H.; Rose, M. J., *Dalton Trans.* **2015,** *44* (29), 13017-13029.
231. Bowman, A. C.; Milsmann, C.; Atienza, C. C. H.; Lobkovsky, E.; Wieghardt, K.; Chirik, P. J., *J. Am. Chem. Soc.* **2010,** *132* (5), 1676-1684.
232. Carmen, C.; Atienza, H.; Milsmann, C.; Semproni, S. P.; Turner, Z. R.; Chirik, P. J., *Inorg. Chem.* **2013,** *52* (9), 5403-5417.
233. Stueber, D.; Patterson, D.; Mayne, C. L.; Orendt, A. M.; Grant, D. M.; Parry, R. W., *Inorg. Chem.* **2001,** *40* (8), 1902-1911.
234. Housecroft, C. E.; Sharpe, A. G., Organometallic compounds of d-block elements. In *Inorganic Chemistry*, Pearson Education Limited: Essex, 2005.
235. Gervasio, G.; Sappa, E.; Secco, A., *J. Organomet. Chem.* **2014,** *751*, 111-152.
236. Bressan, M.; Corain, B.; Rigo, P.; Turco, A., *Inorg. Chem.* **1970,** *9* (7), 1733-&.
237. Ghilardi, C. A.; Midollini, S.; Sacconi, L., *J. Organomet. Chem.* **1980,** *186* (2), 279-287.
238. Wolczanski, P. T., *Polyhedron* **1995,** *14* (22), 3335-3362.
239. Choi, K. M.; Yokoi, T.; Tatsumi, T.; Kuroda, K., *J. Mater. Chem. A* **2013,** *1* (7), 2485-2494.
240. Kriesel, J. W.; Sander, M. S.; Tilley, T. D., *Adv. Mater.* **2001,** *13* (5), 331-335.

241. Brutchey, R. L.; Mork, B. V.; Sirbuly, D. J.; Yang, P. D.; Tilley, T. D., *J. Mol. Catal. Chem.* **2005,** *238* (1-2), 1-12.
242. Conley, M. P.; Delley, M. F.; Siddiqi, G.; Lapadula, G.; Norsic, S.; Monteil, V.; Safonova, O. V.; Coperet, C., *Angew. Chem. Int. Ed.* **2014,** *53* (7), 1872-1876.
243. Jarupatrakorn, J.; Tilley, J. D., *J. Am. Chem. Soc.* **2002,** *124* (28), 8380-8388.
244. Bindl, M.; Stade, R.; Heilmann, E. K.; Picot, A.; Goddard, R.; Furstner, A., *J. Am. Chem. Soc.* **2009,** *131* (27), 9468-9470.
245. Lysenko, S.; Volbeda, J.; Jones, P. G.; Tamm, M., *Angew. Chem. Int. Ed.* **2012,** *51* (27), 6757-6761.
246. Clark, D. L.; Sattelberger, A. P.; Vandersluys, W. G.; Watkin, J. G., *J. Alloys Compd.* **1992,** *180*, 303-315.
247. Bianchini, C.; Mealli, C.; Meli, A.; Sabat, M., *Inorg. Chem.* **1984,** *23* (25), 4125-4127.
248. Lund, H.; Hoyer, E.; Hazell, R. G., *Acta Chem. Scand. B* **1982,** *36* (3), 207-209.
249. Bacher, A. D.; Sens, I.; Muller, U., *Z. Naturforsch. B: Chem. Sci.* **1992,** *47* (5), 702-705.
250. Camp, C.; Pecaut, J.; Mazzanti, M., *J. Am. Chem. Soc.* **2013,** *135* (32), 12101-12111.
251. Camp, C.; Mougel, V.; Pecaut, J.; Maron, L.; Mazzanti, M., *Chem. Eur. J.* **2013,** *19* (51), 17528-17540.
252. Li, B.; Tan, X.; Xu, S. S.; Song, H. B.; Wang, B. Q., *J. Organomet. Chem.* **2008,** *693* (4), 667-674.
253. Mace, W. J.; Main, L.; Nicholson, B. K.; Hagyard, M., *J. Organomet. Chem.* **2002,** *664* (1-2), 288-293.
254. Olk, R. M.; Dietzsch, W.; Kohler, K.; Kirmse, R.; Reinhold, J.; Hoyer, E.; Golic, L.; Olk, B., *Z. Anorg. Allg. Chem.* **1988,** *567* (12), 131-144.
255. Breitzer, J. G.; Chou, J. H.; Rauchfuss, T. B., *Inorg. Chem.* **1998,** *37* (8), 2080-+.
256. Brennan, J. G.; Andersen, R. A.; Zalkin, A., *Inorg. Chem.* **1986,** *25*, 1761-1765.
257. Rosenzweig, M. W.; Scheurer, A.; Lamsfus, C. A.; Heinemann, F. W.; Maron, L.; Andrez, J.; Mazzanti, M.; Meyer, K., *Chem. Sci.* **2016,** *7* (9), 5857-5866.
258. Franke, S. M.; Rosenzweig, M. W.; Heinemann, F. W.; Meyer, K., *Chem. Sci.* **2015,** *6* (1), 275-282.
259. Bugaris, D. E.; Ibers, J. A., *Inorg. Chem.* **2012,** *51* (1), 661-666.
260. Smiles, D. E.; Wu, G.; Hayton, T. W., *Inorg. Chem.* **2014,** *53* (24), 12683-12685.
261. Ward, M. D.; Pozzi, E. A.; Lee, M.; Van Duyne, R. P.; Choi, E. S.; Ibers, J. A., *Inorg. Chem.* **2015,** *54* (6), 3055-3060.
262. Camp, C.; Kefalidis, C. E.; Pecaut, J.; Maron, L.; Mazzanti, M., *Angew. Chem. Int. Ed.* **2013,** *52* (48), 12646-12650.
263. Gardner, B. M.; Balazs, G.; Scheer, M.; Tuna, F.; McInnes, E. J. L.; McMaster, J.; Lewis, W.; Blake, A. J.; Liddle, S. T., *Angew. Chem. Int. Ed.* **2014,** *53* (17), 4484-4488.
264. Franke, S. M.; Heinemann, F. W.; Meyer, K., *Chem. Sci.* **2014,** *5* (3), 942-950.
265. Gombler, W., *Z. Naturforsch. B: Chem. Sci.* **1981,** *36* (12), 1561-1565.
266. Smith, S. J.; Whaley, C. M.; Rauchfuss, T. B.; Wilson, S. R., *Inorg. Chem.* **2006,** *45* (2), 679-687.
267. Kuwata, S.; Hidai, M., *Coord. Chem. Rev.* **2001,** *213*, 211-305.
268. Smiles, D. E.; Wu, G.; Hrobarik, P.; Hayton, T. W., *J. Am. Chem. Soc.* **2016,** *138*, 814-825.
269. Robinson, J. R.; Carroll, P. J.; Walsh, P. J.; Schelter, E. J., *Angew. Chem. Int. Ed.* **2012,** *51* (40), 10159-10163.
270. Robinson, J. R.; Gordon, Z.; Booth, C. H.; Carroll, P. J.; Walsh, P. J.; Schelter, E. J., *J. Am. Chem. Soc.* **2013,** *135* (50), 19016-19024.
271. Levin, J. R.; Dorfner, W. L.; Carroll, P. J.; Schelter, E. J., *Chem. Sci.* **2015,** *6* (12), 6925-6934.

272. Lukens, W. W.; Beshouri, S. M.; Blosch, L. L.; Andersen, R. A., *J. Am. Chem. Soc.* **1996,** *118* (4), 901-902.
273. Halter, D. P.; Heinemann, F. W.; Bachmann, J.; Meyer, K., *Nature* **2016,** *530* (7590), 317-321.
274. Karmazin, L.; Mazzanti, M.; Pecaut, J., *Inorg. Chem.* **2003,** *42* (19), 5900-5908.
275. Franke, S. M.; Tran, B. L.; Heinemann, F. W.; Hieringer, W.; Mindiola, D. J.; Meyer, K., *Inorg. Chem.* **2013,** *52* (18), 10552-10558.
276. Tskhovrebov, A. G.; Solari, E.; Wodrich, M. D.; Scopelliti, R.; Severin, K., *Angew. Chem. Int. Ed.* **2012,** *51* (1), 232-234.
277. Tskhovrebov, A. G.; Solari, E.; Wodrich, M. D.; Scopelliti, R.; Severin, K., *J. Am. Chem. Soc.* **2012,** *134* (3), 1471-1473.
278. Tskhovrebov, A. G.; Solari, E.; Scopelliti, R.; Severin, K., *Inorg. Chem.* **2013,** *52* (20), 11688-11690.
279. Tslchovrebov, A. G.; Vuichoud, B.; Solari, E.; Scopelliti, R.; Severin, K., *J. Am. Chem. Soc.* **2013,** *135* (25), 9486-9492.
280. Fortier, S.; Hayton, T. W., *Coord. Chem. Rev.* **2010,** *254* (3-4), 197-214.
281. Evans, W. J.; Lee, D. S.; Ziller, J. W., *J. Am. Chem. Soc.* **2004,** *126* (2), 454-455.
282. Krempner, C.; McNerney, B., Rare Earth Siloxides. In *The Rare Earth Elements Fundamentals and Applications*, Atwood, D. A., Ed. John Wiley & Sons: West Sussex, 2012.
283. McGeary, M. J.; Coan, P. S.; Folting, K.; Streib, W. E.; Caulton, K. G., *Inorg. Chem.* **1991,** *30* (8), 1723-1735.
284. Mansfeld, D.; Mehring, M., *Z. Anorg. Allg. Chem.* **2005,** *631* (12), 2429-2432.
285. Boyle, T. J.; Bunge, S. D.; Clem, P. G.; Richardson, J.; Dawley, J. T.; Ottley, L. A. M.; Rodriguez, M. A.; Tuttle, B. A.; Avilucea, G. R.; Tissot, R. G., *Inorg. Chem.* **2005,** *44* (5), 1588-1600.
286. Shao, P. C.; Berg, D. J.; Bushnell, G. W., *Inorg. Chem.* **1994,** *33* (16), 3452-3458.
287. Lorenz, V.; Giessmann, S.; Gun'ko, Y. K.; Fischer, A. K.; Gilje, J. W.; Edelmann, F. T., *Angew. Chem. Int. Ed.* **2004,** *43* (35), 4603-4606.
288. Lapadula, G.; Conley, M. P.; Coperet, C.; Andersen, R. A., *Organometallics* **2015,** *34* (11), 2271-2277.
289. Fischbach, A.; Klimpel, M. G.; Widenmeyer, M.; Herdtweck, E.; Scherer, W.; Anwander, R., *Angew. Chem. Int. Ed.* **2004,** *43* (17), 2234-2239.
290. Zimmermann, M.; Froystein, N. A.; Fischbach, A.; Sirsch, P.; Dietrich, H. M.; Tornroos, K. W.; Herdtweck, E.; Anwander, R., *Chem. Eur. J.* **2007,** *13* (31), 8784-8800.
291. Le Roux, E.; Liang, Y. C.; Tornroos, K. W.; Nief, F.; Anwander, R., *Organometallics* **2012,** *31* (18), 6526-6537.
292. Lapadula, G.; Bourdolle, A.; Allouche, F.; Conley, M. P.; del Rosal, I.; Maron, L.; Lukens, W. W.; Guyot, Y.; Andraud, C.; Brasselet, S.; Coperet, C.; Maury, O.; Andersen, R. A., *Chem. Mater.* **2014,** *26* (2), 1062-1073.
293. Le Roux, E.; Michel, O.; Sommerfeldt, H. M.; Liang, Y. C.; Maichle-Mossmer, C.; Tornroos, K. W.; Anwander, R., *Dalton Trans.* **2010,** *39* (36), 8552-8559.
294. Boyle, T. J.; Ottley, L. A. M., *Chem. Rev.* **2008,** *108* (6), 1896-1917.
295. Prasad, E.; Knettle, B. W.; Flowers, R. A., *J. Am. Chem. Soc.* **2002,** *124* (49), 14663-14667.
296. Shabangi, M.; Flowers, R. A., *Tetrahedron Lett.* **1997,** *38* (7), 1137-1140.
297. Allmann, R., *The Chemistry of Hydrazo, Azo. and Azoxy Groups*. Wiley: New York, 1975.
298. Buser, U.; Ess, C. H.; Gerson, F., *Magn. Reson. Chem.* **1991,** *29* (7), 721-725.

299. Labouille, S.; Nief, F.; Maron, L., *J. Phys. Chem. A* **2011,** *115* (29), 8295-8301.
300. Kempe, R., *Angew. Chem. Int. Ed.* **2000,** *39* (3), 468-493.
301. Piers, W. E.; Emslie, D. J. H., *Coord. Chem. Rev.* **2002,** *233*, 131-155.
302. Wichmann, O.; Sillanpaa, R.; Lehtonen, A., *Coord. Chem. Rev.* **2012,** *256* (3-4), 371-392.
303. Natrajan, L.; Pécaut, J.; Mazzanti, M.; LeBrun, C., *Inorg. Chem.* **2005,** *44*, 4756-4765.
304. Benndorf, P.; Schmitt, S.; Koeppe, R.; Ona-Burgos, P.; Scheurer, A.; Meyer, K.; Roesky, P. W., *Angew. Chem. Int. Ed.* **2012,** *51* (20), 5006-5010.
305. Bonnet, F.; Cowley, A. R.; Mountford, P., *Inorg. Chem.* **2005,** *44* (24), 9046-9055.
306. Amgoune, A.; Thomas, C. M.; Roisnel, T.; Carpentier, J. F., *Chem. Eur. J.* **2006,** *12* (1), 169-179.
307. Du, Z.; Zhang, Y.; Yao, Y.; Shen, Q., *Dalton Trans.* **2011,** *40* (29), 7639-7644.
308. Hou, Z. M.; Wakatsuki, Y., *Coord. Chem. Rev.* **2002,** *231* (1-2), 1-22.
309. Delbridge, E. E.; Dugah, D. T.; Nelson, C. R.; Skelton, B. W.; White, A. H., *Dalton Trans.* **2007,** (1), 143-153.
310. Zhou, H.; Guo, H.; Yao, Y.; Zhou, L.; Sun, H.; Sheng, H.; Zhang, Y.; Shen, Q., *Inorg. Chem.* **2007,** *46* (3), 958-964.
311. Yang, S.; Du, Z.; Zhang, Y.; Shen, Q., *Chem. Commun.* **2012,** *48* (78), 9780-9782.
312. Wietzke, R.; Mazzanti, M.; Latour, J. M.; Pecaut, J.; Cordier, P. Y.; Madic, C., *Inorg. Chem.* **1998,** *37* (26), 6690-6697.
313. Bozoklu, G. *Luminescent Lanthanide-Based Molecular and Supramolecular Architectures*. Université de Grenoble, France, **2011**.
314. Jaroschik, F.; Nief, F.; Le Goff, X.-F.; Ricard, L., *Organometallics* **2007,** *26* (14), 3552-3558.
315. Bochkarev, M. N.; Khoroshenkov, G. V.; Schumann, H.; Dechert, S., *J. Am. Chem. Soc.* **2003,** *125* (10), 2894-2895.
316. Wietzke, R.; Mazzanti, M.; Latour, J. M.; Pecaut, J., *Chem. Commun.* **1999,** (2), 209-210.
317. Caravan, P.; Hedlund, T.; Liu, S.; Sjöberg, S.; Orvig, C., *J. Am. Chem. Soc.* **1995,** *117*, 11230-11238.
318. Sinenkov, M. A.; Fukin, G. K.; Cherkasov, A. V.; Ajellal, N.; Roisnel, T.; Kerton, F. M.; Carpentier, J.-F.; Trifonov, A. A., *New J. Chem.* **2011,** *35* (1), 204-212.
319. Selinsky, R. S.; Han, J. H.; Perez, E. A. M.; Guzei, I. A.; Jin, S., *J. Am. Chem. Soc.* **2010,** *132* (45), 15997-16005.
320. Ren, W.; Song, H.; Zi, G.; Walter, M. D., *Dalton Trans.* **2012,** *41* (19), 5965-5973.
321. Ren, W. S.; Zi, G. F.; Fang, D. C.; Walter, M. D., *J. Am. Chem. Soc.* **2011,** *133* (33), 13183-13196.
322. Andrez, J.; Pecaut, J.; Bayle, P.-A.; Mazzanti, M., *Angew. Chem. Int. Ed.* **2014,** *53* (39), 10448-10452.
323. Deacon, G. B.; Tuong, T. D.; Wilkinson, D. L., Lanthanide and actinide complexes. In *Inorganic Syntheses*, sons, J. W., Ed. 1990; Vol. 27.
324. Bryan, A. M.; Long, G. J.; Grandjean, F.; Power, P. P., *Inorg. Chem.* **2013,** *52* (20), 12152-12160.
325. Kiplinger, J. L.; Morris, D. E.; Scott, B. L.; Burns, C. J., *Organometallics* **2002,** *21* (26), 5978-5982.
326. Wu, D. H.; Chen, A. D.; Johnson, C. S., *J. Magn. Reson., Ser. A* **1995,** *115* (2), 260-264.
327. Waldeck, A. R.; Kuckel, P. W.; Lennon, A. J.; Chapman, B. E., *Prog. Nucl. Magn. Reson. Spectrosc.* **1997,** *30*, 39-68.

328. CrysAlisPro CCD, C. R., ABSPACK, CrysAlis PRO. Agilent Technologies, Agilent Yarnton, England, **2010**.
329. Duisenberg, A. J. M.; Kroon-Batenburg, L. M. J.; Schreurs, A. M. M., *J. Appl. Crystallogr.* **2003,** *36*, 220-229.
330. Blessing, R. H., *Acta Crystallogr., Sect. A* **1995,** *51*, 33-38.
331. Sheldrick, G. M., *Acta Crystallogr., Sect. A* **2008,** *64*, 112-122.
332. Palatinus, L.; Chapuis, G., *J. Appl. Crystallogr.* **2007,** *40*, 786-790.
333. PLATON; Spek, A. L., *Acta Crystallogr., Sect. D* **2009,** *65*, 148-155.
334. Chen, H. Y.; Cronin, J. A.; Archer, R. D., *Inorg. Chem.* **1995,** *34* (9), 2306-2315.
335. Cameron, P. A.; Gibson, V. C.; Redshaw, C.; Segal, J. A.; White, A. J. P.; Williams, D. J., *J. Chem. Soc., Dalton Trans.* **2002,** (3), 415-422.
336. Takano, K.; Takahashi, M.; Fukushima, T.; Takezaki, M.; Tominaga, T.; Akashi, H.; Takagi, H.; Shibahara, T., *Bull. Chem. Soc. Jpn.* **2012,** *85* (11), 1210-1221.
337. Mazzanti, M.; Gambarotta, S.; Floriani, C.; Chiesivilla, A.; Guastini, C., *Inorg. Chem.* **1986,** *25* (14), 2308-2314.
338. Zheng, S.; Berto, T. C.; Dahl, E. W.; Hoffman, M. B.; Speelman, A. L.; Lehnert, N., *J. Am. Chem. Soc.* **2013,** *135* (13), 4902-4905.
339. Thapper, A.; Behrens, A.; Fryxelius, J.; Johansson, M. H.; Prestopino, F.; Czaun, M.; Rehder, D.; Nordlander, E., *Dalton Trans.* **2005,** (21), 3566-3571.
340. Toupance, T.; Dubberley, S. R.; Rees, N. H.; Tyrrell, B. R.; Mountford, P., *Organometallics* **2002,** *21* (7), 1367-1382.
341. Tong, Y. L.; Yan, Y.; Chan, E. S. H.; Yang, Q. C.; Mak, T. C. W.; Ng, D. K. P., *J. Chem. Soc. Dalton Trans.* **1998,** (18), 3057-3064.
342. Chomitz, W. A.; Minasian, S. G.; Sutton, A. D.; Arnold, J., *Inorg. Chem.* **2007,** *46* (17), 7199-7209.

# Appendix

## X-Ray structural informations

**Table A1: X-ray crystallographic data**

| **Compound** | **1-Cl.(py)** | **2.$(tol)_2$** | **3.$(py)_{4.5}$** | **4** |
|---|---|---|---|---|
| **Formula** | $C_{47}H_{35}N_5O_2Cl_2U$ | $C_{98}H_{76}N_8O_4U_2$ | $C_{78.5}H_{60.5}N_{8.5}O_4U$ | $C_{84}H_{60}N_8O_8U$ |
| **Crystal size [mm]** | 0.28x0.22x0.15 | 0.32x0.19x0.02 | 0.25x0.10x0.02 | 0.27x0.14x0.03 |
| **Crystal system** | Triclinic | Triclinic | Monoclinic | Monoclinic |
| **Space group** | P -1 | P -1 | C 2/c | P $2_1$/c |
| **V [Å$^3$]** | 1977.10(13) | 1897.75(15) | 12586.6(13) | 3319.99(15) |
| **a [Å]** | 10.0338(4) | 11.1583(6) | 45.625(2) | 16.2723(5) |
| **b [Å]** | 12.7361(5) | 13.4999(7) | 15.8387(9) | 11.8342(3) |
| **c [Å]** | 16.6880(7) | 13.5383(5) | 18.5959(13) | 18.1568(5) |
| **α [°]** | 101.098(3) | 97.421(3) | 90 | 90 |
| **β [°]** | 101.394(3) | 107.177(4) | 110.506(5) | 108.281(3) |
| **γ [°]** | 102.627(3) | 98.029(4) | 90 | 90 |
| **Z** | 2 | 1 | 8 | 2 |
| **Absorption coefficient [mm$^{-1}$]** | 4.287 | 4.324 | 2.640 | 4.941 |
| **T [K]** | 150(2) | 150(2) | 150(2) | 150(2) |
| **Total no. reflexions** | 41283 | 14739 | 31319 | 39686 |
| **Unique reflexions [R(int)]** | 12067 [0.0592] | 7739 [0.0961] | 9013 [0.1193] | 10126 [0.0740] |
| **Final R indice [I>2σ(I)]** | 0.0511 | 0.0780 | 0.0623 | 0.0450 |
| **Largest diff. peak and hole [eA$^{-3}$]** | 5.549 and -2.664 | 2.983 and -1.895 | 2.465 and -1.712 | 1.340 and -1.248 |
| **GOF** | 1.155 | 0.939 | 1.063 | 1.012 |

**Table A2: X-ray crystallographic data (continued)**

| **Compound** | **5-THF.(THF)$_{1.5}$** | **5-Py** | **6-THF.(THF)$_{1.5}$** | **7-THF** |
|---|---|---|---|---|
| **Formula** | $C_{54}H_{56}CoN_4O_{7.5}U$ | $C_{50}H_{38}CoN_6O_4U$ | $C_{54}H_{56}N_4NiO_{7.5}U$ | $C_{44}H_{36}CoN_4NdO_5$ |
| **Crystal size [mm]** | 0.42x0.37x0.27 | 0.38x0.22x0.09 | 0.17x0.10x0.08 | 0.26x0.08x0.02 |
| **Crystal system** | Monoclinic | Monoclinic | Monoclinic | Orthorhombic |
| **Space group** | C 2/c | C 2/c | C 2/c | P nma |
| **V [Å$^3$]** | 9138(5) | 8466.5(3) | 9151.8(4) | 3568.9(4) |
| **a [Å]** | 26.2903(17) | 26.5567(6) | 26.2314(8) | 24.759(2) |
| **b [Å]** | 12.927(7) | 11.9483(2) | 12.9229(3) | 19.8895(8) |
| **c [Å]** | 27.0396(12) | 26.6871(5) | 27.1920(7) | 7.2474(5) |
| **α [°]** | 90 | 90 | 90 | 90 |
| **β [°]** | 96.065(6) | 91.1024(16) | 96.858(3) | 90 |
| **γ [°]** | 90 | 90 | 90 | 90 |
| **Z** | 8 | 8 | 8 | 4 |
| **Absorption coefficient [mm$^{-1}$]** | 3.965 | 4.267 | 4.008 | 1.959 |
| **T [K]** | 150(2) | 150(2) | 150(2) | 150(2) |
| **Total no. reflexions** | 26327 | 25630 | 28607 | 10859 |
| **Unique reflexions [R(int)]** | 13941 [0.0474] | 12885 [0.0341] | 13862 [0.0485] | 3751 [0.0823] |
| **Final R indice [I>2σ(I)]** | 0.0581 | 0.0369 | 0.0467 | 0.0526 |
| **Largest diff. peak and hole [e.A$^{-3}$]** | 2.382 and -1.368 | 1.163 and -0.827 | 1.114 and -1.166 | 1.570 and -1.589 |
| **GOF** | 1.058 | 1.022 | 1.027 | 1.017 |

**Table A3: X-ray crystallographic data (continued)**

| **Compound** | **7-Py.(py)$_2$** | **8** | **9.hex** |
|---|---|---|---|
| **Formula** | $C_{100}H_{76}Co_2N_{12}Nd_2O_8$ | $C_{70}H_{58}Co_2Li_2N_{10}O_4$ | $C_{102}H_{130}Co_3N_6Na_6O_{18}$ |
| **Crystal size [mm]** | 0.35x0.16x0.04 | 0.23x0.16x0.031 | 0.453x0.299x0.054 |
| **Crystal system** | Monoclinic | Monoclinic | Monoclinic |
| **Space group** | P $2_1$/c | P $2_1$/n | C 2/c |
| **V [Å$^3$]** | 8393.6(12) | 2864.2(4) | 10271(3) |
| **a [Å]** | 18.1658(16) | 11.9653(8) | 18.508(3) |
| **b [Å]** | 11.8172(8) | 13.6748(9) | 29.695(5) |
| **c [Å]** | 39.203(4) | 17.7417(15) | 18.979(4) |
| **α [°]** | 90 | 90 | 90 |
| **β [°]** | 94.148(9) | 99.374(7) | 100.017(15) |
| **γ [°]** | 90 | 90 | 90 |
| **Z** | 4 | 2 | 4 |
| **Absorption coefficient [mm$^{-1}$]** | 1.673 | 0.642 | 0.572 |
| **T [K]** | 150(2) | 150(2) | 100(2) |
| **Total no. reflexions** | 53438 | 13162 | 56773 |
| **Unique reflexions [R(int)]** | 17129 [0.1719] | 5840 [0.0618] | 9452 [0.1401] |
| **Final R indice [I>2σ(I)]** | 0.0997 | 0.0714 | 0.0852 |
| **Largest diff. peak and hole [e.A$^{-3}$]** | 2.427 and -1.519 | 1.502 and -0.455 | 1.047 and -0.554 |
| **GOF** | 1.068 | 1.101 | 1.081 |

**Table A4: X-ray crystallographic data (continued)**

| **Compound** | **10** | **11.(THF)$_2$** | **[(K18c6)$_2$($C_2S_4$)].Py** |
|---|---|---|---|
| **Formula** | $C_{98}H_{144}Co_2N_{10}Na_4O_{26}$ | $C_{90}H_{124}Co_2N_8Na_4O_{26}$ | $C_{31}H_{53}K_2NO_{12}S_4$ |
| **Crystal size [mm]** | 0.025x0.045x0.288 | 0.168×0.062×0.041 | 1.07x0.13x0.02 |
| **Crystal system** | Monoclinic | Monoclinic | Monoclinic |
| **Space group** | P $2_1$/c | P $2_1$/c | C 2/c |
| **V [Å$^3$]** | 12982.7(15) | 9062.5(8) | 4109.4(7) |
| **a [Å]** | 22.2322(16) | 22.0036(13) | 23.321(3) |
| **b [Å]** | 12.7790(7) | 14.5281(6) | 10.1497(5) |
| **c [Å]** | 46.954(3) | 28.4397(14) | 21.907(3) |
| **α [°]** | 90 | 90 | 90 |
| **β [°]** | 103.289(7) | 94.568(5) | 127.579(19) |
| **γ [°]** | 90 | 90 | 90 |
| **Z** | 4 | 4 | 4 |
| **Absorption coefficient [mm$^{-1}$]** | 2.791 | 0.468 | 0.489 |
| **T [K]** | 140(2) | 140(2) | 150(2) |
| **Total no. reflexions** | 59483 | 104214 | 20966 |
| **Unique reflexions [R(int)]** | 13854 [0.1462] | 22915 [0.1984] | 5082 [0.0672] |
| **Final R indice [I>2σ(I)]** | 0.1172 | 0.0972 | 0.0611 |
| **Largest diff. peak and hole [e.A$^{-3}$]** | 0.897 and -0.787 | 0.802 and -0.606 | 0.967 and -0.471 |
| **GOF** | 1.033 | 1.021 | 1.034 |

**Table A5: X-ray crystallographic data (continued)**

| **Compound** | **12.(tol)$_4$** | **13.hex** | **[$K_2C_2S_4(DMSO)_3$]$_n$** |
|---|---|---|---|
| **Formula** | $C_{101}H_{188}K_2O_{28}S_3Si_4U$ | $C_{57}H_{122}K_2O_{16}S_5Si_4U$ | $C_8H_{18}K_2O_3S_7$ |
| **Crystal size [mm]** | 0.544x0.440x0.349 | 0.050x0.010x0.010 | 0.522x0.265x0.020 |
| **Crystal system** | Triclinic | Monoclinic | Triclinic |
| **Space group** | P -1 | P $2_1$/n | P-1 |
| **V [Å$^3$]** | 6545.9(5) | 8345(4) | 1008.95(6) |
| **a [Å]** | 14.8483(6) | 24.370(4) | 9.9182(3) |
| **b [Å]** | 17.9359(8) | 13.958(5) | 10.2993(4) |
| **c [Å]** | 25.5598(12) | 25.659(5) | 10.3745(4) |
| **α [°]** | 81.725(4) | 90 | 90.141(3) |
| **β [°]** | 85.150(3) | 107.035(16) | 107.571(3) |
| **γ [°]** | 76.692(4) | 90 | 92.782(3) |
| **Z** | 2 | 4 | 2 |
| **Absorption coefficient [mm$^{-1}$]** | 1.449 | 2.279 | 1.194 |
| **T [K]** | 150(2) | 150(2) | 150(2) |
| **Total no. reflexions** | 59744 | 22393 | 12179 |
| **Unique reflexions [R(int)]** | 26722 [0.0880] | 8691 [0.3291] | 6084 [0.0408] |
| **Final R indice [I>2σ(I)]** | 0.0919 | 0.1173 | 0.0472 |
| **Largest diff. peak and hole [e.A$^{-3}$]** | 3.509 and -1.881 | 1.414 and -0.693 | 0.459 and -0.400 |
| **GOF** | 1.070 | 0.973 | 1.023 |

**Table A6: X-ray crystallographic data (continued)**

| **Compound** | **14.tol** | **15.tol** | **16.tol** |
|---|---|---|---|
| **Formula** | $C_{55}H_{116}K_2O_{16}S_2Si_4U$ | $C_{79}H_{170}K_2O_{24}S_{4.36}Si_4U_2$ | $C_{103}H_{224}K_4O_{32}S_2Si_4U_2$ |
| **Crystal size [mm]** | 0.288x0.171x0.018 | 0.230x0.230x0.180 | 0.80x0.70x0.60 |
| **Crystal system** | Orthorombic | Monoclinic | Triclinic |
| **Space group** | P bca | P $2_1$/n | P -1 |
| **V [Å$^3$]** | 15151.7(6) | 5644.5(6) | 3592.8(3) |
| **a [Å]** | 19.2882(5) | 14.1455(8) | 13.2622(7) |
| **b [Å]** | 19.3780(5) | 18.0590(13) | 15.3715(6) |
| **c [Å]** | 40.5378(9) | 22.1126(12) | 20.3762(10) |
| **α [°]** | 90 | 90 | 76.530(4) |
| **β [°]** | 90 | 92.218(5) | 74.270(4) |
| **γ [°]** | 90 | 90 | 65.093(4) |
| **Z** | 8 | 2 | 1 |
| **Absorption coefficient [mm$^{-1}$]** | 2.425 | 3.142 | 2.525 |
| **T [K]** | 150(2) | 150(2) | 150(2) |
| **Total no. reflexions** | 89393 | 34303 | 43383 |
| **Unique reflexions [R(int)]** | 23090 [0.0718] | 17040 [0.0446] | 21655 [0.0499] |
| **Final R indice [I>2σ(I)]** | 0.0550 | 0.0475 | 0.0449 |
| **Largest diff. peak and hole [e.A$^{-3}$]** | 2.555 and -1.221 | 1.400 and -1.013 | 2.712 and -2.218 |
| **GOF** | 1.082 | 1.034 | 1.017 |

**Table A7: X-ray crystallographic data (continued)**

| **Compound** | **17.tol** | **18.hex** | **19** |
|---|---|---|---|
| **Formula** | $C_{122}H_{256}K_4O_{38}S_2Si_8U_2$ | $C_{72}H_{158}K_2N_2O_{22}SSi_4U$ | $C_{90}H_{198}K_4N_2O_{30}S_3Si_6U_2$ |
| **Crystal size [mm]** | 0.216x0.095x0.020 | 0.39x0.26x0.21 | 0.231x0.177x0.063 |
| **Crystal system** | Monoclinic | Triclinic | Orthorhombic |
| **Space group** | P $2_1$/n | P-1 | P $2_12_12$ |
| **V [Å$^3$]** | 8250.6(11) | 4919.2(13) | 7250.0(3) |
| **a [Å]** | 16.3304(14) | 14.610(2) | 27.6846(8) |
| **b [Å]** | 26.8000(19) | 17.221(3) | 17.5786(4) |
| **c [Å]** | 18.8582(15) | 19.8684(19) | 14.8975(4) |
| **α [°]** | 90 | 84.563(10) | 90 |
| **β [°]** | 91.476(9) | 84.218(9) | 90 |
| **γ [°]** | 90 | 83.002(12) | 90 |
| **Z** | 2 | 2 | 2 |
| **Absorption coefficient [mm$^{-1}$]** | 2.209 | 1.864 | 2.495 |
| **T [K]** | 150(2) | 100(2) | 150(2) |
| **Total no. reflexions** | 37944 | 75038 | 43886 |
| **Unique reflexions [R(int)]** | 16850 [0.1343] | 27810 [0.0677] | 21867 [0.0851] |
| **Final R indice [I>2σ(I)]** | 0.0778 | 0.0677 | 0.0752 |
| **Largest diff. peak and hole [e.A$^{-3}$]** | 1.422 and -1.071 | 3.508 and -1.868 | 1.995 and -1.027 |
| **GOF** | 0.931 | 1.181 | 1.021 |

**Table A8: X-ray crystallographic data (continued)**

| **Compound** | **20** | **21.(tol)$_2$** | **22.tol** |
|---|---|---|---|
| **Formula** | $C_{66}H_{144}KN_2O_{22}Si_4U$ | $C_{79}H_{170}K_2O_{24}S_{4.66}Si_6U_2$ | $C_{67}H_{141}KO_{22}SSi_4U$ |
| **Crystal size [mm]** | 0.080x0.060x0.010 | 0.42×0.32×0.25 | 0.890x0.144x0.027 |
| **Crystal system** | Orthorhombic | Monoclinic | Monoclinic |
| **Space group** | P $2_12_12_1$ | P 2/n | C c |
| **V [Å$^3$]** | 17950.5(14) | 11415(3) | 8891.0(8) |
| **a [Å]** | 26.0324(13) | 28.669(3) | 13.8962(5) |
| **b [Å]** | 26.2136(9) | 13.985(2) | 24.5807(16) |
| **c [Å]** | 6.3048(13) | 28.721(4) | 26.1417(14) |
| **α [°]** | 90 | 90 | 90 |
| **β [°]** | 90 | 97.583(9) | 95.317(5) |
| **γ [°]** | 90 | 90 | 90 |
| **Z** | 8 | 4 | 4 |
| **Absorption coefficient [mm$^{-1}$]** | 1.970 | 3.113 | 2.011 |
| **T [K]** | 150(2) | 100(2) | 150(2) |
| **Total no. reflexions** | 83574 | 157549 | 20499 |
| **Unique reflexions [R(int)]** | 32897 [0.1083] | 32538 [0.0515] | 11450 [0.0559] |
| **Final R indice [I>2σ(I)]** | 0.0372 | 0.0540 | 0.0674 |
| **Largest diff. peak and hole [e.A$^{-3}$]** | 1.421 and -1.297 | 4.982 and -4.181 | 1.676 and -1.648 |
| **GOF** | 0.464 | 1.146 | 1.075 |

**Table A9: X-ray crystallographic data (continued)**

| **Compound** | **23.tol** | **25-THF.tol** | **26** | **27** |
|---|---|---|---|---|
| **Formula** | $C_{79}H_{170}K_2O_{24}S_3Si_6U_2$ | $C_{59}H_{124}LiO_{17}Si_4U$ | $C_{48}H_{108}NaO_{16}Si_4U$ | $C_{48}H_{108}CsO_{16}Si_4U$ |
| **Crystal size [mm]** | 0.147x0.143x0.096 | 0.506x0.417x0.012 | 0.591x0.442x0.245 | 0.633x0.339x0.152 |
| **Crystal system** | Monoclinic | Monoclinic | Triclinic | Triclinic |
| **Space group** | P $2_1$ | P $2_1$/n | P-1 | P-1 |
| **V [Å$^3$]** | 5642.4(11) | 7622.3(7) | 3349.49(18) | 3460.1(7) |
| **a [Å]** | 13.9735(17) | 13.9291(8) | 12.8185(4) | 13.3400(13) |
| **b [Å]** | 18.2720(11) | 23.8285(12) | 13.8946(4) | 14.0020(17) |
| **c [Å]** | 22.168(3) | 23.0735(13) | 20.6221(6) | 20.165(3) |
| **α [°]** | 90 | 90 | 88.407(2) | 88.454(12) |
| **β [°]** | 94.534(12) | 95.554(5) | 89.539(2) | 89.945(10) |
| **γ [°]** | 90 | 90 | 65.824(3) | 66.782(9) |
| **Z** | 2 | 4 | 2 | 2 |
| **Absorption coefficient [mm$^{-1}$]** | 3.117 | 2.249 | 2.555 | 2.986 |
| **T [K]** | 100(2) | 150(2) | 150(2) | 120(2) |
| **Total no. reflexions** | 72530 | 66485 | 80782 | 44663 |
| **Unique reflexions [R(int)]** | 22269 [0.0680] | 15552 [0.0805] | 20426 [0.0492] | 15238 [0.0640] |
| **Final R indice [I>2σ(I)]** | 0.0463 | 0.0443 | 0.0433 | 0.0632 |
| **Largest diff. peak and hole [e.A$^{-3}$]** | 2.307 and -1.485 | 1.824 and -1.083 | 2.664 and -1.44 | 3.131 and -3.331 |
| **GOF** | 1.156 | 1.066 | 1.109 | 1.265 |

**Table A10: X-ray crystallographic data (continued)**

| **Compound** | **28.DIPE** | **29.tol** | **30** | **32** |
|---|---|---|---|---|
| **Formula** | $C_{153}H_{336}Na_6O_{58}Si_{12}U_3$ | $C_{79}H_{170}O_{27}Si_6K_2U_2$ | $C_{72}H_{162}NO_{25}Si_6U_2$ | $C_{48}H_{108}KO_{16}Si_4Yb$ |
| **Crystal size [mm]** | 0.374x0.266x0.103 | 0.606x0.365x0.293 | 0.862x0.491x0.453 | 0.49x0.43x0.13 |
| **Crystal system** | Trigonal | Monoclinic | Triclinic | Triclinic |
| **Space group** | R -3 | P $2_1$ | P-1 | P -1 |
| **V [Å$^3$]** | 139689(15) | 5542.1(13) | 4988.7(13) | 3415.9(2) |
| **a [Å]** | 74.436(4) | 13.945(2) | 13.3490(13) | 12.9906(5) |
| **b [Å]** | 74.436(4) | 18.1921(19) | 16.186(3) | 14.1745(5) |
| **c [Å]** | 29.1115(13) | 21.896(4) | 25.445(3) | 20.1312(7) |
| **α [°]** | 90 | 90 | 71.541(13) | 87.905(3) |
| **β [°]** | 90 | 93.900(13) | 80.482(9) | 88.583(3) |
| **γ [°]** | 120 | 90 | 73.743(9) | 67.247(4) |
| **Z** | 18 | 2 | 2 | 2 |
| **Absorption coefficient [mm$^{-1}$]** | 1.664 | 3.120 | 3.376 | 1.553 |
| **T [K]** | 150(2) | 100(2) | 100(2) | 150(2) |
| **Total no. reflexions** | 164408 | 83801 | 133436 | 41570 |
| **Unique reflexions [R(int)]** | 63341 [0.1997] | 30662 [0.0728] | 40011 [0.0262] | 20663 [0.0323] |
| **Final R indice [I>2σ(I)]** | 0.0578 | 0.0741 | 0.0304 | 0.0459 |
| **Largest diff. peak and hole [e.A$^{-3}$]** | 1.296 and -0.687 | 5.985 and -4.606 | 0.864 and -1.911 | 1.044 and -0.765 |
| **GOF** | 0.580 | 1.207 | 1.266 | 1.021 |

**Table A11: X-ray crystallographic data (continued)**

| Compound | 33-Eu.THF | 33-Yb.tol | 33-Sm | KPhNNPh |
|---|---|---|---|---|
| Formula | $C_{52}H_{116}EuK_2O_{17}Si_4$ | $C_{55}H_{116}K_2O_{16}Si_4Yb$ | $C_{48}H_{108}K_2O_{16}Si_4Sm$ | $C_{12}H_{10}KN_2$ |
| Crystal size [mm] | 0.97x0.94x0.72 | 0.77x0.56x0.05 | 0.28x0.19x0.03 | 0.22x0.08x0.01 |
| Crystal system | Monoclinic | Triclinic | Monoclinic | Orthorhombic |
| Space group | P $2_1$/c | P -1 | P $2_1$/c | P bca |
| V [Å$^3$] | 7296.7(3) | 3758.2(2) | 7115.9(2) | 1021.3(3) |
| a [Å] | 14.9751(3) | 13.1340(4) | 20.2557(3) | 6.5686(6) |
| b [Å] | 23.7045(5) | 14.4973(5) | 14.5768(3) | 7.0512(11) |
| c [Å] | 21.2011(6) | 22.6747(8) | 24.2662(4) | 22.049(5) |
| α [°] | 90 | 76.599(3) | 90 | 90 |
| β [°] | 104.177(3) | 78.058(3) | 96.7062(17) | 90 |
| γ [°] | 90 | 64.359(3) | 90 | 90 |
| Z | 4 | 2 | 4 | 4 |
| Absorption coefficient [mm$^{-1}$] | 1.094 | 1.472 | 1.061 | 0.483 |
| T [K] | 150(2) | 150(2) | 150(2) | 150(2) |
| Total no. reflexions | 87992 | 45739 | 83477 | 3506 |
| Unique reflexions [R(int)] | 22230 [0.0447] | 22784 [0.0544] | 21699 [0.0773] | 1553 [0.1163] |
| Final R indice [I>2σ(I)] | 0.0450 | 0.0844 | 0.0485 | 0.0730 |
| Largest diff. peak and hole [e.A$^{-3}$] | 1.770 and -0.822 | 2.487 and -2.446 | 1.882 and -1.429 | 0.319 and -0.328 |
| GOF | 1.165 | 1.167 | 0.995 | 0.939 |

**Table A12: X-ray crystallographic data (continued)**

| **Compound** | **34.hex** | **$[(K_2CS_3)_5(DMSO)_{12}]_n$** | **35** |
|---|---|---|---|
| **Formula** | $C_{63}H_{125}EuK_2N_2O_{16}Si_4$ | $C_{29}H_{72}K_{10}O_{12}S_{27}$ | $C_{52}H_{118}O_{18}Si_4Yb_2$ |
| **Crystal size [mm]** | 0.53x0.33x0.03 | 0.40x0.14x0.08 | 0.22x0.18x0.11 |
| **Crystal system** | Monoclinic | Triclinic | Triclinic |
| **Space group** | P $2_1$/n | P 1 | P -1 |
| **V [Å$^3$]** | 8461.9(5) | 2048.44(8) | 7268.7(17) |
| **a [Å]** | 15.9738(6) | 10.5764(2) | 13.8950(17) |
| **b [Å]** | 22.4611(7) | 14.2351(3) | 18.933(3) |
| **c [Å]** | 23.6457(8) | 14.2982(3) | 27.899(2) |
| **α [°]** | 90 | 84.4166(17) | 90.191(10) |
| **β [°]** | 94.122(4) | 82.5117(18) | 97.701(9) |
| **γ [°]** | 90 | 74.1047(19) | 91.962(12) |
| **Z** | 4 | 1 | 4 |
| **Absorption coefficient [mm$^{-1}$]** | 0.950 | 1.251 | 2.680 |
| **T [K]** | 150(2) | 150(2) | 150(2) |
| **Total no. reflexions** | 75645 | 42486 | 49711 |
| **Unique reflexions [R(int)]** | 17273 [0.1116] | 20224 [0.0360] | 49711 [0.1154] |
| **Final R indice [I>2σ(I)]** | 0.0681 | 0.0493 | 0.0779 |
| **Largest diff. peak and hole [e.A$^{-3}$]** | 3.520 and -1.731 | 0.892 and -0.516 | 2.814 and -2.282 |
| **GOF** | 1.086 | 1.020 | 0.840 |

**Table A13: X-ray crystallographic data (continued)**

| **Compound** | **36.$(CH_3CN)_{0.5}$** | **37** | **38-Eu** | **38-Yb.$(CH_3CN)_3$** |
|---|---|---|---|---|
| **Formula** | $C_{21}H_{22.5}I_2N_{5.5}Yb$ | $C_{36}H_{36}Eu_2I_4N_8$ | $C_{36}H_{36}EuI_2N_8$ | $C_{42}H_{45}I_2N_{11}Yb$ |
| **Crystal size [mm]** | 0.68x0.44x0.27 | 0.26x0.07x0.06 | 0.21x0.12x0.08 | 0.24x0.10x0.03 |
| **Crystal system** | Triclinic | Orthorhombic | Monoclinic | Monoclinic |
| **Space group** | P -1 | P bca | P $2_1$/c | C c |
| **V [Å$^3$]** | 1299.35(9) | 4273.0(2) | 1823.80(7) | 4459.54(13) |
| **a [Å]** | 9.7066(4) | 18.7333(5) | 9.6921(2) | 20.9808(4) |
| **b [Å]** | 11.8441(5) | 9.8963(2) | 10.6794(2) | 17.9897(3) |
| **c [Å]** | 13.2726(5) | 23.0485(8) | 18.2566(4) | 11.8325(2) |
| **α [°]** | 81.086(3) | 90 | 90 | 90 |
| **β [°]** | 67.813(4) | 90 | 105.171(3) | 93.1003(16) |
| **γ [°]** | 66.875(4) | 90 | 90 | 90 |
| **Z** | 2 | 4 | 2 | 4 |
| **Absorption coefficient [mm$^{-1}$]** | 5.991 | 5.833 | 3.449 | 3.524 |
| **T [K]** | 150(2) | 150(2) | 150(2) | 150(2) |
| **Total no. reflexions** | 11849 | 42811 | 22764 | 24007 |
| **Unique reflexions [R(int)]** | 7790 [0.0243] | 13402 [0.0665] | 6113 [0.0367] | 10194 [0.0351] |
| **Final R indice [I>2σ(I)]** | 0.0361 | 0.0411 | 0.0337 | 0.0420 |
| **Largest diff. peak and hole [e.A$^{-3}$]** | 1.708 and -0.998 | 1.827 and -1.360 | 1.592 and -0.504 | 1.544 and -0.509 |
| **GOF** | 1.021 | 1.002 | 0.884 | 0.858 |

**Table A14: X-ray crystallographic data (continued)**

| **Compound** | **38-Sm** | **39** | **40** | **41.$(CH_3CN)_{0.4}$** |
|---|---|---|---|---|
| **Formula** | $C_{36}H_{36}I_2N_8Sm$ | $C_{39}H_{36}EuF_3N_6O_5S$ | $C_{38}H_{36}EuN_6O_2$ | $C_{42.8}H_{43.2}I_2N_{8.4}O_2Yb_2$ |
| **Crystal size [mm]** | 0.37x0.18x0.08 | 0.57x0.45x0.39 | 0.56x0.28x0.10 | 0.34x0.20x0.18 |
| **Crystal system** | Monoclinic | Monoclinic | Monoclinic | Monoclinic |
| **Space group** | P $2_1$/c | P $2_1$/n | P $2_1$/n | P $2_1$/n |
| **V [Å$^3$]** | 1879.6(4) | 3829.80(11) | 3330.6(3) | 2205.2(6) |
| **a [Å]** | 9.7886(11) | 12.4858(2) | 10.5841(5) | 11.6761(14) |
| **b [Å]** | 10.8139(12) | 14.8216(2) | 24.1684(15) | 12.6175(16) |
| **c [Å]** | 18.363(2) | 20.7654(3) | 13.1318(7) | 15.621(3) |
| **α [°]** | 90 | 90 | 90 | 90 |
| **β [°]** | 104.764(12) | 94.7180(17) | 97.474(5) | 106.621(12) |
| **γ [°]** | 90 | 90 | 90 | 90 |
| **Z** | 2 | 4 | 4 | 2 |
| **Absorption coefficient [mm$^{-1}$]** | 3.240 | 1.759 | 1.927 | 5.660 |
| **T [K]** | 150(2) | 150(2) | 150(2) | 100(2) |
| **Total no. reflexions** | 8052 | 18325 | 16951 | 55009 |
| **Unique reflexions [R(int)]** | 3795 [0.0396] | 11573 [0.0242] | 10045 [0.0403] | 9690 [0.0800] |
| **Final R indice [I>2σ(I)]** | 0.0631 | 0.0385 | 0.0494 | 0.0427 |
| **Largest diff. peak and hole [e.A$^{-3}$]** | 2.082 and -1.039 | 1.867 and -1.370 | 1.153 and -1.287 | 3.918 and -3.409 |
| **GOF** | 1.073 | 1.044 | 1.060 | 1.098 |

**Table A15 : X-ray crystallographic data (continued)**

| Compound | **42.(py)$_{2.5}$** | **43-DME** | **44.DMSO** |
|---|---|---|---|
| **Formula** | $C_{67.5}H_{80.5}EuF_3N_{8.5}O_5S$ | $C_{80}H_{120}KN_4O_8Yb$ | $C_{26}H_{36}EuN_3O_4S_6$ |
| **Crystal size [mm]** | 0.439x0.089x0.026 | 0.889x0.032x0.025 | 0.431x0.239x0.202 |
| **Crystal system** | Monoclinic | Tetragonal | Monoclinic |
| **Space group** | P $2_1$/n | P $4_12_12$ | C 2/c |
| **V [Å$^3$]** | 6669.0(13) | 9323(2) | 6904(2) |
| **a [Å]** | 9.7537(15) | 20.747(3) | 39.121(5) |
| **b [Å]** | 27.649(2) | 20.747(3) | 16.268(3) |
| **c [Å]** | 24.817(2) | 21.6594(16) | 10.908(3) |
| **α [°]** | 90 | 90 | 90 |
| **β [°]** | 94.836(11) | 90 | 96.042(14) |
| **γ [°]** | 90 | 90 | 90 |
| **Z** | 4 | 4 | 8 |
| **Absorption coefficient [mm$^{-1}$]** | 1.034 | 1.093 | 2.214 |
| **T [K]** | 150(2) | 150(2) | 100(2) |
| **Total no. reflexions** | 21533 | 24168 | 51467 |
| **Unique reflexions [R(int)]** | 21533 [0.1239] | 9513 [0.1454] | 10016 [0.0876] |
| **Final R indice [I>2σ(I)]** | 0.1142 | 0.0987 | 0.0787 |
| **Largest diff. peak and hole [e.A$^{-3}$]** | 12.779 and -5.258 | 1.980 and -0.673 | 5.229 and -2.235 |
| **GOF** | 0.926 | 0.873 | 1.204 |

# NMR spectra

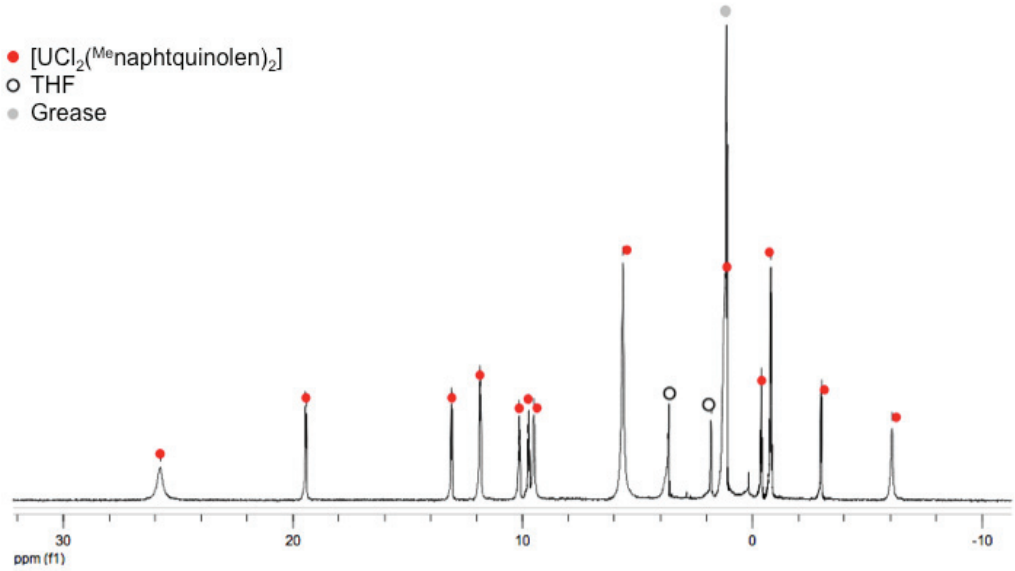


**Figure A1: $^{1}$H NMR spectrum (200 MHz, THF-$d_8$, 298) of [$UCl_2$($^{Me}$naphtquinolen)$_2$] 1-Cl.**

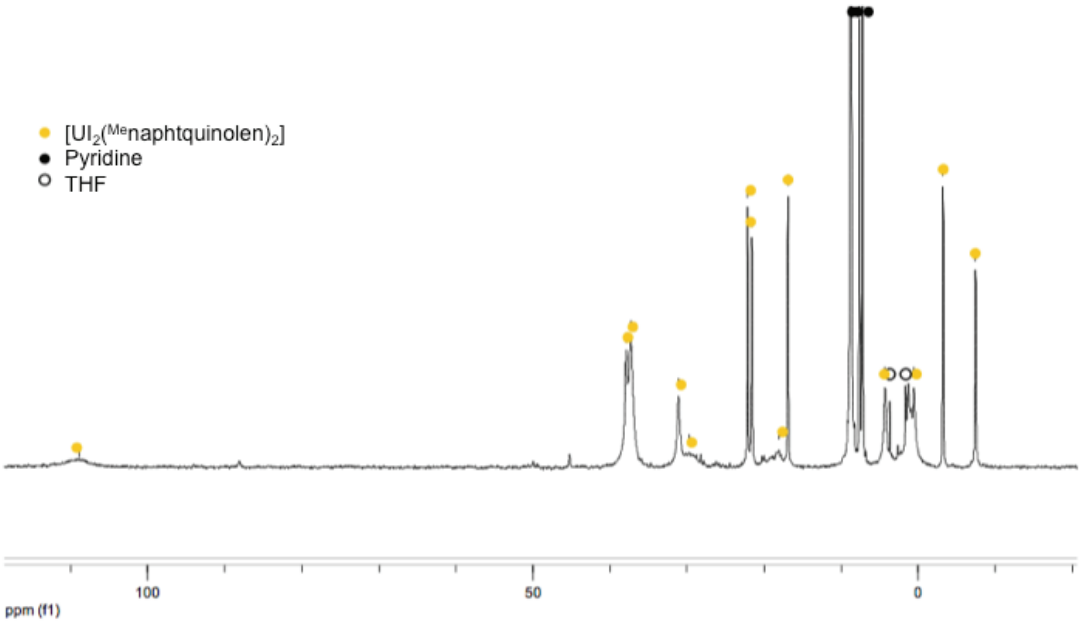


**Figure A2: $^{1}$H NMR spectrum (200 MHz, py-$d_5$, 298K) of [$UI_2$($^{Me}$naphtquinolen)$_2$] 1-I.**

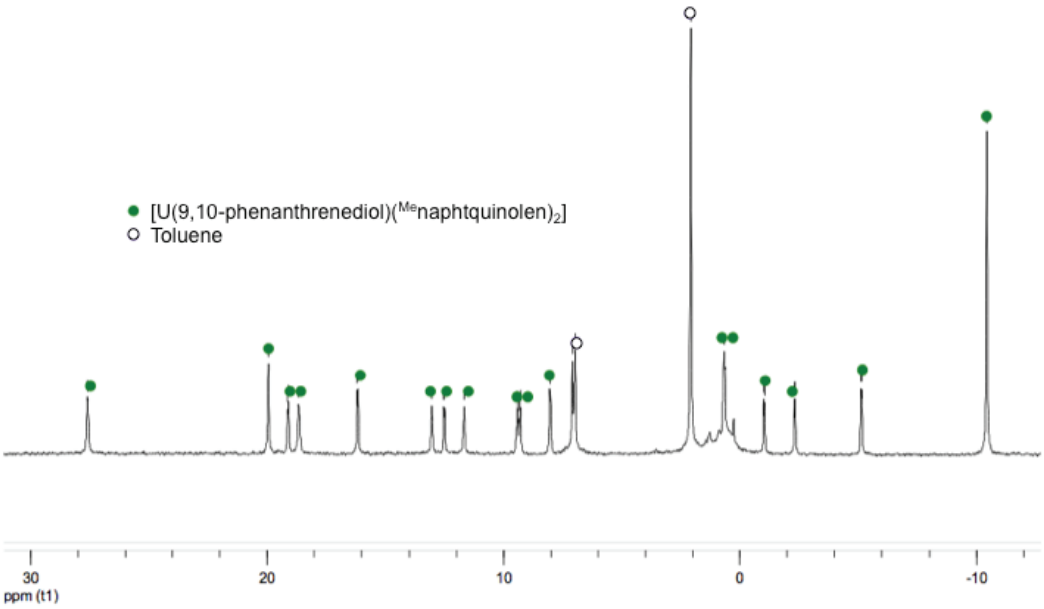


**Figure A3: $^{1}$H NMR spectrum (200 MHz, tol-$d_8$, 298K) of [U(9,10- phenanthrenediol) ($^{Me}$naphtquinolen)$_2$] 3.**

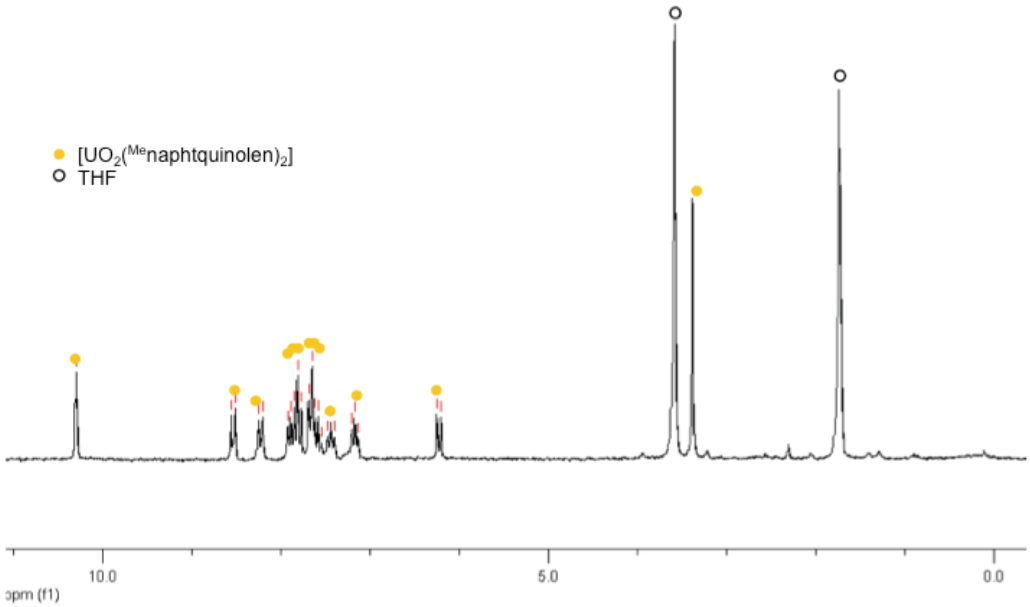


**Figure A4: $^{1}$H NMR spectrum (200 MHz, THF-$d_8$, 298K) of [$UO_2$($^{Me}$naphtquinolen)$_2$] 4.**

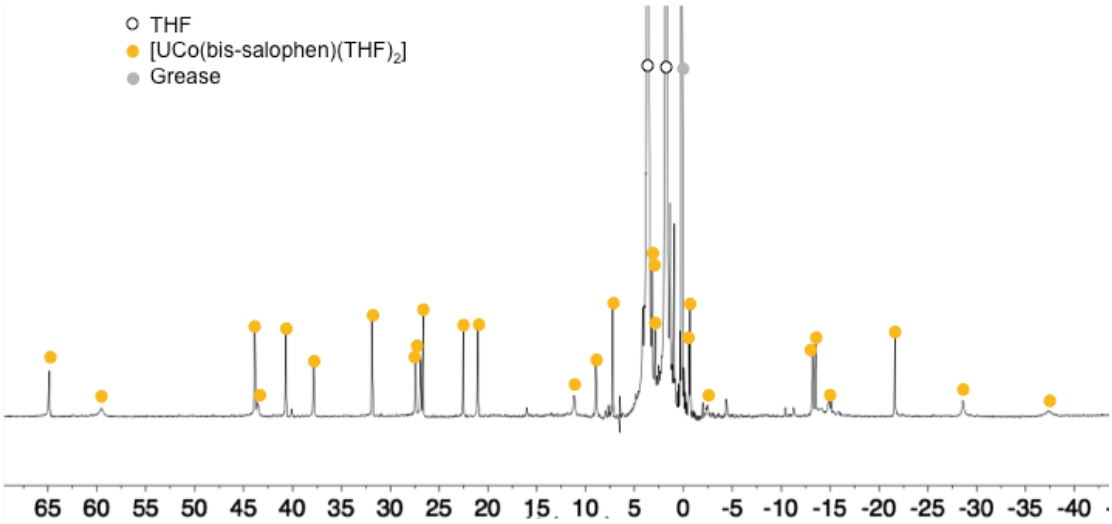


**Figure A5: $^{1}$H NMR spectrum (200 MHz, THF-$d_8$, 298K) of [UCo(bis-salophen)(THF)$_2$] 5.**

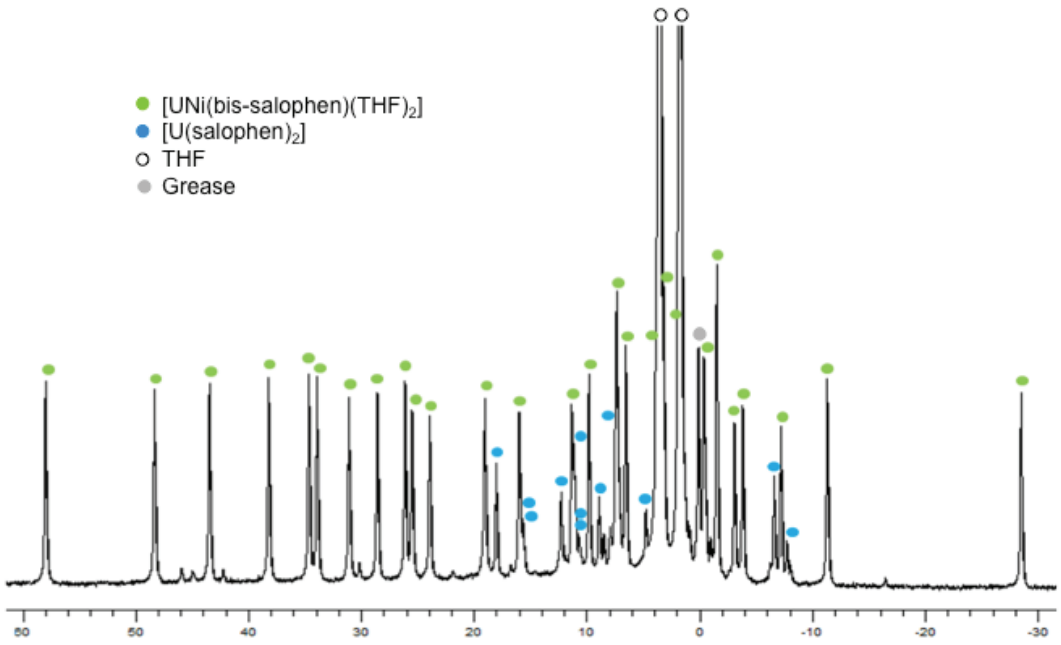


**Figure A6: $^{1}$H NMR spectrum (200 MHz, THF-$d_8$, 298 K) of the 1:1 crude reaction mixture of $Na_2$[U(bis-salophen)] and [$NiI_2(THF)_{0.2}$].**

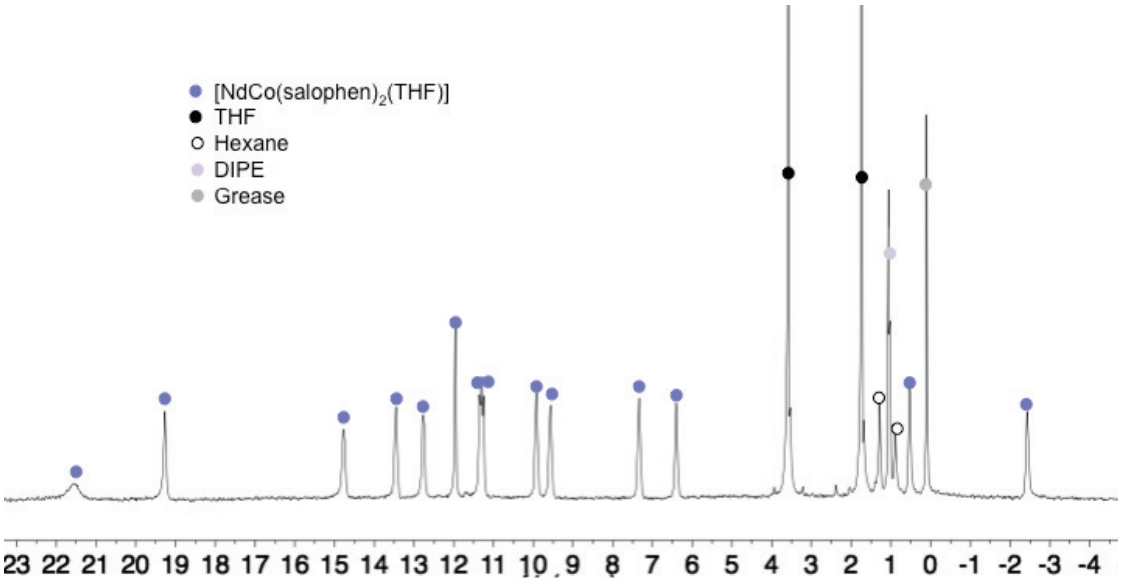


**Figure A7: $^{1}$H NMR spectrum (200 MHz, THF-$d_8$, 298 K) of [NdCo(salophen)$_2$(THF)] 7.**

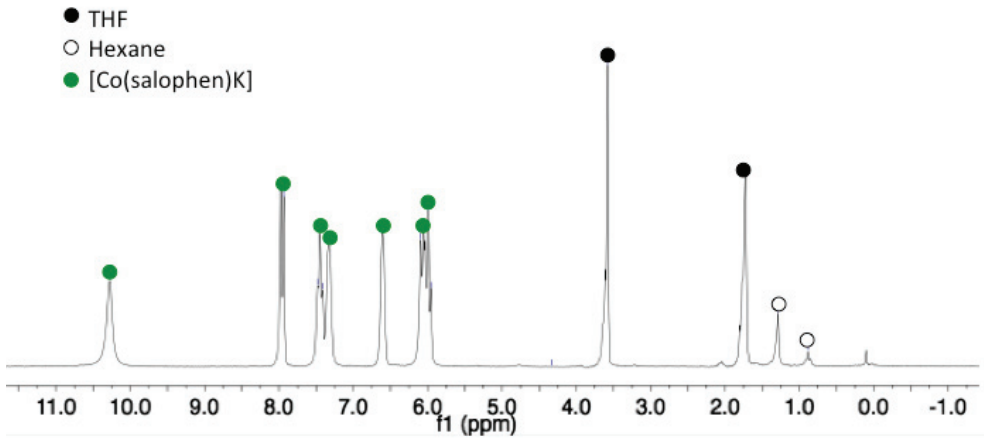


**Figure A8: $^{1}$H NMR spectrum (400 MHz, THF-$d_8$, 298 K) of the complex [Co(Salophen)K)(THF)].**

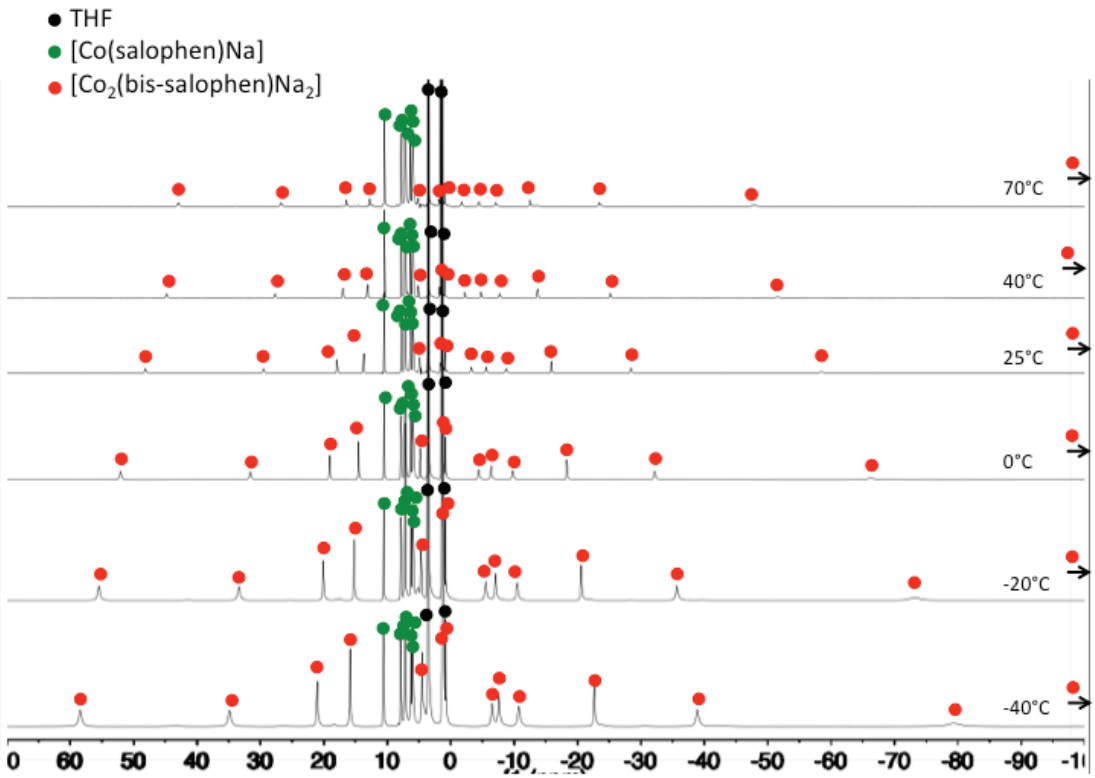


**Figure A9: Variable temperature $^{1}$H NMR spectra (400 MHz, THF-$d_8$) from -40°C to 70°C of a 0.353M solution of [Co(salophen)] reacted with one equivalent of Na.**

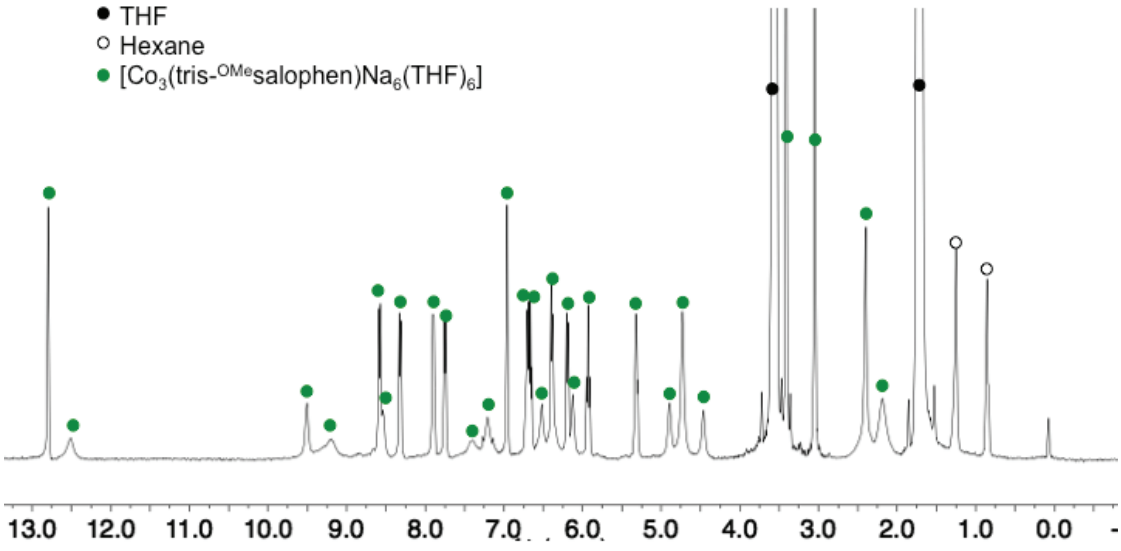


**Figure A10: $^{1}$H NMR spectrum (400 MHz, THF-$d_8$, 298K) of [$Co_3$(tris-$^{OMe}$salophen)$Na_6$], 9.**

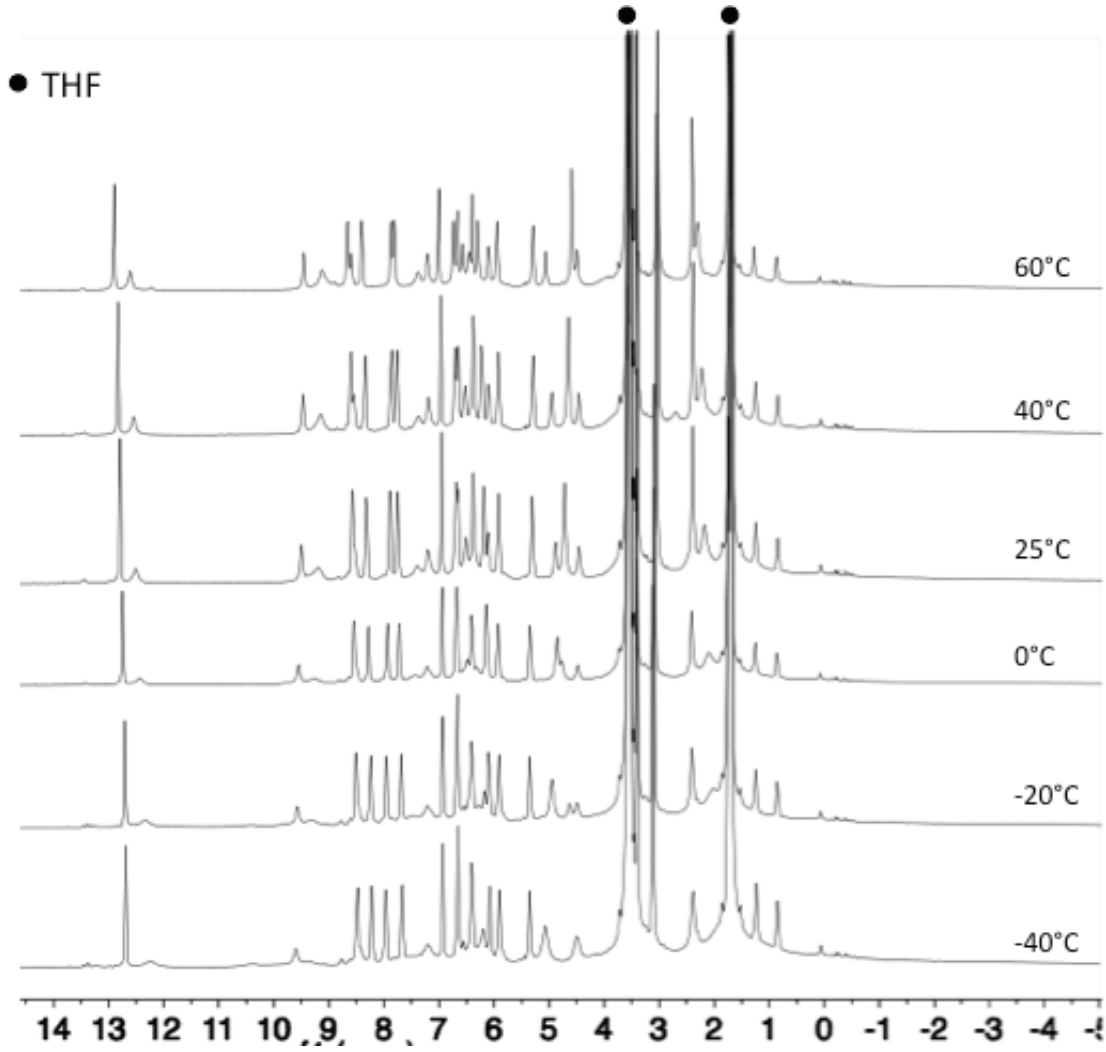


**Figure A11: Variable temperature NMR spectrum (400 MHz, THF-$d_8$) from -40°C to 60°C of a 15 mM solution of [$Co_3$(tris-$^{OMe}$salophen)$Na_6$], 9.**

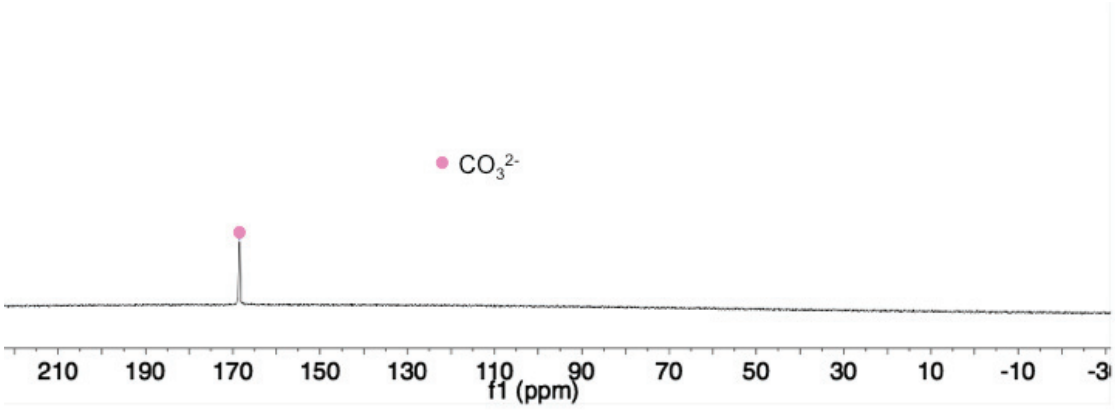


**Figure A12: $^1$H NMR spectrum (100 MHz, $D_2O$, 298 K) of the 1:1 crude reaction mixture of [$Co_3$(tris-$^{OMe}$salophen)$Na_6$], 9 and excess $CO_2$.**

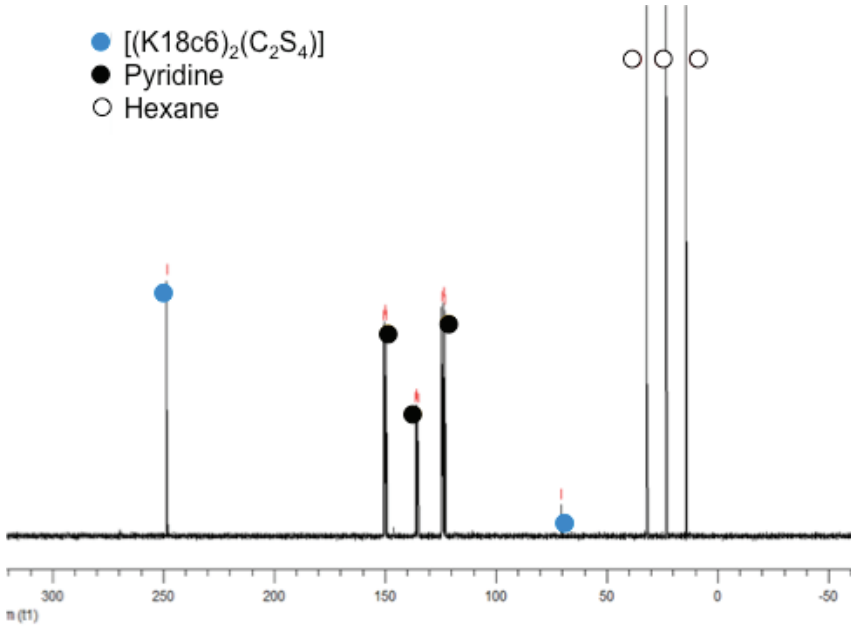


**Figure A13 : $^{13}$C NMR spectrum (100 MHz, py-$d_5$, 298K) of the crystals of [(K18c6)$_2$C$_2$S$_4$].Py isolated from pyridine/hexane.**

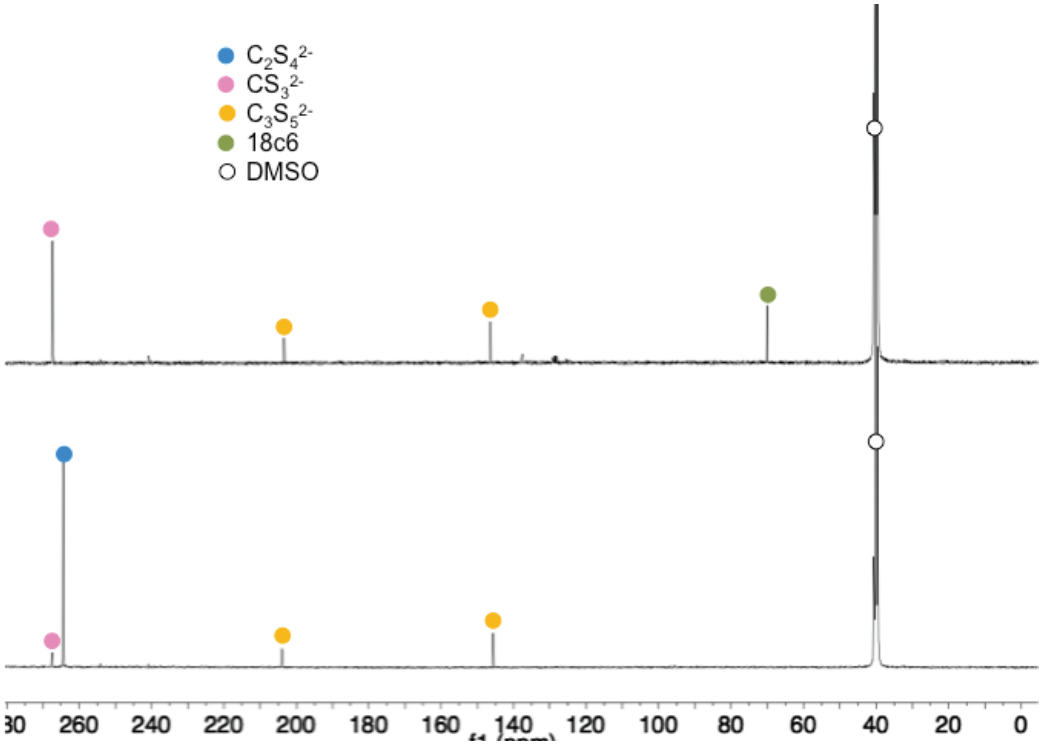


**Figure A14: $^{13}$C NMR spectra (100 MHz, DMSO-$d_6$, 298K) of the reaction mixture of [U(OSi(OtBu)$_3$)$_4$K] (bottom) and [K18c6][U(OSi(OtBu)$_3$)$_4$] (top) with 4eq $^{13}CS_2$.**

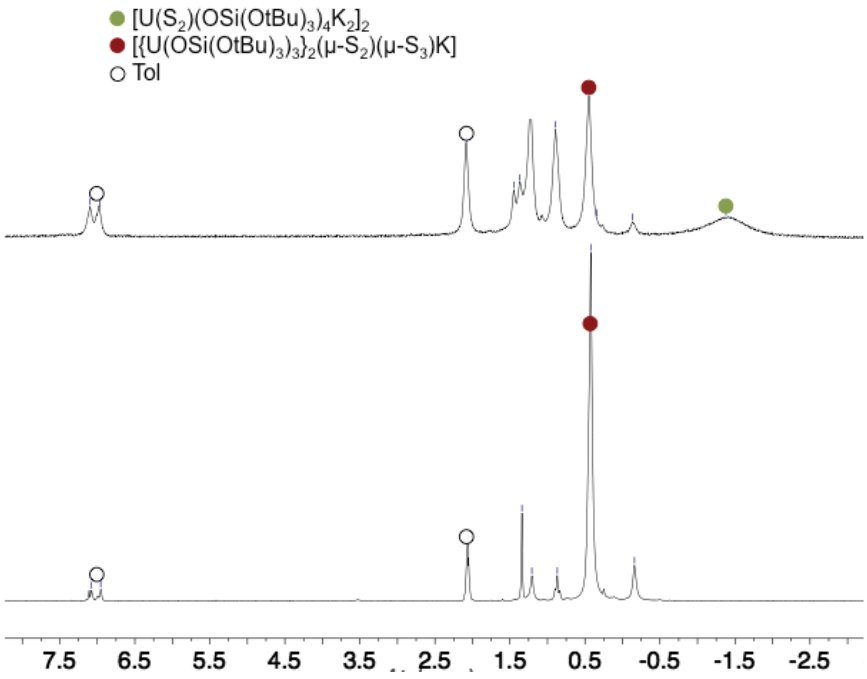


**Figure A15: 1H NMR spectra (400 MHz, tol-$d_8$, 298K) of the reaction mixture of $[U(OSi(OtBu)_3)_4K]$ with 0.125eq (top) and 0.25eq (bottom) of $S_8$.**

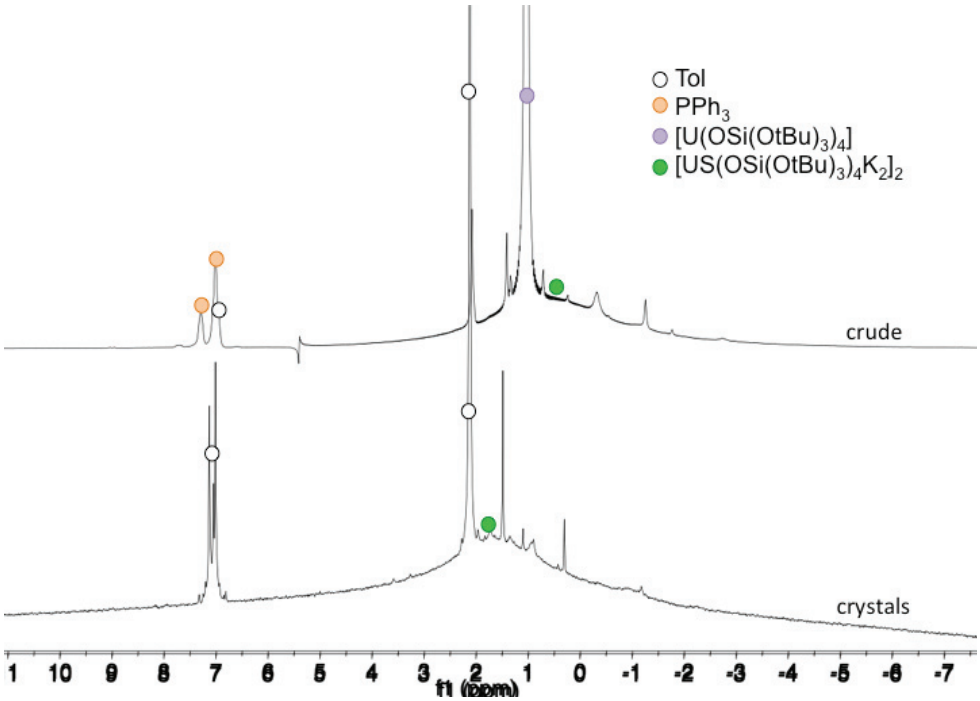


**Figure A16: $^1$H NMR spectrum (200 MHz, tol-$d_8$, 298K) of the 1:0.5 reaction mixture of $[U(OSi(OtBu)_3)_4K]$ and $Ph_3PS$ (top) and of $[US(OSi(OtBu)_3)_4K_2]_2$ 16 (bottom).**

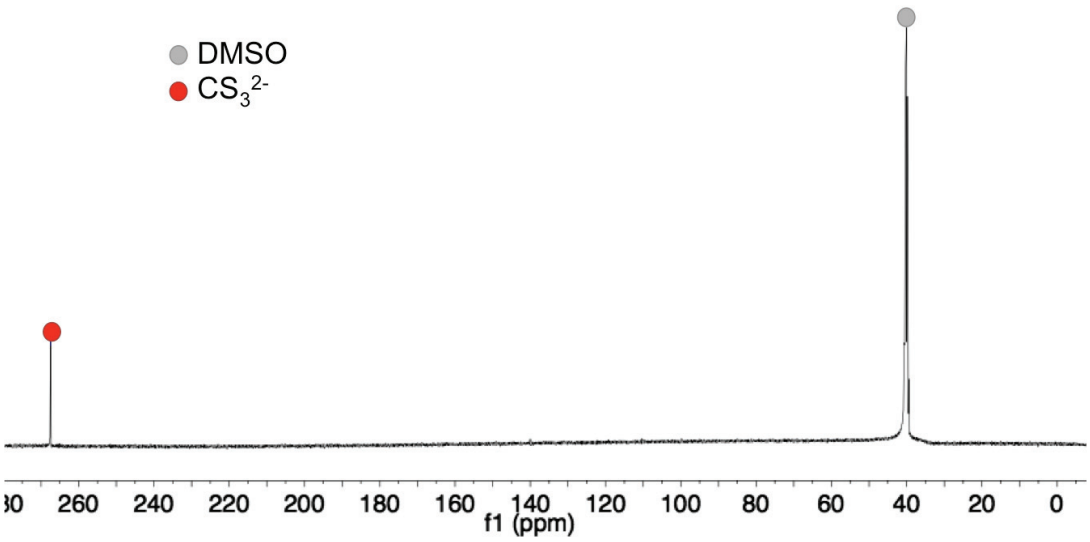


**Figure A17: $^{13}C$ NMR spectrum (100 MHz, DMSO-$d_6$, 298K) of the 1:2 reaction mixture of complex $[US(OSi(OtBu)_3)_4K_2]_2$ 16 and $^{13}CS_2$.**

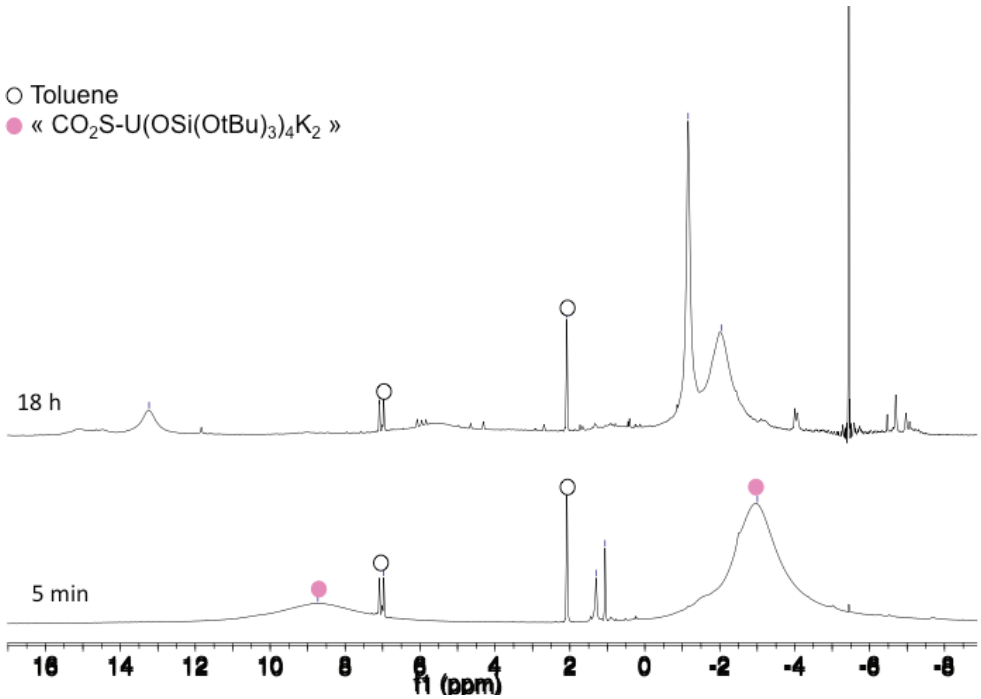


**Figure A18: $^{1}H$ NMR spectrum (400 MHz, tol-$d_8$, 298 K) of the crude mixture after addition of an excess of $^{13}CO_2$ to $[US(OSi(OtBu)_3)_4K_2]_2$ 16 after 5 min (bottom) and after 18 h (top).**

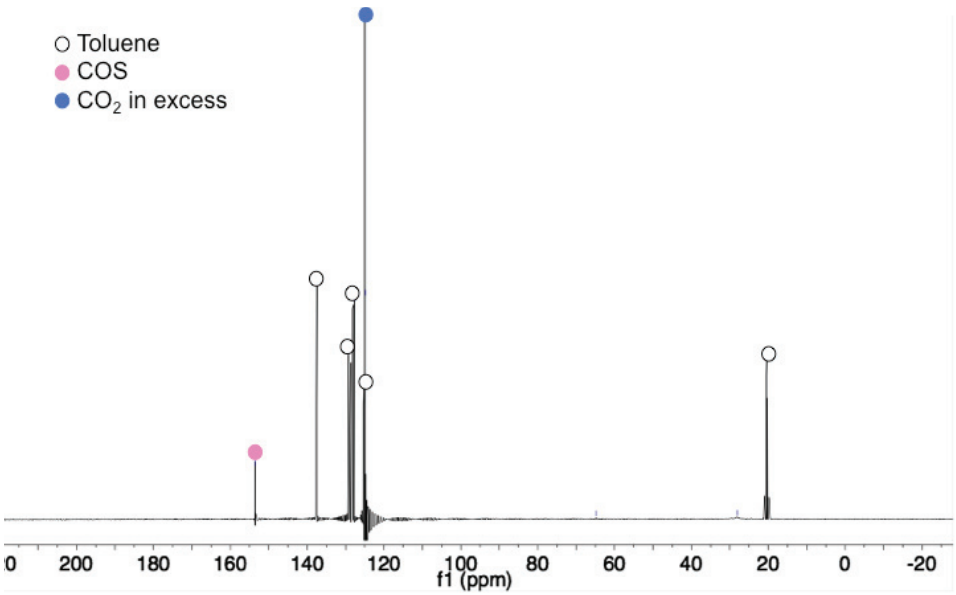


**Figure A19: $^{13}C$ NMR spectrum (100 MHz, tol-$d_8$, 298 K) of the crude mixture after addition of an excess of $^{13}CO_2$ to $[US(OSi(OtBu)_3)_4K_2]_2$ 16.**

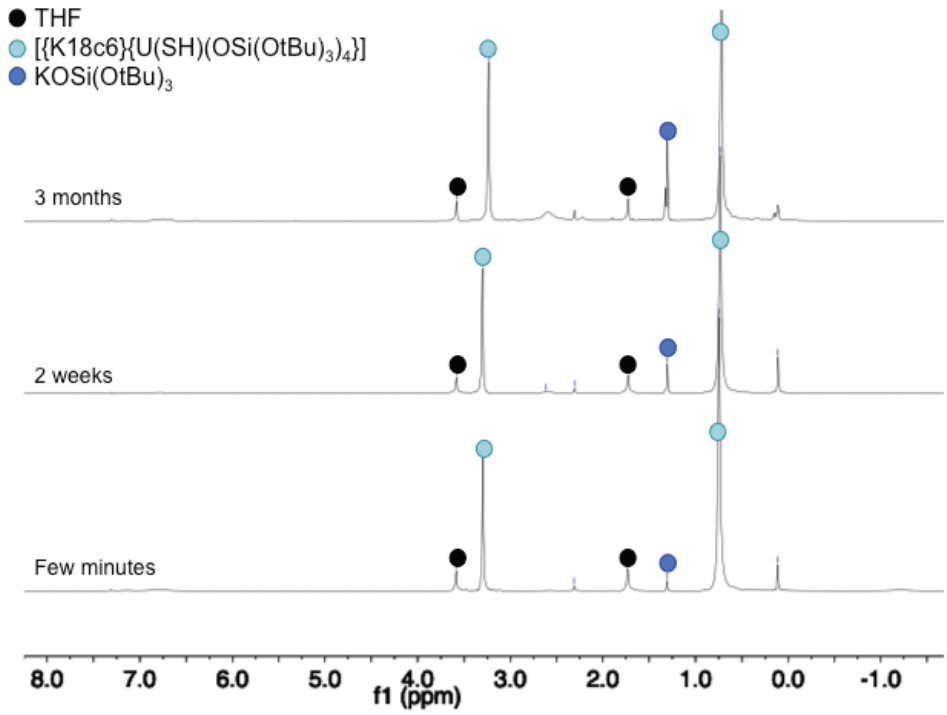


**Figure A20: $^{1}H$ NMR spectra (400 MHz, THF-$d_8$, 298 K) of the stability follow up of [{K18c6}{U(SH)(OSi(OtBu)$_3$)$_4$}], 22, over time.**

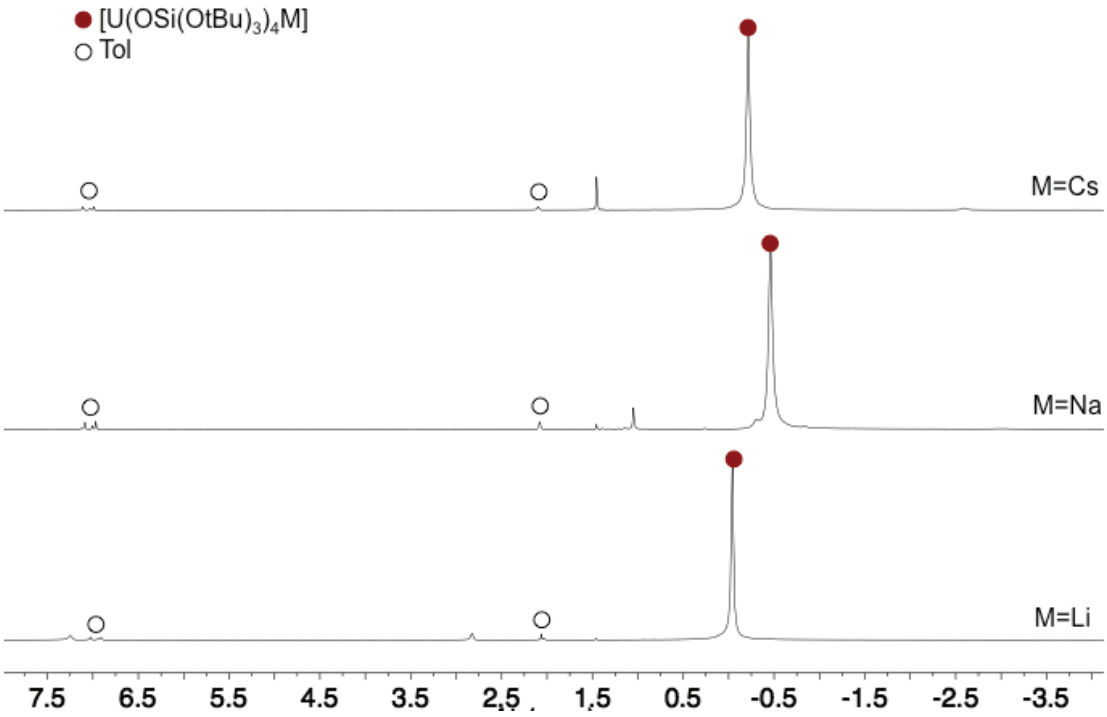


**Figure A21: $^{1}$H NMR spectra (400 MHz, tol-$d_8$, 298 K) of the [U(OSi(OtBu)$_3$)$_4$M] complexes M=Li 25 (bottom), M=Na 26 (middle), M=Cs 27 (top).**

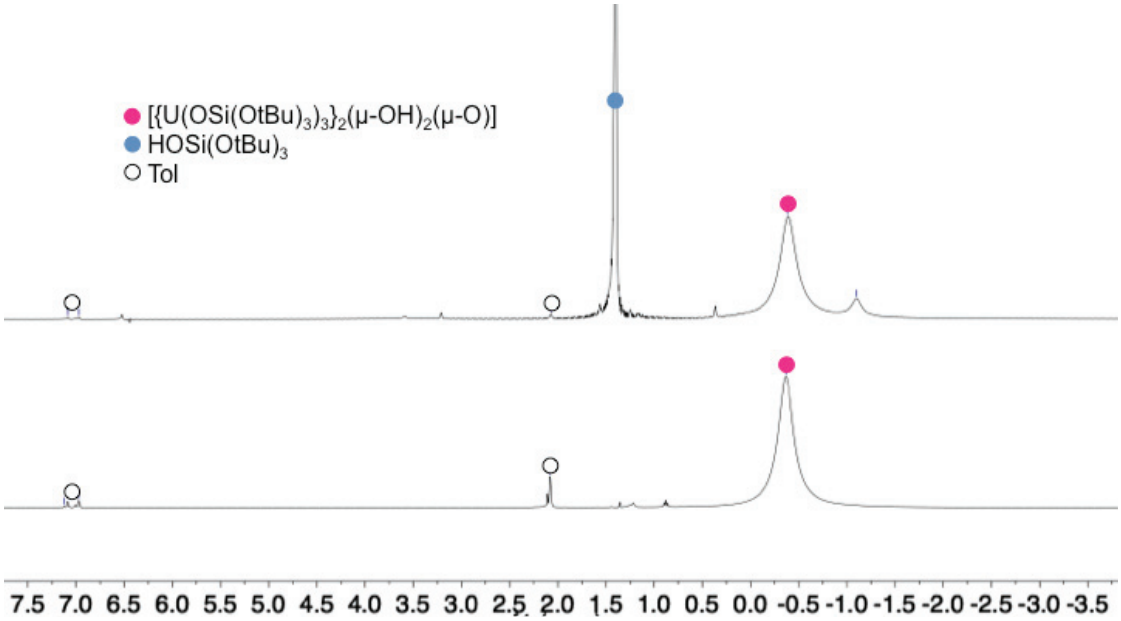


**Figure A22: $^{1}$H NMR spectra (400 MHz, tol-$d_8$, 298K) of the crude reaction mixture of [U(OSi(OtBu)$_3$)$_4$K] with 1.5eq of H2O (top) and of [{U(OSi(OtBu)$_3$)$_3$}$_2$(μ-OH)$_2$(μ-O)] 29 (bottom).**

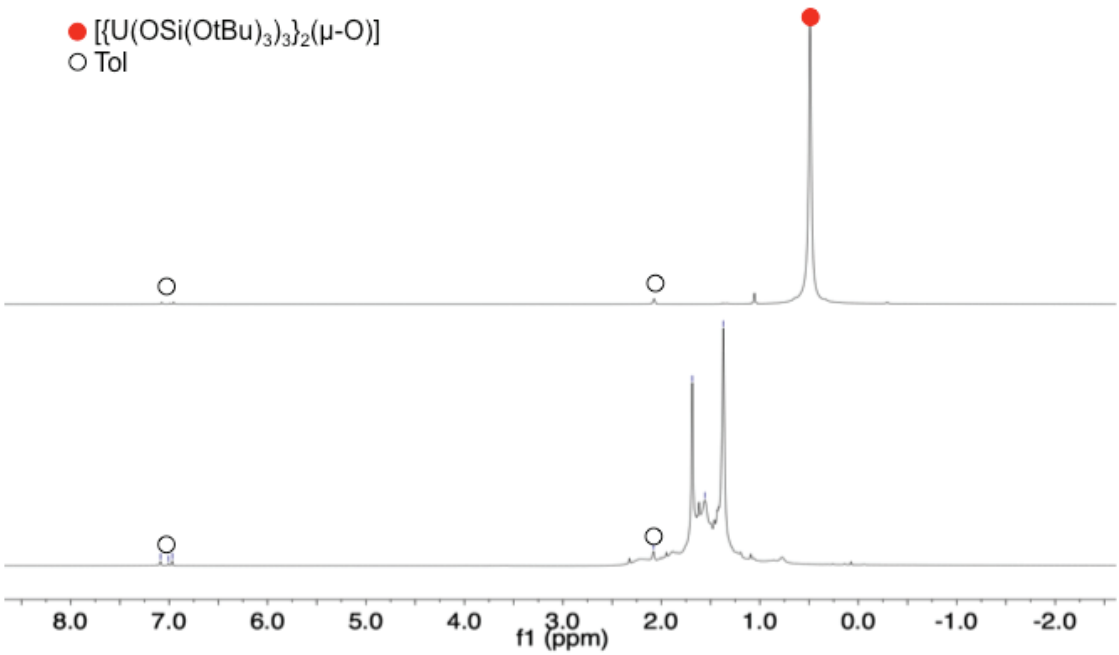


**Figure A23: $^{1}$H NMR spectrum (400 MHz, tol-$d_8$, 298K) of the crude reaction mixture of $[U(OSi(OtBu)_3)_3]_2$ with excess $N_2O$ (bottom) and of $[\{U(OSi(OtBu)_3)_3\}_2(\mu\text{-}O)]$ 30 (top).**

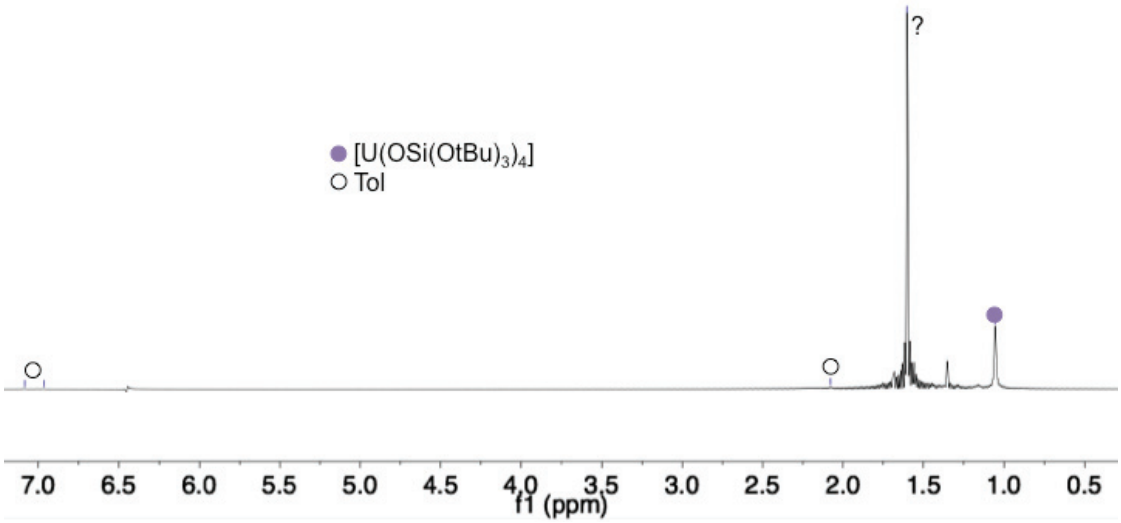


**Figure A24: $^{1}$H NMR spectrum (400 MHz, tol-$d_8$, 298K) of the crude reaction mixture of $[U(OSi(OtBu)_3)_4]$ with excess $N_2O$.**

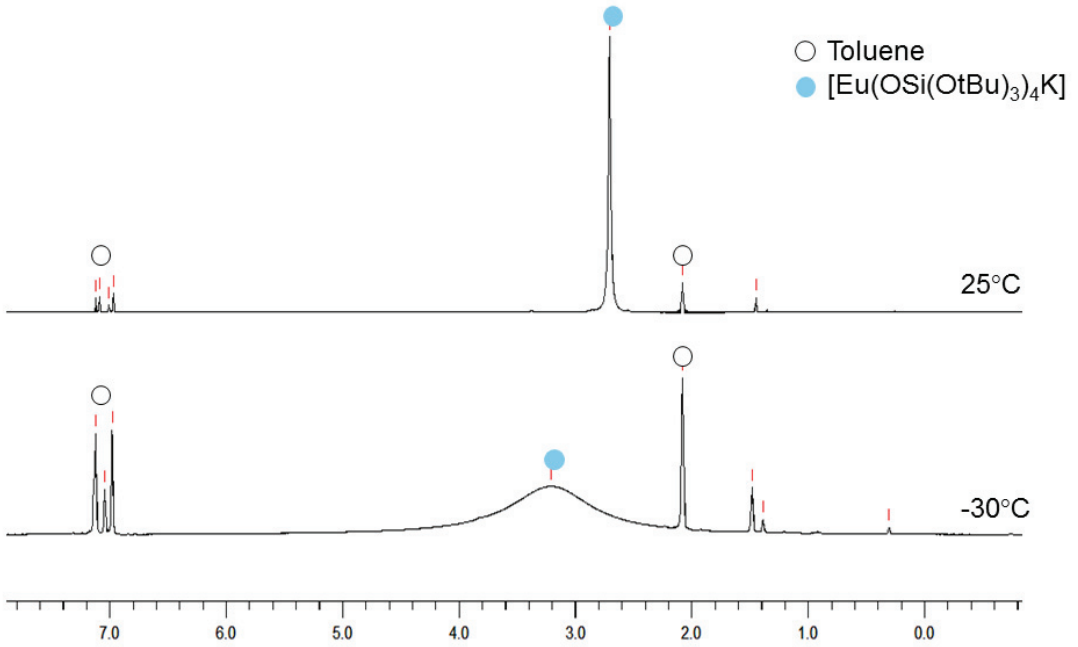


**Figure A25: $^{1}$H NMR spectra (400 MHz, tol-$d_8$) of [Eu(OSi(OtBu)$_3$)$_4$K] 32-Eu at -30°C (bottom) and 25°C (top).**

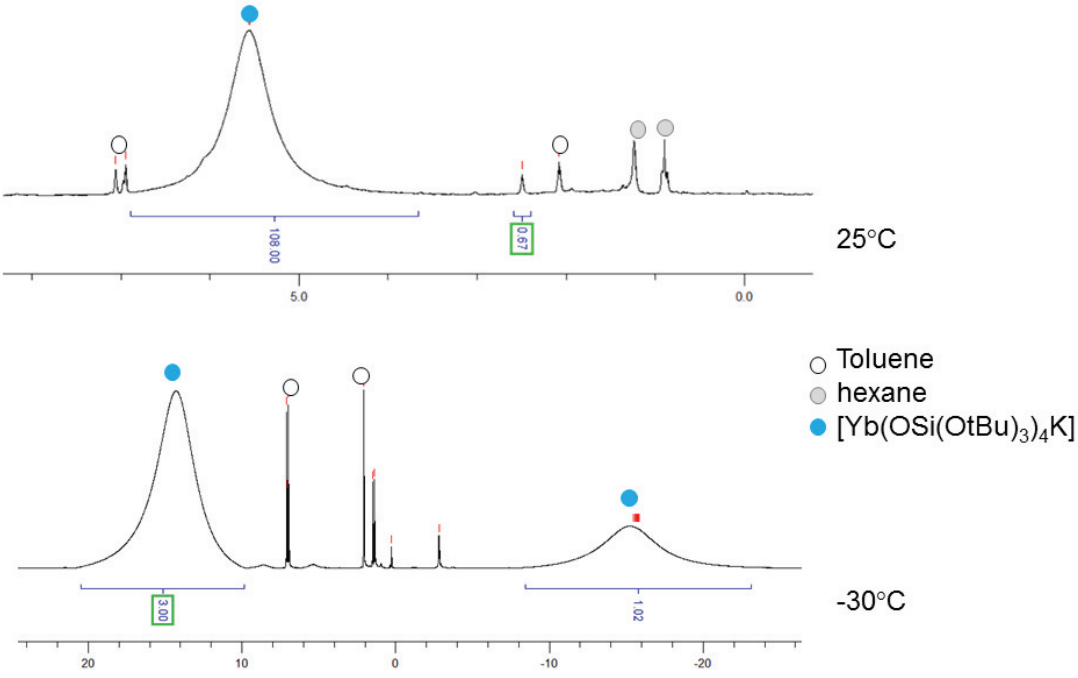


**Figure A26: $^{1}$H NMR spectra (400 MHz, tol-$d_8$) of [Yb(OSi(OtBu)$_3$)$_4$K] 32-Yb at -30°C (bottom) and 25°C (top).**

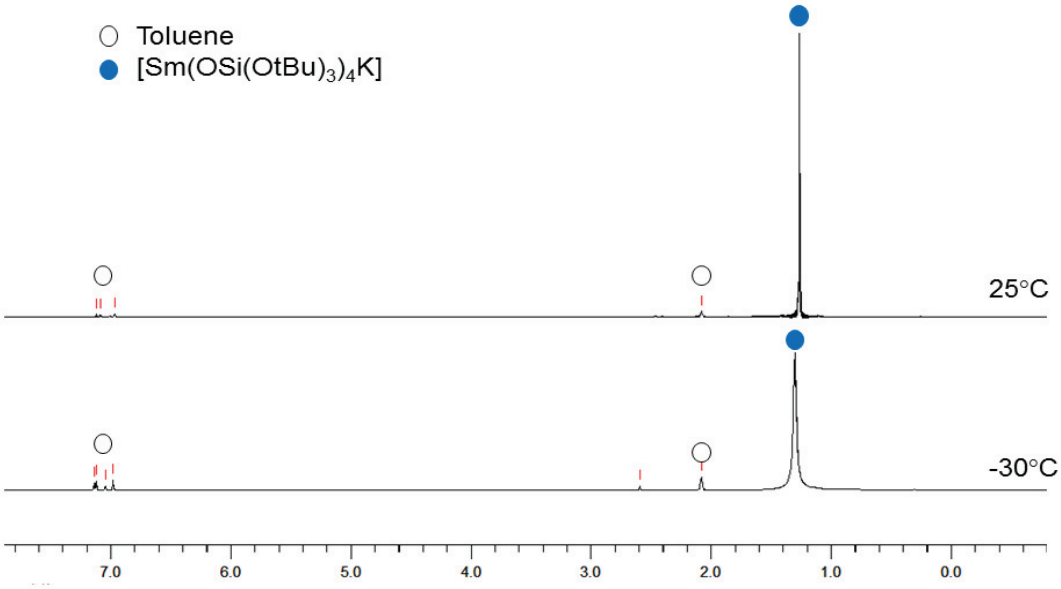


**Figure A27: $^{1}$H NMR spectra (400 MHz, tol-$d_8$) of [Sm(OSi(OtBu)$_3$)$_4$K] 32-Sm at -30°C (bottom) and 25°C (top).**

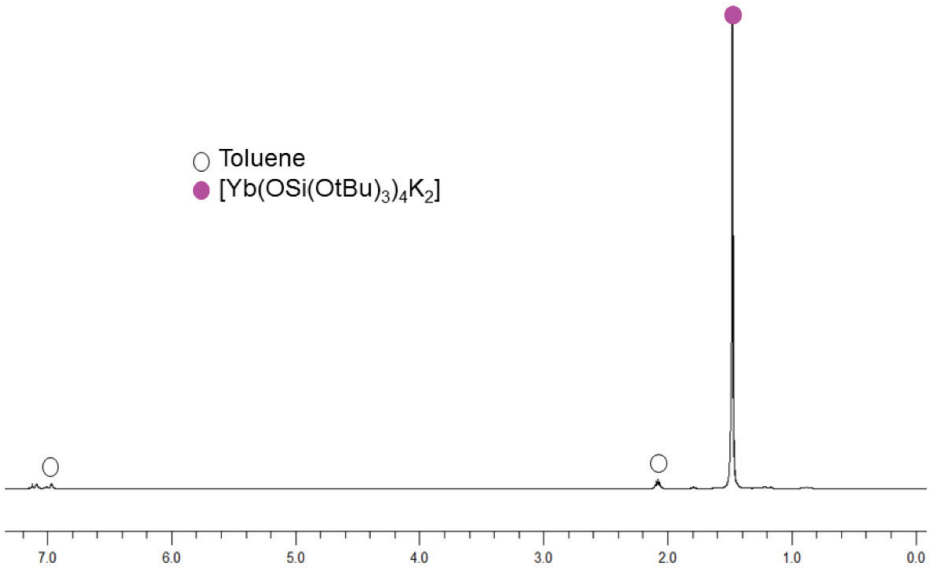


**Figure A28: $^{1}$H NMR spectrum (400 MHz, tol-$d_8$, 298K) of [Yb(OSi(OtBu)$_3$)$_4$K$_2$] 33-Yb.**

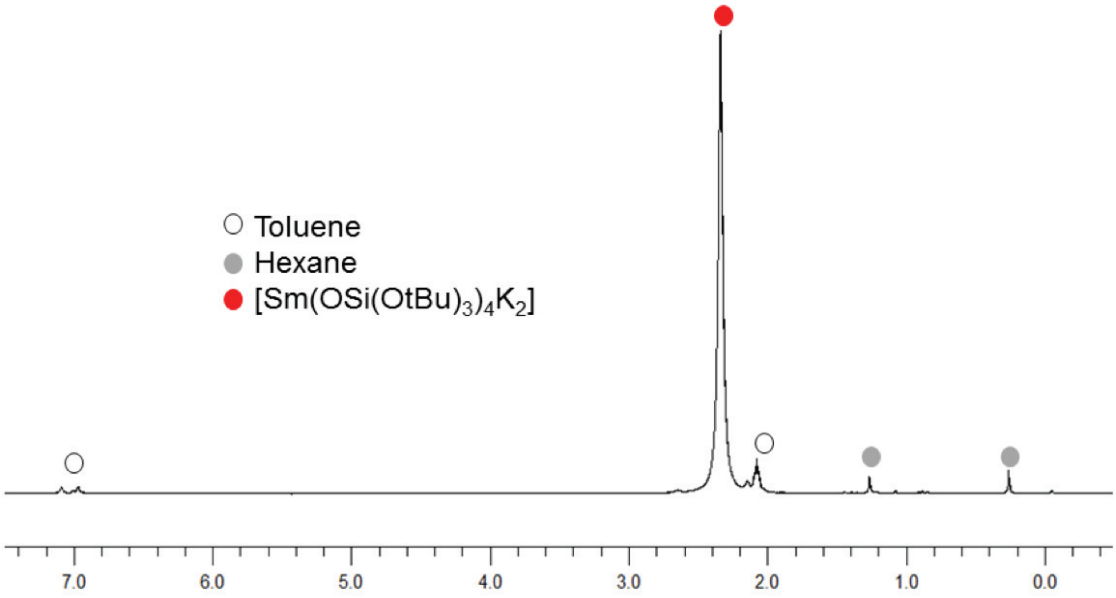


**Figure A29: $^{1}$H NMR spectrum (400 MHz, tol-$d_8$, 298K) of [Sm(OSi(OtBu)$_3$)$_4$K$_2$] 33-Sm.**

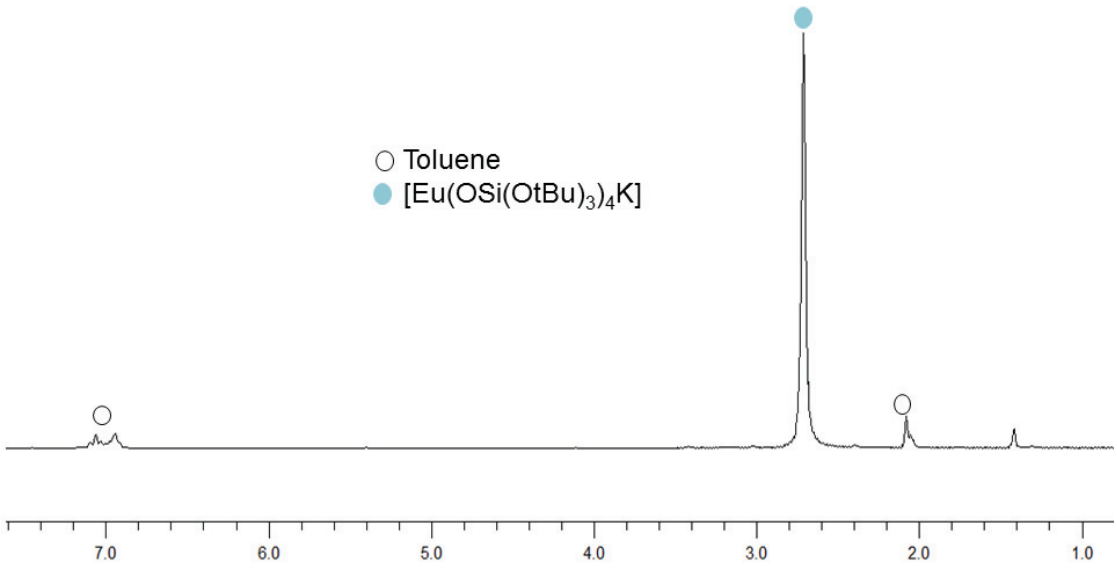


**Figure A30: $^{1}$H NMR spectrum (200 MHz, tol-$d_8$, 298K) of the supernatant of the reaction of [Eu(OSi(OtBu)$_3$)$_4$K$_2$] 33-Eu with 1eq of PhNNPh.**

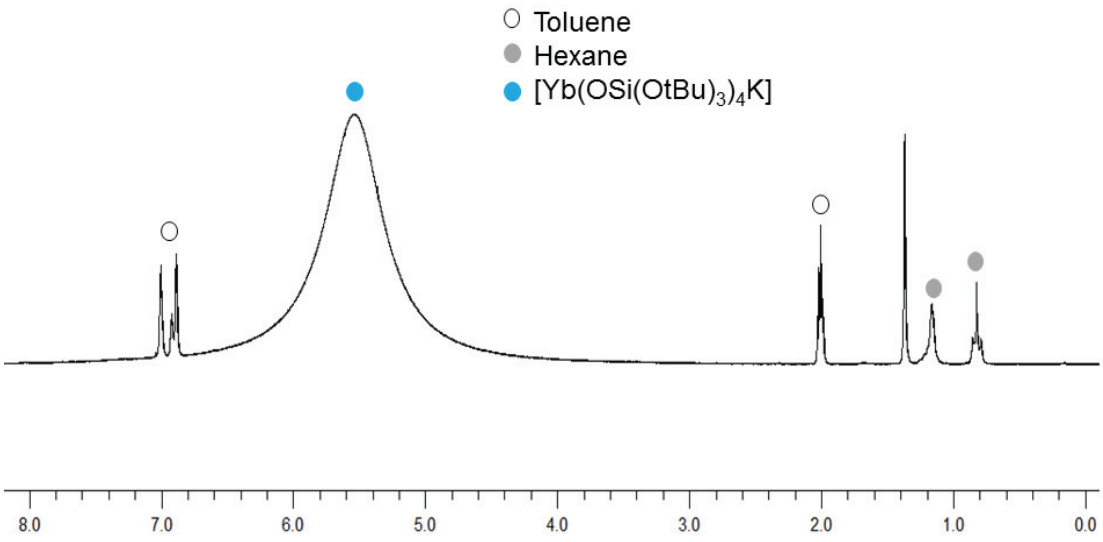


**Figure A31: In situ $^{1}$H NMR spectrum (200MHz, tol-$d_8$, 298K) after the addition of 1eq of $CS_2$ to $[Yb(OSi(OtBu)_3)_4K_2]$ 33-Yb, after 1 hour.**

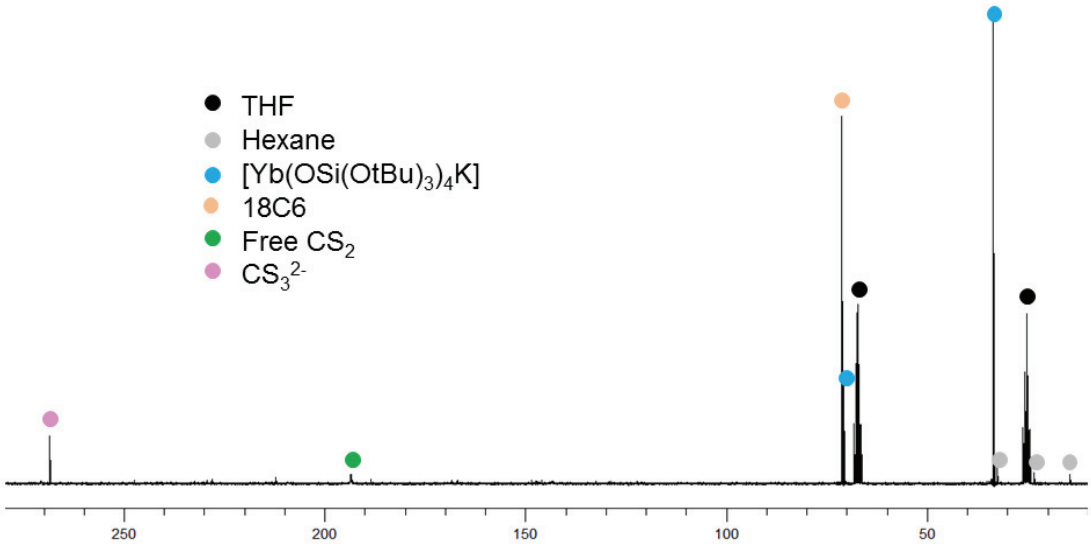


**Figure A32: In situ $^{13}$C NMR spectrum (50 MHz, THF-$d_8$, 298K) of the crude mixture reaction after the addition of 1eq of $^{13}CS_2$ to $[Yb(OSi(OtBu)_3)_4K_2]$ + 2eq 18C6.**

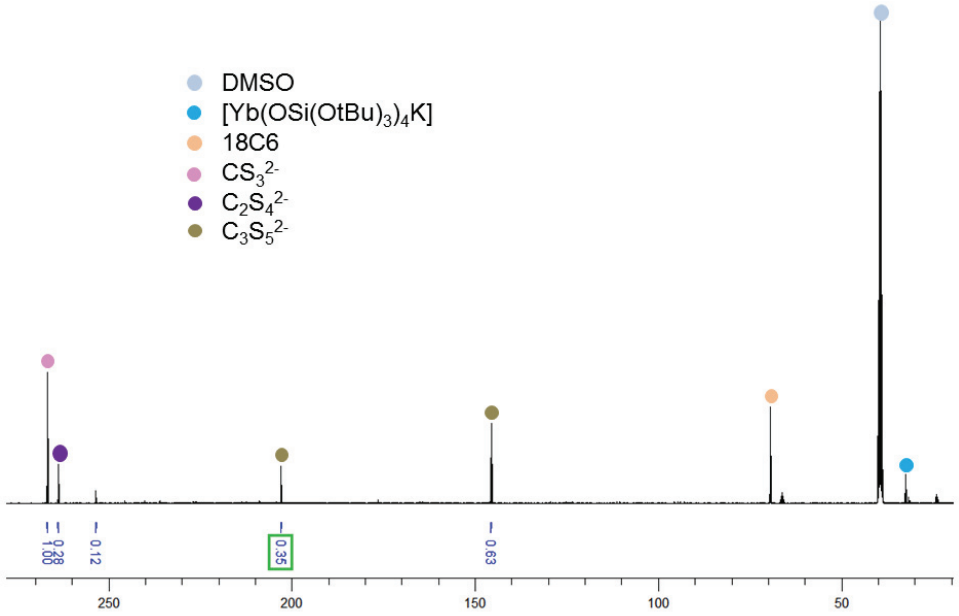


**Figure A33: Quantitative $^{13}C$ NMR spectrum (100MHz, DMSO-$d_6$, 298K) of the crude mixture reaction after the addition of 1eq of $^{13}CS_2$ to [$Yb(OSi(OtBu)_3)_4K_2$] + 2eq 18C6 after the removal of THF.**

.

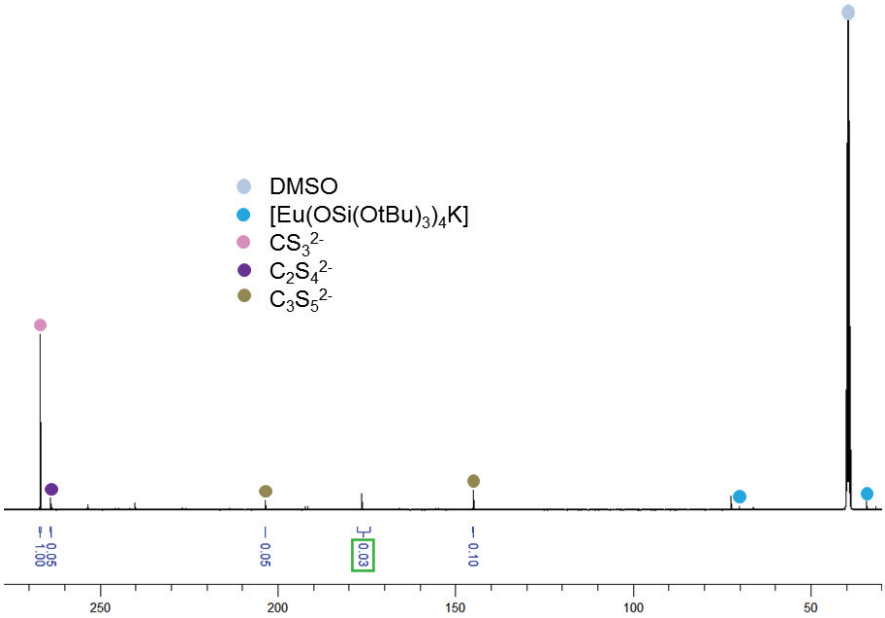


**Figure A34: Quantitative $^{13}C$ NMR spectrum (100MHz, DMSO-$d_6$, 298K) of the crude mixture reaction after the addition of 1eq of $^{13}CS_2$ to [$Eu(OSi(OtBu)_3)_4K_2$] 33-Eu after the removal of THF.**

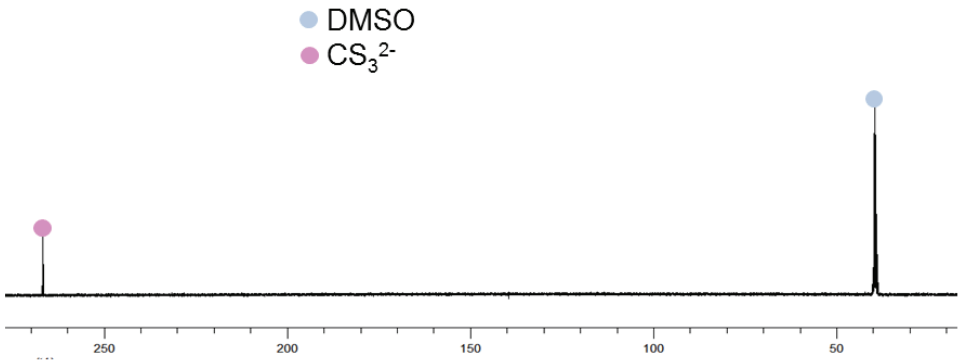


**Figure A35: $^{13}$C NMR spectrum (100MHz, DMSO-$d_6$, 298K) of the crystals of $[(K_2CS_3)_5(DMSO)_{12}]_n$.**

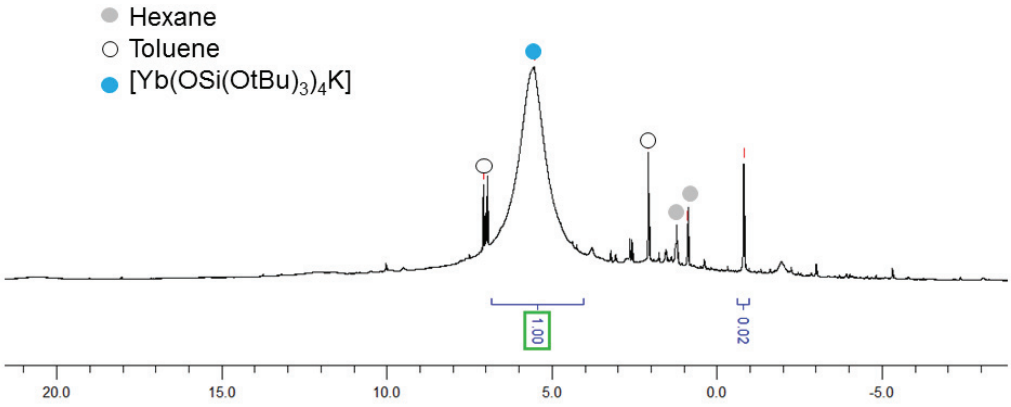


**Figure A36: In situ $^1$H NMR spectrum (400 MHz, tol-$d_8$, 298K) after addition of $CO_2$ to $[Yb(OSi(OtBu)_3)_4K_2]$ 33-Yb.**

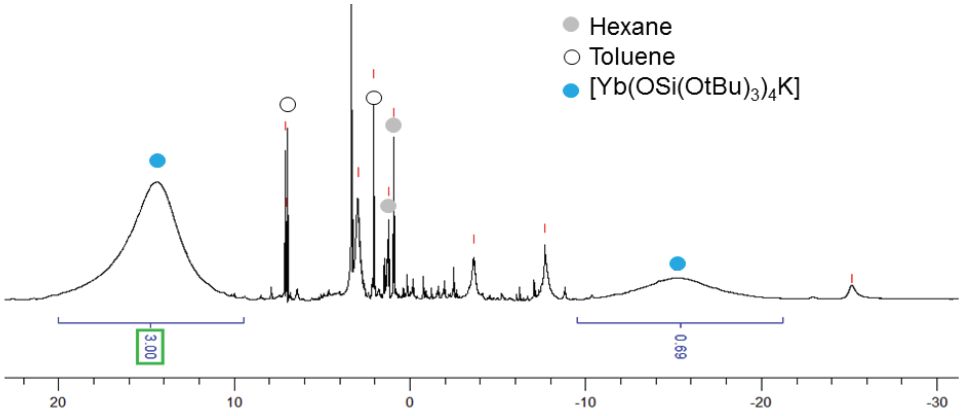


**Figure A37: In situ $^1$H NMR spectrum (400 MHz, tol-$d_8$) after addition of $CO_2$ to $[Yb(OSi(OtBu)_3)_4K_2]$ 33-Yb at -40°C.**

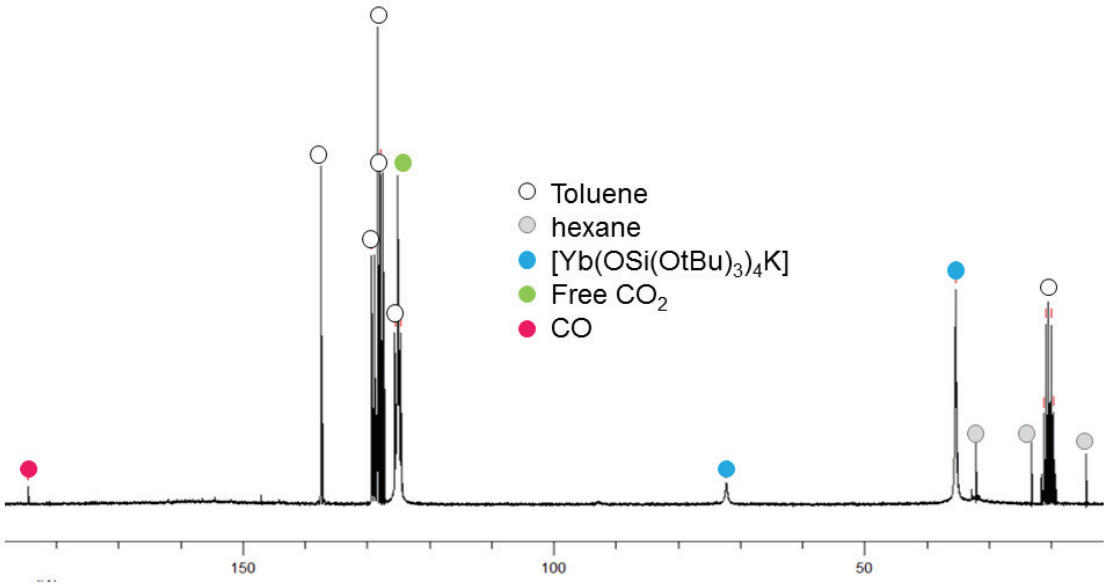


**Figure A38: $^{13}C$ NMR spectrum (50MHz, tol-$d_8$, 298K) of the crude mixture reduction of $^{13}CO_2$ by $[Yb(OSi(OtBu)_3)_4K_2]$ 33-Yb.**

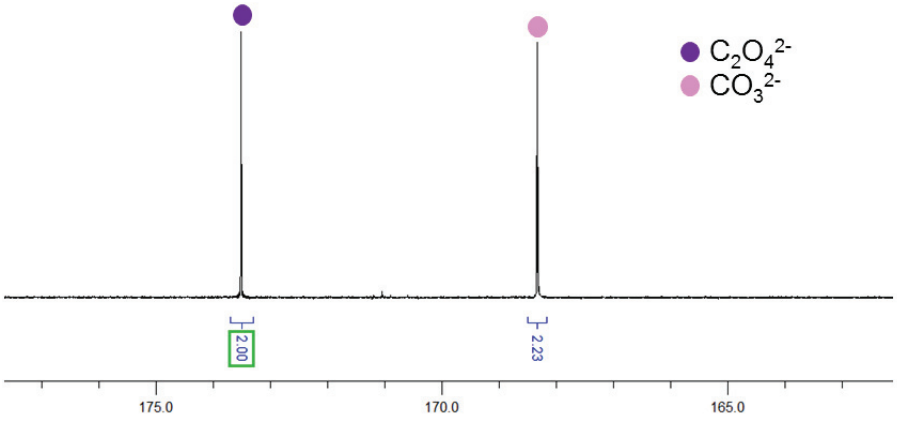


**Figure A39: Quantitative $^{13}C$ NMR spectrum (100MHz, $D_2O$, 298K) of the crude mixture reduction of $^{13}CO_2$ by $[Yb(OSi(OtBu)_3)_4K_2]$ 33-Yb after removal of toluene (158mM concentration).**

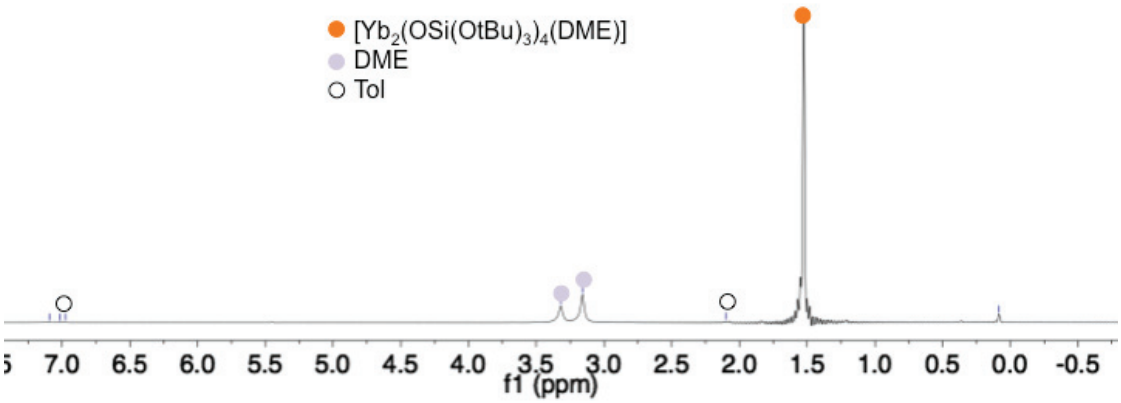


**Figure A40: $^{1}$H NMR spectrum (200MHz, tol-$d_8$, 298K) of the 1:2 reaction mixture of [Yb(HMDS)$_2$] and HOSi(OtBu)$_3$.**

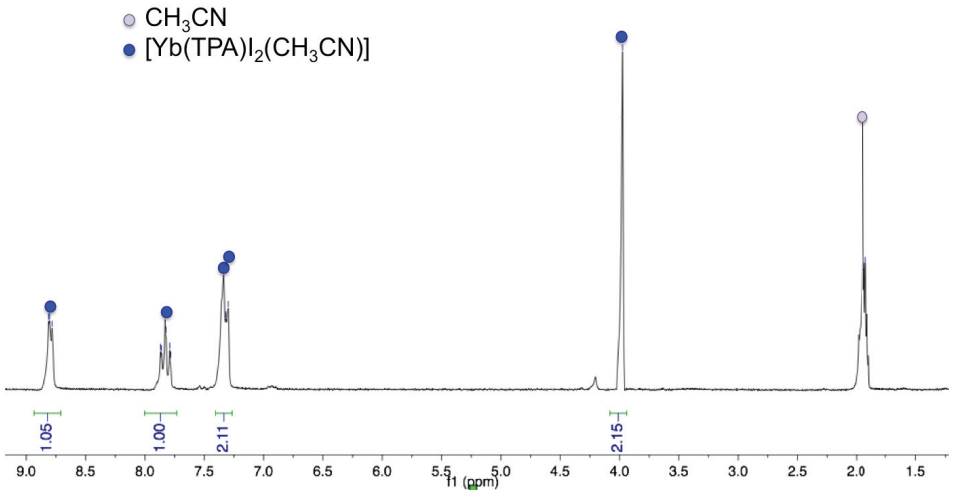


**Figure A41: $^{1}$H NMR spectrum (200 MHz, $CD_3CN$, 298K) of [Yb(TPA)$I_2$($CH_3CN$)] 36.**

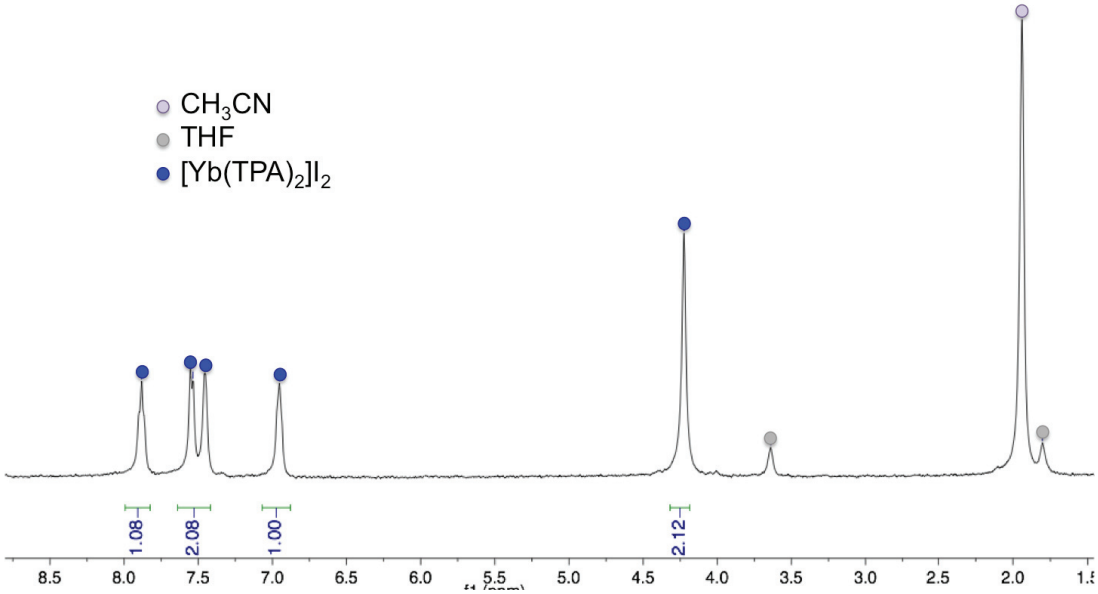


**Figure A42: $^{1}$H NMR spectrum (200 MHz, $CD_3CN$, 298K) of $[Yb(TPA)_2]I_2$ 38-Yb.**

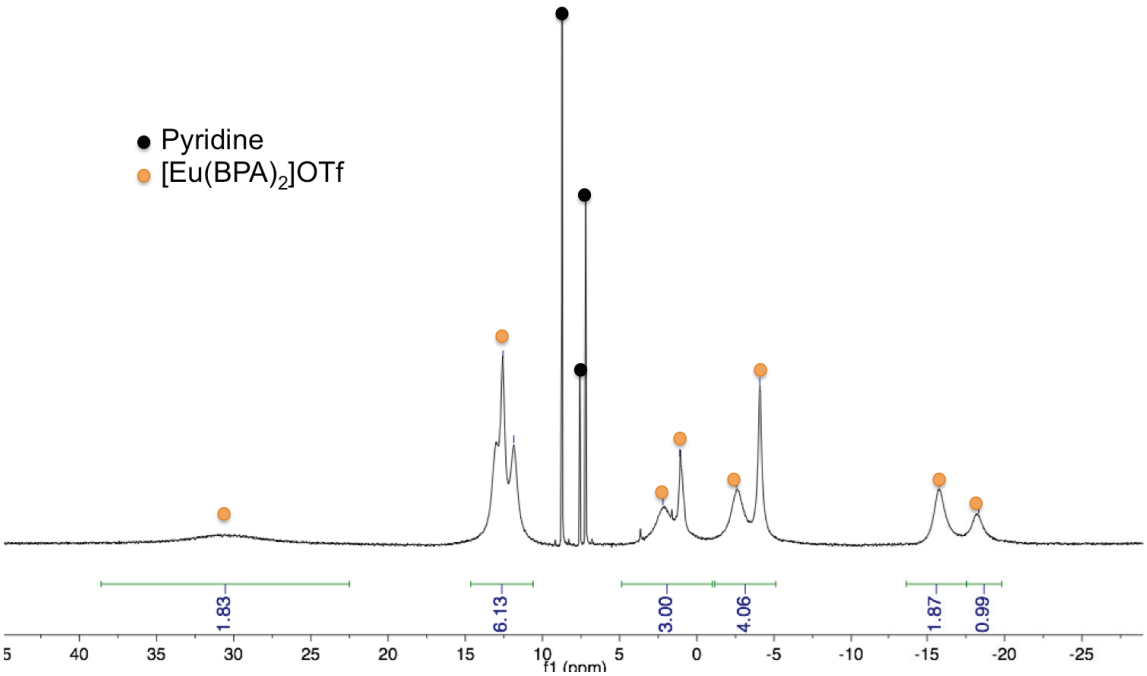


**Figure A43: $^{1}$H NMR spectrum (200 MHz, py-$d_5$, 298K) of $[Eu(BPA)_2]OTf$ 39.**

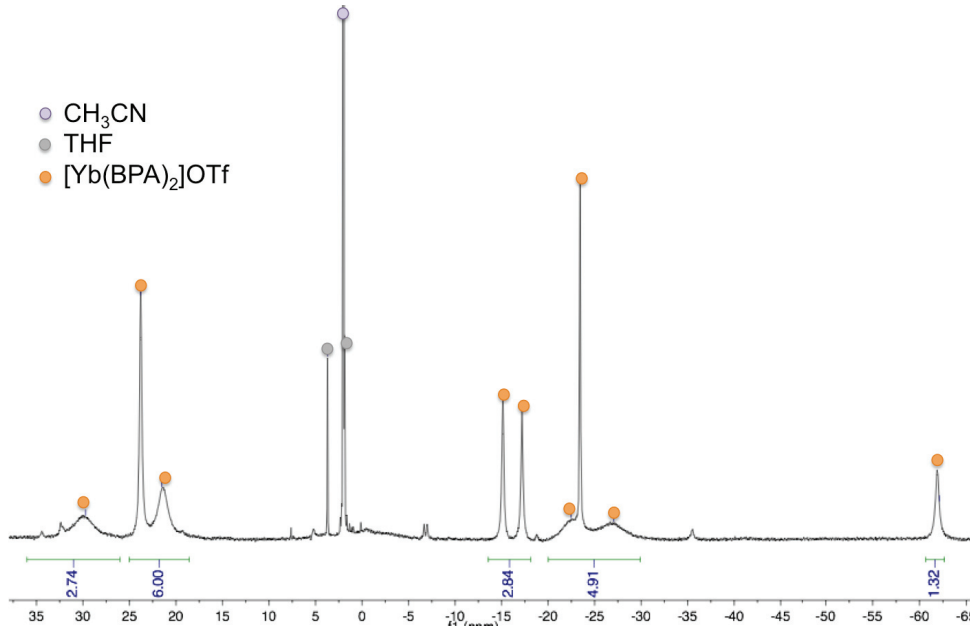


**Figure A44: $^{1}$H NMR spectrum (200 MHz, $CD_3CN$, 298K) of the 1:2 reaction mixture of $Yb(OTf)_3$ and KBPA.**

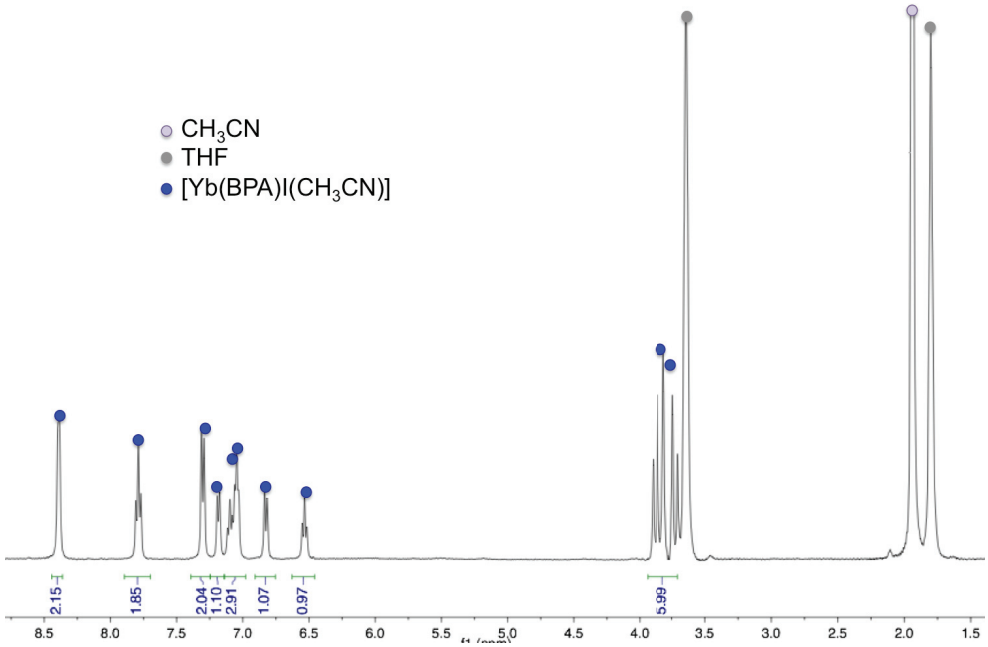


**Figure A45: $^{1}$H NMR spectrum (200 MHz, $CD_3CN$, 298K) of the 1:1 reaction mixture of $YbI_2$ and KBPA.**

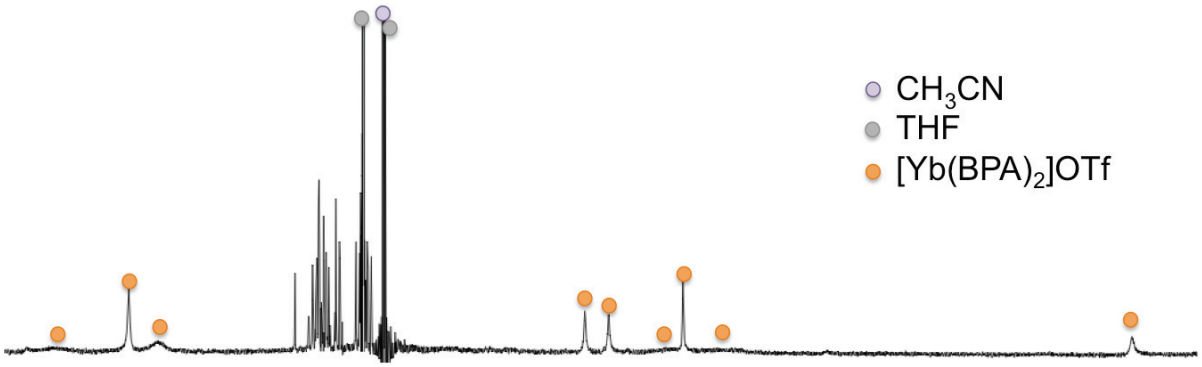


**Figure A46: $^1$H NMR spectrum (200 MHz, $CD_3CN$, 298K) of the 1:2 reaction mixture of $YbI_2$ and KBPA.**

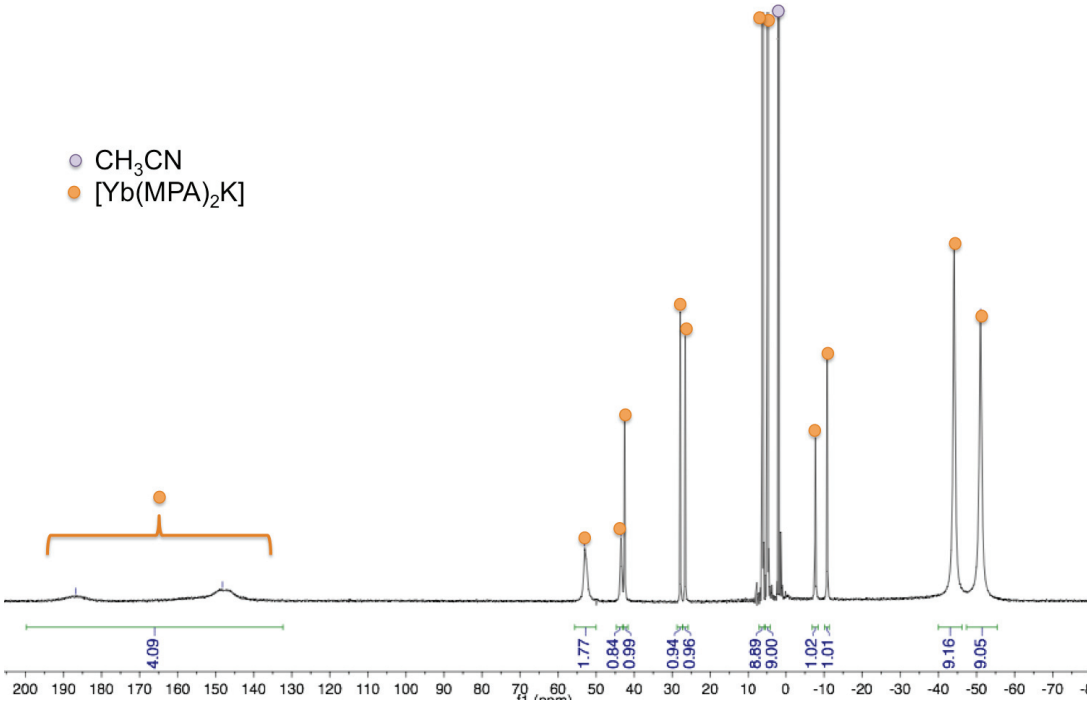


**Figure A47: $^1$H NMR spectrum (200 MHz, $CD_3CN$, 298K) of $[Yb(MPA)_2K]$ 43.**

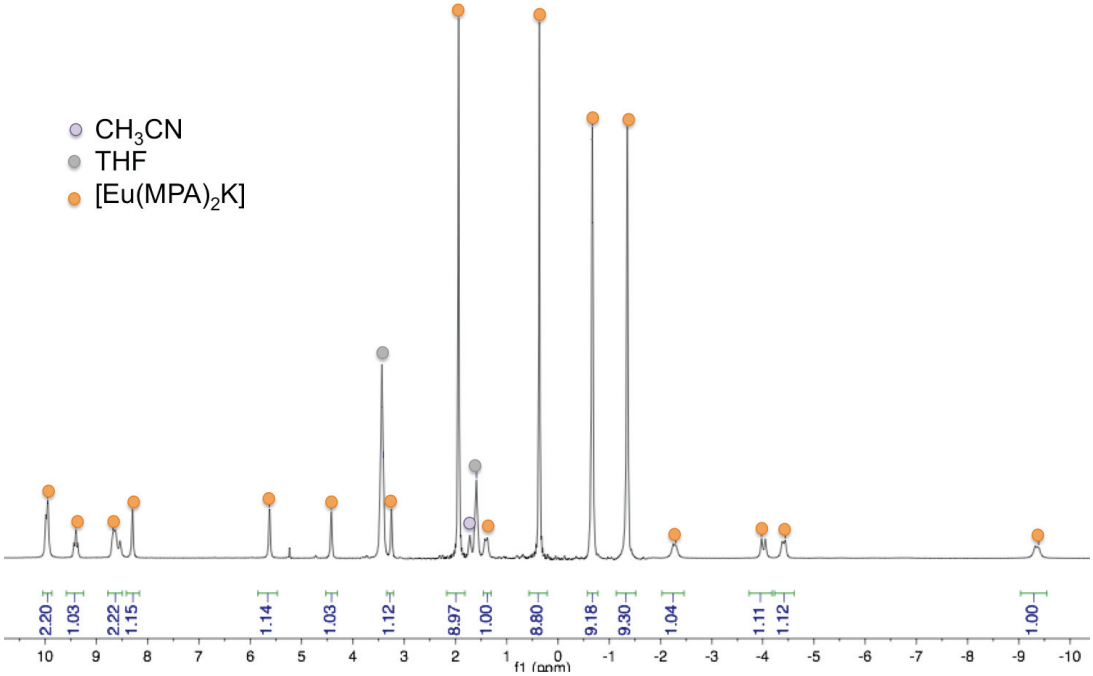


**Figure A48: $^{1}$H NMR spectrum (200 MHz, THF-$d_8$, 298K) of the 1:2 reaction mixture of $Eu(OTf)_3$ and $K_2MPA$.**

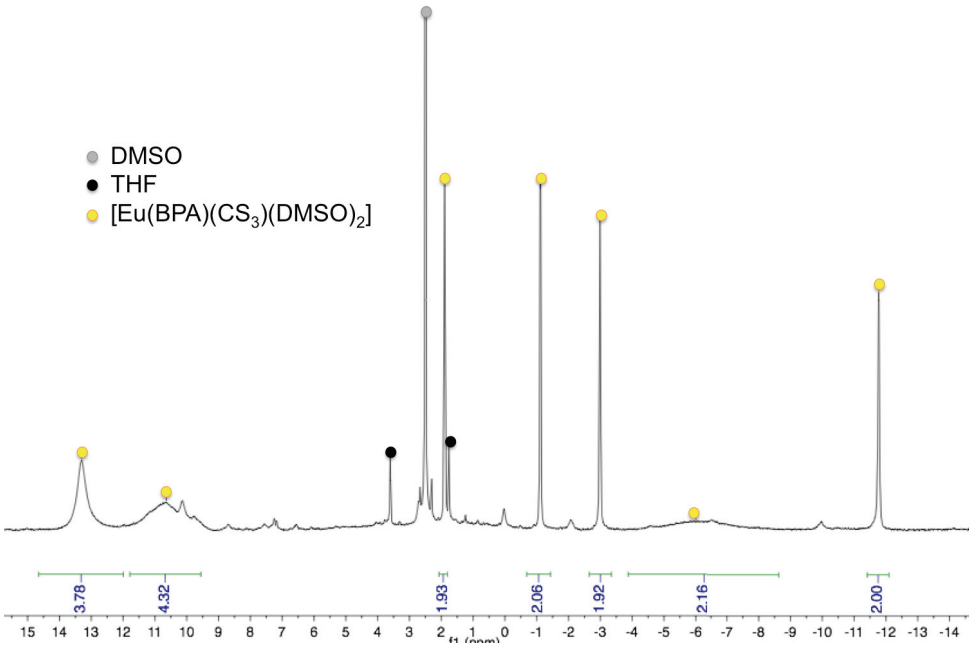


**Figure A49: $^{1}$H NMR spectrum (400 MHz, DMSO-$d_6$, 298K) of $[Eu(BPA)(CS_3)(DMSO)_2]$ 44.**

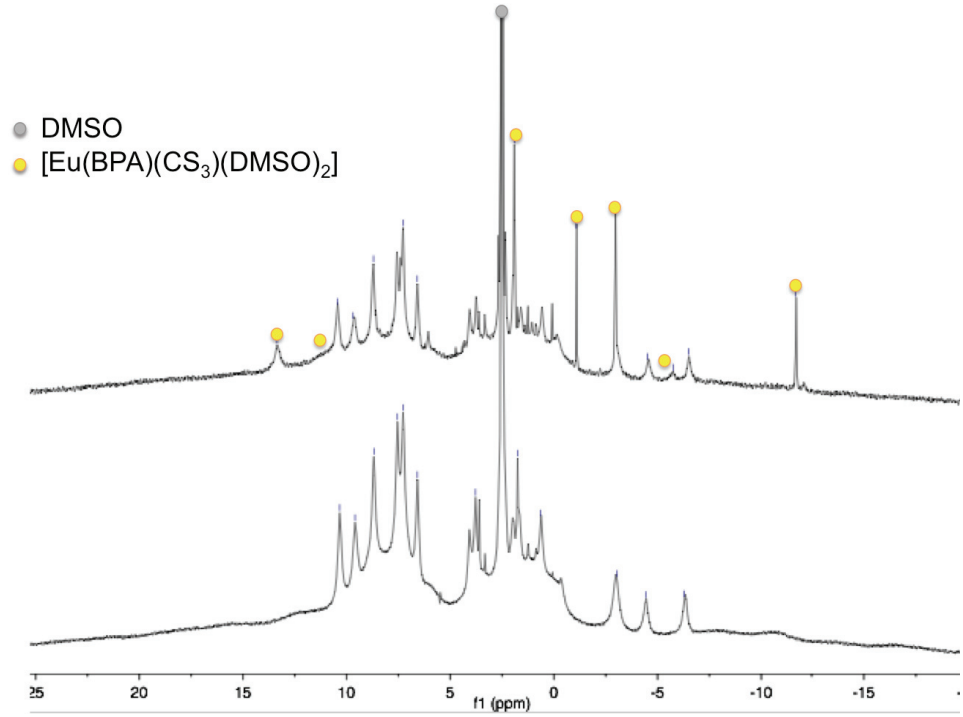


**Figure A50: $^{1}$H NMR spectra (400 MHz, DMSO-$d_6$, 298K) of the 1:2 reaction mixture of $EuI_2$ and KBPA after addition of 1eq of $CS_2$ (top) and the 1:3 reaction mixture of $Eu(OTf)_3$ and KBPA (bottom).**

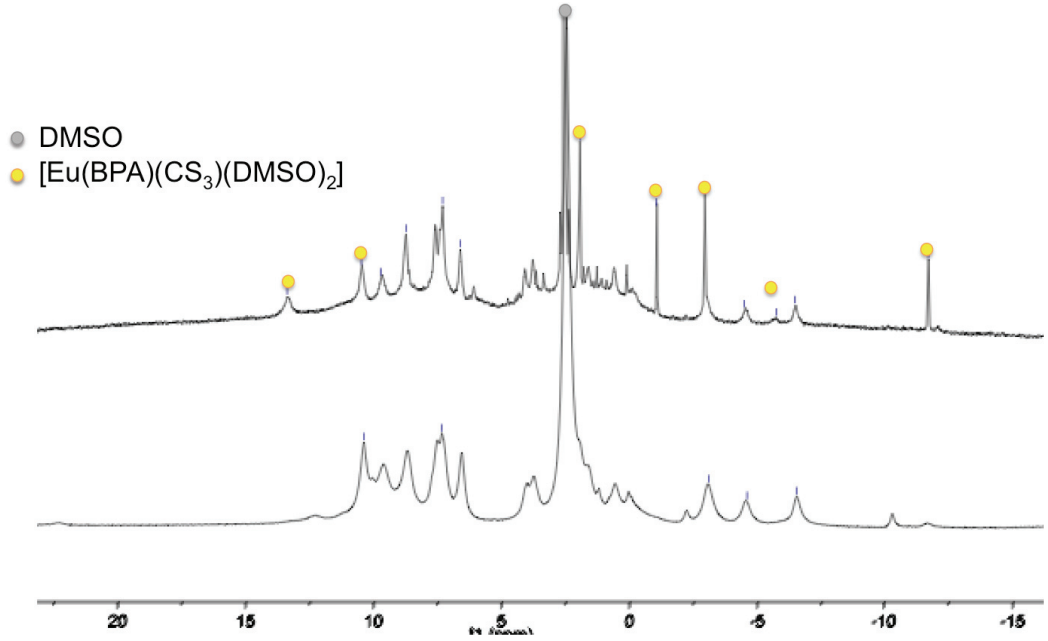


**Figure A51: $^{1}$H NMR spectra (400 MHz, DMSO-$d_6$, 298K) of the 1:2 (top) and 1:1 (bottom) reaction mixture of $EuI_2$ and KBPA after addition of 1eq of $CS_2$.**

# Electrochemistry

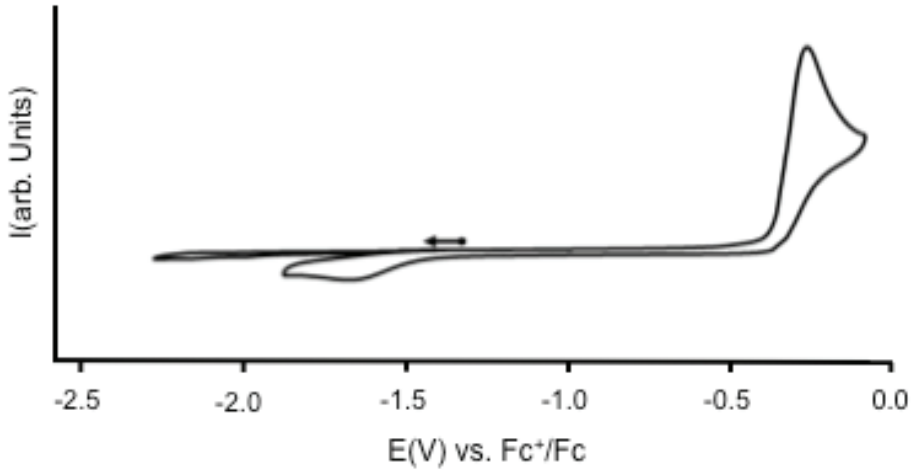


**Figure A52: Cyclic voltammogram for K-$^{Me}$naphtquinolen in ~0.1 M [$Bu_4N$][$PF_6$] pyridine solution at 100 mV.$s^{-1}$ scan-rate. No reduction event is observed when the voltammogram is swept initially from -1.4 V to the negative direction. An irreversible oxidation process attributed to the oxidation of the phenol moiety occurs at E = -0.26 V and is associated to the irreversible reduction occurring at -1.67 V.**

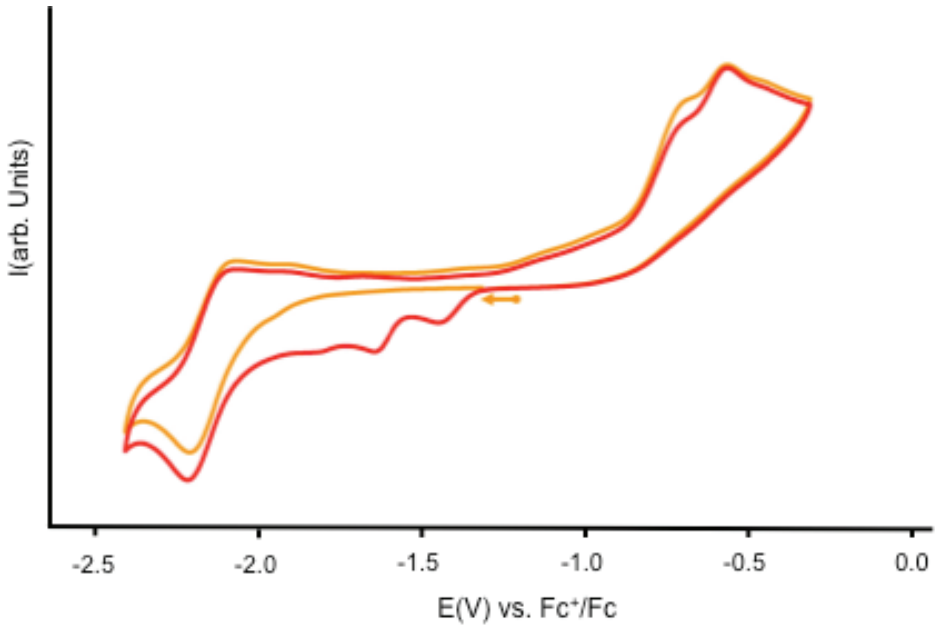


**Figure A53: Cyclic voltammograms of [U(bis-$^{Me}$naphtquinolen)]$_2$, 2 in ~0.1 M [$Bu_4N$][$PF_6$] pyridine solution at 100 mV.$s^{-1}$ scan-rate. First scan: orange ; second scan : red.**

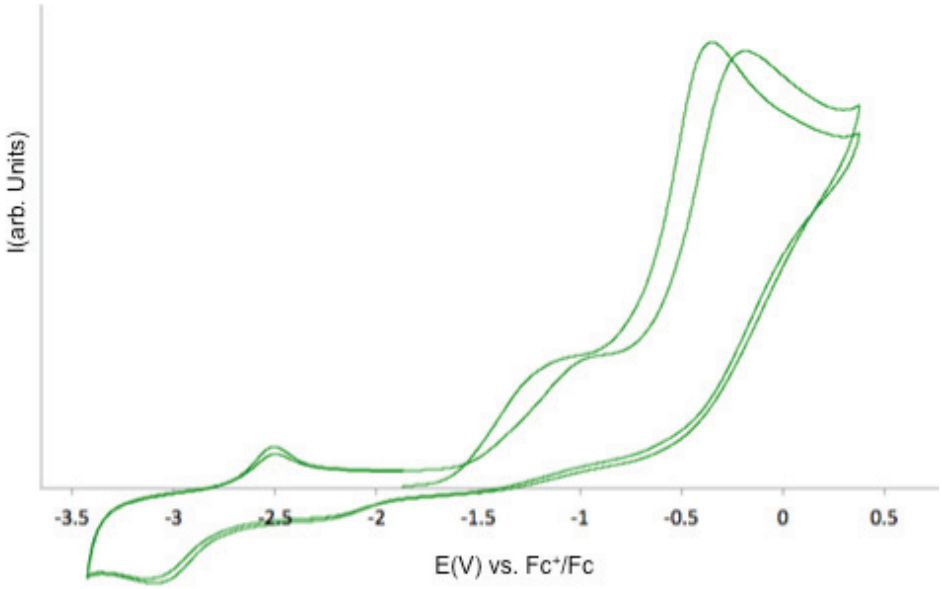


**Figure A54: Cyclic voltammograms of $[US(OSi(OtBu)_3)_4K_2]_2$, 16 in ~0.1 M $[Bu_4N][PF_6]$ THF solution at 100 $mV.s^{-1}$ scan-rate**

# Curriculum Vitae

# Julie Andrez

9 rue Marquian
38100 Grenoble, France
andrez.julie@gmail.com
☎ : +33 6 21 53 51 96

- Chemical engineer (ENSIACET) & PhD in chemistry (EPFL)
- Inorganic and green chemistry specialist
- Skills in project management and leadership

LinkedIn Profile here

## EDUCATION

2012 – oct. 2016 : **PhD** in chemistry at Ecole Polytechnique Fédérale de Lausanne (**EPFL**, Switzerland) in association with Commissariat à l'Energie Atomique (**CEA Grenoble**, France).

2012 : **Master's Degree** "Fundamental and applied chemistry" undertaken concurrently with my engineering degree. Université Paul Sabatier, Toulouse, France.

2009 – 2012 : **Chemical engineering degree**, specializing in **green chemistry**.
National Polytechnic Institute of Chemistry, Industrial and Chemical Engineering, and Technology (INP-**ENSIACET**), Chemistry Department, Toulouse, France.

2007 – 2009 : **Preparatory classes** for entrance exams into national engineering schools.
**Physics-Chemistry** section, Lycée Michel de Montaigne, Bordeaux, France.

2007 : **Scientific Baccalauréat** with a focus on **Physics-Chemistry** graduated with "very high honours".
Lycée Grand Air, Arcachon, France.

## PROFESSIONAL EXPERIENCE

2012 – Oct. 2016 : **PhD in Chemistry, CEA** Grenoble (France) and then the **laboratory moved to the EPFL** (Switzerland).

- **Management of a research project** aiming to reuse nuclear waste to prepare complexes, ideally catalysts, able to transform carbon dioxide ($CO_2$) into valuable products.
- **Management** and training of new PhD and Msc students.
- **Communication**: Oral presentations of my results to assemblies of experts.
- **Supervision of the equipment transfer:**
  - Packaging of the compounds.
  - Specialized transport organisation for radioactive compounds.
  - Ordering of new equipment.
  - Liaising with contractors.
  - Maintenance of the laboratory equipment.

Mars à Août 2012 : **Master's-degree internship (M2)**, CEA Grenoble.
The subject of this internship was similar to the one of my PhD thesis and it was a perfect introduction to my PhD studies.

Jui. et Sept. 2011 : **2nd year Internship (M1)**, **University of Siena** (Italy).
This internship, done in the Applied Pharmaceutical Chemistry Department, focused on an **innovative synthetic strategy** (organocatalysis) for the preparation of **drug active principles** (statin-like compounds).

## PUBLICATIONS

- J. Andrez, J. Pécaut, R. Scopelliti, C. E. Kefalidis, L. Maron, K. Meyer and M. Mazzanti « Synthesis and reactivity of a terminal uranium(IV) sulfide supported by siloxide ligands», *Chem. Sci.*, **2016**, *7*, 5846–5856.

- M. W. Rosenzweig, A. Scheurer, F. Heinemann, C. A. Lamsfus, L. Maron, J. Andrez, M. Mazzanti and K. Meyer « Uranium(IV) Terminal Hydrosulfido and Sulfido Complexes : The Nature of the Uranium-Sulfur Bond», *Chem. Sci.*, **2016**, *7*, 5857–5866.

- J. Andrez, G. Bozoklu, G. Nocton, J. Pécaut, R. Scopelliti, L. Dubois and M. Mazzanti « Lanthanide(II) Complexes Supported by N,O-Donor Tripodal Ligands : Synthesis, Structure, and Ligand-Dependent RedoxBehavior » *Chem. Eur. J.* **2015**, *21*, 15188 –15200. **Inside front cover**.


- C. Camp, O. Cooper, J. Andrez, J. Pécaut and M. Mazzanti « $CS_2$ activation at uranium(III) siloxide ate complexes: the effect of a Lewis acidic site » *Dalton Trans*., **2015**, *44*, 2650–2656.

- J. Andrez, J. Pécaut, P.-A. Bayle, and M. Mazzanti « Tuning Lanthanide Reactivity Towards Small Molecules with Electron- Rich Siloxide Ligands » *Angew. Chem. Int. Ed.* **2014**, *53*, 10448 –10452.

- C. Camp, J. Andrez, J. Pécaut, and M. Mazzanti « Synthesis of Electron-Rich Uranium(IV) Complexes Supported by Tridentate Schiff Base Ligands and Their Multi-Electron Redox Chemistry » *Inorg. Chem.*, **2013**, *52* (12), 7078–7086.

## TECHNICAL SKILLS

**Practical work and safety**:

- Rigour and meticulousness needed for the manipulation of radioactive, toxic and highly reactive compounds.
- Method and anticipation essential for syntheses under inert atmosphere (glovebox, Schlenk techniques).
- Work on system under pressure, gazes manipulations.
- Experience in enantioselective organic synthesis.
- Safety linked to radiological risks.

**Characterisation techniques**:

X-Ray Diffraction (XRD), electrochemistry, nuclear magnetic resonance spectroscopy (NMR), electron paramagnetic resonance spectroscopy (EPR), Fourier transform infrared spectroscopy (FTIR), and electrospray ionisation mass spectrometry (ESI-MS), polarimetry.

## LANGUAGES

- French, mother tongue.
- English, high level.

# Publications

Inorganic Chemistry

Article

pubs.acs.org/IC

# Synthesis of Electron-Rich Uranium(IV) Complexes Supported by Tridentate Schiff Base Ligands and Their Multi-Electron Redox Chemistry

Clément Camp, Julie Andrez, Jacques Pécaut, and Marinella Mazzanti*

Laboratoire de Reconnaissance Ionique et Chimie de Coordination, SCIB, UMR-E CEA/UJF-Grenoble 1, INAC, CEA-Grenoble, 17 rue des Martyrs, Grenoble, F-38054, France

Supporting Information

**ABSTRACT:** The synthesis, structure, and reactivity of a new complex of U(IV) with the tridentate Schiff base ligand Menaphtquinolen are reported. The reduction of the bis-ligand complexes $[UX_2(^{Me}naphtquinolen)_2]$ (X = Cl, (**1-Cl**) ; I (**1-I**)) with potassium metal affords the U(IV) complex of the new tetranionic hexadentate ligand $\mu$-bis-$^{Me}$naphtquinolen formed through the intramolecular reductive coupling of the imino groups of each $^{Me}$naphtquinolen unit. The solid state structure of the $[U(\mu\text{-bis-}^{Me}naphtquinolen)]_2$ dimer **2** isolated from toluene confirms the presence of a U(IV) complex of the reduced ligand. Reactivity studies with molecular oxygen and 9,10-phenanthrenequinone show that complex **2** can act as a multielectron reducing agent releasing two electrons through the cleavage of the C−C bond to restore the original imino function of the ligand. In the resulting U(IV) and U(VI) complexes [U(9,10-phenanthrenediol)$(^{Me}naphtquinolen)_2$], **3**, and $[UO_2(^{Me}naphtquinolen)_2]$, **4**, the restored tridentate Schiff base allows for the coordination of the reduced substrate to the metal. Electrochemical studies of complex **2** show the presence of irreversible ligand centered reduction processes and of a reversible U(IV)/U(III) couple.

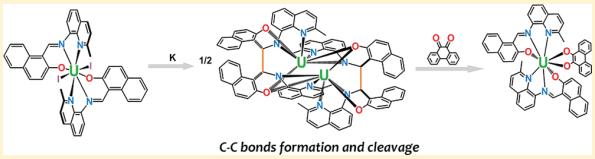


## INTRODUCTION

Complexes of low valent uranium are attracting increasing interest because they can promote the activation and functionalization of small molecules[1−3] such as CO,[4−9] $CO_2$,[1,10−17] $N_2$[18−20] and azides[21−24] in mild conditions. Because of the unique coordination and bonding properties of uranium, its compounds could also provide an attractive alternative to transition metals for the catalytic transformation of small molecules.[4,7,12,25,26]

However, metal based multielectron processes remain uncommon in uranium chemistry[2,27,28] especially in comparison with the d-block metals, the chemistry of low-valent uranium being dominated by single-electron transfers. In this context, the association of uranium to a noninnocent ligand acting as an independent electron reservoir at the same molecule represents an attractive alternative that should render multielectron reactivity possible while stabilizing highly reactive formally low-valent oxidation states. Accordingly, in recent years ligand based redox processes have been increasingly combined with metal centered redox transfers to promote multielectron reductions in uranium complexes.[29−40] In most of these systems the electrons stored on the coordinated aromatic ligands become available to oxidizing substrates either through metal mediated processes or by a sterically induced reduction mechanism.

An alternative ligand-based mechanism for storing and transferring electrons in metal complexes involves the reversible formation and cleavage of C−C bonds in tetradentate Schiff base ligands that can function as two electron reservoir in redox reactions.[41−45]

Multidentate Schiff bases have been extensively used as supporting ligands in the chemistry of d-block metals. In uranium chemistry the use of Schiff base ligands has been mostly limited to the complexation of $UO_2^{2+}$.[46,47] Recently our group and others have shown that tetradentate and pentadentate Schiff bases are also effective ligands for the stabilization of the elusive pentavalent uranyl.[48−55]

In contrast only very few examples of U(III)[56] and U(IV)[47,57−59] complexes of Schiff base ligands have been reported. Polynucleating hexadentate Schiff bases have been used to promote the formation of heteropolymetallic complexes of U(IV) with 3d metals which show interesting magnetic properties.[60] However, to the best of our knowledge, the study of the redox reactivity of U(IV) Schiff base complexes is limited to one example.[45] We have recently reported redox reactivity studies of U(IV) complexes of the tetradentate ligand salophen (salophen = *N,N′*-disalicylidene-*o*-phenylenediaminate) which demonstrate that the salophen ligand behaves as a redox-active ligand able to store and release up to 4 electrons through the reversible formation and cleavage of one or two C−C bonds.[45]

Here we report a new U(IV) complex supported by a redox-active tridentate Schiff-base ligand $^{Me}$naphtquinolen. The tridentate nature of the ligand was chosen to render available two coordination sites at the metal center which were not present in the previously reported salophen system. The presence of available coordination sites should allow the coordination of potential

**Received:** March 13, 2013
**Published:** June 4, 2013

   dx.doi.org/10.1021/ic4006218 | *Inorg. Chem.* 2013, 52, 7078−7086

substrates to the metal center leading to a better control of the reactivity. Notably, it might favor reaction pathways involving the metal-mediated inner-sphere transfer to the coordinate substrate of the electrons stored upon reduction in the C−C bond. We show that this Schiff base behaves as a redox active ligand when coordinated to U(IV) and that the reduction of the bis-ligand complex of U(IV) proceeds with the reductive coupling of the imino function of the ligand to afford a new U(IV) complex with two electrons stored in a C−C bond. The ligand-based multielectron redox activity of the system was confirmed by reactivity studies of the reduced system with different oxidizing substrates.

## EXPERIMENTAL SECTION

**General Considerations.** Unless otherwise noted, all manipulations were carried out at ambient temperature under an inert argon atmosphere using Schlenk techniques and an MBraun glovebox equipped with a purifier unit. The water and oxygen levels were always kept at less than 1 ppm. Glassware was dried overnight at 130 °C before use.

**$^1$H NMR Experiments.** were carried out using NMR tubes adapted with J. Young valves. $^1$H NMR spectra were recorded on Bruker 200 and 500 MHz and Varian Mercury 400 MHz spectrometers. NMR chemical shifts are reported in ppm with solvent as internal reference.

**UV−visible Spectra.** UV−vis measurements were carried out with a Varian Cary 50 Probe spectrophotometer in quartz cells (optical path lengths: 1 mm) adapted with Young valves.

**Elemental Analyses.** Elemental analyses were performed under argon by Analytische Laboratorien GMBH at Lindlar, Germany.

**Starting Materials.** Unless otherwise noted, reagents were purchased from commercial suppliers and used without further purification. The solvents were purchased from Aldrich or Eurisotop (deuterated solvents) in their anhydrous form, conditioned under argon and vacuum distilled from K/benzophenone (toluene, hexane, pyridine, and thf). All reagents were dried under high-vacuum for 7 days prior to use. 9,10-phenanthrenequinone was purified by recrystallization in toluene prior to use. Dry dioxygen was prepared upon storing an $O_2$ atmosphere upon $P_4O_{10}$ for one week prior to use. Depleted uranium turnings were purchased from the "Société Industrielle du Combustible Nucléaire" of Annecy (France). $UCl_4$[61] and $UI_4(OEt_2)_2$[62] were prepared according to the published procedures.

***Caution!*** *Depleted uranium (primary isotope $^{238}U$) is a weak α-emitter (4.197 MeV) with a half-life of 4.47 × $10^9$ years. Manipulations and reactions should be carried out in monitored fume hoods or in an inert atmosphere glovebox in a radiation laboratory equipped with α- and β-counting equipment.*

**H-$^{Me}$naphtquinolen.** The ligand was prepared by a modified literature procedure.[63,64] A solution of 2-methylquinolin-8-amine (1.0 g, 6.32 mmol, 1 equiv) and 3-hydroxy-2-naphtaldehyde (1.1 g, 6.39 mmol, 1.01 equiv) in 30 mL of anhydrous toluene was stirred in a Dean−Stark setup at 110 °C during 2 days. Then the solvent was removed under vacuum giving an orange-brown solid. This solid was suspended in 100 mL of cyclohexane and heated to reflux. Toluene was added dropwise until most solid was soluble, and the temperature was raised to maintain the reflux. A hot filtration was carried out to remove the black insoluble impurities, and the mixture was cooled down to room temperature, affording red crystals that were filtered and dried under vacuum to give H-$^{Me}$naphtquinolen (1.38 g, 4.42 mmol, 70% yield).

$^1$H NMR (200 MHz, CDCl3, 298 K): $\delta$ = 15.8 (br s, 1H, OH), 9.3 (d, 1H), 8.1 (d, 1H), 8.0 (d, 1H), 7.7−7.4 (m, 7H), 7.3−7.2 (m, 1H), 6.9 (d, 1H), 2.9 (s, 3H, $CH_3$). $^{13}$C NMR (200 MHz, CDCl3, 298 K): $\delta$ = 182.3 (C═N), 159.3 ($C_{aro}$), 145.9 ($C_{aro}$), 139.5 ($C_{aro}$), 139.3 ($C_{aro}$), 136.6 ($C_{aro}$), 136.0 ($C_{aro}$), 134.5 ($C_{aro}$), 129.5 ($C_{aro}$), 128.4 ($C_{aro}$), 127.2 ($C_{aro}$), 126.9 ($C_{aro}$), 126.7 ($C_{aro}$), 125.7 ($C_{aro}$), 124.1 ($C_{aro}$), 123.6 ($C_{aro}$), 122.3 ($C_{aro}$), 118.4 ($C_{aro}$), 113.2 ($C_{aro}$), 8.0 ($C_{aro}$), 25.9 ($CH_3$). ES-MS: $m/z$ = 313.2 [M+H$^+$].

**K-$^{Me}$naphtquinolen.** To a stirring solution of H-$^{Me}$naphtquinolen (1.2 g, 3.84 mmol, 1 equiv) in 30 mL of anhydrous tetrahydrofuran (THF) was added portion wise potassium hydride (0.15 g, 3.84 mmol, 1 equiv). The solution turned from deep orange to deep red. After 12 h stirring, an orange solid deposited. This solid was filtered and dried under vacuum for 5 h to give K-$^{Me}$naphtquinolen (0.88 g, 2.51 mmol, 65% yield).

$^1$H NMR (200 MHz, py-$d_5$, 298 K): $\delta$ = 9.7 (s, 1H, HC═N), 8.6 (d, 1H), 8.0 (d, 1H), 7.7 (m, 2H), 7.5−7.7 (m, 3H), 7.3−7.0 (m, 4H), 2.5 (s, 3H, $CH_3$).

**[$UCl_2$($^{Me}$naphtquinolen)$_2$], 1-Cl.** A solution of K-$^{Me}$naphtquinolen (92.3 mg, 0.263 mmol, 2 equiv) in THF (10 mL) was added to $UCl_4$ (50.0 mg, 0.132 mmol, 1 equiv), and the reaction mixture was stirred at room temperature overnight, affording an orange suspension. The mixture was filtered to remove KCl, the THF volume of the filtrate was reduced to 2 mL, and the solution was layered with hexane. The resulting orange precipitate was filtered and dried under vacuum to afford an orange solid (89.0 mg, 0.096 mmol, 72% yield). $^1$H NMR (200 MHz, THF-$d_8$, 298 K): $\delta$ = 25.7 (s, 2H), 19.4 (d, 2H), 13.0 (d, 2H), 11.8 (d, 2H), 10.1 (t, 2H), 9.7 (t, 2H), 9.5 (m, 2H), 5.6 (s, 6H), 1.0 (d, 2H)-0.4 (t, 2H), −0.8 (m, 2H), −3.0 (d, 2H), −6.1 (s, 2H). Anal. Calcd for [$UCl_2$($^{Me}$naphtquinolen)$_2$] $C_{42}H_{30}Cl_2N_4O_2U$: C, 54.15; H, 3.25; N, 6.01. Found: C, 54.03; H, 3.41; N, 6.06. Single crystals suitable for X-ray diffraction were obtained by slow diffusion of hexane into a pyridine solution of [$UCl_2$($^{Me}$naphtquinolen)$_2$].

**Reduction of [$UCl_2$($^{Me}$naphtquinolen)$_2$], 1-Cl.** To a solution of **1-Cl** (24.5 mg, 0.026 mmol, 1 equiv) in THF (4 mL) was added a potassium chunk (2.1 mg, 0.053 mmol, 2 equiv), and the reaction mixture was stirred at room temperature overnight, affording a deep brown suspension. The $^1$H NMR spectrum (200 MHz, THF-$d_8$, 298 K) recorded for the crude reaction mixture showed that a complex mixture of compounds had formed, among which the resonances of **2** and **2b** could be identified (see Supporting Information).

A suspension of potassium graphite (7.1 mg, 0.053 mmol, 2 equiv) in THF (2 mL) was added to a solution of **1-Cl** (24.5 mg, 0.026 mmol, 1 equiv) in THF (2 mL), and the reaction mixture was stirred at room temperature for 15 min, affording a deep brown suspension. Graphite was removed by centrifugation. The $^1$H NMR spectrum (200 MHz, THF-$d_8$, 298 K) recorded for the crude reaction mixture (see Supporting Information) showed the formation of **2** and **2b** as the only $^{Me}$naphtquinolen-containing species.

**[U(μ-bis-$^{Me}$naphtquinolen)]$_2$, 2.** A solution of $^{Me}$naphtquinolen-K (150.0 mg, 0.428 mmol, 2 equiv) in THF (8 mL) was added to [$UI_4(OEt_2)_2$] (191.3 mg, 0.214 mmol, 1 equiv), and the reaction mixture was stirred at room temperature overnight, affording a yellowish-brown suspension. Intermediate data for [$UI_2$($^{Me}$naphtquinolen)$_2$], **1-I**: $^1$H NMR (200 MHz, pyridine-$d_5$, 298 K): $\delta$ = 108.9 (br s, 2H), 37.9 (s, 2H), 37.3 (s, 6H), 31.1 (s, 2H), 29.7 (br s, 2H), 22.1 (s, 2H), 21.6 (s, 2H), 18.0 (br s, 6H), 16.9 (s, 2H), 4.3 (s, 4H), 0.6 (s, 2H), −3.2 (s, 2H) −7.4 (s, 2H). This mixture was added onto potassium chunks and then stirred at room temperature for 12 h. The reaction mixture gradually turned dark olive brown. The mixture was filtered to remove KI, and the filtrate evaporated to dryness. The resulting brown solid was extracted with toluene (12 mL) to give a brown suspension that was filtered. The filtrate was taken to dryness to give [U(μ-bis-$^{Me}$naphtquinolen)]$_2$, **2**, as a brown solid (122.9 mg, 0.071 mmol, 67% yield). $^1$H NMR (200 MHz, toluene-$d_8$, 298 K): $\delta$ = 88.0 (s, 2H), 46.2 (s, 2H), 41.7 (m, 4H), 33.1 (d, 2H), 31.2 (d, 2H), 30.9 (d, 2H), 20.0 (t, 2H), 17.8 (d, 2H), 15.1 (d, 2H), 14.9 (m, 2H), 13.2 (t, 2H), 12.3 (t, 2H), 10.4 (t, 2H), 8.9 (dt, 2H), 7.2 (d, 2H), 5.6 (d, 2H), 5.2 (d, 2H), 2.5 (d, 2H), −3.9 (d, 2H), −5.1 (d, 2H), −5.9 (t, 2H), −7.7 (s, 6H, $CH_3$), −9.0 (d, 2H), −13.8 (d, 2H), −25.8 (s, 6H, $CH_3$). Anal. Calcd for **2** $C_{84}H_{60}N_8O_4U_2$: C, 58.61; H, 3.51; N, 6.51. Found: C, 58.37; H, 3.73; N, 6.38. Single crystals suitable for X-ray diffraction were obtained by slow diffusion of hexane into a toluene solution of **2**.

Upon dissolution of **2** into pyridine, 2 sets of proton signals are observed in solution assigned to the dimeric complex **2** and the monomeric analogue **2b**: $^1$H NMR (500 MHz, pyridine-$d_5$, 298 K):

Ratio of complexes **2**: **2b**: 3:1 after 30 min, 0.5:1 after 4 days.

Complex **2**: $\delta$ = 85.7 (s, 2H), 47.4 (d, 2H), 41.1 (d, 2H), 35.2 (d, 2H), 32.3 (d, 2H), 28.9 (s, 2H), 28.1 (d, 2H), 18.4 (t, 2H), 16.7 (d, 2H), 15.2 (t, 2H), 11.3 (t, 2H), 11.2 (t, 2H), 11.1 (t, 2H), 10.9 (d, 2H), 9.8 (d, 2H),


dx.doi.org/10.1021/ic4006218 | Inorg. Chem. 2013, 52, 7078−7086

**Table 1. X-ray Crystallographic Data**

| compound | **1-Cl**·(pyridine) | **2**·(toluene)$_2$ | **3**·(pyridine)$_{4.5}$ | **4** |
|---|---|---|---|---|
| formula | C47 H35 N5 O2 Cl2 U | C98 H76 N8 O4 U2 | C78.5 H60.5 N8.5 O4 U | C84 H60 N8 O8 U |
| crystal size [mm] | 0.28 × 0.22 × 0.15 | 0.32 × 0.19 × 0.02 | 0.25 × 0.10 × 0.02 | 0.27 × 0.14 × 0.03 |
| crystal system | triclinic | triclinic | monoclinic | monoclinic |
| space group | $P\bar{1}$ | $P\bar{1}$ | $C2/c$ | $P2_1/c$ |
| $V$ [Å$^3$] | 1977.10(13) | 1897.75(15) | 12586.6(13) | 3319.99(15) |
| $a$ [Å] | 10.0338(4) | 11.1583(6) | 45.625(2) | 16.2723(5) |
| $b$ [Å] | 12.7361(5) | 13.4999(7) | 15.8387(9) | 11.8342(3) |
| $c$ [Å] | 16.6880(7) | 13.5383(5) | 18.5959(13) | 18.1568(5) |
| $\alpha$ [deg] | 101.098(3) | 97.421(3) | 90 | 90 |
| $\beta$ [deg] | 101.394(3) | 107.177(4) | 110.506(5) | 108.281(3) |
| $\gamma$ [deg] | 102.627(3) | 98.029(4) | 90 | 90 |
| $Z$ | 2 | 1 | 8 | 2 |
| absorption coefficient [mm$^{-1}$] | 4.287 | 4.324 | 2.640 | 4.941 |
| $F$ (000) | 988 | 936 | 5720 | 1736 |
| $T$ [K] | 150(2) | 150(2) | 150(2) | 150(2) |
| total no. reflexions | 41283 | 14739 | 31319 | 39686 |
| unique reflexions [$R$(int)] | 12067 [0.0592] | 7739 [0.0961] | 9013 [0.1193] | 10126 [0.0740] |
| final $R$ indices [$I > 2\sigma(I)$] | 0.0511 | 0.0780 | 0.0623 | 0.0450 |
| largest diff. peak and hole [e A$^{-3}$] | 5.549 and −2.664 | 2.983 and −1.895 | 2.465 and −1.712 | 1.340 and −1.248 |
| GOF | 1.155 | 0.939 | 1.063 | 1.012 |

8.9 (d, 2H), 8.1 (d, 2H), 6.3 (d, 2H), 5.2 (d, 2H), 0.9 (s, 6H, $CH_3$), −0.7 (d, 2H), −3.8 (t, 2H), −6.7 (d, 2H), −9.5 (d, 2H), −10.0 (d, 2H), −13.9 (s, 6H, $CH_3$).

Complex **2b**: $\delta$ = 91.3 (s, 2H), 47.6 (d, 2H), 45.9 (d, 2H), 44.1 (s, 2H), 35.6 (d, 2H), 32.1 (d, 2H), 20.2 (d, 2H), 19.3 (d, 2H), 19.1 (t, 2H), 17.5 (m, 2H), 14.3 (t, 2H), 13.9 (t, 2H), 13.7 (d, 2H), 13.4 (t, 2H), 13.3 (d, 2H), 6.5 (s, 6H, $CH_3$), 5.7 (d, 2H), 4.6 (d, 2H), 3.7 (t, 2H), 2.2 (s, 2H), 1.6 (d, 2H), −5.3 (t, 2H), −5.7 (d, 2H), −7.0 (d, 2H), −11.8 (d, 2H), −15.0 (s, 6H, $CH_3$).

**Reaction of 2 with 9,10-Phenanthrenequinone.** A toluene (6 mL) 9,10-phenanthrenequinone (12.2 mg, 0.059 mmol, 2 equiv) solution was prepared and added to a toluene (4 mL) solution of complex **2** (50.6 mg, 0.029 mmol, 1 equiv). Immediately the deep brown solution turned yellowish green. The mixture was stirred 3 h before filtration. The brown solid was washed with 2 × 0.5 mL of toluene and dried in vacuo to give [U(9,10-phenanthrenediol)-($^{Me}$naphtquinolen)$_2$] **3** as a brown-gold solid (33.8 mg, 0.032 mmol, 54% yield). Similar results were obtained when performing the reaction in pyridine. Single crystals suitable for X-ray diffraction were obtained by slow evaporation of a saturated pyridine solution of the complex. $^1$H NMR (200 MHz, toluene-d$_8$, 298 K): $\delta$ = 27.6 (s, 2H), 19.9 (s, 2H), 19.1 (s, 2H), 18.6 (s, 2H), 16.2 (d, 2H), 13.0 (t, 2H), 12.5 (d, 2H), 11.7 (t, 2H), 9.4 (t, 2H), 9.3 (t, 2H), 8.0 (d, 2H), 0.7 (t, 2H), 0.6 (d, 2H), −1.1 (d, 2H), −2.4 (d, 2H), −5.2 (d, 2H), −10.5 (s, 6H). Anal. Calcd for **3**·(toluene$_{0.2}$) $C_{57.2}H_{39.6}N_4O_4U$: C, 63.32; H, 3.68; N, 5.16. Found: C, 63.54; H, 3.85; N, 5.25.

**Reaction of 2 with $I_2$.** A solution of iodine (2.9 mg, 0.011 mmol, 2 equiv.) in toluene (1 mL) was added dropwise to a stirred solution of **2** (9.7 mg, 0.006 mmol, 1 equiv.) in toluene (0.5 mL). Immediately, the dark brown solution turned pale brown. After 10 min stirring, the crude reaction was taken to dryness and dissolved into pyridine. The $^1$H NMR spectrum (200 MHz, py-d$_5$, 298 K) recorded for the crude reaction mixture showed that complex **1-I** was restored.

**Reaction of 2 with Dry $O_2$.** A pyridine (6 mL) solution of complex **2** (58.0 mg, 0.034 mmol, 1 equiv) was transferred into a reaction vessel. The suspension was degassed using a freeze−pump−thaw procedure. Then 1 atm of dry dioxygen was introduced into the flask. Immediately, a color change from dark brown to dark red/orange was observed. The reaction was stirred for 12 h at room temperature before the solvent was removed in vacuo. The solid was washed with toluene (3 × 2 mL), recovered and dried in vacuo to afford **4** as a bright orange solid (42.0 mg, 0.047 mmol, 69% yield). $^1$H NMR (200 MHz, THF-d$_8$, 298 K): $\delta$ = 10.3 (s, 2H, N=CH), 8.5 (d, 2H, H$_{aro}$), 8.2 (d, 2H, H$_{aro}$), 7.9−7.8 (m, 6H, H$_{aro}$), 7.7−7.5 (m, 6H, H$_{aro}$), 7.4 (t, 2H, H$_{aro}$), 7.2 (t, 2H, H$_{aro}$), 6.2 (d, 2H, H$_{aro}$), 3.4 (s, 6H, $CH_3$). Anal. Calcd for **4**·($KI_{0.25}$) $C_{42}H_{30}N_4O_4UK_{0.25}I_{0.25}$: C, 54.00; H, 3.24; N, 6.00. Found: C, 53.88; H, 3.49; N, 5.98. The presence of KI arises from the residual presence of KI in the batch of complex **2** used in this reaction.

**Electrochemical Methods.** Cyclic voltammetry data were carried out at room temperature in an argon-filled glovebox described above. Data were collected using a Biologic SP-300 potentiostat connected to a personal computer. All samples were 10 mM in complex with 0.1 M [$Bu_4N$][$PF_6$] supporting electrolyte in pyridine solution. The experiments were carried out with a platinum disk ($d$ = 5 mm) working electrode, a platinum wire counter electrode, and an Ag/AgCl reference electrode. The experiments were repeated on independently synthesized samples to assess the reproducibility of the measurement. Potential calibration was performed at the end of each data collection cycle using the ferrocene/ferrocenium [$(C_5H_5)_2Fe$]$^{+/0}$ couple as an internal standard.

**X-ray Crystallography.** Diffraction data were taken using an Oxford-Diffraction XCallibur S kappa geometry diffractometer (Mo−K$\alpha$ radiation, graphite monochromator, $\lambda$ = 0.71073 Å). To prevent evaporation of cocrystallized solvent molecules the crystals were coated with light hydrocarbon oil, and the data were collected at 150 K. The cell parameters were obtained with intensities detected on three batches of 5 frames. The crystal-detector distance was 4.5°cm. The number of settings and frames has been established taking in consideration the Laue symmetry of the cell by CrysAlisPro Oxford-diffraction software.[65] A total of 866 for **1-Cl**, 430 for **2**, 377 for **3**, and 498 for **4** narrow data were collected for 1° increments in $\omega$ with a 15 s exposure time for **1-Cl**, 100 s for **2**, 200 s for **3**, and 80 s for **4**. Unique intensities detected on all frames using the Oxford-diffraction Red program were used to refine the values of the cell parameters. The substantial redundancy in data allows empirical absorption corrections to be applied using multiple measurements of equivalent reflections with the ABSPACK Oxford-diffraction program.[65] Space groups were determined from systematic absences. The structures were solved by direct methods using the SHELXTL 6.14 package.[66] All non-hydrogen atoms were found by difference Fourier syntheses and refined on $F^2$. For **1-Cl** hydrogen atoms were found by Fourier synthesis and refined except for methyl groups which were fixed in ideal position. For **2**, **3**, and **4** hydrogen atoms were fixed in ideal position. Full crystallographic details for complexes **1**−**4** are given in Table 1.


dx.doi.org/10.1021/ic4006218 | Inorg. Chem. 2013, 52, 7078−7086

## RESULTS AND DISCUSSION

**$[UX_2(^{Me}naphtquinolen)_2]$ Complexes.** Proton NMR spectra of the reaction mixture of 2 equiv of $^{Me}$naphtquinolenK and 1 equiv of $[UI_4(OEt_2)_2]$ or $[UCl_4]$ in deuterated THF shows only one set of signals assigned to the heteroleptic mononuclear $[UX_2(^{Me}naphtquinolen)_2]$ **1-X** complexes (Scheme 1) where X = I

**Scheme 1. Synthesis of $[UX_2(^{Me}naphtquinolen)_2]$ 1-X (X = Cl, I)**

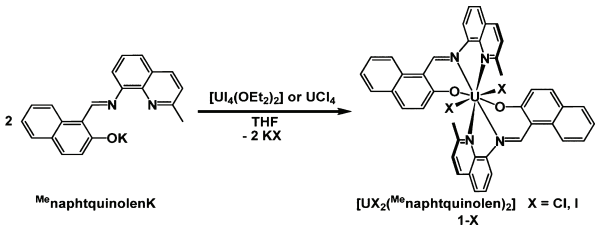


or Cl respectively. The UV−visible spectra for **1-Cl** and **1-I** display a series of intense absorptions below 450 nm ($\varepsilon \approx$ 25000 L cm$^{-1}$ mol$^{-1}$) that we assign to ligand-based $\pi-\pi^*$ transitions. The solubility of **1-Cl** in organic solvents (fully soluble in THF, partially soluble in toluene) is much higher than the one of **1-I** (sparingly soluble in THF, insoluble in toluene) facilitating its separation from KX salts. Accordingly, the complex $[UCl_2(^{Me}naphtquinolen)_2]$ was also isolated pure in high yield. The X-ray structural analysis of **1-Cl** shows that the uranium atom is octa-coordinated by two $^{Me}$naphtquinolen and two chloride ligands in a slightly distorted square antiprism possessing a pseudo $C_2$ axis (Figure 1). The mean values of U−O (2.20(2) Å), U−N (2.6(1) Å), and U−Cl (2.67(4) Å) bond distances (Table 2) are in the range of the ones found in other U(IV) Schiff base complexes,[45,57,58] and bond valence calculations are in agreement with a +IV oxidation state for the metal (see Supporting Information). The $^{Me}$naphtquinolen ligands are strongly distorted from planarity with about 70° between the quinoleine and the naphtol planes. This is most probably due to sterical repulsion between the two tridentate ligands in the present coordination environment. The two $^{Me}$naphtquinolen ligands are arranged perpendicular to each other with the two halide anions lying on the same face of the square antiprism. This geometry is very different from the one reported for analogous tridentate ligands bound to Yb(III) or Y(III).[67] In the crystal structure of the $[L_2Ln(N(TMS)_2)]$ (Ln = Yb(III) or Y(III) L = bis(3,5-di-*tert*-butylsalicylidene)-8-aminoquinoline) the two tridentate Schiff bases are almost planar and bind the metal in a parallel fashion. These two binding modes are reminiscent of those found in sandwich and meridional isomers of uranium bis-ligand complexes of tetradentate Schiff bases.[45,57]

**Synthesis and Structure of $[U(\mu\text{-bis-}^{Me}naphtquinolen)]_2$.** The proton NMR spectrum in THF of the reaction mixture after reduction of the complex **1-I** with 2 equiv of potassium in deuterated THF shows the presence of two sets of 26 signals (ratio 66:34) (see Supporting Information, Figure S.A.3). The proton NMR in toluene of the reaction mixture after removal of THF shows the presence of only one set of 26 signals. Recrystallization from toluene affords the complex $[U(\mu\text{-bis-}^{Me}naphtquinolen)]_2$ **2** pure in 67% yield (Scheme 2).

The solid state structure of **2** determined by X-ray structural studies is presented in Figure 2. It shows that the dimeric compound **2** is composed of two [U(IV)bis-$^{Me}$naphtquinolen] complexes bridged by the phenolate oxygens of the two tetra-anionic bis-$^{Me}$naphtquinolen ligands. The crystal structure is centrosymmetric, with an inversion center located halfway between the two uraniums. Each metal cation is hepta-coordinated in a distorted capped trigonal prismatic environment by the four nitrogen (mean U−N = 2.5(1) Å) and two oxygen atoms from a bis-$^{Me}$naphtquinolen ligand (mean U−O = 2.3(1) Å) and by a bridging phenolate oxygen form the other [U(IV)-bis-$^{Me}$naphtquinolen] complex. The two bidentate phenolate bridging ligands hold the two uranium centers in the dimer at 3.7983(8) Å apart (Figure 3). The analysis of the structural parameters of the complex clearly shows that the reduction has occurred on the imino groups of the ligands rather than on the metal ions. Notably, the two electron reduction of the ligand results in the formation of two C−C bonds, 1.64(1) Å long, by intramolecular coupling of the original imino groups. The value of the C−C bond distance is larger than those found in the $Na_2$[U(bis-salophen)] (1.559(7) Å) and $[U_2$(cyclo-salophen)-$(py)_4]$ (1.609(5) Å) complexes for the C−C bonds formed after reductive coupling of the imino groups[45] but remains in the range of reported values for C−C bonds. Reductive coupling mediated by low valent uranium has been previously reported for carbonyl compounds,[68] heterocycles,[69] CO,[6] and $CS_2$.[70] The C−$N_{am}$ bond distances (mean C−$N_{am}$ = 1.474(5) Å) of the ligand

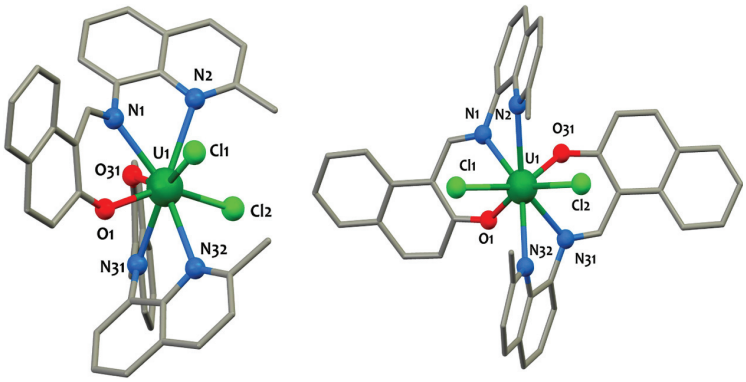


**Figure 1.** Mercury diagrams (side and top views) of the solid-state molecular structure of $[UCl_2(^{Me}naphtquinolen)_2]$ in **1-Cl**. Hydrogen atoms and solvent molecules are omitted for clarity. Color code: uranium (deep green), chlorine (bright green), nitrogen (blue), oxygen (red), and carbon (gray).


dx.doi.org/10.1021/ic4006218 | Inorg. Chem. 2013, 52, 7078−7086

Table 2. Mean Values of Selected Bond Lengths (Å) in the U(IV) Complexes 1-Cl, 2, 3, and 4

| compound | $U-N_{aro}$ | $U-N_{imino/amido}$ | $U-O_{phenolate}$ | U−X | $C-C_{link}$ | $C-N_{imino/amido}$ |
|---|---|---|---|---|---|---|
| 1-Cl | 2.70(3) | 2.51(3) | 2.204(18) | $2.67(4)_{X = Cl}$ | | 1.293(2) |
| 2 | 2.538(3) | 2.36(2) | 2.26(10) | | 1.636(14) | 1.474(5) |
| 3 | 2.58(7) | 2.52(2) | 2.227(13) | $2.26(4)_{X = O}$ | | 1.294(9) |
| 4 | 2.646(4) | 2.55(2) | 2.238(6) | $1.776(3)_{X = O^{2-}}$ | | 1.292(2) |

Scheme 2. Synthesis of $[U(\mu\text{-bis-}^{Me}\text{naphtquinolen})]_2$ 2 and Schematic Representation of the Tetranionic Hexadentate Ligand Bis-$^{Me}$naphtquinolen$^{4-}$

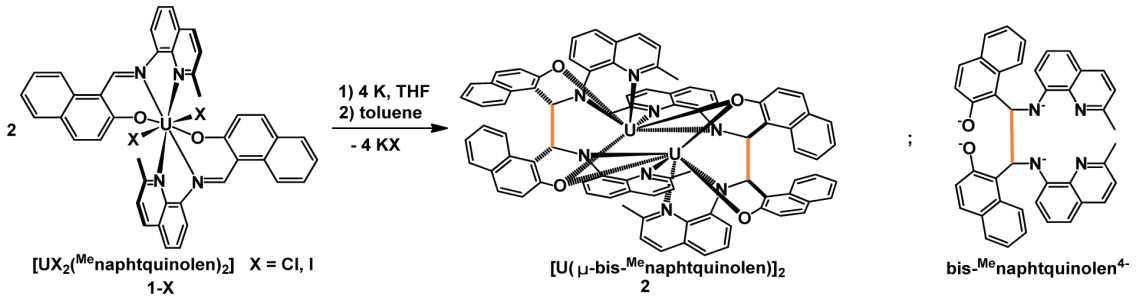


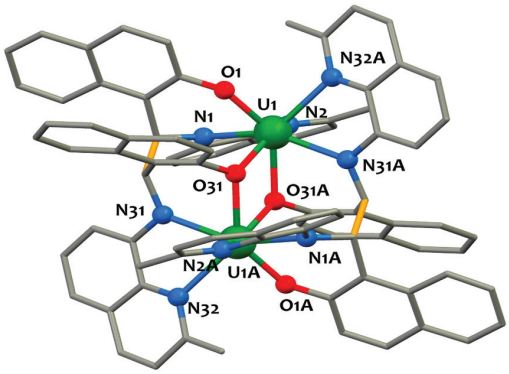


Figure 2. Mercury diagram of the solid-state molecular structure of $[U(\mu\text{-bis-}^{Me}\text{naphtquinolen})]_2$ in 2. Hydrogen atoms and solvent molecules are omitted for clarity. The C−C bond formed by reduction of the imine moieties of the ligands is represented in yellow. Color code: uranium (green), nitrogen (blue), oxygen (red), and carbon (gray). (U1A = U1 $-x+1,-y+1,-z+2$).

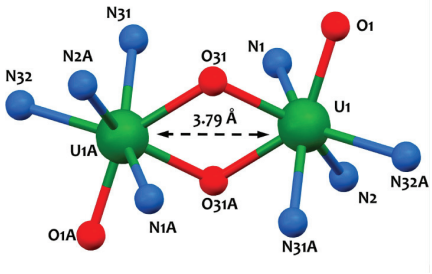


Figure 3. View of the dinuclear core of complex $[U(\mu\text{-bis-}^{Me}\text{naphtquinolen})]_2$ 2.

backbone are much longer than the one observed in **1-Cl**, and are in agreement with the presence of two amido groups. This is further confirmed by the analysis of the values of the U−N bond distances, with the $U-N_{am}$ distances in **2** ($U-N_{am}$ = 2.36(2) Å) being significantly shorter than the $U-N_{py}$ distances in **2** ($U-N_{py}$ = 2.538(3) Å) and the $U-N_{im}$ distances in **1-Cl** ($U-N_{im}$ = 2.51(3) Å). This distance compares well with the $U-N_{am}$ (2.387(8) Å) and $U-N_{im}$ (2.624(7) Å) found in $Na_2[U(\text{bis-salophen})]$.[45] Finally, bond valence calculations are in agreement with a +IV oxidation state for the uraniums in **2** (see Supporting Information). The value of the magnetic moment (2.44 $\mu_\beta$) per uranium measured using the Evans method[71] for a toluene solution of **2** is also in the range of values reported for U(IV) complexes.[30] Thus, the formula $[U(\mu\text{-bis-}^{Me}\text{naphtquinolen})]_2$ where bis-$^{Me}$naphtquinolen is a tetra-anionic hexadentate ligand provides a good description of this neutral complex.

Compound **2** is stable for weeks at room temperature in the solid state or in toluene solution under inert atmosphere. In addition to the ligand-based $\pi-\pi^*$ transitions below 450 nm, a long tail absorption extending to 750 nm is observed in the UV−visible spectrum of **2** (see Supporting Information), responsible for its dark-brown color in solution. The proton NMR spectrum of **2** in toluene solution shows only one set of 26 signals assigned to a centrosymmetric dimeric solution species in agreement with the solid state structure of **2**. The $^1$H NMR spectrum of **2** in deuterated THF or pyridine shows the presence of two sets of 26 resonances indicating that two forms of the complex are present in coordinating polar solvents (Scheme 3). Evaporation of the pyridine and THF solutions and dissolution of the resulting solid in toluene result again in the presence of only one species in the proton NMR spectrum. The monitoring of the $^1$H NMR spectrum of complex **2** in pyridine solution at different times after dissolution shows that the ratio between the two isomers evolves in time, going from 3:1 after 30 min, to a final stable ratio of 0.5:1 after 4 days. The proton chemical shifts for the initially major species are close to the ones measured for complex **2** in deuterated toluene. This suggests that the initially major species in pyridine solution is a dinuclear complex which with time undergoes a rearrangement in pyridine solution. The second set of 26 resonances could either correspond to a solvent adduct of the dinuclear complex **2** or to a monomeric form of the complex. Pulsed-field-gradient stimulated-echo diffusion NMR spectroscopy (see Supporting Information) was used to measure the diffusion coefficients of both species in pyridine solution. $D$ is a function of the molecular weight and has been successfully used to discriminate metallosupramolecular


dx.doi.org/10.1021/ic4006218 | Inorg. Chem. 2013, 52, 7078−7086

architectures in solution.[72,73] The values measured in pyridine ($(D_A/D_B)^3$ = 1.63 ; $M_A/M_B$ = 1.69) are in agreement with the presence of a mononuclear and a dinuclear complexes in solution. Attempts to isolate crystals of the monomeric complex from pyridine or thf were not successful.

**Scheme 3. Equilibrium between the Dimeric and the Monomeric Forms of 2 in Coordinating Solvents**

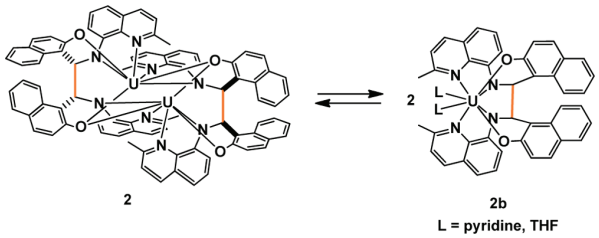


The most probable pathway for the formation of **2** (see Supporting Information) from the reduction of **1** involves the reduction of the two imino group to afford two U(IV) radical anion complexes which then undergo intramolecular C−C coupling. This produces a U(IV) complex of the new hexadentate tetranionic bis-phenolato bis-amido bis-$^{Me}$naphtquinolen ligand where at least two coordination sites are available at the metal center for solvent or substrate binding. In the absence of coordinating solvents this complex dimerizes through phenolate bridging to yield **2**.

Isolation of a pure product from the reduction of the chloride analogue **1-Cl** with potassium proved more difficult. Proton NMR in deuterated THF of the reaction mixture after reduction of **1-Cl** with 2 equiv of potassium metal shows the presence of several sets of signals. Two sets of signals were assigned to the reduced species **2** and **2b**, the other signals remain unidentified. The presence of additional species can be explained in terms of a competition of an intermolecular C−C coupling process leading to complex mixtures as a result of the presence of the more coordinating chloride ligand. Although the ligands could rearrange in solution, the conformation adopted by the two tridentate ligands in the solid state structure of the complex **1-Cl** with the two carbons of the imino groups situated at a distance of 5.995(6) Å is not favorable to intramolecular C−C bond formation. However, proton NMR studies show that the reduction of **1-Cl** with $KC_8$ in THF leads cleanly to the formation of complexes **2** and **2b**. These results show that clean ligand based reduction followed by intramolecular C−C coupling is not limited to uranium complexes of tetradentate Schiff bases. However in the case of tridentate Schiff bases the choice of the halide precursor plays an important role in the outcome of the reduction reaction. Moreover, the final complex presents free coordination sites at the metal center which are not available in the previously reported $Na_2$[U(bis-salophen)] complex obtained from the intramolecular C−C coupling of two reduced imino groups from the [U(salophen)$_2$] precursor.[42]

Complex **2** provides an interesting precursor for the synthesis of more reduced species. The possibility of further reduction of the metal center in **2** was explored by electrochemical studies.

**Electrochemistry.** Cyclic voltammetry data were collected for complexes **1-I** and **2** in ∼0.1 M [$Bu_4N$][$PF_6$] pyridine solution and are presented in Figure 4 and Table 3. All redox potentials are referenced against the $[(C_5H_5)_2Fe]^{+/0}$ redox couple. While the free ligand in K-$^{Me}$naphtquinolen does not exhibits reduction process in the range −0.5 to −2.4 V (see Supporting Information), the voltammogram of complex **1-I** shows three distinct reduction events. A first reduction process occurs at $E_{pc1}$ = −1.45 V and is followed by a reduction at $E_{pc2}$ = −1.65 V. These two waves are associated with an irreversible oxidation process occurring at $E_{pa}$ = −0.56 V which is not observed when the voltammogram is swept initially from −1.2 V toward the positive direction. These data indicate the presence of a system with a limited degree of chemical reversibility as one could expect because of the formation of the C−C bond after ligand reduction. Finally, a third reversible process is observed at $E_{1/2}$ = −2.16 V. Similar redox processes are observed on the voltammogram of the reduced species **2** which can be reversibly reduced at $E_{1/2}$ = −2.17 V and irreversibly oxidized at $E_{pa}$ = −0.56 V. The latter wave has a shoulder at −0.68 V that can be reasonably assigned to the oxidation of the monomeric form in equilibrium with the dimeric one in pyridine solution. Notably, it has been observed that the intensity of the shoulder was increasing 1 h after dissolution of **2** in pyridine, in agreement with a higher ratio of monomer/dimer in pyridine solution as observed in the NMR studies. The two irreversible reduction waves at $E_{pc1}$ = −1.49 V and $E_{pc2}$ = −1.70 V are not observed when the voltammogram is swept initially from −1.3 V to the negative direction and are thus associated to the reduction of the oxidation product.

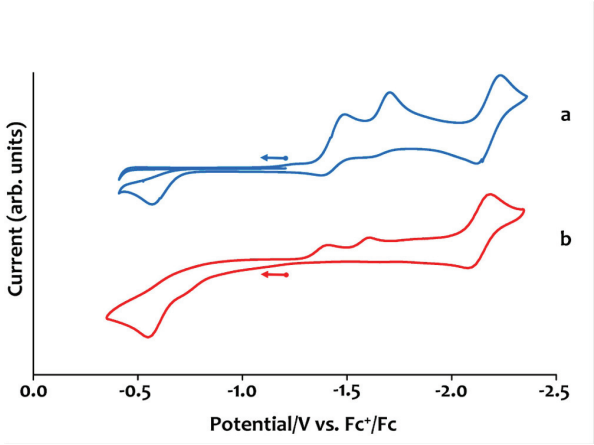


**Figure 4.** Cyclic voltammogram for 10 mM solutions of (a) **1-I** and (b) **2** in ∼0.1 M [$Bu_4N$][$PF_6$] pyridine solution at 100 mV $s^{-1}$ scan-rate.

**Table 3. Voltammetric Data for 1-I and 2**

| | ligand-based waves | | | metal-based wave |
|---|---|---|---|---|
| compd | $E_{pa}$ (V) | $E_{pc1}$ (V) | $E_{pc2}$ (V) | $E_{1/2}$(V) |
| **1-I** | −0.56 | −1.45 | −1.65 | −2.16 |
| **2** | −0.56 | −1.49 | −1.70 | −2.17 |

Taking into account that both the ligand and the uranium center are electroactive species, distinguishing ligand-based and metal-based processes is critical. The values of the redox potentials of the first two reduction waves are not compatible with metal based reductions (U(IV)/U(III) and U(III)/U(II)). The pseudoreversible reduction processes in the −1.45 to −1.70 V range probably correspond to two successive one electron transfers to the bis-$^{Me}$naphtquinolen ligand platform. Thus, the irreversible oxidation occurring at $E_{pa}$ = −0.56 V corresponds to the oxidation of the bis-$^{Me}$naphtquinolen platform, that is, to the oxidative cleavage of the C−C bond.


dx.doi.org/10.1021/ic4006218 | Inorg. Chem. 2013, 52, 7078−7086

The irreversibility of the ligand-based processes suggests that the electrochemical reduction is followed by a rapid chemical transformation involving the formation or cleavage of the C−C bond between two reduced imino groups. This process confers a strong stabilization to the system, as is expressed by the much lower potential required for transferring an electron to the $^{Me}$naphtquinolen ligand than the one required for oxidizing the bis-$^{Me}$naphtquinolen platform ($\Delta Ep$ = 0.9 V).

The reversible wave at $E_{1/2}$ = −2.16 V corresponds to a further reduction of **2** and is attributed to a U(IV)/U(III) couple. This fits with the range of values of redox potentials reported for other U(IV)/U(III) reversible systems.[74−76] Future studies will be directed to identify the chemical conditions allowing the isolation of this reduced species and to investigate its reactivity.

**Reactivity of [U($\mu$-bis-$^{Me}$naphtquinolen)]$_2$ with Oxidizing Agents.** The reaction of [U($\mu$-bis-$^{Me}$naphtquinolen)]$_2$ **2** with different oxidizing substrates has been investigated to assess if the electrons stored in the C−C bond can become available. Complex **2** can act as a multielectron reductant when reacted with 9,10-phenanthrenequinone, iodine, or molecular oxygen (Scheme 4).

**Scheme 4. Reactivity of [U($\mu$-$^{Me}$bis-naphtquinolen)]$_2$ 2 with Oxidizing Agents**

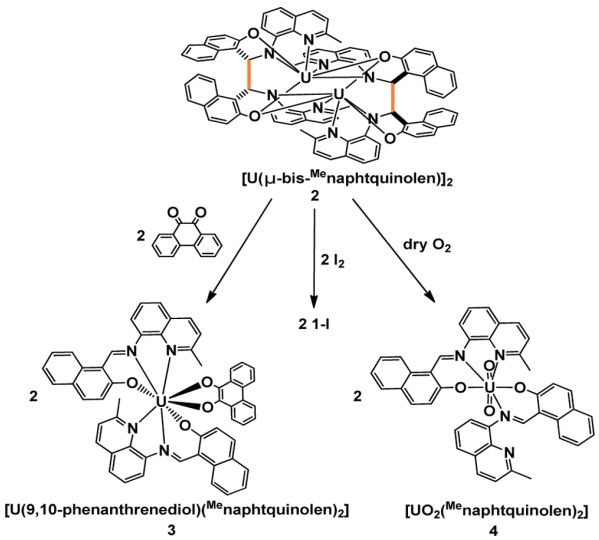


Complex [U(9,10-phenanthrenediol)($^{Me}$naphtquinolen)$_2$] **3** is obtained in 54% yield from the reaction of **2** with 9,10-phenanthrenequinone in toluene. The same reactivity is observed when using pyridine as solvent. The UV−visible spectrum for **3** is very similar to the one of **1-I**, with two strong absorption bands centered at 420 and 334 nm ($\varepsilon \approx 25000$ L cm$^{-1}$ mol$^{-1}$) that we assign to ligand-based $\pi-\pi^*$ transitions. Notably, the tail absorption extending to 750 nm, characteristic of the reduced form of the ligand, is not present in **3**, in agreement with an oxidation of the ligand platform. Single crystals suitable for X-ray diffraction were obtained by slow evaporation of a pyridine solution of **3**, allowing its structural characterization. The molecular structure, as shown in Figure 5, consists of a $C_2$-symmetric complex where the uranium atom is octa-coordinated in a distorted square antiprismatic fashion by two tridentate monoanionic $^{Me}$naphtquinolen ligands and one dianionic 9,10-phenanthrenediol ligand. The reduction of the quinone to its cathecolate form is confirmed by the analysis of the metrical

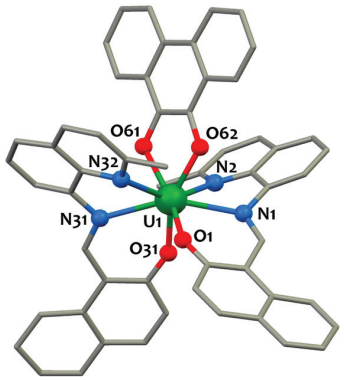


**Figure 5.** Mercury diagram of the solid-state molecular structure of [U(9,10-phenanthrenediol)($^{Me}$naphtquinolen)$_2$] **3**. Hydrogen atoms and solvent molecules are omitted for clarity. Color code: uranium (green), nitrogen (blue), oxygen (red), and carbon (gray).

parameters for the ligand. The average U−O$_{9,10\text{-phenanthrenediol}}$ bond distances (2.26(4) Å) are relatively short, as expected for a doubly charged phenolate ligand, and are in the same range of the U−O$_{phenolate}$ moieties from the $^{Me}$naphtquinolen ligand (2.23(1) Å). The C−O bond distances for this ligand (1.359(1) Å) are in agreement with the presence of simple C−O bonds. The imino moieties of the $^{Me}$naphtquinolen ligands have been restored, as is illustrated by the short C−N double bond distances (1.294(9) Å) and long U−N bond distances (2.52(1) Å) which compare well with those found in **1-Cl**. The overall neutral charge of the complex and the bond valence sum calculations are in agreement with a +IV oxidation state of the uranium cation in **3**.

The reduction of 9,10-phenanthrenequinone is likely to proceed through the coordination of the substrate to the metal center and disruption of the dimeric structure of **2** followed by the cleavage of the two ligand C−C bonds. Thus each mononuclear uranium(IV) complex [U($\mu$-bis-$^{Me}$naphtquinolen)] acts as a two electron reducing agent without undergoing a variation of the oxidation state of the metal center. In contrast to what was observed for the previously reported U(IV) multielectron redox system based on a tetradentate Schiff base, the presence of available coordination sites at the metal center allows a direct coordination of the incoming substrate to the uranium as shown by the structure of the oxidation product. This should provide a more controlled reaction pathway.

Proton NMR studies also show that the reaction of **2** with $I_2$ in toluene leads to the cleavage of the C−C bond restoring the original Schiff base structure and affords the **1-I** complex demonstrating the chemical reversibility of this redox system.

The number of transferred electrons can be increased when both the ligand and the metal are participating in the electron transfer. The reaction of a dark brown solution of **2** with excess dry oxygen in pyridine (where **2** is mostly present in its monomeric form **2b**) proceeds instantly to give a dark red/orange solution. The $^1$H NMR spectrum recorded for the reaction mixture shows 13 resonances in the diamagnetic region, in agreement with the presence of the new uranyl(VI) complex [UO$_2$($^{Me}$naphtquinolen)$_2$] **4**.

The solid-state structure of **4**, determined by single crystal X-ray diffraction, is represented in Figure 6. The uranium atom has a pentagonal bipyramidal coordination provided by the two oxo groups in axial positions and five O and N-donor atoms from two $^{Me}$naphtquinolen ligands in the equatorial plane.


dx.doi.org/10.1021/ic4006218 | Inorg. Chem. 2013, 52, 7078−7086

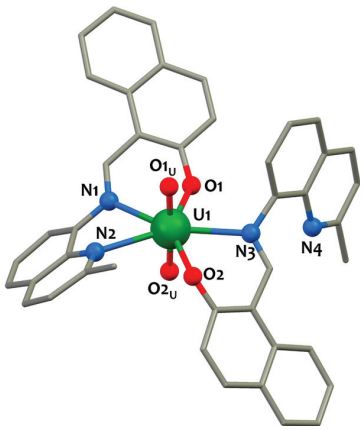


**Figure 6.** Mercury diagram of the solid-state molecular structure of $[UO_2(^{Me}naphtquinolen)_2]$ **4**. Hydrogen atoms are omitted for clarity. Color code: uranium (green), nitrogen (blue), oxygen (red) and carbon (gray).

While the first $^{Me}$naphtquinolen ligand adopts a classical tridentate ONN coordination mode, as found in **1-Cl** and **3**, the second $^{Me}$naphtquinolen ligand is bound to the uranium center in a bidentate fashion by the phenolate and the imino group with the nitrogen atom from the quinoline remaining noncoordinated. Pentagonal bipyramid is the most common coordination geometry for uranyl(VI) compounds, higher coordination numbers in the equatorial plane being disfavored for sterical reasons. The C−$N_{im}$ (1.276(6) and 1.308(6) Å) bond distances from both $^{Me}$naphtquinolen ligands are in the same range than the ones found in **1-Cl** and **3**, confirming their imino character. U−$N_{im}$, U−$N_{aro}$, and U−$O_{naphtol}$ mean bond distances (respectively 2.547(2), 2.646(4), and 2.238(6) Å) compare well with those found in other uranyl(VI) Schiff base complexes.[47,54]

The uranyl $UO_2$ group in **4** is nearly linear (O−U−O angle 177.3(1)°) with uranyl bond distances (mean U−O distance 1.776(3) Å) falling in the characteristic range of seven-coordinate hexavalent uranyl complexes.[47,54]

The formation of complex **4** from **2b** provides a rare example of a transfer of 4 electrons from a mononuclear uranium(IV) complex.

## SUMMARY

Here we have prepared and characterized new examples of U(IV) complexes containing a tridentate Schiff base. Redox reactivity studies show that the reduction of the $[UX_2(^{Me}naphtquinolen)_2]$ halides proceeds cleanly for the iodide precursor while multiple products are formed for the chloride derivative. The reduction leaves the oxidation state of the metal center unchanged and occurs on the imino function of the ligand leading to intramolecular C−C bond formation. The two electrons stored in the resulting amidophenolate U(IV) complex are released in the presence of oxidizing agents. In the U(IV) and U(VI) complexes [U(9,10-phenanthrenediol)($^{Me}$naphtquinolen)$_2$], **3**, and $[UO_2(^{Me}naphtquinolen)_2]$, **4**, obtained respectively in the two- and four-electron reduction of oxidizing substrates, the restored tridentate Schiff base allows for the coordination of the reduced substrate to the metal. Thus tridentate Schiff bases provide a new example of redox active ligands which enable multielectron reductions at a U(IV) center. This shows that ligand centered reductions are not limited to tetradentate Schiff bases, and that controlled ligand centered reactivity can be achieved with lower denticity ligands by a careful choice of the reaction condition and ligand structure. Electrochemical studies suggest that the new U(IV) amidophenolate complex might provide a suitable precursor for the synthesis of highly reactive U(III) complexes. Future studies will be directed to investigate how the ligand structure affects the reducing properties in these systems.

## ASSOCIATED CONTENT

### Supporting Information

Selected $^1$H NMR and UV−vis spectra, pulsed-field-gradient stimulated-echo diffusion NMR data, selected cyclovoltammograms, bond valence sum calculations, X-ray crystallographic data, and files in CIF format. This material is available free of charge via the Internet at http://pubs.acs.org.

## AUTHOR INFORMATION

### Corresponding Author

*E-mail: marinella.mazzanti@cea.fr.

### Author Contributions

All authors have given approval to the final version of the manuscript.

### Notes

The authors declare no competing financial interest.

## ACKNOWLEDGMENTS

We acknowledge Pierre-Alain Bayle for his help with NMR characterizations, Lionel Dubois for his help with cyclic voltammetry measurements, and support from the Commissariat à l'Energie Atomique, Direction de l'Energie Nucléaire, RBPCH program and by the "Agence Nationale de la Recherche", (ANR-10-BLAN-0729).

## REFERENCES

(1) Lam, O. P.; Meyer, K. *Polyhedron* **2012**, *32*, 1−9.
(2) Evans, W. J.; Kozimor, S. A. *Coord. Chem. Rev.* **2006**, *250*, 911−935.
(3) Arnold, P. L. *Chem. Commun.* **2011**, *47*, 9005−9010.
(4) Gardiner, M. B.; Stewart, J. C.; Davis, A. L.; McMaster, J.; Lewis, W.; Blake, A. J.; Liddle, S. T. *Proc. Nat. Acad. Sci. U.S.A.* **2012**, *109*, 9265−9270.
(5) Summerscales, O. T.; Cloke, F. G. N.; Hitchcock, P. B.; Green, J. C.; Hazari, N. *J. Am. Chem. Soc.* **2006**, *128*, 9602−9603.
(6) Summerscales, O. T.; Cloke, F. G. N.; Hitchcock, P. B.; Green, J. C.; Hazari, N. *Science* **2006**, *311*, 829−831.
(7) Frey, A. S. P.; Cloke, F. G. N.; Coles, M. P.; Maron, L.; Davin, T. *Angew. Chem., Int. Ed.* **2011**, *50*, 6881−6883.
(8) Arnold, P. L.; Turner, Z. R.; Bellabarba, R. M.; Tooze, R. P. *Chem. Sci.* **2011**, *2*, 77−79.
(9) Mansell, S. M.; Kaltsoyannis, N.; Arnold, P. L. *J. Am. Chem. Soc.* **2011**, *133*, 9036−9051.
(10) Castro-Rodriguez, I.; Meyer, K. *J. Am. Chem. Soc.* **2005**, *127*, 11242−11243.
(11) Zuend, S. J.; Lam, O. P.; Heinemann, F. W.; Meyer, K. *Angew. Chem., Int. Ed.* **2011**, *50*, 10626−10630.
(12) Schmidt, A. C.; Nizovtsev, A. V.; Scheurer, A.; Heinemann, F. W.; Meyer, K. *Chem. Commun.* **2012**, *48*, 8634−8636.
(13) Castro-Rodriguez, I.; Nakai, H.; Zakharov, L. N.; Rheingold, A. L.; Meyer, K. *Science* **2004**, *305*, 1757−1759.
(14) Summerscales, O. T.; Frey, A. S. P.; Geoffrey, F.; Cloke, N.; Hitchcock, P. B. *Chem. Commun.* **2009**, 198−200.
(15) Mougel, V.; Camp, C.; Pecaut, J.; Coperet, C.; Maron, L.; Kefalidis, C. E.; Mazzanti, M. *Angew. Chem., Int. Ed.* **2012**, *51*, 12280−12284.
(16) Matson, E. M.; Forrest, W. P.; Fanwick, P. E.; Bart, S. C. *J. Am. Chem. Soc.* **2011**, *133*, 4948−4954.

(17) Mora, E.; Maria, L.; Biswas, B.; Camp, C.; Santos, I.; Pécaut, J.; Cruz, A.; Carretas, J. M.; Marçalo, J.; Mazzanti, M. *Organometallics* **2013**, *32*, 1409−1422.
(18) Korobkov, I.; Gambarotta, S.; Yap, G. P. A. *Angew. Chem., Int. Ed.* **2002**, *41*, 3433−3436.
(19) Cloke, G., F. N.; Hitchcock, P. B. *J. Am. Chem. Soc.* **2002**, *124*, 9352−9353.
(20) Roussel, P.; Scott, P. *J. Am. Chem. Soc.* **1998**, *120*, 1070−1071.
(21) Nocton, G.; Pecaut, J.; Mazzanti, M. *Angew. Chem., Int. Ed.* **2008**, *47*, 3040−3042.
(22) Evans, W. J.; Kozimor, S. A.; Ziller, J. W. *Science* **2005**, *309*, 1835−1838.
(23) Fortier, S.; Wu, G.; Hayton, T. W. *J. Am. Chem. Soc.* **2010**, *132*, 6888−6889.
(24) King, D. M.; Tuna, F.; McInnes, E. J. L.; McMaster, J.; Lewis, W.; Blake, A. J.; Liddle, S. T. *Science* **2012**, *337*, 717−720.
(25) Fox, A. R.; Bart, S. C.; Meyer, K.; Cummins, C. C. *Nature* **2008**, *455*, 341−349.
(26) Andrea, T.; Eisen, M. S. *Chem. Soc. Rev.* **2008**, *37*, 550−567.
(27) Castro-Rodriguez, I.; Olsen, K.; Gantzel, P.; Meyer, K. *J. Am. Chem. Soc.* **2003**, *125*, 4565−4571.
(28) Castro-Rodriguez, I.; Nakai, H.; Meyer, K. *Angew. Chem., Int. Ed.* **2006**, *45*, 2389−2392.
(29) Schelter, E. J.; Wu, R. L.; Veauthier, J. M.; Bauer, E. D.; Booth, C. H.; Thomson, R. K.; Graves, C. R.; John, K. D.; Scott, B. L.; Thompson, J. D.; Morris, D. E.; Kiplinger, J. L. *Inorg. Chem.* **2010**, *49*, 1995−2007.
(30) Schelter, E. J.; Wu, R. L.; Scott, B. L.; Thompson, J. D.; Cantat, T.; John, K. D.; Batista, E. R.; Morris, D. E.; Kiplinger, J. L. *Inorg. Chem.* **2010**, *49*, 924−933.
(31) Kraft, S. J.; Walensky, J.; Fanwick, P. E.; Hall, M. B.; Bart, S. C. *Inorg. Chem.* **2010**, *49*, 7620−7622.
(32) Evans, W. J.; Kozimor, S. A.; Ziller, J. W. *Chem. Commun.* **2005**, 4681−4683.
(33) Evans, W. J.; Kozimor, S. A.; Ziller, J. W.; Kaltsoyannis, N. *J. Am. Chem. Soc.* **2004**, *126*, 14533−14547.
(34) Evans, W. J.; Traina, C. A.; Ziller, J. W. *J. Am. Chem. Soc.* **2009**, *131*, 17473−17481.
(35) Diaconescu, P. L.; Arnold, P. L.; Baker, T. A.; Mindiola, D. J.; Cummins, C. C. *J. Am. Chem. Soc.* **2000**, *122*, 6108−6109.
(36) Diaconescu, P. L.; Cummins, C. C. *J. Am. Chem. Soc.* **2002**, *124*, 7660−7661.
(37) Zi, G. F.; Jia, L.; Werkema, E. L.; Walter, M. D.; Gottfriedsen, J. P.; Andersen, R. A. *Organometallics* **2005**, *24*, 4251−4264.
(38) Korobkov, I.; Gorelsky, S.; Gambarotta, S. *J. Am. Chem. Soc.* **2009**, *131*, 10406−10420.
(39) Kraft, S. J.; Williams, U. J.; Daly, S. R.; Schelter, E. J.; Kozimor, S. A.; Boland, K. S.; Kikkawa, J. M.; Forrest, W. P.; Christensen, C. N.; Schwarz, D. E.; Fanwick, P. E.; Clark, D. L.; Conradson, S. D.; Bart, S. C. *Inorg. Chem.* **2011**, *50*, 9838−9848.
(40) Patel, D.; Moro, F.; McMaster, J.; Lewis, W.; Blake, A. J.; Liddle, S. T. *Angew. Chem., Int. Ed.* **2011**, *50*, 10388−10392.
(41) Mazzanti, M.; Gambarotta, S.; Floriani, C.; Chiesivilla, A.; Guastini, C. *Inorg. Chem.* **1986**, *25*, 2308−2314. Gambarotta, S.; Mazzanti, M.; Floriani, C.; Zehnder, M. *J. Chem. Soc., Chem. Commun.* **1984**, 1116−1118.
(42) Camp, C.; Guidal, V.; Biswas, B.; Pecaut, J.; Dubois, L.; Mazzanti, M. *Chem. Sci.* **2012**, *3*, 2433−2448.
(43) Dube, T.; Gambarotta, S.; Yap, G. *Organometallics* **1998**, *17*, 3967−3973.
(44) Rosi, M.; Sgamellotti, A.; Franceschi, F.; Floriani, C. *Chem.—Eur. J.* **1999**, *5*, 2914−2920.
(45) Camp, C.; Mougel, V.; Horeglad, P.; Pecaut, J.; Mazzanti, M. *J. Am. Chem. Soc.* **2010**, *132*, 17374−17377.
(46) Gaunt, A. J.; Jones, M. B. *Chem. Rev.* **2013**, *113*, 1137−1198.
(47) Sessler, J. L.; Melfi, P. J.; Pantos, G. D. *Coord. Chem. Rev.* **2006**, *250*, 816−843.
(48) Arnold, P. L.; Love, J. B.; Patel, D. *Coord. Chem. Rev.* **2009**, *253*, 1973−1978.
(49) Arnold, P. L.; Pecharman, A. F.; Hollis, E.; Yahia, A.; Maron, L.; Parsons, S.; Love, J. B. *Nat. Chem.* **2010**, *2*, 1056−1061.
(50) Arnold, P. L.; Hollis, E.; White, F. J.; Magnani, N.; Caciuffo, R.; Love, J. B. *Angew. Chem., Int. Ed.* **2011**, *50*, 887−890.
(51) Nocton, G.; Horeglad, P.; Vetere, V.; Pecaut, J.; Dubois, L.; Maldivi, P.; Edelstein, N. M.; Mazzanti, M. *J. Am. Chem. Soc.* **2010**, *132*, 495−508.
(52) Mougel, V.; Horeglad, P.; Nocton, G.; Pecaut, J.; Mazzanti, M. *Chem.—Eur. J.* **2010**, *16*, 14365−14377.
(53) Mougel, V.; Horeglad, P.; Nocton, G.; Pecaut, J.; Mazzanti, M. *Angew. Chem., Int. Ed.* **2009**, *48*, 8477−8480.
(54) Mougel, V.; Pecaut, J.; Mazzanti, M. *Chem. Commun.* **2012**, *48*, 868−870.
(55) Takao, K.; Kato, M.; Takao, S.; Nagasawa, A.; Bernhard, G.; Hennig, C.; Ikeda, Y. *Inorg. Chem.* **2010**, *49*, 2349−2359.
(56) Arnold, P. L.; Potter, N. A.; Magnani, N.; Apostolidis, C.; Griveau, J. C.; Colineau, E.; Morgenstern, A.; Caciuffo, R.; Love, J. B. *Inorg. Chem.* **2010**, *49*, 5341−5343.
(57) Salmon, L.; Thuery, P.; Ephritikhine, M. *Dalton Trans.* **2004**, 4139−4145.
(58) Salmon, L.; Thuery, P.; Ephritikhine, M. *Dalton Trans.* **2004**, 1635−1643.
(59) Arnold, P. L.; Potter, N. A.; Carmichael, C. D.; Slawin, A. M. Z.; Roussel, P.; Love, J. B. *Chem. Commun.* **2010**, *46*, 1833−1835.
(60) Le Borgne, T.; Riviere, E.; Marrot, J.; Girerd, J. J.; Ephritikhine, M. *Angew. Chem., Int. Ed.* **2000**, *39*, 1647−1649.
(61) Kiplinger, J. L.; Morris, D. E.; Scott, B. L.; Burns, C. J. *Organometallics* **2002**, *21*, 5978−5982.
(62) Carmichael, C. D.; Jones, N. A.; Arnold, P. L. *Inorg. Chem.* **2008**, *47*, 8577−8579.
(63) Takano, K.; Takahashi, M.; Fukushima, T.; Takezaki, M.; Tominaga, T.; Akashi, H.; Takagi, H.; Shibahara, T. *Bull. Chem. Soc. Jpn.* **2012**, *85*, 1210−1221.
(64) Cameron, P. A.; Gibson, V. C.; Redshaw, C.; Segal, J. A.; White, A. J. P.; Williams, D. J. *J. Chem. Soc., Dalton Trans.* **2002**, 415−422.
(65) *CrysAlisPro CCD; CrysAlisPro RED ; ABSPACK; CrysAlis PRO*; Agilent Technologies: Yarnton, England, 2010.
(66) Sheldrick, G. M. *SHELXTL*, 6.14th ed.; Bruker: Madison, WI, 1997.
(67) Han, F. B.; Li, B. Y.; Zhang, Y.; Wang, Y. R.; Shen, Q. *Organometallics* **2010**, *29*, 3467−3470.
(68) Maury, O.; Villiers, C.; Ephritikhine, M. *Angew. Chem., Int. Ed.* **1996**, *35*, 1129−1130.
(69) Monreal, M. J.; Diaconescu, P. L. *J. Am. Chem. Soc.* **2010**, *132*, 7676−7683.
(70) Lam, O. P.; Heinemann, F. W.; Meyer, K. *Angew. Chem., Int. Ed.* **2011**, *50*, 5965−5968.
(71) Evans, D. F. *J. Am. Chem. Soc.* **1959**, 2003−2005.
(72) Bozoklu, G.; Gateau, C.; Imbert, D.; Pecaut, J.; Robeyns, K.; Filinchuk, Y.; Memon, F.; Muller, G.; Mazzanti, M. *J. Am. Chem. Soc.* **2012**, *134*, 8372−8375.
(73) Allouche, L.; Marquis, A.; Lehn, J.-M. *Chem.—Eur. J.* **2006**, 7520−7525.
(74) Sonnenberger, D. C.; Gaudiello, J. G. *Inorg. Chem.* **1988**, *27*, 2747−2748.
(75) Morris, D. E.; Da Re, R. E.; Jantunen, K. C.; Castro-Rodriguez, I.; Kiplinger, J. L. *Organometallics* **2004**, *23*, 5142−5153.
(76) Schelter, E. J.; Yang, P.; Scott, B. L.; Thompson, J. D.; Martin, R. L.; Hay, P. J.; Morris, D. E.; Kiplinger, J. L. *Inorg. Chem.* **2007**, *46*, 7477−7488.

Small-Molecule Activation

DOI: 10.1002/anie.201405031

# Tuning Lanthanide Reactivity Towards Small Molecules with Electron-Rich Siloxide Ligands**

*Julie Andrez, Jacques Pécaut, Pierre-Alain Bayle, and Marinella Mazzanti**

***Abstract:*** *The synthesis, structure, and reactivity of stable homoleptic heterometallic $LnL_4K_2$ complexes of divalent lanthanide ions with electron-rich tris(tert-butoxy)siloxide ligands are reported. The $[Ln(OSi(OtBu)_3)_4K_2]$ complexes (Ln = Eu, Yb) are stable at room temperature, but they promote the reduction of azobenzene to yield the KPhNNPh radical anion as well as the reductive cleavage of $CS_2$ to yield $CS_3^{2-}$ as the major product. The $Eu^{III}$ complex of the radical anion PhNNPh is structurally characterized. Moreover, $[Yb(OSi(OtBu)_3)_4K_2]$ can reduce $CO_2$ at room temperature. Release of the reduction products in $D_2O$ shows the quantitative formation of both oxalate and carbonate in a 1:2.2 ratio. The bulky siloxide ligands enforce the labile binding of the reduction products providing the opportunity to establish a closed synthetic cycle for the $Yb^{II}$-mediated $CO_2$ reduction. These studies show that the presence of four electron-rich siloxide ligands renders their $Eu^{II}$ and $Yb^{II}$ complexes highly reactive.*

Metal complexes capable of reducing small molecules, such as $CO_2$ and $CS_2$, in a controlled manner and under ambient conditions are a very attractive current target.[1] The majority of research into metal-mediated transformations of small molecules has focused on d-block transition metals, and is comparatively much less developed for f-block elements.[2] Notably, the use of f-block elements in the activation and reduction of $CO_2$ and $CS_2$ is limited to a few interesting and unprecedented examples.[2a,b,3] In particular, there are only three reported examples of $CO_2$ reduction and one example of $CS_2$ reduction mediated by complexes of lanthanides.[4] The reduction of diazobenzene, an interesting model substrate for $N_2$ reduction, was also reported for $Sm^{II}$ complexes,[2c] but has never been observed for the less-reducing $Eu^{II}$ complexes.

[*] J. Andrez, Dr. J. Pécaut, P.-A. Bayle
Laboratoire de Reconnaissance Ionique et
Chimie de Coordination SCIB
UMR-E3 CEA-UJF, INAC, CEA-Grenoble
17 rue des Martyrs, 38054 Grenoble Cedex 09 (France)
Dr. M. Mazzanti
EPFL, ISIC
Batiment CH J2 490
1015 Lausanne (Switzerland)
E-mail: marinella.mazzanti@epfl.ch

[**] We thank C. LeBrun, S. Gambarelli, and L. Dubois for their contribution to the spectroscopic characterizations. We thank L. Plassais for technical support. We acknowledge support from Labex Arcane (ANR-11-LABX-003-01). This work was also supported by COST Action CM1006–EUFEN: European F-Element Network).

Supporting information for this article is available on the WWW under http://dx.doi.org/10.1002/anie.201405031.

The optimization of the ion size in a given ligand environment provides a versatile tool for tuning the reactivity which is unique to lanthanide ions.[5] However, out of the 14 lanthanide ions that display similar coordination properties but a range of different ionic radii, the metal-centered reduction of heteroallenes has only been reported for the $Sm^{II}$ ion. This is probably a result of the fact that the highly reducing lanthanide ions, such as $Nd^{II}$, $Tm^{II}$, and $Dy^{II}$,[2b,5] are difficult to handle and have different reactivities compared to $Sm^{II}$. The $Eu^{II}$ and $Yb^{II}$ ions provide easier access to complexes of differently sized ions because of the higher stability of $Eu^{II}$ and $Yb^{II}$ precursors. However, the reductive chemistry of $Eu^{II}$ and $Yb^{II}$ has been limited by the $Ln^{3+}/Ln^{2+}$ redox potential of Eu and Yb ions (−0.35 V and −1.15 V versus NHE respectively, NHE = normal hydrogen electrode) that is significantly lower than the $Sm^{III}/Sm^{II}$ redox potential (−1.55 V versus NHE).

Electron-rich ligands were found to impart unusual reducing properties to the $Ce^{3+}$ ion,[6] but the use of electron-rich ligands to impart greater reducing ability to $Ln^{II}$ ions with poor reducing ability has not been investigated. In the search for suitable ligands that could confer higher reducing ability to the $Eu^{II}$ and $Yb^{II}$ ions, we have identified tris(*tert*-butoxy)siloxides as attractive bulky, electron-rich ligands that can adopt mono- or bidentate forms and which can support unusual reactivity at reduced metal centers.[3c,7] Siloxides have rarely been used as ancillary ligands in lanthanide chemistry[8] with only two structurally characterized examples of dinuclear divalent lanthanide complexes.[8d,9]

Herein, we show that electron-rich tris(*tert*-butoxy)siloxide ligands (L) can impart stability and unusual reactivity to homoleptic heterodimetallic[8b,10] $LnK_2$ "ate" complexes of $Yb^{II}$ and $Eu^{II}$ ions. We report the syntheses and structures of mononuclear $[Ln^{II}(OSi(OtBu)_3)_4K_2]$ complexes for Sm, Eu, and Yb ions and the first example of heteroallene activation by a $Yb^{II}$ complex. The $[Yb(OSi(OtBu)_3)_4K_2]$ complex is found to promote the reduction of PhNNPh, $CS_2$, and $CO_2$. Moreover, the bulky siloxide ligands enforce the labile binding of the reduction products providing the opportunity to establish a closed synthetic cycle for the reduction of $CO_2$.

The reaction of the trivalent lanthanide salts $LnX_3$ (Ln = Eu or Yb, X = OTf; Ln = Sm, X = I) with $KOSi(OtBu)_3$ (L; 4 equivalents) affords the "ate" $[Ln(OSi(OtBu)_3)_4K]$ ($Ln^{III}L_4K$) complexes (Scheme S1, Supporting Information). The structure of complex $Yb^{III}L_4K$ was determined by single-crystal X-ray diffraction analysis and is shown in Figure 1 a. In this structure, the $Yb^{III}$ ion is tetracoordinated by four siloxide ligands bound to the Yb ion in a $\kappa^1$ fashion. Three siloxide ligands bridge the Yb and K ions, binding the K ion in a $\kappa^2$ mode. The Ln–O bond lengths are in the range of the

  

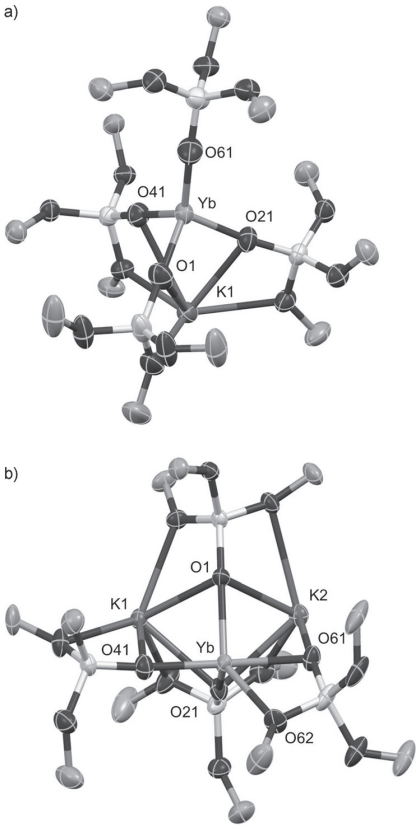


***Figure 1.*** Molecular structures of $Yb^{III}L_4K$ (a) and $Yb^{II}L_4K_2$ (b). Thermal ellipsoids are set at 50% probability. Hydrogens atoms, methyl groups, and disorder are omitted for clarity. Selected bond lengths [Å] in $Yb^{III}L_4K$: Yb-O1 2.060(2), Yb-O21 2.075(2), Yb-O41 2.070(2), Yb-O61 2.041(2); and in $Yb^{II}L_4K_2$: Yb-O1 2.271(5), Yb-O21 2.272(5), Yb-O41 2.251(6), Yb-O61 2.422(5), Yb-O62 2.571(6).

values reported for mononuclear $Yb^{III}$ phenoxide and siloxide complexes.[8c,d]

The $^1$H NMR spectra of $Ln^{III}L_4K$ at 25 °C in deuterated toluene and THF show, in both solvents, one single resonance signal for the 108 protons of the complexes, in agreement with the presence of solution species with tetrahedral symmetry. The addition of [18]crown-6 (18C6; 1 equivalent) to a solution of $Yb^{III}L_4K$ in [$D_8$]THF results in a shift of the $^1$H NMR signal of the siloxide from $\delta = 5.48$ to 1.94 ppm. These results suggest the presence in THF of a heterobimetallic structure where the potassium cation adopts a fluxional coordination. The $^1$H NMR spectrum of $Yb^{III}L_4K$ shows a significantly broader resonance signal in toluene compared to THF suggesting the presence of fluxional coordination in toluene.

When the temperature is decreased to −30 °C, the $^1$H NMR spectrum of the $Yb^{III}L_4K$ complex shows the appearance of two different broad resonance signals with an integration ratio of 3:1, in agreement with the solid-state structure and the presence of a heterobimetallic LnK structure in toluene solution (Supporting Information). Variable-temperature $^1$H NMR experiments carried out in toluene for the $Eu^{III}L_4K$ complex show that the resonance signal of the siloxide broadens and shifts slightly. The $^1$H NMR spectrum of the $Sm^{III}L_4K$ complex in toluene is not significantly affected by the temperature, in agreement with an increased potassium fluxionality. Reduction of $Ln^{III}L_4K$ in hexane at −40 °C with potassium (1 equivalent) affords the divalent complexes [$Ln(OSi(OtBu)_3)_4(THF)_xK_2$] ($Ln^{II}L_4K_2$; Ln = Eu, $x = 1$; Ln = Yb or Sm, $x = 0$), which were isolated as pure compounds and in high yield after recrystallization (Scheme 1). The compound $Sm^{II}L_4K_2$ decomposes at 25 °C

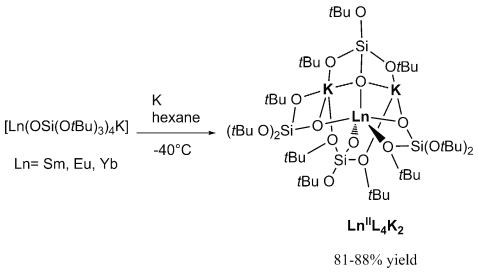


***Scheme 1.*** Synthesis of $Ln^{II}$ tris(*tert*-butoxy)siloxide complexes $Ln^{II}L_4K_2$.

in toluene solution but complexes $Eu^{II}L_4K_2$ and $Yb^{II}L_4K_2$ are stable for weeks in toluene at 25 °C and can be prepared at ambient temperature. Interestingly, only $Yb^{II}L_4K_2$ has a low solubility in THF which can be increased by the addition of 18C6 (2 equivalents).

Single crystals suitable for X-ray diffraction analysis were obtained from a concentrated solution of $Ln^{II}L_4K_2$ in toluene at −40 °C for $Yb^{II}L_4K_2$, in hexane at −40 °C for $Sm^{II}L_4K_2$, and in a hexane/THF 100:1 mixture at −40 °C for $Eu^{II}L_4K_2$. The structure of $Yb^{II}L_4K_2$ (Figure 1 b) shows that the $Yb^{II}$ center is pentacoordinated with five siloxide oxygen atoms in the coordination sphere in a highly distorted geometry. The siloxide ligands bridge the Yb center to two potassium cations, affording a neutral heterobimetallic structure. The solid-state structure of $Sm^{II}L_4K_2$ is isostructural to the $Yb^{II}$ complex, whereas in the $Eu^{II}L_4K_2$ complex an additional THF molecule binds one potassium cation (Supporting Information). The Ln–O bond lengths in the $Ln^{II}L_4K_2$ complexes (Table S2) are consistent with the values previously reported for lanthanide phenoxide and siloxide compounds.[8c,d,9]

The $^1$H NMR spectrum of $Ln^{II}L_4K_2$ in deuterated toluene shows only one resonance signal for the 108 protons of the siloxide ligands. Variable-temperature $^1$H NMR studies show that the spectrum of $Yb^{II}L_4K_2$ in toluene is only slightly affected by the temperature. Addition of crown ether to the $Yb^{II}L_4K_2$ complex in deuterated toluene reduces dramatically the solubility of the divalent Yb complex in toluene, suggesting that in the absence of crown ether the potassium remains bound to the siloxide, as found in the solid-state structure. Thus the presence of one unique signal for all the siloxide ligands in toluene solution can be interpreted in term of a fluxional coordination of the potassium cation.

In view of the higher stability of the $Eu^{II}$ and $Yb^{II}$ complexes compared to the $Sm^{II}$ complex, we investigated if

  

the electron-rich environment provided by the four siloxide ligands could promote the reduction of small molecules. Notably, cyclic voltammetry studies in THF solution (with or without the presence of 18C6) show a large shift of the oxidation potential for the $Ln^{II}L_4K_2$ complexes (Eu: $E_{ox} = -1.26$ V; Yb: $E_{ox} = -2.19$ V) compared to $LnI_2$ (Eu: $E_{ox} = -0.14$ V; Yb: $E_{ox} = -0.68$ V), clearly showing the enhancement in reducing ability provided by the siloxide ligand.[11]

The reaction of $Ln^{II}L_4K_2$ (Ln = Eu, Yb) with azobenzene (1 equivalent) in toluene at room temperature affords the trivalent lanthanide complexes $Ln^{III}L_4K$ (Ln = Eu, Yb) and the reduced potassium radical anion of azobenzene KPhNNPh (Scheme 2).

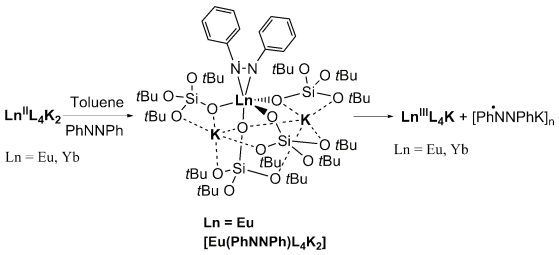


***Scheme 2.*** Reaction of $Ln^{II}$ siloxide complexes ($Ln^{II}L_4K_2$; Ln = Eu, Yb) with diazobenzene (PhNNPh).

The solid-state EPR spectrum of the isolated KPhNNPh radical in suspension in a mixture of toluene/hexane (20/1 v/v) at 19 °C shows an intense signal at approximately $g = 2$, characteristic of an organic radical (see Supporting Information). The solution-state EPR spectrum measured in DME/THF (DME = 1,2-dimethoxyethane) shows a hyperfine structure consistent with the spectrum previously reported for the KPhNNPh radical anion generated in DME solution (see Supporting Information).[12] The structure of KPhNNPh was determined by X-ray diffraction studies and shows a 2D polymeric structure (Figure 2). The nitrogen atoms of the azobenzene radical are found on two positions with occupation coefficients of 0.66(2) and 0.34(2), respectively. The structural data shows that the N–N bond length between the principal position of the nitrogen atoms N1 (1.331(17) Å) is elongated compared to free azobenzene (1.25 Å),[13] in agreement with the presence of a monoanionic reduced ligand. The value of the N–N bond length in KPhNNPh is in the range of those found[14] in carbocyclic complexes of $Tm^{III}$ or $Sm^{III}$ containing a monoanionic reduced diazobenzene (1.32–1.39 Å).

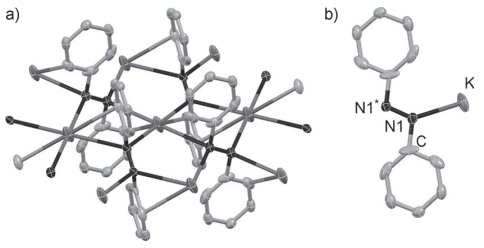


***Figure 2.*** Molecular structure of the 2D polymer (a) and detailed unit (b) of KPhNNPh (thermal ellipsoids set at 50% probability). Disorder and hydrogen atoms were omitted for clarity. Selected bond lengths [Å]: N1-N1* 1.331(17), N1-C 1.432(12), N1-K 2.921(7) (* = $-x$, $-y+1$, $-z+1$).

Some crystals of the intermediate [Eu($\eta^2$-PhNNPh)-(OSi(O*t*Bu)$_3$)$_4$K$_2$], [Eu(PhNNPh)$L_4K_2$], were isolated by carrying out the reaction at −40 °C in hexane. In the structure of [Eu(PhNNPh)$L_4K_2$] (Figure 3) the europium ion is hexacoordinated in a highly distorted trigonal-prismatic fashion. The N81–N82 bond length (1.450(8) Å) is longer than in the free radical KPhNNPh (1.331(17) Å) and is similar to the N–N simple bond length in hydrazine (1.45 Å).[13] The Eu–N82 distance is significantly shorter than Eu–N81, suggesting the presence of a radical localized on N82. The azobenzene radical-anion complex, $[(C_5Me_5)_2Sm(N_2Ph_2)(THF)]$, has been previously obtained from the single-electron reduction of azobenzene by the $Sm^{II}$ $[(Cp)_2Sm(THF)_2]$ complex.[14b] The analogous $Yb^{II}$ complex leads to the two-electron-reduction product only.[14b] In all cases, the reduced diazobenzene ligand forms a stable complex and the release of the reduced diazobenzene ligand is not detected.

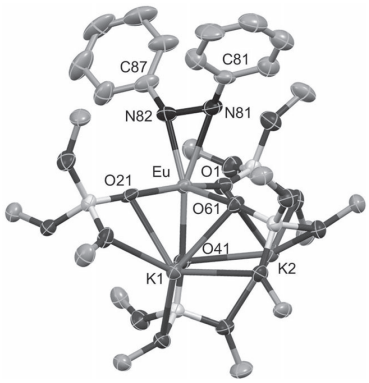


***Figure 3.*** Molecular structure of [Eu(PhNNPh)$L_4K_2$] (thermal ellipsoids set at 50% probability). Hydrogen atoms, methyl groups, and solvent molecule were omitted for clarity. Selected bond lengths [Å]: Eu-O1 2.276(5), Eu-O21 2.244(4), Eu-O41 2.357(4), Eu-O61 2.237(4), Eu-N81 2.599(5), Eu-N82 2.328(5), N81-N82 1.450(8), N81-C81 1.429(8), N82-C87 1.377(8).

The structure of [Eu(PhNNPh)$L_4K_2$] (Figure 3) shows that in spite of the presence of four bulky siloxide ligands, the lanthanide center is still accessible for binding coordinating substrates. Moreover, the presence of four electron-rich siloxide ligands renders their $Eu^{II}$ and $Yb^{II}$ complexes highly reactive. Notably, this reactivity provides the first example of the reduction of azobenzene by a $Eu^{II}$ complex.

This unprecedented reactivity prompted us to investigate the reaction of these complexes with heteroallenes. NMR spectroscopic studies show that the stoichiometric addition of $^{13}CS_2$ to a THF/18C6 solution of the divalent $Ln^{II}L_4K_2$ (Ln = Eu, Yb) complexes affords the trivalent $Ln^{III}L_4K$ (Ln = Eu, Yb) species in 94% yield (determined

  

by NMR spectroscopy using naphthalene as an internal standard). The $^{13}C$ NMR spectrum in deuterated THF of the soluble fraction of the reaction mixture after reaction of the $Ln^{II}L_4K_2$ complex with $^{13}CS_2$ in THF/18C6 shows the presence of the $Ln^{III}L_4K$ complex and a signal at $\delta = 266.97$ ppm which is assigned to the $^{13}CS_3^{2-}$ anion.[15] The fraction of the reaction mixture which was insoluble in THF was dissolved in [D$_6$]DMSO. The $^{13}C$ NMR spectrum of this fraction showed the presence of $^{13}CS_3^{2-}$ as a major species. The compounds $C_2S_4^{2-}$ (with a resonance signal at $\delta = 264$ ppm) and $C_3S_5^{2-}$ (with resonance signals at $\delta = 203$ and 145 ppm)[16] are also present as minor products. Diffusion of toluene into a DMSO solution of $^{13}CS_3K_2$ afforded single crystals suitable for X-ray diffraction of the 3D polymer $[(K_2CS_3)_5(DMSO)_{12}]_n$ (Figure S3). Thus, the $Ln^{III}L_4K$ complexes promote both the reductive coupling of $CS_2$ to form $C_2S_4^{2-}$ and the reductive disproportionation of $CS_2$ to form $CS_3^{2-}$ and CS. The low stability of CS often prevents its characterization but in this case CS is partly trapped in the $C_3S_5^{2-}$ by-product.

The relative ratio of the products obtained from the reduction of $CS_2$ by $Yb^{II}L_4K_2$ in THF/18C6 is $CS_3^{2-}$:$C_2S_4^{2-}$:$C_3S_5^{2-}$ = 1:0.14:0.35. The selectivity for the formation of the $CS_3^{2-}$ species is significantly higher when the complex $Eu^{II}L_4K_2$ is used to reduce $CS_2$ ($CS_3^{2-}$:$C_2S_4^{2-}$:$C_3S_5^{2-}$ = 1:0.025:0.05) clearly showing that the nature of the lanthanide ion plays a role in the reduction mechanism (Scheme 3). The relative ratio of the products

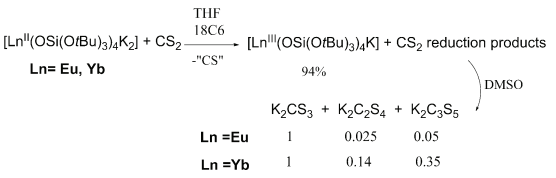


***Scheme 3.*** Reaction of $Ln^{II}L_4K_2$ with $CS_2$ and ratio of reduction products.

does not change when the reaction is carried out in toluene or in the presence of an excess of $CS_2$. The difference in selectivity probably arises from the difference in size (ionic radii of $Yb^{II}$ = 1.02 Å, $Eu^{II}$ = 1.17 Å)[17] of the two metal ions leading to different steric demands in the respective $CS_2$-bound reaction intermediates, though the different $Ln^{3+}/Ln^{2+}$ redox potentials of the two ions (Yb = −1.15 V, Eu = −0.35 V versus NHE)[18] might also play a role. These results highlight the advantage of having access to complexes of different $Ln^{II}$ ions in the same ligand environment for tuning selectivity.

Attempts to isolate intermediates with lanthanide-bound reaction products from these reactions were not successful. The steric bulk of the siloxide ligands and the dianionic charge of the thiocarbonate and tetrathioxalate products are likely to promote the decoordination of the reaction product. However, this selectivity in the reduction of $CS_2$ by the $Ln^{II}L_4K_2$ complexes suggests that the reaction is indeed occurring by an inner-sphere mechanism. The structure of the intermediate [Eu(PhNNPh)L$_4$K$_2$] isolated from the reaction of $Eu^{II}$ with diazobenzene also supports the fact that sterically less-demanding substrates, such as $CS_2$ and $CO_2$, can coordinate the metal center. Herein, the electron-rich environment provided by the siloxide ligands leads to a reactivity unprecedented for the $Eu^{II}$ and $Yb^{II}$ ions.

The ability of $Ln^{II}L_4K_2$ (Ln = Eu, Yb) to reduce $CS_2$ prompted us to investigate their reactivity with carbon dioxide. The $Eu^{II}$ complex does not react with $CO_2$ whereas an immediate reaction was observed when a toluene solution of the divalent $Yb^{II}L_4K_2$ complex was exposed to excess $CO_2$. The $^1H$ NMR spectra of the reaction mixture after reaction of a toluene solution of $Yb^{II}L_4K_2$ with excess $^{13}CO_2$ show the formation of the trivalent complex $Yb^{III}L_4K$ (Scheme 4) in

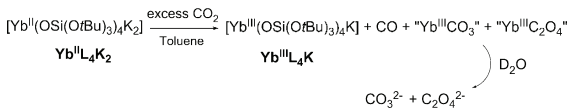


***Scheme 4.*** Reaction of $Yb^{II}L_4K_2$ with $CO_2$.

approximately 50% yield (evaluated by $^1H$ NMR spectroscopy using naphthalene as an internal standard). The $^{13}C$ NMR spectra of these reaction mixtures in toluene or THF show only the presence of the trivalent complex and of free $^{13}CO$. This data suggests that mononuclear $Yb^{III}$ complexes containing bound reduction products are also present in solution. Attempts to isolate single crystals of these compounds lead only to the isolation of the $Yb^{III}L_4K$ complex, suggesting a labile binding of the $CO_2$ reduction products.

When toluene and excess $CO_2$ are removed and $D_2O$ is added to release the coordinated reaction products, $^{13}C$ NMR spectroscopic studies clearly show two resonance signals corresponding to potassium oxalate ($\delta = 173$ ppm) and potassium carbonate ($\delta = 168$ ppm) present in a 1:2.2 ratio. Quantitative $^{13}C$ NMR spectra measured using $^{13}C$-labelled sodium acetate show a total yield (of oxalate and carbonate) of approximately 95%. This confirms that the reaction of the $Yb^{III}L_4K$ complex with $CO_2$ leads quantitatively to the reduction of $CO_2$ to CO, oxalate, and carbonate.

As the reduction of $CO_2$ by $Yb^{II}L_4K_2$ leads to the trivalent $Yb^{III}L_4K$ complex, we envisaged the possibility to implement this reduction in a closed synthetic cycle.

After $Yb^{II}L_4K_2$ undergoes reaction with $CO_2$ to afford $Yb^{III}L_4K$ and unidentified substrate-bound $Yb^{III}$ compounds, the addition of $KC_8$ to the reaction mixture yields $Yb^{II}L_4K_2$ with the concomitant formation of side products (some free potassium siloxide is detected). This cycle can be repeated several times and each time $Yb^{III}L_4K$ is formed in 50% yield. After 5 cycles (see Supporting Information for experimental conditions), the $^1H$ NMR spectra clearly show a decreased concentration of the active divalent complex and an increased concentration of side products. This experiment suggests that the $Yb^{III}L_4K$ complex is quantitatively reduced back to the $Yb^{II}L_4K_2$ compound. The synthetic cycle is probably terminated by the formation of carbonate- and oxalate-bound $Yb^{III}$ species that are not further reduced to yield the $Yb^{II}L_4K_2$

  

precursor.[19] Future studies will be directed to investigate the mechanism of $CO_2$ reduction and to optimize the steric bulk to prevent the coordination of the reaction products to the final complex and to improve selectivity. Such optimization should allow the implementation of a catalytic cycle.

In conclusion, the tris(*tert*-butoxy)siloxide ligand can be used to isolate the heterobimetallic $[Ln^{II}(OSi(OtBu)_3)_4K_2]$ complexes (Ln = Sm, Eu, and Yb). The $Eu^{II}$ complex promotes the reduction of azobenzene and $CS_2$, affording the first example of azobenzene reduction by $Eu^{II}$ and the first example of trithiocarbonate formation from the reductive splitting of $CS_2$ promoted by a lanthanide ion. The $Yb^{II}$ complex reduces $CO_2$ to carbonate and oxalate, to afford the first example of $CO_2$ reduction by a $Yb^{II}$ center. Thus, these studies show that the electron-rich environment provided by the siloxide ligands leads to a reactivity unprecedented for the $Eu^{II}$ and $Yb^{II}$ ions, and that siloxide "ate" complexes of $Eu^{II}$ and $Yb^{II}$ are very attractive stable precursors for the reduction of heteroallenes. In these systems the bulky siloxide ligands prevent the strong coordination to the final lanthanide complex of the products of the reduction of $CS_2$ and the azobenzene reaction, setting the basis for the ready exchange of substrates which is a prerequisite for the implementation of catalytic cycles. A suitable tuning of the steric demand should prove very effective for the optimization of selectivity and promote the release of carbonate and oxalate.

Received: May 6, 2014
Revised: June 4, 2014
Published online: July 30, 2014

**Keywords:** carbon dioxide reduction · carbon disulfide reduction · lanthanide complexes · siloxide ligands · small-molecule activation

[1] W. B. Tolman, *Activation of Small Molecules*, Wiley-VCH, Weinheim, **2006**.

[2] a) H. S. La Pierre, K. Meyer in *Progress in Inorganic Chemistry* (Ed.: K. D. Karlin), Wiley-VCH, Hoboken, **2014**, *58*, 303 – 416; b) W. J. Evans, *Coord. Chem. Rev.* **2000**, *206*, 263 – 283; c) M. G. Gardiner, D. N. Stringer, *Materials* **2010**, *3*, 841 – 862; d) W. J. Evans, *J. Alloys Compd.* **2009**, *488*, 493 – 510; e) B. M. Gardner, S. T. Liddle, *Eur. J. Inorg. Chem.* **2013**, 3753 – 3770; f) R. K. Thomson, T. Cantat, B. L. Scott, D. E. Morris, E. R. Batista, J. L. Kiplinger, *Nat. Chem.* **2010**, *2*, 723 – 729; g) D. M. King, F. Tuna, E. J. L. McInnes, J. McMaster, W. Lewis, A. J. Blake, S. T. Liddle, *Science* **2012**, *337*, 717 – 720; h) A. S. P. Frey, F. G. N. Cloke, M. P. Coles, L. Maron, T. Davin, *Angew. Chem.* **2011**, *123*, 7013 – 7015; *Angew. Chem. Int. Ed.* **2011**, *50*, 6881 – 6883.

[3] a) O. P. Lam, L. Castro, B. Kosog, F. W. Heinemann, L. Maron, K. Meyer, *Inorg. Chem.* **2012**, *51*, 781 – 783; b) O. P. Lam, F. W. Heinemann, K. Meyer, *Angew. Chem.* **2011**, *123*, 6088 – 6091; *Angew. Chem. Int. Ed.* **2011**, *50*, 5965 – 5968; c) V. Mougel, C. Camp, J. Pecaut, C. Coperet, L. Maron, C. E. Kefalidis, M. Mazzanti, *Angew. Chem.* **2012**, *124*, 12446 – 12450; *Angew. Chem. Int. Ed.* **2012**, *51*, 12280 – 12284; d) J. G. Brennan, R. A. Andersen, A. Zalkin, *Inorg. Chem.* **1986**, *25*, 1756 – 1760; e) L. Castro, S. Labouille, D. R. Kindra, J. W. Ziller, F. Nief, W. J. Evans, L. Maron, *Chem. Eur. J.* **2012**, *18*, 7886 – 7895; f) O. T. Summerscales, A. S. P. Frey, F. G. N. Cloke, P. B. Hitchcock, *Chem. Commun.* **2008**, 198 – 200; g) W. S. Ren, H. B. Song, G. F. Zi, M. D. Walter, *Dalton Trans.* **2012**, *41*, 5965 – 5973; h) W. S. Ren, G. F. Zi, D. C. Fang, M. D. Walter, *J. Am. Chem. Soc.* **2011**, *133*, 13183 – 13196; i) I. Castro-Rodriguez, H. Nakai, L. N. Zakharov, A. L. Rheingold, K. Meyer, *Science* **2004**, *305*, 1757 – 1759; j) Z. M. Hou, K. Takamine, O. Aoki, H. Shiraishi, Y. Fujiwara, H. Taniguchi, *J. Org. Chem.* **1988**, *53*, 6077 – 6084; k) K. Takaki, S. Tanaka, Y. Fujiwara, *Chem. Lett.* **1991**, *20*, 493 – 494.

[4] a) W. J. Evans, J. M. Perotti, J. C. Brady, J. W. Ziller, *J. Am. Chem. Soc.* **2003**, *125*, 5204 – 5212; b) W. J. Evans, C. A. Seibel, J. W. Ziller, *Inorg. Chem.* **1998**, *37*, 770 – 776; c) N. W. Davies, A. S. P. Frey, M. G. Gardiner, J. Wang, *Chem. Commun.* **2006**, 4853 – 4855; d) D. Heitmann, C. Jones, D. P. Mills, A. Stasch, *Dalton Trans.* **2010**, *39*, 1877 – 1882.

[5] a) W. J. Evans, G. Zucchi, J. W. Ziller, *J. Am. Chem. Soc.* **2003**, *125*, 10 – 11; b) W. J. Evans, D. S. Lee, *Can. J. Chem.* **2005**, *83*, 375 – 384; c) F. Nief, *Dalton Trans.* **2010**, *39*, 6589 – 6598.

[6] a) J. R. Robinson, Z. Gordon, C. H. Booth, P. J. Carroll, P. J. Walsh, E. J. Schelter, *J. Am. Chem. Soc.* **2013**, *135*, 19016 – 19024; b) B. D. Mahoney, N. A. Piro, P. J. Carroll, E. J. Schelter, *Inorg. Chem.* **2013**, *52*, 5970 – 5977.

[7] a) P. T. Wolczanski, *Polyhedron* **1995**, *14*, 3335 – 3362; b) C. Krempner, *Eur. J. Inorg. Chem.* **2011**, 1689 – 1698; c) C. Camp, J. Pecaut, M. Mazzanti, *J. Am. Chem. Soc.* **2013**, *135*, 12101 – 12111; d) C. Camp, V. Mougel, J. Pecaut, L. Maron, M. Mazzanti, *Chem. Eur. J.* **2013**, *19*, 17528 – 17540.

[8] a) A. Fischbach, G. Eickerling, W. Scherer, E. Herdtweck, R. Anwander, *Z. Naturforsch. B* **2004**, *59*, 1353 – 1364; b) E. Le Roux, O. Michel, H. M. Sommerfeldt, Y. C. Liang, C. Maichle-Mossmer, K. W. Tornroos, R. Anwander, *Dalton Trans.* **2010**, *39*, 8552 – 8559; c) T. J. Boyle, L. A. M. Ottley, *Chem. Rev.* **2008**, *108*, 1896 – 1917; d) M. Nishiura, Z. M. Hou, Y. Wakatsuki, *Organometallics* **2004**, *23*, 1359 – 1368; e) G. Lapadula, A. Bourdolle, F. Allouche, M. P. Conley, I. del Rosal, L. Maron, W. W. Lukens, Y. Guyot, C. Andraud, S. Brasselet, C. Copéret, O. Maury, R. A. Andersen, *Chem. Mater.* **2014**, *26*, 1062 – 1073.

[9] D. J. Duncalf, P. B. Hitchcock, G. A. Lawless, *J. Organomet. Chem.* **1996**, *506*, 347 – 349.

[10] a) B. R. Elvidge, S. Arndt, T. P. Spaniol, J. Okuda, *Dalton Trans.* **2006**, 890 – 901; b) O. Michel, S. Konig, K. W. Tornroos, C. Maichle-Mossmer, R. Anwander, *Chem. Eur. J.* **2011**, *17*, 11857 – 11867; c) M. Zimmermann, N. A. Froystein, A. Fischbach, P. Sirsch, H. M. Dietrich, K. W. Tornroos, E. Herdtweck, R. Anwander, *Chem. Eur. J.* **2007**, *13*, 8784 – 8800.

[11] a) E. Prasad, B. W. Knettle, R. A. Flowers, *J. Am. Chem. Soc.* **2002**, *124*, 14663 – 14667; b) M. Shabangi, R. A. Flowers, *Tetrahedron Lett.* **1997**, *38*, 1137 – 1140.

[12] U. Buser, C. H. Ess, F. Gerson, *Magn. Reson. Chem.* **1991**, *29*, 721 – 725.

[13] R. Allmann, *The Chemistry of the Hydrazo, Azo, and Azoxy Groups*, Wiley, New York, **1975**.

[14] a) D. Turcitu, F. Nief, L. Ricard, *Chem. Eur. J.* **2003**, *9*, 4916 – 4923; b) W. J. Evans, D. K. Drummond, L. R. Chamberlain, R. J. Doedens, S. G. Bott, H. M. Zhang, J. L. Atwood, *J. Am. Chem. Soc.* **1988**, *110*, 4983 – 4994.

[15] D. Stueber, D. Patterson, C. L. Mayne, A. M. Orendt, D. M. Grant, R. W. Parry, *Inorg. Chem.* **2001**, *40*, 1902 – 1911.

[16] a) J. G. Breitzer, J. H. Chou, T. B. Rauchfuss, *Inorg. Chem.* **1998**, *37*, 2080 – 2081; b) R. M. Olk, W. Dietzsch, K. Kohler, R. Kirmse, J. Reinhold, E. Hoyer, L. Golic, B. Olk, *Z. Anorg. Allg. Chem.* **1988**, *567*, 131 – 144.

[17] R. D. Shannon, *Acta Crystallogr. Sect. A* **1976**, *32*, 751 – 767.

[18] L. R. Morss, *Chem. Rev.* **1976**, *76*, 827 – 841.

[19] A. C. Schmidt, A. V. Nizovtsev, A. Scheurer, F. W. Heinemann, K. Meyer, *Chem. Commun.* **2012**, *48*, 8634 – 8636.

  

Dalton Transactions

PAPER

View Article Online
View Journal | View Issue

Cite this: *Dalton Trans.*, 2015, **44**, 2650

# $CS_2$ activation at uranium(III) siloxide ate complexes: the effect of a Lewis acidic site†

Clément Camp,[a,b] Oliver Cooper,[a,b] Julie Andrez,[a,b] Jacques Pécaut[a,b] and Marinella Mazzanti*[c]

Received 26th August 2014,
Accepted 10th November 2014

DOI: 10.1039/c4dt02585g

www.rsc.org/dalton

Multimetallic cooperative binding of heteroallenes provides an attractive route to their activation, but the reduction of $CS_2$ at heterobimetallic sites, associating an electron-rich metal with a main group Lewis acid has not been explored. Here we show that the presence of a heterometallic U, K site plays an important role in the $CS_2$ reduction by uranium(III) complexes of the electron-rich and the sterically demanding tris(*tert*-butoxy)siloxide ligand. Specifically, the ion-pair complex [K(18c6)][U(OSi(O$^t$Bu)$_3$)$_4$], **1**, leads preferentially to the reductive disproportionation of $CS_2$ to $K_2CS_3$ and CS. The crystal structure of the thiocarbonate intermediate complex [U(OSi(O$^t$Bu)$_3$)$_4$ ($\mu_3$–$\kappa^2$:$\kappa^2$:$\kappa^2$–$CS_3$)$K_2$(18c6)$_2$], **3**, isolated from the toluene reaction mixture has been determined. In contrast, the heterobimetallic complex [U(OSi(O$^t$Bu)$_3$)$_4$K], **2**, promotes preferentially the reductive dimerization of $CS_2$ to $K_2C_2S_4$ and $K_2C_3S_5$. The $[K_2C_2S_4(DMSO)_3]_n$, **5**, and $[U(OSi(O^tBu)_3)_4K_2(C_3S_5)]_n$, **6**, polymeric compounds were isolated from this reaction and structurally characterized.

## Introduction

The metal-mediated activation of heteroallenes ($CO_2$, $CS_2$) is an area of growing interest due to the potential use of $CO_2$ as a low cost renewable C1 source.[1] Due to the higher reactivity of $CS_2$ compared to the thermodynamically stable $CO_2$ molecule, the chemistry of d-block transition metals with $CS_2$ has attracted a significant number of studies as a pertinent model for $CO_2$ reactivity.[2] Depending on the nature of the metal ion and the ancillary ligand, metal complexes have been shown to promote $CS_2$ disproportionation to $CS_3^{2-}$ and CS,[3] reductive dimerization to afford tetrathioxalate[4] or $CS_2$ reduction to sulphido complexes[5] with CS or thiocarbonate complexes as by-products.

A few examples of insertion[6] and reduction reactions of $CS_2$ promoted by f element complexes have been reported so far.[5b,7]

Notably reduction of $CS_2$ has been observed only for three U(III) systems.[7a–d] An unusual behaviour was reported for the reduction of $CS_2$ by the U(III) complex [((Ad ArO)$_3$N)U(DME)] which promotes both the reductive dimerization and the reductive disproportionation of $CS_2$ affording two different products (80% $C_2S_4^{2-}$ and 20% $CS_3^{2-}$)[7b]. In contrast the reaction of the U(III) complex [(RC$_5$H$_4$)$_3$U] (R = Me; SiMe$_3$) with $CS_2$ was found to afford the U(IV)–U(IV) dimer [(RC$_5$H$_4$)$_3$U]$_2$-[$\mu$-$\kappa^1$:$\kappa^2$-$CS_2$].[7a]

We have recently reported an analogous behaviour for the dinuclear homoleptic siloxide complex [U(OSi(O$^t$Bu)$_3$)$_2$($\mu$-OSi-(O$^t$Bu)$_3$)]$_2$ (Scheme 1), which also reduces $CS_2$ yielding a uranium(IV) dimer that features a reduced $CS_2^{2-}$ bridging group.[7d] Bulky siloxide ligands such as tris(*tert*-butoxy)siloxide have proven to be attractive ancillary ligands in the chemistry of trivalent uranium[7d,8,9] and in particular in the controlled reduction of heteroallenes.[7d,10] Notably, the electronic properties and steric demand of the uranium center can be tuned by changing the number of the siloxides and their denticity.[9a]

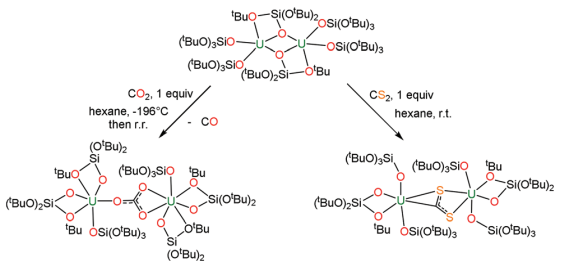


**Scheme 1** Reaction of [U$^{III}$(OSi(O$^t$Bu)$_3$)$_2$($\mu$-OSi(O$^t$Bu)$_3$)]$_2$ with $CO_2$ and $CS_2$.

[a]*Univ. Grenoble Alpes, INAC-SCIB, RICC, F-38000 Grenoble, France*
[b]*CEA, INAC-SCIB, F-38000 Grenoble, France*
[c]*Institut des Sciences et Ingénierie Chimique, Ecole Polytechnique Fédérale de Lausanne (EPFL), CH-1015 Lausanne, Switzerland.*
*E-mail: marinella.mazzanti@epfl.ch*

† Electronic supplementary information (ESI) available: $^1$H and $^{13}$C NMR spectra, and crystallographic data. CCDC 1012567–1012569. For ESI and crystallographic data in CIF or other electronic format see DOI: 10.1039/c4dt02585g

Moreover, tris(*tert*-butoxy)siloxides due to their multiple binding modes provide a route to heterobimetallic U, K complexes.[10] In particular we have recently shown that the neutral homodimetallic complex $[U(OSi(O^tBu)_3)_2(\mu\text{-}OSi(O^tBu)_3)]_2$ (Scheme 1),[7d] the "ate" complex $[K(18c6)][U(OSi(O^tBu)_3)_4]$, **1**, and the heterodimetallic U, K complex $[U(OSi(O^tBu)_3)_4K]$, **2** (Scheme 2) reduce $CO_2$ leading to different reaction products. Particularly remarkable is the observed effect of the presence of the potassium site on the reactivity of **2** which highlights the multimetallic cooperativity taking place in the reduction of $CO_2$ by such heterodimetallic complex.[10] Cooperative binding of heteroallenes at polymetallic complexes provides an attractive route for promoting their activation and reduction.[3b,4b,11,12]

However, while the seminal work by Bianchini and co-workers indicated that the presence of Lewis acid is important to achieve $CS_2$ dimerization,[13] the effect of cooperative binding of $CS_2$ at heterobimetallic sites, associating an electron-rich metal with a main group Lewis acid has not been explored.

In view of the multimetallic cooperative effect observed in $CO_2$ reduction for the U, K complex $[U(OSi(O^tBu)_3)_4K]$, **2** we have now explored its reactivity with $CS_2$ and compared it with that of the "ate" complex **1**. Here we show that complex **1** favors the reductive disproportionation pathway compared to the reductive dimerization yielding trithiocarbonate as the major product, while for the heterodimetallic complex **2** the dimerization of $CS_2$ is the favored pathway affording the tetrathioxalate as the major product. We were able to isolate intermediates presenting the $CS_2$ reaction products coordinated to the resulting uranium(IV) centres but these products quickly dissociate, laying the basis for kinetically accessible exchange of substrates and products required in catalytic processes.

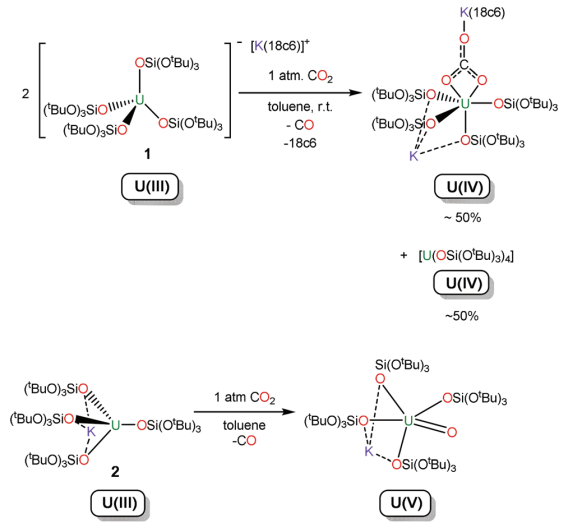


**Scheme 2** Reaction of $[K(18c6)][U(OSi(O^tBu)_3)_4]$, **1** (top) and of $[U(OSi(O^tBu)_3)_4K]$, **2** (bottom) with $CO_2$.

## Results and discussion

The reaction of the bulky and electron-rich tetrasiloxide complex $[K(18c6)][U(OSi(O^tBu)_3)_4]$, **1**, with $CS_2$ (Scheme 3) leads to the reductive cleavage of $CS_2$ affording trithiocarbonate as the major product. The tetrathioxalate is also formed as a by-product of this reaction. $[K(18c6)]_2C_2S_4$ can be isolated from the reaction mixture after 30 minutes, but all $C_2S_4^{2-}$ is transformed into the $C_3S_5^{2-}$ dianion ($dmit^{2-}$ = 1,3-dithiole-2-thione-4,5-dithiolate) after 48 hours.

The $^1H$ NMR and $^{13}C$ NMR spectra of the toluene crude mixture from the reaction of **1** with one to four equivalents of $^{13}CS_2$ for two days shows the presence of the U(IV) complex $[U(OSi(O^tBu)_3)_4]$ as the major product (65%). The $^{13}C$ NMR spectra in deuterated pyridine or in DMSO of this reaction mixture after toluene evaporation reveal the presence of free $^{13}CS_3^{2-}$ as the major species (resonance at +267.7 ppm[14]). This suggests that the thiocarbonate is released from uranium(IV) intermediates in the presence of coordinating solvents. The formation of $^{13}CS_3^{2-}$ indicates that complex **1** promotes the disproportionation of $^{13}CS_2$ to $^{13}CS_3^{2-}$ and $^{13}CS$, but the high reactivity of CS[15] prevents its direct characterization. The $^{13}C$ NMR spectrum of the reaction mixture shows also resonances at roughly +146 and +203 ppm assigned to the $^{13}C_3S_5^{2-}$ dianion.[16] The presence of $dmit^{2-}$ is probably the result of the reaction of the dimerization product $^{13}C_2S_4^{2-}$ with CS. The reaction of $^{13}C_2S_4^{2-}$ with excess $^{13}CS_2$ could also contribute to the formation of the $^{13}C_3S_5^{2-}$ dianion.[16,17] A $^{13}CS_3^{2-}$ : $^{13}C_3S_5^{2-}$ ratio of 10 : 1 was determined by quantitative carbon NMR spectroscopy. The $^{13}CS_3^{2-}$ : $^{13}C_3S_5^{2-}$ ratio is independent of complex concentration, but varies with the number of equivalents of $^{13}CS_2$ added. Thus, complex **1** promotes both the reductive disproportionation of $CS_2$ to $CS_3^{2-}$ and CS and the reductive coupling of $CS_2$ to $C_2S_4^{2-}$ with the reductive disproportionation being the favoured pathway.

When the reaction of **1** with one equivalent of $CS_2$ in toluene is followed over time by $^1H$ NMR spectroscopy (see ESI†) it is evident that several uranium(IV) intermediate species, in addition to the $[U(OSi(O^tBu)_3)_4]$ complex, are present in solution after 2 hours. After 48 hours only the

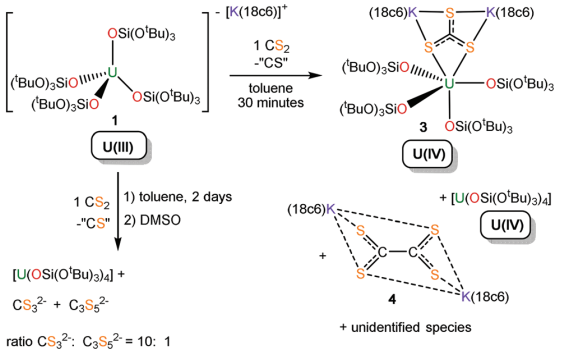


**Scheme 3** Reaction of $[K(18c6)][U(OSi(O^tBu)_3)_4]$ **1** with $CS_2$.

signals assigned to the $[U(OSi(O^tBu)_3)_4]$ complex are present in the $^1H$ NMR spectrum. The presence of multiple reaction products and the labile coordination of the reduction products to the uranium center (observed during the reactions work up) renders the isolation of uranium complexes containing $CS_2$ reduction products very difficult.

Thus, in order to isolate intermediate reaction species we worked up the reaction mixture shortly after reacting **1** with $CS_2$. Evaporation of the reaction mixture after reacting **1** with $CS_2$ for 30 minutes in toluene and extraction of the residue with hexane allows the separation of the hexane soluble species from an insoluble residue. The $^{13}C$ NMR spectrum of this residue in deuterated pyridine before recrystallization shows only the presence of one peak assigned to $[K(18c6)]_2{}^{13}C_2S_4$. The presence of the tetrathioxalate was confirmed by recrystallization from pyridine/hexane which produced dark-green crystals of $\{[K(18c6)]_2C_2S_4\}\cdot Py$, **4·Py**, suitable for X-ray diffraction studies. (The $^{13}C$ NMR spectrum of the isolated crystals is shown in Fig. S3.†)

In spite of the fact that the major component of the hexane extract even after 30 minutes is $[U(OSi(O^tBu)_3)_4]$, recrystallization from toluene at −40 °C of the hexane extract afforded few yellow crystals of the tetravalent uranium trithiocarbonate species $[U(OSi(O^tBu)_3)_4(\mu_3\text{-}\kappa^2\text{:}\kappa^2\text{:}\kappa^2\text{-}CS_3)K_2(18c6)_2]$, **3**.

The $^{13}C$ NMR spectrum of the hexane extract (after solvent evaporation) in deuterated DMSO shows the presence of $[K(18c6)]_2{}^{13}CS_3$ confirming that the latter is released from complex **3** in DMSO.

The crystal structure of $\{[K(18c6)]_2C_2S_4\}\cdot Py$, **4·Py** is presented in Fig. 1. The $C_2S_4{}^{2-}$ unit lies on a crystallographically imposed centre of symmetry and is coordinated to two $[K(18c6)]^+$ cations in a bridging $\kappa^3\text{:}\kappa^3$ mode which, to our knowledge, has not been reported before for this ligand. The $C_2S_4{}^{2-}$ moiety adopts a non-planar structure, with a torsion S2–C1S–C1SA–S2A angle of 83.8(3)°. A similar feature is found in the related $[PPh_4]_2[C_2S_4]$[18] and $[NEt_4]_2[C_2S_4]$[19] structures. The central C–C bond length and the C–S bond distances (C1S–C1SA 1.511(6) Å, S1–C1S 1.670(3) Å and S2–C1S 1.679(3) Å) are also in agreement with the presence of a dianionic tetrathioxalate.[18]

The structure of **3**, set out in Fig. 2, shows the presence of a uranium(IV) six-coordinated by the two S atoms of a trithiocarbonate unit and the four oxygen atoms of four terminal

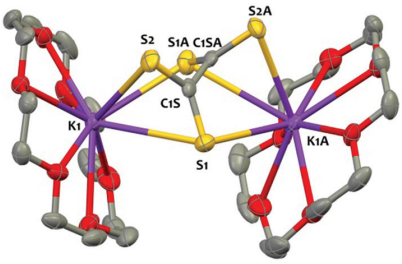


**Fig. 1** Ellipsoid plot for $\{[K(18c6)]_2C_2S_4\}$ crystallized from pyridine; probability 50%. Hydrogen atoms and solvent molecules are omitted for clarity.

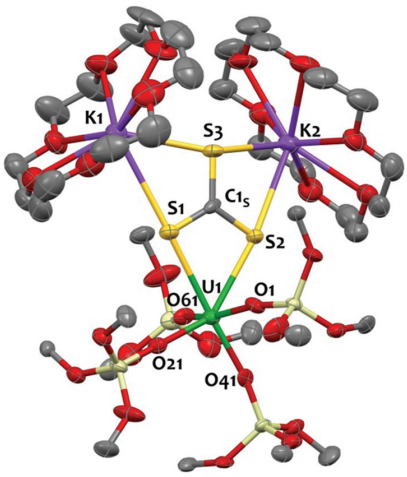


**Fig. 2** Ellipsoid plot for $[U(OSi(O^tBu)_3)_4$ $(\mu_3\text{-}\kappa^2\text{:}\kappa^2\text{:}\kappa^2CS_3)K_2(18c6)_2]$ **3** crystallized from toluene; probability 50%. Hydrogen atoms, methyl groups and solvent molecules are omitted for clarity.

siloxide ligands. The trithiocarbonate unit bridges in a $\mu_3\text{-}\kappa^2\text{:}\kappa^2\text{:}\kappa^2$ fashion the uranium and two $[K(18c6)]^+$ cations. Overall, the metrical parameters for **3** and its neutral charge are in agreement with a tetravalent oxidation state for uranium. Notably, the average U–O bond distance (2.199(14) Å) falls in the range of those typically found for U(IV) siloxy systems.[7d,9a,b] The C–S bond lengths are comparable (1.727(8), 1.709(9) and 1.706(8) Å), and are in agreement with an electronic delocalisation over the $CS_3{}^{2-}$ unit. These values are also similar to those found in other trithiocarbonate complexes.[3a,b,7b] Unfortunately, attempts to isolate cleanly compound **3** failed in preventing further characterization.

Complex **3** is only the second example of an f-element complex containing a coordinated trithiocarbonate ligand. In complex **3**, the thiocarbonate adopts a very different binding mode from that found in the crystal structure of the previously reported diuranium(IV) complex of a tripodal tris-aryloxide ligand, where the trithiocarbonate bridges the two U(IV) ions in a $\mu\text{-}\kappa^2\text{:}\kappa^2$ mode.[7b] The terminal binding of the trithiocarbonate to the U(IV) ion in complex **3** is probably the result of the sterical demand of the four siloxide ligands combined in the presence of potassium counterions stabilizing the mononuclear complex.

The reactivity of the "ate" tetrasiloxide complex $[K(18c6)][U(OSi(O^tBu)_3)_4]$, **1** with $CS_2$ differs from the one reported for the less bulky, neutral analogue $[U(OSi(O^tBu)_3)_2(\mu\text{-}OSi(O^tBu)_3)]_2$ where a $CS_2{}^{2-}$ bridged diuranium(IV) complex was obtained as a sole product. This shows the versatility of siloxide ligands in tuning the reactivity of U(III) complexes with heteroallenes and the important effect of sterical demand and charge on the outcome of the reaction.

In view of the presence of the $K(18c6)^+$ cation binding the uranium-bound trithiocarbonate in complex **3** and of its potential role in stabilizing the thiocarbonate complex, we decided to investigate the reactivity of the heterometallic U, K complex **2** with $CS_2$ (Scheme 4).

 

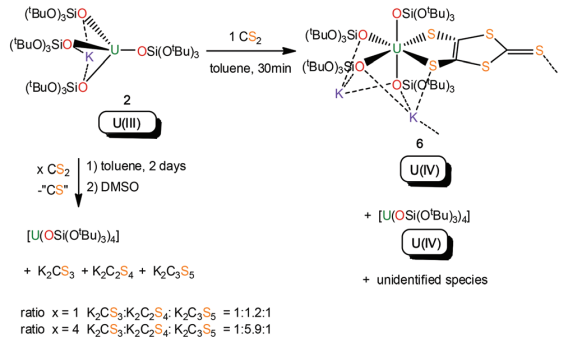


**Scheme 4** Reaction of $[U(OSi(O^tBu)_3)_4K]$, **2** with $CS_2$.

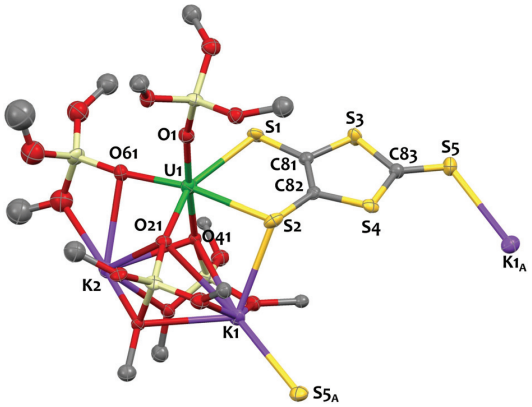


**Fig. 3** Ellipsoid plot of the coordination environment of the uranium center in the $[U(OSi(O^tBu)_3)_4K_2(C_3S_5)]_n$, **6** polymer crystallized from hexane; probability 50%. Hydrogen atoms, methyl groups and solvent molecules are omitted for clarity.

The $^1H$ NMR spectrum immediately after the addition of 1 equivalent of $^{13}CS_2$ to a toluene solution of **2** reveals the formation of a new paramagnetic species and $[U(OSi(O^tBu)_3)_4]$. Following the reaction over time shows a decreasing amount in the new paramagnetic species and after 48 hours the only product observed in solution is $[U(OSi(O^tBu)_3)_4]$. The $^{13}C$ NMR spectrum of the reaction mixture (reacted for 30 minutes or 48 hours) measured in deuterated DMSO after the removal of all volatiles shows the presence of free $^{13}CS_3^{2-}$, $^{13}C_2S_4^{2-}$ and $C_3S_5^{2-}$ in the ratio 1 : 1.2 : 1. However, when the reaction is carried out in the presence of excess $CS_2$ (4 equiv.) the $^{13}CS_3^{2-}$, $^{13}C_2S_4^{2-}$ and $^{13}C_3S_5^{2-}$ compounds are formed in ratio 1 : 5.9 : 1.

When the reaction mixture obtained from the reaction of 1 equivalent of $CS_2$ with **2** in toluene is evaporated, the recrystallization of the residue from THF, after separation of the soluble by-products, affords the tetrathiooxalate potassium salt in 65% yield. Recrystallization of this solid in DMSO layered with toluene affords yellow crystals of $[K_2C_2S_4(DMSO)_3]_n$, **5**. X-ray diffraction studies (Fig. S9 in ESI†) show the presence of a 2D polymeric structure. Each $C_2S_4^{2-}$ ligand bridges three potassium cations yielding a 1-D polymer chain. Two DMSO molecules bridge two potassium cations from adjacent chains to afford the 2-D polymeric structure. The central C–C bond length and the C–S bond distances (C1–C3 1.496(3) Å, S1–C1 1.700(2) Å and S2–C1 1.671(2) Å, S3–C3 1.678(3) Å and S4–C3 1.686(2) Å) are in agreement with the presence of a dianionic tetrathioxalate.[18]

Attempts to isolate a uranium(IV) complex of the tetrathioxalate ligand from the toluene reaction mixture were not successful. However, evaporation to dryness of the toluene reaction mixture 30 minutes after the addition of $CS_2$ to **2**, and extraction with hexane of the residue resulted in the isolation of few crystals of the U(IV) complex $[U(OSi(O^tBu)_3)_4K_2(C_3S_5)]_n$, **6** which crystallizes as an infinite 1D polymer.‡ While the quality of the structure is not sufficient to discuss the metrical parameter, it clearly shows the atom connectivity. In the structure of **6**, presented in Fig. 3, the uranium center is hexacoordinated by the four oxygens of the siloxide ligands and the two sulfur atoms of the $C_3S_5^{2-}$ ligand. Two potassium cations are bound in the pockets formed by five oxygen atoms from the siloxide ligands. The thione sulfur of the $C_3S_5^{2-}$ ligand binds one of the potassium cations of the adjacent complex yielding a 1-D chain. The structure of **4** shows that the coordination environment provided by the siloxide ligands can adapt allowing the coordination of the dmit dianion to the uranium center. Dmit complexes of transition metals have attracted considerable attention due to their electrical conductivities.[20,21] However, to the best of our knowledge dmit complexes of f-elements have not so far been structurally characterized.

Moreover complex **6** provides the first example of a dmit complex formed from the reduction of $CS_2$ by a metal complex. The mechanism of formation of **6** remains unclear although it should involve reductive dimerization of $CS_2$ as a first step.

Thus, the presence of the bound potassium cation in the heterometallic complex **2** leads to a different reduction pathway being preferred in the reaction of the U(III) tetrasiloxide with $CS_2$ in toluene. Notably, the reaction affords preferentially the reductive $CS_2$ coupling product tetrathiooxalate rather than the reductive cleavage product, the trithiocarbonate, found to be the major reaction product in the reaction of **1** with $CS_2$. Future DFT studies should be performed to investigate the mechanism of $CS_2$ reduction by complexes **1** and **2**.

Several examples of U(III) mediated C–C coupling are known[7c,22] but only one example of the mediated U(III) reductive coupling of $CS_2$ has been reported to date.[7c]

## Concluding remarks

In summary the "ate" complex $[K(18c6)][U(OSi(O^tBu)_3)_4]$, **1**, and the heterodimetallic U, K complex $[U(OSi(O^tBu)_3)_4K]$,

‡Unit cell parameters for **6·hexane**: *a*, 24.370(4) Å; *b*, 13.958(5) Å; *c*, 25.659(5) Å; *α*, 90°; *β*, 107.035(16)°; *γ*, 90°; unit cell volume 8345(4) Å$^3$; formula, $C_{57}H_{122}K_2O_{16}S_5Si_4U$.

**2** both engage in the parallel reductive dimerization and reductive disproportionation of $CS_2$. In these bulky systems the reduction products are easily displaced from the uranium coordination sphere by coordinating ligands, suggesting that these systems might be well poised for the development of catalytic cycles. This reactivity differs significantly from that previously observed for the analogous homoleptic tris-siloxide complex $[U(OSi(O^tBu)_3)_2(\mu\text{-}OSi(O^tBu)_3)]_2$ which reduces $CS_2$ to a $CS_2^{2-}$ group that remains tightly bound to two U(IV) centers in a bridging mode. Moreover, the presence of the bound Lewis acidic potassium cation in the heterodimetallic U, K complex leads preferentially to the reductive dimerization of $CS_2$ while the reductive disproportionation pathway is favoured by the "ate" complex $[K(18c6)][U(OSi(O^tBu)_3)_4]$. The coordination of $K^+$ and $[K(18c6)]^+$ in the structure of the isolated complexes $[U(OSi(O^tBu)_3)_4(\mu_3\text{–}CS_3)K_2(18c6)_2]$ and $[U(OSi(O^tBu)_3)_4K_2(C_3S_5)]_n$ suggest that in both systems the alkali ion plays an important, if different, role. Future studies will be directed to elucidate the mechanism of $CS_2$ reduction in these systems.

## Experimental

### General experimental procedures

All manipulations were carried out at ambient temperature under an inert argon atmosphere using Schlenk techniques and an MBraun glovebox equipped with a purifier unit. The water and oxygen level were always kept at less than 0.1 ppm. Glassware was systematically dried in an oven overnight at 130 °C followed by 3 vacuum/argon cycles before use. Unless otherwise noted, reagents were purchased from commercial suppliers and used without further purification. The solvents were purchased from Aldrich in their anhydrous form, conditioned under argon and vacuum distilled from K/benzophenone (toluene and pyridine) or sodium dispersion (hexane) and degassed by three freeze–pump–thaw cycles. DMSO was dried over activated molecular sieves for one week. The deuterated solvents were purchased from Eurisotop and prepared identically. $CS_2$ was degassed by three freeze–pump–thaw cycles and stored over molecular sieves. Depleted uranium turnings were purchased from the "Société Industrielle du Combustible Nucléaire" of Annecy (France). Complexes $[K(18c6)][U(OSi(O^tBu)_3)_4]$, **1**[9a] and $[U(OSi(O^tBu)_3)_4K]$, **2**[10] were prepared according to the published procedures. $^1H$ and $^{13}C$ NMR experiments were carried out using NMR tubes adapted with J. Young valves and the spectra were recorded on Bruker 200 MHz and Bruker 400 MHz spectrometers. NMR chemical shifts are reported in ppm with a solvent as an internal reference.

**Caution:** Depleted uranium (primary isotope $^{238}U$) is a weak α-emitter (4.197 MeV) with a half-life of $4.47 \times 10^9$ years. Manipulations and reactions should be carried out in monitored fume hoods or under an inert atmosphere glovebox in a radiation laboratory equipped with α- and β-counting equipment.

**Reaction of $[K(18c6)][U(OSi(O^tBu)_3)_4]$ (1) with $CS_2$.** 100 μL of a 0.15 M toluene solution of $CS_2$ (0.015 mmol, 1 eq.) were added to a 2 mL suspension of **1** (25.0 mg, 0.015 mmol, 1 eq.) in toluene to afford a red/pink solution. After 30 min stirring, the solvent was removed *in vacuo*. The residue was extracted with hexane to give a pink/red solution (A) and an insoluble brown solid. The solid was recovered by centrifugation and then dissolved in pyridine to give a brown solution; slow diffusion of hexane into this pyridine solution produced deep green needles of $\{[K(18c6)]_2C_2S_4\}\cdot$Py, **4·Py** suitable for X-ray diffraction (13% yield). $^1H$ NMR (200 MHz, pyridine-$d_5$, 298 K): $\delta$ 3.58 (s, 24H, C$H_2$-18c6). $^{13}C\{^1H\}$ NMR (200 MHz, pyridine-$d_5$, 298 K): $\delta$ 70.57 (s, $CH_2$-18c6), 248.45 (s, $C_2S_4$). $^{13}C\{^1H\}$ NMR (200 MHz, water-$d_2$, 298 K): $\delta$ 70.00 (s, $CH_2$-18c6), 251.03 (s, $C_2S_4$).

After removing all volatiles from the pink/red hexane extract A the solid was dissolved in toluene and left standing at −40 °C to afford crystals of $[K(18c6)]_2[U(\mu\text{-}\kappa^1\text{:}\kappa^2\text{:}\kappa^2CS_3)(OSi(O^tBu)_3)_4]$ (**3**) suitable for X-ray diffraction. Unfortunately, attempts to separate **3** from $[U(OSi(O^tBu)_3)_4]$ were unsuccessful, preventing further characterization of this species.

The quantitative $^1H$ NMR spectrum recorded on a toluene solution of **1** reacted with one equivalent of $CS_2$ for 30 minutes after addition of an internal standard (naphthalene) shows the formation of $[U(OSi(O^tBu)_3)_4]$ in 50% yield.

The quantitative $^1H$ NMR spectrum of the toluene reaction mixture after two days shows the presence of the U(IV) complex $[U(OSi(O^tBu)_3)_4]$ as the major product (65%).

Quantitative $^{13}C$ NMR: 10.4 μL of a 0.64 M toluene solution of $^{13}CS_2$ (0.006 mmol, 1 eq.) were added to a 0.5 mL suspension of **1** (9.5 mg, 0.006 mmol, 1 eq.) in toluene to afford a red/pink solution. $^{13}C$ NMR spectra in deuterated DMSO of the reaction mixture after toluene evaporation show the presence of free $^{13}CS_3^{2-}$ as the major species, compared to $^{13}C_3S_5^{2-}$ in a 10 : 1 ratio. Quantitative $^{13}C$ NMR using naphthalene as an internal standard shows the quantitative transformation of $CS_2$ into the reduction products $^{13}CS_3^{2-}$, and $^{13}C_3S_5^{2-}$.

**Reaction of $[U\{OSi(O^tBu)_3\}_4K]$ (2) with $CS_2$**

*A – short reaction times.* 30 μL (0.038 mmol) of a 1.25 M toluene-$d_8$ solution of $^{13}CS_2$ were added to a solution of **2** (25.4 mg, 0.019 mmol, 2 eq.) in toluene-$d_8$ (0.5 mL) and stirred for 30 minutes. All volatiles were then removed *in vacuo*. The residue was suspended in hexane and the undissolved solid was discarded. Pink/red crystals of $[U(OSi(O^tBu)_3)_4K_2(C_3S_5)]_n$, **6** suitable for X-ray diffraction were isolated by letting this hexane solution to stand for few days at room temperature. Attempts to separate **6** from the other reaction products were unsuccessful, preventing further characterization of this species.

*B – long reaction times.* 30 μL (0.038 mmol) of a 1.25 M toluene-$d_8$ solution of $^{13}CS_2$ were added to a solution of **2** (50.8 mg, 0.038 mmol, 1 eq.) in toluene-$d_8$ (0.5 mL) to afford an orange solution. After letting the solution stand at room temperature for 2 days a few red crystals formed which were identified by $^{13}C$ NMR as $K_2CS_3$. The $^1H$ NMR spectrum of the toluene reaction mixture shows the presence of the U(IV) complex $[U(OSi(O^tBu)_3)_4]$ as the major product (66%). All the volatiles were then removed *in vacuo* to afford a brown solid.

 

Recrystallization of this residue by slow diffusion of toluene (4 mL) into DMSO (0.5 mL) affords $[K_2C_2S_4(DMSO)_3]_n$, **5**, as yellow crystals suitable for X-ray diffraction. $^{13}C\{^1H\}$ NMR (200 MHz, DMSO-$d_5$, 298 K): $\delta$ = 264.46 (s, $C_2S_4$).

An analogous reaction performed with a 1 : 2 ratio complex **2**:$CS_2$ allows the isolation of the insoluble $K_2C_2S_4$·5THF salt (5 THFs confirmed from the $^1$H NMR spectrum in dmso-$d_6$) as yellow crystals in 65% yield (a yield consistent with the 1 : 3.7 : 1 $^{13}CS_3^{2-}$ : $C_2S_4^{2-}$ : $^{13}C_3S_5^{2-}$ ratio obtained from the quantitative $^{13}$C NMR spectra as indicated below).

The quantitative $^{13}$C NMR spectrum recorded in deuterated pyridine or in DMSO immediately after solvent evaporation of a toluene solution of **2** reacted with one equivalent of $CS_2$ shows the presence of free $^{13}CS_3^{2-}$, $C_2S_4^{2}$ and $^{13}C_3S_5^{2-}$ in a 1 : 1.2 : 1 ratio. The quantitative $^{13}$C NMR spectrum recorded in deuterated pyridine or in DMSO immediately after solvent evaporation of toluene solutions of **2** reacted with two or four equivalents of $CS_2$, showing the presence of an increasingly higher amount of free $C_2S_4^{2-}$ compared to $^{13}CS_3^{2-}$ and $^{13}C_3S_5^{2-}$. (A 1 : 3.7 : 1 $^{13}CS_3^{2-}$ : $C_2S_4^{2-}$ : $^{13}C_3S_5^{2-}$ ratio was found for 2 equiv. $CS_2$ and a 1 : 5.9 : 1 for 4 equivalents.)

### X-Ray crystallography

Diffraction data were taken using an Oxford-Diffraction XCallibur S kappa geometry diffractometer (Mo-Kα radiation, graphite monochromator, $\lambda$ = 0.71073 Å). To prevent evaporation of the co-crystallised solvent molecules, the crystals were coated with light hydrocarbon oil and the data were collected at 150 K. The cell parameters were obtained with intensities detected on three batches of 5 frames. The crystal–detector distance was 4.5 cm. The number of settings and frames has been established taking into consideration the Laue symmetry of the cell using CrysAlisPro Oxford-diffraction software.[23] 503 for **4·Py**, 508 for **3**, 495 for **5** and 266 for **6** were collected for 1° increments in $\omega$ with 150 s, 10 s, 50 s and 300 s, respectively, exposure times. Unique intensities detected on all frames using the Oxford-diffraction Red program were used to refine the values of the cell parameters. Modelisation of the crystal shape in CrysAlisPro software allows analytical absorption correction for **4·Py** and **5**. In the case of imprecise shape modelisation, substantially redundancy in measured intensities allows empirical multi-scan absorption correction for **3·4** toluene and **5**. Space groups were determined from systematic absences, and they were confirmed by the successful solution of the structure. The structures were solved using Superflip software,[24] and refined with the Olex package.[25] All non-hydrogen atoms were found by difference Fourier syntheses and refined on $F^2$. Hydrogen atoms were fixed in an ideal position for **3·4** toluene, **4·Py** and **5** and refined using a riding model. In complex **3·4** toluene 835 restraints were applied: The methyl distances, and all thermal coefficients of the toluene molecules were restrained with SIMU instruction. The carbon atoms of three toluene molecules (C151, C251 and C241) were restrained to be planar with FLAT instruction. The thermal coefficients of the carbon atoms of three toluene molecules (C121, C151, and C251) were restrained to be closer to a sphere with ISOR instruction. The thermal coefficients of the carbon atoms of the toluene C251 were constrained to be equal. The thermal coefficients of the following atoms of the silanol ligands were restrained to be closer to a sphere with ISOR instruction: O21B C30 C10B O1B O41 C10 C24 C27B C30B C31B C46 C48 C50 C50B C52B C67 C70B C69B C71 C72 C72B C87 C88 O1 O21 O43 O43B C5B C6B C7B C8B C9 C9B C11B C12 C12B C29B.

The C9–C10 bonds of the *tert*-butyl group of a silanol ligand were restrained to be symmetric with DELU instruction.

For structure **5** at position 000 a 169 Å$^3$ empty space was found where 30 electrons were modeled by SQUEEZE.[26] The quality of structure **6** is not sufficient for publication in Cambridge Structural Database due to the poor quality of the crystals.

Experimental details for X-ray data are given in Table S2.†

## Acknowledgements

This work benefited from COST Action CM1006 – EUFEN: European F-Element Network. We acknowledge support from the Labex Arcane, ANR-11-LABX-003-01.

## Notes and references

1 (*a*) W. B. Tolman, *Activation of small molecules*, Wiley-VCH, Weinheim, Germany, 2006; (*b*) C. Finn, S. Schnittger, L. J. Yellowlees and J. B. Love, *Chem. Commun.*, 2012, **48**, 1392–1399; (*c*) E. E. Benson, C. P. Kubiak, A. J. Sathrum and J. M. Smieja, *Chem. Soc. Rev.*, 2009, **38**, 89–99.

2 (*a*) J. A. Ibers, *Chem. Soc. Rev.*, 1982, **11**, 57–73; (*b*) K. K. Pandey, *Coord. Chem. Rev.*, 1995, **140**, 37–114; (*c*) I. S. Butler and A. E. Fenster, *J. Organomet. Chem.*, 1974, **66**, 161–194.

3 (*a*) B. Li, X. Tan, S. Xu, H. Song and B. Wang, *J. Organomet. Chem.*, 2008, **693**, 667–674; (*b*) W. J. Mace, L. Main, B. K. Nicholson and M. Hagyard, *J. Organomet. Chem.*, 2002, **664**, 288–293; (*c*) A. Shaver, B. El Mouatassim, F. Mortini, F. Belanger-Gariepy and A. Lough, *Organometallics*, 2007, **26**, 4229–4233.

4 (*a*) H. A. Harris, A. D. Rae and L. F. Dahl, *J. Am. Chem. Soc.*, 1987, **109**, 4739–4741; (*b*) P. V. Broadhurst, B. F. G. Johnson, J. Lewis and P. R. Raithby, *J. Chem. Soc., Chem. Commun.*, 1982, 140–141.

5 (*a*) A. R. Johnson, W. M. Davis, C. C. Cummins, S. Serron, S. P. Nolan, D. G. Musaev and K. Morokuma, *J. Am. Chem. Soc.*, 1998, **120**, 2071–2085; (*b*) W. S. Ren, H. B. Song, G. F. Zi and M. D. Walter, *Dalton Trans.*, 2012, **41**, 5965–5973.

6 (*a*) E. M. Matson, W. P. Forrest, P. E. Fanwick and S. C. Bart, *J. Am. Chem. Soc.*, 2011, **133**, 4948–4954; (*b*) D. Heitmann, C. Jones, D. P. Mills and A. Stasch, *Dalton Trans.*, 2010, **39**, 1877–1882; (*c*) W. S. Ren, G. F. Zi, D. C. Fang and M. D. Walter, *J. Am. Chem. Soc.*, 2011, **133**, 13183–13196.

7 (*a*) J. G. Brennan, R. A. Andersen and A. Zalkin, *Inorg. Chem.*, 1986, **25**, 1756–1760; (*b*) O. P. Lam, L. Castro, B. Kosog, F. W. Heinemann, L. Maron and K. Meyer, *Inorg. Chem.*, 2012, **51**, 781–783; (*c*) O. P. Lam, F. W. Heinemann and K. Meyer, *Angew. Chem., Int. Ed.*, 2011, **50**, 5965–5968; (*d*) V. Mougel, C. Camp, J. Pecaut, C. Coperet, L. Maron, C. E. Kefalidis and M. Mazzanti, *Angew. Chem., Int. Ed.*, 2012, **51**, 12280–12284.

8 D. L. Clark, A. P. Sattelberger, W. G. Vandersluys and J. G. Watkin, *J. Alloys Compd.*, 1992, **180**, 303–315.

9 (*a*) C. Camp, J. Pecaut and M. Mazzanti, *J. Am. Chem. Soc.*, 2013, **135**, 12101–12111; (*b*) C. Camp, V. Mougel, J. Pecaut, L. Maron and M. Mazzanti, *Chem. – Eur. J.*, 2013, **19**, 17528–17540; (*c*) C. Camp, C. E. Kefalidis, J. Pecaut, L. Maron and M. Mazzanti, *Angew. Chem., Int. Ed.*, 2013, **52**, 12646–12650; (*d*) S. M. Mansell, J. H. Farnaby, A. I. Germeroth and P. L. Arnold, *Organometallics*, 2013, **32**, 4214–4222.

10 O. Cooper, C. Camp, J. Pecaut, C. E. Kefalidis, L. Maron, S. Gambarelli and M. Mazzanti, *J. Am. Chem. Soc.*, 2014, **136**, 6716–6723.

11 (*a*) G. Fachinetti, C. Floriani and P. F. Zanazzi, *J. Am. Chem. Soc.*, 1978, **100**, 7405–7407; (*b*) S. Gambarotta, F. Arena, C. Floriani and P. F. Zanazzi, *J. Am. Chem. Soc.*, 1982, **104**, 5082–5092.

12 (*a*) P. Haack, C. Limberg, T. Tietz and R. Metzinger, *Chem. Commun.*, 2011, **47**, 6374–6376; (*b*) J. P. Krogman, B. M. Foxman and C. M. Thomas, *J. Am. Chem. Soc.*, 2011, **133**, 14582–14585; (*c*) J. H. Jeoung and H. Dobbek, *Science*, 2007, **318**, 1461–1464.

13 C. Bianchini, C. Mealli, A. Meli and M. Sabat, *Inorg. Chem.*, 1984, **23**, 4125–4127.

14 D. Stueber, D. Patterson, C. L. Mayne, A. M. Orendt, D. M. Grant and R. W. Parry, *Inorg. Chem.*, 2001, **40**, 1902–1911.

15 E. K. Moltzen, K. J. Klabunde and A. Senning, *Chem. Rev.*, 1988, **88**, 391–406.

16 (*a*) R. M. Olk, W. Dietzsch, K. Kohler, R. Kirmse, J. Reinhold, E. Hoyer, L. Golic and B. Olk, *Z. Anorg. Allg. Chem.*, 1988, **567**, 131–144; (*b*) J. G. Breitzer, J. H. Chou and T. B. Rauchfuss, *Inorg. Chem.*, 1998, **37**, 2080–2081.

17 N. Svenstrup and J. Becher, *Synthesis*, 1995, 215–235.

18 H. Lund, E. Hoyer and R. G. Hazell, *Acta Chem. Scand. Ser. B-Org. Chem. Biochem.*, 1982, **36**, 207–209.

19 A. D. Bacher, I. Sens and U. Muller, *Z. Naturforsch., B*, 1992, **47**, 702–705.

20 M. Bousseau, L. Valade, J. P. Legros, P. Cassoux, M. Garbauskas and L. V. Interrante, *J. Am. Chem. Soc.*, 1986, **108**, 1908–1916.

21 A. E. Pullen and R. M. Olk, *Coord. Chem. Rev.*, 1999, **188**, 211–262.

22 (*a*) C. Camp, V. Mougel, P. Horeglad, J. Pecaut and M. Mazzanti, *J. Am. Chem. Soc.*, 2010, **132**, 17374–17377; (*b*) C. Camp, J. Andrez, J. Pecaut and M. Mazzanti, *Inorg. Chem.*, 2013, **52**, 7078–7086; (*c*) M. J. Monreal, S. Khan and P. L. Diaconescu, *Angew. Chem., Int. Ed.*, 2009, **48**, 8352–8355; (*d*) B. M. Gardner, J. C. Stewart, A. L. Davis, J. McMaster, W. Lewis, A. J. Blake and S. T. Liddle, *Proc. Natl. Acad. Sci. U. S. A.*, 2012, **109**, 9265–9270; (*e*) A. S. Frey, F. G. N. Cloke, P. B. Hitchcock, I. J. Day, J. C. Green and G. Aitken, *J. Am. Chem. Soc.*, 2008, **130**, 13816–13817; (*f*) P. L. Arnold, Z. R. Turner, R. M. Bellabarba and R. P. Tooze, *Chem. Sci.*, 2011, **2**, 77–79.

23 CrysAlisPro CCD, *CrysAlisPro RED and ABSPACK, CrysAlis PRO*, Agilent Technologies, Yarnton, England, 2010.

24 L. Palatinus and G. Chapuis, *J. Appl. Crystallogr.*, 2007, **40**, 786–790.

25 O. V. Dolomanov, L. J. Bourhis, R. J. Gildea, J. A. K. Howard and H. Puschmann, *J. Appl. Crystallogr.*, 2009, **42**, 339–334.

26 (*a*) A. L. Spek, *J. Appl. Crystallogr.*, 2003, **36**, 7–13; (*b*) A. L. Spek, *Acta Crystallogr., Sect. D: Biol. Crystallogr.*, 2009, **65**, 148–155.

 

ChemPubSoc Europe

DOI: 10.1002/chem.201502204

CHEMISTRY
A European Journal
Full Paper

Lanthanides |*Hot Paper*|

# Lanthanide(II) Complexes Supported by N,O-Donor Tripodal Ligands: Synthesis, Structure, and Ligand-Dependent Redox Behavior

Julie Andrez,[a] Gülay Bozoklu,[b] Grégory Nocton,[b] Jacques Pécaut,[b] Rosario Scopelliti,[a] Lionel Dubois,[b] and Marinella Mazzanti*[a]

**Abstract:** The preparation and characterization of a series of complexes of the Yb and Eu cations in the oxidation state II and III with the tetradentate N,O-donor tripodal ligands (tris(2-pyridylmethyl)amine (TPA), $BPA^-$ (HBPA = bis(2-pyridylmethyl)(2-hydroxybenzyl)amine), $BPPA^-$ (HBPPA = bis(2-pyridylmethyl)(3.5-di-*tert*-butyl-2-hydroxybenzyl)amine), and $MPA^{2-}$ ($H_2MPA$ = (2-pyridylmethyl)bis(3.5-di-*tert*-butyl-2-hydroxybenzyl)amine) is reported. The X-ray crystal structures of the heteroleptic $Ln^{2+}$ complexes $[Ln(TPA)I_2]$ (Ln = Eu, Yb) and $[Yb(BPA)I(CH_3CN)]_2$, of the $Ln^{2+}$ homoleptic $[Ln(TPA)_2]I_2$ (Ln = Sm, Eu, Yb) and $[Eu(BPA)_2]$ complexes, and of the $Ln^{3+}$ $[Eu(BPPA)_2]OTf$ and $[Yb(MPA)_2K(dme)_2]$ (dme = dimethoxyethane) complexes have been determined. Cyclic voltammetry studies carried out on the bis-ligand complexes of $Eu^{3+}$ and $Yb^{3+}$ show that the metal center reduction occurs at significantly lower potentials for the $BPA^-$ ligand as compared with the TPA ligand. This suggests that the more electron-rich character of the $BPA^-$ ligand results in a higher reducing character of the lanthanide complexes of $BPA^-$ compared with those of TPA. The important differences in the stability and reactivity of the investigated complexes are probably due to the observed difference in redox potential. Preliminary reactivity studies show that whereas the bis-TPA complexes of $Eu^{2+}$ and $Yb^{2+}$ do not show any reactivity with heteroallenes, the $[Eu(BPA)_2]$ complex reduces $CS_2$ to afford the first example of a lanthanide trithiocarbonate complex.

## Introduction

The molecular chemistry of $Eu^{2+}$, $Yb^{2+}$, and $Sm^{2+}$ has been successfully used in a wide variety of applications and has afforded original reactivity.[1–4] Furthermore, several examples of activation of small molecules such as $CO_2$,[5] $CS_2$,[5c,6] and $N_2$[7] by $Ln^{2+}$ complexes have been reported. Because of the recognized importance of steric and electronic factors in the control of $Ln^{2+}$ reactivity,[4b,c] the association of the high reducing ability of divalent lanthanides with a range of appropriate supporting ligands is crucial for establishing new $Ln^{2+}$-mediated transformations. Carbocyclic ligands[1c,4b,8] have been extensively and successfully used as supporting ligands in divalent lanthanide chemistry. However, reactivity studies associating $Ln^{2+}$ with N,O-donor chelating ligands are less developed.[2b,5c,d,9,6a,b,10] Tripodal polypyridyl ligands such as TPA[11] (Scheme 1) and tripodal aminophenolate ligands[12] have been largely used as supporting ligands in d-block chemistry but they are rarer in f element chemistry.[12,13] $Ln^{3+}$ complexes of tripodal aminophenolates[12] and of the TPA ligand[13c,d,14] have been reported and were shown to promote original stoichiometric and catalytic transformations.[15–17] In contrast, the complexation of divalent lanthanides by the tris(2-pyridylmethyl)-amine (TPA) ligand has never been explored. Moreover, only a few examples of $Ln^{2+}$ complexes of tripodal aminobisphenolates have been reported.[16,18] Furthermore, although some of these complexes demonstrated attractive catalytic activity[16,18a,19] and the ability of activating organic molecules,[18a] their reactivity with heteroallenes has not been investigated.

Recent results from our group show that electron-rich siloxide ligands can impart high reducing power to $Ln^{2+}$ ions ($E_a$ = −1.56 V for Yb-siloxide, $E_a$ = −0.63 V for Eu-siloxide vs. NHE), with relatively high $Ln^{3+}/Ln^{2+}$ redox potential ($E_{1/2\,Ln3+/Ln2+}$ calcd for aqueous ions = −0.35 V for Eu and = −1.15 for Yb vs. NHE and $E_{1/2}$ measured = −0.05 V ($YbI_2$), 0.49 V ($EuI_2$) vs. NHE) and promote unusual reactivity in homoleptic "ate" complexes of the classical lanthanide ions $Eu^{2+}$, $Yb^{2+}$.[5c] In the search for new ligand systems capable of promoting a higher reactivity in $Eu^{2+}$ and $Yb^{2+}$ complexes, in this work, we investigate the influence of tripodal tetradentate ligands of different charge (Scheme 1) on the redox properties of the $Eu^{2+}$ and $Yb^{2+}$ ions in homoleptic bis-ligand complexes.

[a] *J. Andrez, Dr. R. Scopelliti, Dr. M. Mazzanti*
*Institut des Sciences et Ingénierie Chimiques*
*Ecole Polytechnique Fédérale de Lausanne (EPFL)*
*1015 Lausanne (Switzerland)*
*E-mail: marinella.mazzanti@epfl.ch*

[b] *Dr. G. Bozoklu, Dr. G. Nocton, Dr. J. Pécaut, Dr. L. Dubois*
*Univ. Grenoble Alpes, INAC-SCIB, F-38000 Grenoble*
*France, CEA, INAC-SCIB, 38000 Grenoble (France)*

*Supporting information for this article is available on the WWW under http://dx.doi.org/10.1002/chem.201502204.*

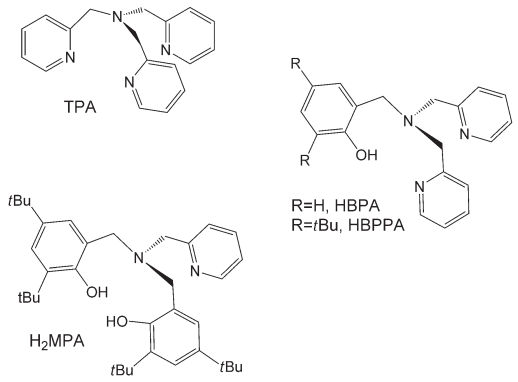


**Scheme 1.** Targeted N- and O-donor tripodal ligands.

The previously reported tripodal tetradentate ligands presented in Scheme 1, the neutral TPA (tris(2-pyridylmethyl)-amine),[11] the monoanionic $BPA^-$ (HBPA = bis(2-pyridylmethyl)(2-hydroxybenzyl)amine) and $BPPA^-$ (HBPPA = bis(2-pyridylmethyl) (3.5-di-*tert*-butyl-2-hydroxybenzyl)amine) ligands,[13b,20] and the dianionic $MPA^{2-}$ ligand ($H_2MPA$ = (2-pyridylmethyl)-bis(3.5-di-*tert*-butyl-2-hydroxybenzyl)amine),[21] provide a series of analogous ligands with different charge that allow us to investigate the effects of electronics on the stability and reactivity of divalent lanthanides. Here we report the first examples of heteroleptic mono-ligand and homoleptic bis-ligand complexes of TPA with $Sm^{2+}$, $Eu^{2+}$, and $Yb^{2+}$ ions. We also report the synthesis and crystal structure of the $[Eu^{II}(BPA)_2]$ complex and its reactivity with $CS_2$. The redox properties of the bis-ligand complexes of $Eu^{3+}$ and $Yb^{3+}$ have been investigated for all the tetradentate ligands presented in Scheme 1.

## Results and Discussion

### TPA complexes

The $Ln^{2+}$ heteroleptic mono-ligand complexes $[Ln(TPA)I_2]$ were obtained by treating divalent lanthanide iodide salts $LnI_2$ (Ln = $Sm^{2+}$, $Yb^{2+}$, $Eu^{2+}$) with one equivalent of TPA in THF. Crystals suitable for X-ray diffraction of $[Yb(TPA)I_2(CH_3CN)]\cdot(CH_3CN)_{0.5}$ and of $[Eu(TPA)(\mu\text{-}I)I]_2$ were obtained by slow diffusion of diisopropyl ether into acetonitrile solutions of the $Yb^{2+}$ and $Eu^{2+}$ complexes.

The complex $[Yb(TPA)I_2(CH_3CN)]\cdot(CH_3CN)_{0.5}$ crystallizes in the triclinic space group $P\bar{1}$. An ellipsoid diagram of the complex is given in Figure 1 (top). The metal ion is seven-coordinated with a distorted monocapped octahedron geometry by four nitrogen atoms of TPA, two cis coordinated iodide ions, and a nitrogen atom of an acetonitrile molecule. The coordination of the acetonitrile is nearly linear, with an Yb-N21-C21 angle of 172.7(4)°. The triangular face N3, N2, N4 is capped by the N1 atom. The Yb–$N_{amine}$ bond (2.620(4) Å) is longer than the average Yb–$N_{pyridyl}$ bond (2.565(6) Å). The complex $[Eu(TPA)(\mu\text{-}I)I]_2$, crystallizes as a dimer in the orthorhombic *Pbca* space group (Figure 1, bottom). The europium ion is situated 1.2532(18) Å above the plane defined by the $N_{pyridyl}$ atoms. This value is larger than that observed for the $Yb^{2+}$ in $[Yb(TPA)I_2(CH_3CN)]$ (1.087(2) Å) because of the smaller ionic radius of the $Yb^{2+}$ ion as compared with $Eu^{2+}$. These differences are probably responsible for the observed nuclearity of the Yb and Eu complexes in the solid-state crystal structure. The structure of the $[Eu(TPA)(\mu\text{-}I)I]_2$ has an inversion center in the middle of the Eu2I2 core relating two $Eu(TPA)(\mu\text{-}I)I$ units. The europium atoms are seven-coordinated, with a distorted monocapped octahedron geometry, by the four nitrogens of the TPA ligand, one terminal and two bridging iodide ligands. The ligand TPA adopts an helical arrangement around the metal cation as found in the in the $Eu^{3+}$ complex $[Eu(TPA)]Cl_3$.[13d] The average Eu–$N_{pyridyl}$ distance is 2.67(1) Å and is significantly shorter than the Eu–$N_{amine}$ distance (2.748(3) Å). Significantly shorter Eu–N distances were found in the $Eu^{3+}$ complex $[Eu(TPA)]Cl_3$[13d] (Eu–$N_{amine}$ = 2.612(1) Å; mean Eu–$N_{pyridyl}$ = 2.57(2) Å) but the difference in bond lengths remains smaller that the difference in ionic radii (0.2 Å).[22] The Eu–I distance is shorter for the terminal iodide (Eu–I2 = 3.2888(3) Å) than for the bridging ones (Eu-I1 3.3142(1) and 3.3111(1) Å).

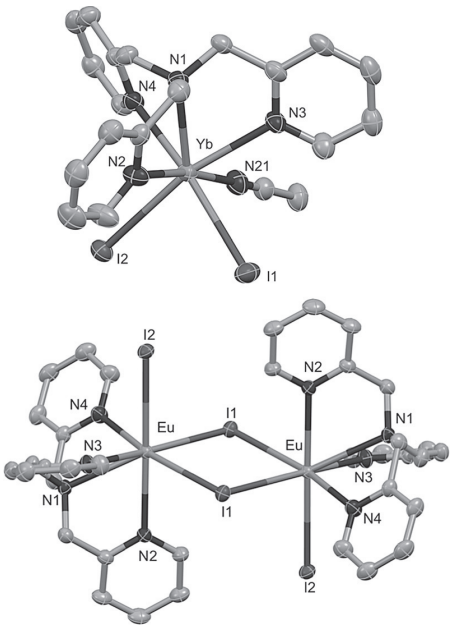


**Figure 1.** Ellipsoid diagram of the complex $[Yb(TPA)I_2(CH_3CN)]$ (top) and $[Eu(TPA)(\mu\text{-}I)I]_2$ (bottom) (50% probability ellipsoids). Hydrogen atoms and solvent molecules are omitted for clarity.

Because of the strong paramagnetism of the $4f^7$ electronic configuration of $Eu^{2+}$, an informative NMR spectrum could not be obtained for the europium complexes. In contrast, the $^1H$ NMR spectrum of the $Yb^{2+}$ complex in deuterated acetonitrile shows a set of 5 (with two signals overlapping) signals in the diamagnetic region from $\delta$ = 4.0 to 8.8 ppm in agreement with the presence of dynamically averaged $C_{3v}$ symmetric solu-

tion species. The $[Eu(TPA)I_2]$ and $[Yb(TPA)I_2]$ complexes are stable both in the solid state and in acetonitrile solution. In contrast, the $[Sm(TPA)I_2]$ complex is stable in the solid state but decomposes rapidly in acetonitrile solution preventing further characterization.

Thus, TPA has proven a suitable ligand for the synthesis of stable heteroleptic complexes of the $Eu^{II}$ and $Yb^{II}$ cations. Therefore, we also investigated the possibility of preparing homoleptic 2:1 complexes of TPA.

The $Ln^{2+}$ homoleptic complexes $[Ln(TPA)_2]I_2$ (Ln = Sm, Yb, Eu) have been obtained by treating the divalent lanthanide iodide salts $LnI_2$ ($Ln = Sm^{2+}$, $Yb^{2+}$, $Eu^{2+}$) with two equivalents of TPA in THF at room temperature (Scheme 2).

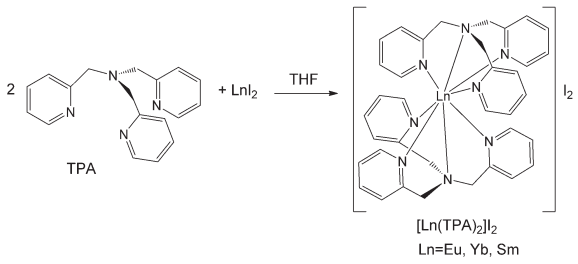


**Scheme 2.** Synthesis of $[Ln(TPA)_2]I_2$.

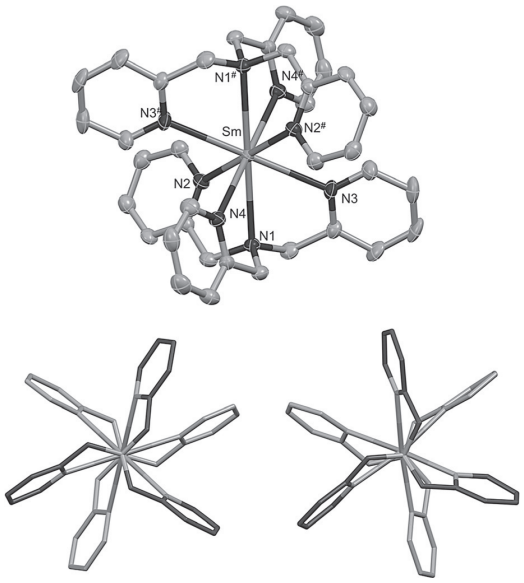


**Figure 2.** Ellipsoid diagram of $[Sm(TPA)_2]^{2+}$ (top) (50% probability ellipsoids). Hydrogen atoms and iodine counterion are omitted for clarity. ($^{\#} = -x+1, -y+1, -z+1$). Ellipsoid diagram of the structures $[Sm(TPA)_2]I_2$ (bottom left) and $[Sm(TPA)_2]I_3$ (bottom right), $S_6$ and $D_3$ symmetric arrangement, respectively. Hydrogen atoms and the iodine counterion are omitted for clarity.

The isolated complexes were characterized by $^1H$ NMR spectroscopy, X-ray crystallography, and elemental analysis. Because of the very low solubility of these complexes in THF, crystals suitable for X-ray diffraction were obtained by slow diffusion of the ligand into a solution of $LnI_2$ in THF (for Eu, Sm) or by slow diffusion of DIPE into a concentrated solution of the complex in acetonitrile (for Yb). The complexes $[Sm(TPA)_2]I_2$ and $[Eu(TPA)_2]I_2$ both crystallize in the monoclinic centrosymmetric $P2_1/c$ space group. The complex $[Yb(TPA)_2]I_2$ crystallizes in the non-centrosymmetric monoclinic $Cc$ space group. The two complexes are isostructural and accordingly only the ellipsoid diagram of $[Sm(TPA)_2]^{2+}$ is given in Figure 2 (top).

In the $[Ln(TPA)_2]^{2+}$ complexes the metal cations are 8-coordinated by the eight nitrogen atoms from the TPA ligands with a distorted cubic geometry. The angle between the two square faces is 1.46° in the Yb complex $[Yb(TPA)_2]I_2$, whereas the two faces are perfectly parallel (0°) in the $[Sm(TPA)_2]I_2$ and $[Eu(TPA)_2]I_2$ complexes, resulting in a less distorted polyhedron. The N–N distances defining the edges of the cube range from 2.77 to 3.48 Å for $[Sm(TPA)_2]I_2$, 2.77 to 3.45 Å for $[Eu(TPA)_2]I_2$, 2.65 to 3.38 Å for $[Yb(TPA)_2]I_2$, and the angles within the cube described by the eight N atoms lie between 72.67 and 96.19° for $[Sm(TPA)_2]I_2$, 73.28 and 96.28° for $[Eu(TPA)_2]I_2$, and 75.42 and 97.12° for $[Yb(TPA)_2]I_2$. The value of the N-Ln-N (Ln = Sm, Eu) *trans* angles is of 180° as required by the presence of an inversion center symmetry in the $[Sm(TPA)_2]I_2$ and $[Eu(TPA)_2]I_2$ complexes. The mean value of the Ln–N distances found for pyridyl nitrogen are 2.69(2) Å for $[Sm(TPA)_2]I_2$, 2.67(2) Å for $[Eu(TPA)_2]I_2$, and 2.60(2) Å for $[Yb(TPA)_2]I_2$. The mean value of the Ln–N distance found for the apical tertiary amine nitrogen is 2.730(8), 2.727(3), and 2.65(2) Å for the Sm, Eu, and Yb complexes, respectively (Tables 1 and 2). Similarly to the previously reported trivalent analogues,[15a] the Ln–N distances show a linear increase with increasing ionic radii as expected in a ionic bonding model and for ligands that can adapt well to metals of different sizes. In the structures of the $[Ln(TPA)_2]^{2+}$ complexes, the two ligands show opposite right- and left-handed helical arrangement around the cation (Figure 2, bottom left). This differs from the structure of the previously reported $Ln^{3+}$ complexes $[Ln(TPA)_2]I_3$ ($Ln = La^{3+}$, $Ce^{3+}$, $Nd^{3+}$), $[Eu(TPA)_2]OTf_3$,[15a] and of the $U^{3+}$ $[U(TPA)_2]I_2$[13a] complex in which both ligands have the same helical arrangement. Such difference in the ligand arrangement is probably the result of the larger ionic radius of the $Ln^{2+}$ ions as compared with the $Ln^{3+}$ ones. Notably, the same difference is also observed between the structure of $[Sm(TPA)_2]I_2$ and that of the $Sm^{3+}$ complex $[Sm(TPA)_2]I_3$ (Figure 2, bottom right) prepared according to the procedure described for $[Ln(TPA)_2]I_3$ complexes.[15a] The Ln–N distances found in the $[Sm(TPA)_2]I_3$ ($Sm–N_{pyridine} = 2.55(3)$ Å and $Sm–N_{amine} = 2.59(2)$ Å) are shorter than those found in $[Sm(TPA)_2]I_2$ ($Sm–N_{pyridine} = 2.69(2)$ Å and $Sm–N_{amine} = 2.730(8)$ Å), in agreement with the difference in the ionic radii between $Sm^{3+}$ (1.079 Å) and $Sm^{2+}$ (1.27 Å).[22]

The proton $^1H$ NMR spectra of the $[Ln(TPA)_2]I_2$ complexes ($Ln = Sm^{2+}$ and $Yb^{2+}$) in $CD_3CN$ shows the presence of one set of signals with four resonances for the pyridyl protons and a single resonance for the methylene protons both at room temperature and at low temperature (283 K), in agreement with the presence of dynamically averaged $D_3h$ symmetric so-

**Table 1.** Selected average bond lengths [Å] for Eu complexes.

| Bonds | $[Eu^{II}(TPA)(\mu\text{-}I)I]_2$ | $[Eu^{II}(TPA)_2I_2]$ | $[Eu^{II}(BPA)_2]$ | $[Eu^{III}(BPA)_2]OTf$ | $[Eu^{III}(BPA)(CS_3)(dmso)_2]$ |
|---|---|---|---|---|---|
| $Eu–N_{amine}$ | 2.748(3) | 2.731(3) | 2.83(5) | 2.64(5) | 2.674(8) |
| $Eu–N_{pyridyl}$ | 2.67(1) | 2.68(2) | 2.749(9) and 2.88(1) | 2.62(3) | 2.61(1) |
| Eu–O | – | – | 2.41(3) | 2.234(8) | 2.273(7) |

**Table 2.** Selected average bond lengths [Å] for Yb complexes.

| Bonds | $[Yb^{II}(TPA)I_2(CH_3CN)]$ | $[Yb^{II}(TPA)_2I_2]$ | $[Yb^{II}(BPA)I(CH_3CN)]_2$ | $[Yb^{III}(MPA)K(dme)_2]$ |
|---|---|---|---|---|
| $Yb–N_{amine}$ | 2.620(4) | 2.65(3) | 2.594(3) | 2.448(16) |
| $Yb–N_{pyridyl}$ | 2.565(6) | 2.68(2) | 2.626(9) | – |
| Yb–O | – | – | 2.346(3) | 2.16(2) |

lution species in which all chelating arms of the TPA ligand are equivalent. The complex $[Sm(TPA)_2]I_2$ is insoluble in THF and unstable at room temperature in acetonitrile. After one day, the color of the acetonitrile solution turned from blue green to yellow and only unidentified decomposition products were found in solution.

The complexes $[Yb(TPA)_2]I_2$ and $[Eu(TPA)_2]I_2$ are stable for weeks in acetonitrile at room temperature. The higher solution stability as compared with the $Sm^{2+}$ analogue is in agreement with the less negative $Ln^{3+}/Ln^{2+}$ redox potential of Eu and Yb ions (−0.35 V and −1.15 vs. NHE, respectively) compared with that of Sm (−1.55 vs. NHE) and with the electrochemistry studies carried out on the homoleptic complexes (see the electrochemistry section).

To investigate how the charge and electron-donor character of the ligand affects the redox properties and reactivity of $Ln^{2+}$ ions, we have studied the complexation of Yb and Eu in the oxidation state +III and +II by the monoanionic tetradentate ligands $BPA^-$ and $BPPA^-$ and by the dianionic $MPA^{2-}$ ligands. Because of their low solution stability, we did not attempt the study of the analogous $BPA^-$ and $BPPA^-$ complexes of $Sm^{2+}$.

## BPA complexes

The $[Ln(BPA)_2]OTf$ complexes (Ln = Eu, Yb) were prepared in situ for electrochemistry studies by treating the trivalent lanthanide salts $[Ln(OTf)_3]$ with 2 equivalents of the KBPA ligand in acetonitrile (Scheme 3). The $Eu^{3+}$ complex $[Eu(BPA)_2]OTf$ was also prepared and characterized. Orange crystals suitable for X-ray diffraction were obtained from a slow diffusion of diisopropyl ether (DIPE) into a THF solution of the complex.

$[Eu(BPA)_2]OTf$ crystallizes in the monoclinic $P2_1/n$ space group. The structure presents an octacoordinated europium surrounded by two BPA ligands in a distorted dodecahedral fashion (Figure 3, left). Similar values are found for the average $Eu–N_{pyridyl}$ bond lengths (mean value = 2.62(3) Å) and the $Eu–N_{amine}$ distance (2.64(5) Å). The mean value of the Eu–O distances is 2.234(8) Å and fall in the range of $Eu–O_{phenoxide}$ bond lengths reported in the literature.[23] The two ligands BPA wrap around the $Eu^{3+}$ cation with a pincer arrangement rather than the helical one found in bis-TPA complexes (Figure 3). The $^1H$ NMR spectrum of the complex in $CD_3CN$ shows a set of very broad signals for the 18 H from $\delta = 31$ to −18 ppm.

The treatment of the divalent $EuI_2$ salt with 2 equivalents of the KBPA ligand in THF leads to isolation of the neutral homoleptic $Eu^{2+}$ complex $[Eu(BPA)_2]$ (Scheme 3). The complex has very low solubility in THF but is partially soluble in acetonitrile and pyridine and is stable in the three solvents for several weeks.

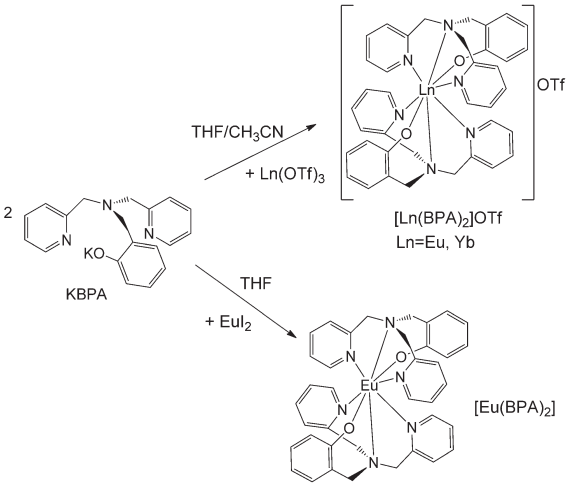


**Scheme 3.** Synthesis of $[Eu(BPA)_2]$ and $[Ln(BPA)_2]OTf$ complexes.

The paramagnetism of the $Eu^{2+}$ ion leads to an uninformative $^1H$ NMR spectrum. Suitable single crystals were obtained from slow diffusion of hexane into a pyridine solution of the complex. The X-ray diffraction studies show the presence of the bis-ligand complex $[Eu(BPA)_2]$, which crystallizes in monoclinic system and $P2_1/n$ space group. The overall neutral charge is in agreement with the presence of the $Eu^{2+}$ cation. The octacoordinated europium is surrounded by two ligands in a distorted cubic fashion (Figure 3, right). The two ligands wrap around the metal ion in a geometry that brings the two oxygen atoms from the phenolate arms side by side. In each ligand, one $Eu–N_{pyridyl}$ distance is significantly shorter than the other: 2.755(3) Å and 2.866(3) for the first ligand, 2.742(3) and 2.887(3) Å for the second one. These distances are slightly elongated as compared with the bis-TPA europium complex in which the average $Eu–N_{pyridyl}$ is 2.68(2) Å. This is probably due to the steric effect of the phenol arms. The average value of the $Eu–N_{amine}$ 2.83(5) Å is 0.1 Å longer than the value found for

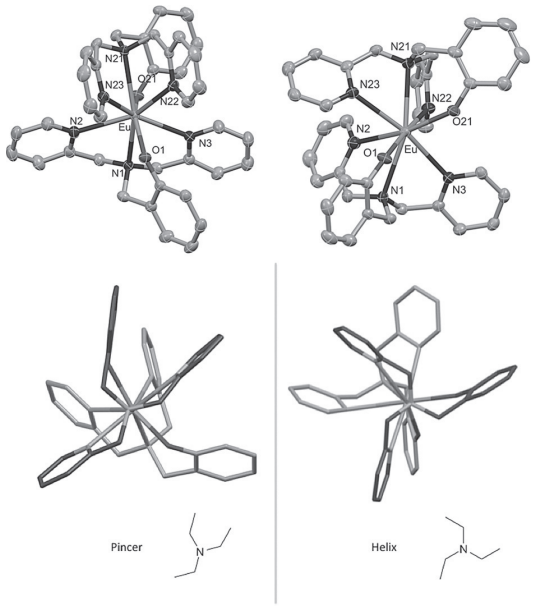


**Figure 3.** Ellipsoid diagrams of $[Eu(BPA)_2]^+$ (left) and $[Eu(BPA)_2]$ (right) (50% probability ellipsoids). Hydrogen atoms and triflate counterion of $[Eu(BPA)_2]^+$ are omitted for clarity.

the bis-ligand complexes $[Eu(TPA)_2]I_2$. The large lengthening of the Eu–N and Eu–O (2.83(5) Å) distances found in $[Eu(BPA)_2]$ as compared with the $Eu^{3+}$ analogue can be interpreted in terms of the difference in ionic radii of the $Eu^{3+}$ and $Eu^{2+}$ cations (0.19 Å).[22] The two ligands in the $Eu^{2+}$ complex adopt the same helical conformation leading to a chiral complex. Both enantiomers $\Lambda\Lambda$ and $\Delta\Delta$ are present in the structure.

Attempts to isolate single crystals of the $Yb^{2+}$ $[Yb(BPA)_2]$ complex failed because of the low stability of this species at −40 °C. Proton NMR studies of the reaction of $YbI_2$ with two equivalents of the KBPA ligand salt in THF at 233 K or at room temperature shows the presence of a complicated mixture of paramagnetic species. However, proton NMR studies of the reaction of $YbI_2$ with two equivalents of the KBPA ligand salt in acetonitrile at 233 K show paramagnetic signals assigned to the $Yb^{3+}$ $[Yb(BPA)_2]^+$ complex. Signals of intermediate diamagnetic species are also observed immediately after mixing the $YbI_2$ and the ligand, but these species decompose even at 233 K. After one night at room temperature or at 233 K, the THF and acetonitrile reaction mixture became deep blue. The deep-blue color of the reaction mixture after complete decomposition is suggestive of the presence of additional reaction products, since the $[Yb(BPA)_2]^+$ complex is colorless. The formation of $[Yb(BPA)_2]^+$ could arise from a disproportionation reaction of a $Yb^{2+}$ intermediate species to $Yb^{3+}$ and $Yb^0$ or from solvent/ligand reduction. Notably, C–C coupling of aromatic heterocycles by $Yb^{2+}$ complexes has been previously reported.[3c] Attempts to isolate potential additional decomposition products were not successful.

These results indicate that the replacement of one pyridine of the TPA ligand with a phenol group reduces significantly the stability of the respective homoleptic $Yb^{2+}$ complexes as compared with their $Yb^{3+}$ analogues. The difference in stability of the $[Eu(BPA)_2]$ and of the $[Yb(BPA)_2]$ complexes can be explained by the difference in redox potential between the two cations (see the electrochemistry section).

However, the proton NMR spectrum in $CD_3CN$ of a solution of $YbI_2$ treated with one equivalent of BPA ligand shows the presence of only one set of signals in the diamagnetic region, in agreement with the formation of a stable heteroleptic $Yb^{2+}$ complex. Indeed, the complex $[Yb(BPA)I(CH_3CN)]_2$ (Figure 4) crystallizes from a saturated acetonitrile solution in the $P2_1/n$ space group. The crystals structure of the $Yb^{2+}$ mono-BPA complex shows that the phenolate oxygen atoms of the ligand BPA bridge two $Yb^{2+}$ ions, affording a dimer with an inversion center in the middle of the YbOOYb diamond core (Figure 4). The two Yb ions are heptacoordinated by three nitrogen and two oxygen atoms from the BPA ligands, one nitrogen from an acetonitrile molecule and one iodide with a distorted pentagonal bipyramidal geometry. The Yb–$N_{amine}$ distance (2.594(3) Å) and the average value of the Yb–$N_{pyridyl}$ distance (2.626(9) Å) are similar to those found for Yb–$N_{amine}$ and Yb–$N_{pyridyl}$ in the $[Yb(TPA)I_2CH_3CN]$ and $[Yb(TPA)_2I_2]$ complexes. The Yb–O distance is 2.346(3) Å and falls in the range of bridging Yb–$O_{phenoxide}$ distances reported in literature.[16]

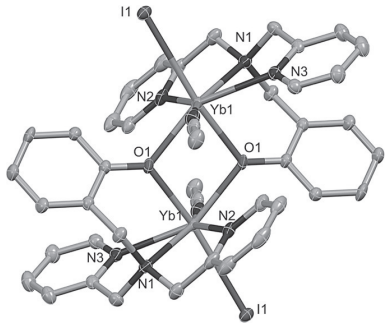


**Figure 4.** Ellipsoid diagrams of $[Yb(BPA)I(CH_3CN)]_2$ (50% probability ellipsoids). Hydrogen atoms and solvent molecule are omitted for clarity.

These results suggest that, in spite of its more electron-rich character as compared with TPA, the BPA ligand can be used in the preparation of stable heteroleptic complexes of divalent ytterbium. Future studies will be directed to investigate the reactivity and catalytic activity of this compound.

### BPPA complexes

The $[Ln(BPPA)_2]OTf$ complexes (Ln = Eu, Yb) were prepared in situ for electrochemistry studies by treating the trivalent lanthanide salt $[Ln(OTf)_3]$ with 2 equivalents of the KBPPA ligand in acetonitrile (Scheme 4).

The $Eu^{3+}$ complex $[Eu(BPPA)_2]OTf$ was also isolated and characterized. The complex is partially soluble in THF but fully solu-

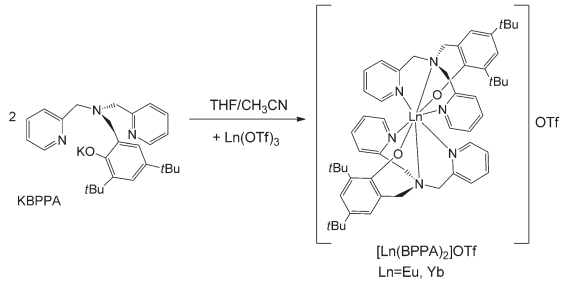


**Scheme 4.** Synthesis of $[Ln(BPPA)_2]OTf$ complexes.

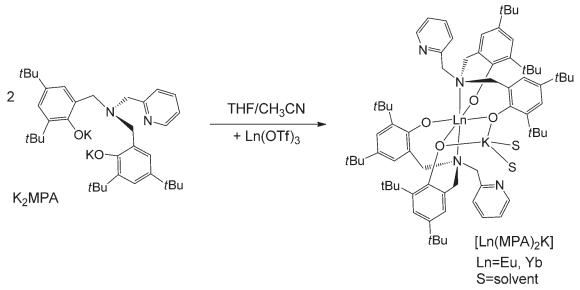


**Scheme 5.** Synthesis of $[Ln(MPA)_2K]$ complexes.

ble in acetonitrile. The $^1H$ NMR spectrum of this complex in $CD_3CN$ shows 34 H broad and sharp signals in the range $\delta = -15$ to $+23$ ppm. The quality of the X-ray data collected for the orange needles, obtained by a slow diffusion of hexane into a pyridine solution of the complex, was good enough to establish the overall structure and connectivity (Figure 5) but insufficient to allow a discussion of the bond lengths.

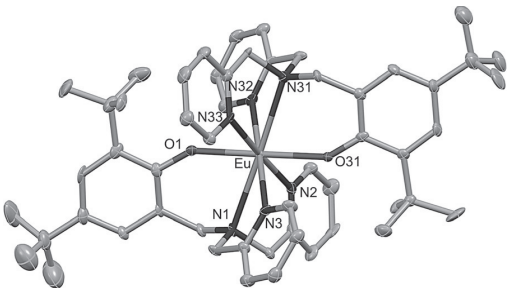


**Figure 5.** Ellipsoid diagrams of $[Eu(BPPA)_2]OTf$ (50% probability ellipsoids). Hydrogen atoms, solvent molecules, disorder, and triflate counteranion are omitted for clarity.

The crystal structure shows that the europium center is octacoordinated by two tetradentate BPPA ligands with a distorted cubic geometry. The ligand arms are both in a helical conformation presenting opposite rotation direction. This results in an achiral complex. The overall monocationic charge of the $Eu^{3+}$ complex is counterbalanced by the triflate anion. The structure of the $[Eu(BPPA)_2]OTf$ complex shows that the presence of the bulky *tert*-butyl substituents do not prevent formation of homoleptic bis-ligand complexes.

### MPA complexes

Proton NMR studies in $CD_3CN$/THF of the reaction of the trivalent lanthanide salts $[Ln(OTf)_3]$ (Ln = Eu, Yb) with 1 or 2 equivalents of the $K_2MPA$ ligand show the formation of the bis-ligand complex independently of the used stoichiometry (Scheme 5).

This suggests a strong preference of the $MPA^{2-}$ for the formation of 2:1 complexes, a behavior rarely encountered in coordination chemistry[24] but previously reported for $Nd^{3+}$ complexes of aminobis-phenolates.[17d] The bis-ligand "ate" complex $[Yb(MPA)_2K]$ was isolated from the treatment of $[Yb(OTf)_3]$ with two equivalents of the $K_2MPA$ ligand in THF. The presence of the *tert*-butyl groups renders the final complex very soluble in non-polar solvents such as hexane. Colorless crystals suitable for X-ray diffraction of the complex $[Yb(MPA)_2K(dme)_2]$ were obtained from a concentrated solution of the complex in hexane/DME (30:1) at 233 K. The X-ray crystal structure (Figure 6) shows that two MPA ligands bind to the $Yb^{3+}$ ion, but in the resulting complex the pyridine nitrogen atoms remain non-binding with a Ln–N distance of 5.393(19) Å.

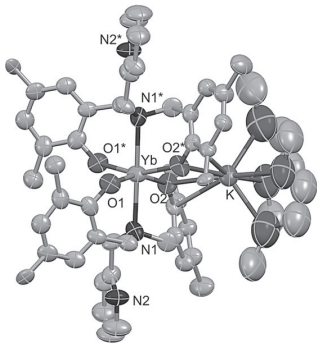


**Figure 6.** Ellipsoid diagram of $[Yb(MPA)_2K(dme)_2]$ (50% probability ellipsoids). Hydrogen atoms, solvent molecules and methyl groups are omitted for clarity. *= *y*, *x*, −*z*.

As a result, the ytterbium center is only hexacoordinated by two MPA ligands in a distorted octahedral fashion. The average values of the Yb–O distance and of the Yb–$N_{amine}$ distance are 2.16(2) and 2.448(16) Å, respectively, and are slightly shorter than the Yb–O and Yb–$N_{amine}$ average distances of the divalent Yb complex $[Yb(BPA)I(CH_3CN)]_2$. This is in agreement with the shorter ionic radii of $Yb^{III}$ center (Table 2). A potassium cation is also present in the structure, binding a phenolate oxygen from each ligand with a K–O distance of 2.794(14) Å. The K coordination sphere is completed by two DME molecules. The $^1H$ NMR spectrum of $[Yb(MPA)_2K]$ in $CD_3CN$ shows the presence of paramagnetically shifted signals in the $\delta = -50$ to $+186$ ppm range, indicative of a $Yb^{3+}$ metal center.

Although X-ray suitable crystals of the [Eu(MPA)$_2$K] complex were not obtained, the $^1$H NMR spectrum of a 1:2 solution of $EuI_2$ and $K_2$MPA in $CD_3CN$ only shows one set of paramagnetically shifted signals in the $\delta = -9$ to $+10$ ppm range.

$^1$H NMR studies of the reaction of $YbI_2$ with one equivalent of $K_2$MPA in THF at 233 K show the formation of a diamagnetic species assigned to the [Yb(MPA)] complex (the Supporting Information, Figure S.A.12). A broad, uninformative proton NMR spectrum is obtained for the reaction of $EuI_2$ with one equivalent of $K_2$MPA in THF at 233 K, suggesting the presence of the $Eu^{2+}$ ion. The neutral [Ln(MPA)] complexes are stable in THF at room temperature, but the addition of small ligand excess leads in both cases to the apparition of the paramagnetic signals of the $Eu^{3+}$ and $Yb^{3+}$ complexes. Stable mono-ligand complexes of $Yb^{2+}$ with bulky aminobisphenolate (*t*Bu substituents on the phenolate groups) containing a methoxy[16,19a] or a dimethylamine arm[18a] have been previously reported and proven to be active catalysts in the ring-opening polymerization of cyclic esters.[16,18a,19a] Attempts to isolate crystal of the neutral [Ln(MPA)] complexes suitable for X-ray diffraction were so far unsuccessful. However, NMR studies suggest that the presence of a pyridyl arm does not lead to a decreased stability of the mono-ligand $Yb^{2+}$ complexes as compared with the methoxy and dimethylamino arms.

Treatment of the divalent $EuI_2$ salt with two equivalents of $K_2$MPA in THF at 233 K leads to the formation of intermediate $Eu^{2+}$ species that decompose slowly to afford the $Eu^{3+}$ complex [Eu(MPA)$_2$K] as identified by NMR spectroscopy. $^1$H NMR studies of the 1:2 $YbI_2$/$K_2$MPA reaction in THF at 233 K show the immediate formation of the $Yb^{3+}$ complex [Yb(MPA)$_2$K], which was also identified by X-ray diffraction studies. The formation of the [Ln(MPA)$_2$K] compounds could arise from a disproportionation process to afford the $Ln^{3+}$ bis-ligand complexes and $Ln^0$ (not unambiguously identified), or from solvent/ligand reduction.

The formation of a bis-ligand complex of $Yb^{3+}$ has also been observed for the reaction of the $YbI_2$ or the [Yb{N(SiMe$_3$)$_2$}$_2$] precursors with tripodal aminobisphenolate ligands containing a methoxide arm[18c] or a dimethylamine arm.[16]

The presented results show that the replacement of two pyridyl groups in the TPA ligand with two phenoxide groups prevents the formation of stable homoleptic bis-ligand complexes for both the $Yb^{2+}$ and $Eu^{2+}$ ions.

To relate the stability properties of the described complexes to their redox properties, cyclic voltammetry studies were performed on the homoleptic complexes of the ligands TPA, BPA, BPPA, and MPA.

### Electrochemistry studies

Cyclic voltammograms were measured in acetonitrile on samples of the trivalent complexes [Yb(TPA)$_2$]OTf$_3$ and [Eu(TPA)$_2$]OTf$_3$ (Figure 7) prepared in situ. These data clearly show the quasi-reversible reduction of the metal center at $E_{1/2} = -1.11$ V and $-0.41$ V versus $Fc^+$/Fc, respectively. The cyclic voltammogram of the Sm complex [Sm(TPA)$_2$]OTf$_3$ prepared in situ shows an irreversible reduction of the metal center at $-1.7$ V versus $Fc^+$/Fc (the Supporting Information, Figure S.C.2). The irreversible character of this event is in agreement with the instability of the divalent Sm complex $[Sm(TPA)_2]^{2+}$ in acetonitrile. The cyclic voltammogram of the free ligand (see the Supporting Information) confirms the absence of redox events at these potentials when the metal ions are missing. The voltammogram of the free ligand also presents an irreversible oxidation feature at $E_{pa} = 0.63$ V, which is attributed to the oxidation of the central tertiary amine. This event is absent in the CV of [Eu(TPA)$_2$]OTf. The coordination of the amine to the metal center probably renders its oxidation more difficult resulting in a shift of this wave from 0.63 V to higher potentials.

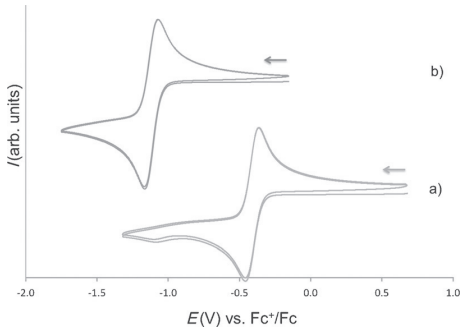


**Figure 7.** Cyclic voltammogram for 4 mM solutions of: a) [Eu(L1)$_2$]OTf; b) [Yb(L1)$_2$]OTf in $\approx$0.1 M [Bu$_4$N][PF$_6$] acetonitrile solution at 100 mV s$^{-1}$ scan rate.

To investigate the impact of the presence of phenolate oxygen donors on the redox properties of their $Yb^{2+}$ and $Eu^{2+}$ complexes, we studied the redox properties of the analogous BPA and MPA complexes.

The cyclic voltammograms obtained in acetonitrile solutions of the trivalent complex [Yb(BPA)$_2$]OTf prepared in situ show an irreversible reduction of the metal center at the very low potential of $-2.41$ V (vs. $Fc^+$/Fc) close to the reduction of the solvent (Figure 8 b). This reduction does not become reversible even at 1 V s$^{-1}$ scan rate, suggesting that a highly reactive $Yb^{2+}$ species is formed. Notably, a shift to more negative potentials of the metal center reduction process is observed for both [Yb(BPA)$_2$]OTf and [Eu(BPA)$_2$]OTf complexes as compared with the TPA analogous complexes (from $E_{pc} = -1.17$ to $-2.41$ V, that is, $-1.24$ V shift for Yb and from $E_{1/2} = -0.48$ to $-1.73$ V, that is, $-1.25$ V shift for Eu). The substitution of a pyridine arm on TPA by an anionic phenolate arm on BPA ligand renders the metal center significantly more electron-rich and thus more difficult to reduce. As a result, the corresponding $Ln^{2+}$ species are much more reductive.

Although the complexes [Yb(TPA)$_2$]OTf$_3$ and [Eu(TPA)$_2$]OTf$_3$ did not exhibit any oxidation process in the range 0.5–1 V, the voltammograms of the complex [Yb(BPA)$_2$]OTf and [Eu(BPA)$_2$]OTf show also an irreversible oxidation at 0.70 and 0.72 V, respectively, attributed to the oxidation of the phenol

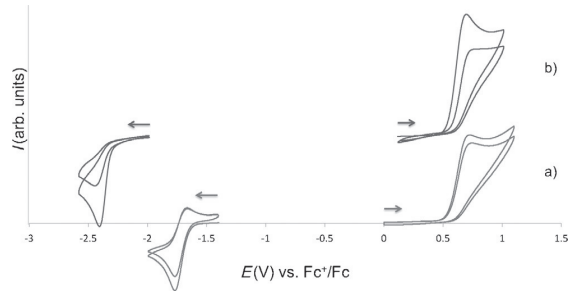


**Figure 8.** Cyclic voltammogram for 4 mM solutions of: a) $[Eu(BPA)_2]OTf$ and b) $[Yb(BPA)_2]OTf$ in ≈0.1 M $[Bu_4N][PF_6]$ acetonitrile solution at 100 mV $s^{-1}$ scan rate.

**Table 3.** Voltammetric data for Eu complexes (vs. $Fc^+/Fc$).

| Compounds | Metal-based wave | | Ligand-based waves | |
|---|---|---|---|---|
| | $E_{pc}$ [V] | $E_{pa}$ [V] | $E_{pa1}$ [V] | $E_{pa2}$ [V] |
| $[Eu(TPA)_2]OTf_3$ | −0.46 | −0.36 | – | – |
| $[Eu(BPA)_2]OTf_3$ | −1.77 | −1.66 | 0.72 | – |
| $[Eu(BPPA)_2]OTf_3$ | −1.78 | −1.52 | $E_{1/2}=0.34$ | $E_{1/2}=0.65$ |

**Table 4.** Voltammetric data for Eu complexes (vs. NHE).

| Compounds | Metal-based wave | | Ligand-based waves | |
|---|---|---|---|---|
| | $E_{pc}$ [V] | $E_{pa}$ [V] | $E_{pa1}$ [V] | $E_{pa2}$ [V] |
| $[Eu(TPA)_2]OTf_3$ | 0.17 | 0.27 | – | – |
| $[Eu(BPA)_2]OTf_3$ | −1.14 | −1.03 | 1.35 | – |
| $[Eu(BPPA)_2]OTf_3$ | −1.15 | −0.89 | $E_{1/2}=0.97$ | $E_{1/2}=1.28$ |

**Table 5.** Voltammetric data for Yb complexes (vs. $Fc^+/Fc$).

| Compounds | Metal-based wave | Ligand-based waves | |
|---|---|---|---|
| | $E_{pc}$ [V] | $E_{pa1}$ [V] | $E_{pa2}$ [V] |
| $[Yb(TPA)_2]OTf_3$ | −1.17 ($E_{1/2}=-1.11$) | – | – |
| $[Yb(BPA)_2]OTf_3$ | −2.41 | 0.70 | – |
| $[Yb(BPPA)_2]OTf_3$ | −2.40 | $E_{1/2}=0.34$ | $E_{1/2}=0.64$ |

**Table 6.** Voltammetric data for Yb complexes (vs. NHE).

| Compounds | Metal-based wave | Ligand-based waves | |
|---|---|---|---|
| | $E_{pc}$ [V] | $E_{pa1}$ [V] | $E_{pa2}$ [V] |
| $[Yb(TPA)_2]OTf_3$ | −0.54 ($E_{1/2}=-0.48$) | – | – |
| $[Yb(BPA)_2]OTf_3$ | −1.78 | 1.33 | – |
| $[Yb(BPPA)_2]OTF_3$ | −1.77 | $E_{1/2}=0.97$ | $E_{1/2}=1.27$ |

function on the BPA ligand, which is easier to oxidize than the tertiary amine (see the Supporting Information).

A summary of the redox potentials is given in Tables 3 to 6. To assess the effect of electron-donor substituents on the redox properties of the $[Yb(BPA)_2]OTf_3$ and $[Eu(BPA)_2]OTf_3$ complexes, the redox properties of the complexes of the BPPA ligand containing electron-donor substituents on the phenolate arm were investigated.

The cyclic voltammograms of solutions of the trivalent complexes $[Yb(BPPA)_2]OTf$ and $[Eu(BPPA)_2]OTf$ in acetonitrile (Figure 9) show that the presence of the *tert*-butyl groups in *meta* and *para* position of the phenolate arm in the BPPA ligand does not affect significantly the reduction potential of the lanthanide ions. Notably, the reduction potentials of both $[Yb(BPPA)_2]OTf$ ($E_{pc}=-2.40$ V) and $[Eu(BPPA)_2]OTf$ ($E_{pc}=-1.78$ V) are similar to those of $[Yb(BPA)_2]OTf$ ($E_{pc}=-2.41$ V) and $[Eu(BPA)_2]OTf$ ($E_{pc}=-1.77$ V), respectively.

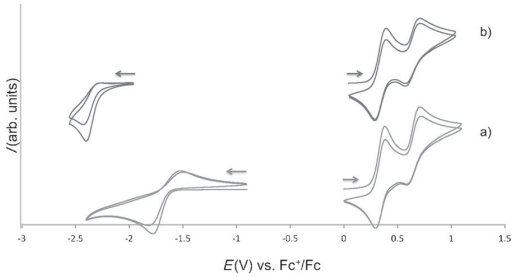


**Figure 9.** Cyclic voltammogram for 4 mM solutions of: a) $[Eu(BPPA)_2]OTf$ and b) $[Yb(BPPA)_2]OTf$ in ≈0.1 M $[Bu_4N][PF_6]$ acetonitrile solution at 100 mV $s^{-1}$ scan rate.

Two quasi-reversible oxidation events occur at $E_{1/2}=0.34$ and 0.65 V, which are attributed to the oxidation of the two phenol groups in phenoxyl radicals stabilized by the *tert*-butyl groups in the *ortho* and *para* positions. Such stabilization explains the reversibility of this oxidation process compared with the irreversible oxidation of the BPA ligand in the analogous $[Yb(BPA)_2]OTf$ and $[Eu(BPA)_2]OTf$ complexes.

The cyclic voltammograms obtained in acetonitrile or THF solutions of the trivalent "ate" complexes $[Yb(MPA)_2K]$ and $[Eu(MPA)_2K]$ prepared in situ do not present any redox event at the metal center (the Supporting Information, Figure S.C.3). These results suggest that the presence of four phenolate oxygen donors shifts the redox potential significantly towards lower values. The second cycle presents some small reduction wave apparently linked to ligand oxidation processes. The ligand-based redox processes are much more difficult to interpret than are those of the analogous BPPA complexes.

## Reactivity

A preliminary study of the reactivity of the isolated $Ln^{2+}$ complexes with heteroallenes has been carried out. The $Ln^{2+}$ complexes $[Ln(TPA)_2]I_2$ do not react with $CO_2$ or $CS_2$. The $[Eu(BPA)_2]$ and $[Eu(MPA)_2K_2]$ complexes do not react with carbon dioxide. In contrast, $[Eu(BPA)_2]$ reduces $CS_2$. When one equivalent of $^{13}CS_2$ was added to a THF suspension or a pyridine solution of $[Eu(BPA)_2]$, a color change from purple to red was observed. Only the signals of the trivalent Eu complex $[Eu(BPA)_2]^+$ appear in the $^1H$ NMR spectrum, probably due to the fluxional nature of a putative $[Eu(CS_3)(BPA)_2]^-$ complex. Dissolution of the reac-

tion mixture in deuterated DMSO leads to the release of the free ligand $BPA^-$ and to the appearance in the proton NMR spectrum of an additional set of paramagnetic signals assigned to the thiocarbonate complex $[Eu(BPA)(CS_3)(dmso)_2]$ (Scheme 6). Slow diffusion of toluene into a DMSO solution of the reaction products lead to the isolation of the analytically pure $[Eu(BPA)(CS_3)(dmso)_2]$ in 33% yield. The structure of the complex was confirmed by X-ray diffraction analysis. When one equivalent of $^{13}CS_2$ is added to a 1:1 solution of $EuI_2$ and KBPA in pyridine, the formation of the $[Eu(BPA)_2]^+$ complex is observed by proton NMR spectroscopy. However the $^1H$ NMR spectrum of the reaction mixture in deuterated DMSO does not show the formation of the $[Eu(BPA)(CS_3)(dmso)_2]$. This suggests that, in this case, different products are formed from the reduction of $CS_2$ that could not be identified.

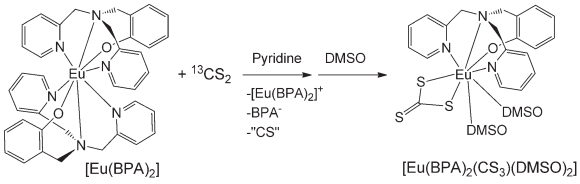


**Scheme 6.** Synthesis of $[Eu(BPA)(CS_3)(dmso)_2]$.

The structure $[Eu(BPA)(CS_3)(dmso)_2]$ (Figure 10) shows the presence a trivalent europium ion surrounded by one BPA ligand and a terminal thiocarbonate moiety. The coordination sphere is completed by two DMSO molecules. The europium center is octacoordinated in a distorted dodecahedral fashion. The $Eu–N_{amine}$, $Eu–N_{pyridyl}$, and $Eu–O_{phenol}$ distances (2.672(6), 2.601(7), 2.588(7) and 2.588(7), and 2.272(5) Å, respectively) are very similar to those found in the $Eu^{3+}$ bis-ligand complex $[Eu(BPA)_2]OTf$. The average Eu–S bond (2.88(1) Å) falls in the range of Eu–S distances previously reported for $Eu^{3+}$ thiocarbamate complexes.[25] The S–C bonds of the thiocarbonate moiety, S1–C2 and S2–C2, measure 1.735(10) and 1.725(10) Å, respectively. The S3 atom is disordered between two positions. The main position (55% occupancy) leads to a C–S distance of 1.748(15) Å, the minor position (45% occupancy) leads to a shorter C–S distance of 1.630(16) Å. The C–S distances remain in the range of previously reported trithiocarbonate complexes.[26,27]

There are two previous reports of trithiocarbonate complexes containing f elements,[28,29] but the complex $[Eu(BPA)(CS_3)(dmso)_2]$ is the first example of a trithiocarbonate complex containing a 4f element. Moreover, only three examples of $CS_2$ reduction by lanthanide complexes have been reported before. The reduction of $CS_2$ by $Eu^{2+}$ and $Yb^{2+}$ tetrasiloxide complexes has been reported by our group[5c] and was found, by $^{13}C$ NMR studies, to afford trithiocarbonate and tetrathioxalate products in different ratios depending on the $Ln^{2+}$ ion. However, the $CS_2$ reduction products are quickly released in the reaction media and no lanthanide-bound product was isolated. Very different results were found for the reaction of

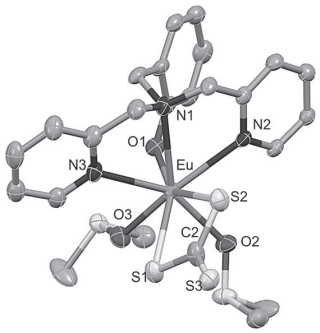


**Figure 10.** Ellipsoid diagram of $[Eu(BPA)(CS_3)(dmso)_2]$ (50% probability ellipsoids). Hydrogen atoms, disorder, and solvent molecules are omitted for clarity.

formamidinato[6a] and guanidinate[6b] complexes of $Sm^{2+}$ with $CS_2$. These compounds were found to promote a C–S coupling reaction affording the thioformyl carbonotrithioate, the ($(SCSCS_2)^{2-}$) bridging ligand.

## Conclusion

Complexation studies were performed with a series of tetradentate tripodal pyridylamine and pyridylaminophenolate ligands for the lanthanide ions Eu and Yb in their oxidation state III and II. Stable mono ligand and bis-ligand complexes of $Eu^{2+}$ and $Yb^{2+}$ were prepared and characterized with the neutral tetradentate ligand TPA. The replacement of one pyridyl group by a phenolate group in the ligand $BPA^-$ leads to a decreased stability of the bis-ligand complex of $Yb^{2+}$ preventing its isolation but the mono-BPA complex of divalent Yb can be isolated and it is stable in acetonitrile solution. The bis-ligand complexes of $Eu^{2+}$ and $Eu^{3+}$ with $BPA^-$ were also isolated and their solid-state structure was characterized. The neutral $Eu^{2+}$ complex $[Eu(BPA)_2]$ is stable in acetonitrile solution. The replacement of two pyridyl groups by two phenolate group in the ligand $MPA^{2-}$ leads to a further decrease of the stability of the bis-ligand complexes of $Eu^{2+}$ and $Yb^{2+}$, preventing their isolation. Cyclic voltammetry studies carried out on the bis-ligand complexes of $Eu^{3+}$ and $Yb^{3+}$ show that the metal center reduction occurs at significantly lower potentials for the $BPA^-$ ligand as compared with the TPA ligands. No metal-centered redox event was observed in the used conditions for the bis-MPA complexes, most likely because metal reduction occurs at even lower potential. These studies show that the successive replacement of pyridyl groups by phenolate groups, leading to more electron-rich ligands, results in significant differences in the reducing character of the lanthanide complexes of TPA, $BPA^-$, and $MPA^{2-}$ ligands. The important differences in the stability and reactivity of the investigated complexes are probably due to the observed difference in redox potential. Preliminary reactivity studies show that, whereas the bis-TPA complexes of $Eu^{2+}$ and $Yb^{2+}$ do not react with heteroallenes, the $[Eu(BPA)_2]$ complex reduces $CS_2$, affording the first example of a lanthanide trithiocarbonate complex. Future work will be

directed to investigate the reactivity of heteroleptic $Ln^{2+}$ complexes of $BPA^{-}$ and $MPA^{2-}$with different substrates.

## Experimental Section

### General considerations

Unless otherwise noted, all manipulations were carried out at ambient temperature under an inert argon atmosphere using Schlenk techniques and an MBraun glovebox equipped with a purifier unit. The water and oxygen levels were always kept at less than 1 ppm. Glassware was dried overnight at 130 °C before use.

$^1$H NMR experiments were performed using NMR tubes adapted with J. Young valves. $^1$H NMR spectra were recorded on Bruker 200 MHz and 400 MHz spectrometers. NMR chemical shifts are reported in ppm with solvent as internal reference.

Elemental analyses were performed under argon by Analytische Laboratorien GMBH at Lindlar, Germany.

Unless otherwise noted, reagents were purchased from commercial suppliers and used without further purification. The solvents were purchased from Aldrich or Eurisotop (deuterated solvents) in their anhydrous form, conditioned under argon and vacuum distilled from K/benzophenone (hexane, pyridine, DIPE, DME, and THF). Acetonitrile was heated at reflux on $CaH_2$ for 2 days prior to being distilled. All reagents were dried under high vacuum for 7 days prior to use. TPA was purchased from Aldrich and recrystallize from $Et_2O$ prior to use. 2-(3,5-Di-*tert*-butyl-2-hydroxybenzylaminomethyl)pyridine was prepared according to the published procedure.[28]

### Syntheses

The ligand HBPPA[29] was prepared according to the published procedure. The previously reported HBPA ligand[30] was prepared in 78% yield with the same procedure[29] used for ligand HBPPA. The previously reported ligand $H_2MPA$[21] was synthesized from 2-(3,5-di-*tert*-butyl-2-hydroxybenzylaminomethyl)pyridine in 24% yield according to the literature procedure used for a similar system.[28] The proton NMR data are in agreement with those reported in the literature. The potassium salts of all ligands were prepared according to a published procedure.[13b] The complexes $[Ln(TPA)_2]OTf_3$ (Ln = Eu and Yb) were prepared in situ according to the published procedure.[15a]

**KBPA**: $^1$H NMR (200 MHz, [D$_5$]py, 298 K): $\delta$ = 8.3 (d, 2H), 7.5–7.1 (m, 7H), 6.9 (dd, 2H), 6.5 (td, 1H), 3.7 ppm (m, 6H).

**KBPPA**: HBPPA (1.1 g, 2.5 mmol, 1 equiv) and potassium hydride (0.11 g, 2.8 mmol, 1.1 equiv) were mixed in anhydrous THF (25 mL). The reaction mixture was heated at reflux under argon for 12 h. The mixture was then filtered to remove the excess of KH, the filtrate was taken to dryness and washed with hexane (10 mL). The obtained solid was dried under vacuum for 2 days to give $KBPPA(THF)_{0.65}$ (0.9 g, 1.7 mmol, 68% yield), in which the amount of THF was determined by quantitative $^1$H NMR spectroscopy. $^1$H NMR (200 MHz, [D$_5$]py, 298 K): $\delta$ = 8.3 (d, 2H), 7.5–7.2 (m, 6H), 6.9 (dd, 2H), 3.9 (s, 2H), 3.8 (s, 4H), 1.8 (s, 9H), 1.5 ppm (s, 9H).

**$K_2MPA$**: $^1$H NMR. $^1$H NMR (200 MHz, [D$_5$]py, 298 K): $\delta$ = 7.9 (d, 1H), 7.4–7.3 (m, 4H), 7.1 (d, 2H), 6.7 (t, 1H), 4.1 (s, 2H), 3.9 (br s, 4H), 1.7 (s, 18H), 1.4 ppm (s, 18H).

**$[Ln(TPA)I_2]$ (Ln = Eu, Sm)**: Addition of a solution of TPA (20.9 mg, 0.071 mmol) in THF (1 mL) to a stirred solution of $LnI_2$ (1 equiv) in THF (1 mL) resulted in an orange suspension for $[Eu(TPA)I_2]$ and a red-purple suspension for $[Sm(TPA)I_2]$. After filtration, the residue was washed several times with THF and hexane and dried under vacuum to yield $[Eu(TPA)I_2]$ as an orange powder in 90% yield and $[Sm(TPA)I_2]$ as a red-purple powder in 82% yield. Crystals suitable for X-ray diffraction were obtained for Ln = Eu by slow diffusion of DIPE into an acetonitrile solution of the complex. Elemental analysis calcd (%) for $[Eu(TPA)I_2]$ ($C_{36}H_{36}I_4N_8Eu_2$): C 31.06, H 2.61, N 8.05; found: C 31.11, H 2.75, N 8.18; elemental analysis calcd (%) for $[Sm(TPA)I_2(THF)_{0.2}]$ ($C_{18.8}H_{19.6}I_2N_8O_{0.2}Sm$): C 31.85, H 2.79, N 7.90; found: C 31.84, H 3.4, N 7.96.

**$[Yb(TPA)I_2]$**: Slow addition of a solution of TPA (11.3 mg, 0.039 mmol) in $CH_3CN$ (2 mL) to a stirred orange solution of $[YbI_2]$ (1 equiv) in $CH_3CN$ (2 mL) resulted in a dark-blue solution. After stirring for 3 h, the reaction mixture was layered with DIPE. Big dark crystals formed in three days and were collected by filtration and dried under vacuum to yield $[Yb(TPA)I_2(CH_3CN)_{0.6}]$ in 69% yield. Crystals suitable for X-ray diffraction were obtained by slow diffusion of DIPE into a $CH_3CN$ solution of the complex. $^1$H NMR (200 MHz, $CD_3CN$, 298 K): $\delta$ = 8.8 (s, 3H), 7.8 (t, 3H), 7.3 (d, 6H), 4.0 ppm (s, 6H); elemental analysis calcd (%) for $[Yb(TPA)I_2(CH_3CN)_{0.6}]$ ($C_{19.2}H_{19.8}I_2N_{4.6}Yb$): C 31.09, H 2.69, N 8.69; found: C 30.86, H 2.80, N 8.84.

**$[Ln(TPA)_2]I_2$ (Ln = Eu, Yb, Sm)**: Addition of TPA (20 mg, 0.068 mmol, 2 equiv) in THF (2 mL) to a stirred solution of $LnI_2$ (1 equiv) in THF (2 mL) resulted in a color change (to dark red for Ln = Eu, to green for Ln = Yb and to purple-violet for Ln = Sm). A solid precipitates out of the solution after few minutes. After filtration, the solids were washed several times with THF and hexane and dried under vacuum to yield $[Ln(TPA)_2]I_2$ as powder in 76% yield. Crystals suitable for X-ray diffraction were obtained by slow diffusion of a solution of TPA in THF into a solution of $LnI_2$ in THF (for Ln = Eu and Sm) and from slow diffusion of DIPE into an acetonitrile solution of $[Yb(TPA)_2]I_2$. $^1$H NMR (200 MHz, $CD_3CN$, 298 K): For Ln = Yb: $\delta$ = 7.9 (s, 6H), 7.5 (d, 6H), 7.4 (s, 6H), 6.9 (s, 6H), 4.2 ppm (s, 12H); For Ln = Sm: $\delta$ = 23.8 (s, 6H), 11.5 (d, 6H), 4.6–4.2 (m, 6H), 3.9–3.6 (m, 6H), −12.2 ppm (s, 12H); elemental analysis calcd (%) for $[Eu(TPA)_2]I_2$ ($C_{36}H_{36}I_2N_8Eu$): C 43.83, H 3.68, N 11.36; found: C 43.53, H 3.85, N 11.44; calcd (%) for $[Yb(TPA)_2]I_2$ ($C_{36}H_{36}I_2N_8Yb$): C 42.92, H 3.60, N 11.12; found: C 42.54, H 3.70, N 11.26; calcd (%) for $[Sm(TPA)_2]I_2$ ($C_{36}H_{36}I_2N_8Sm$): C 43.90, H 3.68, N 11.38; found: C 43.75, H 3.81, N 11.41.

**$[Eu(BPA)_2]OTf$**: A white suspension of KBPA (118.2 mg, 0.34 mmol, 2 equiv) in THF (2 mL) was added to a white suspension of $[Eu(OTf)_3]$ (103.2 mg, 0.17 mmol, 1 equiv) in THF (2 mL) and stirred 30 min. The reaction mixture turned yellow in few seconds and a white precipitate formed (KOTf) that was filtered out. The resulting solution was layered with DIPE. Orange crystals formed in 2 days and they were filtered and dried under vacuum for 24 h leading to 151.3 mg of $[Eu(BPA)_2]OTf{\cdot}(KOTf)_{0.1}$ (0.16 mmol, 95% yield). Orange crystals suitable for X-ray diffraction were obtained by slow diffusion of DIPE into a THF solution of the complex. $^1$H NMR (200 MHz, [D$_5$]py, 298 K): $\delta$ = 30.6 (br s, 4H), 13.0–11.8 (br m, 12H), 2.0–1.0 (br m, 6H), −2.5 to −4.0 (br m, 8H), −15.7 (br s, 4H), −18.2 ppm (br s, 2H); elemental analysis calcd (%) for $[Eu(BPA)_2]OTf{\cdot}(KOTf)_{0.1}$ ($C_{39.1}H_{36}N_6O_{5.3}F_{3.3}S_{1.1}K_{0.1}Eu$): C 50.57, H 3.91, N 9.05; found: C 50.62, H 3.88, N 9.14.

**$[Eu(BPA)_2]$**: A solution of $EuI_2$ (200.0 mg, 0.49 mmol, 1 equiv) in THF (3 mL) was added to a white suspension of KBPA (338.2 mg, 0.98 mmol, 2 equiv) in THF (6 mL), affording a red-brown suspension. After 1 h of stirring, the mixture was filtered. The brown solid obtained was extracted in pyridine (4 mL) to remove KI. The two filtrates were combined, concentrated, and layered with hexane. Brown crystals formed after one week, which were collected, washed with hexane, and dried under vacuum for 24 h to yield

318 mg of [Eu(BPA)$_2$] (0.42 mmol, 85% yield). Dark-brown crystals suitable for X-ray diffraction were obtained by slow diffusion of hexane into a pyridine solution of the complex. Elemental analysis calcd (%) for [Eu(BPA)$_2$] ($C_{38}H_{36}N_6O_2Eu$): C 60.00, H 4.77, N 11.05; found: C 59.61, H 4.74, N 10.95.

**[Yb(BPA)I]**: A white suspension of KBPA (0.051 mmol, 1 equiv) in $CH_3CN$ (1.5 mL) was added dropwise to an orange solution of $YbI_2(thf)_{2.1}$ (0.051 mmol, 1 equiv) in $CH_3CN$ (1.5 mL) and stirred 18 h. The resulting mixture turned dark green in few seconds. The mixture was then concentrated to 2 mL and filtered. The filtrate was layered with DIPE. A dark-green crystalline solid formed after 24 h. The proton NMR spectrum shows the presence of only one set of signals assigned to the [Yb(BPA)I($CH_3CN$)]$_2$ complex. Unfortunately, a satisfactory elemental analysis was not obtained because of the co-crystallization of KI, which we were not able to separate. X-ray quality dark-green crystals of [Yb(BPA)I($CH_3CN$)]$_2$·($CH_3CN$)$_{0.4}$ were obtained from a saturated solution of the complex in $CH_3CN$ (24.3 mM). $^1$H NMR (400 MHz, $CD_3CN$, 298 K) $\delta = 8.40$ (d, 2H), 7.79 (t, 2H), 7.31 (d, 2H), 7.17 (d, 1H), 7.13–7.00 (m, 3H), 6.84 (d, 1H), 6.53 (t, 1H), 3.95–3.69 ppm (m, 6H).

**[Eu(BPPA)$_2$]OTf**: A white suspension of KBPPA(THF)$_{0.65}$ (93.3 mg, 0.18 mmol, 2 equiv) in THF (2 mL) was added to a white suspension of [Eu(OTf)$_3$] (55.6 mg, 0.09 mmol, 1 equiv) in THF (2 mL) and stirred for 1 h. The resulting suspension turned orange in few seconds. The solvent was then removed under vacuum and pyridine (2 mL) was added to afford a deep orange suspension that was filtered to partially remove KOTf. Complete removal of KOTf salt is not possible due to the very similar solubility of the desired complex and KOTf. The filtrate was layered with hexane to yield 96.1 mg of [Eu(BPPA)$_2$]OTf·(KOTf)$_{1.5}$ (52% yield) as an orange solid. X-ray quality orange crystals of [Eu(BPPA)$_2$]OTf were obtained by slow diffusion of hexane into a pyridine solution of the complex. $^1$H NMR (200 MHz, [D$_5$]py, 298 K): $\delta = 30.0$ to $-24.0$ (broad signals 32H), 4.86 (s, 18H), $-15.22$ ppm (s, 18H); elemental analysis calcd (%) for [Eu(BPPA)$_2$]OTf.[KOTf]$_{1.5}$ ($C_{56.5}H_{68}N_6O_{9.5}F_{7.5}S_{2.5}K_{1.5}Eu$): C 47.91, H 4.84, N 5.93; found: C 47.85, H 4.86, N 6.21.

**[Yb(MPA)$_2$K]**: A light-yellow solution of $K_2$MPA (54.9 mg, 0.08 mmol, 2 equiv) in THF (3 mL) was added to a suspension of [Yb(OTf)$_3$] (24.8 mg, 0.04 mmol, 1 equiv) in THF (2 mL), affording a pale-yellow suspension which was stirred for 4 h. The reaction mixture was evaporated and the resulting solid was extracted with hexane. The insoluble KOTf was removed and the colorless filtrate was concentrated and let standing at $-40\,^\circ$C. After 15 h, colorless crystals formed that were washed with cold hexane and dried under vacuum for 24 h to afford 42.5 mg of [Yb(MPA)$_2$K][KOTf]$_{0.3}$ (0.03 mmol, 78% yield). Colorless crystals suitable for X-ray diffraction were obtained from a concentrated solution of the complex in 30:1 hexane/DME. $^1$H NMR (200 MHz, $CD_3CN$, 298 K): $\delta = 187.0$–148.0 (br m, 8H), 52.9 (br m, 4H), 43.3 (br s, 2H), 42.4 (br s, 2H), 27.7 (s, 2H), 26.4 (s, 2H), 6.2 (s, 18H), 4.8 (s, 18H), 1.6 (s, 4H), $-7.6$ (br s, 2H), $-10.8$ (bs, 2H), $-43.9$ (br s, 18H), $-50.9$ ppm (br s, 18H); elemental analysis calcd (%) for [Yb(MPA)$_2$K][KOTf]$_{0.3}$ ($C_{72.3}H_{100}N_4O_{4.9}F_{0.9}S_{0.3}K_{1.3}Yb$): C 64.13, H 7.44, N 4.14; found: C 64.26, H 7.37, N 4.15.

**Reaction of YbI$_2$(thf)$_{2.4}$ with two equivalents of K$_2$MPA**: A light-yellow solution of $YbI_2(thf)_{2.4}$ in [D$_8$]THF and a white suspension of 2 equiv of $K_2$MPA in [D$_8$]THF were prepared separately and cooled down to $-40\,^\circ$C. The cold ligand solution was added to the cold suspension of ytterbium iodide leading to a light orange suspension. The $^1$H NMR spectrum of this reaction mixture show only the presence of the signals assigned to the trivalent Yb complex [Yb(MPA)$_2$K].

**[Eu(BPA)(CS$_3$)(dmso)$_2$]**: $^{13}CS_2$ (4.9 μL) was added to a pyridine solution of [Eu(BPA)$_2$] (0.081 mmol, 1 equiv). The solution turned from red-brown to red. Then pyridine was removed under vacuum and DMSO was added. Red crystals suitable for X-ray diffraction were obtained from a DMSO solution of the reaction mixture layered with toluene. [Eu(BPA)($CS_3$)(dmso)$_2$](DMSO)$_{0.3}$ was recovered (11 mg, 33%); elemental analysis calcd (%) for [Eu(BPA)($CS_3$)(dmso)$_2$](DMSO)$_{0.3}$ ($C_{26.6}H_{37.8}N_3O_{4.3}S_{6.3}Eu$): C 38.85, H 4.63, N 5.11; found: C 38.46, H 4.48, N 4.91.

## Electrochemical methods

Cyclic voltammetry data were performed at room temperature in an argon-filled glovebox as described above. Data were collected using a Biologic SP-300 potentiostat connected to a personal computer. All samples were 4 mM in complex with 0.1 M [Bu$_4$N][PF$_6$] supporting electrolyte in $CH_3CN$ solution. The experiments were carried out with a platinum disk ($d = 1$ mm) working electrode, a platinum wire counter electrode, and an Ag/AgCl reference electrode. Potential calibration was performed at the end of each data collection cycle using the ferrocene/ferrocenium $[(C_5H_5)_2Fe]^{+/0}$ couple as an internal standard ($E^\circ = 0.630$ V/NHE).

The solutions of the trivalent complexes [Ln(TPA)$_2$]OTf$_3$; [Ln(BPA)$_2$]OTf; [Ln(BPPA)$_2$]OTf and [Ln(MPA)$_2$K] (Ln = Eu and Yb) for voltammetric studies were prepared in situ by the addition of 2 equivalents of ligand to the corresponding LnOTf$_3$ salt.

## X-ray crystallography

Diffraction data were taken using an Oxford-Diffraction XCallibur S kappa geometry diffractometer ($Mo_{K\alpha}$ radiation, graphite monochromator, $\lambda = 0.71073$ Å). To prevent evaporation of co-crystallized solvent molecules, the crystals were coated with light hydrocarbon oil and the data were collected at 150 K. The cell parameters were obtained with intensities detected on three batches of 5 frames. The crystal-detector distance was 4.5 cm. The number of settings and frames has been established taking in consideration the Laue symmetry of the cell by CrysAlisPro Oxford-diffraction software.[31] Unique intensities detected on all frames using the Oxford-diffraction Red program were used to refine the values of the cell parameters. The substantial redundancy in data allows empirical absorption corrections to be applied using multiple measurements of equivalent reflections with the ABSPACK Oxford-diffraction program.[31] For, [Sm(TPA)$_2$]I$_2$, [Eu(TPA)I(μI)]$_2$, [Yb(TPA)$_2$]I$_2$·($CH_3CN$)$_3$, [Sm(TPA)$_2$]I$_3$, [Yb(TPA)I$_2$$CH_3CN$]·($CH_3CN$)$_{0.5}$, [Eu(TPA)$_2$]I$_2$, [Eu(BPA)$_2$]OTf, [Eu(BPA)$_2$]. For [Eu(BPPA)$_2$]OTf·Py$_{2.5}$, [Yb(MPA)$_2$K(dme)$_2$] determination of the crystal shape allowed an analytical absorption correction with ABSPACK Oxford-diffraction.[31] Space groups were determined from systematic absences, and they were confirmed by the successful solution of the structure. The structures were solved by direct methods using the SHELXTL 6.14 package for [Sm(TPA)$_2$]I$_2$, [Eu(TPA)I(μI)]$_2$, [Yb(TPA)$_2$]I$_2$·($CH_3CN$)$_3$, [Yb(TPA)I$_2$$CH_3CN$]·($CH_3CN$)$_{0.5}$, [Eu(TPA)$_2$]I$_2$, [Eu(BPA)$_2$]OTf, and by charge flipping method using Superflip[32] for [Sm(TPA)$_2$]I$_3$, [Eu(BPPA)$_2$]OTf·Py$_{2.5}$, and [Yb(MPA)$_2$K(dme)$_2$]. All non-hydrogen atoms were found by difference Fourier syntheses and refined on $F^2$. For [Sm(TPA)$_2$]I$_2$, [Sm(TPA)$_2$]I$_3$, [Yb(TPA)$_2$]I$_2$·($CH_3CN$)$_3$, [Yb(TPA)I$_2$$CH_3CN$]·($CH_3CN$)$_{0.5}$, [Eu(BPPA)$_2$]OTf·Py$_{2.5}$, and [Yb(MPA)$_2$K(dme)$_2$] hydrogen atoms were fixed in ideal position and refined with a riding model. All hydrogen atoms were found by Fourier synthesis and isotropically refined for [Eu(TPA)$_2$]I$_2$, [Eu(TPA)I(μI)]$_2$, [Eu(BPA)$_2$], and [Eu(BPA)$_2$]OTf. For [Eu(BPPA)$_2$]OTf·Py$_{2.5}$ data reduction were driven taking in account a twin law with two components (62 and 38%) and the structure was solved with the concatenated hklf5 file. For [Yb-

$(MPA)_2K(dme)_2]$, a squeeze treatment was applied, modeling an electron number corresponding with a DME molecule. For the [Eu(BPA)$(CS_3)(dmso)_2$](dmso) structure, the diffraction data were measured at low temperature [100(2) K] using $Mo_{K\alpha}$ radiation on a Bruker APEX II CCD diffractometer equipped with a kappa geometry goniometer. The data sets were reduced by EvalCCD[33] and then corrected for absorption.[34] The solution and refinement was performed by SHELX.[35] The crystal structure was refined using full-matrix least-squares based on $F^2$ with all non-hydrogen atoms anisotropically defined. Hydrogen atoms were placed in calculated positions by means of the "riding" model. Additional electron density found in the difference Fourier map (due to highly disordered solvent) was treated by the SQUEEZE algorithm of PLATON.[36] Anion $CS_3^{2-}$ and DSMO molecules (bound and free) showed high disorder and were treated by means of the split model and by applying some restraints to their thermal parameters (SIMU card). A tough constraint was applied to the adp's of C22A and C22B (EADP card).

Experimental details for X-ray data collections of all complexes are given in Table S.B.1. (Supporting Information). Crystallographic data have been deposited for the 12 structures with the Cambridge Crystallographic Data Centre. CCDC 1402199 ([Eu(BPA)2]), 1402200 ([Eu$(BPA)_2$]OTf), 1402201 ([Eu(BPA)$(CS_3)(dmso)_2$](dmso), 1402202 ([Eu$(BPPA)_2$]OTf·$Py_{2.5}$), 1402203 ([Eu$(TPA)_2]I_2$), 1402204 ([Eu(TPA)I(μI)]$_2$), 1402205 ([Sm$(TPA)_2]I_2$), 1402206 ([Sm$(TPA)_2]I_3$), 1402207 ([Yb$(MPA)_2K(dme)_2$]), 1402208 ([Yb$(TPA)_2]I_2$·$(CH_3CN)_3$), 1402209 ([Yb(TPA)$I_2CH_3CN$]·$(CH_3CN)_{0.5}$) and 1404893 ([Yb(BPA)I-$(CH_3CN)]_2(CH_3CN)$) contain the supplementary crystallographic data for this paper. These data are provided free of charge by The Cambridge Crystallographic Data Centre.

## Acknowledgements

We thank L. Plassais for technical support and ligand synthesis, and C. Camp for useful discussions. This work was supported by the Swiss National Science Foundation, and by the EPFL.

**Keywords:** europium · lanthanides · ligands · reduction · ytterbium

[1] a) H. B. Kagan, J. L. Namy, *Tetrahedron* **1986**, *42*, 6573 – 6614; b) G. A. Molander, *Chem. Rev.* **1992**, *92*, 29; c) W. J. Evans, *Coord. Chem. Rev.* **2000**, *206*, 263 – 283.

[2] a) B. Liu, T. Roisnel, L. Maron, J.-F. Carpentier, Y. Sarazin, *Chem. Eur. J.* **2013**, *19*, 3986 – 3994; b) I. V. Basalov, V. Dorcet, G. K. Fukin, J.-F. Carpentier, Y. Sarazin, A. A. Trifonov, *Chem. Eur. J.* **2015**, *21*, 6033 – 6036; c) M. Szostak, N. J. Fazakerley, D. Parmar, D. J. Procter, *Chem. Rev.* **2014**, *114*, 5959 – 6039.

[3] a) M. Nishiura, Z. Hou, *Nat. Chem.* **2010**, *2*, 257 – 268; b) D. J. Berg, J. M. Boncella, R. A. Andersen, *Organometallics* **2002**, *21*, 4622 – 4631; c) G. Nocton, W. W. Lukens, C. H. Booth, S. S. Rozenel, S. A. Medling, L. Maron, R. A. Andersen, *J. Am. Chem. Soc.* **2014**, *136*, 8626 – 8641.

[4] a) J. M. Veauthier, E. J. Schelter, C. N. Carlson, B. L. Scott, R. E. Da Re, J. D. Thompson, J. L. Kiplinger, D. E. Morris, K. D. John, *Inorg. Chem.* **2008**, *47*, 5841 – 5849; b) W. J. Evans, *J. Alloys Compd.* **2009**, *488*, 493 – 510; c) G. Meyer, *Angew. Chem. Int. Ed.* **2008**, *47*, 4962 – 4964; *Angew. Chem.* **2008**, *120*, 5040 – 5042.

[5] a) W. J. Evans, J. M. Perotti, J. C. Brady, J. W. Ziller, *J. Am. Chem. Soc.* **2003**, *125*, 5204 – 5212; b) W. J. Evans, C. A. Seibel, J. W. Ziller, *Inorg. Chem.* **1998**, *37*, 770 – 776; c) J. Andrez, J. Pecaut, P.-A. Bayle, M. Mazzanti, *Angew. Chem. Int. Ed.* **2014**, *53*, 10448 – 10452; *Angew. Chem.* **2014**, *126*, 10616 – 10620; d) N. W. Davies, A. S. P. Frey, M. G. Gardiner, J. Wang, *Chem. Commun.* **2006**, 4853 – 4855.

[6] a) G. B. Deacon, P. C. Junk, J. Wang, D. Werner, *Inorg. Chem.* **2014**, *53*, 12553 – 12563; b) D. Heitmann, C. Jones, D. P. Mills, A. Stasch, *Dalton Trans.* **2010**, *39*, 1877 – 1882; c) L. Castro, S. Labouille, D. R. Kindra, J. W. Ziller, F. Nief, W. J. Evans, L. Maron, *Chem. Eur. J.* **2012**, *18*, 7886 – 7895.

[7] a) W. J. Evans, D. S. Lee, *Can. J. Chem.* **2005**, *83*, 375 – 384; b) M. G. Gardiner, D. N. Stringer, *Materials* **2010**, *3*, 841 – 862; c) T. Dubé, S. Conoci, S. Gambarotta, G. P. A. Yap, G. Vasapollo, *Angew. Chem. Int. Ed.* **1999**, *38*, 3657 – 3659; *Angew. Chem.* **1999**, *111*, 3890 – 3892.

[8] M. E. Fieser, M. R. MacDonald, B. T. Krull, J. E. Bates, J. W. Ziller, F. Furche, W. J. Evans, *J. Am. Chem. Soc.* **2015**, *137*, 369 – 382.

[9] a) M. L. Cole, P. C. Junk, *Chem. Commun.* **2005**, 2695 – 2697; b) M. L. Cole, G. B. Deacon, C. M. Forsyth, P. C. Junk, K. Konstas, J. Wang, H. Bittig, D. Werner, *Chem. Eur. J.* **2013**, *19*, 1410 – 1420; c) R. Kempe, *Angew. Chem. Int. Ed.* **2000**, *39*, 468 – 493; *Angew. Chem.* **2000**, *112*, 478 – 504; d) P. W. Roesky, *Chem. Soc. Rev.* **2000**, *29*, 335 – 345; e) F. T. Edelmann, D. M. M. Freckmann, H. Schumann, *Chem. Rev.* **2002**, *102*, 1851 – 1896; f) W. E. Piers, D. J. H. Emslie, *Coord. Chem. Rev.* **2002**, *233*, 131 – 155; g) G. B. Deacon, C. M. Forsyth, P. C. Junk, B. W. Skelton, A. H. White, *Chem. Eur. J.* **1999**, *5*, 1452 – 1459; h) Z. M. Hou, T. Miyano, H. Yamazaki, Y. Wakatsuki, *J. Am. Chem. Soc.* **1995**, *117*, 4421 – 4422; i) W. J. Evans, D. S. Lee, J. W. Ziller, *J. Am. Chem. Soc.* **2004**, *126*, 454 – 455.

[10] a) J. Jenter, M. T. Gamer, P. W. Roesky, *Organometallics* **2010**, *29*, 4410 – 4413; b) I. V. Basalov, S. C. Rosca, D. M. Lyubov, A. N. Selikhov, G. K. Fukin, Y. Sarazin, J.-F. Carpentier, A. A. Trifonov, *Inorg. Chem.* **2014**, *53*, 1654 – 1661.

[11] G. Anderegg, E. Hubmann, N. G. Podder, F. Wenk, *Helv. Chim. Acta* **1977**, *60*, 123 – 140.

[12] O. Wichmann, R. Sillanpaa, A. Lehtonen, *Coord. Chem. Rev.* **2012**, *256*, 371 – 392.

[13] a) L. Karmazin, M. Mazzanti, J. Pecaut, *Inorg. Chem.* **2003**, *42*, 5900 – 5908; b) W. A. Chomitz, S. G. Minasian, A. D. Sutton, J. Arnold, *Inorg. Chem.* **2007**, *46*, 7199 – 7209; c) R. Wietzke, M. Mazzanti, J.-M. Latour, J. Pécaut, *J. Chem. Soc. Dalton Trans.* **1998**, 4087 – 4088; d) R. Wietzke, M. Mazzanti, J.-M. Latour, J. Pecaut, P.-Y. Cordier, C. Madic, *Inorg. Chem.* **1998**, *37*, 6690 – 6697; e) T. Andrea, E. Barnea, M. Botoshansky, M. Kapon, E. Genizi, Z. Goldschmidt, M. S. Eisen, *J. Organomet. Chem.* **2007**, *692*, 1074 – 1080.

[14] Y. Takashi, S. Shinoda, H. Sugimoto, J.-i. Uenishi, H. Tsukube, *Inorg. Chem.* **2003**, *42*, 7932 – 7937.

[15] a) L. Natrajan, J. Pécaut, M. Mazzanti, C. LeBrun, *Inorg. Chem.* **2005**, *44*, 4756 – 4765; b) P. Benndorf, S. Schmitt, R. Koeppe, P. Ona-Burgos, A. Scheurer, K. Meyer, P. W. Roesky, *Angew. Chem. Int. Ed.* **2012**, *51*, 5006 – 5010; *Angew. Chem.* **2012**, *124*, 5091 – 5095.

[16] D. T. Dugah, B. W. Skelton, E. E. Delbridge, *Dalton Trans.* **2009**, 1436 – 1445.

[17] a) A. Amgoune, C. M. Thomas, T. Roisnel, J. F. Carpentier, *Chem. Eur. J.* **2006**, *12*, 169 – 179; b) F. Bonnet, A. R. Cowley, P. Mountford, *Inorg. Chem.* **2005**, *44*, 9046 – 9055; c) H. E. Dyer, S. Huijser, N. Susperregui, F. Bonnet, A. D. Schwarz, R. Duchateau, L. Maron, P. Mountford, *Organometallics* **2010**, *29*, 3602 – 3621; d) M. A. Sinenkov, G. K. Fukin, A. V. Cherkasov, N. Ajellal, T. Roisnel, F. M. Kerton, J.-F. Carpentier, A. A. Trifonov, *New J. Chem.* **2011**, *35*, 204 – 212; e) Z. Du, Y. Zhang, Y. Yao, Q. Shen, *Dalton Trans.* **2011**, *40*, 7639 – 7644; f) C. E. Willans, M. A. Sinenkov, G. K. Fukin, K. Sheridan, J. M. Lynam, A. A. Trifonov, F. M. Kerton, *Dalton Trans.* **2008**, 3592 – 3598; g) K. Nie, X. Gu, Y. Yao, Y. Zhang, Q. Shen, *Dalton Trans.* **2010**, *39*, 6832 – 6840; h) Y. M. Yao, M. T. Ma, X. P. Xu, Y. Zhang, Q. Shen, W. T. Wong, *Organometallics* **2005**, *24*, 4014 – 4020; i) C. X. Cai, A. Amgoune, C. W. Lehmann, J. F. Carpentier, *Chem. Commun.* **2004**, 330 – 331; j) Z. M. Hou, Y. Wakatsuki, *Coord. Chem. Rev.* **2002**, *231*, 1 – 22.

[18] a) H. Zhou, H. Guo, Y. Yao, L. Zhou, H. Sun, H. Sheng, Y. Zhang, Q. Shen, *Inorg. Chem.* **2007**, *46*, 958 – 964; b) H. Guo, H. Zhou, Y. Yao, Y. Zhang, Q. Shen, *Dalton Trans.* **2007**, 3555 – 3561; c) E. E. Delbridge, D. T. Dugah, C. R. Nelson, B. W. Skelton, A. H. White, *Dalton Trans.* **2007**, 143 – 153.

[19] a) S. Yang, Z. Du, Y. Zhang, Q. Shen, *Chem. Commun.* **2012**, *48*, 9780 – 9782; b) M. Zhang, X. Ni, Z. Shen, *Organometallics* **2014**, *33*, 6861 – 6867.

[20] S. C. Marinescu, T. Agapie, M. W. Day, J. E. Bercaw, *Organometallics* **2007**, *26*, 1178 – 1190.

[21] T. Toupance, S. R. Dubberley, N. H. Rees, B. R. Tyrrell, P. Mountford, *Organometallics* **2002**, *21*, 1367 – 1382.

[22] R. D. Shannon, *Acta Crystallogr. Sect. A* **1976**, *32*, 751 – 767.

[23] a) W. J. Evans, M. A. Greci, J. W. Ziller, *Chem. Commun.* **1998**, 2367 – 2368; b) T. J. Boyle, L. A. M. Ottley, *Chem. Rev.* **2008**, *108*, 1896 – 1917.
[24] a) P. Caravan, T. Hedlund, S. Liu, S. Sjoberg, C. Orvig, *J. Am. Chem. Soc.* **1995**, *117*, 11230 – 11238; b) R. Wietzke, M. Mazzanti, J. M. Latour, J. Pecaut, *Chem. Commun.* **1999**, 209 – 210.
[25] R. S. Selinsky, J. H. Han, E. A. M. Perez, I. A. Guzei, S. Jin, *J. Am. Chem. Soc.* **2010**, *132*, 15997 – 16005.
[26] C. Camp, O. Cooper, J. Andrez, J. Pecaut, M. Mazzanti, *Dalton Trans.* **2015**, *44*, 2650 – 2656.
[27] O. P. Lam, L. Castro, B. Kosog, F. W. Heinemann, L. Maron, K. Meyer, *Inorg. Chem.* **2012**, *51*, 781 – 783.
[28] Y. L. Tong, Y. Yan, E. S. H. Chan, Q. C. Yang, T. C. W. Mak, D. K. P. Ng, *J. Chem. Soc. Dalton Trans.* **1998**, 3057 – 3064.
[29] S. Zheng, T. C. Berto, E. W. Dahl, M. B. Hoffman, A. L. Speelman, N. Lehnert, *J. Am. Chem. Soc.* **2013**, *135*, 4902 – 4905.
[30] A. Thapper, A. Behrens, J. Fryxelius, M. H. Johansson, F. Prestopino, M. Czaun, D. Rehder, E. Nordlander, *Dalton Trans.* **2005**, 3566 – 3571.
[31] CrysAlisPro CCD, CrysAlisPro RED, ABSPACK, CrysAlis PRO, Agilent Technologies, Yarnton, England, Agilent (2010).
[32] L. Palatinus, G. Chapuis, *J. Appl. Crystallogr.* **2007**, *40*, 786 – 790.
[33] A. J. M. Duisenberg, L. M. J. Kroon-Batenburg, A. M. M. Schreurs, *J. Appl. Crystallogr.* **2003**, *36*, 220 – 229.
[34] R. H. Blessing, *Acta Crystallogr. Sect. A* **1995**, *51*, 33 – 38.
[35] SHELX, G. M. Sheldrick, *Acta Crystallogr. Sect. A* **2008**, *64*, 112 – 122.
[36] PLATON, A. L.Spek, *Acta Crystallogr. Sect. D* **2009**, *65*, 148 – 155.

Received: June 5, 2015
Published online on August 21, 2015

Chemical Science

EDGE ARTICLE

View Article Online
View Journal | View Issue



Cite this: *Chem. Sci.*, 2016, **7**, 5846

# Synthesis and reactivity of a terminal uranium(IV) sulfide supported by siloxide ligands†

Julie Andrez,[a] Jacques Pécaut,[bc] Rosario Scopelliti,[a] Christos E. Kefalidis,[d] Laurent Maron,[d] Michael W. Rosenzweig,[e] Karsten Meyer[e] and Marinella Mazzanti*[a]

Received 13th February 2016
Accepted 8th April 2016

DOI: 10.1039/c6sc00675b

www.rsc.org/chemicalscience

The reactions of the tetrasiloxide U(III) complexes [U(OSi(O$^t$Bu)$_3$)$_4$K] and [U(OSi(O$^t$Bu)$_3$)$_4$][K18c6] with 0.5 equiv. of triphenylphosphine sulfide led to reductive S-transfer reactions, affording the U(IV) sulfide complexes [SU(OSi(O$^t$Bu)$_3$)$_4$K$_2$]$_2$, **1**, and [{SU(OSi(O$^t$Bu)$_3$)$_4$K$_2$}$_2$(μ-18c6)], **2**, with concomitant formation of the U(IV) complex [U(OSi(O$^t$Bu)$_3$)$_4$]. Addition of 1 equiv. of 2.2.2-cryptand to complex **1** resulted in the isolation of a terminal sulfide complex, [SU(OSi(O$^t$Bu)$_3$)$_4$K][Kcryptand], **3**. The crucial role of the K$^+$ Lewis acid in these reductive sulfur transfer reactions was confirmed, since the formation of complex **3** from the reaction of the U(III) complex [U(OSi(O$^t$Bu)$_3$)$_4$][Kcryptand] and 0.5 equiv. of PPh$_3$S was not possible. Reactivity studies of the U(IV) sulfide complexes showed that the sulfide is easily transferred to $CO_2$ and $CS_2$ to afford S-functionalized products. Moreover, we have found that the sulfide provides a convenient precursor for the synthesis of the corresponding U(IV) hydrosulfide, {[(SH)U(OSi(O$^t$Bu)$_3$)$_4$][K18c6]}, **5**, after protonation with PyHCl. Finally, DFT calculations were performed to investigate the nature of the U–S bond in complexes **1**, **3** and **5**. Based on various analyses, triple-bond character was suggested for the U–S bond in complexes **1** and **3**, while double-bond character was determined for the U–SH bond in complex **5**.

## Introduction

Actinide complexes containing terminal oxide, sulfide or nitride ligands involved in multiple bonding with actinide ions are of high current interest, due to both their electronic structures and potential applications in atom transfer chemistry and catalysis.[1–11] Though still considerably less numerous than complexes containing bridging oxo or uranyl ($UO_2^{n+}$) groups, the number of well-characterized terminal uranium oxo complexes has been rapidly increasing in recent years.[3,9,12–16] In contrast, the majority of attempts to prepare terminal sulfides have resulted in the formation of di-uranium sulfide-bridged complexes[17–22] or mononuclear disulfide complexes[18,23] because of the nucleophilic character of the terminal sulfide. Such nucleophilic character has been demonstrated by reactivity studies of a bridging sulfide with heteroallenes, leading to thiocarbonates.[24,25]

Chalcogenide complexes of actinides are also attracting increasing interest because of their importance in energy-related research. Additionally, the nature of the bonding between hard actinides and soft donor atoms and especially the involvement of f-orbitals in these bonds are of great relevance for academia and industry.[26,27] Notably, the efficiency of sulfur-containing ligands in the selective extraction of actinides from spent nuclear fuel[28] has been attributed to the presence of covalent An–S interactions, which remains a source of debate.[29–34] However, to date, only one ligand system has been reported that enabled the isolation of a terminal uranium sulfide.[16,35] Hayton and co-workers succeeded in synthesizing the terminal U(IV) sulfide complex [US(NR$_3$)$_3$] (R = SiMe$_3$) by disfavouring the formation of bridging sulfide complexes with an ylide capping group during sulfur transfer from $S_8$.[16] The same complex was also prepared by cleavage of a trityl protecting group.[35] A sodium-capped uranium mononuclear sulfide was also reported (with Cp* as a supporting ligand) that was isolated from the reduction of the thiolate [Cp*$_2$U(S$^t$Bu)$_2$] with Na/Hg amalgam.[36] While bulky ligands are usually used in transition metal chemistry to prevent the formation of bridging oxides and sulfides, this approach has not been successful so far in the preparation of a terminal uranium sulfide complex.

Recently, our group reported the synthesis of a terminal U(V) oxo complex, [UO(OSi(O$^t$Bu)$_3$)$_4$K], *via* cooperative two-electron

[a]*Institut des Sciences et Ingénierie Chimiques Ecole Polytechnique Fédérale de Lausanne (EPFL), 1015 Lausanne, Switzerland. E-mail: marinella.mazzanti@epfl.ch*
[b]*Univ. Grenoble Alpes, INAC-SyMMES, RICC, F-38000 Grenoble, France*
[c]*CEA, INAC-SyMMES, F-38000 Grenoble, France*
[d]*Université de Toulouse et CNRS INSA, UPS, CNRS, UMR 5215, LPCNO, 135 avenue de Rangueil, 31077 Toulouse, France*
[e]*Department of Chemistry and Pharmacy, Inorganic Chemistry, Friedrich-Alexander University Erlangen-Nürnberg, Egerlandstraße 1, 91058 Erlangen, Germany*

† Electronic supplementary information (ESI) available: Full computational details, $^1$H NMR spectra, and detailed X-ray crystallographic data in CIF format. CCDC 1447982–1447990. For ESI and crystallographic data in CIF or other electronic format see DOI: 10.1039/c6sc00675b

reduction of carbon dioxide by the bulky heterobimetallic uranium(III) complex $[U(OSi(O^tBu)_3)_4K]$.[14] Herein, we report the stabilization of a terminal uranium sulfide species by the bulky ligand environment created by four siloxide groups. Moreover, we found that sulfur transfer from the two-electron oxidizing agent $Ph_3PS$ to the highly hindered uranium centre is favoured by the presence of the Lewis acid $K^+$. The reactivity of this U(IV) sulfide with different substrates was also investigated. Additionally, the bonding analysis of the terminal sulfide complex and of the potassium-bound sulfide complex revealed triple-bond character. Most importantly, calculations highlight that the participation of the f-orbitals in the bonding is indeed low.

## Results and discussion

### Syntheses and molecular structures of uranium(IV) sulfides

With the goal of preparing a terminal sulfide complex, the bulky U(III) complex $[U(OSi(O^tBu)_3)_4K]$ (Fig. 1, left) was reacted with elemental sulfur. This reaction led to multiple oxidation products, regardless of the applied stoichiometry (0.125 eq. or 0.25 eq. of $S_8$). The $^1H$ NMR spectra of the crude reaction mixtures show several resonances that are in agreement with the presence of multiple products. Among these products, we were able to crystallographically characterize a dimeric U(IV) persulfide complex, $[(S_2)U(OSi(O^tBu)_3)_4K_2]_2$, and a dimeric tris(siloxide) U(IV) complex, $\{[UK(OSi(O^tBu)_3)_3]_2(\mu\text{-}S_2)(\mu\text{-}S_3)\}$, containing both disulfide and trisulfide ligands (see ESI†). These results show that it is impossible to control the reaction stoichiometry by using elemental sulfur; thus, $Ph_3PS$ was used as the sulphur transfer agent.

The reaction of 0.5 equivalents of $Ph_3PS$ with a brown solution of $[U(OSi(O^tBu)_3)_4K]$ in toluene afforded a green solution from which the uranium(IV) sulfide complex $[SU(OSi(O^tBu)_3)_4K_2]_2$, **1** (Scheme 1), was isolated analytically pure with yields up to 62%. Proton NMR studies reveal that complex **1** is formed with similar conversion rates when $[U(OSi(O^tBu)_3)_4K]$ is reacted with 1 or 0.5 equivalents of $Ph_3PS$. The formation of **1** is accompanied by the formation of the uranium(IV) tetrasiloxide complex $[U(OSi(O^tBu)_3)_4]$,[37] which was identified by NMR spectroscopy. The reaction of the U(III) complex $[U(OSi(O^tBu)_3)_4K]$ with the two-electron oxidizing agent $Ph_3PS$ led to two different U(IV) products rather than one U(V) species. This is due to the fact that U(III) complexes favour one-electron redox reactions to attain the thermodynamically more stable U(IV) ion. In this reaction, each $Ph_3PS$ oxidizes two U(III) complexes to U(IV) and transfers the sulfur atom to one of the two tetrasiloxide

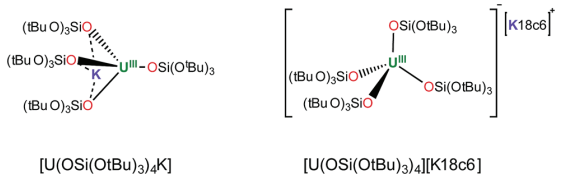


Fig. 1 Drawing of complexes $[U(OSi(O^tBu)_3)_4K]$ (left) and $[U(OSi(O^tBu)_3)_4][K18c6]$ (right).

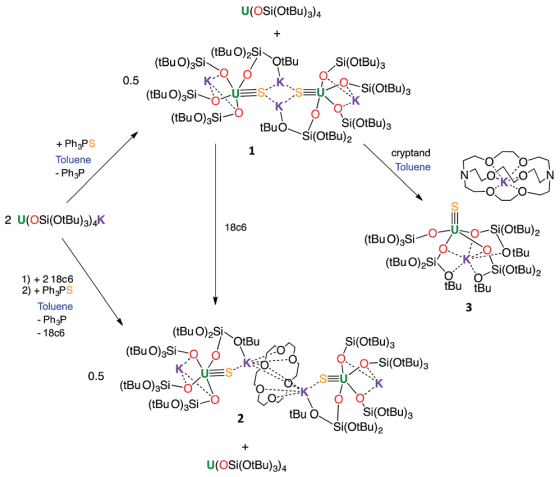


Scheme 1 Synthesis of U(IV) terminal and potassium-capped sulfide complexes.

complexes, generating the U(IV) sulfide complex **1**. Green single crystals of **1**·toluene were obtained from the crude reaction mixture at room temperature.

Complex **1**·toluene crystallized as a dimer in the centrosymmetric, triclinic space group, $P\bar{1}$. The solid-state structure of complex **1** (Fig. 2) shows that two $[SU(OSi(O^tBu)_3)_4K_2]$ moieties are bridged by two potassium cations, capping the sulfides to yield a dimer. Two potassium cations (each one also bound to a $O^tBu$ group) and the two sulfides form an SKSK diamond core around the inversion centre. The second potassium ion of the asymmetric unit is located in an O6 coordination pocket formed by three siloxide ligands. The five-coordinate uranium centre is ligated by four oxygen atoms of the siloxide ligands and one sulfide. The coordination geometry can best be described as distorted trigonal bipyramidal. The U–S bond length (2.5440(8) Å) is significantly longer than those found in the previously reported sodium- or potassium-capped U(IV) sulfide complexes (2.4805(5)–2.4463(6) Å),[35,36] probably due to steric hindrance. The S1–K2 bond length of 3.0455(12) Å is comparable to those

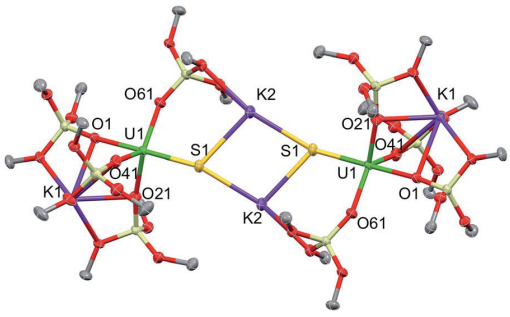


Fig. 2 Thermal ellipsoid diagram of $[SU(OSi(O^tBu)_3)_4K_2]_2$ (**1**) (50% probability ellipsoids). The methyl groups and lattice solvent molecules are omitted for clarity.

found in the U(IV) complex [K(18c6)][U(S)(NR$_2$)$_3$] (R = SiMe$_3$) (3.0684(8) Å and 3.1551(8) Å),[35] in which the sulfide is capped by the K(18c6)$^+$ cation. The average U–O$_{siloxide}$ bond length (2.22(1) Å) falls in the range of U–O bond lengths reported for uranium(IV) siloxide complexes.[14,37–40]

The $^1$H NMR spectrum of crystals of **1** in deuterated toluene shows a very broad signal between 3 and 1 ppm, in agreement with the presence of a fluxional behaviour of the siloxide ligands in solution. Decreasing the temperature down to 233 K did not lead to a fully resolved spectrum. Complex **1** is stable in the solid state at room temperature but slowly decomposes in toluene at room temperature, leading to the formation of [U(OSi(O$^t$Bu)$_3$)$_4$], free ligand and unidentified species (decomposition products are observed after 24 hours). Complex **1** can be isolated analytically pure from toluene due to its lower solubility compared to [U(OSi(O$^t$Bu)$_3$)$_4$].

In order to identify the role of the potassium cation in the stabilization of the U(IV)–S species, and to prepare a terminal sulfide, complex 1 was reacted with 18c6 and 2.2.2-cryptand. The addition of 1 equivalent of 18c6 to **1** in toluene led to the formation of [{SU(OSi(O$^t$Bu)$_3$)$_4$K$_2$}$_2$(μ-18c6)], **2**, containing a U(IV)–S group capped by a K(18c6)$^+$ ion.

Blue-green single crystals of **2** were obtained from a toluene solution of the reaction mixture at 233 K. **2**·tol crystallized in the centrosymmetric, monoclinic space group, $P2_1/n$. In the structure of **2**, a 18c6 bridges two [SU(OSi(O$^t$Bu)$_3$)$_4$K$_2$] units to yield a dimer with the inversion centre located in the middle of the crown ether (Fig. 3). The coordination environment of the U(IV) ion in **2** is very similar to that found in **1**. In contrast, the US$_2$K$_2$ core present in the structure of **1** is disrupted by the presence of the bridging 18c6. Each potassium cation capping the sulfides in **2** is also bound to two O$^t$Bu groups from a siloxide ligand and to four oxygen atoms of the bridging crown ether. Thus, the crown ether is coordinated to two different potassium cations, and adopts a non-planar conformation.

The U–S distance (2.534(2) Å) in **2** is similar to that found in complex **1**, indicating that the presence of the crown ether coordinated to the potassium cation does not significantly affect the U–S bonding interaction. The S1–K2 bond length (3.128(3) Å) in **2** is slightly elongated compared to **1** because of the presence of the crown ether (Table 1).

Table 1 Selected bond distances for complexes **1**, **2**, **3** and **5** (in Å)

| Structural parameters | **1**·tol | **2**·tol | **3**·hex | **5**·tol |
|---|---|---|---|---|
| U–S | 2.5440(8) | 2.534(2) | 2.5220(14) | 2.834(3) |
| S–K | 3.0455(12) | 3.128(3) | — | 3.229(5) |
| Av. U–O$_{bridging}$ | 2.22(1) | 2.22(2) | 2.26(2) | — |
| Av. U–O$_{terminal}$ | — | — | 2.197(4) | 2.15(3) |

Complex **2** can also be prepared by the reaction of 0.5 or 1 equivalent of Ph$_3$PS with the U(III) complex [U(OSi(O$^t$Bu)$_3$)$_4$][K18c6] (Fig. 1, right)[37] in toluene for 12 hours.

The $^1$H NMR spectrum of **2** in deuterated toluene features two signals for the siloxide ligands at −0.9 ppm and −10.3 ppm, respectively, with an integration ratio of 1 : 3. This is in agreement with the presence of a $C_3$-symmetric species and a fluxional binding of the potassium cation in solution.

The solid-state structure of **2** shows that the addition of crown ether to complex **1** does not prevent the binding of potassium to the U(IV)–S. The addition of excess crown ether does not afford a more symmetric solution species, indicating that the binding of the potassium cannot be prevented by crown ether in solution.

In order to inhibit the coordination of potassium to the sulfide, we resorted to the use of 2.2.2-cryptand.

The addition of 1 equivalent of cryptand to a solution of **1** in toluene (Scheme 1) afforded the U(IV) terminal sulfide complex [SU(OSi(O$^t$Bu)$_3$)$_4$K][Kcryptand], **3**.

Green single crystals of **3** were obtained from hexane at room temperature. Complex **3**·hex crystallized in the centrosymmetric, triclinic space group, $P\bar{1}$, as a separated ion pair, consisting of the [Kcryptand]$^+$ cation and the [SU(OSi(O$^t$Bu)$_3$)$_4$K]$^-$ anion (Fig. 4). In **3**, the five-coordinate uranium ion is ligated by four siloxide ligands and a terminal sulfide, giving a distorted trigonal bipyramidal coordination geometry. One potassium atom remains encapsulated in the O6 pocket made by three bridging siloxide ligands. The U–S bond length in **3** (2.5220(14) Å) is comparable to the U–S bond distance in complex **1** (2.5440(8) Å) (Table 1). This indicates that potassium binding and dimer formation only lead to a slight lengthening of the U–S bond. The U–O bond length is 2.197(4) Å for the terminal siloxide oxygen, while the average for the three UK-bridging

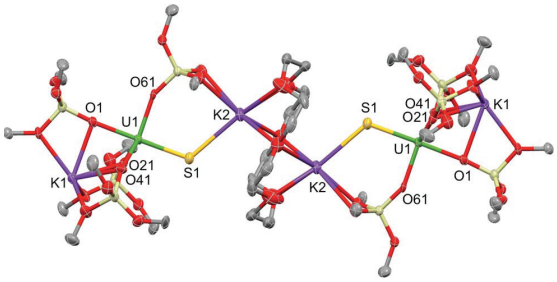


Fig. 3 Thermal ellipsoid diagram of [{SU(OSi(O$^t$Bu)$_3$)$_4$K$_2$}$_2$(μ-18c6)] (**2**·tol) (50% probability ellipsoids). Methyl groups and lattice solvent molecule are omitted for clarity.

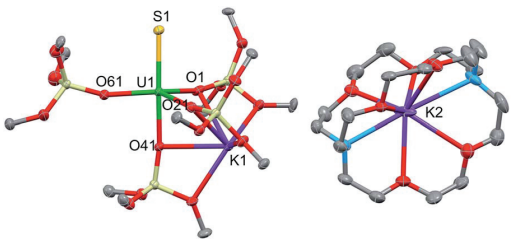


Fig. 4 Thermal ellipsoid diagram of [SU(OSi(O$^t$Bu)$_3$)$_4$K][Kcryptand] (**3**·hex) (50% probability ellipsoids). Methyl groups and lattice solvent molecule are omitted for clarity.

siloxide ligands is 2.26(2) Å, which is in the range of previously reported U–$O_{siloxide}$ bond lengths.[14,37–40]

The $^1$H NMR spectrum of **3** in deuterated toluene shows two signals (ratio 1 : 3) for the siloxide ligands, in agreement with a $C_3$-symmetric species in solution within the NMR timescale. This suggests the presence of a unique chemical environment for the three siloxide ligands that compose the equatorial plane giving rise to one signal and one environment for the siloxide *trans* to the U=S giving rise to the second signal. This can be interpreted in terms of a fluxional binding of the potassium cation. Three additional paramagnetically shifted signals assigned to the cryptand protons are also observed. The paramagnetic shift of the cryptand signals strongly suggests that the terminal sulfide could be in fast exchange in solution with a potassium-capped sulfide species.[41]

The terminal sulfide complex **3** is stable in the solid state at room temperature, but slowly decomposes in toluene (50% decomposition after 1 month), as well as in THF solution (decomposition products already visible in the NMR spectrum after 24 hours), affording the U(IV) complex $[U(OSi(O^tBu)_3)_4]$ and a mixture of other decomposition products. One of the decomposition products of **3** in THF has been identified as the U(IV)–U(IV) complex $[S_3U_2(OSi(O^tBu)_3)_6K_3][Kcryptand]$, **4** (20% conversion in **4** after 7 months determined by NMR spectroscopy). Complex **4** crystallizes as an ion pair consisting of the $[U_2(\mu\text{-}S)_3(OSi(O^tBu)_3)_6K_3]^-$ anion and the $[Kcryptand]^+$ cation. In the $[U_2(\mu\text{-}S)_3(OSi(O^tBu)_3)_6K_3]^-$ anion, three $S^{2-}$ anions bridge the two uranium atoms (see ESI†). Thus, the decomposition of complex **3** leads to the loss of one siloxide ligand from each uranium complex, as well as sulfide redistribution to afford a sulfide-bridged diuranium(IV) complex. Although a terminal U(IV) sulfide is stabilized by the presence of the sterically hindered environment provided by the four siloxide ligands, this complex can slowly eliminate one siloxide ligand and further react to afford a sulfide-bridged diuranium(IV) complex.

### Influence of cation binding on the S-transfer reaction

Interestingly, no reaction is observed when $Ph_3PS$ is added to a solution of the U(III) complex $[U(OSi(O^tBu)_3)_4K]$ that has been pre-treated with cryptand (Scheme 2). This unambiguously shows that the presence of a bound potassium cation is crucial in the S-transfer reaction between $[U(OSi(O^tBu)_3)_4K]$ and $Ph_3PS$.

Notably, in toluene solution, the potassium cation remains bound to the siloxide ligands in complex $[U(OSi(O^tBu)_3)_4K]$, while $[U(OSi(O^tBu)_3)_4][Kcryptand]$ exists as separated ion pair. The solid-state structure of $[U(OSi(O^tBu)_3)_4][K18c6]$[37] reveals an ion pair with $(K18c6)^+$ located in the outer coordination sphere of the complex, but the coordination of potassium is probably still possible in solution.

To confirm the important role of potassium for the reactivity of the complexes, the reactions were studied in the more polar solvent THF. In THF, both $[U(OSi(O^tBu)_3)_4][K18c6]$ and $[U(OSi(O^tBu)_3)_4][Kcryptand]$ most likely exist as ion pairs and therefore do not react with $Ph_3PS$. Reactivity is only observed in THF for the $[U(OSi(O^tBu)_3)_4K]$ complex.

To some extent, such pronounced differences in reactivity arise from steric differences that result in reduced access of the substrate to the metal centre in $[U(OSi(O^tBu)_3)_4][Kcryptand]$. However, the possible role of cooperative binding of the potassium to the sulfur might also be important. Comparing the O–U–O angles in the reported X-ray structures of the heterobimetallic UK complex $[U(OSi(O^tBu)_3)_4K]$ and the ion pair $[U(OSi(O^tBu)_3)_4][K18c6]$,[37] a significant difference is observed. In the ion pair $[U(OSi(O^tBu)_3)_4][K18c6]$ the four ligands form a weakly distorted tetrahedron with three angles having a mean value of 110.6(6)° and three angles having a mean value of 108.3(3)°. In the UK complex, the coordination tetrahedron is highly distorted. The potassium cation coordinates three of the four ligands and brings them closer together, resulting in an average value of the three O–U–O angles of 94.91(7)°. In contrast, the O–U–O angles between the bridging siloxides and the terminal one are significantly larger (127.2(3)°, 122.5(3)° and 115.0(3)°) than those found in $[U(OSi(O^tBu)_3)_4][K18c6]$, rendering the metal centre more accessible to the substrate.

In both complexes, the steric hindrance provided by the four siloxide ligands prevents the rapid formation of sulfide-bridged complexes previously observed when reacting neutral U(III) silylamide- or tacn-based amido or aminophenolato complexes with sulfur transfer agents ($S_8$ or $Ph_3PS$).[17–19,21,42]

However, the presence of the potassium cation in the oxygen pocket of three siloxide ligands in the heterobimetallic UK complex results in easier access to the uranium centre than in the ion pair complex, in which the potassium is encapsulated in the crown ether (Fig. 1 and 5).

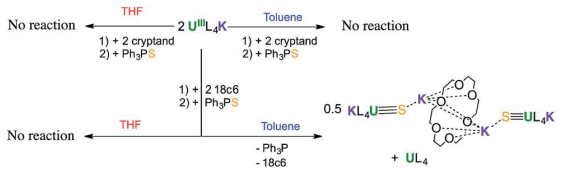


Scheme 2 Reactivity of $[U(OSi(O^tBu)_3)_4K]$ with $Ph_3PS$ in the presence of cryptand and 18C6.

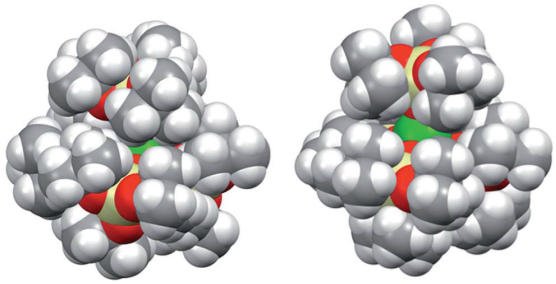

Fig. 5 Space-filling representation of $[U(OSi(O^tBu)_3)_4][K18c6]$ (left) and $[U(OSi(O^tBu)_3)_4K]$ (right). The lattice solvent molecule and the $[K18c6]^+$ cation in $[U(OSi(O^tBu)_3)_4][K18c6]$ are omitted for clarity.

On the other hand, due to the low accessibility of the metal centre in these tetrasiloxide complexes, cooperative binding of potassium might be also important for the S-transfer process to occur. Binding of the sulfur atom to the potassium cation during the sulfur transfer reaction may also reduce the nucleophilic character of the sulfur, rendering reaction pathways leading to bridging sulfides less favourable. The important role of cooperative UK binding in the reduction of $CO_2$ and $CS_2$ by $[U(OSi(O^tBu)_3)_4K]$ has been reported previously.[14,39]

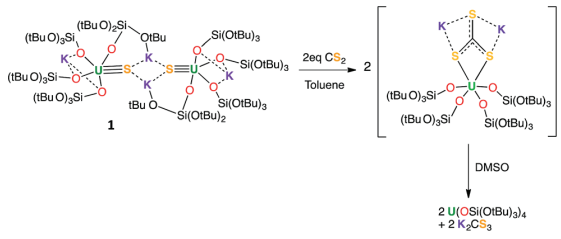


Scheme 4 $CS_2$ insertion into complex **1**.

### Reactivity of the U(IV) sulfide

Previous reactivity studies have shown that sulfide-bridged diuranium(IV) complexes can undergo nucleophilic addition of chalcogens, $CS_2$ and $CO_2$, to afford stable disulfide-,[43] trithiocarbonate-[25] and monothiocarbonate-bridged ($CO_2S^{2-}$)[24] diuranium(IV) complexes, respectively. In order to probe the possibility of sulfur transfer in complexes containing a U–S multiple bond, we investigated the reactivity of the sulfide complex **1** with various substrates (Scheme 3). To date, only chalcogen atom transfer reactivity has been investigated for terminal U(IV) sulfides, affording di-chalcogenide and tri-chalcogenide complexes depending on the stoichiometry.[44]

Complex **1** reacts rapidly with $^{13}CS_2$ (1 equivalent per U atom) in toluene. The $^1$H NMR spectrum of the reaction mixture shows the presence of signals assigned to exchanging species that we were unable to identify due to the low stability of the corresponding compound.

After several hours, the presence of $[U(OSi(O^tBu)_3)_4]$ was observed by $^1$H NMR spectroscopy. Dissolution of the evaporated reaction mixture in DMSO-$d_6$ led to complete dissociation of the reaction products. The $^1$H NMR spectrum in DMSO-$d_6$ only contains one signal, which was assigned to $[U(OSi(O^tBu)_3)_4]$.

The $^{13}$C NMR spectrum of the reaction products in DMSO-$d_6$ shows the presence of only one signal at 267 ppm, which was assigned to free thiocarbonate.[45] This indicates that, in toluene, the $^{13}CS_2$ molecule inserts into the U–S bond to afford a U(IV) thiocarbonate complex (Scheme 4), which dissociates into $[U(OSi(O^tBu)_3)_4]$ and $K_2CS_3$ in DMSO. The labile trithiocarbonate complex $[U(OSi(O^tBu)_3)_4(\mu_3\kappa^2{:}\kappa^2{:}\kappa^2CS_3)K_2(18c6)_2]$[39] was isolated previously from the reaction of $[U(OSi(O^tBu)_3)_4][K18c6]$ with $CS_2$. This complex quickly dissociates in solution, affording $[U(OSi(O^tBu)_3)_4]$ and $K_2CS_3$.

Complex **3** displays the same reactivity towards $^{13}CO_2$ and $^{13}CS_2$ as **1**. The $^{13}$C NMR spectrum in DMSO-$d_6$ of the reaction of **3** with $^{13}CS_2$ only shows the signals of thiocarbonate and 2.2.2-cryptand. The presence of the cryptand in the reaction mixture does not affect the insertion of $CS_2$ into the U–S bond and a terminal thiocarbonate U(IV) complex is also likely to be formed in this case. Formation of a stable trithiocarbonate-bridged di-uranium(IV) complex from the nucleophilic addition of a sulfide-bridged diuranium(IV) complex to $CS_2$ has been previously reported by Meyer *et al.*,[25] but such reactivity has never been reported for terminal sulfides.

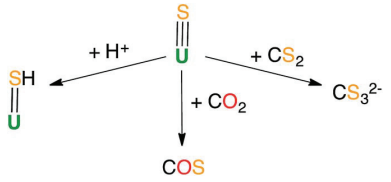


Scheme 3 Reactivity of U(IV) sulfide species.

In light of the observed fast addition of $CS_2$ to **1** and **3**, we also decided to explore the reaction of **1** with $CO_2$. Complex **1** reacted immediately with an excess of $^{13}CO_2$ in toluene, affording a new labile U(IV) species that decomposes rapidly at room temperature. Attempts to crystallize the reaction products were not successful. The $^{13}$C NMR spectrum of the reaction mixture in deuterated toluene shows the presence of a peak at 153.5 ppm that increases over time. This chemical shift corresponds to free COS.[46] The formation of COS can be interpreted as arising from the decomposition of a hypothetical U–$CO_2$S intermediate.

A sulfide complex seemed the ideal precursor for the straightforward synthesis of a U(IV) hydrosulfide complex and therefore we investigated the reactivity of complex **2** with pyHCl. This is a known strategy in transition metal chemistry for the synthesis of hydrosulfide complexes.[47,48] Hydrosulfide complexes of transition metals have attracted considerable attention because of their relevance to metalloenzymes and metal sulfide catalysts for industrial hydrodesulfurization.[48–51] The only crystallographically characterized uranium hydrosulfido complexes to date have been prepared through reduction of $H_2S$ by tacn- and N-anchored tris(aryl oxide) U(III) complexes.[52]

The addition of one equivalent (per U atom) of pyHCl to the $[\{SU(OSi(O^tBu)_3)_4K_2\}_2(\mu\text{-}18c6)]$ complex **2** in THF led to the formation of $\{[(SH)U(OSi(O^tBu)_3)_4][K18c6]\}$, **5**, with 53% conversion determined by $^1$H NMR spectroscopy. Light blue-green single crystals were obtained from the crude toluene mixture at 233 K (Fig. 6). Complex **5**·tol crystallized in the non-centrosymmetric, monoclinic space group, *Cc*. The five-coordinate uranium atom is ligated by four terminal siloxide ligands and one $SH^-$ moiety in a distorted trigonal bipyramidal geometry. The 18c6-encapsulated potassium counter-ion is bound to the sulfur atom with a S1–K1 bond length of 3.229(5) Å. The U1–S1 distance was measured to be 2.834(3) Å, which is much longer than the U–S bond distance in **3** (2.5220(14) Å), but is very similar to that found in the only other example of a mononuclear U(IV)–SH complex that was reported by Meyer *et al.*

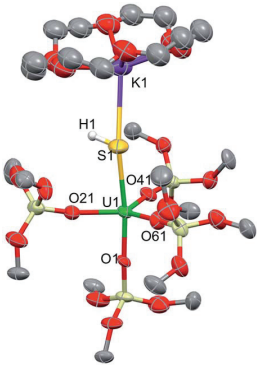


Fig. 6 Thermal ellipsoid diagram of {[(SH)U(OSi(O$^t$Bu)$_3$)$_4$][K18c6]}·(5·tol) (50% probability ellipsoids). Methyl groups and lattice solvent molecule are omitted for clarity.

(2.797(1) Å).[52] The average U–$O_{siloxide}$ bond length (2.15(3) Å) is similar in length to that found for the terminal siloxides in the terminal sulfide complex **3** (2.197(4) Å).

Complex **5** can also be prepared from the reaction of the U(III) complex [U(OSi(O$^t$Bu)$_3$)$_4$][K18c6] with $H_2S$, but in much lower yield, independent of the U : $H_2S$ ratio (17% yield and 22% overall conversion was determined by quantitative NMR spectroscopy). Moreover, this alternative synthetic route requires the handling of a solution of toxic $H_2S$. X-ray quality crystals of a dimeric by-product were also isolated from this reaction. This structure clearly shows the presence of two U(IV) and [U(OSi(O$^t$Bu)$_3$)$_3$K] moieties, bridged by three sulfur atoms (complex **6** in ESI†). The bond valence sum and the intermediate average value of the U–S distances (2.83(2) Å) fall in between the reported values for bridging $S^{2-}$ (2.59(1)–2.736(2) Å)[17,21] and bridging $SH^-$ (2.877(1)–2.964(1) Å)[52] moieties, suggesting that 2 $SH^-$ and 1 $S_2^{2-}$ groups are bridging the uranium centres. The hydrogens of the $SH^-$ moieties are probably fluxional, and therefore very difficult to locate in the crystal structure. The isolation of this by-product suggests that the low yield of the reaction with $H_2S$ is probably associated with the fast reaction of the hydrosulfide with more than one equivalent of $H_2S$ (even using stoichiometric conditions). The further aggregation of the initially formed mononuclear hydrosulfide complexes leads to polynuclear sulfide complexes. This represents a well-recognized problem in the preparation of mononuclear hydrosulfide complexes.[48] Therefore, the protonation of the sulfide **2** provides a more convenient route to the preparation of the hydrosulfide complex **5**.

### Computational bonding analysis

In order to investigate the nature of the U–S bond in complexes **1**, **3** and **6**, we performed calculations at the B3PW91 level. In particular for complex **1**, a small core pseudopotential basis set was chosen for the uranium atom, in which the f-electrons are included in the valence shell. Moreover, the monomeric form of complex **1** was considered for the sake of computational time. To verify the validity of such a theoretical protocol, we compared some important geometrical features to the available X-ray data and found that they are in close agreement (see ESI†). In particular, we found that the calculated values of the U–S bond distances were in agreement with the experimental ones (Fig. S.D.1†). Henceforth, we proceed into the analysis by firstly inspecting the related molecular orbitals (MOs).

As expected, for the U(IV) electron configuration (triplet multiplicity), the $(SOMO)^\alpha$ and $(SOMO-1)^\alpha$ orbitals correspond to pure non-bonding f-orbitals. Interestingly, the subsequent three MOs correspond to two π- (HOMO, HOMO−1) and one σ-type (HOMO−2) singly-occupied MOs of the U–S bond, as depicted in Fig. 9. It is worth noting that in (HOMO−2) the orbital is polarized towards the potassium atom, indicating small, but not negligible, overlap between the K and the S atom. This molecular orbital picture between the dianionic sulfide and the U(IV) centre, which is unconventional for the transition metals, is also found in $H_2U{=}S$ gas phase compounds.[33] Similarly, they closely resemble the shape of the MOs responsible for the U≡$N_{terminal}$ triple bond in $Tren^{TIPS}$-based complexes,[53,54] as well as of the recently reported Th(IV) chalcogenide tris(amide) system.[11] The peculiar triple character bonding situation is also evident based on the natural bond orbital (NBO) analysis. In particular, the contribution of the uranium atom to the σ-bond is 18%, whereas the contribution of the sulfur is 77%. For the two π combinations, the contributions are 23% and 15% for the uranium atom, and 72% and 78% for the sulfur atom, respectively. Additionally, the two highest singly-occupied orbitals based on NBO analysis are almost pure 5f orbitals, with the composition of $(SOMO-1)^\alpha$ being 92% of U, and of $(SOMO)^\alpha$ being 84% of U and 8% of S. In the same way, the Wiberg bond order analysis in a Löwdin orthogonalized basis gave a bond order of 2.25 for the U–S bond, indicating partial triple bond character. In addition, the natural charges of the U and S are 1.39 and −0.86 |e|, respectively. The natural electron configuration (NEC) of the uranium (see Fig. 7) corresponds to what is expected for a formal $f^2$ configuration. At first sight, this seems to indicate a crucial role of the f-orbitals in the bonding.

In order to further investigate the role of the f-orbitals in the bonding, we considered a different pseudopotential for the uranium(IV) atom, the so-called "large-core". By using this f-in-core pseudopotential, the f-electrons are now explicitly included in the core shell configuration, and hence not available for any mixture with other orbitals, with the d-orbitals being the only ones available for bonding. However, even with such a computational strategy, the bonding picture remains essentially the same, as illustrated in Fig. 8. It should be noted that the NBO analysis also predicts that the U–S bond features triple-bond character as well, in line with the corresponding small-core calculations.

Therefore, the triple-bond character is not due to 5f involvement in the bonding. Finally, the spin density (SD) of uranium was found to be 2.19 (being depopulated by 0.19), with most of this residual being donated to the sulfide atom ($SD^{sulfur} = -0.12$).

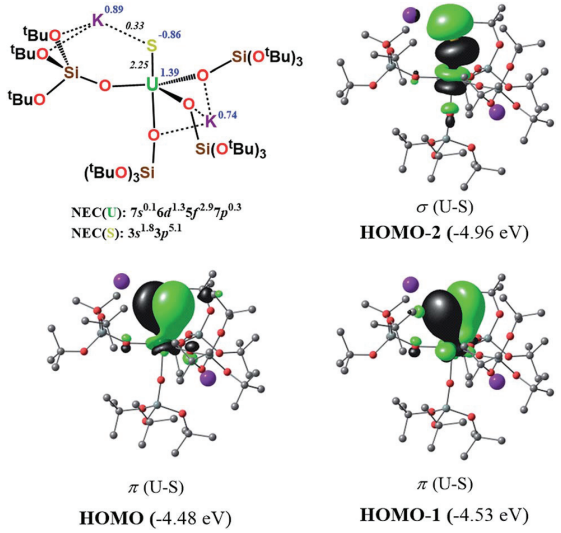


Fig. 7 σ and π molecular orbitals (α-spin) calculated for the monomer-**1** using the small-core pseudopotential. The numbers in blue correspond to the natural charges and those in italics to the Wiberg bond orders. Hydrogen atoms are omitted for clarity.

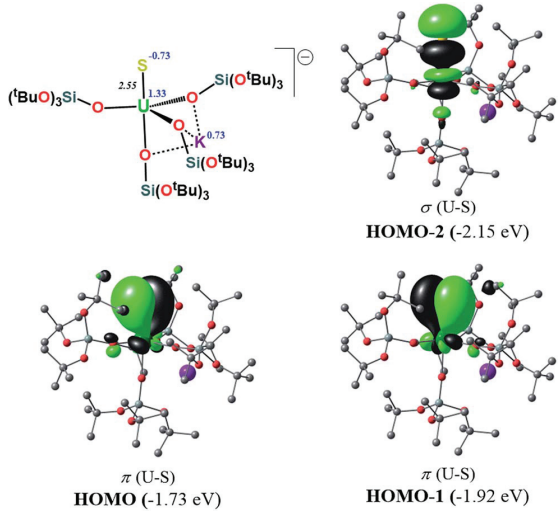


Fig. 9 σ and π molecular orbitals (α-spin) calculated for **3**, using the small-core pseudopotential. The numbers in blue correspond to the natural charges and those in italics to the Wiberg bond orders. Hydrogen atoms are omitted for clarity.

In order to investigate the effect of the presence of S-bound potassium on the U–S bond, we also calculated the electronic structure of complex **3**. The cryptand moiety was excluded from the calculations, and consequently a negative charge was placed on the overall complex. The DFT-predicted structure of the triplet state, which is imposed by the uranium +IV oxidation state, is in close agreement with that found in the solid-state structure (see ESI†). Molecular orbital analysis gave the same picture for the bonding situation between the U and S atoms as for the monomeric structure **1**, as clearly depicted in Fig. 9.

Interestingly, despite the absence of a second potassium atom in the vicinity of the sulfide, the total picture of the bonding remains unchanged with respect to monomer-**1**. Minor differences are apparent, which are mostly linked to the absence of the polarization induced by the potassium atom on the σ-orbital (HOMO−2), and to the slightly smaller natural charge located on the sulfide group. Moreover, there are virtually no changes to the charges of the uranium and potassium atom in **3** with respect to the corresponding ones in monomer-**1**. NBO analysis also predicted a $\sigma^2\pi^4$ U–S configuration, in line with a triple bond. Specifically, the σ-bond has 20% uranium and 76% sulfur character, whereas the contributions of each atom to the two π bonds are 29/18% for U and 67/75% for S, respectively. Again, as found for monomer-**1**, the exclusion of the f-electrons from the valence shell does not change the bonding picture (see ESI†). The bond order of the U–S bond was found to be 2.55, slightly higher than that calculated for monomer-**1**. In addition, the spin density (SD) of uranium was found to be 2.21 and that of the sulfur was found to be −0.14.

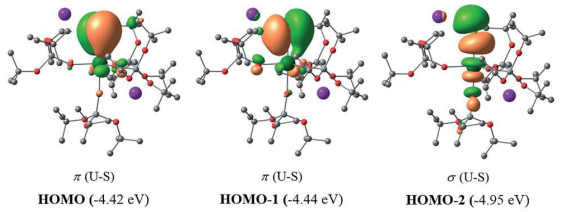


Fig. 8 σ and π molecular orbitals (α-spin) calculated for the monomer-**1** using the "large-core" pseudopotential. Hydrogen atoms are omitted for clarity.

In order to gain insights into the bonding situation in complex **5**, we proceeded to the optimization of the X-ray structure at the B3PW91 level, once again using the "small-core" basis set for the uranium atom. The potassium crown ether (K18C6) cation was excluded from the calculations, and consequently a negative charge was placed on the overall complex. Molecular orbital analysis is consistent with the presence of a double bond between the U and S atoms, as depicted in Fig. 10. This is in line with the previous MO picture found in the monomer-**1** and **3** models, since here the protonation of the strongly nucleophilic sulfide results in the breaking of one of the two π bonds. In particular, the HOMO−1 and HOMO orbitals possess 14% and 12% uranium character, respectively, and 82% sulfur character in both cases. The two SOMOs are mainly composed of pure f-orbitals. This further highlights the strongly polarized nature of this bond. Interestingly, the Wiberg bond orders in a Löwdin orthogonalized basis gave a bond order of 1.39 for the U–S bond, a value that is significantly smaller than in the other complexes, and is fully consistent with the partial double character of such an interaction.

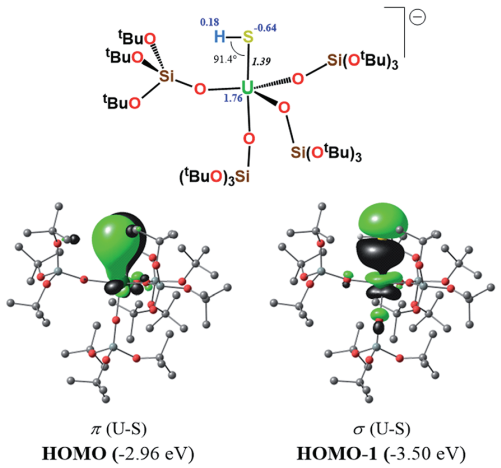


Fig. 10 σ and π molecular orbitals (α-spin) calculated for complex **5** using the small-core pseudopotential. The numbers in blue correspond to the natural charges and those in italics to the Wiberg bond orders. Hydrogen atoms are omitted for clarity.

## Conclusions

In summary, we have isolated a new series of complexes containing a U–S bond from the reaction of the bulky U(III) tetrasiloxide complex [U(OSi(O$^t$Bu)$_3$)$_4$K] with $Ph_3PS$.

This is the first example of a terminal uranium(IV) sulfide complex, which was directly obtained from the reaction of U(III) and a sulfur-transfer agent without the addition of protecting groups. The bulk provided by the four siloxide ligands prevents the formation of sulfide-bridged complexes. Moreover, the presence of bound potassium is essential for the reaction to occur, probably due to both steric effects and cooperative binding of the sulfur-transfer reagent to the K and U centres.

The terminal sulfide can easily be transferred to $CO_2$ and $CS_2$ to afford new thiocarbonates. Moreover, the terminal sulfide provides a convenient precursor for the synthesis of the corresponding hydrosulfide complex upon protonation with PyHCl.

DFT calculations carried out for the potassium-bound sulfide complex **1**, and for the terminal sulfide complex [SU(OSi(O$^t$Bu)$_3$)$_4$K][Kcryptand], **3**, showed that the U–S interactions in both complexes consist of three bonding pairs (σ + 2π bonds) with a Wiberg bond order of 2.25 for **1** and a bond order of 2.55 for **3**. However, the use of the "large-core" pseudopotential indicates that the triple-bond character is not due to 5f involvement in the bonding. For the hydrosulfide complex **5**, the molecular orbital analysis is consistent with the presence of a double bond between the U and S atoms with a Wiberg bond order of 1.39, a value significantly smaller than those found in complexes **1** and **3**.

Future studies will be directed to explore the reactivity of the terminal sulfide with other organic molecules and to isolate terminal sulfide complexes containing uranium in oxidation states higher than +IV and to investigate the nature of the U–S bond in these systems.

## Experimental

### General procedures

Unless otherwise noted, all experiments were carried out at ambient temperature under an inert atmosphere using Schlenk techniques and an MBraun glovebox equipped with a purifier unit. Water and oxygen levels were always kept at less than 1 ppm. Glassware was dried overnight at 150 °C prior to use. Syntheses were performed using glass-covered stirring bars.

### Starting materials

Solvents were purchased in their anhydrous form from Aldrich or Cortecnec (deuterated solvents), conditioned under argon and vacuum distilled from K/benzophenone (toluene, THF) or sodium dispersion (hexane) or dried over molecular sieves for one week (DMSO). All reagents were dried under high-vacuum for 5 days prior to use. Dry $^{13}CO_2$ was prepared by storing over molecular sieves for one week prior to use. HOSi(O$^t$Bu)$_3$ ligand was purchased from Aldrich and purified by sublimation prior to use. Depleted uranium turnings were purchased from the "Société Industrielle du Combustible Nucléaire" of Annecy (France). [U(OSi(O$^t$Bu)$_3$)$_4$K][14] and [U(OSi(O$^t$Bu)$_3$)$_4$][18c6][37] were prepared according to the published procedures.

### $^1$H NMR experiments

NMR spectra were performed in J. Young NMR tubes. $^1$H and $^{13}$C NMR spectra were recorded on a Bruker 400 MHz spectrometer. NMR chemical shifts are reported in ppm and are referenced to the residual $^1$H and $^{13}$C signals of the deuterated solvents.

### Elemental analyses

They were performed under argon by Analytische Laboratorien GMBH at Lindlar (Germany) or by the elemental analyses department of the EPFL using a Thermo Scientific Flash 2000 Organic Elemental Analyzer.

### X-ray analyses

Experimental details for X-ray data collections of all complexes are given in Table S1.† Figure graphics were generated using MERCURY 3.6 supplied by the Cambridge Structural Database; CCDC: Cambridge, U.K., 2001–2015. Diffraction data were taken using Oxford-Diffraction Xcalibur S or Bruker APEX II CCD kappa geometry diffractometers (Mo-Kα radiation, graphite monochromator, $\lambda = 0.71073$ Å). To prevent evaporation of co-crystallized solvent molecules the crystals were coated with light hydrocarbon oil and the data were collected at 150 K or 100 K. The datasets were reduced by CrysAlis[55] or EvalCCD[56] and then corrected for absorption.[57]

The structure resolutions were performed with SHELXS or Superflip and the structure refinement was performed with SHELXL.[58,59] The crystal structures were refined using full-matrix least-squares based on $F^2$ with all non-hydrogen atoms anisotropically defined. Hydrogen atoms were placed in calculated positions by means of the "riding" model. Additional

electron density found in the difference Fourier map (due to highly disordered solvent) was eventually treated by the SQUEEZE algorithm of PLATON.[60]

### Synthesis of complex 1

A colourless solution of $PPh_3S$ (26.3 mg, 0.089 mmol, 0.5 eq.) in toluene (2 mL) was added to a stirred brown solution of $[U(OSi(O^tBu)_3)_4K]$ (238.1 mg, 0.179 mmol, 1 eq.) in toluene (4 mL). The mixture was stirred at room temperature for 18 h. The resulting green solution was concentrated to approximately 3 mL and big green crystals formed overnight from toluene at room temperature. The crystals were filtered and dried for 2 hours (79.3 mg, 62% yield in 2 crops). The yield can be increased by recovering additional crops but it leads to co-crystallization of small amounts of the byproduct $[U(OSi(O^tBu)_3)_4]$. $^1$H NMR (400 MHz, Tol-$d_8$, 298 K): $\delta$ [ppm] $\approx$ 1 (very broad, 216H). Anal. calcd for **1**·$(tol)_{0.6}$ $C_{100.2}H_{220.8}O_{32}Si_8S_2K_4U_2$: C, 42.09; H, 7.78; S, 2.24. Found C, 42.17; H, 7.68; S, 2.10. Green single crystals of **1**·tol suitable for X-ray diffraction were obtained from a concentrated toluene solution of the complex at room temperature.

### Reaction of $[U(OSi(O^tBu)_3)_4]$[K18c6] with 0.5 eq. of $Ph_3PS$: isolation of 2

A colourless solution of $PPh_3S$ (2.1 mg, 0.007 mmol, 0.5 eq.) in toluene (1 mL) was added to a stirred brown suspension of $[U(OSi(O^tBu)_3)_4]$[K18c6] (22.3 mg, 0.014 mmol, 1 eq.) in toluene (0.5 mL). The mixture was stirred at room temperature for 18 h to yield a green solution. The $^1$H NMR spectrum shows the presence of $PPh_3$, $[U(OSi(O^tBu)_3)_4]$ and complex **2** (90% conversion determined by $^1$H NMR spectroscopy using naphthalene as an internal standard) in the reaction mixture. $^1$H NMR (400 MHz, Tol-$d_8$, 298 K): $\delta$ [ppm] = −0.9 (s, 162H), −10.3 (s, 54H). Blue-green single crystals of **2**·tol were obtained from the toluene reaction mixture at 233 K. Due to the similar solubility of $[U(OSi(O^tBu)_3)_4]$ and complex **2**, **2** can only be isolated in low yield from this reaction (25%).

Complex **2** can also be obtained with similar conversion rates by addition of 1 eq. of 18c6 per U atom to complex **1** in toluene.

Anal. Calcd for **2** $C_{108}H_{240}O_{38}Si_8S_2K_4U_2$: C, 42.28; H, 7.88; found C, 42.33; H, 8.07.

### Synthesis of complex 3

A colourless solution of 2.2.2-cryptand (7.8 mg, 0.021 mmol, 2 eq., 1 eq. per U) in toluene (1 mL) was added to a stirred green solution of complex **1** (29.5 mg, 0.010 mmol, 1 eq.) in toluene (1 mL). After 20 min. of stirring, toluene was removed and hexane (1 mL) was added. Green single crystals of complex **3**·hex formed from hexane at room temperature. The crystals were filtered, washed with hexane and dried under vacuum for 1 h (27 mg, 74%). $^1$H NMR (400 MHz, Tol-$d_8$, 298 K): $\delta$ [ppm] = 13.1 (bs, 12H), 12.9 (bs, 12H), 11.8 (bs, 12H), −0.5 (s, 81H), −10.6 (s, 27H). Anal. calcd for **3** $C_{66}H_{144}N_2O_{22}Si_4SK_2U$: C, 44.57; H, 8.16; N, 1.58. Found C, 44.16; H, 8.15; N, 1.65.

### Reaction of complex 1 with 2 eq. of $^{13}CS_2$

To a green solution of complex **1** (8.5 mg, 0.003 mmol, 1 eq.) in deuterated toluene (0.5 mL), 9.3 μL of a 636.5 mM solution of $^{13}CS_2$ (0.006 mmol, 2 eq.) in deuterated toluene was added. The reaction mixture immediately turned light yellow, affording a labile species. $^1$H NMR (400 MHz, Tol-$d_8$, 298 K): $\delta$ [ppm] = 11.1 (bs, 27H), −2.8 (bs, 81H). The solution was periodically monitored by $^1$H NMR spectroscopy over the course of a week, and it showed a decrease in the intensity of the two broad peaks and an increase in the intensity of the signal corresponding to the U(IV) complex $[U(OSi(O^tBu)_3)_4]$. This evolution shows the lability of the likely formed thiocarbonate complex, resulting in the release of the thiocarbonate anion. When toluene was removed and DMSO-$d_6$ added, the $^{13}$C NMR spectrum only showed the signal assigned to thiocarbonate. $^{13}C\{^1H\}$ NMR (100 MHz, DMSO-$d_6$, 298 K): $\delta$ [ppm] = 267.4 (s, $CS_3^{2-}$).

### Reaction of complex 1 with an excess of $^{13}CO_2$

An excess (1 atm) of $^{13}CO_2$ was added to a frozen green solution of complex **1** (11.7 mg, 0.004 mmol, 1 eq.) in deuterated toluene (0.5 mL). The solution was allowed to warm up to room temperature to yield a light pink solution. $^1$H NMR (400 MHz, Tol-$d_8$, 298 K): $\delta$ [ppm] = 8.7 (bs, 27H), −2.9 (bs, 81H). $^{13}C\{^1H\}$ NMR (100 MHz, Tol-$d_8$, 298 K): $\delta$ [ppm] = 153.5 (s, CSO).

### Synthesis of complex 5

A colourless solution of 18c6 (5.2 mg, 0.020 mmol, 2 eq.) in THF (1 mL) was added to a stirred green solution of complex **1** (28.2 mg, 0.010 mmol, 1 eq.) in THF (1 mL). The resulting green solution of complex **2** was stirred for ten minutes and was added to a stirred white suspension of PyHCl (2.3 mg, 0.020 mmol, 2 eq.) in THF (1 mL). The resulting yellow suspension was stirred for 2 h to yield a light green suspension. The $^1$H NMR spectrum of the crude reaction mixture in THF-$d_8$ at 298 K showed the formation of complex **5** with 53% conversion (determined by NMR spectroscopy using naphthalene as an internal standard) as the main reaction product. Blue-green single crystals of complex **5**·tol were obtained by storing the toluene reaction mixture at 233 K. The crystals were collected and dried under vacuum for 2 h (11.1 mg, 34% yield). $^1$H NMR (400 MHz, THF-$d_8$, 298 K): $\delta$ [ppm] = 3.07 (s, 24H, 18c6), 0.74 (s, 108H). Anal. calcd for **5**·$(tol)_{0.5}$ $C_{63.5}H_{137}O_{22}Si_4SKU$: C, 45.55; H, 8.25. Found C, 45.66; H, 8.61.

Complex **5** was also obtained in lower yield (17%) (22% overall conversion determined by NMR spectroscopy using naphthalene as an internal standard) by addition of 1 eq. of $H_2S$ to the U(III) complex $[U(OSi(O^tBu)_3)_4]$[K18c6] in THF.

The reaction of complex **1** with PyHCl was carried out under analogous conditions. The $^1$H NMR spectrum of the crude reaction mixture performed in THF-$d_8$ at 298 K after addition of 18c6 showed the formation of **5** with 48% conversion.

The reaction of **3** with PyHCl affords $\{[(SH)U(OSi(O^tBu)_3)_4]$[Kcrypt]$\}$ with 52% conversion as determined by $^1$H NMR. $^1$H NMR (400 MHz, THF-$d_8$, 298 K): $\delta$ [ppm] = 3.36–3.33 (m, crypt), 2.35 (s, crypt), 0.70 (s, 108H) (the identity of this complex was

 

confirmed by comparing this $^{1}$H NMR spectrum to that obtained after adding cryptand to a solution of complex **5**).

### Computational details

All the structures reported in this study were fully optimized with the Becke's 3-parameter hybrid functional combined with the non-local correlation functional provided by Perdew/Wang (denoted as B3PW91).[61,62] The Stuttgart-Dresden RECP (relativistic effective core potential) 5f-in-valence was used for the uranium atom, in combination with its adapted basis set.[63–65] However, in some cases, the 5f-in-core ECP augmented by a f polarization function ($\alpha = 1.0$) was used for the fixed oxidation state IV of the uranium atom.[66] In addition, silicon atoms were treated with the corresponding Stuttgart-Dresden RECP in combination with its adapted basis sets,[67] each one augmented by an extra set of polarization functions.[68] For the rest of the atoms, the 6-31G(d,p) basis set was used.[69–71] For analysing the bonding situation in the complexes of interest, we mainly used natural bond orbital analysis (NBO) using Weinhold's methodology.[72,73] Also, the Multiwfn program[74] was used for obtaining the composition of the molecular orbitals, based on the natural atomic orbital method,[75] as well as the Wiberg bond order analysis in a Löwdin orthogonalized basis. The Chemcraft program was used for the visualization of the molecular orbitals.[76] Finally, the GAUSSIAN09 program suite was used in all calculations.[77]

## Acknowledgements

We would like to thank Dr Oliver Cooper for preliminary experiments and Dr Euro Solari for elemental analysis. LM is a member of the Institut Universitaire de France. CAlmip is acknowledged for the generous grant of computing time. This work was supported by EPFL, by the Swiss National Science Foundation and by funds of the Joint DFG-ANR projects (ANR-14-CE35-0004-01 and ME1754/7-1).

## Notes and references

1 D. S. J. Arney and C. J. Burns, *J. Am. Chem. Soc.*, 1995, **117**, 9448–9460.
2 D. S. J. Arney and C. J. Burns, *J. Am. Chem. Soc.*, 1993, **115**, 9840–9841.
3 G. F. Zi, L. Jia, E. L. Werkema, M. D. Walter, J. P. Gottfriedsen and R. A. Andersen, *Organometallics*, 2005, **24**, 4251–4264.
4 T. W. Hayton, *Dalton Trans.*, 2010, **39**, 1145–1158.
5 S. T. Liddle, *Angew. Chem., Int. Ed. Engl.*, 2015, **54**, 8604–8641.
6 M. B. Jones and A. J. Gaunt, *Chem. Rev.*, 2013, **113**, 1137–1198.
7 T. Andrea and M. S. Eisen, *Chem. Soc. Rev.*, 2008, **37**, 550–567.
8 M. S. Eisen, *Top. Organomet. Chem.*, 2010, **31**, 157–184.
9 T. W. Hayton, *Chem. Commun.*, 2013, **49**, 2956–2973.
10 W. S. Ren, G. F. Zi, D. C. Fang and M. D. Walter, *J. Am. Chem. Soc.*, 2011, **133**, 13183–13196.
11 D. E. Smiles, G. Wu, P. Hrobarik and T. W. Hayton, *J. Am. Chem. Soc.*, 2016, **138**, 814–825.
12 S. J. Kraft, J. Walensky, P. E. Fanwick, M. B. Hall and S. C. Bart, *Inorg. Chem.*, 2010, **49**, 7620–7622.
13 B. Kosog, H. S. La Pierre, F. W. Heinemann, S. T. Liddle and K. Meyer, *J. Am. Chem. Soc.*, 2012, **134**, 5284–5289.
14 O. Cooper, C. Camp, J. Pecaut, C. E. Kefalidis, L. Maron, S. Gambarelli and M. Mazzanti, *J. Am. Chem. Soc.*, 2014, **136**, 6716–6723.
15 S. Fortier, N. Kaltsoyannis, G. Wu and T. W. Hayton, *J. Am. Chem. Soc.*, 2011, **133**, 14224–14227.
16 J. L. Brown, S. Fortier, R. A. Lewis, G. Wu and T. W. Hayton, *J. Am. Chem. Soc.*, 2012, **134**, 15468–15475.
17 O. P. Lam, F. W. Heinemann and K. Meyer, *Chem. Sci.*, 2011, **2**, 1538–1547.
18 C. Camp, M. A. Antunes, G. Garcia, I. Ciofini, I. C. Santos, J. Pecaut, M. Almeida, J. Marcalo and M. Mazzanti, *Chem. Sci.*, 2014, **5**, 841–846.
19 J. L. Brown, G. Wu and T. W. Hayton, *Organometallics*, 2013, **32**, 1193–1198.
20 D. E. Smiles, G. Wu and T. W. Hayton, *New J. Chem.*, 2015, **39**, 7563–7566.
21 J. G. Brennan, R. A. Andersen and A. Zalkin, *Inorg. Chem.*, 1986, **25**, 1761–1765.
22 L. P. Spencer, P. Yang, B. L. Scott, E. R. Batista and J. M. Boncella, *Inorg. Chem.*, 2009, **48**, 11615–11623.
23 E. M. Matson, M. D. Goshert, J. J. Kiernicki, B. S. Newell, P. E. Fanwick, M. P. Shores, J. R. Walensky and S. C. Bart, *Chem.–Eur. J.*, 2013, **19**, 16176–16180.
24 O. P. Lam, S. M. Franke, F. W. Heinemann and K. Meyer, *J. Am. Chem. Soc.*, 2012, **134**, 16877–16881.
25 O. P. Lam, L. Castro, B. Kosog, F. W. Heinemann, L. Maron and K. Meyer, *Inorg. Chem.*, 2012, **51**, 781–783.
26 M. L. Neidig, D. L. Clark and R. L. Martin, *Coord. Chem. Rev.*, 2013, **257**, 394–406.
27 M. Mazzanti, R. Wietzke, J. Pécaut, J.-M. Latour, P. Maldivi and M. Remy, *Inorg. Chem.*, 2002, **41**, 2389–2399.
28 H. H. Dam, D. N. Reinhoudt and W. Verboom, *Chem. Soc. Rev.*, 2007, **36**, 367–377.
29 A. J. Gaunt, B. L. Scott and M. P. Neu, *Chem. Commun.*, 2005, 3215–3217.
30 K. I. M. Ingram, N. Kaltsoyannis, A. J. Gaunt and M. P. Neu, *J. Alloys Compd.*, 2007, **444**, 369–375.
31 C. C. L. Pereira, C. J. Marsden, J. Marcalo and J. K. Gibson, *Phys. Chem. Chem. Phys.*, 2011, **13**, 12940–12958.
32 M. B. Jones, A. J. Gaunt, J. C. Gordon, N. Kaltsoyannis, M. P. Neu and B. L. Scott, *Chem. Sci.*, 2013, **4**, 1189–1203.
33 X. F. Wang, L. Andrews, K. S. Thanthiriwatte and D. A. Dixon, *Inorg. Chem.*, 2013, **52**, 10275–10285.
34 L. Karmazin, M. Mazzanti and J. Pécaut, *Chem. Commun.*, 2002, 654–655.
35 D. E. Smiles, G. Wu and T. W. Hayton, *J. Am. Chem. Soc.*, 2014, **136**, 96–99.
36 L. Ventelon, C. Lescop, T. Arliguie, P. C. Leverd, M. Lance, M. Nierlich and M. Ephritikhine, *Chem. Commun.*, 1999, 659–660.
37 C. Camp, J. Pecaut and M. Mazzanti, *J. Am. Chem. Soc.*, 2013, **135**, 12101–12111.

38 V. Mougel, C. Camp, J. Pecaut, C. Coperet, L. Maron, C. E. Kefalidis and M. Mazzanti, *Angew. Chem., Int. Ed. Engl.*, 2012, **51**, 12280–12284.
39 C. Camp, O. Cooper, J. Andrez, J. Pecaut and M. Mazzanti, *J. Chem. Soc., Dalton Trans.*, 2015, **44**, 2650–2656.
40 C. Camp, C. E. Kefalidis, J. Pecaut, L. Maron and M. Mazzanti, *Angew. Chem., Int. Ed. Engl.*, 2013, **52**, 12646–12650.
41 B. M. Gardner, G. Balazs, M. Scheer, F. Tuna, E. J. L. McInnes, J. McMaster, W. Lewis, A. J. Blake and S. T. Liddle, *Angew. Chem., Int. Ed. Engl.*, 2014, **53**, 4484–4488.
42 L. R. Avens, D. M. Barnhart, C. J. Burns, S. D. McKee and W. H. Smith, *Inorg. Chem.*, 1994, **33**, 4245–4254.
43 S. M. Franke, F. W. Heinemann and K. Meyer, *Chem. Sci.*, 2014, **5**, 942–950.
44 D. E. Smiles, G. Wu and T. W. Hayton, *Inorg. Chem.*, 2014, **53**, 12683–12685.
45 D. Stueber, D. Patterson, C. L. Mayne, A. M. Orendt, D. M. Grant and R. W. Parry, *Inorg. Chem.*, 2001, **40**, 1902–1911.
46 W. Gombler, *Z. Naturforsch., B: Anorg. Chem., Org. Chem.*, 1981, **36**, 1561–1565.
47 S. J. Smith, C. M. Whaley, T. B. Rauchfuss and S. R. Wilson, *Inorg. Chem.*, 2006, **45**, 679–687.
48 S. Kuwata and M. Hidai, *Coord. Chem. Rev.*, 2001, **213**, 211–305.
49 M. Peruzzini, I. De los Rios and A. Romerosa, *Prog. Inorg. Chem.*, 2001, **49**, 169–453.
50 C. Bianchini and A. Meli, *Acc. Chem. Res.*, 1998, **31**, 109–116.
51 M. R. Dubois, *Chem. Rev.*, 1989, **89**, 1–9.
52 (*a*) S. M. Franke, M. W. Rosenzweig, F. W. Heinemann and K. Meyer, *Chem. Sci.*, 2015, **6**, 275–282; (*b*) M. W. Rosenzweig, A. Scheurer, F. W. Heinemann, C. A. Lamsfus, L. Maron, J. Andrez, M. Mazzanti and K. Meyer, *Chem. Sci.*, 2016, DOI: 10.1039/C6SC00677A.
53 Q.-Y. Wu, J.-H. Lan, C.-Z. Wang, Y.-L. Zhao, Z.-F. Chai and W.-Q. Shi, *J. Phys. Chem. A*, 2015, **119**, 922–930.
54 D. M. King, F. Tuna, E. J. L. McInnes, J. McMaster, W. Lewis, A. J. Blake and S. T. Liddle, *Science*, 2012, **337**, 717–720.
55 CrysAlisPro CCD, CrysAlisPro RED and ABSPACK, CrysAlis PRO. Agilent Technologies, Yarnton, England., Agilent, 2010.
56 A. J. M. Duisenberg, L. M. J. Kroon-Batenburg and A. M. M. Schreurs, *J. Appl. Crystallogr.*, 2003, **36**, 220–229.
57 R. H. Blessing, *Acta Crystallogr., Sect. A: Found. Crystallogr.*, 1995, **51**, 33–38.
58 G. M. Sheldrick, *Acta Crystallogr., Sect. A: Found. Crystallogr.*, 2008, **64**, 112–122.
59 L. Palatinus and G. Chapuis, *J. Appl. Crystallogr.*, 2007, **40**, 786–790.
60 A. L. Spek, *Acta Crystallogr., Sect. D: Biol. Crystallogr.*, 2009, **65**, 148–155.
61 A. D. Becke, *J. Chem. Phys.*, 1993, **98**, 5648–5652.
62 J. P. Perdew and Y. Wang, *Phys. Rev. B: Condens. Matter Mater. Phys.*, 1992, **45**, 13244–13249.
63 W. Kuchle, M. Dolg, H. Stoll and H. Preuss, *J. Chem. Phys.*, 1994, **100**, 7535–7542.
64 X. Y. Cao, M. Dolg and H. Stoll, *J. Chem. Phys.*, 2003, **118**, 487–496.
65 X. Y. Cao and M. Dolg, *J. Mol. Struct.: THEOCHEM*, 2004, **673**, 203–209.
66 A. Moritz, X. Y. Cao and M. Dolg, *Theor. Chem. Acc.*, 2007, **118**, 845–854.
67 A. Bergner, M. Dolg, W. Kuechle, H. Stoll and H. Preuss, *Mol. Phys.*, 1993, **80**, 1431–1441.
68 A. W. Ehlers, M. Böhme, S. Dapprich, A. Gobbi, A. Höllwarth, V. Jonas, K. F. Köhler, R. Stegmann, A. Veldkamp and G. Frenking, *Chem. Phys. Lett.*, 1993, **208**, 111–114.
69 R. Ditchfield, W. J. Hehre and J. A. Pople, *J. Chem. Phys.*, 1971, **54**, 724–728.
70 W. J. Hehre, R. Ditchfield and J. A. Pople, *J. Chem. Phys.*, 1972, **56**, 2257–2261.
71 P. C. Hariharan and J. A. Pople, *Theor. Chim. Acta*, 1973, **28**, 213–222.
72 A. E. Reed, L. A. Curtiss and F. Weinhold, *Chem. Rev.*, 1988, **88**, 899–926.
73 F. Weinhold, in *The Encyclopedia of Computational Chemistry*, ed. P. v. R. Schleyer, John Wiley & Sons, Chichester, 1998, p. 1792.
74 T. Lu and F. Chen, *J. Comput. Chem.*, 2012, **33**, 580–592.
75 T. Lu and F. Chen, *Acta Chim. Sin.*, 2011, **69**, 2393–2406.
76 http://www.chemcraftprog.com.
77 M. J. Frisch, G. W. Trucks, H. B. Schlegel, G. E. Scuseria, M. A. Robb, J. R. Cheeseman, G. Scalmani, V. Barone, B. Mennucci, G. A. Petersson, H. Nakatsuji, M. Caricato, X. Li, H. P. Hratchian, A. F. Izmaylov, J. Bloino, G. Zheng, J. L. Sonnenberg, M. Hada, M. Ehara, K. Toyota, R. Fukuda, J. Hasegawa, M. Ishida, T. Nakajima, Y. Honda, O. Kitao, H. Nakai, T. Vreven, J. A. Montgomery Jr, J. E. Peralta, F. Ogliaro, M. Bearpark, J. J. Heyd, E. Brothers, K. N. Kudin, V. N. Staroverov, R. Kobayashi, J. Normand, K. Raghavachari, A. Rendell, J. C. Burant, S. S. Iyengar, J. Tomasi, M. Cossi, N. Rega, J. M. Millam, M. Klene, J. E. Knox, J. B. Cross, V. Bakken, C. Adamo, J. Jaramillo, R. Gomperts, R. E. Stratmann, O. Yazyev, A. J. Austin, R. Cammi, C. Pomelli, J. W. Ochterski, R. L. Martin, K. Morokuma, V. G. Zakrzewski, G. A. Voth, P. Salvador, J. J. Dannenberg, S. Dapprich, A. D. Daniels, Ö. Farkas, J. B. Foresman, J. V. Ortiz, J. Cioslowski and D. J. Fox, *Gaussian 09, Revision A.02*, Gaussian, Inc., Wallingford CT, 2009.

Chemical Science

EDGE ARTICLE

View Article Online
View Journal | View Issue



CrossMark click for updates

Cite this: *Chem. Sci.*, 2016, **7**, 5857

# Uranium(IV) terminal hydrosulfido and sulfido complexes: insights into the nature of the uranium–sulfur bond†

Michael W. Rosenzweig,[a] Andreas Scheurer,[a] Carlos A. Lamsfus,[c] Frank W. Heinemann,[a] Laurent Maron,[c] Julie Andrez,[b] Marinella Mazzanti[b] and Karsten Meyer*[a]

Received 13th February 2016
Accepted 9th May 2016

DOI: 10.1039/c6sc00677a

www.rsc.org/chemicalscience

Herein, we report the synthesis and characterization of a series of terminal uranium(IV) hydrosulfido and sulfido complexes, supported by the hexadentate, tacn-based ligand framework $(^{Ad,Me}ArO)_3tacn^{3-}$ (= trianion of 1,4,7-tris(3-(1-adamantyl)-5-methyl-2-hydroxybenzyl)-1,4,7-triazacyclononane). The hydrosulfido complex $[((^{Ad,Me}ArO)_3tacn)U–SH]$ (**2**) is obtained from the reaction of $H_2S$ with the uranium(III) starting material $[((^{Ad,Me}ArO)_3tacn)U]$ (**1**) in THF. Subsequent deprotonation with potassium bis(trimethylsilyl)amide yields the mononuclear uranium(IV) sulfido species in good yields. With the aid of dibenzo-18-crown-6 and 2.2.2-cryptand, it was possible to isolate a terminal sulfido species, capped by the potassium counter ion, and a "free" terminal sulfido species with a well separated cation/anion pair. Spectroscopic and computational analyses provided insights into the nature of the uranium–sulfur bond in these complexes.

## Introduction

The anhydrous coordination chemistry of the light actinides has become an active field of research since the discovery of suitable starting materials.[1–3] Research has mainly focused on the chemistry of the mildly radioactive isotopes of uranium and thorium, rendering the resulting complexes suitable for practical applications ranging from catalysis to materials science.[4–13] In contrast to the extensive uranium coordination chemistry with hard oxygen and nitrogen based ligands, bonding between uranium and the heavier chalcogens (S, Se, Te) was assumed to be disfavored due to the hard–soft mismatch. With the synthesis of stable uranium thiolate complexes in the late 1950s this theory was revoked[14] and soft chalcogen containing ligands were developed for the selective complexation and separation of actinides and lanthanides in spent nuclear fuel. The selective complexation of 5f metal ions compared to 4f ions is based on the fundamentally different bonding and degree of covalency of the actinide *versus* lanthanide chalcogen bonds.[15–18] In recent years, the number of actinide compounds with soft chalcogen ligands has been increasing steadily.[19] DFT calculations of compounds with uranium–sulfur single bonds reveal this bond to be strongly polarized, thus essentially ionic in nature, whereas uranium–chalcogen multiple bonding is considered to be more covalent. Considerable academic as well as industrial interest in uranium chalcogenide multiple bonding has triggered efforts to synthesize well-defined mononuclear U=E compounds (E = O, S, *etc.*), enabling a more detailed insight into the electronic structure and degree of covalency in this structural motif.[20–32]

In contrast to the rapidly increasing number of reported terminal uranium oxo complexes,[20–26] the number of fully characterized terminal uranium sulfido complexes remains scarce.[27,29,32] This is likely due to the proclivity of uranium(III) to undergo one electron oxidation resulting in dinuclear, sulfido-bridged diuranium(IV/IV) complexes rather than stabilizing the terminal sulfido ligand, $S^{2-}$.[28,33–35] Recently, our group established a facile synthetic route to mononuclear uranium(IV) hydrochalcogenido complexes employing $H_2E$ (E = S, Se, and Te) as the chalcogenido ligand source.[36] Analogous to other known examples in transition metal chemistry, these uranium hydrosulfido complexes are suitable precursor molecules for the high-yield synthesis of terminal chalcogenido complexes, since the proton can be conveniently removed.[37,38] Additionally, the U–EH species can be seen as "proton-capped" terminal chalcogenido complexes and spectroscopic comparison to the

[a]*Department of Chemistry and Pharmacy, Inorganic Chemistry, Friedrich-Alexander University Erlangen-Nürnberg, Egerlandstraße 1, 91058 Erlangen, Germany. E-mail: karsten.meyer@fau.de*

[b]*Institut des Sciences et Ingénierie Chimiques, Ecole Polytechnique Fédérale de Lausanne (EPFL), 1015 Lausanne, Switzerland*

[c]*LPCNO, Université de Toulouse, INSA Toulouse, 135 Avenue de Rangueil, 31077 Toulouse, France*

† Electronic supplementary information (ESI) available: Full synthetic and experimental details, spectroscopic data for $^1$H NMR, SQUID, UV/vis/NIR, electrochemistry, and detailed X-ray crystallographic data. CCDC 1452972–1452974. For ESI and crystallographic data in CIF or other electronic format see DOI: 10.1039/c6sc00677a

analogous, truly terminal species provides unique insight into the nature of the chemical bond between uranium and the soft chalcogenido ligand.[27–29,32] Until today, there is only one structurally characterized uranium hydrosulfido complex reported in the literature, namely [(($^{Ad,Me}$ArO)$_3$N)U–SH(DME)] (with ($^{Ad,Me}$ArO)$_3$N$^{3-}$ = trianion of tris(2-hydroxy-3-(1-adamantyl)-5-methylbenzyl)amine). Due to their potential application as catalysts, transition metal hydrochalcogenido complexes (E = O, S, Se, and Te) have received considerable interest in recent years.[37–45] Most recently a uranium(IV) hydroxo complex, namely [(($^{Ad,Me}$ArO)$_3$mes)-U–OH], was found to be the key intermediate in the electrocatalytic production of dihydrogen from water.[9]

## Results and discussion

We previously demonstrated that the uranium(III) complexes [(($^{tBu,tBu}$ArO)$_3$tacn)U] (with ($^{tBu,tBu}$ArO)$_3$tacn$^{3-}$ = trianion of 1,4,7-tris-(3,5-di-*tert*-butyl-2-hydroxybenzyl)-1,4,7-triazacyclononane) and [(($^{Ad,Me}$ArO)$_3$N)U(DME)] (with $^{Ad,Me}$ArO)$_3$N$^{3-}$ = trianion of tris(2-hydroxy-3-(1-adamantyl)-5-methylbenzyl)amine) efficiently activate the elemental chalcogens (E = O, S, Se, and Te)[34] as well as their hydrogen chalcogenides $H_2E$.[36] Uranium-mediated reductive transformations with the employed ligand systems, however, did not facilitate the formation of terminal uranium chalcogenido complexes. Instead, dimerization of the complexes *via* (poly-)chalcogenido as well as bis-hydrochalcogenido bridges was observed.[34,36,46] In order to prevent dimerization reactions, we made use of a well-established tacn anchored ligand, the sterically encumbered adamantyl derivative ($^{Ad,R}$ArO)$_3$tacn)$^{3-}$ (R = *tert*-butyl, methyl).[29] Accordingly, the uranium(III) precursor [(($^{Ad,Me}$ArO)$_3$tacn)U] (**1**) (($^{Ad,Me}$ArO)$_3$-tacn$^{3-}$ = trianion of 1,4,7-tris(3-(1-adamantyl)-5-methyl-2-hydroxybenzyl)-1,4,7-triazacyclononane) allowed for synthesis of the here reported monomeric uranium (hydro-) chalcogenido complexes. More importantly, the bulky adamantyl groups effectively prevent dimerization upon deprotonation of the SH$^-$ ligand; thus, yielding the targeted uranium terminal sulfido complex for direct comparison to the bonding situation in U complexes with $\eta^1$-SH and $\eta^1$-S ligands. The presence of crown ethers or cryptands in the deprotonation step not only increases the solubility of the formed metal salts, but additionally allows for the quantitative evaluation of the bonding situation in a U–S–H *versus* a U–S···K complex.

### Syntheses and molecular structures of terminal uranium(IV) hydrosulfido and sulfido complexes

Reaction of the uranium(III) complex [(($^{Ad,Me}$ArO)$_3$tacn)U] (**1**) with various S atom transfer reagents, such as $Ph_3P{=}S$ or elemental sulfur, does not yield terminal U≡S complexes. Either a reaction was not observed at all or an intractable mixture of compounds without any isolable product was received. Finally, the synthesis of terminal uranium(IV) hydrosulfido and sulfido complexes was successfully achieved by treatment of complex **1** with one equivalent of $H_2S$. The dropwise addition of 0.8 M $H_2S$ in THF to a red-brown solution of **1** in THF reproducibly affords the uranium(IV) hydrosulfido complex [(($^{Ad,Me}$ArO)$_3$tacn)U–SH] (**2**) in excellent yields with concomitant evolution of $H_2$ gas (Scheme 1). After stirring for two hours, the blue-green precipitate was collected by filtration to afford the analytically pure complex **2** in 82% yield. The solid-state molecular structure of **2**·3.25 $CH_2Cl_2$ was unambiguously established by single-crystal X-ray diffraction analysis of the light green prisms, obtained by *n*-pentane diffusion into a concentrated DCM solution of **2**.

Complex **2**·3.25 $CH_2Cl_2$ crystallizes in the chiral hexagonal space group $P6_3$ with two independent molecules per asymmetric unit ($Z = 4$). The mononuclear complex [(($^{Ad,Me}$ArO)$_3$tacn)U–SH] exhibits a seven-coordinate uranium ion in a face-capped octahedral coordination environment (Fig. 1).[47] The U–S bond lengths of the two independent molecules in the crystals of **2** were determined to be 2.844(4) and 2.775(2) Å, respectively. This is in good agreement with other reported uranium–sulfur single bonds (2.588(1)–2.907(3) Å)[36] but distinctly longer than published uranium species with terminal sulfido ligands (2.382(11)–2.481(1) Å).[27–29,32] The SH$^-$ ligand is situated on the $C_3$ axis of the molecule in the axial position, *trans* to the tacn anchor. Since the chalcogen-bound H atom could be located in the difference Fourier map, the U–S–H angle was determined to be 152° and 156°, respectively. The U–$O_{aryloxide}$ distances are 2.152(4) Å and 2.188(3) Å, respectively, and the U–$N_{tacn}$ bond lengths are 2.680(5) Å and 2.650(4) Å. The uranium out-of-plane shift ($U_{oop}$), defined by the displacement of the uranium ion below the plane of the three aryloxide oxygen atoms, was measured to be −0.282 and −0.268 Å, respectively. All these parameters are in good agreement with other uranium(IV) complexes supported by the ($^{R,R'}$ArO)$_3$tacn$^{3-}$ ligand system (R = 1-adamantyl, *tert*-butyl, neopentyl; R′ = *tert*-butyl, methyl).[22,48–52]

In order to obtain a terminal uranium(IV) sulfido species, complex **2** was treated with potassium bis(trimethylsilyl)amide in THF to deprotonate the –SH moiety. In order to encapsulate the potassium counterion, the reaction was performed in the presence of either dibenzo-18-crown-6 (= 6,7,9,10,17,18,20,21-octahydrodibenzo[*b*,*k*]-[1,4,7,10,13,16]hexaoxacyclooctadecine; db-18-c-6) or 2.2.2-cryptand (= 4,7,13,16,21,24-hexaoxa-1,10-diazabicyclo[8.8.8]-hexacosane; 2.2.2-crypt) (Scheme 2). Single-crystal X-ray crystallographic structure determinations of the resulting orange products [(($^{Ad,Me}$ArO)$_3$tacn)U≡S···K(db-18-c-6)] (**3**) and [K(2.2.2-crypt)] [(($^{Ad,Me}$ArO)$_3$tacn)U≡S] (**4**) were carried out. The uranium(IV) sulfido complex **3**·0.62 benzene·0.38 $Et_2O$ crystallizes in the

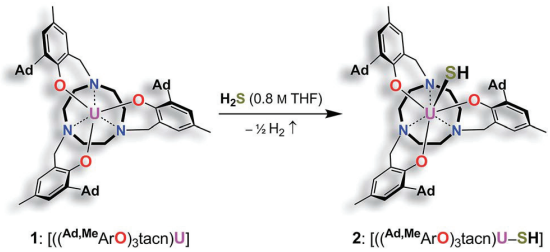


**1**: [(($^{Ad,Me}$ArO)$_3$tacn)U] **2**: [(($^{Ad,Me}$ArO)$_3$tacn)U–SH]

Scheme 1 Synthesis of the uranium(IV) hydrosulfido complex [(($^{Ad,Me}$ArO)$_3$tacn)U–SH] (**2**).

 

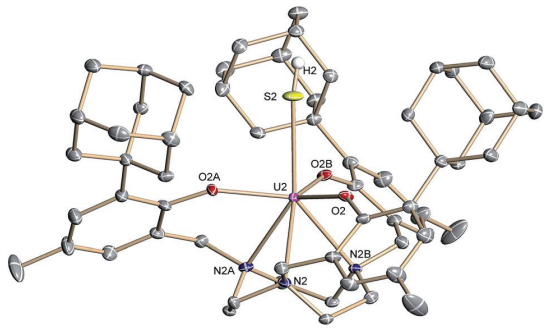


Fig. 1 Molecular structure of the uranium(IV) hydrosulfido complex [((Ad,MeArO)3tacn)U–SH] (2) with the chalcogen-bound H atom located in the difference Fourier map. All other hydrogen atoms and the solvent molecules are omitted for clarity (50% probability ellipsoids).

monoclinic space group $P2_1/c$ with one molecule per asymmetric unit, whereas **4** crystallizes in the chiral, hexagonal space group $P6_3$ with a third of one independent molecules per asymmetric unit. Both the uranium complex and the [K(2.2.2-crypt)] moiety were found on a crystallographic threefold axes. As anticipated, the sulfido ligand of the uranium(IV) complex [((Ad,MeArO)3tacn)U≡S···K(db-18-c-6)] (**3**) is capped by the [K(db-18-c-6)]$^+$ cation, whereas complex [K(2.2.2-crypt)][((Ad,MeArO)3tacn)U≡S] (**4**) features a genuine terminal sulfido ligand with the [K(2.2.2-crypt)]$^+$ cation in the outer coordination sphere of the complex anion (Fig. 2).

Like complex **2**, $U^{IV}$ complex **3** features a seven-coordinate uranium ion with the sulfido ligand occupying the axial position. The S–K distance is 3.136(1) Å, demonstrating a bonding interaction between the $S^{2-}$ ligand and the $K^+$ counter ion (Fig. 2, left). The U–S bond length is 2.507(1) Å, which is significantly shorter compared to [((Ad,MeArO)3tacn)U–SH] (**2**, d(U–SH)$_{av}$ = 2.810(4) Å), but slightly longer than those of other reported uranium(IV) sulfido complexes (2.442(2)–2.4805(5) Å).[27–29,32] While the $^1$H NMR spectrum of **3** reveals a $C_3$-symmetrical molecule in solution (*vide infra*), coordination of the [K(db-18-c-6)]$^+$ crown ether leads to a loss of $C_3$ symmetry in the crystal structure. The average U–O$_{aryloxide}$ distance of 2.219 Å and the mean U–N$_{tacn}$ bond length of 2.819 Å are slightly longer compared to $U^{IV}$ hydrosulfido complex **2**. Interestingly, the U out-of-plane shift (U$_{oop}$) significantly decreases from −0.275 in **2** to −0.055 Å in **3**; hence, the uranium center is positioned almost perfectly in the plane of the three oxygen donors. This observation is quite unusual for uranium(IV) ions in the tacn-based ligand system, and is typically only seen for high-valent $U^V$ and $U^{VI}$ complexes with strong π-donor ligands, such as the oxo and isoelectronic imido functionality.[22,49] However, as shown before, the U out-of-plane shift correlates well with the degree of U–L multiple bond character and bond strength; and thus, might be indicative of significant multiple bonding and covalent character of the U–S bond in **3** (*vide infra*).[22,53]

The connectivity of the $N_3O_3S$ ligand donor set in the anionic complex [((Ad,MeArO)3tacn)U≡S]$^-$ (**4**)$^-$ is analogous to that found for complex **3**. In the case of **4**, however, the potassium cation is encapsulated by the sterically encumbered 2.2.2-cryptand and located in the outer coordination sphere of the anionic $U^{IV}$ complex, leading to a discrete ion pair with isolated [K(2.2.2-crypt)]$^+$ cations and [((Ad,MeArO)3tacn)U≡S]$^-$ anions (Fig. 2, right). Surprisingly, although the sulfido ligand is no longer engaged in cationic interactions, the tetravalent complex **4** exhibits a slightly longer uranium–sulfido distance of 2.536(2) Å and—along with the longer U–S distance—a slightly but noticeably larger U$_{oop}$ of −0.086 Å compared to **3** (d(U–S)$_{av}$ = 2.507(1) and U$_{oop}$ = −0.055 Å). It is suggested that the diphenyl-18-crown-6 moiety exerts a considerable steric strain that might push the sulfur atom slightly deeper into the cavity of the [((AdArO)3tacn)U] moiety, while at the same time, the uranium reduces its negative out-of-plane shift and moves closer to the sulfur atom in order to accommodate the sterically demanding potassium diphenyl-18-crown-6 moiety in the complex periphery. In addition, the seven-coordinate uranium center is chiral with an idealized $C_3$ symmetry, affording a racemate of complex **4**. After crystallization, a conglomerate of enantiomerically pure crystals was found for **4** with an A-configuration

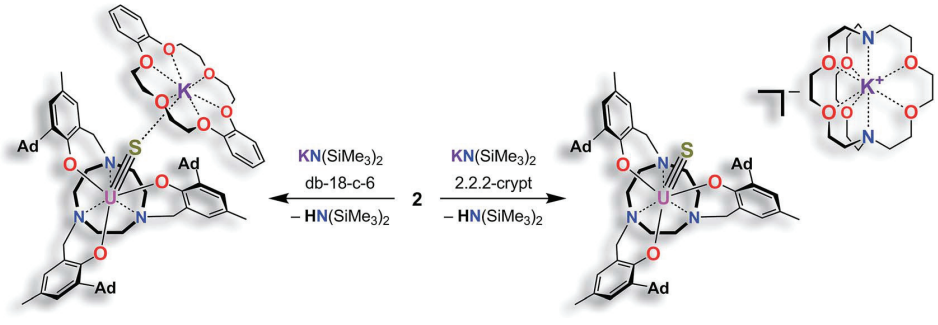


Scheme 2 Synthesis of the terminal uranium(IV) sulfido complexes [((Ad,MeArO)3tacn)U≡S···K(db-18-c-6)] (**3**) and [K(2.2.2-crypt)][((Ad,MeArO)3-tacn)U≡S] (**4**).

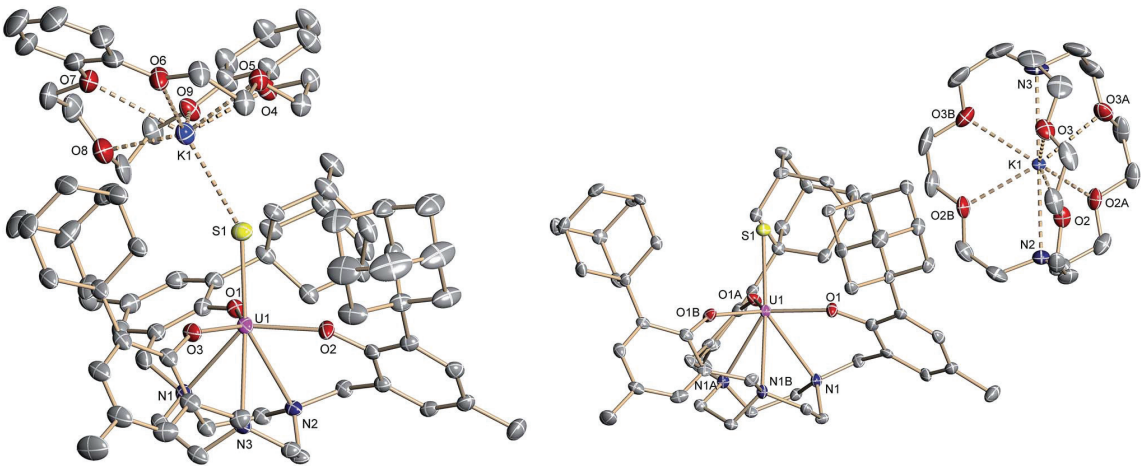


Fig. 2 Molecular structure of the uranium(IV) sulfido complex [(($^{Ad,Me}$ArO)$_3$tacn)U≡S···K(db-18-c-6)] (**3**) (left), and [K(2.2.2-crypt)][(($^{Ad,Me}$ArO)$_3$tacn)U≡S] (**4**) (right). All hydrogen atoms and the solvent molecules are omitted for clarity (50% probability ellipsoids).

of the uranium center in the analyzed crystal.[47,51] Complexes **2–4** are stable in the solid form or in THF solution for at least 3 weeks without any notable decomposition.

### $^1$H NMR spectroscopy

$^1$H NMR spectroscopy shows that compounds **2–4** possess $C_3$ symmetry in solution, induced by coordination of the tacn ligand to the metal center with the hydrosulfido/sulfido ligand situated in the axial position on the $C_3$ axis (see ESI†). Hence, complexes **2–4** are chiral in solution and the methylene protons of the tacn system as well as the benzyl groups are diastereotopic. Hydrosulfido complex **2** recorded in pyridine-$d_5$ at 25 °C features 15 paramagnetically broadened and shifted signals from 10.31 to −32.84 ppm assigned to the 79 protons of the complex. The sulfur-bound hydrogen was assigned by integration to the broadened resonance at −32.84 ppm. The $^1$H NMR spectra of compounds **3** and **4** exhibit 14 proton signals in the range of 107 to −118 ppm, which could not be unequivocally assigned to certain protons of the complex. Furthermore, four additional resonances assigned to the [db-18-c-6] crown ether as well as three resonances for 2.2.2-crypt were observed. Apart from the crown ether/cryptand signals, the spectra of both terminal sulfido complexes **3** and **4** are almost perfectly superimposable, with only slight differences in the chemical shifts. It is noteworthy that—in contrast to the coronate signals of **3**—the cryptate $^1$H-NMR signals of **4** are not paramagnetically shifted, indicating a separated ion pair in solution. Interestingly, the solid state structure of **3** displays the sulfido ligand capped by the potassium counter ion with a U–S–K angle of 142°, thereby breaking the $C_3$ symmetry of the molecule. However, $^1$H NMR spectroscopy clearly reveals a threefold symmetrical species in solution and the paramagnetically shifted coronate signals prove the sustained S···K interaction.[54] Low-temperature VT-NMR measurements were performed on **3** (+20 °C to −80 °C in THF-$d_8$) in order to investigate the complexes' symmetry at low temperatures. Upon cooling the $^1$H-NMR signals broaden and shift, but coalescence is not observed. The VT-NMR experiments thus suggest that, in solution, the crown ether complexated potassium ion remains in the vicinity of the paramagnetic uranium complex anion. It is further suggested that the potassium crown ether moiety fluctuates around the anion's threefold axis faster than the NMR timescale; even at very low temperatures. As a consequence, the U–S bond distance of **3** relaxes in solution, leading to a weaker uranium–sulfur bonding interaction (see computational analysis in the gas-phase, *vide infra*).

### Absorption spectroscopy

The electronic structure of complexes **2–4** was studied by UV/vis near-infrared spectroscopy. In the high-energy region ($\lambda$ < 600 nm) broad and rather intense ligand-based absorption bands as well as charge-transfer transitions are observed. In the UV region of the spectra, all three complexes exhibit an absorption band at 298 nm with an extremely high extinction coefficient (Fig. S14†). This spin- and parity-allowed transition most likely arises from ligand π–π* transitions.[55] Based on the assumption that the sulfido ligand has a certain degree of π-bonding character, this intensified electronic interaction between metal center and ancillary ligand should also be reflected in the electronic absorption spectrum. Indeed, both sulfido complexes **3** and **4** possess an additional absorption band in the visible region at 524 nm ($\varepsilon$ = 190 M$^{-1}$ cm$^{-1}$ (**3**); 300 M$^{-1}$ cm$^{-1}$ (**4**)), absent in **2**. This absorption band is most likely due to a metal to ligand charge-transfer transition (MLCT) of a metal-centered 5f electron into a sulfido-based orbital.[56] The unusually low intensity of this spin- and parity-allowed transition can be explained by the poor overlap of the diffuse 5f orbitals with the ligand orbital.[57] This MLCT transition in the visible region is likely to be responsible for the color differences of the orange sulfido complexes **3** and **4** compared to the pale blue-green color

 

of **2**. The visible near-IR electronic absorption spectra of complexes **2–4** in pyridine (5 mM) are shown in Fig. 3. Uranium(IV) complexes possess a $5f^2$ electron configuration, and therefore display rather complicated electronic absorption spectra with multiple low-intensity absorption bands and fine structure in the vis/NIR region.[58] However, the Laporte forbidden f–f transitions with small extinction coefficients ($\varepsilon$ = 6–116 $M^{-1}$ $cm^{-1}$) give rise to signature absorption bands characteristic of tetravalent uranium complexes. This is particularly true for a series of complexes, in which the symmetry around the metal center remains constant ($C_3$ for all complexes in solution) and the core structure is dominated by the $((ArO)_3tacn)^{3-}$ chelate, and thus, quite similar.[55,59] The terminal sulfido complexes **3** and **4** exhibit 10 absorption bands with nearly identical absorption patterns in the vis/NIR region between 540 and 2100 nm, with three relatively strong absorption peaks at around 990, 1111, and 1990 nm. Noticeably, the molar extinction coefficients observed in the spectra of the separate ion pair **4** are consistently larger than those of complex **3**, with the capped terminal sulfido ligand. The NIR spectra have been reproduced multiple times and the differences in extinction coefficient are significantly larger than the experimental error. Further inspection of the NIR spectra reveals approximately equal line width for the absorption bands in complexes **3** and **4**; thus, excluding an intensity stealing mechanism.‡ A reduced symmetry also cannot account for different extinction coefficients in **3** and **4**, since both possess $C_3$ symmetry in solution (as established by (VT) $^1$H NMR spectroscopy, *vide supra*). However, it is worth noting that the timescale of electronic absorption spectroscopy is significantly shorter compared to proton NMR spectroscopy, therefore complex **3** could lose its $C_3$ symmetry. Regardless, in the latter case, absorption bands of complex **3** should be more intense than those of complex **4**. Since the intensity of an electronic absorption band in the NIR region is considered indicative of the degree of covalency of the uranium ligand multiple bond in a conserved ligand field,[59,60] the spectral data imply a less covalent bonding interaction for the potassium-capped uranium(IV) sulfido complex, **3**. This is in contrast to the shorter U≡S bond observed in the solid-state structure of **3** implying a stronger, more covalent bond compared to **4**. Therefore, one can only conclude—and reiterate—that the mere bond distance is not a valid measure of covalency.

Hydrosulfido complex **2** shows about the same number of absorption bands as **3** and **4**, but the f–f transitions occur at slightly different energies and a charge-transfer transition is not observed. Additionally, the intensities of the bands are significantly lower ($\varepsilon$ = 6–48 $M^{-1}$ $cm^{-1}$) and, in accordance with the lack of charge-transfer transitions, indicate the presence of a ligand with predominantly σ-donor character.

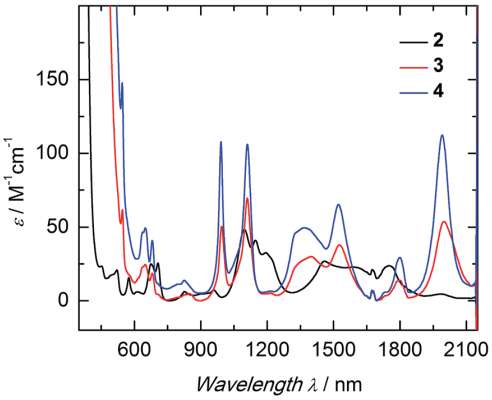


Fig. 3 Electronic absorption spectra of the uranium hydrosulfido complex [((Ad,Me ArO)$_3$tacn)U–SH] (**2**, black) and terminal sulfido complexes [((Ad,Me ArO)$_3$tacn)U≡S···K(db-18-c-6)] (**3**, red) and [K(2.2.2-crypt)][((Ad,Me ArO)$_3$tacn)U≡S] (**4**, blue); all complexes 5 mM in pyridine, measured at RT.

## Magnetic investigations

SQUID magnetization measurements were carried out to study the temperature behavior of trivalent **1** and tetravalent **2–4** from 2 to 300 K (Fig. 4 bottom). Although the room temperature magnetic moments of transition metals and lanthanides can be accurately predicted by the spin-only ($\mu_S$) and total angular momentum approximations ($\mu_J$), respectively, there is currently no approximation to predict the magnetic moment for actinide coordination complexes, since ligand-field effects cannot be ignored and spin–orbit coupling is large.[50,61,62] Tetravalent uranium ions possess an $f^2$ valence electron configuration, which results in a non-magnetic ground state at very low temperatures; and consequently, strongly temperature-dependent magnetic moments, $\mu_{eff}$, with values typically ranging from 0.3 $\mu_B$ at 2 K to 2.8 $\mu_B$ at room temperature.[36,46,50,51,53,61,63,64]

In contrast, trivalent $U^{III}$ ions ($f^3$) possess a half integer spin with a doublet, EPR-active ground state ($g_\perp = 1.912$, $g_\parallel = 2.421$ (Fig. 4 top)) and should approach non-zero values at low temperatures.[53,65] Accordingly, only the effective magnetic moment at low temperatures, as well as the temperature-dependency of the complexes, can provide reasonable hints to the ions' formal oxidation state. Complex **1** displays a strong temperature-dependent magnetic moment, varying from 1.42 $\mu_B$ at 2 K to 2.82 $\mu_B$ at room temperature. As already mentioned, the magnetic moment of 2.82 $\mu_B$ at room temperature is significantly smaller than the calculated moment ($\mu_J = 3.62$ $\mu_B$), but the low temperature effective magnetic moment together with an EPR signal confirms a trivalent uranium ion in complex **1** (Fig. 4 top).

At room temperature, complexes **2–4** possess nearly the same magnetic moment with 2.85 $\mu_B$, 2.90 $\mu_B$, and 2.87 $\mu_B$, respectively, but show significantly different temperature-dependent behavior. These results support the notion that the room temperature magnetic moments cannot be used to determine the oxidation state of the uranium ion, since trivalent **1** at room temperature shows nearly the same (or even slightly lower) magnetic moment as tetravalent **2–4**. At 2 K, however, uranium(IV) complexes with the $f^2$ ion typically show distinctively lower magnetic moments, which are due to the ions' non-magnetic singlet ground state.[61] Complex **2** exhibits temperature-

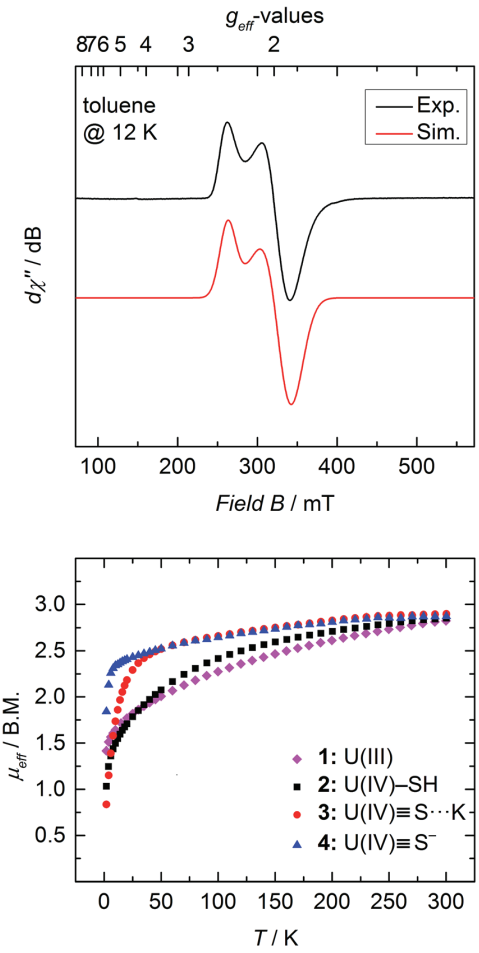


Fig. 4 Top: X-band EPR spectrum of **1** recorded in toluene glass at 12 K. Experimental conditions: microwave frequency, 8.9641 GHz; power, 0.0997 mW; modulation, 1 mT. The spectrum was simulated with $g_\perp = 1.912$ and $g_\parallel = 2.421$ and Gaussian lines with $W_\perp = 20.1$ and $W_\parallel = 11.4$ mT; bottom: temperature dependent SQUID magnetometry of complexes [(($^{Ad,Me}$ArO)$_3$tacn)U] (**1**, magenta diamonds), [(($^{Ad,Me}$ArO)$_3$tacn)U–SH] (**2**, black squares), [(($^{Ad,Me}$ArO)$_3$tacn)U≡S···K(db-18-c-6)] (**3**, red circles), and [K(2.2.2-crypt)][(($^{Ad,Me}$ArO)$_3$tacn)U≡S] (**4**, blue triangles) plotted as $\mu_{eff}$ *vs.* *T*.

dependency overall typical for a uranium(IV) compound. The low magnetic moment, $\mu_{eff}$, of 1.03 $\mu_B$ at 2 K continually increases with increasing temperature. On the contrary, sulfido complexes **3** and **4** reveal an unusually strong temperature-dependency in the range of 2 to 50 K, with a subsequent moderate increase from 50 to 300 K. Notably, complex **3** shows a typically low magnetic moment of 0.84 $\mu_B$ at 2 K, whereas complex **4** possesses an unusually high $\mu_{eff}$ value of 1.84 $\mu_B$. Despite this high magnetic moment, complex **4** is EPR silent (in X band, between 300 and 5 K). Similar high magnetic moments have been observed for $U^{IV}$ complexes with separate ion pairs like [Cp*$_2$Co]-[U(O)(N(SiMe$_3$)$_2$)$_3$],[27] [Li(DME)]-[U(NC$_5$H$_{10}$)$_5$],[66] [Li(THF)$_4$]-[U(CH$_2$$^t$Bu)$_5$], and [Li(DME)$_3$]-[U(CH$_2$SiMe$_3$)$_5$].[67]

On the other hand, complex **2** possesses a more isolated magnetic ground state, where the higher magnetic states slowly become thermally accessible with increasing temperature. Hence, the low-lying magnetic states of complexes **3** and **4** appear to be closer in energy, and are already thermally accessible at temperatures below 50 K. Consequently, the magnetic moment increases rapidly from 2 to 50 K, and merely increases with increasing temperatures above 50 K. The intriguing difference in the temperature dependency of the magnetic moments of complexes **2–4** is due to the different crystal-field-splitting caused by the purely σ-type SH$^-$ *versus* the σ- and π-type S$^{2-}$ ligands.[67]

## Electrochemistry

Cyclic and linear sweep voltammetry were performed on **3** in THF in the presence of ~0.1 M [N(*n*-Bu)$_4$][BPh$_4$] electrolyte and the ferrocenium/ferrocene redox couple ($Fc^+$/Fc) acting as internal standard. The cyclic voltammogram of **3** reveals a quasi-reversible redox process at a half-step potential, $E_{1/2}$, of −1.494 V (Fig. 5). A positive current in the linear-sweep measurement confirms an oxidative process of the compound (see ESI†). Accordingly, this redox process is tentatively assigned to the uranium(IV/V) redox couple, with the half-step potential in the range of other published $U^{IV/V}$ couples (−1.81 to 0.12 V *vs.* $Fc^+$/Fc).[35,50,55,58,59,68] Electrochemical data of uranium–chalcogenido complexes are exceedingly rare and reports on uranium–sulfido complexes are, to the best of our knowledge, not reported at all. However, dimeric uranium–oxo complex [{(($^{nP,Me}$ArO)$_3$tacn)U}$_2$(μ-O)$_2$] (nP = neopentyl) shows a comparable $U^{IV/V}$ couple at a half-step potential of −1.55 V (*vs.* $Fc^+$/Fc).[50]

Due to the poor solubility of **2** and **4** in polar solvents, such as THF, cyclic voltammetry experiments could not be performed with these complexes. Given the lack of characterized terminal uranium(V) sulfido complexes in the literature, and the expectation that the covalency of the uranium–chalcogenide bond

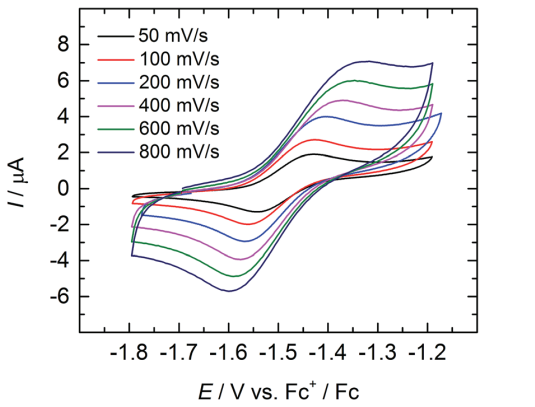


Fig. 5 Quasi-reversible oxidation wave of **3** at different scan rates. Measurement conducted in THF with ~0.1 M [N(*n*-Bu)$_4$][BPh$_4$] electrolyte, using $Fc^+$/Fc couple as internal standard.

increases with increasing valence,[62] the chemical oxidation of **3** is desirable. Unfortunately, all attempts to chemically oxidize **3** and **4** have not yet been met with success and resulted in decomposition of the compounds.

## Theoretical studies

In order to gain further insight into the nature of the U–S bond, theoretical investigations were carried out on complexes **2–4**. Geometry optimizations were conducted on [(($^{Ad,Me}$ArO)$_3$tacn)U–SH] (**2**), [(($^{Ad,Me}$ArO)$_3$tacn)U≡S···K(db-18-c-6)] (**3**), and [K(2.2.2-crypt)][(($^{Ad,Me}$ArO)$_3$tacn)U≡S] (**4**) at the DFT level without any symmetry constraints. Subsequently, molecular orbital (MO) and natural bond orbital (NBO) analyses were performed.

Initially, bond analysis was carried out on the hydrosulfido species **2**. The NBO analysis of **2** clearly indicates a single bond between U and S and a single bond between S and H (Wiberg bond indices (WBI) of 0.77 and 0.92, respectively). Accordingly, the molecular orbitals are consistent with a single U–S bond (Fig. 6), revealing the two non-bonding lone pairs to reside at the sulfur atom. A comparable terminal uranium(IV) hydrochalcogenido complex, namely [((*t*BuO)$_3$SiO)$_4$U(SH)]$^-$ obtained by Andrez *et al.*, exhibits significant double bond character of the uranium sulfur interaction (determined by MO and WBI).[69] In order to understand the origin of these electronic differences of **2** and [((*t*BuO)$_3$SiO)$_4$U(SH)]$^-$, these two complexes were analyzed in more detail.

The U–S σ-bond of complex **2** is strongly polarized with 10% uranium and 90% sulfur orbital character. The metal orbital is a hybrid sdf orbital with 12% 7s, 38% 6d, and 50% 5f contribution. This is comparable to the hybrid orbital composition of the hydrosulfido complex [((*t*BuO)$_3$SiO)$_4$U(SH)]$^-$ exhibiting a σ (and π) orbital with 14% uranium character (12% for the π) and a strongly hybridized orbital (10% 7s, 40% 6d and 50% 5f). As evidenced by the X-ray structure, the geometry of **2** differs significantly from the trigonal bipyramidal complex [((*t*BuO)$_3$SiO)$_4$U(SH)]$^-$. The computational analysis suggests that the pyramidalized uranium ion of **2** has an efficient overlap with the N donor atoms of the tacn ring. This, in turn, results in a *trans*-effect reducing the U–SH bond strength, which is rather unusual for uranium complexes. In order to emphasize the importance of the *trans*-influence of the tacn ligand, a hypothetical tris(aryloxide) complex, **2*** (without the triazacyclononane ligand) was also computed. Interestingly, this model complex adopts a tetrahedral geometry at the uranium center, and a U–S double bond character is found (see ESI† for the complete MO pictures and geometry).

Bonding analysis of uranium(IV) complex **3** clearly reveals a formal U≡S triple bond with one σ and two π-type interactions (Fig. 7). The molecular structure of **3** (and **4**) illustrates that the uranium ion is situated almost perfectly in the trigonal plane of the three aryloxides with a weaker U–N$_{tacn}$ interaction and more efficient uranium–sulfur orbital interaction resulting in the observed U–S multiple bond. NBO analysis shows that the U–S bond is strongly polarized with more than 75% charge on the sulfur. A σ-bond is formed by an sp orbital of sulfur (77%) and a d$_{z2}$/f$_{z3}$ hybrid orbital (41% 6d, 59% 5f) of uranium (23%), and two π orbitals are formed by the interaction of a p lone pair of sulfur (either p$_x$ or p$_y$, 77%) and a hybrid d$_\pi$/f$_\pi$ orbital (40% 6d, 60% 5f) of uranium (23%). This formal uranium sulfur triple bond is virtually unaffected by the minor interaction of the sulfido ligand with the potassium counterion (WBI of 0.1). To further substantiate the effect of the weakly associated K$^+$ ion in **3**, the bonding analysis of **4** with an encrypted and well-isolated potassium ion was carried out. As expected, a triple bond between uranium and the sulfido ligand was found with the orbitals closely resembling those of **3** (see Fig. S17† for the MOs of **4**). The experimentally determined U–S bond length of **4** (without the S···K interaction) is elongated compared to **3**. However, this result is not reproduced by the calculations that show the bond in **3** to be slightly longer (0.02 Å) than in **4** (see Table S4 in ESI,† molecules calculated in the gas-phase).

In the calculation, a weak S···K interaction (10 kcal mol$^{-1}$ at the second order donor–acceptor NBO) in **3** leads to a stronger negative charge on the sulfido ligand (−0.1 unit difference), which is formally interacting with two positively charged ions. Since the charge at the uranium ion is the same for **3** and **4**, the coordination of the potassium ion leads to a higher negative charge on the sulfido ligand in **3**, counterbalancing the charge. Consequently, a higher charge on the sulfido ligand in complex **3** leads to a smaller orbital overlap, and therefore less covalent

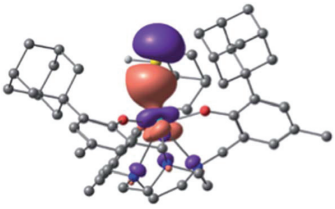

Fig. 6 Bonding σ orbital of [(($^{Ad,Me}$ArO)$_3$tacn)U–SH] (**2**).

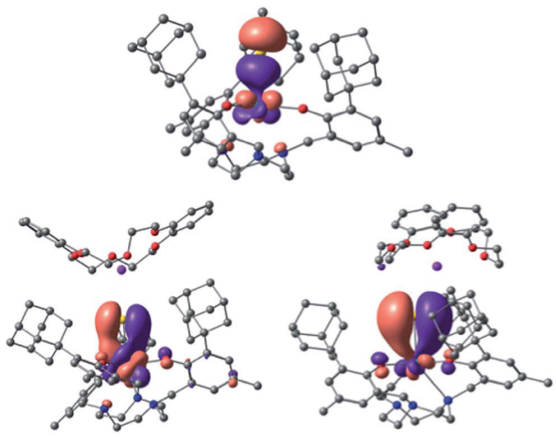

Fig. 7 U–S bonding orbitals in [(($^{Ad,Me}$ArO)$_3$tacn)U≡S···K(db-18-c-6)] (**3**), with the σ (top) and the set of two π orbitals (bottom).

interaction. In order to determine the nature of this discrepancy between experiment and theory, calculations were carried out on the putative anionic complex $[(({}^{Ad,Me}ArO)_3tacn)U(S)]^-$ ($\mathbf{4}^-$). The bonding analysis confirmed the negligible influence of the $K^+$ ion on the electronic structure of the U≡S bond of **3** and **4**, but not on the U–S bond length (see Fig. S18† for the MOs of the putative complex anion $\mathbf{4}^-$). Complex $\mathbf{4}^-$ possesses the shortest U–S distance, in line with the influence of the $K^+$ bonding, but contrary to the bond lengths observed in the solid state (see Table S4 in the ESI†). Complex **3** was optimized taking dispersion interactions into account by applying the empirical Grimme corrections.[70] This leads to a decrease in the U–S bond length by 0.02 Å in complex **3**. Hence, the computational analysis suggests that the experimentally observed shorter bond length of **3** is likely due to crystal packing effects that were not considered in the calculations (*vide supra*). Perrin *et al.* reported a similar effect for the distorted geometry of an amido lanthanide complex.[71]

Based on all of these results, we assign a significant degree of covalency to the U–S bond of complexes **2–4**. The uranium covalency contribution is defined by up to 60% 5f orbital character with the remainder being due to 7s and 6d orbital involvement. The dominating role of the latter orbitals is demonstrated by f-in-core calculations with the f-electrons included in the core shell configuration and unavailable for bonding. The results are essentially the same for complexes **2–4**. For instance, for **3**, a triple U≡S bond is obtained, which is strongly polarized towards S (between 70 and 75%) with hybrid s/d orbital involvement of the metal (roughly 80% 6d). Interestingly, the nature of the U≡S bond of complexes **3** and **4** appears to be quite similar to other computed uranium(IV) chalcogenido complexes with different supporting ligand systems.[72,73] These results indicate that the ligand field, induced by the supporting ligand system, does not significantly affect the bonding within the U≡S entity, regardless of whether aryloxide, siloxide, or supporting amide ligands are applied. In all reported complexes, the geometries at the uranium center are either distorted tetrahedral or trigonal pyramidal. Quite surprisingly, the atomic 5f and 6d orbitals experience a very similar ligand field effect in all complexes.

In order to investigate the possible influence of the chalcogenido ligand, the bonding analyses of the oxo-homologs of **3** and $\mathbf{4}^-$ were carried out. Based on the report by Andersen on a $Cp^*_2UO$ compound, a more ionic bonding description can be expected for the oxo complex.[74] The NBO analysis is in line with a single U–O σ-bond (found for the second order donor–acceptor interaction of an sp-lone pair on O and an s/d/f hybrid orbital). The second order donor–acceptor calculation also hints at a small interaction between a π lone pair of O and an empty d/f orbital on U, but is too small in energy to be considered a bonding interaction (40 kcal $mol^{-1}$, in line with a strong agostic interaction, see Table S4 ESI†). Hence, the oxo complexes are strongly ionic, whereas the sulfur analogs are more covalent. These results are in accordance with an increase in valence orbital energy of the heavier chalcogen homologs.

## Conclusion

In summary, we here present a new and high-yield synthetic protocol and the characterization of the terminal uranium hydrosulfido and sulfido complexes **2–4**, supported by the $({}^{Ad,Me}ArO)_3tacn^{3-}$ ligand system. Proton NMR spectroscopy reveals $C_3$ symmetry of the complexes in solution, and the vis/NIR electronic absorption spectroscopy, together with the SQUID magnetization measurements, allow for the unambiguous assignment of the uranium ion to the +IV oxidation state. The differences in temperature-dependency of complexes **3** and **4** at low temperatures ($T$ < 50 K) also suggest a significant influence of the potassium counter ion on the crystal field splitting of the terminal sulfido complexes as well as the nature of the U–S bond. DFT computational analyses further provided detailed insight into the bonding properties of complexes **2–4**, and reveal a non-negligible degree of covalency in the uranium–sulfur bond of **3** and **4**. This is supported by the complexes' structural parameters, vis/NIR electronic absorption spectroscopy, and SQUID magnetometry. The electrochemical studies show that complex **3** can be electrochemically oxidized, most likely to a $U^V$≡S species, which is expected to exhibit an even greater degree of covalency of the uranium sulfur bond.[62] However, initial attempts to chemically oxidize and isolate a U(V) sulfido complex led to decomposition products.

The synthesis of a complete series of uranium(IV) complexes with terminal hydrochalcogenido and chalcogenido ligands is part of our on-going studies.

## Acknowledgements

This work was supported by funds of the German Federal Ministry of Education and Research (BMBF 2020+ support codes 02NUK012C and 02NUK020C), the Joint DFG-ANR projects (ME1754/7-1, ANR-14-CE35-0004-01) as well as the FAU Erlangen-Nürnberg.

## Notes and references

‡ Complex **3**: $FWHM_{994\ nm}$ = 26 nm, $FWHM_{1111\ nm}$ = 40 nm, $FWHM_{1998\ nm}$ = 106 nm; complex **4**: $FWHM_{991\ nm}$ = 24 nm, $FWHM_{1111\ nm}$ = 38 nm, $FWHM_{1990\ nm}$ = 76 nm.

1 D. L. Clark, A. P. Sattelberger, S. G. Bott and R. N. Vrtis, *Inorg. Chem.*, 1989, **28**, 1771–1773.
2 L. R. Avens, S. G. Bott, D. L. Clark, A. P. Sattelberger, J. G. Watkin and B. D. Zwick, *Inorg. Chem.*, 1994, **33**, 2248–2256.
3 M. J. Monreal, R. K. Thomson, T. Cantat, N. E. Travia, B. L. Scott and J. L. Kiplinger, *Organometallics*, 2011, **30**, 2031–2038.
4 J. Q. Wang, A. K. Dash, J. C. Berthet, M. Ephritikhine and M. S. Eisen, *Organometallics*, 1999, **18**, 2407–2409.
5 J. Wang, A. K. Dash, M. Kapon, J.-C. Berthet, M. Ephritikhine and M. S. Eisen, *Chem.–Eur. J.*, 2002, **8**, 5384–5396.
6 Y. Shiokawa, T. Yamamura, D. Aoki, Y. Homma and Y. Onuki, *Nihon Genshiryoku Gakkaishi*, 2007, **49**, 755–761.

 

7 I. S. R. Karmel, M. Tamm and M. S. Eisen, *Angew. Chem., Int. Ed.*, 2015, **54**, 12422–12425.
8 I. S. R. Karmel, N. Fridman, M. Tamm and M. S. Eisen, *J. Am. Chem. Soc.*, 2014, **136**, 17180–17192.
9 D. P. Halter, F. W. Heinemann, J. Bachmann and K. Meyer, *Nature*, 2016, **530**, 317–321.
10 A. K. Dash, J. X. Wang, J. C. Berthet, M. Ephritikhine and M. S. Eisen, *J. Organomet. Chem.*, 2000, **604**, 83–98.
11 G. J. P. Britovsek, V. C. Gibson and D. F. Wass, *Angew. Chem., Int. Ed.*, 1999, **38**, 428–447.
12 R. J. Batrice, J. McKinven, P. L. Arnold and M. S. Eisen, *Organometallics*, 2015, **34**, 4039–4050.
13 E. Barnea, T. Andrea, M. Kapon, J.-C. Berthet, M. Ephritikhine and M. S. Eisen, *J. Am. Chem. Soc.*, 2004, **126**, 10860–10861.
14 R. G. Jones, G. Karmas, G. A. Martin and H. Gilman, *J. Am. Chem. Soc.*, 1956, **78**, 4285–4286.
15 M. Roger, N. Barros, T. Arliguie, P. Thuéry, L. Maron and M. Ephritikhine, *J. Am. Chem. Soc.*, 2006, **128**, 8790–8802.
16 H. H. Dam, D. N. Reinhoudt and W. Verboom, *Chem. Soc. Rev.*, 2007, **36**, 367–377.
17 A. J. Gaunt, S. D. Reilly, A. E. Enriquez, B. L. Scott, J. A. Ibers, P. Sekar, K. I. M. Ingram, N. Kaltsoyannis and M. P. Neu, *Inorg. Chem.*, 2008, **47**, 29–41.
18 L. Karmazin, M. Mazzanti and J. Pecaut, *Chem. Commun.*, 2002, 654–655.
19 F. Nief, *Coord. Chem. Rev.*, 1998, **178–180**, 13–81.
20 D. S. J. Arney and C. J. Burns, *J. Am. Chem. Soc.*, 1993, **115**, 9840–9841.
21 D. S. J. Arney and C. J. Burns, *J. Am. Chem. Soc.*, 1995, **117**, 9448–9460.
22 S. C. Bart, C. Anthon, F. W. Heinemann, E. Bill, N. M. Edelstein and K. Meyer, *J. Am. Chem. Soc.*, 2008, **130**, 12536–12546.
23 S. Fortier, N. Kaltsoyannis, G. Wu and T. W. Hayton, *J. Am. Chem. Soc.*, 2011, **133**, 14224–14227.
24 G. Zi, L. Jia, E. L. Werkema, M. D. Walter, J. P. Gottfriedsen and R. A. Andersen, *Organometallics*, 2005, **24**, 4251–4264.
25 S. J. Kraft, J. Walensky, P. E. Fanwick, M. B. Hall and S. C. Bart, *Inorg. Chem.*, 2010, **49**, 7620–7622.
26 B. Kosog, H. S. La Pierre, F. W. Heinemann, S. T. Liddle and K. Meyer, *J. Am. Chem. Soc.*, 2012, **134**, 5284–5289.
27 J. L. Brown, S. Fortier, R. A. Lewis, G. Wu and T. W. Hayton, *J. Am. Chem. Soc.*, 2012, **134**, 15468–15475.
28 J. L. Brown, G. Wu and T. W. Hayton, *Organometallics*, 2013, **32**, 1193–1198.
29 D. E. Smiles, G. Wu and T. W. Hayton, *J. Am. Chem. Soc.*, 2014, **136**, 96–99.
30 D. E. Smiles, G. Wu and T. W. Hayton, *Inorg. Chem.*, 2014, **53**, 12683–12685.
31 D. E. Smiles, G. Wu and T. W. Hayton, *Inorg. Chem.*, 2014, **53**, 10240–10247.
32 L. Ventelon, C. Lescop, T. Arliguie, M. Ephritikhine, P. C. Leverd, M. Lance and M. Nierlich, *Chem. Commun.*, 1999, 659–660.
33 O. P. Lam, S. M. Franke, F. W. Heinemann and K. Meyer, *J. Am. Chem. Soc.*, 2012, **134**, 16877–16881.
34 O. P. Lam, F. W. Heinemann and K. Meyer, *Chem. Sci.*, 2011, **2**, 1538–1547.
35 C. Camp, M. A. Antunes, G. Garcia, I. Ciofini, I. C. Santos, J. Pécaut, M. Almeida, J. Marcalo and M. Mazzanti, *Chem. Sci.*, 2014, **5**, 841–846.
36 S. M. Franke, M. W. Rosenzweig, F. W. Heinemann and K. Meyer, *Chem. Sci.*, 2015, **6**, 275–282.
37 P. J. Lundmark, G. J. Kubas and B. L. Scott, *Organometallics*, 1996, **15**, 3631–3633.
38 V. Jancik and H. W. Roesky, *Inorg. Chem.*, 2005, **44**, 5556–5558.
39 R. J. Angelici, *Acc. Chem. Res.*, 1988, **21**, 387–394.
40 C. Bianchini and A. Meli, *Acc. Chem. Res.*, 1998, **31**, 109–116.
41 R. R. Chianelli, T. A. Pecoraro, T. R. Halbert, W. H. Pan and E. I. Stiefel, *J. Catal.*, 1984, **86**, 226–230.
42 M. D. Curtis and S. H. Druker, *J. Am. Chem. Soc.*, 1997, **119**, 1027–1036.
43 M. R. DuBois, *Chem. Rev.*, 1989, **89**, 1–9.
44 E. J. M. Hensen, G. M. H. J. Lardinois, V. H. J. de Beer, J. A. R. van Veen and R. A. van Santen, *J. Catal.*, 1999, **187**, 95–108.
45 M. Peruzzini, I. D. L. Rios and A. Romerosa, *Prog. Inorg. Chem.*, 2001, **49**, 169–453.
46 S. M. Franke, F. W. Heinemann and K. Meyer, *Chem. Sci.*, 2014, **5**, 942–950.
47 S. Parsons, H. D. Flack and T. Wagner, *Acta Crystallogr., Sect. B: Struct. Sci., Cryst. Eng. Mater.*, 2013, **69**, 249–259.
48 I. Castro-Rodriguez, K. Olsen, P. Gantzel and K. Meyer, *Chem. Commun.*, 2002, 2764–2765.
49 I. Castro-Rodriguez and K. Meyer, *Chem. Commun.*, 2006, 1353–1368.
50 A.-C. Schmidt, F. W. Heinemann, W. W. Lukens and K. Meyer, *J. Am. Chem. Soc.*, 2014, **136**, 11980–11993.
51 A. V. Nizovtsev, A. Scheurer, B. Kosog, F. W. Heinemann and K. Meyer, *Eur. J. Inorg. Chem.*, 2013, 2538–2548.
52 A.-C. Schmidt, A. V. Nizovtsev, A. Scheurer, F. W. Heinemann and K. Meyer, *Chem. Commun.*, 2012, **48**, 8634–8636.
53 I. Castro-Rodriguez, K. Olsen, P. Gantzel and K. Meyer, *J. Am. Chem. Soc.*, 2003, **125**, 4565–4571.
54 M. J. Wilson, R. A. Pethrick, D. Pugh and M. Saiful Islam, *J. Chem. Soc., Faraday Trans.*, 1997, **93**, 2097–2104.
55 D. E. Morris, R. E. Da Re, K. C. Jantunen, I. Castro-Rodriguez and J. L. Kiplinger, *Organometallics*, 2004, **23**, 5142–5153.
56 R. E. Da Re, K. C. Jantunen, J. T. Golden, J. L. Kiplinger and D. E. Morris, *J. Am. Chem. Soc.*, 2005, **127**, 682–689.
57 K. C. Jantunen, C. J. Burns, I. Castro-Rodriguez, R. E. Da Re, J. T. Golden, D. E. Morris, B. L. Scott, F. L. Taw and J. L. Kiplinger, *Organometallics*, 2004, **23**, 4682–4692.
58 E. J. Schelter, P. Yang, B. L. Scott, J. D. Thompson, R. L. Martin, P. J. Hay, D. E. Morris and J. L. Kiplinger, *Inorg. Chem.*, 2007, **46**, 7477–7488.
59 R. K. Thomson, B. L. Scott, D. E. Morris and J. L. Kiplinger, *C. R. Chim.*, 2010, **13**, 790–802.
60 B. Vlaisavljevich, P. L. Diaconescu, W. L. Lukens, L. Gagliardi and C. C. Cummins, *Organometallics*, 2013, **32**, 1341–1352.
61 D. R. Kindra and W. J. Evans, *Chem. Rev.*, 2014, **114**, 8865–8882.

62 S. T. Liddle, *Angew. Chem., Int. Ed.*, 2015, **54**, 8604–8641.
63 A.-C. Schmidt, F. W. Heinemann, L. Maron and K. Meyer, *Inorg. Chem.*, 2014, **53**, 13142–13153.
64 D. P. Halter, H. S. La Pierre, F. W. Heinemann and K. Meyer, *Inorg. Chem.*, 2014, **53**, 8418–8424.
65 S. M. Franke, B. L. Tran, F. W. Heinemann, W. Hieringer, D. J. Mindiola and K. Meyer, *Inorg. Chem.*, 2013, **52**, 10552–10558.
66 L. A. Seaman, S. Fortier, G. Wu and T. W. Hayton, *Inorg. Chem.*, 2011, **50**, 636–646.
67 S. Fortier, B. C. Melot, G. Wu and T. W. Hayton, *J. Am. Chem. Soc.*, 2009, **131**, 15512–15521.
68 C. R. Graves, P. Yang, S. A. Kozimor, A. E. Vaughn, D. L. Clark, S. D. Conradson, E. J. Schelter, B. L. Scott, J. D. Thompson, P. J. Hay, D. E. Morris and J. L. Kiplinger, *J. Am. Chem. Soc.*, 2008, **130**, 5272–5285.
69 J. Andrez, J. Pécaut, R. Scopelliti, C. E. Kefalidis, L. Maron, M. W. Rosenzweig, K. Meyer and M. Mazzanti, *Chem. Sci.*, 2016, DOI: 10.1039/c6sc00675b.
70 S. Grimme, *J. Comput. Chem.*, 2006, **27**, 1787–1799.
71 L. Perrin, E. L. Werkema, O. Eisenstein and R. A. Andersen, *Inorg. Chem.*, 2014, **53**, 6361–6373.
72 J. L. Brown, S. Fortier, G. Wu, N. Kaltsoyannis and T. W. Hayton, *J. Am. Chem. Soc.*, 2013, **135**, 5352–5355.
73 S. Fortier, J. L. Brown, N. Kaltsoyannis, G. Wu and T. W. Hayton, *Inorg. Chem.*, 2012, **51**, 1625–1633.
74 N. Barros, D. Maynau, L. Maron, O. Eisenstein, G. Zi and R. A. Andersen, *Organometallics*, 2007, **26**, 5059–5065.